

APPENDIX 2.3

9965 CONE-SEAL CLOSURE PERFORMANCE AT -40°F

This Page Intentionally Left Blank

9965 Cone Seal Closure Performance at -40°F

April 2, 1990

SRL-PTG-90-0047

To: E. K. Opperman, 730-A
Manager, Packaging and Transportation (P&T) Group

From: J. E. Cox, 730-A
Associate Engineer, P&T Group

9965 Cone Seal Closure Performance at -40°F

Ref: U. S. DOE Memo to G. W. May, from J. G. Leonard, Acting Chief-Packaging Certification Staff-Office of Security Evaluations-Defense Programs, "Questions from Q0 Review of 9965, 9966, 9967, and 9968 Packages, Docket 88-4-9965", 4/7/89.

A question from the Central Certification Office (3.1 of Reference) concerning the Viton seal low temperature performance of the 9965-9968 shipping packages initiated a P&T investigation.

P&T evaluated the information in the SARP (DPSPU 83-124-1, Sec 2.6.2) and determined that additional information was necessary to qualify the Viton "GLT" O-rings at -40°F. The P&T Group and Equipment Engineering Section (EES) of SRL developed hardware and wrote a test procedure, EES Special Procedure No. 407, Rev. 0, to perform helium leak testing on the 9965 Cone Seal Closure at -40°F.

EES performed an initial helium leak test (EES-900055, Record No. 465) at room temperature according to DPSOL 324-3-3404. P&T and EES then cooled the 9965 primary containment vessel (PCV) to -40°F and repeated the leak test. The results (EES-900055, Record No. 458) document that the PCV was leak tight (less than 1×10^{-7} atm cc/sec air per ANSI N 14.5-1987) for 10 minutes with an internal pressure of 15 psig. P&T and EES warmed the PCV to room temperature and installed a new set of O-rings. EES performed an initial leak test (EES-900055, Record No. 463) on the reassembled 9965 at room temperature. After cooling the PCV, EES and P&T repeated the -40°F leak test (EES-900055, Record No. 462) with leak tight results.

P&T documented the tests in the 9965-9968 QA file 810000574 located in SRL and revised Section 2.6.2 of the SARP. DOE/Savannah River will transmit the revised SARP to the Central Certification Office for review after P&T addresses all of the QOs and incorporates the changes into the SARP. All "scoping" work leading up to the final tests will be on file in the P&T Group files.

If you have any questions, please contact me, extension 5-1713.

CC G. Cadelli

APPENDIX 2.4
EVALUATION OF 9975 SHIPPING CONTAINER FLANGE CLOSURE

This Page is Intentionally Left Blank

OSR 45-24# (Rev 1-10-2000)

Calculation Cover Sheet

Project NA	Calculation No. T-CLC-F-00172	Project Number NA		
Title Evaluation of 9975 Shipping Container Flange Closure		Functional Classification SC	Sheet 1 of 68 (including attachments)	
Discipline Structural Mechanics				
<input type="checkbox"/> Preliminary <input checked="" type="checkbox"/> Confirmed				
Computer Program No. ABAQUS <input type="checkbox"/> N/A		Version/Release No. 5.8		
Purpose and Objective The purpose of this analysis is to provide analytical justification for the flange closure modification on the 9975 series package assembly. This analysis will show that the assembly, with the flange closure, will perform as well as the DOE approved DT-22 assembly when evaluated to design requirements.				
Summary of Conclusion The proposed flange closure design for the 9975 series shipping packages has been shown to provide acceptable performance for the requirements of 10CFR71. The conclusion is based on analytical comparison to the flange closure of the DT-22 shipping package. Specific results are shown in Table 3.1. The modification to the drum closure is documented in drawing R-R2-F-0025 and R-R2-F-0026. The increase in weight of the assembly is 6.2 lbs. The evaluation provided supports use of the flange closure on the 9975 shipping package without additional testing.				
Revision(s)				
Rev. No.	Revision Description			
0	Initial Issue			
1	See Revision Page			
2	See Revision Page			
Sign Off				
Rev. No.	Originator (Print) Sign / Date	Verification / Checking Method	Verifier / Checker (Print) Sign / Date	Manager (Print) Sign / Date
0	C. A. McKeel	Document Review	R. R. Rothermel	G. B. Rawls
	<i>Signature on File</i>		<i>Signature on File</i>	<i>Signature on File</i>
1	C.A. McKeel	Document Review	R.R. Rothermel	Fred Loceff
	<i>Signature on File</i>		<i>Signature on File</i>	<i>Signature on File</i>
2	C.A. McKeel	Document Review	George Antaki	Fred Loceff
	<i>CA McKeel 10-6-03</i>		<i>Antaki 10-7-03</i>	<i>Loceff 10-7-03</i>
Release to Outside Agency - Design Authority (Print)			Signature	Date
NA			NA	NA
Security Classification of the Calculation				
NA				

1 PURPOSE 7

2 SCOPE 7

3 CONCLUSIONS 7

4 METHODOLOGY 8

4.1 Analytical Methodology8

4.2 Acceptance Criteria.....8

5 INPUTS 8

5.1 Structural Details.....8

5.2 Material Properties 11

6 ANALYSIS 12

6.1 Evaluation of Previous Test Data..... 12

6.2 Drop Evaluation..... 14

6.2.1 FEA Model Description..... 14

6.2.2 Load Cases..... 19

6.2.3 Results 19

6.2.4 Evaluation of Closure Screws for Container Crush Loads 37

6.2.5 Evaluation of Lid Curvature 39

6.3 Axial Compression Evaluation 42

6.3.1 Five Times Load Compression Test 42

6.3.2 Buckling Analysis..... 49

6.4 Weight Evaluation 50

6.5 Closure Fastener Evaluation 52

6.6 Vibratory Loads on 9975 Package During Normal Conditions of Transport..... 54

6.7 Loosening of Drum Bolts During Normal Conditions of Transport..... 57

6.8 Evaluation of Flange to Drum Weld 59

7 REFERENCES 63

OPEN ITEMS

None

RECORD OF REVISION					
REV. NO.	PAGES SUPERSEDED	PAGES ADDED	PAGES DELETED	PAGES REVISED	DESCRIPTION OF REVISIONS
0					Original Issue
1					Pages 1-75 of revision 0 replaced by pages 1-67 of revision 1.
2					Complete Revision, all pages replaced to incorporate regulator comments on ASME Code compliance. (Pages 1-67 of rev 1 replaced by 1-68 of revision 2)

1 Purpose

The purpose of this analysis is to provide analytical justification for the flange closure modification on the 9975 series package assembly. This analysis will show that the assembly, with the flange closure, will perform as well as the DOE approved DT-22 assembly when evaluated to design requirements.

2 Scope

The items addressed in this calculation are those directly related to the flange closure. Existing test data and analysis qualifies all aspects of the 9975 package except for the existing banded closure design. This analysis will evaluate the 9975 package flange closure design by comparison to the DT-22 flange design, whenever possible. The items evaluated are:

1. The acceptable performance of the flange closure, including meeting the requirements of 10 CFR71.71 NCT and 10 CFR71.73 HAC testing.
2. Maintenance of 2 inches of undamaged Celotex between the drum and the package internals.
3. Compressive load capability.
4. Closure fastener pre-load.
5. Closure fastener integrity during NCT vibrations.
6. Closure fastener loosening due to thermal cycles.
7. Additional weight of modifications.

3 Conclusions

The proposed flange closure design for the 9975 series shipping packages has been shown to provide acceptable performance for the requirements of 10CFR71. The conclusion is based on analytical comparison to the flange closure of the DT-22 shipping package. This comparison is based on applying loads statically to a non-linear model of the DT-22 container to achieve a comparable level of permanent deformation with the tested DT-22 containers, for both the 45° drop and a horizontal drop from a height of 30 feet. Then a similar model of the 9975 package was loaded to achieve a comparable level of deformation and the resulting closure bolt loads were determined and compared.

The analysis shows that because of the stiffer geometry (from the smaller radius of the 9975 container) the closure screw loads are greater. In order to provide the same level of safety, this 9975 design specifies ½” closure screws, rather than the 3/8” used in the DT-22 package. The modification to the drum closure is documented in drawings R-R2-F-0025 and R-R2-F-0026. The increase in weight of the package is 6.2 lbs.

The evaluation provided supports use of the flange closure on the 9975 shipping package without additional testing. If additional testing is specified, this analysis suggests that the 45° inclination, top down, drop produces worst case loads on the closure screws. It is also recommended that the impact points used in the pre-condition drop and the 30 foot drop be spaced a minimum of 15 degrees and a maximum of 30 degrees apart.

4 Methodology

4.1 Analytical Methodology

The closure screw pre-load and the integrity of the screw during vibratory and thermal loads are evaluated using standard mechanical and stress analysis techniques.

The loads on the 9975 package closure screws are evaluated by comparison to the closure screw loads on a DT-22 package under similar permanent deformations. This is achieved in two steps. First, a finite element model of the DT-22 package is made, with the emphasis being on the closure ring area. This model incorporates non-linear material properties, non-linear geometry, and contact surface definitions between the impact surface and closure ring and also between the various parts of the container which could experience "self-contact." The ring is then loaded statically, until a permanent deformed shape is achieved that is comparable to the tested DT-22 container. This is performed for both the 45° drop orientation and the horizontal drop orientation. Second, a finite element model of the 9975 package is made and subjected to the same loading scheme. The results of the two load cases for each model are then compared. The results are also used to justify the applicability of equal deformations as being a valid comparison basis.

Because of the extensive non-linear nature of the analysis, a quarter model of the drum is made for improved computer speed. A combination of symmetry and fixed boundary conditions are imposed to represent the complete drum. The loads are applied along the edge with symmetry boundary conditions. This modeling technique is acceptable since the impact is localized to a limited area of one side of the drum and the influence of the deformation will not affect the opposite side of the package.

Three-dimensional finite element models of the 9975 assembly and the proven DT-22 assembly were developed for the ABAQUS finite element program. The models consisted of a detailed mesh of the interfacing regions of the lid, ring, and flange assembly. The model also incorporates the drum wall and rolled hoop. The Celotex insulation is not modeled. Though Celotex is the major energy absorber for the drop condition, inclusion of the Celotex would not result in significantly different loads in the drum structure. This is particularly true for the closure screws. A detailed discussion of the model is presented in Section 6.2.1.

4.2 Acceptance Criteria

As the justification of the flange closure on the 9975 package is based on comparison to the DT-22 flange closure, the acceptance criteria is to show that the 9975 closure will perform as well as the DT-22 closure for the hypothetical drop requirements.

5 Inputs

5.1 Structural Details

The 9975 package consists of a cylindrical outer drum constructed of 18 Ga stainless steel. The drum has an inner diameter of 18.25 inches and a height of just under 35 inches. The drum has two rolled hoops for cylindrical stiffness, one near bottom and one near top, located 8.88 inches from the respective ends. The drum bottom is an 18 ga stainless steel circular plate, with edges rolled and

crimped (double seamed) and welded continuously to the drum bottom. The top lid is also an 18 ga. circular plate. The lid incorporates a 0.55" offset hat section. The hat section diameter is 17.87 inches. The outer section of the lid is welded to a 1/8 inch thick x 1.25 inch wide circular ring of 20.85 inch outer diameter. The ring has 24 holes, equally spaced on a 19.84 inch diameter. The maximum gross weight of the 9975 is 404 lbs.

The DT-22 package consists of a cylindrical outer drum constructed of 18 Ga stainless steel. The drum has an inner diameter of 22.4 inches and a height of just under 28 inches. The drum has two rolled hoops for cylindrical stiffness. The hoops are located 3 inches from each end. The drum bottom is an 18 ga stainless steel circular plate, with edges rolled and crimped (double seamed) and welded continuously to the drum bottom. The top lid is also an 18 ga. circular plate. The lid incorporates a 0.75" offset hat section. The hat section diameter is 22 inches. The outer section of the lid is welded to a 1/8 inch thick x 1.25 inch wide circular ring of 25.2 inch outer diameter. The ring has 24 holes, equally spaced on a 24.2 inch diameter. The maximum gross weight of the DT-22 is 412 lbs. as tested.

**Table 5-1
Summary of Structural Details**

	DT-22	9975 w/ Flange
Package Design Weight	412 lbs	404 lbs
Drum		
Outer Diameter of Body	22.4 in	18.35 in
Height (to TOF) ^a	27.68 in	34.78 in
Wall Thickness	0.048 in	0.048 in
# Rolled Hoops	2	2
Rolled Hoop Locations (from Bottom)		8.88 in, 25.9 in
Material	304L ASME SA-240	304L ASME SA-240
Lid		
Thickness	0.048 in	0.048 in
Bend Radius		
Hat Section Depth	0.75 in	0.75 in
Material Specification	304L ASME SA-240	304L ASME SA-240
Lid-to-Ring Weld	0.05" fillet, 1" - 6"	0.05" fillet, 1" - 6"
Ring		
Width	1.25 in	1.25 in
Thickness	0.125 in	0.125 in
Material Specification	304L ASME SA-240	304L ASME SA-240
Flange		
Angle	1¼" x 1¼" x 1/8"	1¼" x 1¼" x 1/8"
Material	304 or 304L ASME SA-479	304 or 304L ASME SA-479
Screws		
Specification	Hex Head Screw, ASME SA-320 L7	Hex Head Screw, ASME SA-320 L7
Screw Size	0.375-16UNC-2A	0.500-13UNC-2A
Bolt Circle Diameter	24.10 in	19.84 in
Number of Bolts	24	24
Bolt-to-Bolt Spacing	3.15 in	2.60 in

a- Top of Flange

5.2 Material Properties

The material properties used for the stainless steel drum, flange, lid and ring, the closure screws, and the screw nuts are shown below. Parametric studies to show the effects of median or upper bound material properties are not performed, as this analysis is comparative in nature. On the same basis, the increased material strength due to the high strain rates was also not considered.

Stainless Steel

The material of construction for the drum body, lid, and ring are ASME SA-240 304L stainless steel. The rolled angle used for the flange is ASME SA-479 304 or 304L stainless steel. The elastic modulus of 28.3E6 psi is obtained from ASME II-D, using room temperature conditions. Design value for true stress-strain curves are developed from room temperature data obtained from the Aerospace Structural Metals Handbook. The data was curve fit to the equation

$$\sigma_t = K \epsilon_t^n$$

where: σ_t = true stress

K = Strength Coefficient = 125,862 psi at room temperature

ϵ_t = true strain

n = strain-hardening exponent = 0.2297 at room temperature.

A plot of the resulting true stress-strain curve is shown below. This stress-strain curve corresponds to lower bound data.

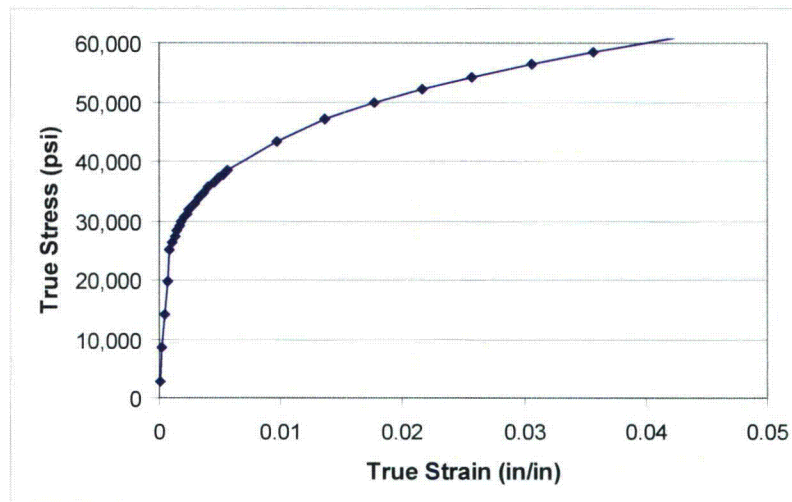


Figure 5-1 True-Stress Strain Curve Used in Analysis for 304L Material

Closure Screws

Material : SA-320, Grade L7

S_y = 105 ksi

S_u = 120 ksi

S_m = 20 ksi

Nut

Material : Carbon Steel

S_y = 30 ksi

S_u = 60 ksi

S_m = 14.5 ksi

6 Analysis

6.1 Evaluation of Previous Test Data

In preparation for developing computer models of the redesigned 9975 closure details, the drop test results of containers having similar closures were reviewed. This included review of test reports and photographs of the tested specimen's damaged state with specific recognition of any breaching of the closure seal, as well as, to assess the expected deformed state of tested containers. The reports for the tested containers that have similar closure flanges to the proposed 9975 modification that were available for review were:

- “Test Report for Certification of the DC-1 Shipping Package” (YMA-93-20), and
- “Test Report for the Certification of the DT-22 Shipping Package” (YMA-93-15).

Both the DC-1 and the DT-22 shipping containers have larger diameters than the 9975 container. Table 6-1 lists pertinent geometry and weight differences between the tested containers and the 9975 container.

TABLE 6-1 Drum Structural Data

Container	Height (inch)	OD-Bolt Ring Diameter (inch)	No. of Bolts	Size of Bolts (inch)	Closure Ring	Wall & Lid Thickness (inch)	Tested Weight
DC-1	≈ 40	≈ 31	30	3/8	NA	.06	754-780 lbs.
DT-22	27.8	25.1	24	3/8	1¼ x 1/8	.048	412 lbs (min)
9975	≈ 35	20.85	24	3/8	1¼ x 1/8	.048	(404 lbs)*

* maximum design weight

The 9975 container has the smallest diameter of the three, and as such will have the highest lateral stiffness of its bolt closure ring for lateral loading.

The features for the 30-foot drop test that are significant when developing computer models are:

- Type of permanent deformation.
- Amount of permanent deformation.
- Breach of confinement.
- Mode of failure.
- Possible bolt failures.

In all of the 30 foot drop tests, there were no reported bolt failures, nor any evidence of bolt failures in the test photographs.

Table 6-2 lists the permanent damage from the DC-1 30 foot drop test and Table 6-3 lists the permanent damage from the DT-22 30 foot drop test as identified in the test reports.

TABLE 6-2 DC-1 30 Foot Drop Tests

Test Orientation	Impact Surface	Note
Horizontal	Side	3/16" opening between drum flange and lid between bolts.
18° Horizontal	Side	Weld broken on top ring to cover plate
47°	Oblique	4-broken weld top ring ≈5" permanent deformation
47°	Oblique	Two broken welds in top ring. ≈5" permanent deformation on impact side

TABLE 6-3 DT-22 30 Foot Drop Tests

Test Orientation	Impact Surface	Note
Horizontal	Side	No broken bolts or welds
Oblique 10° to Horizontal	Side	Flanges separated approximately 5/16 inch between bolts
44.2°	Oblique	6.5 in permanent deformation
Vertical	Top	Barrel buckling at suspended hoop

The DC-1 drop tests resulted in failure of some welds between the bolt ring and the lid. There was no similar failure in the DT-22. This is attributed to the significantly higher weight of the DC-1 package (780 lb vs 412 lbs).

Inspection of Photographs 1 through 4 (see Appendix A) of the DT-22 30-foot drop test indicates that there are no broken bolts or welds. However, there is significant permanent deformation of the bolt ring, container wall and lid.

The horizontal side drop and the 10° oblique drop as shown in Photographs 1 and 2 of the DT-22 container indicates a classical compressive buckling mechanism with permanent deformation of the bolt ring between the bolts. This results in separation between the bolt ring and the angle at the top of the barrel and potential shear loading on the bolt. Observation of the flame path in Photographs 5 and 6, taken during the fire test, show that these openings allow a pathway between the interior and exterior of the vessel.

The plastic buckling mode of the bolt ring was duplicated in the analysis report for the 9975 and the DT-22 computer models. However, because of the decreased closure bolt spacing in the 9975 bolt ring, the shear forces in these bolts are more than proportionally increased with respect to the geometry changes.

The oblique drop, as shown in Photograph 3, resulted in significant inward bending of the bolt closure flange/ring, as the bolt closure flange angles towards the drum wall. The drum wall deforms into the lid offset section. This deformation behavior is captured by the computer models.

The deformation of the bolt closure lid for the horizontal and 10° oblique drop show the bolt closure ring and the bolt closure flange in an upward direction towards the top of the container. This deformation behavior is also captured by the computer models.

6.2 Drop Evaluation

The structural response of the drum closure for the 30 foot drop loading is evaluated in this section. The finite element method is utilized to make mathematical models to represent the drum structural components of the DT-22 and the 9975 assemblies. This evaluation does not consider the dynamics of the 30 foot drop, but rather makes a comparison by confirming that an imposed static deformation via displaced rigid surface on the Finite Element Model (FEM) reasonably duplicates the deformed shape of the test results of the DT-22. The evaluation is by comparison of the response of the 9975 closure to that of the response of the proven DT-22 closure under the same load deflections.

6.2.1 FEA Model Description

The 30 foot drop of the shipping packages induces large, localized, deformations on the exterior shell. Significant plastic behavior and non-linear geometric effects result from the drop testing. In order to analyze this nonlinear behavior, the finite element method is used. A three-dimensional model of each drum is created and coded for the ABAQUS/Standard finite element program. The intent of the modeling is to compare the forces on the closure assembly during the expected crushing. The crush is imposed onto the model using a static analysis procedure.

Element Description

The basic construction of the model employs first order shell elements. The model consists of the closure ring, the closure lid, the drum flange and the drum itself. The closure screws are modeled as beam elements. Each of these components are modeled as completely separate modules. The closure ring is tied to the closure lid intermittently using Multi-Point-Constraints (MPC's). These MPC's represent the stitch welding to be used on the actual drum. Similarly, the drum flange is joined to the drum shell using MPC's at the weld attachment points. The drum/flange assembly and the lid/ring assembly are then joined via ABAQUS contact surfaces and with the (closure screw) beam elements.

A quarter model is used to represent the full drum. Symmetry boundary conditions are imposed along one edge of the quarter model, while the other edge has the symmetry condition plus a restraint in the direction parallel with the drum axis. The imposed deformations are applied along the edge with the pure symmetry condition, as shown in Figure 6-5. This modeling technique is acceptable since the impact deformation is localized to a limited area of one side of the drum and the influence of the deformation will not affect the opposite side of the drum. The specific screw hole locations are modeled in the vicinity of the applied load. Away from the load application point, the model becomes more coarse and the bolt holes are not explicitly modeled. However, all the attachment screws are modeled such that the shear and tensile load can be obtained.

Contact

ABAQUS provides modeling of mechanical contact between bodies. Mechanical contact describes cases where bodies may touch or separate during an analysis. Contact is modeled by defining surfaces (or nodes) which may interact. These surfaces are used in Contact Pair definitions, in which one surface is "slaved" to a "master" surface. Each contact pair is linked to a specific SURFACE INTERACTION option to describe the interaction effects (e.g. friction, heat).

The package assembly is modeled using frictionless contact, such that the bolts are the only shear connection between the drum/flange portion and the lid/ring portion of the model. Softened contact is used. The "softened contact" option allows the contact pressure to build once the involved nodes are

within a user specified distance. A stiffness of the surface is also specified with “soft contact”. Since the shell elements are modeled at their actual centerline, the distance specified in the model is the sum of the half thickness of the slave element and the half thickness of the master element. A stiffness based on the plate thickness and elastic modulus is used.

In addition to the contact elements, non-linear, compression only springs were modeled between the surfaces at the fastener locations. These elements were chosen to simplify the model. Because of the refinement of the mesh at the hole locations, the use of contact surfaces in these areas would have involved too many nodes, creating a penalty in run time and overall performance. The spring stiffness was chosen on the same basis as the contact stiffness.

Because contact introduces a severe non-linearity, only the minimum amount of contact surfaces are used. Contact is specified between the flange and lid by partitioning the surface into several regions. The first region is a band along the outer edge of the flange upper surface, which is paired to a similar region on the lower surface of the lid. The second region is along the inner edge of the mating surfaces. Additional regions include a portion of the mid-span between each bolt. The regions are segmented in order to minimize the nodes involved in contact. Because the bolts have been shown to perform well at keeping the components mated together, the small sliding option is used on the flange to lid surface. With small sliding, ABAQUS minimizes the contact search algorithm by establishing a specific segment of the master surface for each slave node, versus the more general approach of searching an entire region of the master surface for each slave node. Small sliding is appropriate for this surface, since the surfaces do not exhibit significant relative sliding.

Contact using the large sliding algorithm is also specified between the offset section of the lid, and the inner drum wall.

To apply the load, contact is also specified between a rigid surface representing the drop target and contacted portions of the drum. These portions of the drum include the top surface of the ring, the bottom surface of the flange, and the upper region of the drum wall. The surfaces are defined to cover the circumferential distance likely to contact the target surface ($\approx \pm 15^\circ$). The large sliding algorithm is used. No friction is used between the rigid surface and the drum body.

Material Properties

Plastic material properties are used for the ring, lid, flange, and drum. The bolts are modeled strictly elastically. The plastic material properties used for the drum assembly are described in section 5.2.

Pre-Load

The closure screws are modeled explicitly using beam elements. The upper beam end is tied to the ring and the lower end is tied to the flange. Pre-load of the screw creates tension in the screw and forces the flange and lid surfaces together. The pre-load is applied by specifying a thermal contraction of the bolt. Since friction effects between the surface are not explicitly modeled, and the screw is modeled elastically, the actual magnitude of pre-load is not critical to the analysis results. Table 6-4 below shows the required temperature change to impose the pre-load on the bolt. Because of the flexibility created by the softened contact, the actual required temperature change will be slightly higher than that computed. The following calculations are shown using a 3/8” closure screw, as incorporated in the finite element model. The conclusion of this analysis shows that a larger bolt is

required. The model with the smaller screw is still valid in terms of shear loads. As the only shear load path between the lid/ring and the drum/flange are the closure screws, the actual stiffness used will not influence the load magnitude. The change in tensile pre-load is also not significant, since contact friction is not incorporated into the model.

**Table 6-4
Preload Calculations**

		DT-22	9975
Pre-Load	F	1350 lbs	1350 lbs
Bolt Tensile Area	A	0.078 in ²	0.078 in ²
Young's Modulus	E	29E6 psi	29E6 psi
Mechanical Strain in Bolt, =(F/A) / E	ϵ_m	0.000612	0.000612
Modeled Thermal Expansion Coefficient	α	$7.E-6 \frac{in}{in \circ F}$	$7.E-6 \frac{in}{in \circ F}$
Initial Temperature	T_i	70 °F	70 °F
Required Temperature change = ϵ_m/α	ΔT	-87.4 °F	-87.4 °F
Specified Temperature = $T_i - \Delta T$	T	-17.4 °F	-17.4 °F

Model Plots

The following plots show the various components of the finite element model. The model shown is of the DT-22 assembly. The 9975 model is identical, except for the drum diameter and the location of the upper rolled hoop in the drum wall.

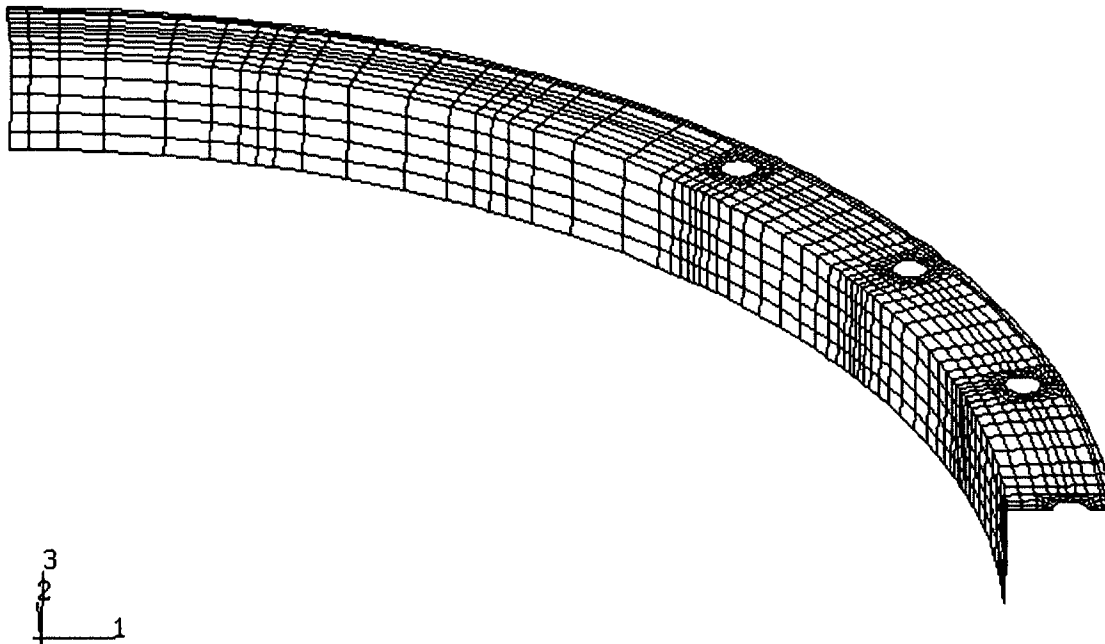


Figure 6-1 Finite Element View of Drum Flange (1.25" x 1.25" x 1/8" Angle)

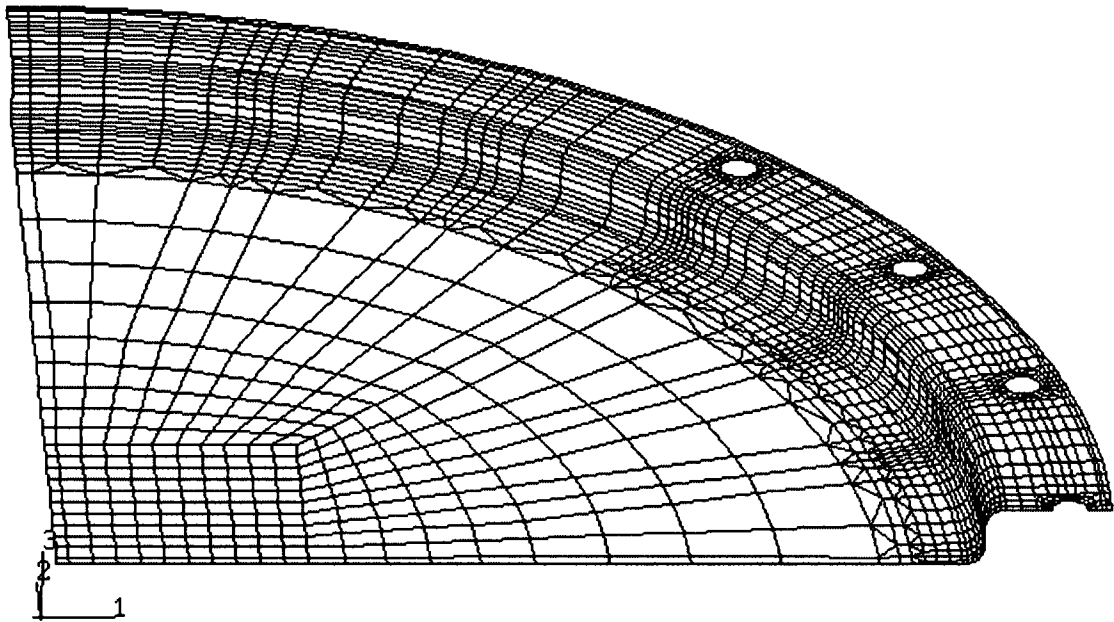


Figure 6-2 Finite Element View of Closure Lid.

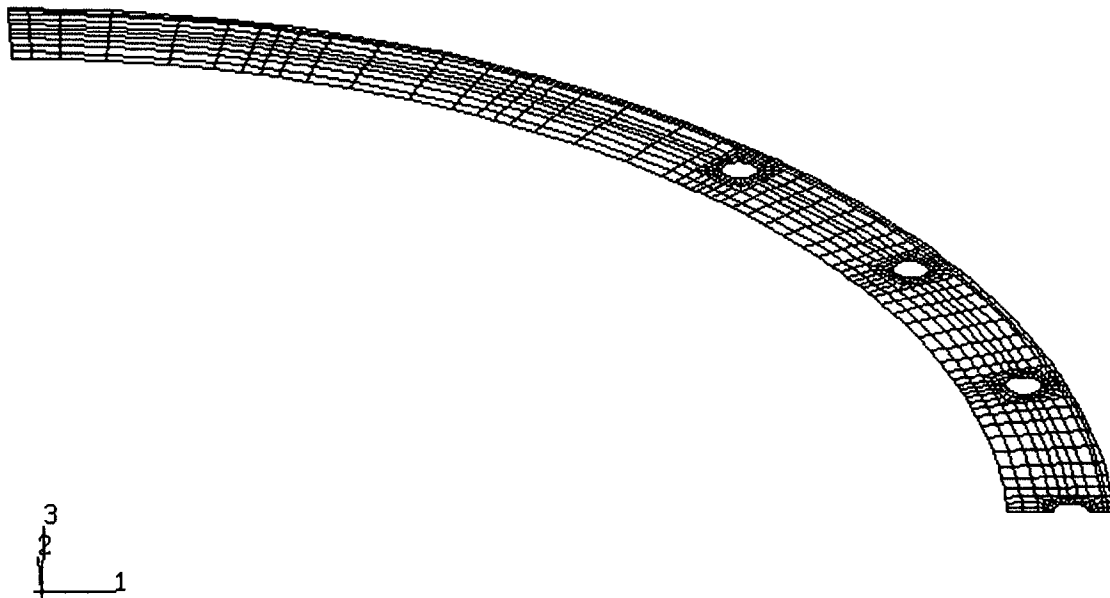


Figure 6-3 Finite Element View of Closure Ring

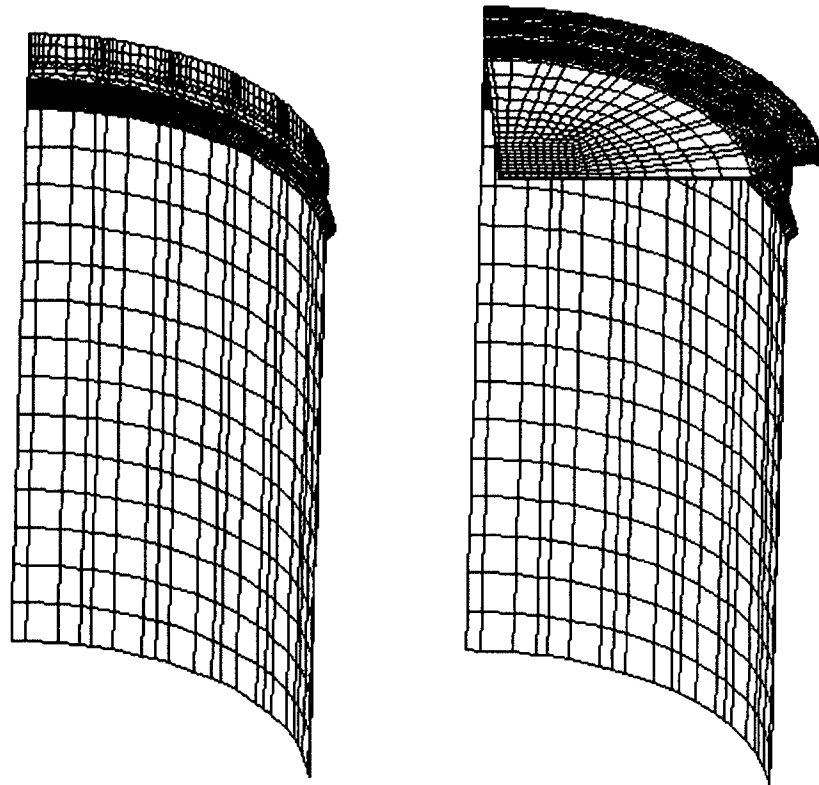


Figure 6-4 Finite Element View of Drum Cylinder and Complete Model.

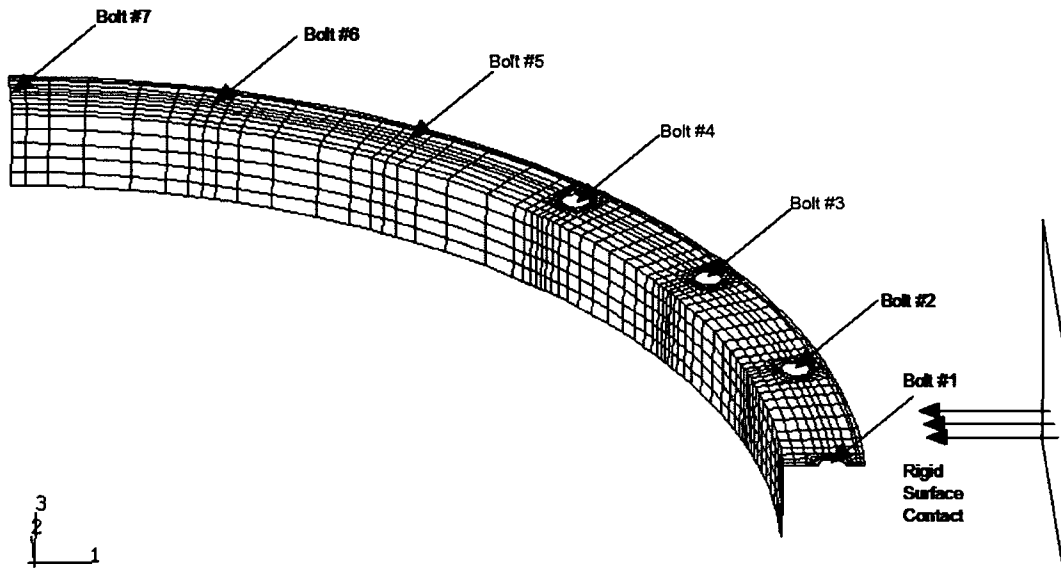


Figure 6-5 Finite Element View of Drum Flange, Showing Closure Screw Numbering Scheme and Location of Rigid Surface.

6.2.2 Load Cases

Two load cases are analyzed on the overall model for each drum:

- Low Angle (horizontal) Impact
- 45° Angle Impact

In the low angle impact, the rigid surface is oriented to be parallel to the drum wall. Contact is initiated at the outer edge of the flange. The overall relative displacement between the drum and surface is specified to be 2.5 inches from initial contact.

In the 45° angle impact, the rigid surface is placed at the tip of the flange and oriented at 45°. The displacement is specified to simulate 3.5 inches of movement of the surface into the drum at the 45 angle. The actual radial and axial displacement at the flange tip will depend on the relative drum assembly stiffnesses in the respective directions.

The analysis procedure is completed in two steps. The first step applies the thermal load to the bolts to provide pre-load. The second step is a static procedure to displace the drum into the rigid surface.

6.2.3 Results

The results of the FEA drop simulations includes the crush forces as a function of displacement, the bolt tensile and shear loads as a function of displacement and the energy absorbed as a function of displacement. In addition to these quantitative results, the deflected shapes of the crushed drums is shown for a qualitative comparison to the photographs from previous drop test. These results are shown for each drop simulation on both the 9975 assembly with flange and for the DT-22 assembly.

Low Angle Drop Simulation

The results of the crush simulations show the two drums behave similarly in terms of deflected shape. The low angle (Zero degree) drop simulation results in the flange bending upwards, duplicating the mode shape indicated in the photographs of existing drop tests. The computer simulation also captures the ring buckling between bolts as the ring is forced inward and into compression. The load histories for the 9975 drop simulation are shown in figures 6-6 through 6-8. The corresponding results for the DT-22 are shown in figures 6-9 though 6-11. A comparison of the results are shown in Figures 6-12 though 6-14. A summary of the results are shown in the following tables. A plot of the displaced shapes are shown in Figures 6-15 though 6-18.

The data for the zero angle simulation shows the 9975 develops more shear force in the screws for a given crush distance. On both drums, the shear load histories show a couple of peaks and dips, a result of the assembly passing through the drum wall buckling mode and the lid/ring buckling mode. The same variances are seen on the crush load histories. It is also seen that the variance of the tensile loads is such that a net tensile load is always maintained. The maximum tensile variance for all screws on either drum was a reduction of less than 500 lbs to an increase of 1200 lbs. Given the nominal values of pre-load, (3360 to 3840 lbs for 9975 {see sec 6.5}, ≈1300 to 1500 lbs DT-22), and the maximum sustainable tensile load of the screws (> 9000 lbs), the screws are shown to be structurally qualified.

The energy absorption history is shown on Figure 6-14 and shows that the 9975 absorbs slightly more energy than the DT-22 for a given deflection. This shows that comparing the 9975 closure screw load response to that of the DT-22 on an equal deflection basis is bounding. The magnitude of the absorbed energy (18,000 in-lbs) is only a small fraction of the total 145,400 in-lb drop energy. This implies that the Celotex, not modeled in this analysis, is the main contributor to the energy absorption. Any difference in structural stiffness between the banded closure design and the flange closure design would not influence the amount of drum crush during the drop. Therefore, the qualification of the Celotex damage measured during the banded closure design drop test is still valid for the flanged closure.

Table 6-5 Summary of Load Data for Zero Angle Imposed Deformation.

	9975 Drum	DT-22 Drum	Ratio of Max Values, 9975 to DT
Shear, Bolt #1	0 to 5950 lbs	0 to 5314 lbs	1.12
Shear, Bolt #2	0 to 5420 lbs	0 to 3230 lbs	1.68
Tension, Bolt #1 (See Note)	-200 lbs to 1000 lbs	-148 lbs to 807 lbs	1.24
Tension, Bolt #2	-30 to 770 lbs	0 to 1184 lbs	0.65
Tension, Bolt #3,4,5	-100 to +330 lbs	< +/-500 lbs	Na
Energy Absorbed (@ 2.5" Crush)	18,730 in-lbs	18,400 in-lbs	1.02

Note: Bolt tension is shown relative to pre-load

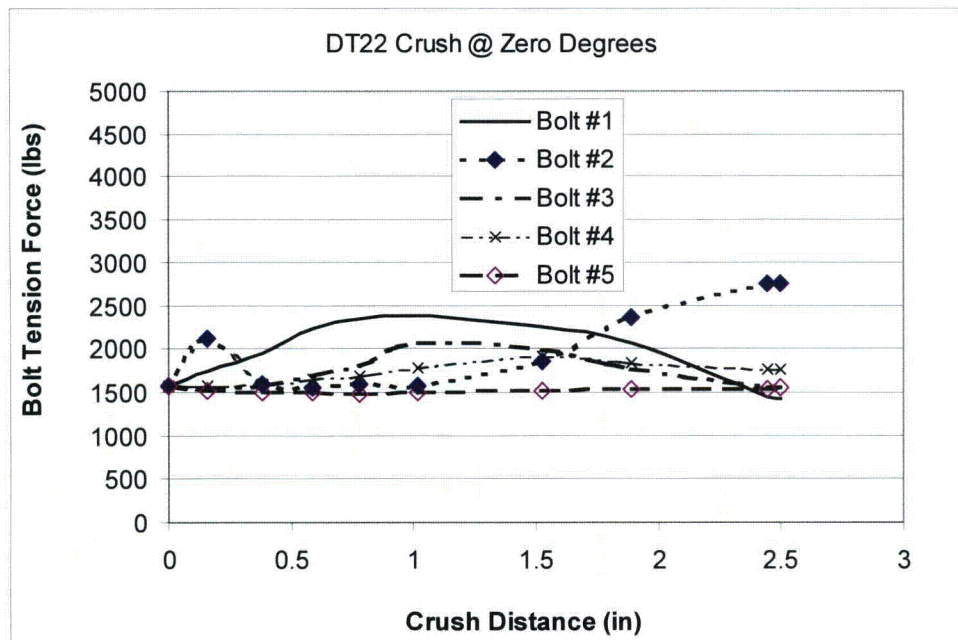


Figure 6-6 Tensile Load History for DT-22 Package Closure Screws For Zero Angle Drop Simulation, Showing Insignificant Variations in Tension Relative to Allowable Load. (Tension Allowable = 6550 lbs for 3/8" screw, Scale Set to ≈ 70% of Max allowable as a Visual Aid).



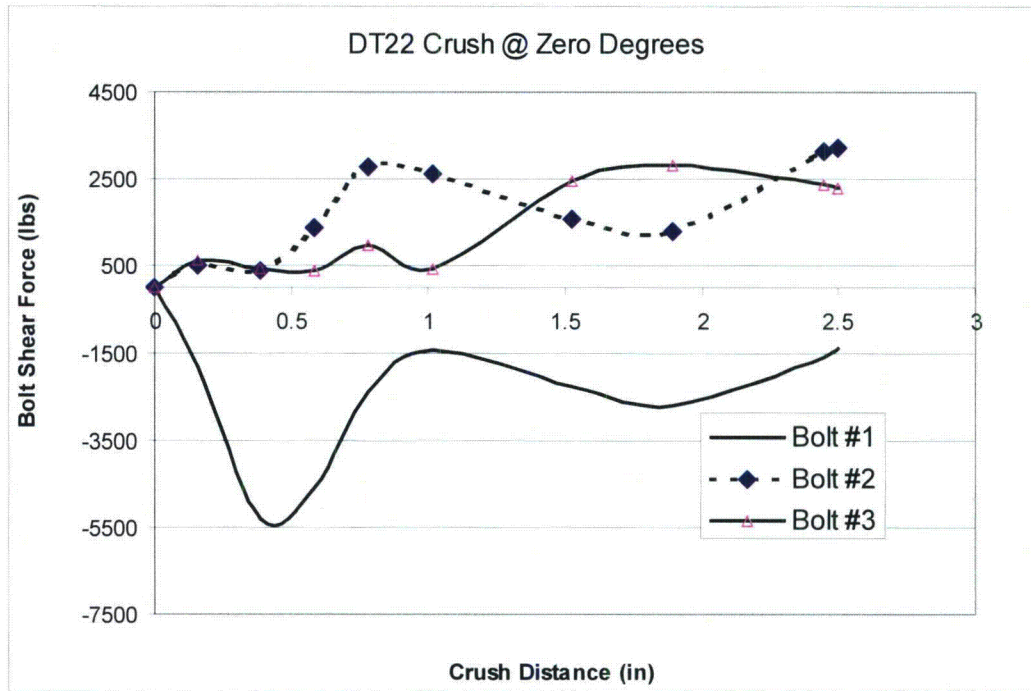


Figure 6-7 Shear Load History for DT-22 Package Closure Screws For Zero Angle Drop Simulation. (Max Shear Allowable for 3/8" Screw is 3427 lbs).

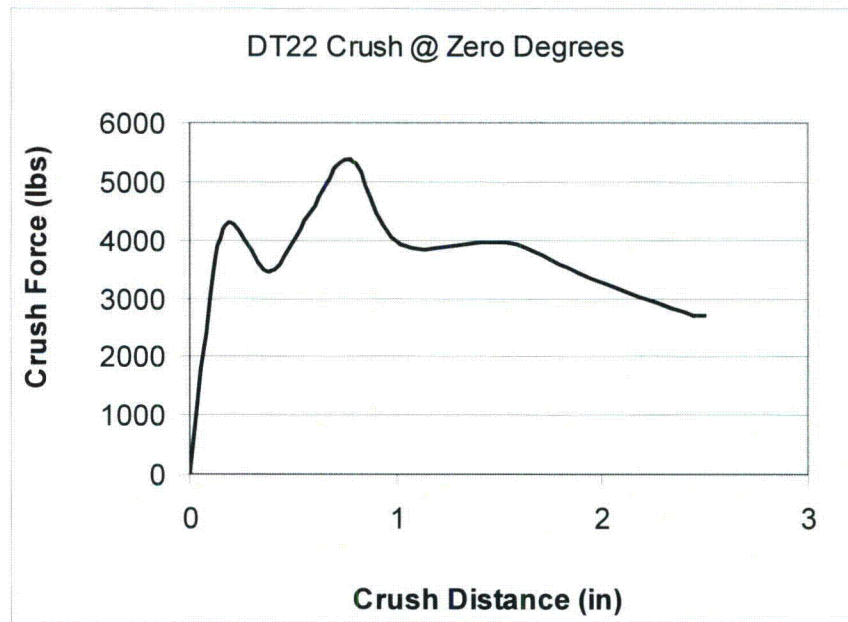


Figure 6-8 Crush Force History for DT-22 Package Closure Screws For Zero Angle Drop Simulation.

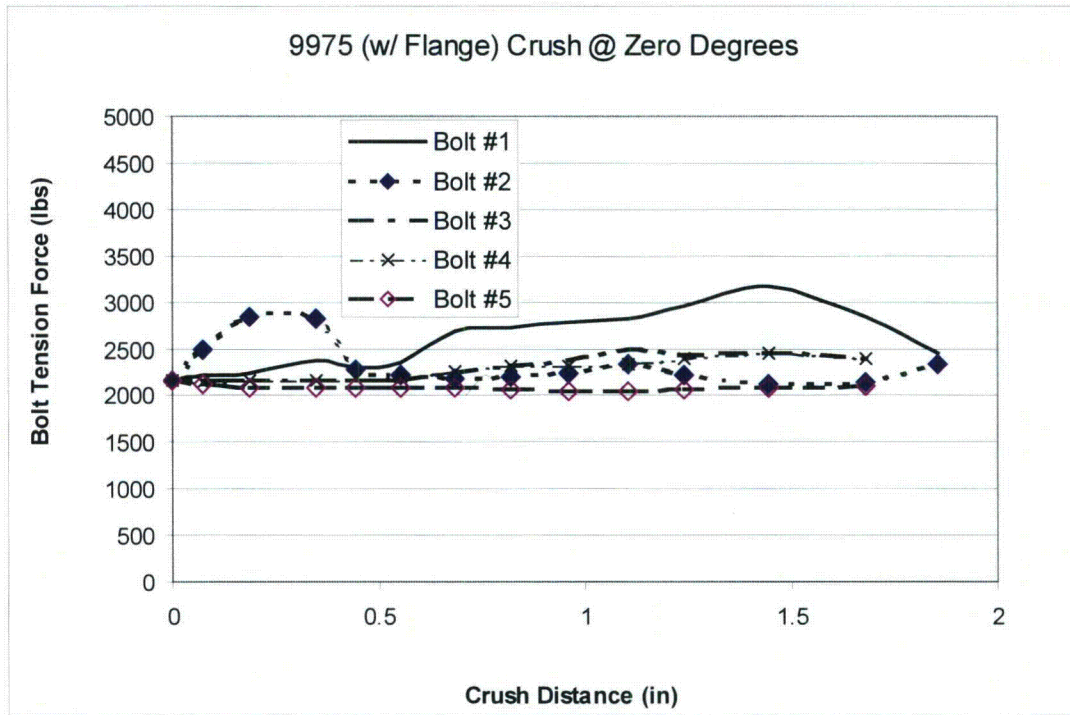


Figure 6-9 Tensile Load History for 9975 Package Closure Screws For Zero Angle Drop Simulation (Scale Based on DT-22 Parameters for Comparison).

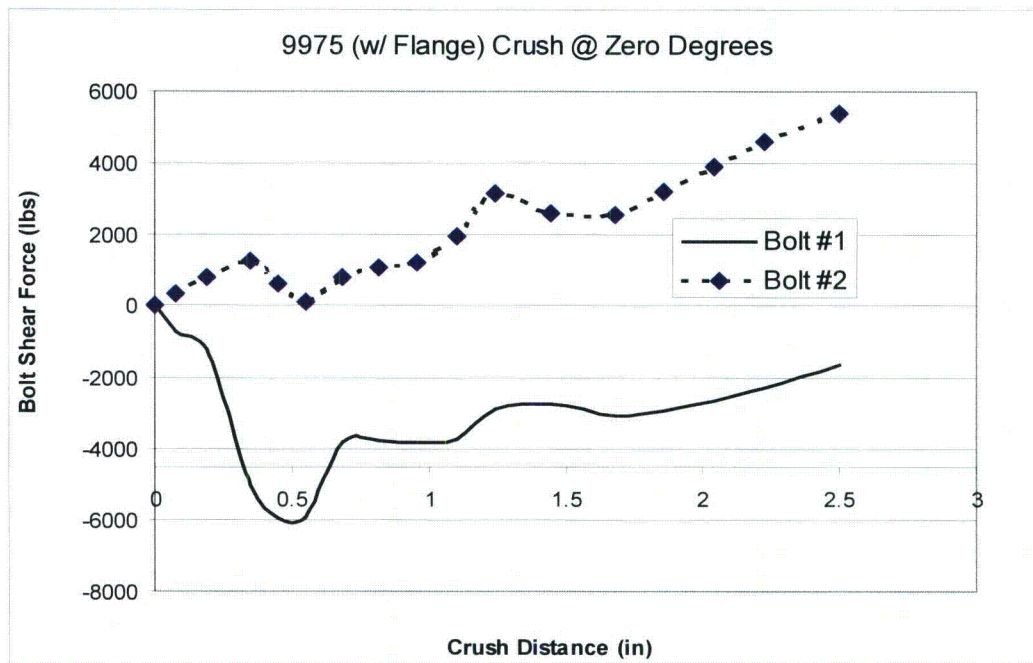


Figure 6-10 Shear Load History for 9975 Package Closure Screws For Zero Angle Drop Simulation.

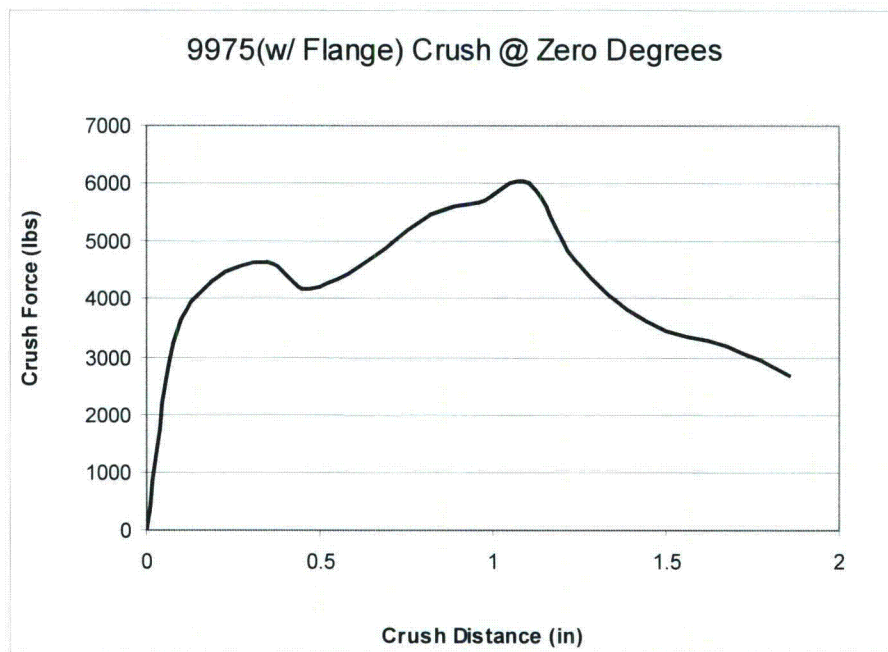


Figure 6-11 Crush Force History for 9975 Package Closure Screws For Zero Angle Drop Simulation.

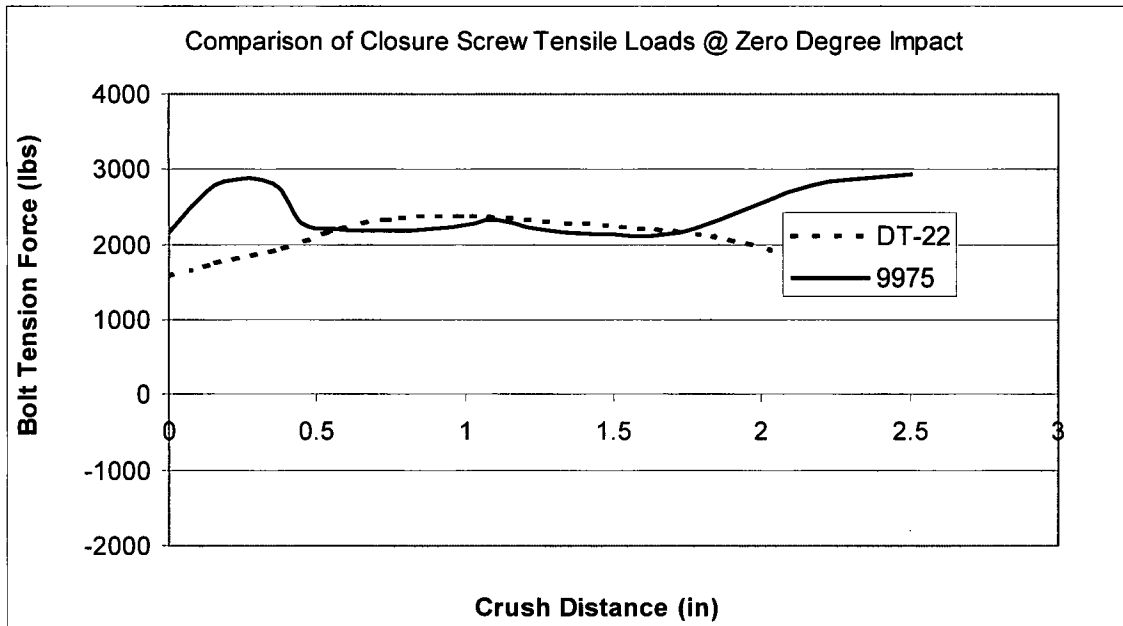


Figure 6-12 Comparison of Closure Screw Tensile Load Histories for Zero Angle Drop Simulation (Bolt #1 Shown)

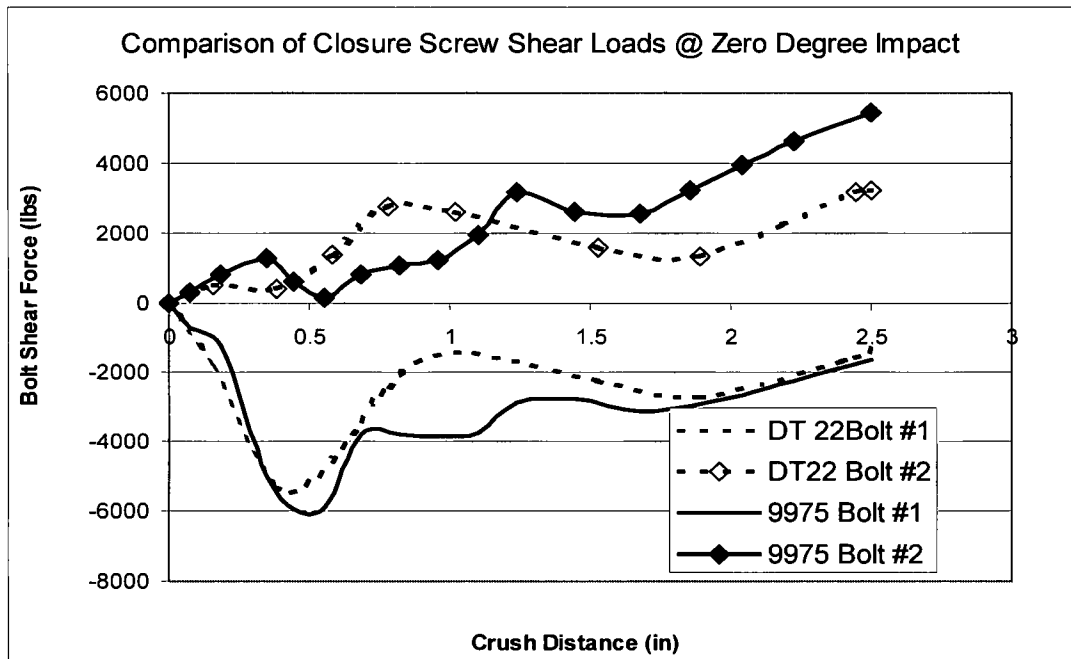


Figure 6-13 Comparison of Closure Screw Shear Load Histories for Zero Angle Drop Simulation.

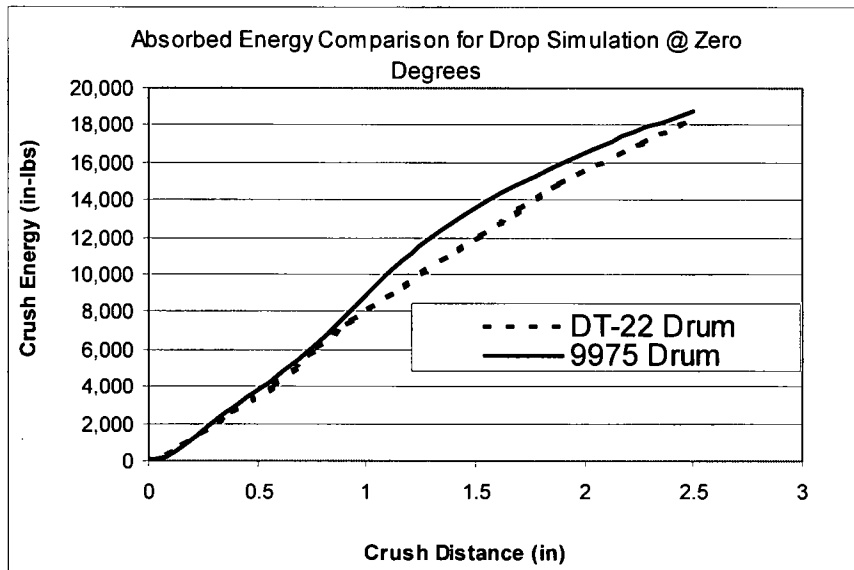


Figure 6-14 Comparison of Absorbed Energy for Zero Angle Drop Simulation.

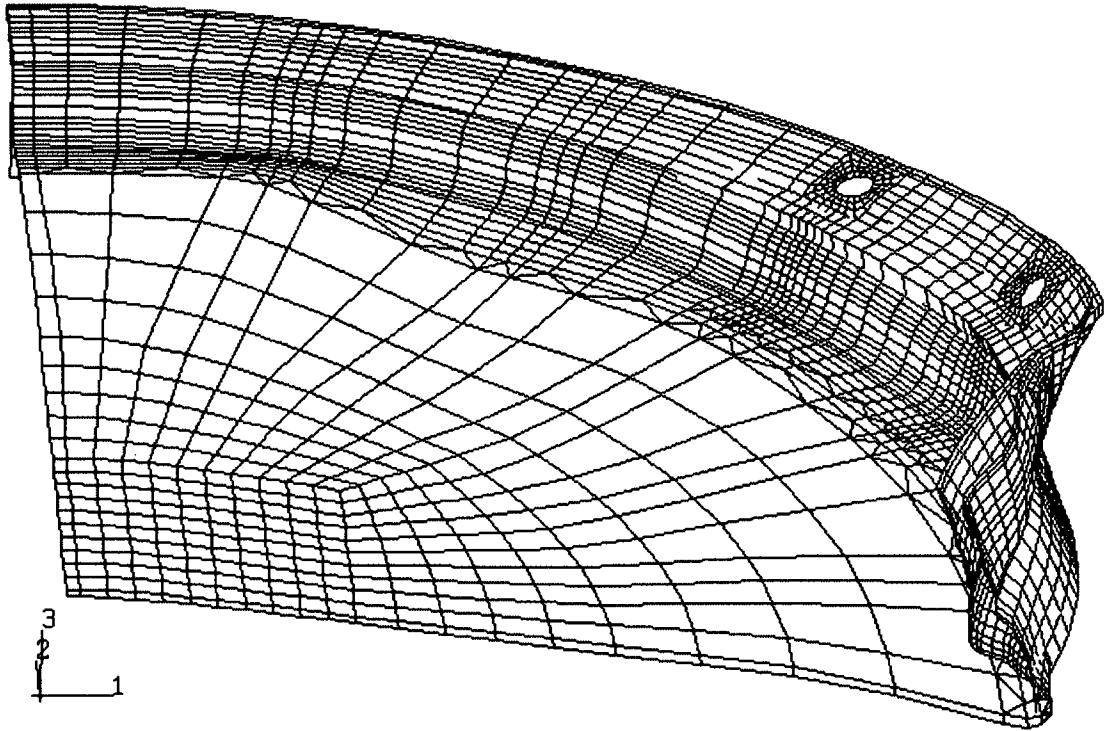


Figure 6-15 Detail View of Deformed Shape for Lid and Flange of Drum Assembly During 2.5 inch Zero Angle Imposed Deformation.

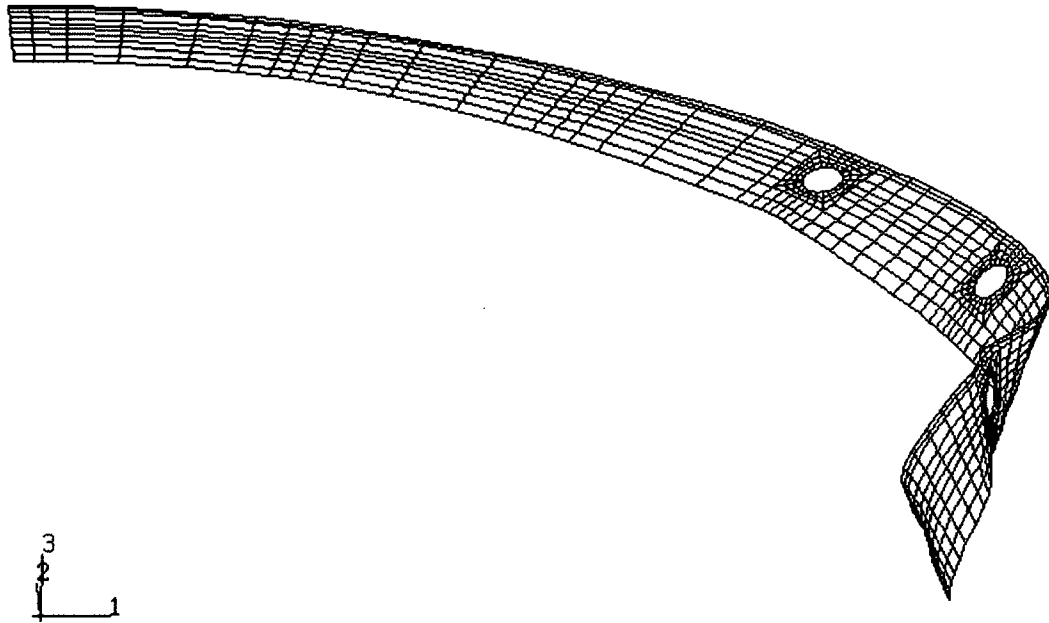


Figure 6-16 Detail View of Deformed Shape for Clamp Ring of Drum Assembly During 2.5 inch Zero Angle Imposed Deformation.

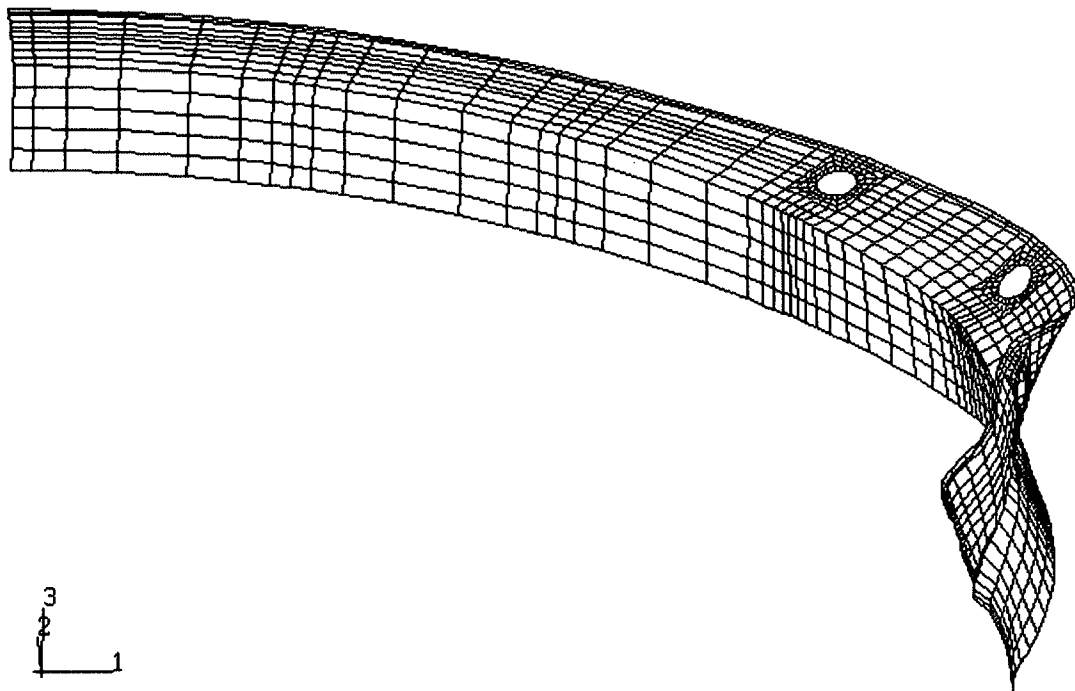


Figure 6-17 Detail View of Deformed Shape for Flange of Drum Assembly During 2.5 inch Zero Angle Imposed Deformation.

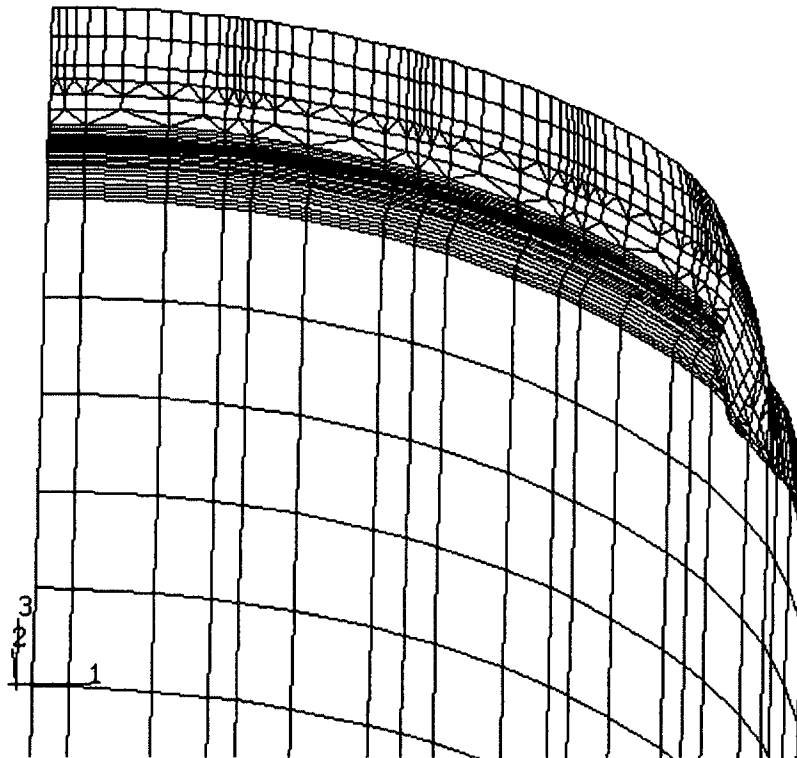


Figure 6-18 Detail View of Deformed Shape Shell Wall of Drum Assembly During 2.5 inch Zero Angle Crush Simulation.

45° Angle Drop Simulation

The results of the crush simulations show the two drums again behave similarly in terms of deflected shape. The 45 degree drop simulation results in the flange bending downwards, duplicating the mode shape indicated in the photographs of existing drop test. The computer simulation captures the drum wall and lid closure buckling, as shown in Figures 6-28 through 6-31. The load results for the 9975 drop simulation are shown in figures 6-19 through 6-21. The corresponding results for the DT-22 are shown in figures 6-22 though 6-24. A comparison of the results are shown in Figures 6-25 though 6-27. A summary of the results are shown in Table 6-6.

As for the zero angle drop simulation, the data for the 45° angle simulation shows the 9975 develops more shear force in the screws for a given crush distance. On both drums, the shear load histories show a couple of peaks and dips, a result of the assembly passing through the drum wall buckling mode and the lid/ring buckling mode. The same variances are seen on the crush load histories. It is also seen that the variance of the tensile loads is such that a net tensile load is always maintained. The maximum tensile variance for all screws on either drum was a reduction of less than 900 lbs to an increase of 530 lbs. Given the nominal values of pre-load, (3360 to 3840 lbs for 9975, \approx 1500 lbs DT-22), and the maximum sustainable tensile load of the screws/nut assembly ($>$ 5000 lbs for the 9975), the screws are shown to be structurally qualified.

The energy absorption history is shown on Figure 6-27 and shows that the 9975 absorb slightly more energy than the DT-22 for a given deflection. This shows that comparing the 9975 closure screw load response to that of the DT-22 on an equal deflection basis is conservative. As for the zero degree drop simulation, the small fraction of the total 145,400 in-lb drop energy absorbed implies that the Celotex is the main contributor to the energy absorption. Therefore, the qualification of the celotex damage measured during the banded closure design drop test is still valid for the flanged closure.

Table 6-6 Summary of Load Data for 45 Degree Drop Simulation

	9975 Drum	DT-22 Drum	Ratio of Max Values, 9975 to DT
Shear, Bolt #1	2930 lbs	2700 lbs	1.09
Shear, Bolt #2	6431 lbs	3550 lbs	1.81
Tension, Bolt #1 (See Note)	-1000 lbs to +500 lbs	-1300 lbs to +0 lbs	Na
Tension, Bolt #2	-800 to +400 lbs	-1000 to 0 lbs	na
Tension, Bolt #3,4,5	< +/-900 lbs	< +/-525 lbs	na
Energy Absorbed (@ 3" Crush)	23,200 in-lbs	18,300 in-lbs	1.27

Note: Range of Bolt Tension is shown relative to Pre-load, Ratio not Computed for Tension as DT-22 shown Zero Increase over the initial Pre-load.

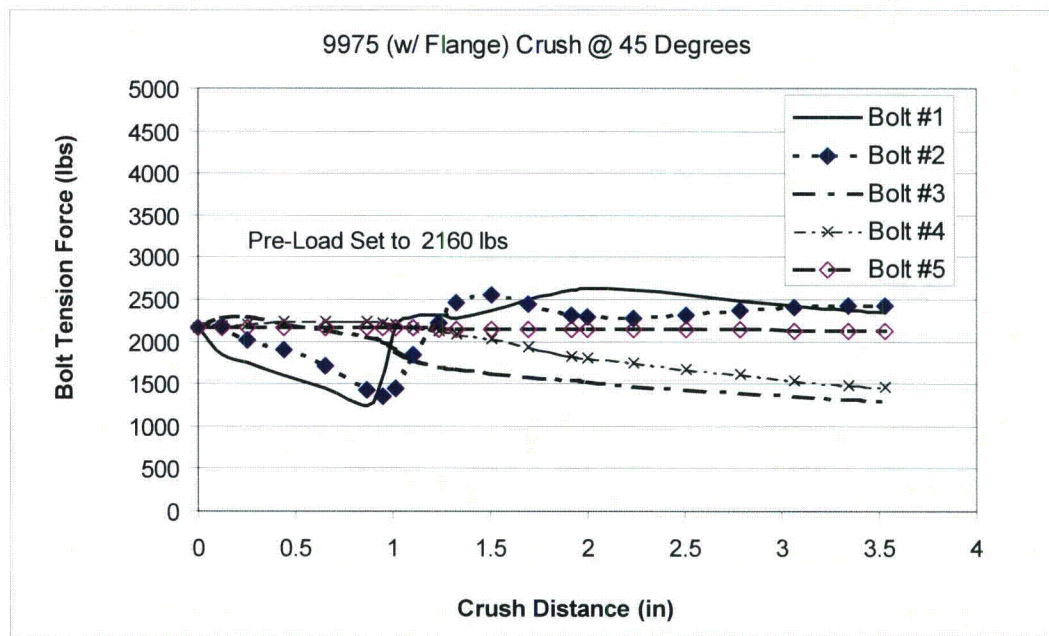


Figure 6-19 Tensile Load History for 9975 Package Closure Screws For 45 Degree Load Case (Pre-Load Shown is For 3/8 Closure Screw, See Section 6.2.1 for Technical Discussion).

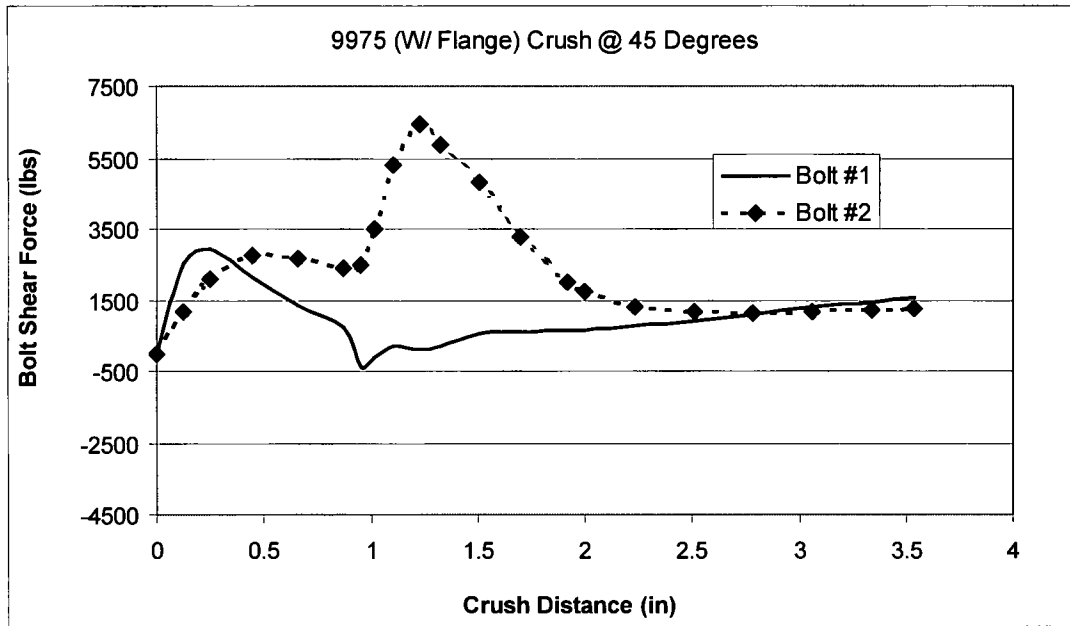


Figure 6-20 Shear Load History for 9975 Package Closure Screws For 45 Degree Load Case.

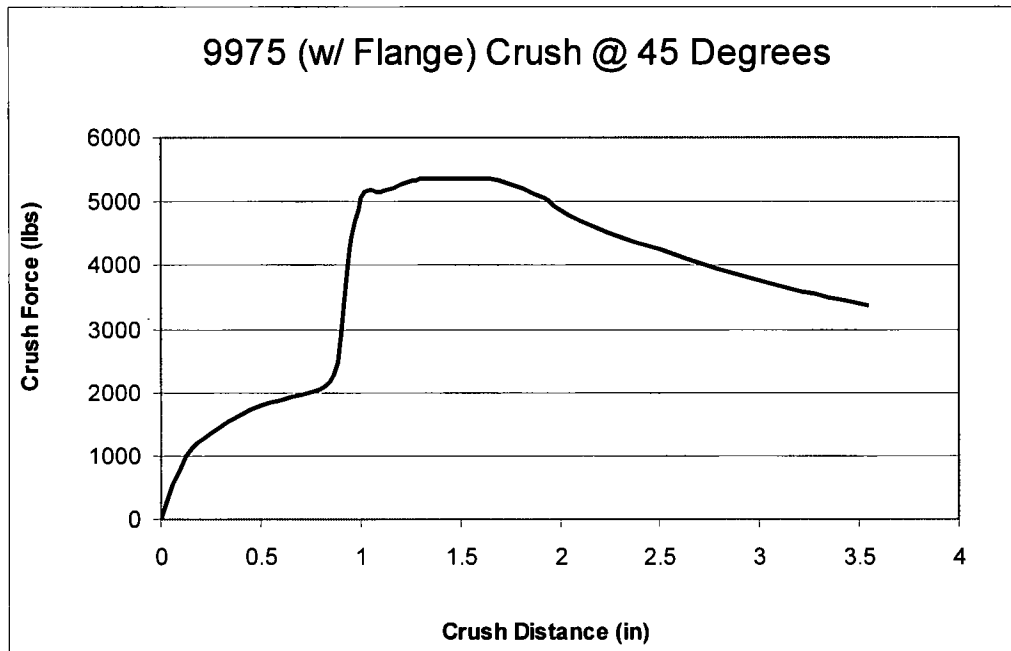


Figure 6-21 Crush Force History for 9975 Package Closure Screws For 45 Degree Load Case.

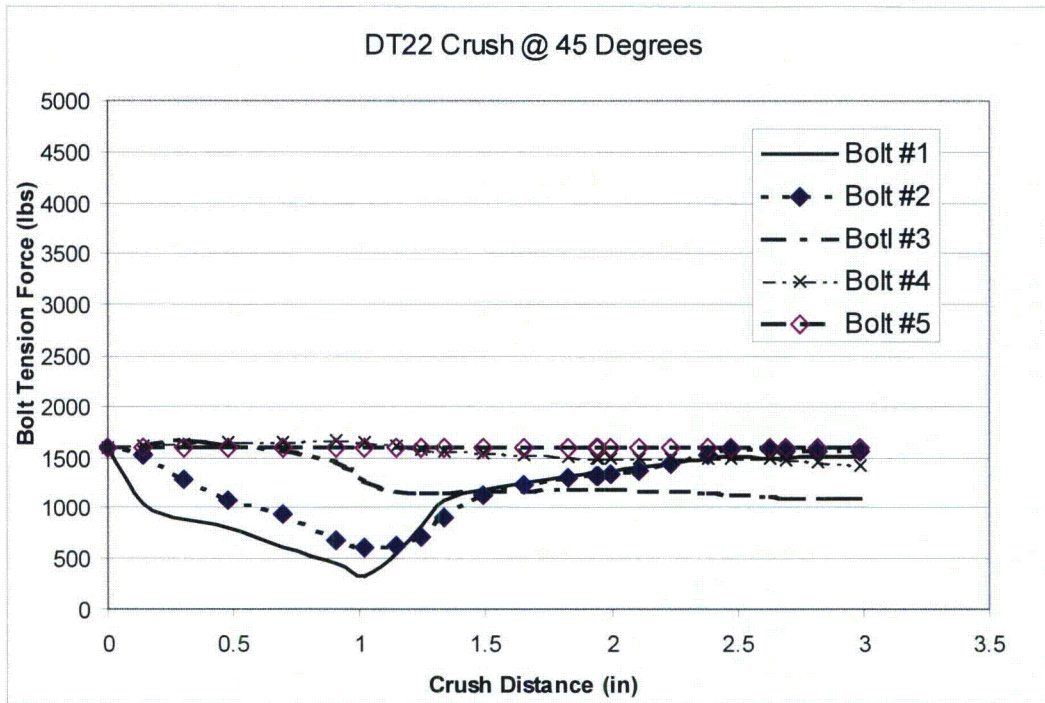


Figure 6-22 Tensile Load History for DT-22 Package Closure Screws For 45 Degree Load Case, Showing Small Variations in Tension Relative to Allowable Load. (Tension Allowable = 6550 lbs, Scale Set to \approx 70% of Allowable as Visual Aid).

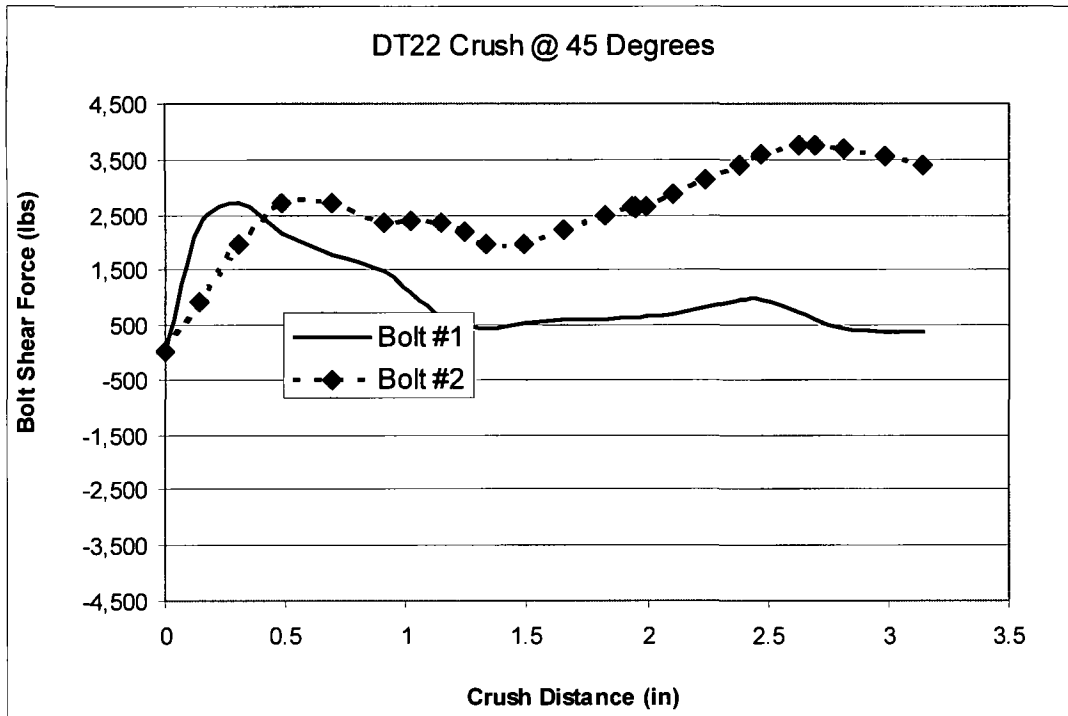


Figure 6-23 Shear Load History for DT-22 Package Closure Screws For 45 Degree Load Case.

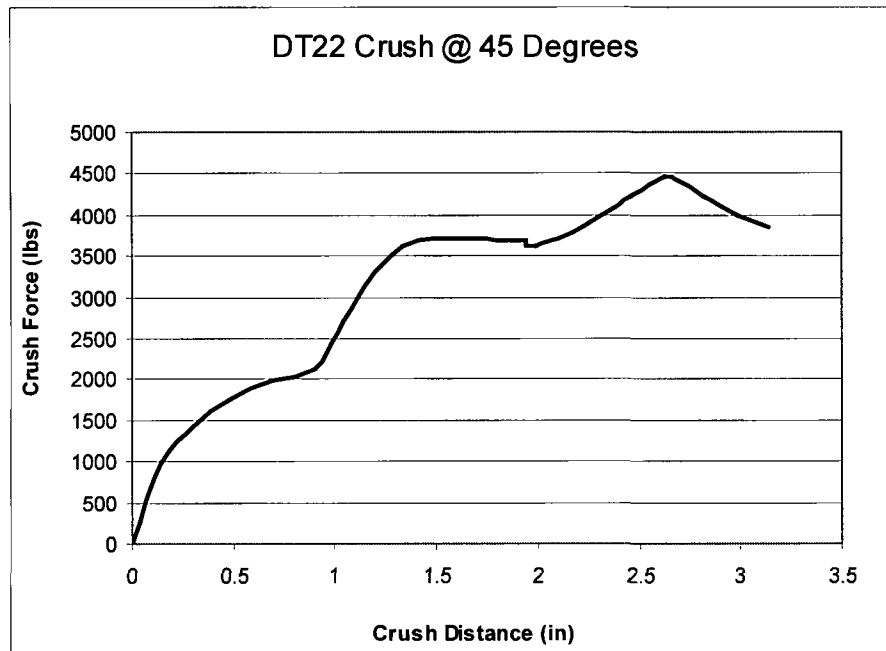


Figure 6-24 Crush Force History for DT-22 Package Closure Screws For 45 Degree Load Case.

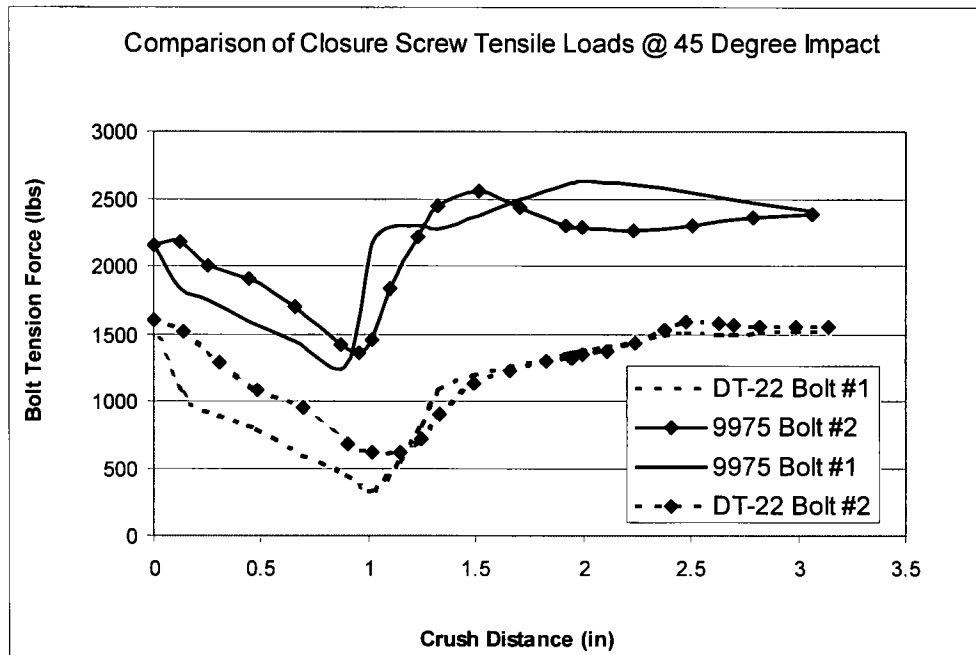


Figure 6-25 Comparison of Closure Screw Tensile Load Histories for 45 Degree Drop Simulation (9975 Pre-load Shown at 2160 lbs, DT-22 Pre-load Shown at 1600 lbs).

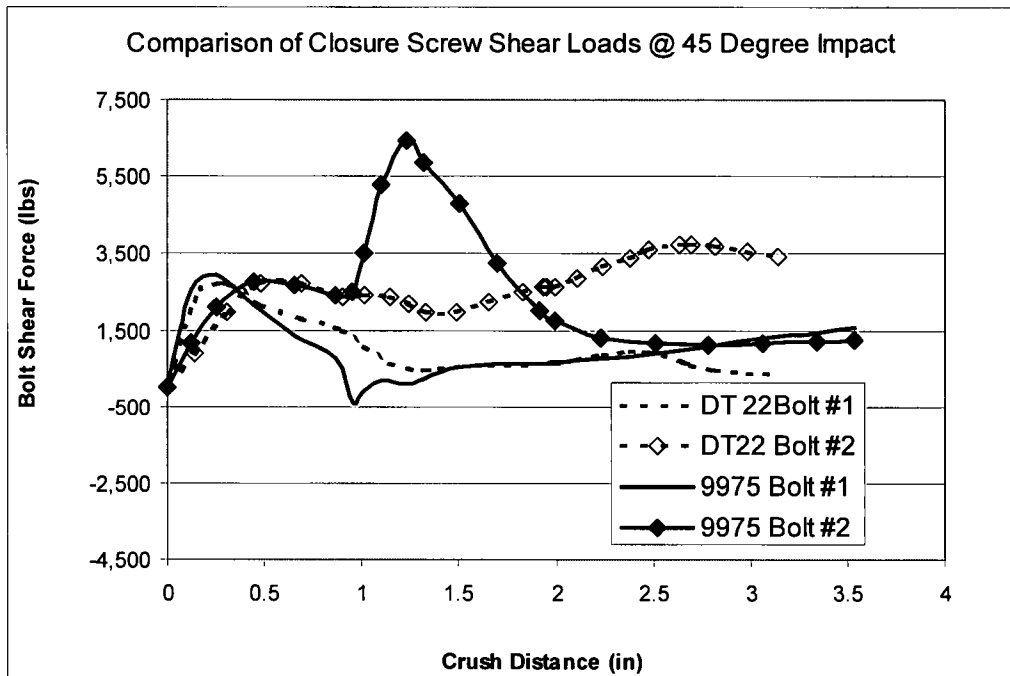


Figure 6-26 Comparison of Closure Screw Shear Load Histories for 45 Degree Drop Simulation.

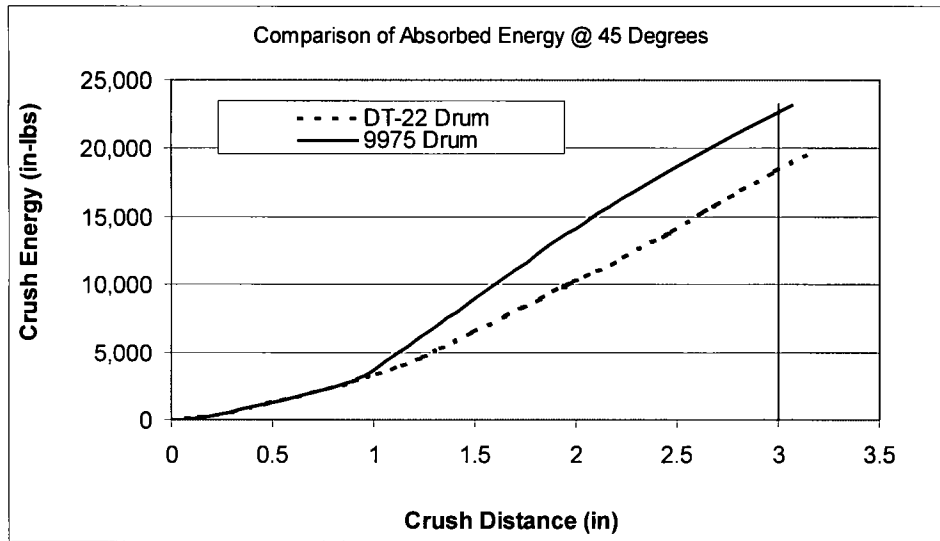


Figure 6-27 Comparison of Absorbed Energy Histories for 45 Degree Drop Simulation.

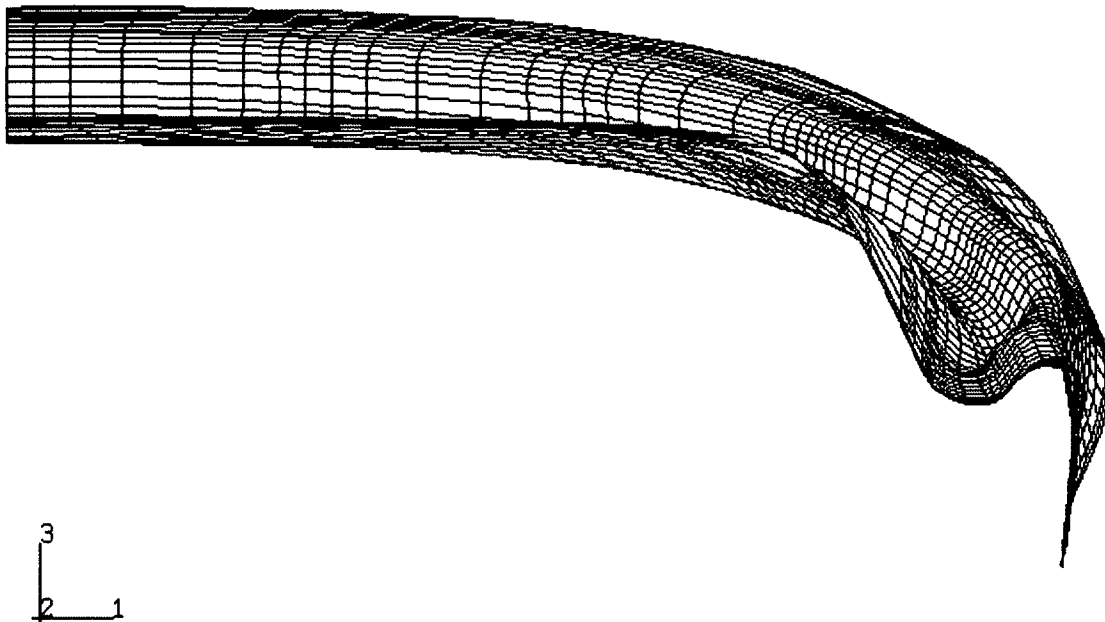


Figure 6-28 Detail View of Deformed Shape for Lid of Drum Assembly During 45 Degree Imposed Deformation (9975 Assembly Shown @ Three Inches Deformation).

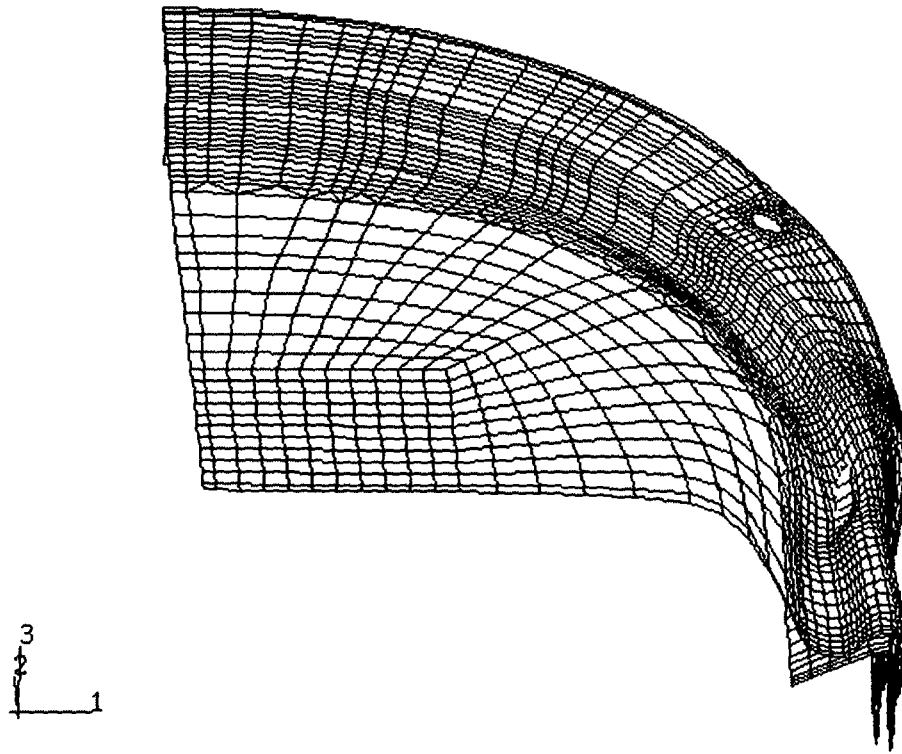


Figure 6-29 Detail View of Deformed Shape for Lid and Flange of Drum During 45 Degree Imposed Deformation (9975 Assembly Shown @ Three Inches Deformation).

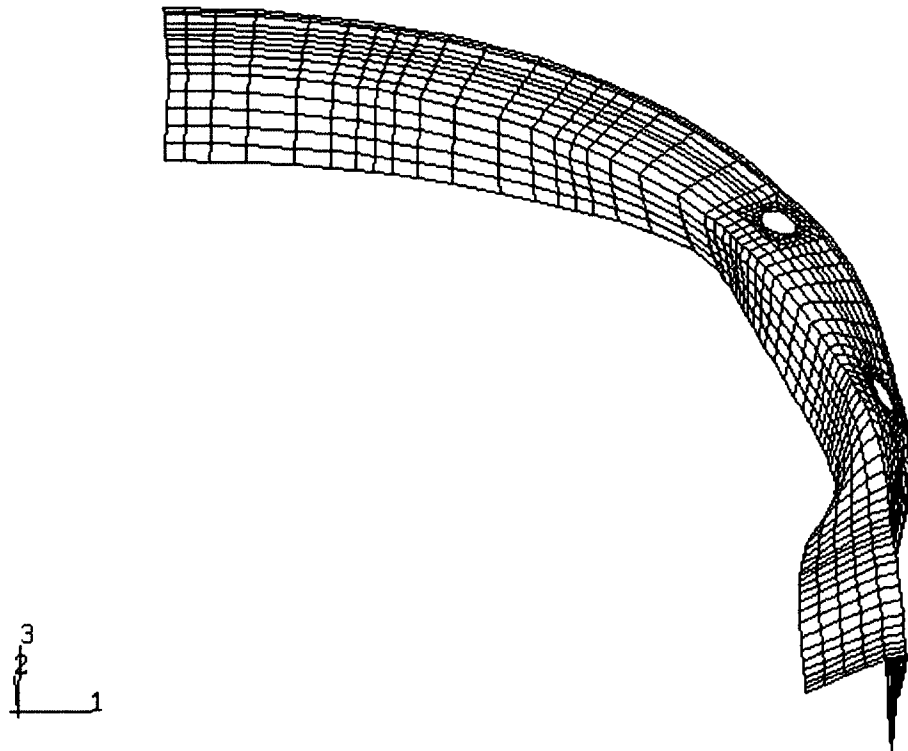


Figure 6-30 Detail View of Deformed Shape for Flange of Drum During 45 Degree Imposed Deformation (9975 Assembly Shown @ Three Inches Deformation).

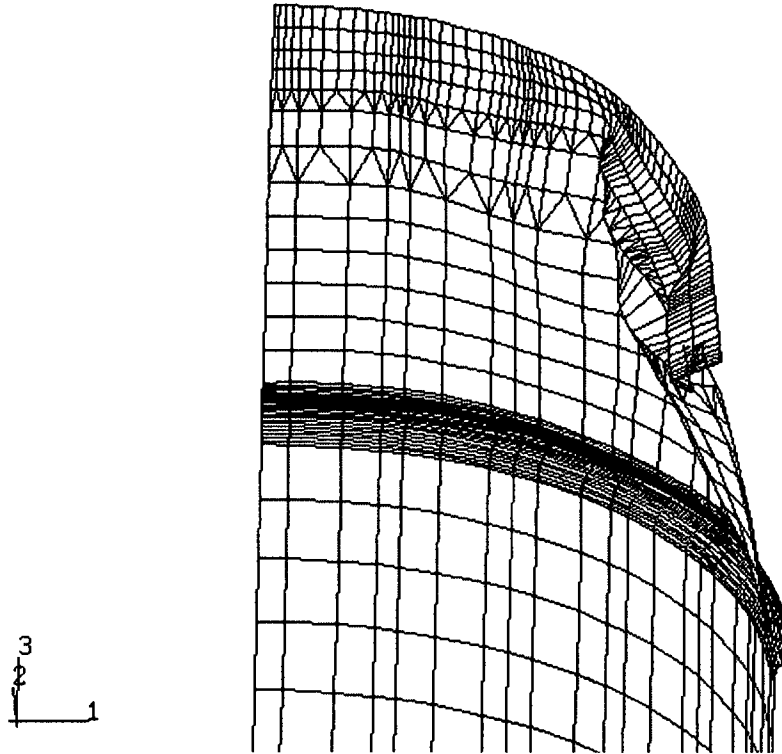


Figure 6-31 Detail View of Deformed Shape for Shell Wall of Drum Assembly During 45 Degree Imposed Deformation (9975 Assembly Shown @ Three Inches Deformation).

6.2.4 Evaluation of Closure Screws for Container Crush Loads

The shear and tensile loads on the 9975 closure screws and nuts are evaluated by both a comparative basis and also by ASME Section III criteria. The comparative basis compares the 9975 loads to the DT-22. Code criteria is based on Section III, Appendix F.

6.2.4.1 Comparative Evaluation

The crush simulation performed within this calculation predicts that the shear loads in the closure screws will be higher in the 9975 package than in the DT-22. This increase is judged to be due to the closer bolt spacing used on the 9975 and the resulting higher load to achieve buckling of the flange between bolts. Table 6-5 shows the shear loads are 68% higher for the zero angle drop and Table 6-6 shows the shear loads are 81% higher for the 45 Degree drop. Because of this increase, the closure screws used on the 9975 flange closure were increased to ½ diameter. The following chart shows the increased bolt size results in sufficient strength increase to accommodate the higher loads.

	Shear Area	Tensile Area
3/8 inch screw	0.068 in ²	0.078 in ²
½ inch screw	0.126 in ²	0.142 in ²
Ratio, 3/8 to ½	1.85	1.82

6.2.4.2 Code Evaluation

In addition to the comparative evaluation of the closure screw loads, the shear and tensile loads are evaluated to ASME B&PV Code Section III Appendix F acceptance criteria. The Code specified limits based on both ultimate and yield strengths. For the bolt material, the ultimate strength controls:

Shear \Rightarrow lesser of 42% of Ultimate, 70% Yield = $0.42 * 120,000 \text{ psi} = F_v = 50,400 \text{ psi}$

Tension \Rightarrow lesser of 70% of Ultimate, 100% Yield = $0.70 * 120,000 \text{ psi} = F_t = 84,000 \text{ psi}$

$$\text{Combined} \Rightarrow \frac{f_t^2}{F_t^2} + \frac{f_v^2}{F_v^2} \leq 1$$

Closure Screws – Zero Degree Drop

Table 6-5 shows that the bolt nearest the impact point is the highest loaded bolt. The shear load is 5950 lbs and the tension load increases to 1000 lbs above the pre-load value. The maximum pre-load is determined to be 3,840 lbs (section 6.5)

Shear Stress = $5950 \text{ lbs} / 0.126 \text{ in}^2 = 40,397 \text{ psi}$ (less than allowable of 50,400 psi)

Tension Stress = $1000 \text{ lbs} / 0.142 \text{ in}^2 = 7,042 \text{ psi}$ (less than allowable of 84,000 psi)

$$\text{Combined} \Rightarrow \frac{7042^2}{84,000^2} + \frac{40397^2}{50,400^2} = 0.65 \leq 1 \quad (\text{Meets the combined interaction equation})$$

Closure Screws – 45 Degree Drop

Table 6-6 shows that the highest loaded bolt is bolt #2, the one adjacent to the point of impact. The shear load is 6431 lbs and the tension load increases to 400 lbs above the pre-load value. The maximum pre-load is determined to be 3,840 lbs (section 6.5)

Shear Stress = $6431 \text{ lbs} / 0.126 \text{ in}^2 = 51,039 \text{ psi}$ (just above the allowable of 50,400 psi)

Tension Stress = $400 \text{ lbs} / 0.142 \text{ in}^2 = 2,817 \text{ psi}$ (less than allowable of 84,000 psi)

$$\text{Combined} \Rightarrow \frac{2,817^2}{84,000^2} + \frac{51,039^2}{50,400^2} = 1.027 > 1$$

The Code evaluation shows that the predicted bolt loads exceed Code allowables by less than 3%. The bolted flange closure is judged to be acceptable because:

- The comparative evaluation shows the 9975 meets the performance target of the DT-22
- The overstress would occur only on 2 non-adjacent bolts of the total of 24 bolts.
- The predicted stress level is below the ultimate capacity of the bolt material by more than 25%.

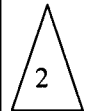
Screw-Nuts

The threads of the welded nut are evaluated for the imposed tensile loads. The maximum tensile load obtained from the imposed formation load cases is an increase of 1000 lbs above the initial pre-load. The allowable load is limited to the shear out of the nut threads controlled by ultimate shear strength of the nut. The nut shear out area is 0.462 in^2 (see Section 6.5)

Load = Pre-Load + Enveloping increase of 1000 lbs = $3840 + 1000 \text{ lb.} = 4840 \text{ lb.}$

Allowable = $42\% * 60,000 \text{ psi} * .462 \text{ in}^2 = 11,642 \text{ lb}$

The actual load of 4840 lbs is less than the 11,642 lb allowable.



6.2.5 Evaluation of Lid Curvature

The effects of lid curvature are quantified in this section. The proven DT-22 package design incorporates a lid with a flat (no curvature) center section (the “hat” or “offset” section). The redesign 9975 package will use the same basic design, with the exception that the center section has curvature. By evaluating two lids, each sized for the 9975 package, one with curvature and one without, it is shown that the curvature of the center section does not create a significant stiffness difference.

An evaluation of the 9975 lid design is conducted by determining the limit load of the lid when subjected to a lateral load applied along one edge of the lid. The limit load of the lid is determined by running a Riks Load Procedure within the Abaqus finite element software. The lid model is the same as described in Section 6.2.1. The limit load of the 9975 flat lid is found to be 808 lbf. The limit load of the curved lid is slightly higher at 828 lbf.

A stiffness comparison of the designs is done by looking at the behavior of the lids under increasing load up to the limit load. Figure 6-32 shows that there is no significant difference between the force-displacement behavior of the lids. Figures 6-33 through 6-37 show the flat and curved lid models undeformed and deformed geometry plots.

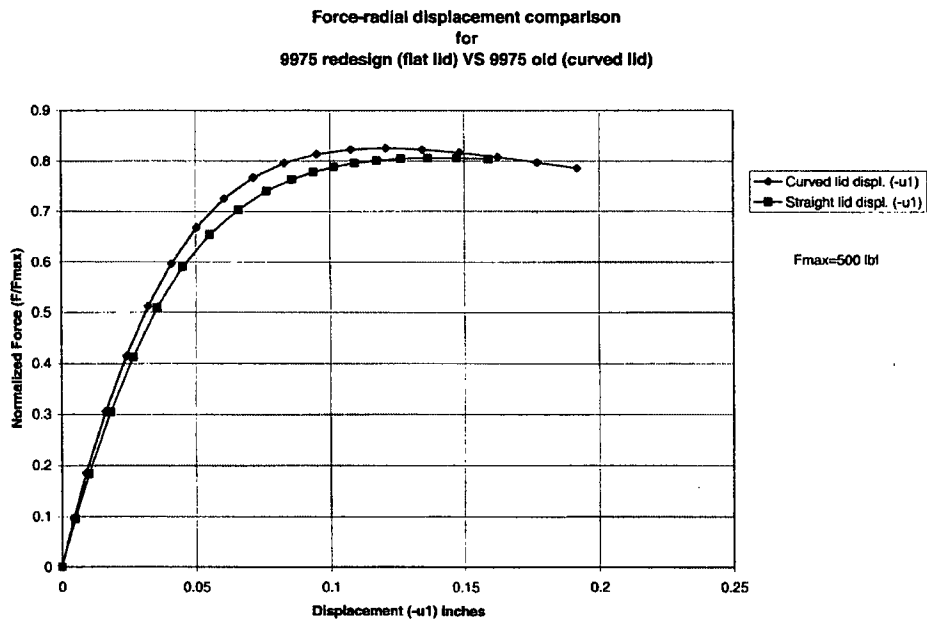


Figure 6-32 Comparison Showing Effects of Curvature of Center Lid Region.

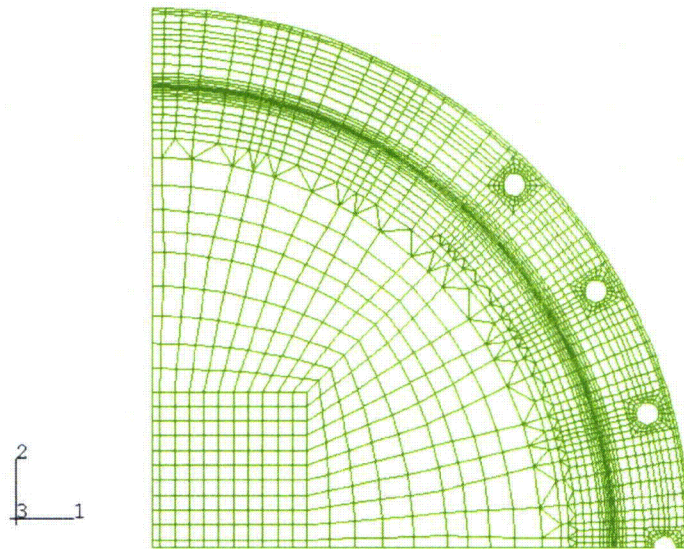


Figure 6-33 Plan View of Uncurved Lid Finite Element Model Used For Limit Load

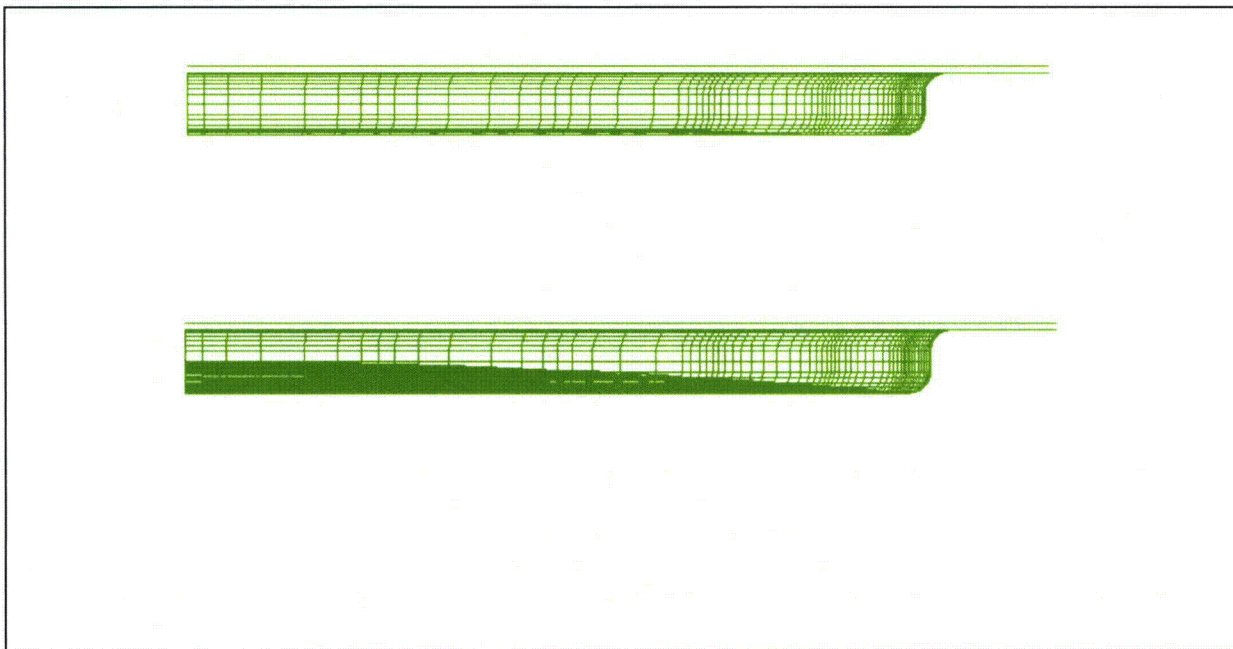
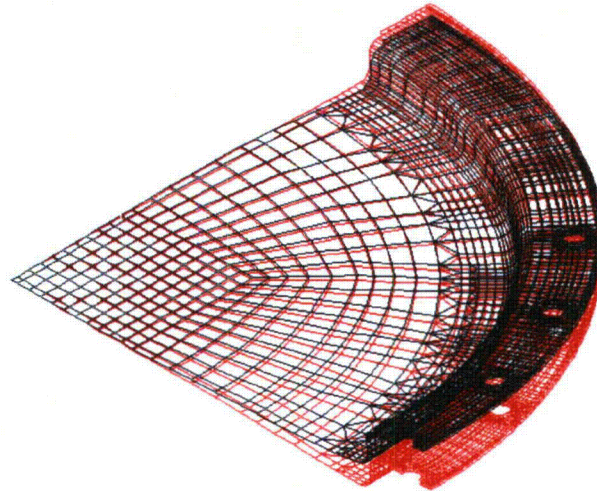


Figure 6-34 Elevation View of Lid With and Without Curvature



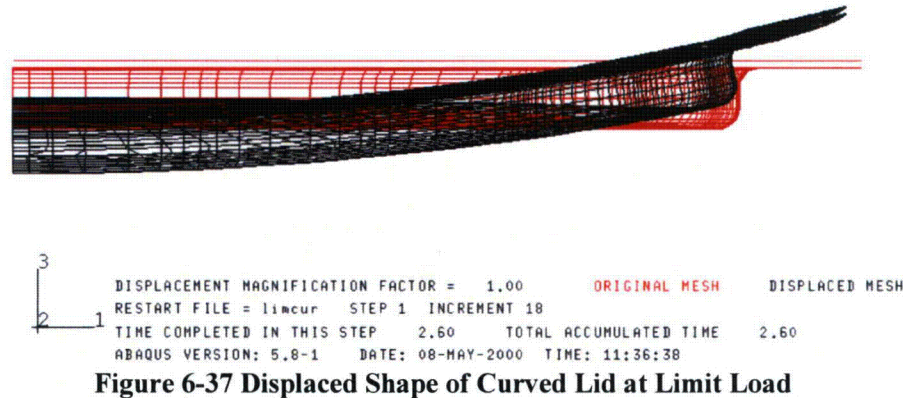
3
2 1
DISPLACEMENT MAGNIFICATION FACTOR = 1.00 ORIGINAL MESH DISPLACED MESH
RESTART FILE = riksstrt STEP 1 INCREMENT 18
TIME COMPLETED IN THIS STEP 2.60 TOTAL ACCUMULATED TIME 2.60
ABAQUS VERSION: 5.8-1 DATE: 07-MAY-2000 TIME: 16:24:59

Figure 6-35 Displaced Shape For Uncurved Lid



3
2
1
DISPLACEMENT MAGNIFICATION FACTOR = 1.00 ORIGINAL MESH DISPLACED MESH
RESTART FILE = riksstrt STEP 1 INCREMENT 18
TIME COMPLETED IN THIS STEP 2.60 TOTAL ACCUMULATED TIME 2.60
ABAQUS VERSION: 5.8-1 DATE: 07-MAY-2000 TIME: 16:24:59

Figure 6-36 Isometric View of Deformed Shape



6.3 Axial Compression Evaluation

6.3.1 Five Times Load Compression Test

In order to test compressive load capability of the 9975 redesign, a finite element model of the container is subjected to a compressive load of 5 times the container's weight. The 5X compressive load requirement is per 10CFR71.71(c)(9). The finite element model and boundary conditions are described in detail section 6.2.1 of this report. Weight stacked on top of the container will be transferred through the bolt heads, which are the earliest point of contact for any flat loading platform. To simulate this loading, the total compressive load is applied as a pressure to a 1 inch wide annular region of the flange with mean diameter equal to the flange's bolt circle diameter. The model is solved in ABAQUS finite element software as a nonlinear static analysis problem.

Input Data:

Flange and Drum Material is A479 304

Allowable Design stress Intensity = 16.7 ksi at atmospheric conditions (Based on 304L grade)

Container weight = 404 lbf

Total compressive load = 5 X 404lbf
= 2020 lbf

Bolt circle diameter = 19.84 in (used in FEM, final location may be moved slightly w/ no effect on this analysis)

Pressure loaded area = $2\pi Rt$
= $(19.84)(1)(\pi)$
= 62.3 sq. in

Pressure value = load / loading area
= 2020/62.3
= 32.4 psi

Results Summary:

The maximum observed stress in the model is a 15.3 ksi axial stress (Fig. 6.45). It occurs at the 0.5 in radius hoop located along the drum shell and is due to bending. The maximum principal stress in the flange area is 14.3 ksi. The maximum displacement of .0079 inches in the downward direction is observed at the top of the flange. The maximum rotation of the flange is 0.15 degrees occurring at the maximum radius of the flange. Figures 6.38 to 6.46 show stress and displacement contour plots of the flange and hoop regions of the container. These regions are presented because they are the most critical for stresses and deformation. Results may be summarized thus:

Flange Region summary:

The principal stresses are:

- First Principal Stress = $\sigma_1 = 5.8$ ksi (Shell top, Figure 6-40)
- 2nd Principal Stress = $\sigma_2 = 14.3$ ksi (Shell top, Figure 6-41)
- 3rd Principal Stress = $\sigma_3 = 0.0$ ksi on FEA Model, actually = to pressure value of -32 psi.

The stress intensity is, $\sigma_m = (\sigma_1 - \sigma_3) \approx 14,300$ psi

The allowable stress is 16,700 psi, D/C ratio = $14,300/16,700 = 0.86$

Max axial displacement = $-7.9 \text{ E-}03$ in Max rotation = 0.15 deg

Hoop Region summary:

Max hoop stress = $\sigma_{11} = 15.3$ ksi (Figure 6.45)

Min axial stress = $\sigma_{22} = 15.8$ ksi (Figure 6.46)

Through Thickness Stress = $\sigma_3 = 0.0$ ksi

For the outer drum shell in the rolled hoop region in which the max stresses occur, the hoop stresses and axial stresses are essentially identical to the principal stresses. As shown in the flange evaluation above, the maximum principal stress is equal to the maximum stress intensity.

The allowable stress is 16,700 psi, D/C ratio = $15,800/16,700 = 0.95$

Max axial displacement = $-3.9 \text{ E-}03$ in

The observed stresses and displacements in the 9975 redesign are below the ASME Code allowable limit of 16.7 ksi. The container will carry a load 5 times its weight without sustaining large rotations or displacements.



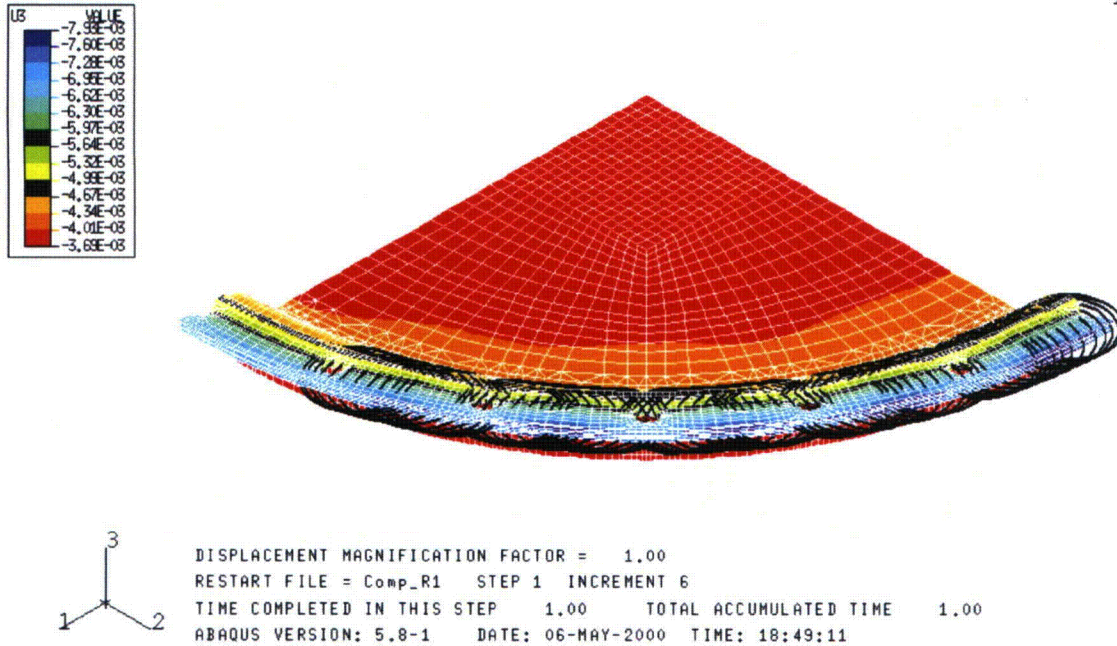


Figure 6.38 Contour Plot of Vertical Displacement for Lid Under 5X Dead Load.

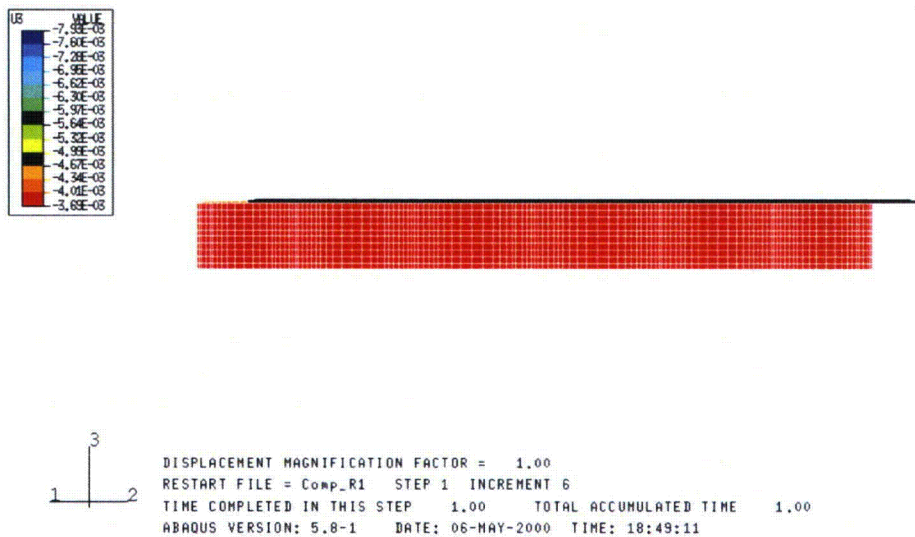


Figure 6.39 Contour Plot (Plan View) of Vertical Displacement for Lid Under 5X Dead Load.

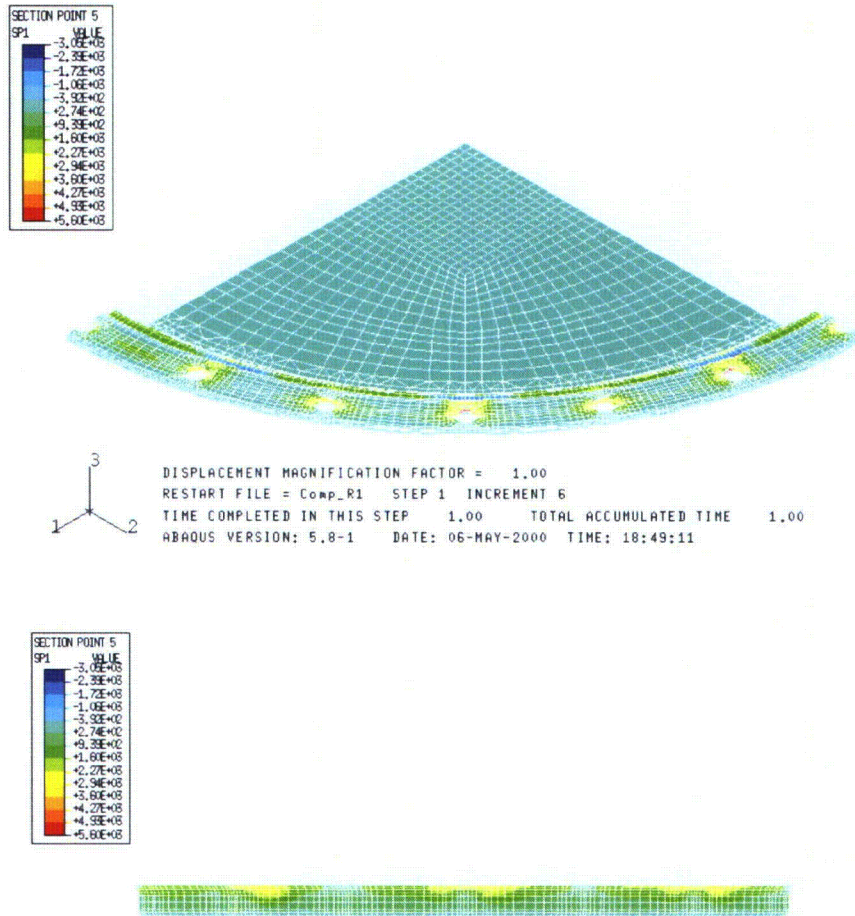


Figure 6.40 Contour Plots (Isometric and Elevation) of Minimum Principal Stress (SP1) for Lid Under 5X Dead Load.

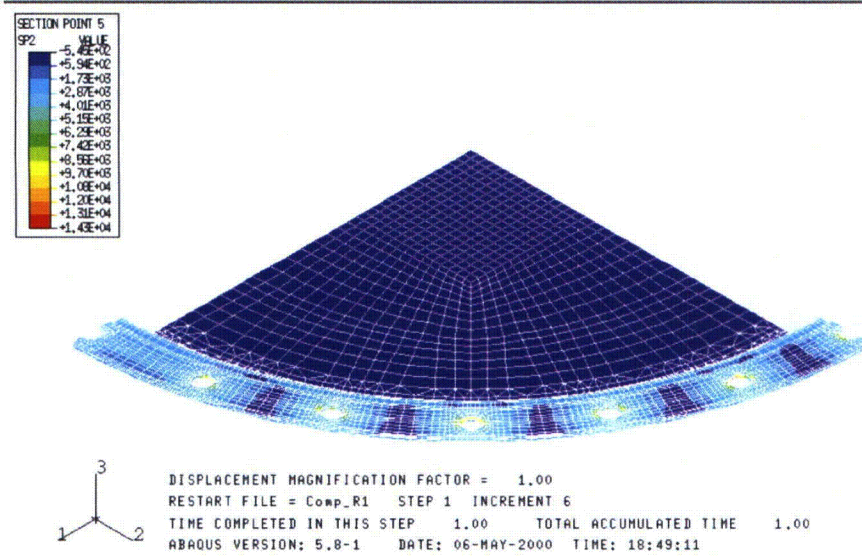


Figure 6.41 Contour Plot (Isometric) of Maximum Principal Stress (SP2) for Lid Under 5X Dead Load.

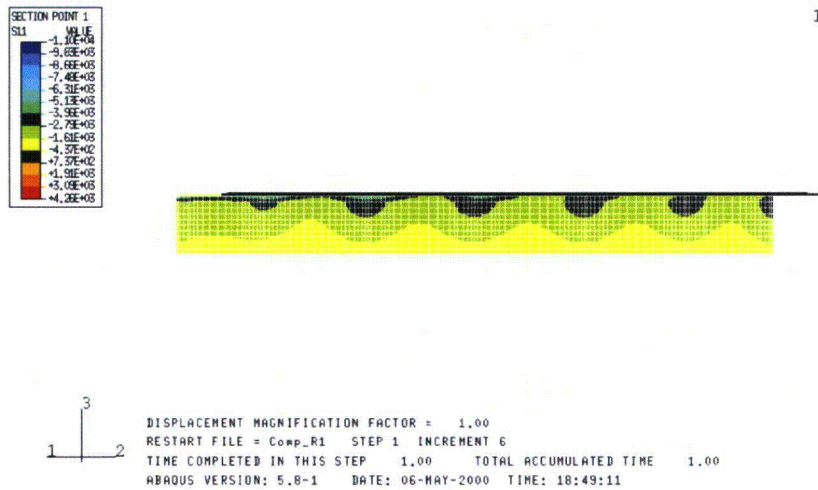


Figure 6.42 Contour Plot (Elevation View) of Hoop Component Stress (S11) for Lid Under 5X Dead Load.

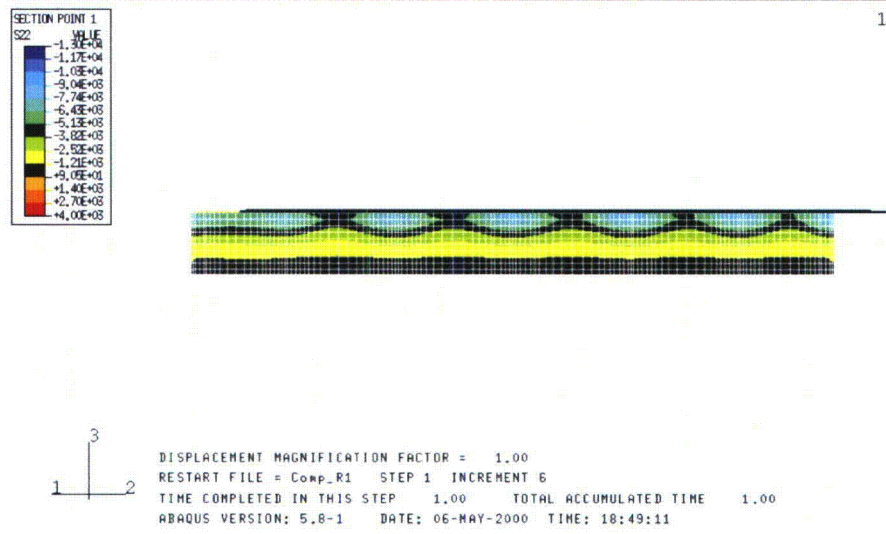


Figure 6.43 Contour Plot (Elevation View) of Radial Component Stress (S22) for Lid Under 5X Dead Load.

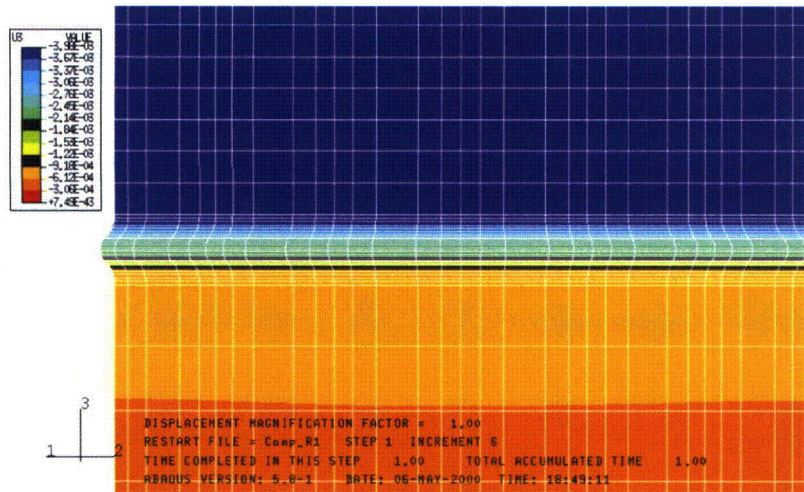


Figure 6.44 Contour Plots (Elev. View) of Vertical Displacement for Drum Wall Under 5X Dead Load.

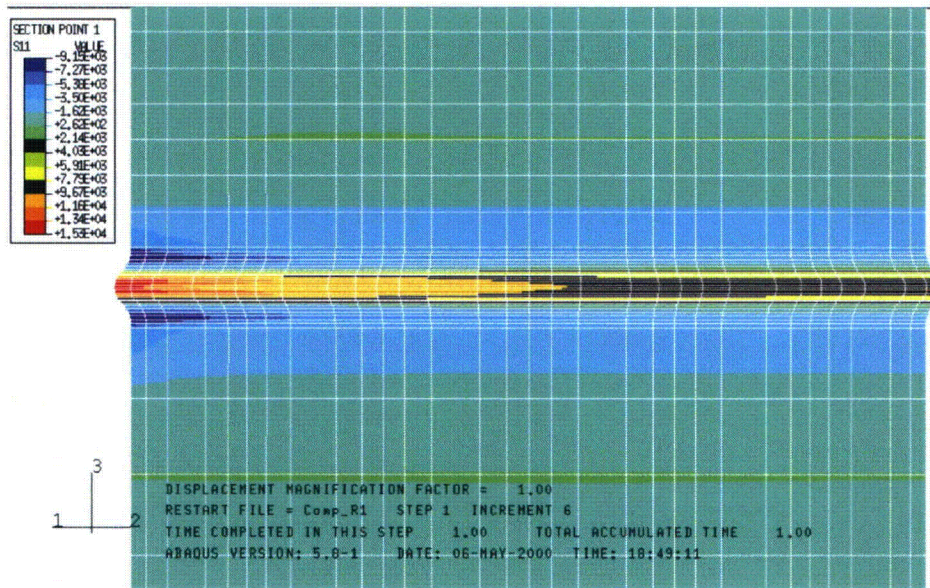


Figure 6.45 Contour Plots (Elev. View) of Hoop Component Stress (S11) for Drum Wall Under 5X Dead Load.

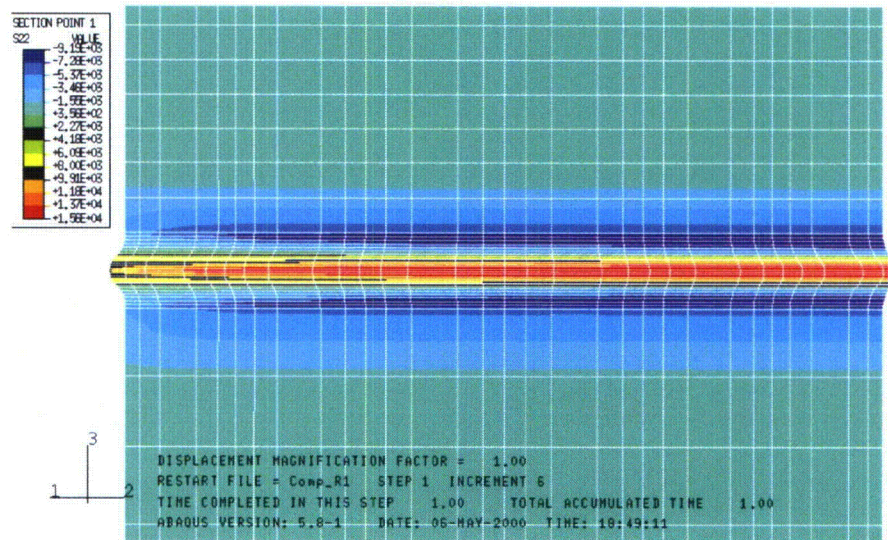


Figure 6.46 Contour Plots (Elev. View) of Radial Component Stress (S22) for Drum Wall Under 5X Dead Load.

1.1.2 Buckling Analysis

A buckling analysis of the container is also conducted. The model is similar to that of the compression test but loading continues until buckling occurs. Results indicate that a geometric buckling will occur at a load of approximately 68 kips while the plastic limit load is found to be 12.3 kips. It is therefore concluded that the maximum compressive capacity for the container is 12.3 kips load.

6.4 Weight Evaluation

Compute the Weight Removed:

1 - Existing Closure Band

The effective diameter of the ring is calculated based on observations that the inside edge of the ring is approximately 1/16" from the drum when clamped. The ¼ gap at the band ends is neglected.

$$\begin{aligned} \text{Band Mean Diameter} &= D_m \\ &= 18.25'' + 2 * 0.048'' + 2 * 1/16'' + 2 * (0.5 - 0.313) \\ &= 18.85'' \end{aligned}$$

Cross-sectional Area = Circular part + straight parts ⇒

$$\begin{aligned} \text{Circular part} &\Rightarrow \left\{ \begin{aligned} &2\pi r_m t \times \text{arcratio} = \\ &2\pi \left(0.313 + \frac{0.105}{2}\right) (0.105) \left(\frac{2 \times 80}{360}\right) \\ &= 0.1072 \text{ in}^2 \end{aligned} \right. \end{aligned}$$

$$\begin{aligned} \text{Straight Parts} &\Rightarrow \text{Length} = L_s = (0.50'' - 0.313'' + 0.313 \sin(20^\circ)) / \cos(20^\circ) = 0.3130 \text{ in} \\ \text{Area} &= 2 \text{ ends} * L_s * t = 2 * 0.313'' * 0.105'' = 0.0657 \text{ in}^2 \end{aligned}$$

$$\begin{aligned} \text{Weight} &= \text{volume} \times \text{density} = \text{Circumferential length} * \text{area} * \text{density} \\ &= \pi D_m \text{Area} \times \rho = \pi (0.18.85'') (0.1072 \text{ in}^2 + 0.0657 \text{ in}^2) (0.283 \text{ lb/in}^3) = \underline{2.90 \text{ lbs}} \end{aligned}$$

2. Closure Ring Extensions (Two extensions are included in total weight, Table 6.7)

$$\begin{aligned} \text{Weight} &= \text{length} \times \text{width} \times \text{thickness} \times \text{density} \\ &\Rightarrow \text{length} \approx (0.63'' - 0.25'') + (0.98'' - 0.25'') + \pi * 0.25/2 = 1.50 \\ &= (1.50 \text{ inches}) \times 2 \text{ inch} \times 11 \text{ ga} \times 0.283 = \underline{0.10 \text{ lbs}} \quad \{11 \text{ ga} = 0.12 \text{ in}\} \end{aligned}$$

3. Closure Bolt (5/8-11UNC-2A x 4")

Use effective length of 5" to account for bolt head and lock nut

$$\text{Weight} \approx \frac{\pi}{4} (0.625'')^2 \times 5'' \times 0.283 \text{ lb/in}^3 = \underline{0.43 \text{ lbs}}$$

4. Closure Bolt Lugs (1.5" dia x 5/8 thick)

$$\text{Weight} = \frac{\pi}{4} (1.5^2 - 0.625^2) \times 0.625'' \times 0.283 \text{ lb/in}^3 = \underline{0.26 \text{ lbs each}}$$

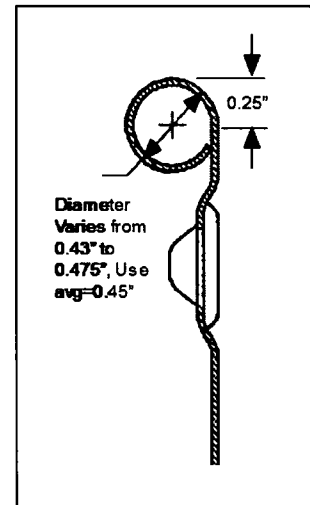
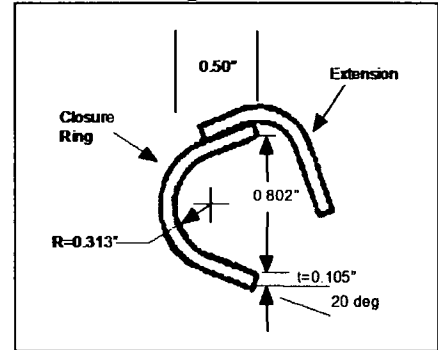
5. Top Drum Curl to be Removed (Cut ≈ 0.25" below top):

$$\text{Circumferential Diameter} = D_m = 18.25 + 2 * 0.048 + 0.45'' = 18.8''$$

$$\text{Diameter of Cross Section} = d = 0.45'' \text{ (average)}$$

$$\text{Cross-Section Area} = A = \pi dt = \pi \times 0.45'' \times 0.048'' = 0.0679 \text{ in}^2$$

$$\text{Weight} = \pi D_m A \rho = \pi \times 18.8 \text{ in} \times 0.0679 \text{ in}^2 \times 0.283 \text{ lb/in}^3 = \underline{1.13 \text{ lbs}}$$



Compute Weight Added:

1. Rolled Angle Flange (1.25 x 1.25 x 0.125")

$$\text{Vertical Portion} \Rightarrow \text{Area} = A = 1.25 \times 0.125 = 0.1563 \text{ in}^2$$

$$\text{Average Diameter} = D_m = 18.35'' + 0.125'' = 18.48''$$

$$\text{Weight} = \pi D_m A \rho = \pi \times 18.48 \text{ in} \times 0.1563 \text{ in}^2 \times 0.283 \frac{\text{lb}}{\text{in}^3} = \underline{2.57 \text{ lbs}}$$

$$\text{Horizontal Portion} \Rightarrow \text{Area} = A = 1.25 \times 0.125 - 0.125^2 = 0.1406 \text{ in}^2$$

$$\text{Average Diameter} = D_m = 18.35'' + 2 \times 0.125'' + 2 \times (1.25 - 0.125'')/2 = 19.73''$$

$$\text{Weight} = \pi D_m A \rho = \pi \times 19.73 \text{ in} \times 0.1406 \text{ in}^2 \times 0.283 \frac{\text{lb}}{\text{in}^3} = \underline{2.47 \text{ lbs}}$$

$$\text{Total} = 2.57 \text{ lbs} + 2.47 \text{ lbs} = 5.04 \text{ lbs}$$

2. Top Ring (1.25" x 0.125")

$$\text{Cross Section Area} = 1.25'' \times 0.125 = 0.1563 \text{ in}^2$$

$$\text{Effective Diameter} = 18.35'' + 1.25'' = 19.60 \text{ in}$$

$$\text{Weight} = \pi D_m A \rho = \pi \times 19.60 \text{ in} \times 0.1563 \text{ in}^2 \times 0.283 \frac{\text{lb}}{\text{in}^3} = \underline{2.72 \text{ lbs}}$$

3. Closure Screws (0.5-13UNC-2A x 0.75" long)

$$\text{Weight} \approx \frac{\pi}{4} \left\{ (0.5^2 \times 1.0'') + (.875^2 \times 0.375) \right\} \times 0.283 \frac{\text{lb}}{\text{in}^3} = \underline{0.12 \text{ lbs each}}$$

4. Closure Screw Weld Nuts and washers

The weight of the weldnuts and washers is estimated as 25% of that of the bolt = .03 lb each

Table 6-7 Summary of Weight Removed from 9975 Drum Assembly

Item	Unit Weight	Quantity	Total Weight
Closure Band	2.9 lbs	1	2.90 lbs
Closure Band Extensions	0.1 lbs	2	0.20 lbs
Closure Bolt	0.43 lbs	1	0.43 lbs
Closure Bolt Lugs	0.26 lbs	2	0.52 lbs
Drum Curl	1.13 lbs	1	1.13 lbs
Total			5.18 lbs

Table 6-8 Summary of Weight Added to 9975 Drum Assembly

Item	Unit Weight	Quantity	Total Weight
Rolled Angle Flange	5.04 lbs	1	5.04 lbs
Top Ring	2.72 lbs	1	2.72 lbs
Closure Screws	0.12 lbs	24	2.87 lbs
Weld Nuts	0.03 lbs	24	0.72 lbs
Total			11.35 lbs

Since the lid is essentially the same size, before and after the modification, it was omitted from detailed weight calculations. Based on the above, the total weight can per drum is:

$$\underline{\text{Additional Weight} = 11.35 \text{ lbs} - 5.18 \text{ lbs} \approx 6.2 \text{ lbs}}$$

6.5 Closure Fastener Evaluation

The 9975 package closure assembly is preloaded during assembly by torque-up of the closure bolts. The preload torque to be applied during assembly of the closure is determined based on the shear capability of the nut threads.

Tensile loads in the bolt produce shear loads in the bolt and nut threads, which attempt to “strip” the threads. Since the nuts (carbon steel) are of significantly lower strength than the bolts (SA-320, Grade L7 alloy steel), maximum stresses must be evaluated with consideration to the weaker nut threads. Reference (2) provides the following relationship for the shear area of the nut, A_{TS} , when the nut material is weaker than the bolt material:

$$A_{TS} = \pi \cdot n \cdot L_e \cdot D_{smin} \cdot \left[\frac{1}{2 \cdot n} + 0.57735 \cdot (D_{smin} - E_{nmax}) \right]$$

where:

D_{smin} = minimum OD of bolt threads = .4876, Reference (3)

E_{nmax} = maximum pitch diameter of nut = .4565, Reference (3)

n = threads per inch = 13

L_e = length of engagement of the bolt/nut threads = nut height for full engagement
= .427 - .016 = .411 in (Reference: Machinery Handbook, 22 ed)

Substituting:

$$A_{TS} = \pi \cdot (13) \cdot (.4111) \cdot (.4876) \cdot \left[\frac{1}{2 \cdot (13)} + (.57735) \cdot (.4876 - .4565) \right] = .462 \text{ in}^2$$

The weldnut is made carbon steel. Using minimum properties from reference (4) for A36 steel and the stress limit for pure shear from reference (5), the maximum allowable stress for temperatures up to 100 °F is limited to $S_{sall} = 0.6 S_m = 0.6 (14,500 \text{ psi}) = 8,700 \text{ psi}$. The maximum load in the joint is limited to:

$$P_{max} = A_{TS} S_{sall} = (.462) (8,700) = 4019 \text{ lb.}$$

6.5.1.1.1 Bolt assembly Torque

The required assembly torque for the bolt is determined using Equation 7.4 of Reference (2)

$$T_{in} = F_p K D$$

where:

T_{in} = input torque, lb.-in.

F_p = achieved preload = 4019 lb.

D = nominal fastener diameter = .5 in

K = nut factor (dimensionless), taken as 0.2 for steel surfaces, reference (2)

The required torque is:

$$T_{in} = (4019) (0.2) (.5) = 402 \text{ lb.-in.} = 33.5 \text{ lb.ft}$$

An assembly torque of 28-32 ft.-lbs. is specified on the drawing. For this torque range, the bolt preload is:

$$P_{min} = \frac{T_{min}}{K \cdot D_{nom}} = \frac{(28) \cdot (12)}{(0.2) \cdot (.5)} = 3360 \text{ lb.}$$

$$P_{max} = \frac{T_{max}}{K \cdot D_{nom}} = \frac{(32) \cdot (12)}{(0.2) \cdot (.5)} = 3840 \text{ lb.}$$

Evaluation of the thermal loads and vibratory loosening (Section 6.7) are performed based on the minimum pre-load of 3360 lb.

To achieve the above pre-load, the bolts shall be tightened using two torquing passes around the circumference of the drum. The first pass is to snug the bolts to a torque of approximately 10% of the final torque. The second pass is to impart full torque to the bolts.

6.6 Vibratory Loads on 9975 Package During Normal Conditions of Transport

Road induced vibrations are random vibrations. A random vibration analysis is followed to determine a root mean square (RMS) value of the acceleration felt by the package. Random vibration analysis is based on the power spectral density for the transport vehicle, given in Figure 3.30 of reference (6) and reproduced as Figure 6-47.

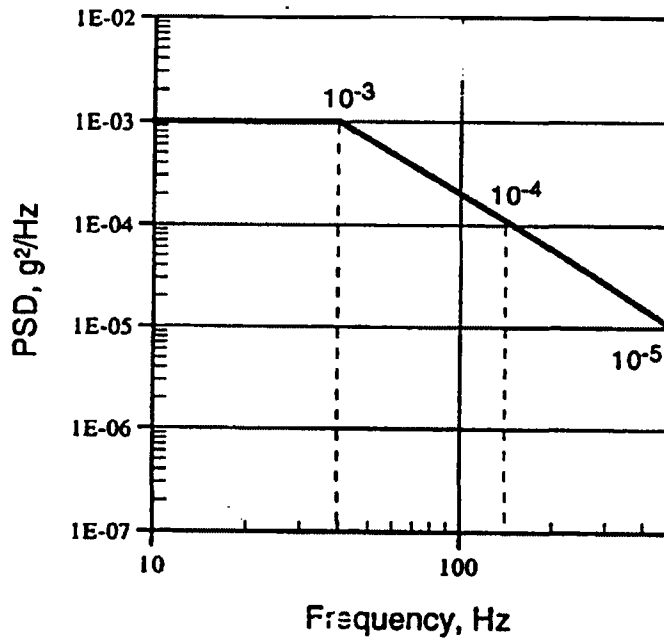


Figure 6-47 Safe-Secure Trailer Power Spectral Density

For a single degree of freedom and a damped system, RMS response of a mass to the broad-band random vibration input is given by (reference (7)):

$$G_{out} = \sqrt{\frac{\pi \cdot P \cdot f \cdot Q}{2}}$$

where:

- G_{out} = acceleration response (g units)
- P = power spectral density (g^2/Hz)
- f = resonance frequency of the system (Hz)
- Q = transmissibility at the resonance frequency

Input for the solution of the above equation are discussed and determined below:

Resonance Frequency of the Package, f

Vibratory response of the 9975 package is evaluated by assuming the natural frequency to coincide with the peak of the power spectral density curve shown in Figure 6-47. This corresponds to a frequency of 40 hz and a PSD of 1E-3 g²/Hz. The degree of conservatism in the above approach, compared to standard practices in evaluating drum vibratory loads, is evaluated by considering the containment vessels with mass M associated with its contained vessel assembly, and structural stiffness k, characterized by the supporting Celotex insulation. The natural frequency is:

$$f = \frac{1}{2 \cdot \pi} \cdot \sqrt{\frac{k \cdot g}{w}}$$

where:

- k = stiffness of Celotex insulation (determined below)
- w = weight of the combined vessel assembly = 283 lb, reference (1)
- g = acceleration of gravity = 386.4 in/sec²

The stiffness of the Celotex insulation is determined by examination of test results reported in reference (1). For a 2 x 2 x 2 inch cubic specimen, progressively loaded in compression, loading of the specimen increased from 20 to 600 pounds as a deflection of 0.5 inch was imposed. The equivalent elastic modulus, E is calculated as:

$$E = \frac{P_t \cdot L_s}{A_s \cdot \Delta} = \frac{(600 - 20) \cdot (2.0)}{(2.0 \cdot 2.0) \cdot (0.5)} = 580 \text{ lb./in}^2$$

where:

- P_t = applied load, lbs.
- L_s = specimen length = 2 inches
- A_s = specimen cross-section area = 2.0 x 2.0 = 4 inches²

The vessel assemblies are supported by an 11.2 inch diameter aluminum plate, which bears on a 4.00 inch thick layer of Celotex. The stiffness of the supporting Celotex, k is calculated below:

$$k = \frac{A_c \cdot E}{L_c} = \frac{\left[\frac{\pi \cdot (11.2)^2}{4} \right] \cdot (580)}{4.00} = 14,300 \text{ lb./in.}$$

where:

- A_c = area of the supporting Celotex (taken as the area of the aluminum support plate)
- L_c = height of the column of Celotex under the support plate (Drawing R-R2-F-0019)

The natural frequency of the package is now calculated using the above relation:

$$f = \frac{1}{2 \cdot \pi} \cdot \sqrt{\frac{k \cdot g}{w}} = \frac{1}{2 \cdot \pi} \cdot \sqrt{\frac{(14,300) \cdot (386.4)}{283}} = 22.2 \text{ Hz}$$

Transmissibility, Q

From reference (7), the transmissibility, Q (also known as magnification factor) is determined as:

$$Q = \left[(1 - r^2)^2 + (2 \cdot r \cdot d)^2 \right]^{-.5} = \left[(1 - 1^2)^2 + (2 \cdot 1 \cdot .10)^2 \right]^{-.5} = 5.0$$

where:

d = damping coefficient = 0.10

r = frequency ratio = $f / f_n = 1$, where f_n = natural frequency

The package acceleration, G_{out} is now calculated below:

$$G_{out} = \sqrt{\frac{\pi \cdot P \cdot f \cdot Q}{2}} = \sqrt{\frac{\pi \cdot (0.001 \text{ g}^2 / \text{hz}) \cdot (40 \text{ hz}) \cdot (5.0)}{2}} = .56 \text{ g}$$

where P = 0.001 from Figure 6-47. Using the computed frequency of 22 Hz results in 0.42 g.

The maximum vibration of the containment vessels and contents is about 3 to 4 times the root mean square, or about 1.7 g to 2.25 g. Conservatively assuming 100% of the package mass is acting at this acceleration level yields a maximum load of less than 1000 lbs. The resistance of the container lid to this load is from the bolt pre-load, as documented in Section 6.5.

6.7 Loosening of Drum Bolts During Normal Conditions of Transport

The only known mechanism for bolt loosening in the 9975 package bolts is vibration-caused motion of the lid flange relative to the drum. If motion occurs, and is properly directed, then turning of the bolt head could be possible. However, motion of the lid flange is prevented by bolt preload as discussed below.

Bolt preload in the drum lid is caused by torque applied to the bolts during assembly. The minimum load on the bolts due to torque-up is given in Section 6.4 as 3360 lbs.

The tensile stress in the bolt, S due to torque-up at 70° F is determined below:

$$S = \frac{F}{A_b} = \frac{3360}{0.1419} = 23,680 \text{ psi}$$

where A_b is the bolt tensile stress area = 0.1419 in., reference (2)

The bolt strain, ϵ is:

$$\epsilon = \frac{S}{E} = \frac{23,680}{30,000,000} = .0007893 \text{ in/in}$$

where E is the modulus of elasticity of the bolt material = 30,000,000 psi

At ambient temperature, the bolt length will increase as it is preloaded by the amount, ΔL_1 , calculated as follows:

$$\Delta L_1 = L \cdot \epsilon = (0.435) \cdot (0.0007893) = 0.0003433 \text{ in.}$$

where:

L = effective loaded length of the bolt = $t_{lf} + t_l + t_{df} + h_w = .125 + 0.048 + .125 + .137 = .435$ in.
 t_{lf} is the thickness of the lid flange = 0.125 in., Drawing R-R2-F-0025
 t_l is the thickness of the lid = 0.048 in., Drawing R-R2-F-0025
 t_{df} is the thickness of the drum flange = 0.125 in., Drawing R-R2-F-0025
 h_w is the washer thickness = .137 in. (reference: ASTM F436-94)

At -40° F, some of the tension in the bolt will relax. Using the coefficients of thermal expansion for the flanges and the bolts, the change in length of the bolt, ΔL_2 with decreased temperature is determined below:

$$\begin{aligned} \Delta L_2 &= (\alpha_f - \alpha_b) \cdot \Delta T \cdot (L - h_w) \\ &= (8.46 \times 10^{-6} - 5.6 \times 10^{-6}) \cdot [70 - (-40)] \cdot (0.435 - .137) = 0.0001108 \text{ in.} \end{aligned}$$

where

α_f is the coefficient of thermal expansion for the flange material (304L)
 $= 8.46 \times 10^{-6}$ in/in/°F (ASME Code, Section II, Part D)

α_b is the coefficient of thermal expansion for the bolt and nut material (carbon/alloy steel)
 $= 5.6 \times 10^{-6}$ in/in/°F (ASME Code, Section II, Part D)

ΔT is the temperature change from bolt-up (70 °F) to minimum service temperature (-40 °F)

This tells us that the flange thickness contracts 5.03×10^{-6} inch more than the bolts, thus reducing the pre-load. However, at minus 40 degrees Fahrenheit the bolt is still in tension because of the remaining pre-load, which is calculated below. The remaining elongation of the bolt, ΔL_3 is calculated as follows:

$$\Delta L_3 = \Delta L_1 - \Delta L_2 = 0.0003433 - 0.0001108 = 0.0002325 \text{ in.}$$

The remaining pre-load is calculated as follows:

$$F_3 = S_3 \cdot A = \epsilon_3 \cdot E \cdot A = \frac{(\Delta L_3) \cdot E \cdot A}{L} = \frac{(0.0002325) \cdot (30 \times 10^6) \cdot (.1419)}{0.435} = 2275 \text{ lb.}$$

where the subscript 3 denotes the values of the previously defined variables at -40 °F.

The remaining preload at minus 40 degrees Fahrenheit is 2275 pounds per bolt. This remaining preload can now be compared with the vibratory load on the drum lid to determine if loosening can occur.

The weight of the drum lid is estimated from details given on Drawing R-R2-F-0025, as follows:

$$W_1 = (0.29)[\pi/4(18.1)^2(.048) + \pi(18.1)(.048)(.75) + \pi/4(20.75^2 - 18.1^2)(.048) + \pi/4(20.85^2 - 18.85^2)(.125)] = 7.6 \text{ lb.}$$

The vibratory load tending to loosen the bolts is calculated as the product of the maximum acceleration, 2.25 g (see Section 6.6) and the lid weight, or $P_{\max} = 2.25 (7.6) \approx 20$ lbs. Conservatively assuming this load is applied in a lateral direction, friction at the lid to drum bolted joint must be sufficient to prevent relative motion between the closure assembly parts, which is the postulated loosening mechanism for the closure bolts. Assuming a metal-to-metal coefficient of friction between the closure parts, the resistance of the closure to slip is calculated as:

$$P_{res} = \mu \cdot F_3 \cdot N_b = (0.1) \cdot (2275) \cdot (24) = 5687.5 \text{ lb.}$$

It is seen that the resistance to slip in the closure assembly, 5687 lbs. is significantly greater than the vibratory load tending to cause slip, 20 lb., and vibration will not be a problem during Normal Conditions of Transport.

6.8 Evaluation of Flange to Drum Weld

The bolting flange is attached to the drum by a fillet weld on the edge of the drum, and a 1-in-4 stitch weld on the drum outer diameter (see Figure 6-48) below. The weld stresses are evaluated based on a limit moment in the drum wall, to account for anticipated plastic deformation of the drum during end impacts. The limit moment in the drum is assumed to be caused by radial loading of the flange at the flange outer diameter. This force and the resulting limit moment on the drum wall, plus the maximum axial load the drum wall is capable of sustaining (12.3 Kips, Section 6.3.2), are applied to the weld to verify the weld can withstand the applied loads.

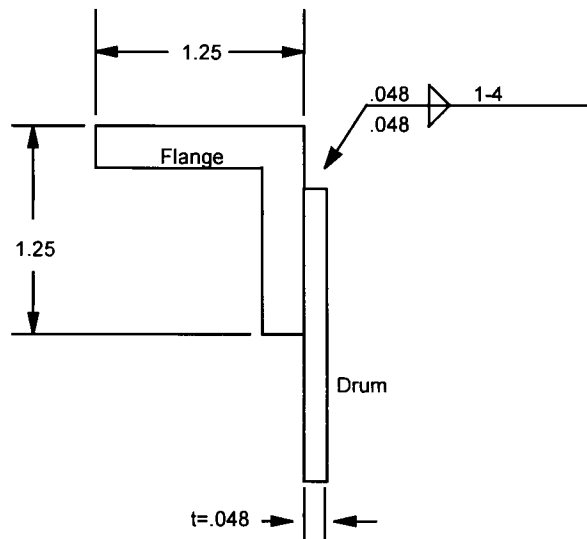


Figure 6-48 Flange to Drum Weld Configuration

The drum is made of Type 304 stainless steel, which has a minimum specified yield strength $S_y = 30,000$ psi, and a minimum specified tensile strength $S_u = 75,000$ psi. The flow stress for this strain hardening stainless steel may be assumed to be equal to $S_f = (S_y + S_u)/2 = 52,500$ psi.

- Bending Moment - Under limit conditions, a fully plastic cross-section exists, with a constant stress throughout the cross-section, equal to the flow stress. For a rectangular cross section, the plastic moment is related to the flow stress by the following relation, reference (8):

$$M_L = \frac{S_f \cdot t^2}{4} = \frac{(52,500) \cdot (.048)^2}{4} = 30 \text{ in} - \text{lb}/\text{in}$$

where:

M is the unit moment acting along the circumference of the drum, and
t is the drum thickness = 0.048 inch (Drawing R-R2-F-0025).

The axisymmetric moment in the drum is assumed to be caused by radial loading of the flange at the flange outer diameter. The flange is comprised of a 1.25 x 1.25 inch angle section, and the force is:

$$F_R = \frac{M_L}{w_f} = \frac{30}{1.25} = 24 \text{ lb}/\text{in.} \quad \text{where } w_f \text{ is the width of the flange.}$$

- Axial Force

In section 6.3.2, the limit load of the drum for the axial direction was determined. The buckling load and the plastic limit load were both computed and compared. It was found that controlling load was the plastic limit load. The maximum value was 12.3 Kips. This was controlled by the induced plasticity in the drum rolled hoops.

$$F_a = \frac{12,300\text{lbs}}{\pi 18.35"} = 213 \text{ lb./in.}$$

Forces on Weld Pattern

The flange to drum weld consists of a repeating pattern as shown in Figure 6-49 below, around the circumference of the drum. This pattern repeats every 4 inches. The unit forces and moments computed above will be expressed in terms of total force and moment on the four inch pattern.

$$\text{Axial Direction Force} = FA = F_a \times 4" = 213\text{lbs/in} \times 4" = \underline{FA = 852\text{lbs}}$$

$$\text{Radial Direction Force} = FR = F_r \times 4" = 24\text{lbs/in} \times 4" = \underline{FR = 96\text{lbs}}$$

$$\text{Axial Direction Force} = ML = M_L \times 4" = 30\text{in}\cdot\text{lbs/in} \times 4" = \underline{ML = 120\text{in}\cdot\text{lbs}}$$

Evaluation of Weld

The weld area and section modulus for the 4 inch pattern are computed. The section modulus is based on the minimum overlap (distance between weld lines):

$$\text{Drum height after Maximum cutoff (Drawing R-R2-F-0025)} = 34.52 - .12 = 34.40 \text{ in.}$$

$$\text{Maximum overall length of drum with flange} = 34.75 + .13 = 34.88 \text{ in.}$$

$$\text{Minimum overlap between flange and drum} = 1.25 - (34.88 - 34.4) = 0.77 \text{ in}$$

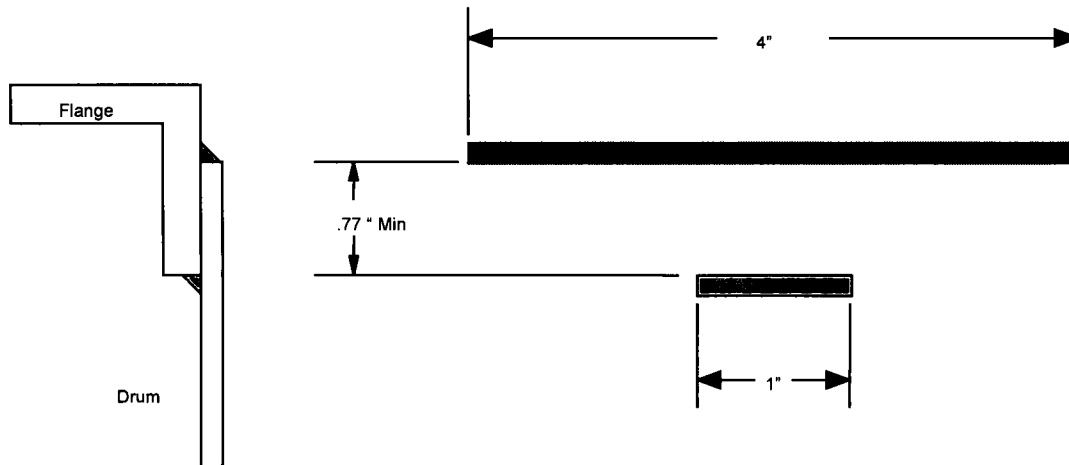


Figure 6-49 Weld Pattern Around Drum Circumference

The methodology of reference (9) is used to evaluate the stresses in the welds. The welds are evaluated as lines, and the section properties are determined on a unit basis.

Weld Area

The total weld area for a four inch length is the sum of the top and bottom weld lengths (4" plus 1"), multiplied by the appropriate weld throat:

$$A_s = .707 \cdot h \cdot (d_1 + d_2) = .707 \cdot (.048) \cdot (4.0 + 1.0) = 0.170 \text{ in.}^2$$

h is the weld leg height = 0.048 in.

d₁ is the length of the upper weld = 4.0 in.

d₂ is the length of the lower weld = 1.0 inch

Weld Section Modulus

The area moment of inertia of the weld group about its centroid is first determined. The centroid is located at a distance from a given datum as follows:

$$\bar{x} = \frac{\sum A \cdot \bar{y}}{\sum A}$$

For a datum located midway between the welds:

$$\bar{x} = \frac{(4.0) \cdot (.77/2) - (1.0) \cdot (.77/2)}{4.0 + 1.0} = 0.231$$

The centroid is located $.77/2 + .231 = .616$ inches above the stitch weld, and $.77/2 - .231 = .154$ inches below the upper weld. The moment of inertia of the weld group about the centroid is:

$$I_u = \sum A \cdot \bar{y}^2 = 1.0 \cdot (.616)^2 + 4.0 \cdot (.154)^2 = .474 \text{ in.}^4 / \text{in}$$

The moment of inertia of the 4" pattern is equal to the width of the weld throat times the unit moment of inertia. The section modulus is the moment of inertia divided by the maximum distance from weld to centroid (c1 = 0.616")

$$I = 0.707 \cdot h \cdot I_u = 0.707 \cdot (.048) \cdot (.474) = 0.0161 \text{ in.}^4$$

$$S = I/c = 0.0161 \text{ in.}^4 / 0.616" = 0.0261 \text{ in}^3$$

Weld Stress

The weld stress due to the radial load and the bending moment combine directly. The stress due to the axial load is perpendicular to the bending and radial stress and is combined by SRSS methods.

$$\text{Stress due to Radial Load} = S_R = \frac{FR}{A_s} = \frac{96 \text{ lbs}}{.170 \text{ in}^2} = 565 \text{ psi}$$

$$\text{Stress due to Axial Load} = S_A = \frac{FA}{A_s} = \frac{852 \text{ lbs}}{.170 \text{ in}^2} = 5012 \text{ psi}$$

$$\text{Stress due to Bending} = S_M = \frac{ML}{S} = \frac{120 \text{ in} \cdot \text{lbs}}{.0261 \text{ in}^3} = 4598 \text{ psi}$$

Evaluation of Combined Stresses

The combined stress from the two forces and one moment is computed below:

$$\sigma_{weld} = \left\{ (S_R + S_M)^2 + (S_A)^2 \right\}^{1/2} = \left\{ (565 + 4598)^2 + (5012)^2 \right\}^{1/2} = 7196 \text{ psi}$$

The shear stress is evaluated to the limits provided in ASME Code, Section III, Division I, Appendix F, Paragraph 1331.1(d), which identifies a limit of 0.42 S_u for pure shear for faulted conditions. For the Type 304 stainless steel weld material, $S_u = 75,000$ psi, and the allowable shear stress is 0.42 (75,000) = 31,500 psi. The maximum shear stress is well within the maximum allowable, and the drum/flange welds are therefore acceptable for loading due to drum deformation. The margin is calculated below:

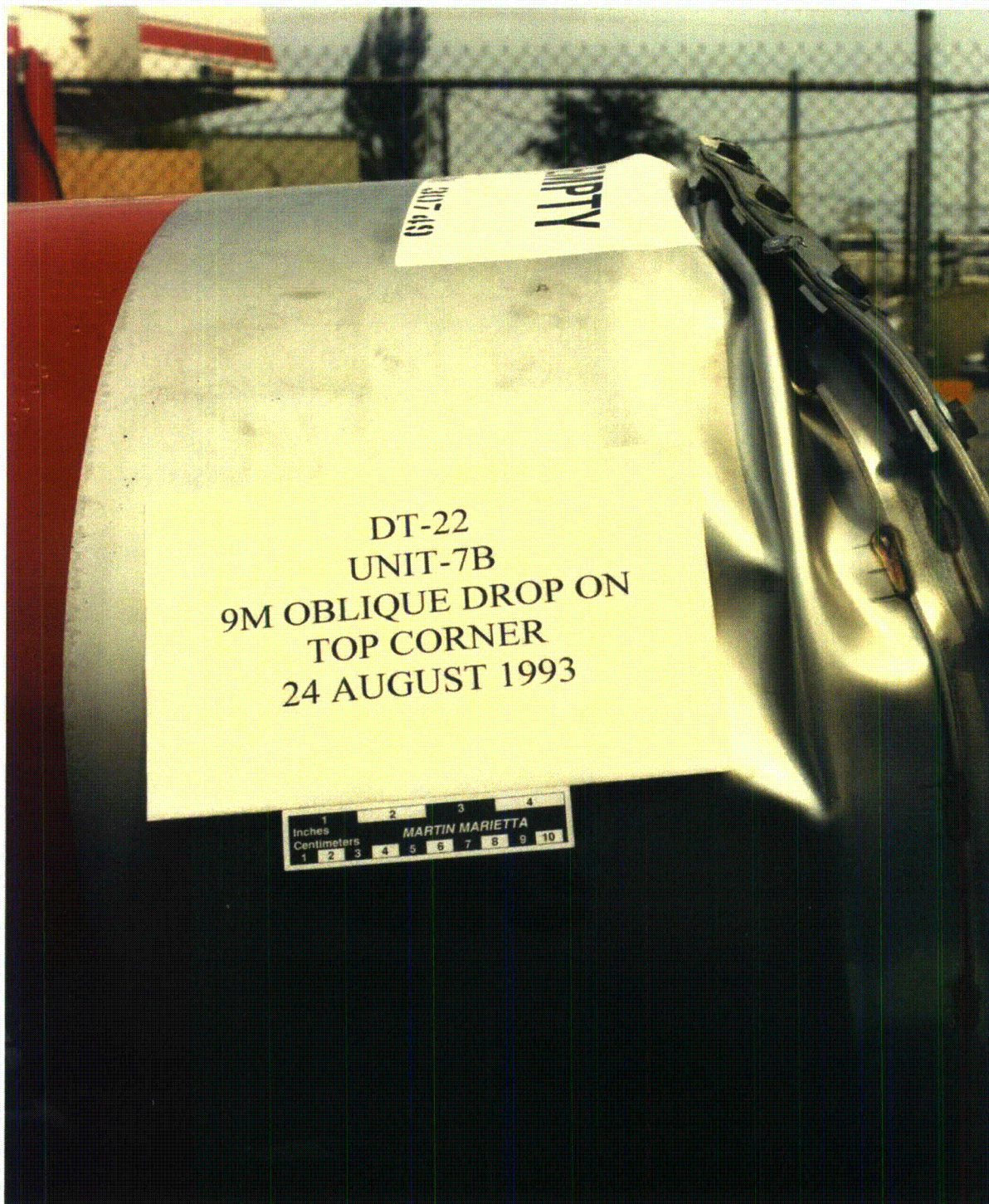
$$\text{margin} = (31,500/7196 - 1) = 3.4$$

7 References

1. *Safety Analysis Report – Packages 9965, 9968, 9972-9975 Packages (U)*, WSRC-SA-7, Revision 8, August 1999
2. An Introduction to the Design and Behavior of Bolted Joints, J. H. Bickford; 3rd Ed.;Dekker, 1995
3. Machinery's Handbook, Twentieth Edition; Industrial Press, 1975
4. ASME Code, Section II, Part D (1998)
5. ASME Code, Section III, Subsection NB (1998)
6. C. F. Magnuson. *Manufacture-to-Stockpile Sequence*. SAND83-0480, Sandia National Laboratory, Albuquerque, NM 87115 (June 1983)
7. *Shock and Vibration Handbook*, C. M. Harris and C. E. Crede; 2nd Ed; McGraw-Hill, 1976
8. Engineering Design; 2nd Edition; J. H. Faupel & F. E. Fisher. Wiley, 1981
9. Mechanical Engineering Design; 3rd Edition; J. E. Shigley. McGraw-Hill, 1977

Appendix A

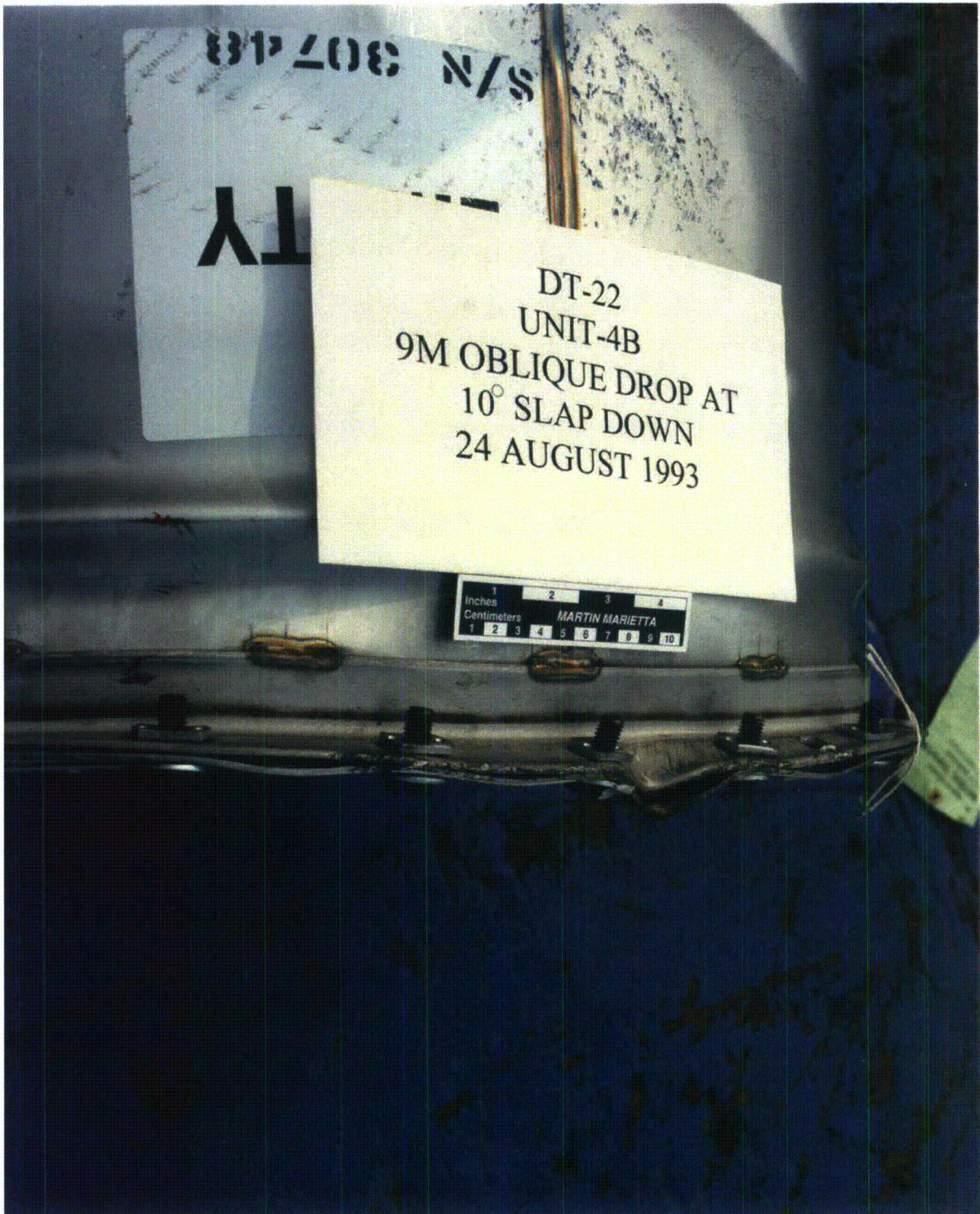
DT-22 Test Photographs



Photograph 1



Photograph 2



Photograph 3



Photograph 4



Photograph 5



Photograph 6

APPENDIX 2.5
9975 PACKAGING COMPARISONS
WITH THE 9966, 9967, 9968, 9973, 9974, AND 9975 PROTOTYPE

This Page Intentionally Left Blank

9975 PACKAGING COMPARISONS WITH THE 9966, 9967, 9968, 9973, 9974, AND 9975 PROTOTYPE

This appendix provides comparisons between the 9975 packaging and packagings of similar design^[1,2] to show that results from Hypothetical Accident Condition (HAC) impact testing and HAC thermal testing are applicable to the 9975. Comparisons of package components and configurations are shown in the following figures and tables.

HAC testing consists of subjecting the packaging to a series of structural and thermal events. 10 CFR 71.41 authorizes evaluation by subjecting a specimen to these tests. Accordingly, the following comparisons and the package test results summarized in Chapter 2 demonstrate that the 9975 package is compliant with 10 CFR 71.

The comparisons are presented in a manner consistent with Regulatory Guide 7.9, Section 2.7.1.d, *Comparison to Similar Packages*.

The principal results from testing of comparable packages that support the HAC evaluation of the 9975 are:

- The integrity of the drum enclosure (9967, 9968, 9974 and 9975 Prototype)
- The integrity of the containment vessels (9967, 9968, 9974 and 9975 Prototype)
- Thermal performance of packaging (9967, 9973 and 9975 Prototype)

The 9967 and 9974 packages are based on 55-gallon drums and include lead shielding over twice as thick as that of the 9975 design. Hence, these packages are significantly heavier than the 9975. Because of heavier weight, the HAC impact responses of the 9967 and the 9974 documented in previous SARPs^[1,2] involve more severe damage than the lighter 9975. However, both the PCVs and SCVs are the same basic designs except for approximately 5-inch shorter lengths than those employed in the 9975 design.

Since impact energy is linear with mass, the resulting impact energy absorbed by the 9967 and 9974 from a 30-ft drop is over 50% greater than that of the 9975. In addition, since the impact characteristics of a Celotex-insulated drum are common to these packages, the impact forces transmitted to the respective containment systems are in the same proportion. Satisfactory performance of the heavier 9974 and 9967 packages establishes that the performance of the lighter 9975 is acceptable by comparison.

The 9968 is a predecessor and largely identical to the 9975 with the exceptions of the carbon steel drum material, bolt/nut/ring drum closure and tie rods for assembling the insulation layers used in the 9968. The carbon steel drum has lower tensile strength than the 9975's 304L stainless steel drum and as a result is more susceptible to structural damage. Therefore, favorable results from 9968 drop testing that demonstrated continued drum integrity and leak-tightness of the containment vessels are applicable to the 9975.

The 9967 and 9973 are lighter and absorb lower impact energy than the 9975 package. While general comparisons of structural damage to the containment features are not applicable to the

9975, a comparison can be made between the thermal features of the packages. The thermal loadings on the containment system of the 9973 are more severe than on the 9975 as follows:

- Less Celotex axial thickness in the 9973 nearest the containment vessel closures
- Absence of lead shield in the 9973 (absence of hot vapor barrier)

A 9973 package was chosen to evaluate fire testing on a drop-damaged package. A 9975 package was chosen to evaluate the effect of preheated contents on fire testing but it was not drop tested before the fire test. Therefore, it is necessary to use the results from the 9973 fire test to provide confirmation that the 9975 will pass the HAC regulatory test sequence.

Compared to the 9975, the 9973 has a lower thermal capacity because there is no lead shielding and the containment vessels are lighter. Although the 9973 has slightly larger radial insulation material (5.5 inches versus 4.75 for the 9975), the increased insulating effect for the 9973 has a minor effect. This is seen in the 9973 test results from Appendix 3.5, which show that the increase in temperature from steady state at the SCV seal is substantially greater (~50°F) than the 9975 at the same location. If the 9973 had contained heat generating contents, the maximum seal temperature could reach 235°F or slightly higher, which would not challenge its limit or any of the component temperature limits.

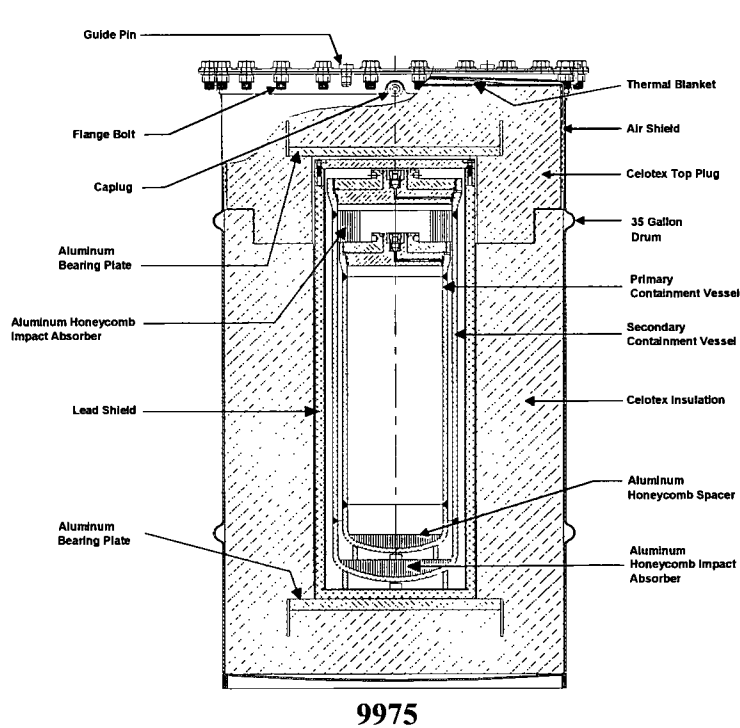
Therefore, results of thermal tests on the 9973 package are more severe on the containment function of the package and consequently bound the 9975 thermal behavior. It may be concluded that if the 9975 had undergone a drop test followed by a fire test with a 19-watt heat load, it would be expected to meet the regulatory HAC performance requirements.

The 9966 package is nearly identical to the 9973 except there is no air-shield on the 9966, which lessens the protection of the Celotex during the fire. The result of the fire test on the 9966^[1] showed no damage to the containment vessels and temperatures were well within limits for these components. Therefore, thermal testing of the 9966 package is more severe on the containment function of the package and consequently results of bound the 9975 thermal behavior.

The 9975 prototype package is exactly like the current 9975 design except for the drum closure. Drop tests performed on the 9975 prototype demonstrated a potential failure mode for the ring closure. As a result of these tests, the drum closure was redesigned to a bolted-flange, characteristic of the type used on Oak Ridge Y-12 Plant packages of the same or heavier weight. The drum closure style has no effect on the loads and stresses of the containment vessels or the temperatures of the drum internals, therefore not all tests were re-run.

REFERENCES:

1. *Safety Analysis Report - Packages: USA/9965/B(U)F (DOE), USA/9966/B(U)F (DOE), USA/9967/B(U)F (DOE), USA/9968/B(U)F (DOE), (Packaging of Fissile and Other Radioactive Materials)*, DPSPU 83-124-1, Rev. 0, Savannah River Site, Aiken, SC (June 1984).
2. *Safety Analysis Report - Packages: 9965, 9968, 9972-9975 Packages (U)*, WSRC-SA-7, Rev. 0, Savannah River Site, Aiken, SC (December 1994).



Not to Scale

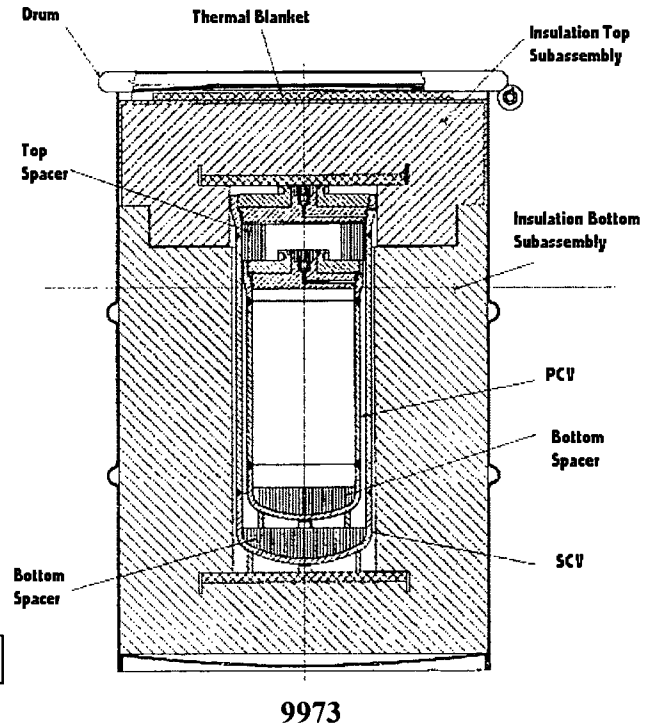


Table 1 - 9975 and 9973 Summary Package Comparison

Packaging Model	Packaging Gross Weight	Drum						Shielding Lead Thickness (inch)	No. of Containment Vessels	Insulation thicknesses (inch)		
		Capacity (gal)	Gauge (18 ga)	Material (304 SS)	Dia. (in.)	Height (in.)	Closure			Top	Bottom	Radial
9975	404	35	√	√	19.6	35.5	Bolted Flange	0.5	2	3.7	3.4	4.75
9973	231	30	√	√	19.6	29.1	Ring	none	2	3.3	3.1	5.5

Table 2 - 9975 and 9973 Detailed Package Comparison

Assembly, Design Features and Materials, Overall Weights and Dimensions					
	Drum	Air Shield Bearing Plate Spacer/Absorber	Insulation	Shielding	Containment Vessels
9975	<p>Drum Material: 18-Gage, 304 Stainless Steel, ASME SA-240</p> <p>Nominal Capacity: 35 gal.</p> <p>Max Gross Weight: 404 lb.</p> <p>Overall Dimensions: 19.6-dia x 35.5(in)</p> <p>Closure: Bolted Flange, 24-Hex Cap Screws, .5- 13UNC-2A x 1.25 in.</p>	<p>Air Shield: 24 -Gage Stainless Steel, ASME SA-480</p> <p>Bearing Plate: 0.5-in, 1100 Al, ASTM B-209 (top and bottom)</p> <p>Spacer/Absorber Al-Tube Honeycomb, Crush strength 1500 ± 500 psi (top and bottom)</p>	<p>Material: Cane fiberboard, 15 lb/ft3 (nominal), ASTM C-208- 75</p> <p>Thickness: Radial - 4.75-in, Axial - 3.7-in (top), 3.4-in (bottom)</p> <p>Assembly Method & Geometry: Glue, stepped geometry</p> <p>Thermal Blanket: Stainless steel encapsulated Kaowool.</p>	<p>Material: 0.5-in Cast Lead, ASTM B- 749, Lined With 20-Gage 304 Stainless Steel Sheet Metal</p> <p>Lid: 0.5-in, 0.5-in, 1100 Al, ASTM B-209</p>	<p>Material: 304L Stainless Steel</p> <p>Dimensions Overall: PCV - 5.87-in dia x 18.63-in SCV - 7.12-in dia x 24.0 in</p> <p>ASME Code: Section III</p>
9973	<p>Drum Material: 18-Gage, 304 Stainless Steel, ASME SA-240</p> <p>Nominal Capacity: 30 gal.</p> <p>Max Gross Weight: 231 lb.</p> <p>Overall Dimensions: 19.6-dia x 29.1(in)</p> <p>Closure: Bolt-Type Locking Ring, 12-Gage, 304 Stainless Steel</p>	<p>Air Shield: 24 -Gage Stainless Steel, ASME SA-480</p> <p>Bearing Plate: 0.5-in, 1100 Al, ASTM B-209 (top and bottom)</p> <p>Spacer/Absorber Al-Tube Honeycomb, Crush strength 1500 ± 500 psi (top and bottom)</p>	<p>Material: Cane fiberboard, 15 lb/ft3 (nominal), ASTM C-208- 75</p> <p>Thickness: Radial - 5.5-in, Axial - 3.3-in (top), 3.1-in (bottom)</p> <p>Assembly Method & Geometry: Glue, stepped geometry</p> <p>Thermal Blanket: Stainless steel encapsulated Kaowool.</p>	None	<p>Material: 304L Stainless Steel</p> <p>Dimensions Overall: PCV - 5.87-in dia x 13.63-in SCV - 7.12-in dia x 19.0 in</p> <p>ASME Code: Section III</p>

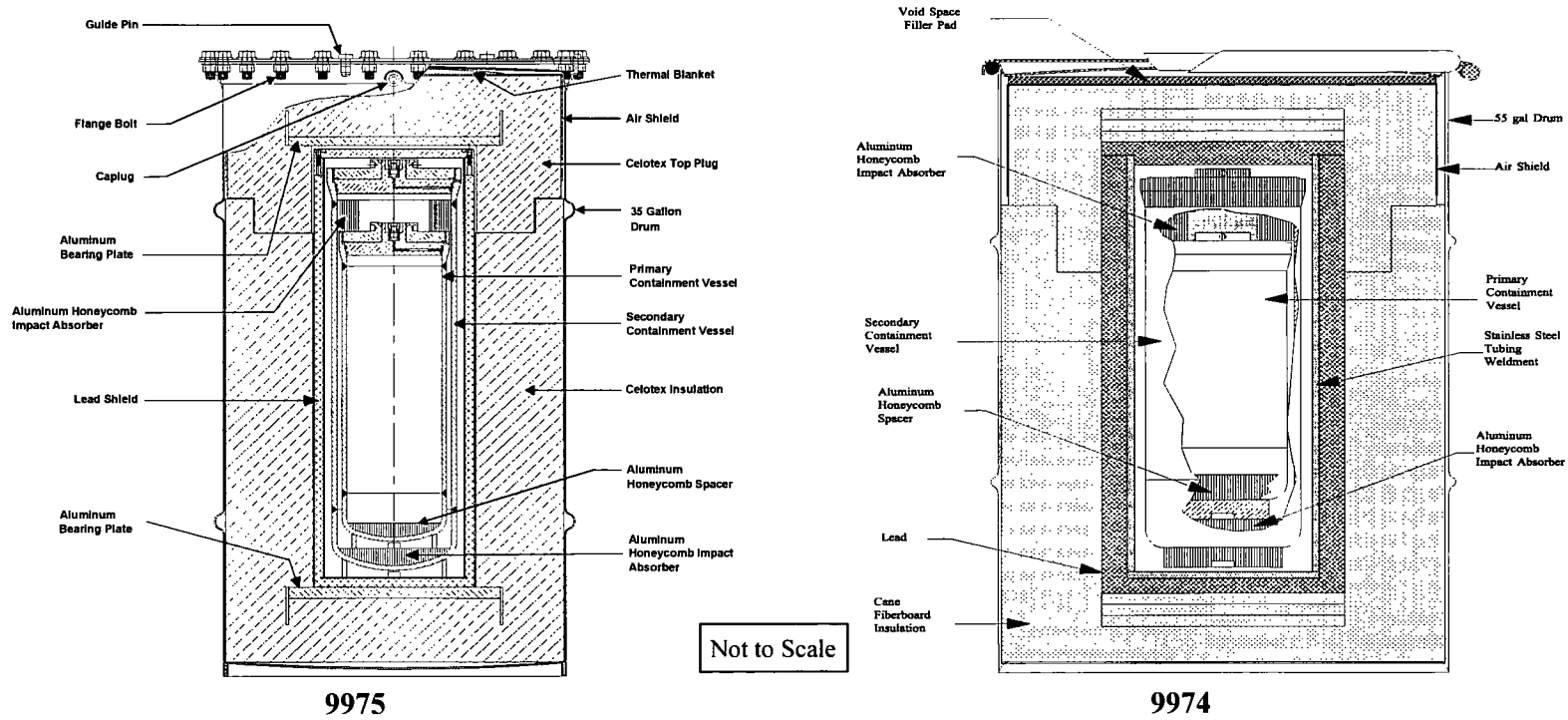
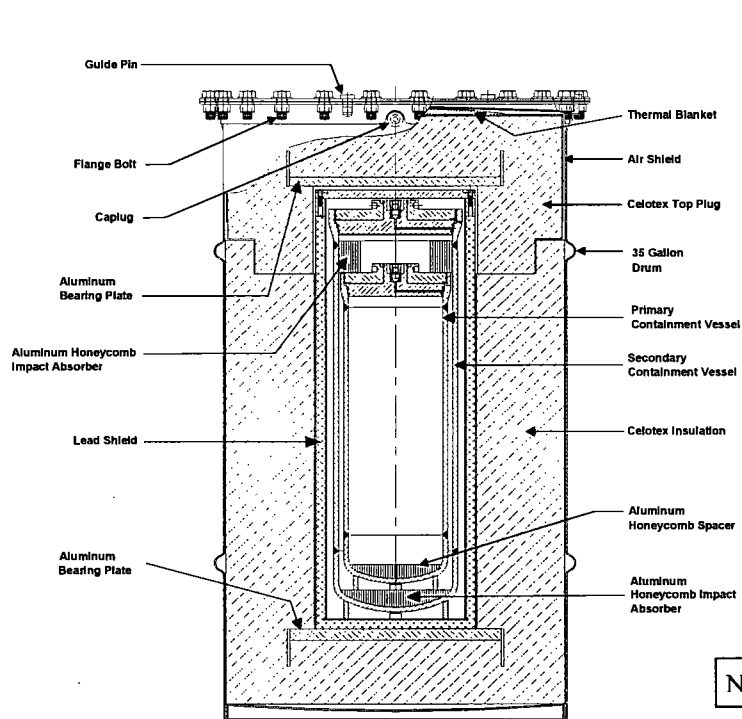


Table 3 - 9975 and 9974 Summary Package Comparison

Packaging Model	Packaging Gross Weight	Drum						Shielding Lead Thickness (inch)	No. of Containment Vessels	Insulation thicknesses (inch)		
		Capacity (gal)	Gauge (ga)	Material	Dia. (in.)	Height (in.)	Closure			Top	Bottom	Radial
9975	404	35	18	304SS	19.6	35.5	Bolted Flange	0.5	2	3.7	3.4	4.75
9974	673	55	16	304SS	23.9	34.8	Ring	1.1	2	3.3	3.1	5.5

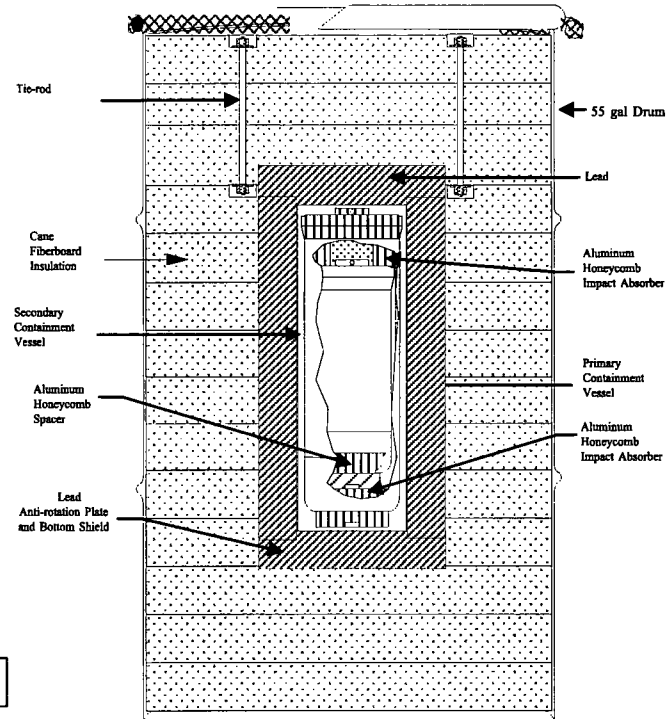
Table 4 - 9975 and 9974 Package Comparison

Assembly, Design Features and Materials, Overall Weights and Dimensions					
	Drum	Air Shield Bearing Plate Spacer/Absorber	Insulation	Shielding	Containment Vessels
9975	<p>Drum Material: 18-Gage, 304 Stainless Steel, ASME SA-240</p> <p>Nominal Capacity: 35 gal.</p> <p>Max Gross Weight: 404 lb.</p> <p>Overall Dimensions: 19.6-dia x 35.5(in)</p> <p>Closure: Bolted Flange, 24-Hex Cap Screws, .5- 13UNC-2A x 1.25 in.</p>	<p>Air Shield: 24 -Gage Stainless Steel, ASME SA-480</p> <p>Bearing Plate: 0.5-in, 1100 Al, ASTM B-209 (top and bottom)</p> <p>Spacer/Absorber Al-Tube Honeycomb, Crush strength 1500 ± 500 psi (top and bottom)</p>	<p>Material: Cane fiberboard, 15 lb/ft³ (nominal), ASTM C-208-75</p> <p>Thickness: Radial - 4.75-in, Axial - 3.7-in (top), 3.4-in (bottom)</p> <p>Assembly Method & Geometry: Glue, stepped geometry</p> <p>Thermal Blanket: Stainless steel encapsulated Kaowool.</p>	<p>Material: 0.5-in Cast Lead, ASTM B-749, Lined With 20- Gage 304 Stainless Steel Sheet Metal</p> <p>Lid: 0.5-in, 0.5-in, 1100 Al, ASTM B-209</p>	<p>Material: 304L Stainless Steel</p> <p>Dimensions Overall: PCV - 5.87-in dia x 18.63-in SCV - 7.12-in dia x 24.0 in</p> <p>ASME Code: Section III</p>
9974	<p>Drum Material: 16-Gage, 304 Stainless Steel, ASME SA-240</p> <p>Nominal Capacity: 55 gal.</p> <p>Max Gross Weight: 673 lb.</p> <p>Overall Dimensions: 23.9-dia x 34.8(in)</p> <p>Closure: Bolt-Type Locking Ring, 12-Gage, 304 Stainless Steel</p>	<p>Air Shield: 24 -Gage Stainless Steel, ASME SA-480</p> <p>Bearing Plate: 0.5-in, 1100 Al, ASTM B-209 (top and bottom)</p> <p>Spacer/Absorber Al-Tube Honeycomb, Crush strength 1500 ± 500 psi (top and bottom)</p>	<p>Material: Cane fiberboard, 15 lb/ft³ (nominal), ASTM C-208-75</p> <p>Thickness: Radial - 5.5-in, Axial - 3.3-in (top), 3.1-in (bottom)</p> <p>Assembly Method & Geometry: Glue, stepped geometry</p> <p>Thermal Blanket: Stainless steel encapsulated Kaowool.</p>	<p>Material: 1.1-in (min) Cast Lead, ASTM B- 749, Lined With 0.250in 304 Stainless Steel Sheet Tubing</p> <p>Lid: 1.5-in, Cast Lead, ASTM B- 749</p>	<p>Material: 304L Stainless Steel</p> <p>Dimensions Overall: PCV - 5.87-in dia x 13.63-in SCV - 7.12-in dia x 19.0 in</p> <p>ASME Code: Section III</p>



9975

Not to Scale



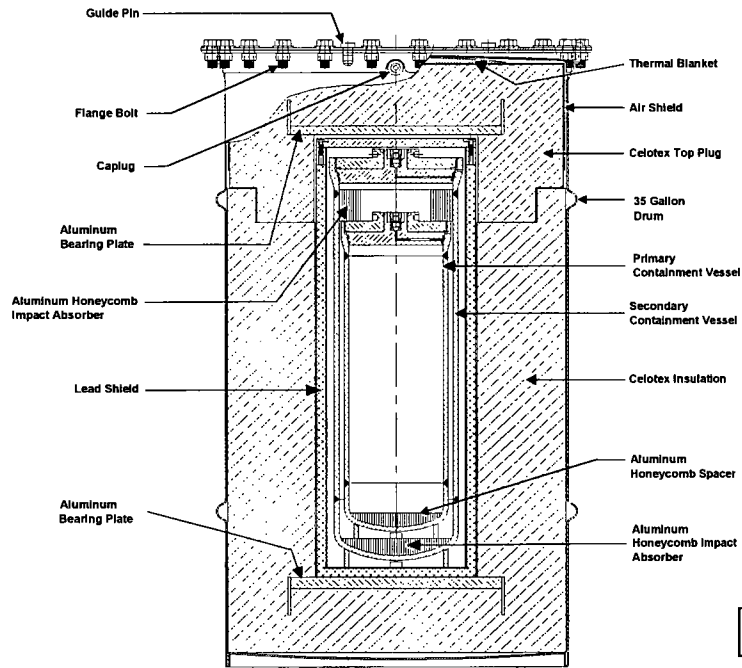
9967

Table 5 - 9975 and 9967 Summary Package Comparison

Packaging Model	Packaging Gross Weight	Drum						Shielding Lead Thickness (inch)	No. of Containment Vessels	Insulation thicknesses (inch)		
		Capacity (gal)	Gauge (ga)	Material	Dia. (in.)	Height (in.)	Closure			Top	Bottom	Radial
9975	404	35	18	304SS	19.6	35.5	Bolted Flange	0.5	2	3.7	3.4	4.75
9967	627	55	16	Gal. CS	23.9	34.8	Ring	1.5	2	6	6	6.6

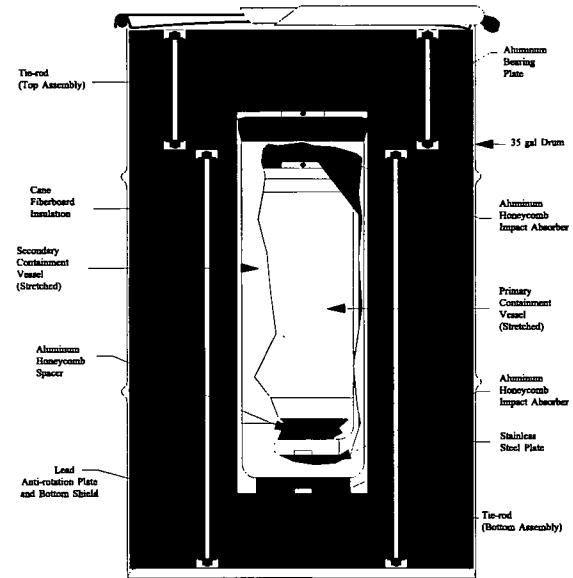
Table 6 - 9975 and 9967 Package Comparison

Assembly, Design Features and Materials, Overall Weights and Dimensions					
	Drum	Air Shield Bearing Plate Spacer/Absorber	Insulation	Shielding	Containment Vessels
9975	<p>Drum Material: 18-Gage, 304 Stainless Steel, ASME SA-240</p> <p>Nominal Capacity: 35 gal.</p> <p>Max Gross Weight: 404 lb.</p> <p>Overall Dimensions: 19.6-dia x 35.5(in)</p> <p>Closure: Bolted Flange, 24-Hex Cap Screws, .5- 13UNC-2A x 1.25 in.</p>	<p>Air Shield: 24 -Gage Stainless Steel, ASME SA-480</p> <p>Bearing Plate: 0.5-in, 1100 Al, ASTM B-209 (top and bottom)</p> <p>Spacer/Absorber Al-Tube Honeycomb, Crush strength 1500 ± 500 psi (top and bottom)</p>	<p>Material: Cane fiberboard, 15 lb/ft³ (nominal), ASTM C-208-75</p> <p>Thickness: Radial - 4.75-in, Axial - 3.7-in (top), 3.4-in (bottom)</p> <p>Assembly Method & Geometry: Glue, stepped geometry.</p> <p>Thermal Blanket: Stainless steel encapsulated Kaowool.</p>	<p>Material: 0.5-in Cast Lead, ASTM B-749, Lined With 20- Gage 304 Stainless Steel Sheet Metal</p> <p>Lid: 0.5-in, 0.5-in, 1100 Al, ASTM B-209</p>	<p>Material: 304L Stainless Steel</p> <p>Dimensions Overall: PCV - 5.87-in dia x 18.63-in SCV - 7.12-in dia x 24.0 in</p> <p>ASME Code: Section III</p>
9967	<p>Drum Material: 16-Gage, Galvanized Carbon Steel, ASTM A-366</p> <p>Nominal Capacity: 55 gal.</p> <p>Max Gross Weight: 627 lb.</p> <p>Overall Dimensions: 23.9-dia x 34.8(in)</p> <p>Closure: Bolt-Type Locking Ring, 12-Gage, Galvanized Carbon Steel, ASTM A-366</p>	<p>Air Shield: None</p> <p>Bearing Plate: Shielding used as top and bottom bearing plates. 0.5 x 0.38-in 304 SST bar-stock, ASTM A-749, attached to bottom of shield assembly to prevent rotation of SCV</p> <p>Spacer/Absorber Al-Tube Honeycomb, Crush strength 1500 ± 500 psi (top and bottom)</p>	<p>Material: Cane fiberboard, 15 lb/ft³ (nominal), ASTM C-208-75</p> <p>Thickness: Radial - 6.6-in, Axial - 6-in (top), 6-in (bottom)</p> <p>Assembly Method & Geometry: glue tie-rods (upper), stacked.</p> <p>Thermal Blanket: None</p>	<p>Material: 2.5-in (min) Cast Lead, ASTM B- 749, coated with weather barrier</p> <p>Lid: 1.5-in, Cast Lead, ASTM B- 749</p>	<p>Material: 304L Stainless Steel</p> <p>Dimensions Overall: PCV - 5.87-in dia x 13.63-in SCV - 7.12-in dia x 19.0 in</p> <p>ASME Code: Section VIII</p>



9975

Not to Scale



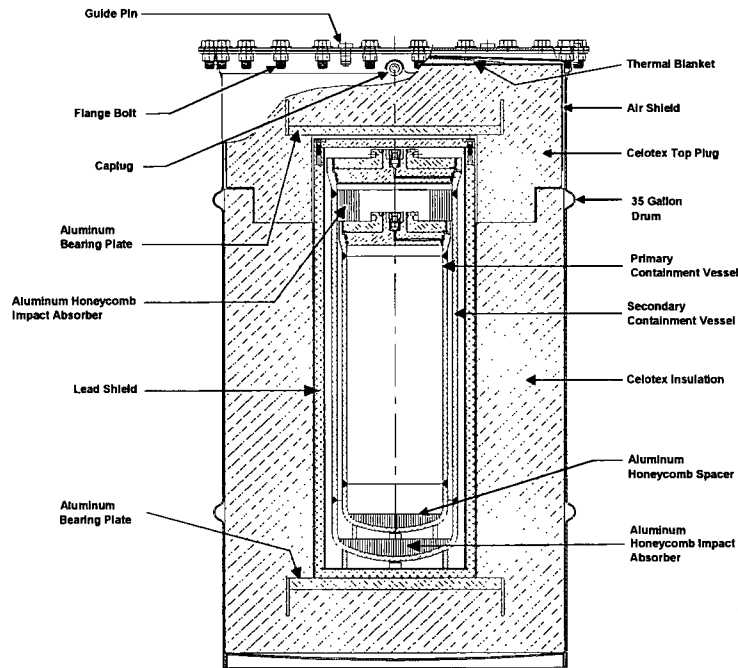
9968

Table 7 - 9975 and 9968 Summary Package Comparison

Packaging Model	Packaging Gross Weight	Drum						Shielding Lead Thickness (inch)	No. of Containment Vessels	Insulation thicknesses (inch)		
		Capacity (gal)	Gauge (ga)	Material	Dia. (in.)	Height (in.)	Closure			Top	Bottom	Radial
9975	404	35	18	304SS	19.6	35.5	Bolted Flange	0.5	2	3.7	3.4	4.75
9968	406	35	18	Gal. CS	19.6	35	Ring	0.5	2	6	6	6.6

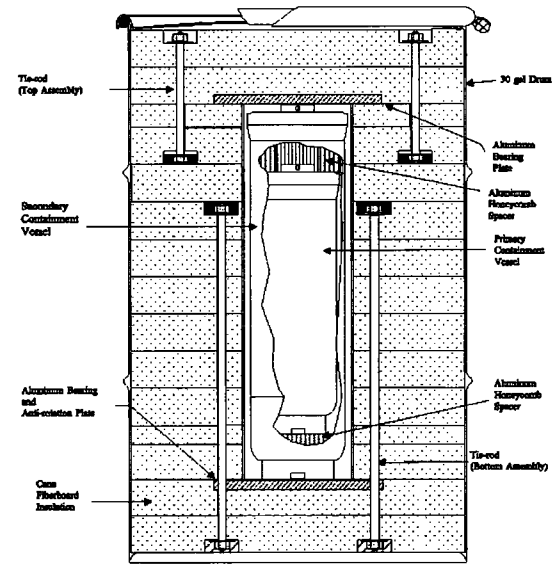
Table 8 - 9975 and 9968 Package Comparison

Assembly, Design Features and Materials, Overall Weights and Dimensions					
	Drum	Air Shield Bearing Plate Spacer/Absorber	Insulation	Shielding	Containment Vessels
9975	<p>Drum Material: 18-Gage, 304 Stainless Steel, ASME SA-240</p> <p>Nominal Capacity: 35 gal.</p> <p>Max Gross Weight: 404 lb.</p> <p>Overall Dimensions: 19.6-dia x 35.5(in)</p> <p>Closure: Bolted Flange, 24-Hex Cap Screws, .5- 13UNC-2A x 1.25 in.</p>	<p>Air Shield: 24 -Gage Stainless Steel, ASME SA-480</p> <p>Bearing Plate: 0.5-in, 1100 Al, ASTM B-209 (top and bottom)</p> <p>Spacer/Absorber Al-Tube Honeycomb, Crush strength 1500 ± 500 psi (top and bottom)</p>	<p>Material: Cane fiberboard, 15 lb/ft3 (nominal), ASTM C-208-75</p> <p>Thickness: Radial - 4.75-in, Axial - 3.7-in (top), 3.4-in (bottom)</p> <p>Assembly Method & Geometry: Glue, stepped geometry.</p> <p>Thermal Blanket: Stainless steel encapsulated Kaowool.</p>	<p>Material: 0.5-in Cast Lead, ASTM B-749, Lined With 20- Gage 304 Stainless Steel Sheet Metal</p> <p>Lid: 0.5-in, 0.5-in, 1100 Al, ASTM B-209</p>	<p>Material: 304L Stainless Steel</p> <p>Dimensions Overall: PCV - 5.87-in dia x 18.63-in SCV - 7.12-in dia x 24.0 in</p> <p>ASME Code: Section III</p>
9968	<p>Drum Material: 18-Gage, Galvanized Carbon Steel, ASTM A-366</p> <p>Nominal Capacity: 35 gal.</p> <p>Max Gross Weight: 406 lb.</p> <p>Overall Dimensions: 19.6-dia x 35(in)</p> <p>Closure: Bolt-Type Locking Ring, 12-Gage, Galvanized Carbon Steel, ASTM A-366</p>	<p>Air Shield: None</p> <p>Bearing Plate: Shielding used as top and bottom bearing plates. 0.5 x 0.25-in 304 SST bar-stock , ASTM A-749, attached to bottom of shield assembly to prevent rotation of SCV</p> <p>Spacer/Absorber Al-Tube Honeycomb, Crush strength 1500 ± 500 psi (top and bottom)</p>	<p>Material: Cane fiberboard, 15 lb/ft3 (nominal), ASTM C-208-75</p> <p>Thickness: Radial - 6.6-in, Axial - 6-in (top), 6-in (bottom)</p> <p>Assembly Method & Geometry: glue and tie rods (upper and lower), stacked geometry.</p> <p>Thermal Blanket: None</p>	<p>Material: Sleeve:1-in (min) Cast Lead, ASTM B-749, coated with weather barrier</p> <p>Bottom: 0.5-in Cast Lead, ASTM B-749, coated with weather barrier</p> <p>Lid: 0.5-in, 0.5-in, 1100 Al, ASTM B-209</p>	<p>Material: 304L Stainless Steel</p> <p>Dimensions Overall: PCV - 5.87-in dia x 13.63-in SCV - 7.12-in dia x 19.0 in</p> <p>ASME Code: Section VIII</p>



9975

Not to Scale



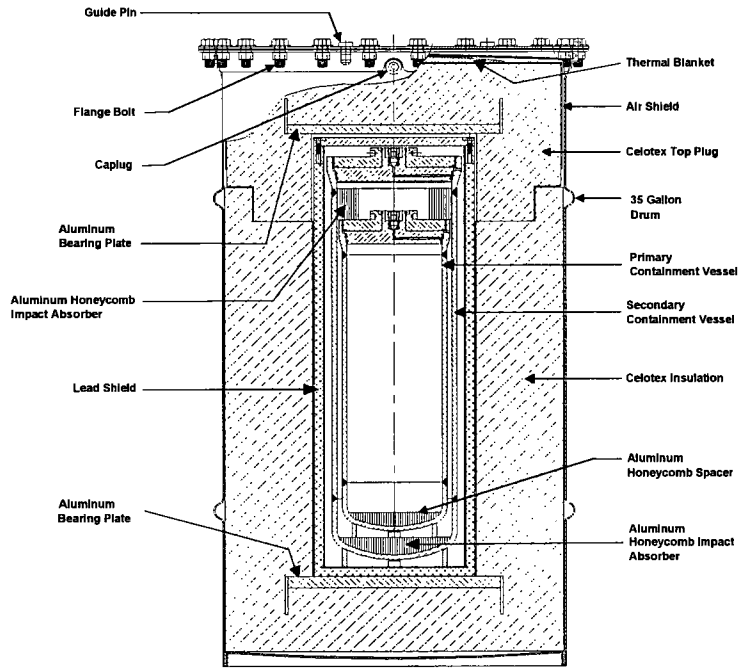
9966

Table 9 - 9975 and 9966 Summary Package Comparison

Packaging Model	Packaging Gross Weight	Drum						Shielding Lead Thickness (inch)	No. of Containment Vessels	Insulation thicknesses (inch)		
		Capacity (gal)	Gauge (ga)	Material	Dia. (in.)	Height (in.)	Closure			Top	Bottom	Radial
9975	404	35	18	304SS	19.6	35.5	Bolted Flange	0.5	2	3.7	3.4	4.75
9966	250	30	18	Gal. CS	19.6	29.3	Ring	None	2	4	4	5.6

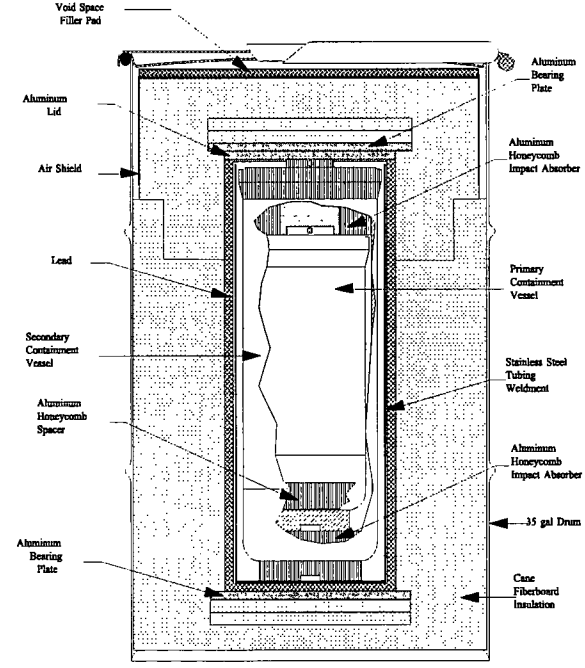
Table 10 - 9975 and 9966 Package Comparison

Assembly, Design Features and Materials, Overall Weights and Dimensions					
	Drum	Air Shield Bearing Plate Spacer/Absorber	Insulation	Shielding	Containment Vessels
9975	<p>Drum Material: 18-Gage, 304 Stainless Steel, ASME SA-240</p> <p>Nominal Capacity: 35 gal.</p> <p>Max Gross Weight: 404 lb.</p> <p>Overall Dimensions: 19.6-dia x 35.5(in)</p> <p>Closure: Bolted Flange, 24-Hex Cap Screws, .5- 13UNC-2A x 1.25 in.</p>	<p>Air Shield: 24 -Gage Stainless Steel, ASME SA-480</p> <p>Bearing Plate: 0.5-in, 1100 Al, ASTM B-209 (top and bottom)</p> <p>Spacer/Absorber Al-Tube Honeycomb, Crush strength 1500 ± 500 psi (top and bottom)</p>	<p>Material: Cane fiberboard, 15 lb/ft³ (nominal), ASTM C-208-75</p> <p>Thickness: Radial - 4.75-in, Axial - 3.7-in (top), 3.4-in (bottom)</p> <p>Assembly Method & Geometry: Glue, stepped geometry.</p> <p>Thermal Blanket: Stainless steel encapsulated Kaowool.</p>	<p>Material: 0.5-in Cast Lead, ASTM B-749, Lined With 20- Gage 304 Stainless Steel Sheet Metal</p> <p>Lid: 0.5-in, 0.5-in, 1100 Al, ASTM B-209</p>	<p>Material: 304L Stainless Steel</p> <p>Dimensions Overall: PCV - 5.87-in dia x 18.63-in SCV - 7.12-in dia x 24.0 in</p> <p>ASME Code: Section III</p>
9966	<p>Drum Material: 18-Gage, Galvanized Carbon Steel, ASTM A-366</p> <p>Nominal Capacity: 30 gal.</p> <p>Max Gross Weight: 250 lb.</p> <p>Overall Dimensions: 19.6-dia x 29.3(in)</p> <p>Closure: Bolt-Type Locking Ring, 12-Gage, Galvanized Carbon Steel, ASTM A-366</p>	<p>Air Shield: None</p> <p>Bearing Plate: 0.5-in, 1100 Al, ASTM B-209 (top and bottom)</p> <p>Spacer/Absorber Al-Tube Honeycomb, Crush strength 1500 ± 500 psi (top and bottom)</p>	<p>Material: Cane fiberboard, 15 lb/ft³ (nominal), ASTM C-208-75</p> <p>Thickness: Radial - 5.6-in, Axial - 4-in (top), 4-in (bottom)</p> <p>Assembly Method & Geometry: glue and tie rods (upper and lower), stacked geometry.</p> <p>Thermal Blanket: None</p>	<p>None</p>	<p>Material: 304L Stainless Steel</p> <p>Dimensions Overall: PCV - 5.87-in dia x 13.63-in SCV - 7.12-in dia x 19.0 in</p> <p>ASME Code: Section VIII</p>



9975 Current

Not to Scale



9975 Early Model

Table 11 – 9975 Current and 9975 Early Model Summary Package Comparison

Packaging Model	Packaging Gross Weight	Drum						Shielding Lead Thickness (inch)	No. of Containment Vessels	Insulation thicknesses (inch)		
		Capacity (gal)	Gauge (ga)	Material	Dia. (in.)	Height (in.)	Closure			Top	Bottom	Radial
9975 current	404	35	18	304SS	19.6	35.5	Bolted Flange	0.5	2	3.7	3.4	4.75
9975 Early	404	35	18	304SS	19.6	35.5	Ring	0.5	2	3.5	3.4	4.75

Table 12 - 9975 (Current) and 9975 (Early) Package Comparison


Assembly, Design Features and Materials, Overall Weights and Dimensions					
	Drum	Air Shield Bearing Plate Spacer/Absorber	Insulation	Shielding	Containment Vessels
9975 Dwg. R-R2-F-0026 Rev. 0	Drum Material: 18-Gage, 304 Stainless Steel, ASME SA-240 Nominal Capacity: 35 gal. Max Gross Weight: 404 lb. Overall Dimensions: 19.6-dia x 35.5(in) Closure: Bolted Flange, 24-Hex Cap Screws, .5- 13UNC-2A x 1.25 in.	Air Shield: 24 -Gage Stainless Steel, ASME SA-480 Bearing Plate: 0.5-in, 1100 Al, ASTM B-209 (top and bottom) Spacer/Absorber Al-Tube Honeycomb, Crush strength 1500 ± 500 psi (top and bottom)	Material: Cane fiberboard, 15 lb/ft3 (nominal), ASTM C-208-75 Thickness: Radial - 4.75-in, Axial - 3.7-in (top), 3.4-in (bottom) Assembly Method & Geometry: Glue, stepped geometry. Thermal Blanket: Stainless steel encapsulated Kaowool.	Material: 0.5-in Cast Lead, ASTM B-749, Lined With 20- Gage 304 Stainless Steel Sheet Metal Lid: 0.5-in, 0.5-in, 1100 Al, ASTM B-209	Material: 304L Stainless Steel Dimensions Overall: PCV - 5.87-in dia x 18.63-in SCV - 7.12-in dia x 24.0 in ASME Code: Section III
9975 Dwg. R-R1-F-0005 Rev. 0	Drum Material: 18-Gage, 304 Stainless Steel, ASME SA-240 Nominal Capacity: 35 gal. Max Gross Weight: 404 lb. Overall Dimensions: 19.6-dia x 35.5(in) Closure: Bolt-Type Locking Ring, 12-Gage, Stainless Steel, ASME SA-240	Air Shield: 24 -Gage Stainless Steel, ASME SA-480 Bearing Plate: 0.5-in, 1100 Al, ASTM B-209 (top and bottom) Spacer/Absorber Al-Tube Honeycomb, Crush strength 1500 ± 500 psi (top and bottom)	Material: Cane fiberboard, 15 lb/ft3 (nominal), ASTM C-208-75 Thickness: Radial - 4.75-in, Axial - 3.5-in (top), 3.4-in (bottom) Assembly Method & Geometry: Glue, stepped geometry. Thermal Blanket: Stainless steel encapsulated Kaowool.	Material: 0.5-in Cast Lead, ASTM B-749, Lined With 20- Gage 304 Stainless Steel Sheet Metal Lid: 0.5-in, 0.5-in, 1100 Al, ASTM B-209	Material: 304L Stainless Steel Dimensions Overall: PCV - 5.87-in dia x 18.63-in SCV - 7.12-in dia x 24.0 in ASME Code: Section III

APPENDIX 3.1
NCT THERMAL ANALYSIS BENCHMARKING

This Page Intentionally Left Blank

OSR 45-24# (Rev 5-19-2003)

Calculation Cover Sheet

Project 9975 SARP		Calculation No. M-CLC-F-00901	Project No. <i>N/A</i>	
Title MODEL OF THERMAL TESTS FOR THE 9975 PACKAGE		Functional Classification SC	Sheet 1 of <u>12</u>	
Calc Level <input checked="" type="checkbox"/> Type 1 <input type="checkbox"/> Type 2		Discipline Mechanical Engineering		
Computer Program No. MSC/Patran-Thermal 2001 <input type="checkbox"/> N/A		Type 1 Calc Status <input type="checkbox"/> Preliminary <input checked="" type="checkbox"/> Confirmed		
Version/Release No. MSC/Patran-Thermal 2001				
Purpose and Objective Purpose: To compare thermal predictions made by the MSC/Patran-Thermal software model for the 9975 package with the test data. Objective: Demonstrate the ability of the model to accurately predict temperatures for the 9975 shipping package.				
Summary of Conclusion With two exceptions, the model for the 9975 shipping package predicts temperatures that are close to the data. The two cases with large temperature differences occur at the bottom of the package and for the maximum Celotex® temperature. In each case, the predicted temperatures are conservatively higher than those in the data, and may be the result of the boundary condition applied to the bottom of the package. Specifically, in the model it was assumed that the bottom of the package was adiabatic, as though it were set against an insulated surface. However, if the bottom of the package were elevated above the surface, so that heat transfer by convection and radiation could occur, the temperatures would be significantly reduced.				
ENGINEERING DOC. CONTROL - SRS  00756001				
Revisions				
Rev No.	Revision Description			
0	Base comparison of thermal model with test data.			
Sign Off				
Rev No.	Originator (Print) Sign/Date	Verification/ Checking Method	Verifier/Checker (Print) Sign/Date	Manager (Print) Sign/Date
0	<i>Bruce Hardy</i> <i>10/7/03</i>	DOCUMENT REVIEW	<i>N. K. Gupta</i> <i>N. K. GUPTA 10/7/03</i>	<i>C. R. Helms Smith</i> <i>10/7/03</i>
Design Authority — (Print) <i>N/A</i>		Signature		Date
Release to Outside Agency — (Print) <i>N/A</i>		Signature		Date
Security Classification of the Calculation Unclassified, No UCNI				

Revisions

Revision	Description
0	Original Issue

MODEL OF THERMAL TESTS FOR THE 9975 PACKAGE

1.0 Conclusions

In the previous version of the SARP [1], thermal models were used to evaluate the 9975 package for the NCT, HAC and the Post-Fire Transient. These models, which were based on the MSC/ Patran-Thermal[®] general purpose heat transfer software, utilized an orthotropic thermal conductivity for the Celotex[®] insulation. In these models the thermal conductivity of the Celotex[®] was represented by an orthotropic tensor because it was inserted into the drum as horizontal layers, which were glued together. To demonstrate the accuracy of the model, it was benchmarked against thermal tests conducted at Sandia National Laboratories on a mockup of the 9975 package [2]. However, the model utilized a scalar thermal conductivity for the Celotex[®]. To ensure consistency with the NCT, HAC and the Post-Fire Transient models, the benchmark comparison was repeated with the thermal conductivity of the Celotex[®] changed to an orthotropic tensor having identical components to those used for the other tests. In addition, discrepancies between the dimensions of the benchmark model and the package used in the test were corrected.

The ambient temperature for this analysis was set to 77°F to match the test environment. The power to the heater was 21 Watts and was applied as a surface heat flux on the heater element, assumed to be composed of ceramic. In the model, natural convection and thermal radiation boundary conditions were applied to the top and side of the package. There was no heat conduction from the bottom of the package, as though it were standing on an insulated surface. Of course, if the package were raised so that the base was no longer insulated, the temperatures predicted by the model would be somewhat lower. This may explain the relatively large differences between the predicted and measured temperature at the bottom of the package and the maximum Celotex[®] temperature, see Table 1.

There was no indication whether air filled gaps existed where the Celotex[®] contacted the drum and the lead shield. Therefore several models were created. The results presented in this document were obtained from a model that assumed no air gaps existed where the Celotex[®] contacted the shield and the drum.

The comparison with Sandia test data from Table 1 of Appendix 3.8, Section 1.2 of Reference 1 is given in Table 1 below. Figure 1 shows the steady state temperature profile predicted by the model.

Table 1 Comparison Between Temperatures From Current NCT Model and Test Data

Channel	Position	Test (°F)	Current Model (°F)	Node Number	Comments
1	Drum Bottom	85	107	70	At bottom center
2	Drum Side	88	87	5144	Mid-height
4	Drum Lid	86	81	8214	Top center
6	Celotex®	107	130	5371	Approx. maximum
8	Lead Side	134	134	5324	Center height
10	PCV Lid	168	169	5970	Package centerline
11	SCV Seal	149	162	6909	
13	SCV Side	149	157	5329	Mid height
15	Top Bearing Plate	122	120	7452	At package centerline

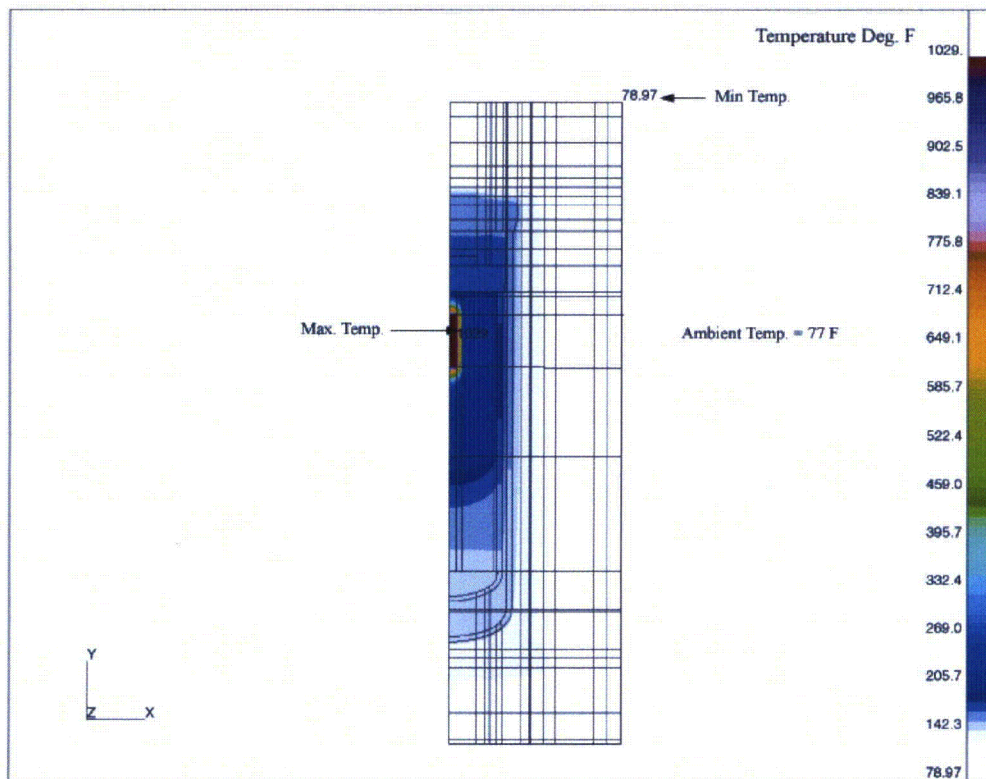


Figure 1 Steady-state temperature profile predicted by the model.

2.0 Input

In Reference 1, a comparison was made between the results of a thermal test conducted on a mockup of the 9975 package at Sandia National Laboratories [2] and a thermal model. The purpose of the comparison was to demonstrate the adequacy of the thermal model for the NCT, HAC and the post fire transient in Reference 1. Because the Celotex[®] is placed into the drum in horizontal sheets, which are glued together, the thermal conductivity of the Celotex[®] was input as an orthotropic tensor. However, the model compared with the test employed a scalar, rather than an orthotropic tensor for the thermal conductivity. In addition, there were a number of geometric discrepancies between the mockup and the model. In this calculation, temperatures predicted by a corrected thermal model are compared to the temperatures measured in the Sandia test. In the model developed for this document, the Celotex[®] thermal conductivity was input as an orthotropic tensor and the dimensions accurately represent the mockup.

In the Sandia tests a 21 W heater was used to simulate the effects of decay heat and a steel annulus with an outside diameter of 4.7 in., inside diameter of 1.38 in., and length of 8.4 in. was used to replicate the mass of the isotopic sources. A photograph of the heater and the replicate mass is shown in Figure 2. The mockup was exposed to an ambient temperature of approximately 77°F and was assumed to be in an upright position, standing on a solid base so that heat transfer through the bottom was negligible. There were air filled gaps of 0.25 in. between the top of the steel annulus and PCV lid, 0.345 in. between the heater and the steel annulus, and 1.18 in. between the heater and PCV lid. The aluminum plate attached to the lead sleeve in the 9975 package was left out of the mockup and was represented in the model as an air space. The duration of the thermal test was 120 hours and temperatures measured at the end of that period were compared to those predicted by the steady-state model.

The thermal model for the mockup used in the Sandia thermal test was created with the MSC/Patran-Thermal[®] general purpose heat transfer software. The model was built in 2D, axisymmetric geometry and utilized dimensions shown in Figure 3, which is also Figure 1 in Appendix 3.8, Section 3.8-5 of Reference 1. The geometric locations of materials in the model are shown schematically in Figure 4 and material thermal properties are listed in Table 2. There was no indication whether air filled gaps existed where the Celotex[®] contacted the drum and the lead shield. Therefore several models were created. The results presented in this document were obtained from a model that assumed no air gaps existed where the Celotex[®] contacted the shield and the drum.

The 21-W heat source was modeled as a ceramic cylinder with a radius of 0.345 in. and a length of 2.8 in. The heat source was uniformly applied at the curved surface of the cylinder to give a total power of 21 W. Heat was transferred within the package by conduction and radiation. In all models, thermal radiation heat transfer was applied across all gaps filled with gas while natural convection was neglected in the internal gas spaces. Further, all gasses were assumed non-absorbing for thermal radiation and, hence, were treated as non-participating media in the radiation calculations..

Both the heater and the replicate mass exchange heat with one another, and the PCV, by radiation and conduction. In the current model, the emissivities for the heater, the steel annulus and the outer surface of the drum were those used in Appendix 3.8 of Reference 1. It should be remarked that in this reference, the emissivity of the heater was assigned a value of 0.05 to provide the best fit to the data. However, it was claimed that analyses showed the package temperatures were relatively insensitive to the heater thermal properties. In Appendix 3.8 Reference 1 the emissivity of the steel annulus was taken to be 0.6 and the surface emissivity of the drum was set to 0.21. Emissivities used in the current model are listed in Table 3.

In the current model, natural convection and thermal radiation boundary conditions were applied to the top and side of the mockup. There was no heat conduction from the bottom of the mockup, as though it were standing on an insulated surface. Of course, if the mockup were raised so that the base was no longer insulated, the temperatures predicted by the model would be somewhat lower.

To avoid the excessively small elements that would be required to model the thin steel of the drum, it was not included in the model. As stated above, it was assumed that there were no air gaps between the Celotex[®] and the steel drum. It was further assumed that the drum and Celotex[®] were in good thermal contact, so that thermal resistances were very small. Hence, it was possible to apply natural convection and thermal radiation boundary conditions directly to the exterior of the Celotex[®] at the top and side of the mockup. That is, the outer surface emissivity of the drum, $\epsilon=0.21$, was applied to the Celotex[®]. This approximation is reasonable because the high thermal conductivity of the steel, coupled with the small thickness of the steel layer, results in a very small temperature gradient across the drum wall.

Natural convection along the vertical side of the mockup is given by the correlations

$$Nu = 0.68 + \frac{0.670Ra^{0.25}}{\left[1 + \left(\frac{0.492}{Pr}\right)^{9/16}\right]^{4/9}} \quad \text{for } Ra < 1 \times 10^9$$

or

$$Nu = \left(0.825 + \frac{0.387Ra^{0.25}}{\left[1 + \left(\frac{0.492}{Pr}\right)^{9/16}\right]^{8/27}} \right)^2 \quad \text{for } Ra > 1 \times 10^9$$

Natural convection at the top of the mockup is given by the correlations

$$Nu = 0.54Ra^{0.25} \quad \text{for } 2.6 \times 10^4 < Ra < 1 \times 10^7$$

or

$$Nu = 0.15Ra^{1/3} \quad \text{for } 1 \times 10^7 < Ra < 3 \times 10^{10}$$

where: Ra = Rayleigh number, dependent on film temperature (based on wall height for the correlations applied to the vertical side)

Nu = Nusselt number, dependent on film temperature

Pr = Prandtl number, dependent on film temperature



Figure 2 Photograph of the heater and replicate mass used in the Sandia test.

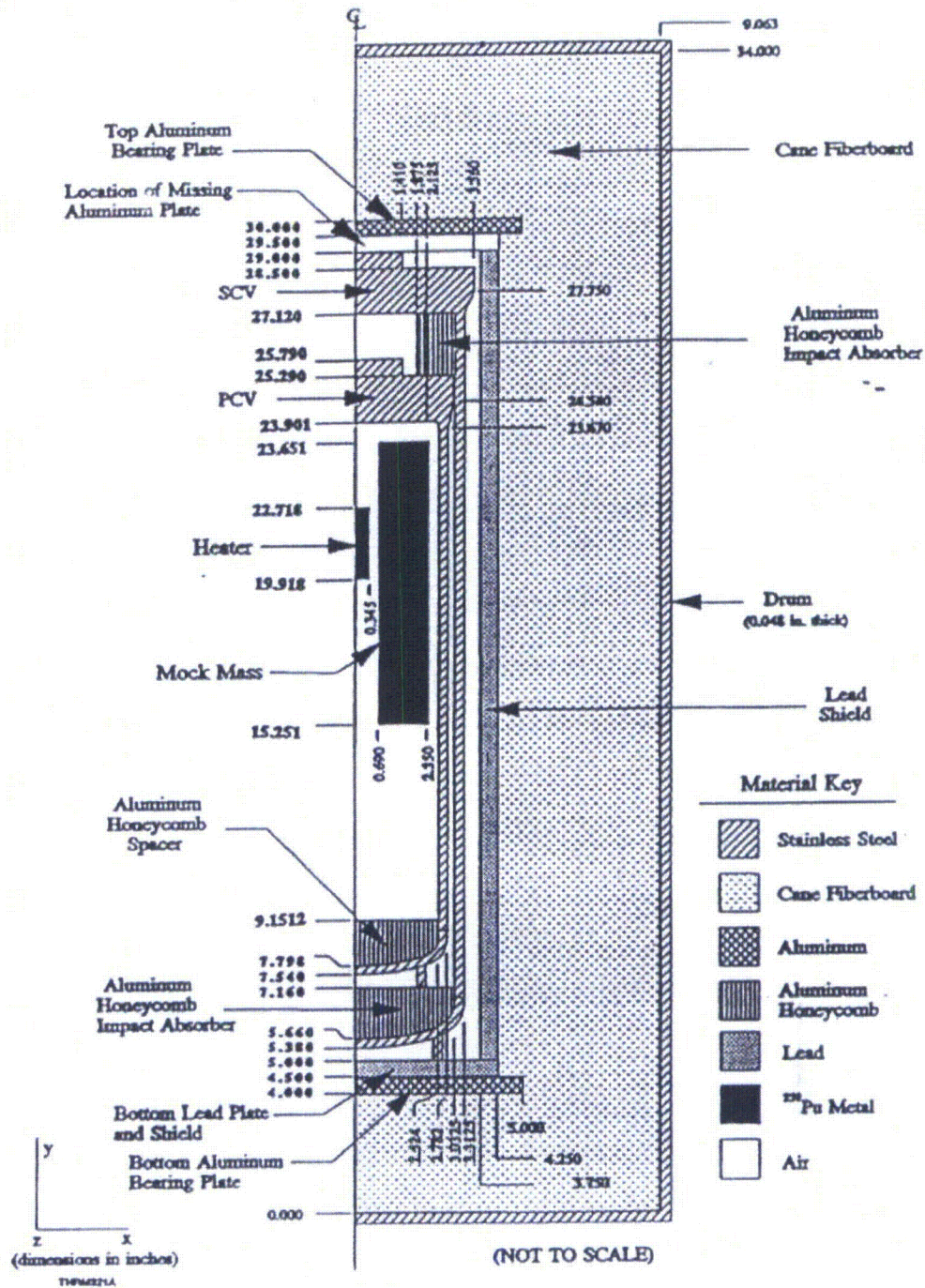


Figure 3 Schematic of model for Sandia test of 9975 package

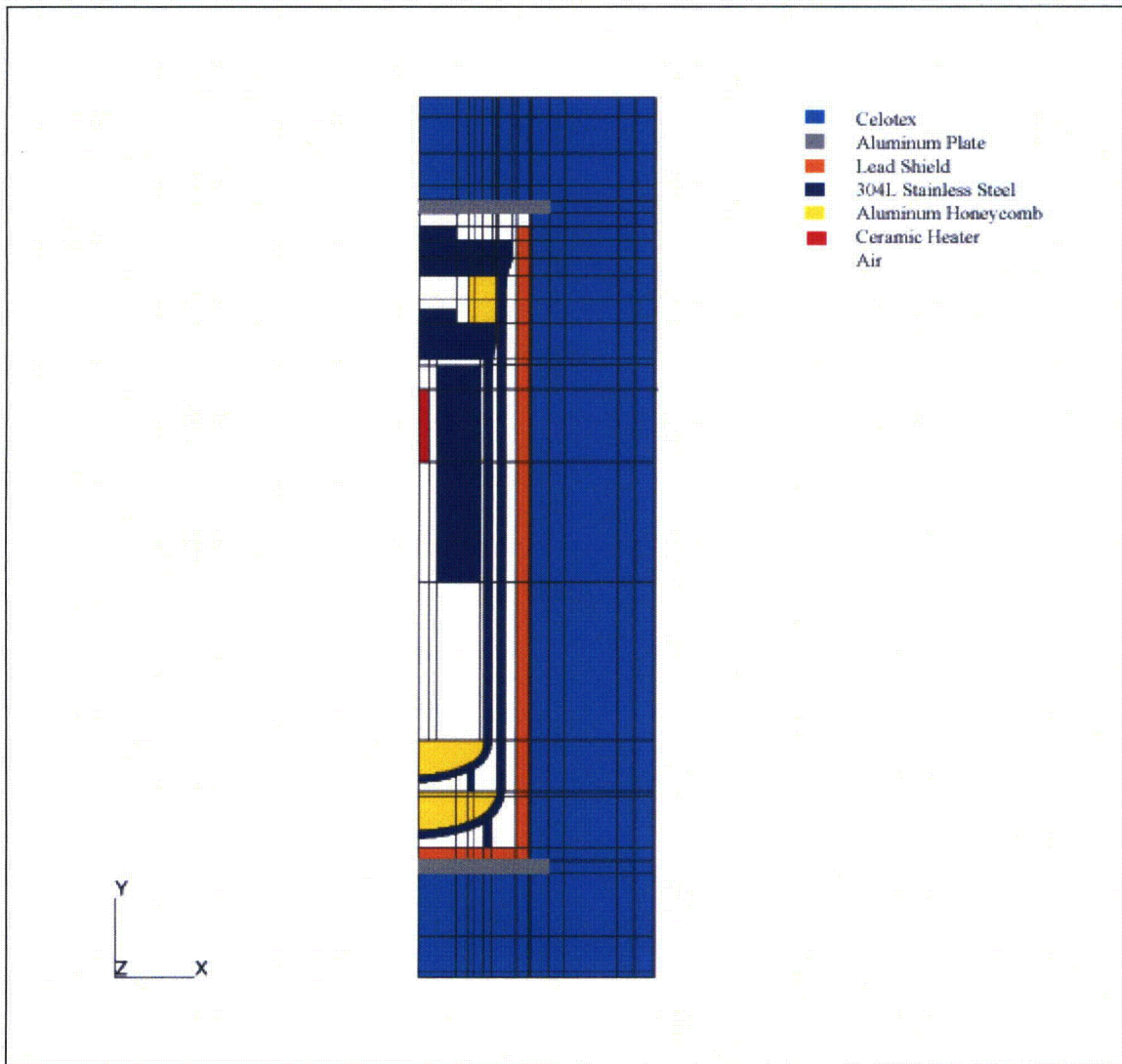


Figure 4 Schematic of material locations in model of Sandia test mockup.

Table 2 Constitutive Properties of Packaging Materials

Material	Density (lbm/ft ³) @ T(°F)	Conductivity (Btu/hr.-ft.- °F) @ T(°F)	Heat Capacity (Btu/lbm °F) @ T(°F)
Air	0.080532	0.01396 @ 32 0.01839 @ 212 0.02238 @ 392 0.02593 @ 572	0.237 @ 212
Honeycomb energy absorber (radial)	7.62	3.82	16.2
Honeycomb energy absorber (axial)	7.62	7.62	16.2
Pre-fire fiberboard (radial)	16.86 @ 77 17.36 @ 187 17.86 @ 295	0.0723	0.306 @ 77 0.360 @ 187 0.417 @ 295
Pre-fire fiberboard (axial)	16.86 @ 77 17.36 @ 187 17.86 @ 295	0.031 @ 77 0.034 @ 187 0.029 @ 533	0.306 @ 77 0.360 @ 187 0.417 @ 295
Aluminum	169.3	126.0	0.216
Stainless steel (304)	494.4	7.74 @ 32 9.43 @ 212 12.58 @ 932	0.12 @ 32 0.135 @ 752
Lead	708.5	19.6 @ 209 18.3 @ 400	0.0305 @ 32 0.0315 @ 212 0.0338 @ 621.5
Ceramic	32.0	7.8 @ 100 10.2 @ 1000 13.2 @ 1500 15.6 @ 2000 19.2 @ 2500 22.2 @ 3000	0.25

Table 3 Surface Emissivities

Surface	Emissivity
Exterior of drum	0.21
Aluminum plate	0.2
Lead shield	0.28
Replicate mass	0.6
Ceramic heater	0.05
Stainless steel (PCV, SCV)	0.3
Celotex	0.5

3.0 Analytical Methods and Computations

The general purpose conduction-radiation computer code MSC/Patran-Thermal[®] was used to perform the computations [3]. Work was performed in accordance with the WSRC E-7 manual [4]. The thermal models of the storage configurations were created using the general purpose finite element pre and post processor MSC/Patran[®] [5].

4.0 Results

The steady state temperature profile predicted by the model is shown in Fig. 1. Predicted steady-state temperatures are compared to measurements in Table 1.

5.0 References

1. Safety Analysis Report – Packages, 9972-9975 (U), WSRC-SA-7, Rev 15, Westinghouse Savannah River Company, Aiken, SC (May 2003).
2. Schulze, D.H. and R. Moreno, “Test Report Simulated Fire Tests of the 9973 and 9975 Packagings”, Report No. 6324AK2801, Sandia National Laboratory, Albuquerque, NM (June 1994).
3. MSC/Thermal, MacNeal-Schwendler Corporation, Los Angeles, CA 90041.
4. Westinghouse Savannah River Co., Conduct of Engineering Manual, E-7, 1998.
5. Patran 2001, MacNeal-Schwendler Corporation, Los Angeles, CA 90041.

APPENDIX 3.2
HAC FIRE ANALYSIS BENCHMARKING
OF THE 9973 AND 9975 PACKAGES

This Page Intentionally Left Blank

**WESTINGHOUSE SAVANNAH RIVER COMPANY
INTER-OFFICE MEMORANDUM**

SRT-EMS-940065

September 12, 1994

TO: R. J. Gromada, 773-53A

FROM: S. J. Hensel, 773-42A *SH*

J. W. Jerrell

J. W. Jerrell Technical Reviewer *9-14-94*
Date

J. R. Pelfrey

J. R. Pelfrey Manager *9-14-94*
Date

**HAC Fire Analysis Benchmarking
Of The 9973 And 9975 Packages (U)****Abstract**

Two packages were fire tested in the Sandia radiant heat facility to benchmark the fiberboard HAC fire analysis model against package test data, and provide evidence of satisfactory package performance during the HAC fire. The 9973 was tested after a 30 ft. top down drop and puncture, and an undamaged 9975 containing a heater was tested to determine heat source effects. A previously developed cane fiberboard HAC fire model was used as the basis to benchmark against the test results. Analysis results using a refined version of the HAC model compared well against the test data from both the damaged 9973 without a heat source and the undamaged 9975 containing a heat source. This analysis will be included as an Appendix in Chapter 3 of the 9965, 9968, 9972, 9973, 9974, and 9975 SARP.

SRT-EMS-940065

P. 2 of 17

HAC Fire Analysis Benchmarking Of The 9973 And 9975 Packages

A damaged 9973 package and undamaged 9975 package containing a heater were fire tested in the Sandia Radiant Heat Facility [1]. The 9973 was tested laying on its side and the 9975 was tested upright. The purpose of the test was to demonstrate package survivability and to benchmark the Hypothetical Accident Condition (HAC) fire model developed by Hensel and Gromada [2]. Analysis of the 9972-75 packages will be performed upon successful benchmarking of the HAC fiberboard model to package test data.

A schematic of the 9973 and 9975 axisymmetric models used in the analysis are shown in Figures 1 and 2. Although the 9973 package was fire tested after a 30 ft. top down drop and puncture, it was modeled as an undamaged package. The 9973 was loaded with 45 lbs. of lead to simulate contents. The thermal properties of the contents portion of the model were adjusted to account for the added mass. The 9975 package was inadvertently assembled without one of the top bearing plates. The 9975 model accurately reflects this oversight and the resulting air gap. The 9975 also contains a heater surrounded by a steel cylinder, and both are included in the model.

All thermal analyses were performed using the general purpose conduction based analysis software package P/Thermal [3]. Analysis of the 9973 began with an initial temperature of 75°F throughout the package, and boundary condition temperature data was supplied by the test report [1]. The 9975 package was heated for a few days (until temperatures leveled off) prior to the test by the internal heat source. A preliminary steady-state normal condition analysis (without solar) was required to obtain the initial temperature distribution in the 9975 package. Results of this normal condition analysis overpredicted internal package temperatures when the cane fiberboard thermal properties in the literature were used. The fiberboard conductivity was increased by a factor of 2 to more accurately compute the temperature profiles in the 9975 package. An accurate initial condition is essential to benchmarking the HAC fire test results.

The cane fiberboard HAC fire properties ultimately used in the benchmarking are presented in Tables 1 and 2. These properties are similar to the initial set developed against 1-D fiberboard fire tests [2]. The fiberboard properties in Table 1 are used throughout the package during the fire (heating) portion of the test. During the cooling, special char properties are used on the first 1.4 inches from the drum wall both radially inward from the drum side and axially inward from the top and bottom. The char properties are presented in Table 2. The fiberboard

SRT-EMS-940065

P. 3 of 17

properties in Table 1 are used throughout the non-char region (within 1.4 inches from the drum wall) throughout the cooling. In the 9973 an air gap between the secondary vessel and cane fiberboard exists. The conductivity of the cane fiberboard HAC fire model was used in this air gap to simulate the flow of hot gases out of the cane fiberboard.

Results of the HAC fire analysis of the 9973 are presented in Figures 3 through 5. All of these Figures are of the same format where the data from the test is referenced as "Data", and the analysis results contain symbols at times in which temperatures written to a file. All temperatures are in °F and all times are in hours. The analysis ended at 4.5 hours.

Figure 3 is a transient plot of the drum wall temperature. Four thermocouples were located circumferentially around the outer drum wall during the test. The data varied slightly around the drum wall due to circumferential heating variations. The drum wall temperature during the analysis compares well with the data. Drum wall analysis temperatures verify that adequate boundary conditions were used during the analysis. Actual benchmarking comparisons must be made with internal package temperature data.

In Figures 4 and 5 analyses results are compared with test temperatures at the Secondary Containment Vessel (SCV) seal and SCV side. The transient temperatures compare well at the SCV seal and SCV wall. The analysis predicts a peak temperature at both locations within 20°F of the measured values. The calculated peak temperatures occur about one half hour later than the measured ones. The measured curves illustrate the circumferential variations at both locations. These variations are likely caused by asymmetric heating (as shown by the drum wall transient temperature curves) and small air gaps because the package is laying on its side during the test.

Results of the HAC fire analysis of the 9975 are presented in Figures 6 through 11. Again, all of these Figures are of the same format where the data from the test is referenced by "Data", and the analysis results contain symbols at times in which temperatures were written to a file. The temperatures are in °F, times are in hours, and the analysis ended at 4.5 hours.

Figure 6 is a transient plot of the drum wall temperature. Two thermocouples were located circumferentially around the outer drum wall during the test. The drum wall temperature during the analysis compares well with the data, and circumferential variation in the data is minimal because the package was tested upright.

In Figures 7 through 11 analyses results are compared with test temperatures at the fiberboard middle, lead side, SCV seal, SCV side, and Primary Containment Vessel (PCV) lid. All measured temperatures compare fairly well with the analysis. The measured temperatures at

SRT-EMS-940065

P. 4 of 17

the fiberboard middle show extensive circumferential variation. Post test evaluation of the package showed uneven charring in the package circumferentially, although little circumferential temperature variation exists elsewhere. Post test evaluation also suggested minimal thermocouple movement. The measured temperatures of internal package components all compare fairly well with the calculated values, although the calculated values tend to somewhat overpredict peak temperatures and cool more quickly. The overprediction and excessive cooling were observed in the 9973 comparison between calculated and measured values. The 9975 benchmark demonstrates that internal package component temperatures can be calculated including heat source effects.

The fiberboard HAC fire thermal model has been benchmarked against a damaged 9973 and undamaged 9975 with an internal heater by comparison with measurements taken during a test at SNL. The internal package temperature transients compare well with the calculations. Damage appears to have relatively minimal effects on package internal temperatures, although this may not be true for a poorly designed package in which the damage included extensive gaps in the fiberboard or significant fiberboard thickness reduction between the vessel and drum wall. An air gap between the fiberboard and vessel wall, as in the 9973, requires special treatment to negate the usual insulating effects of the air gap. The model presented in Tables 1 and 2 will be used to analyze the 9972, 9973, 9974, and 9975 packages including internal heat sources under HAC fire conditions. This analysis will be included as an Appendix in Chapter 3 of the 9965, 9968, 9972-75 SARP.

SRT-EMS-940065

P. 5 of 17

Table 1: Non-Char Fiberboard Properties

Property	Temperature (°F) / Value
Conductivity Btu/ft.-hr.-°F	80/0.035 200/0.55
	115/0.16 210/0.09
	150/0.37 220/0.09
	170/0.45 450/0.07
	185/0.55 500/0.07
Density lb/ft. ³	80/15.4
	475/15.4
	810/8.5
	1500/3.5
Specific Heat Btu/lb-°F	70/0.25
	400/0.50
	500/0.50

Phase Change: 50 Btu/lb @ 200°F

Table 2: Char Fiberboard Properties

Property	Temperature (°F) / Value
Conductivity Btu/ft.-hr.-°F	100/0.07
	140/0.07
	200/1.0
	300/0.30
	500/0.07
	600/0.07
Density lb/ft. ³	8.1
Specific Heat Btu/lb-°F	0.25

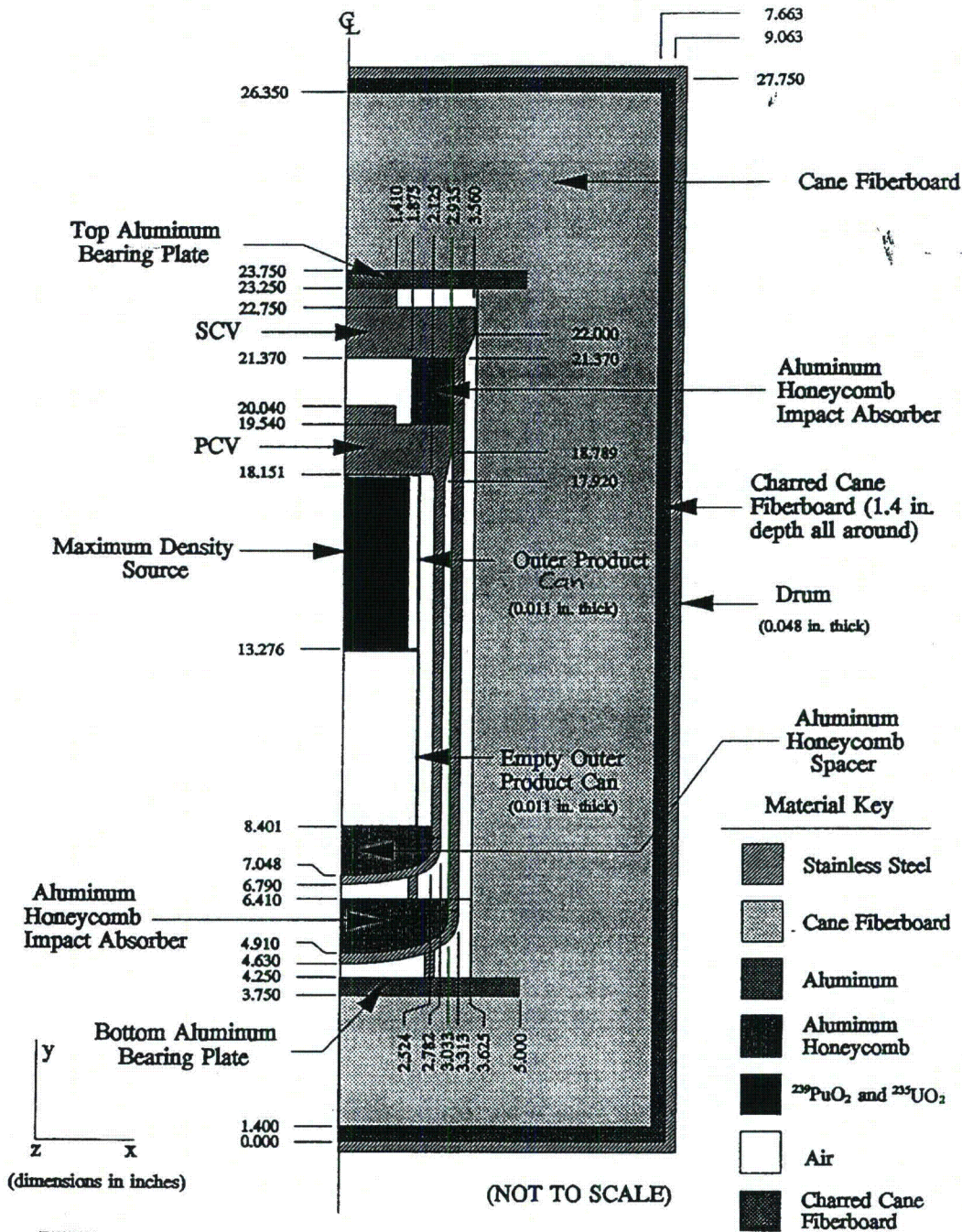
No phase Change.

SRT-EMS-940065

P. 6 of 17

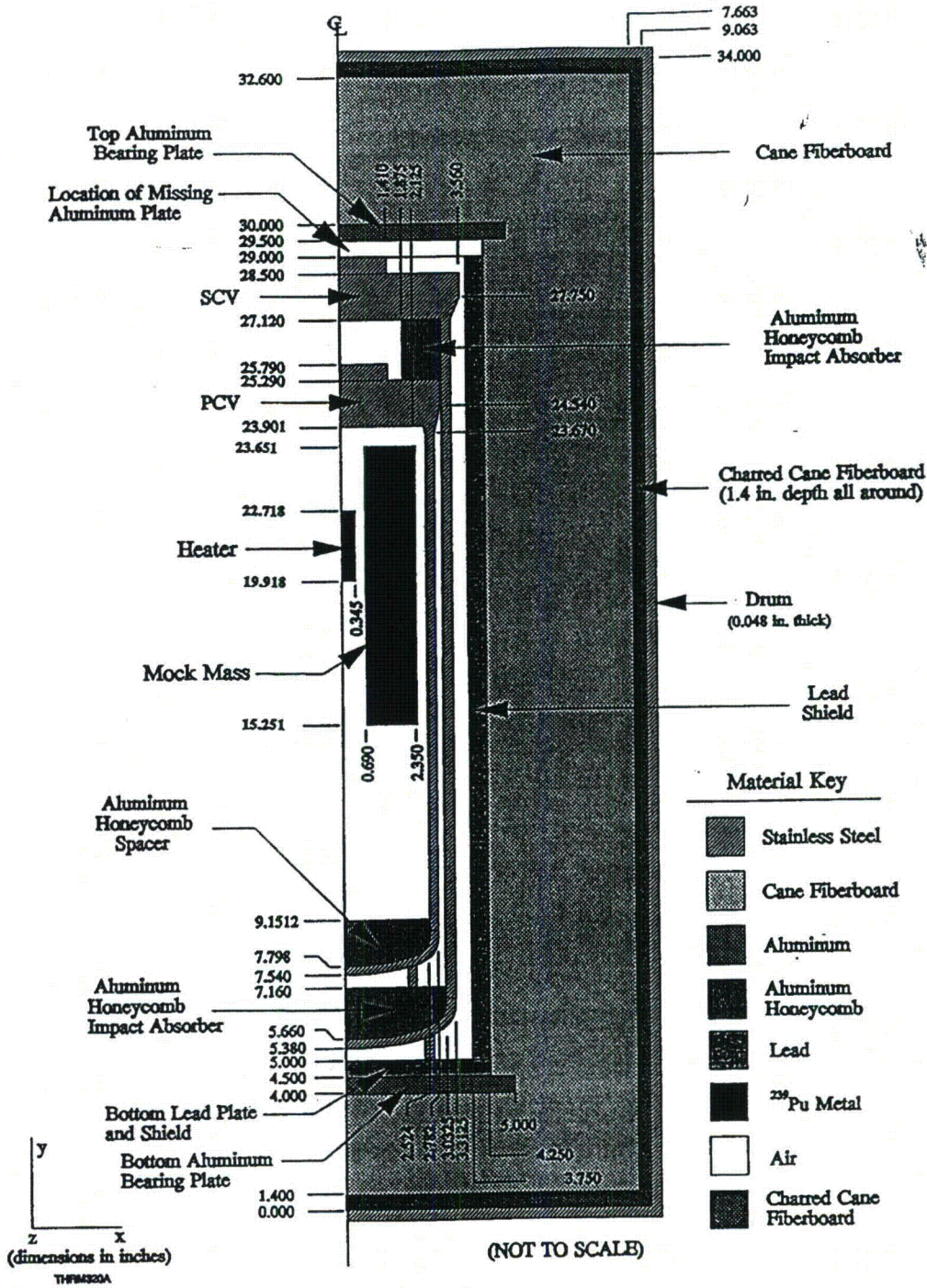
References:

- [1] M. N. Van Alstine, SRT-PTG-94-0058, "9973 and 9975 Packaging Thermal Test Report (U)", July 25, 1994.
- [2] S. J. Hensel and R. J. Gromada, "Development of A Simulation (Thermophysical Property) Model For Cane Fiberboard Packages Subjected to A Hypothetical Accident Condition Fire", 1994 DOE Defense Programs Packaging Workshop, Knoxville, TN.
- [3] P/Thermal 2.6, PDA Engineering, PATRAN Division, Costa Mesa, CA (March 1993).



Schematic of 9973 Model

FIGURE 1



Schematic of 9975 Model

FIGURE 2

9973 Drum Wall Temperatures

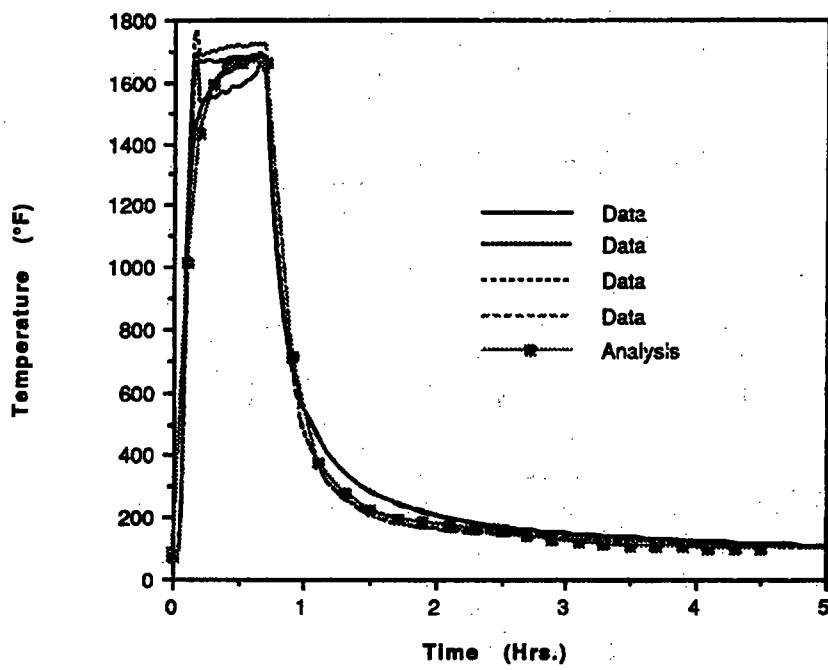


Figure 3

9973 SCV SEAL TEMPERATURE

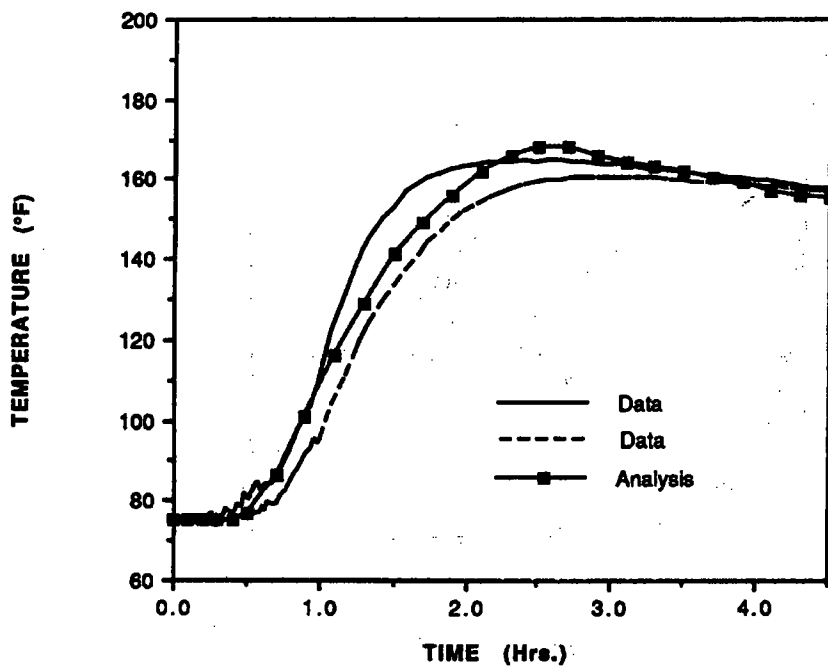


Figure 4

9973 SCV SIDE TEMPERATURE

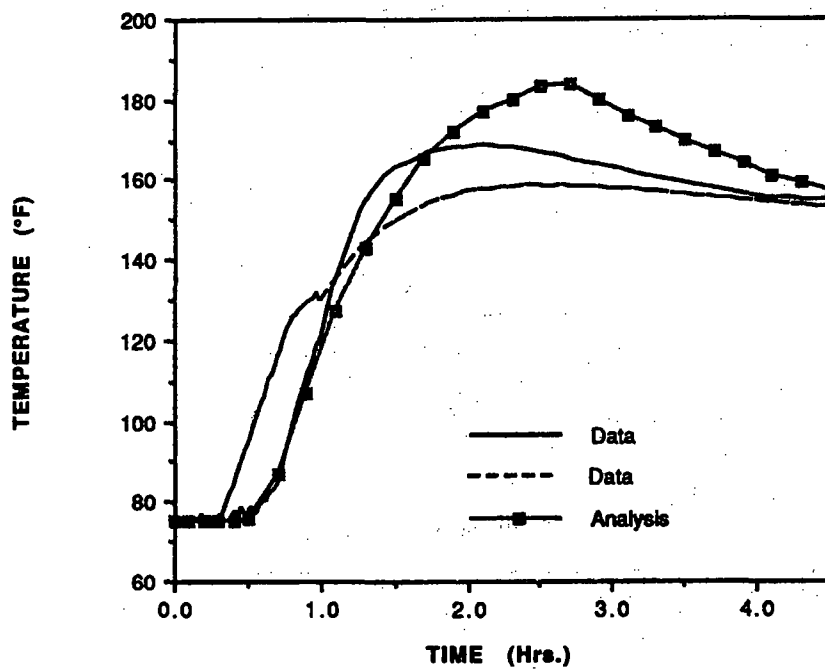


Figure 5

9975 DRUM SIDE TEMPERATURE

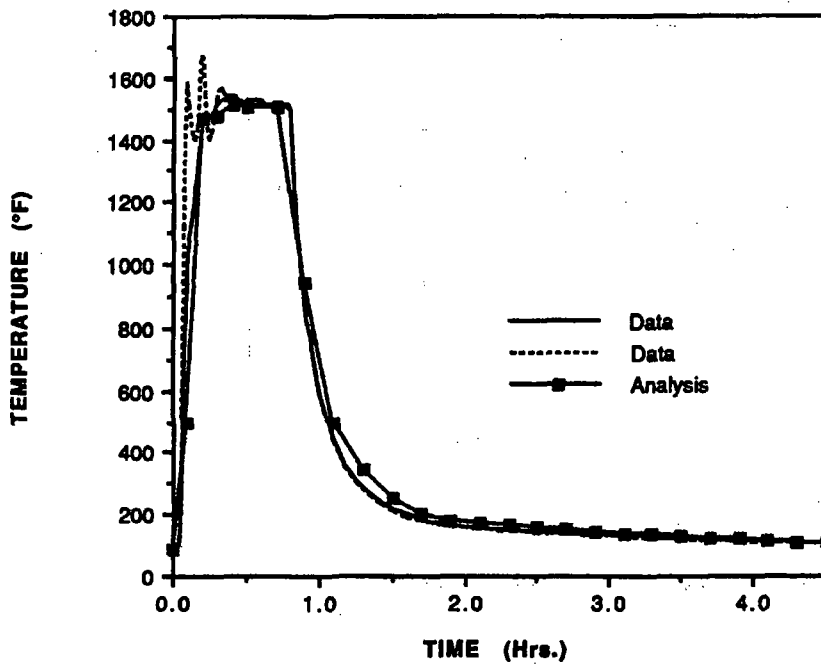


Figure 6

9975 MID FIBERBOARD TEMPERATURE

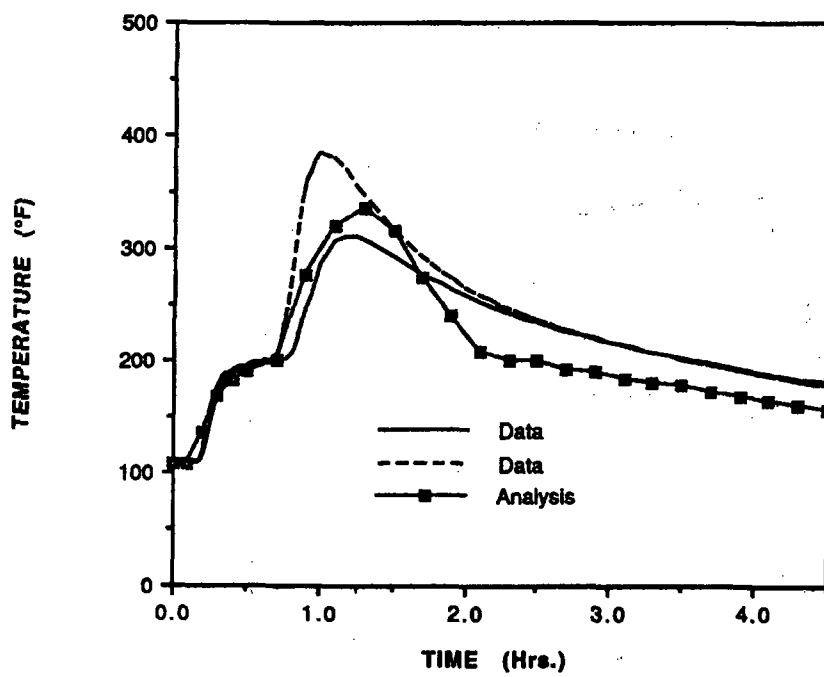


Figure 7

SRT-EMS-940065

P. 14 of 17

9975 LEAD SIDE TEMPERATURE

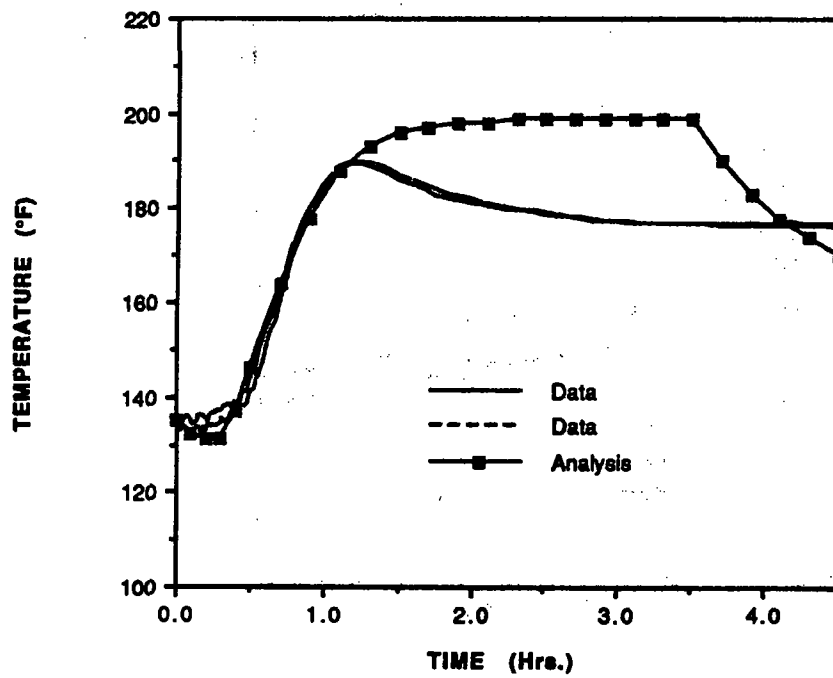


Figure 8

9975 SCV SEAL TEMPERATURE

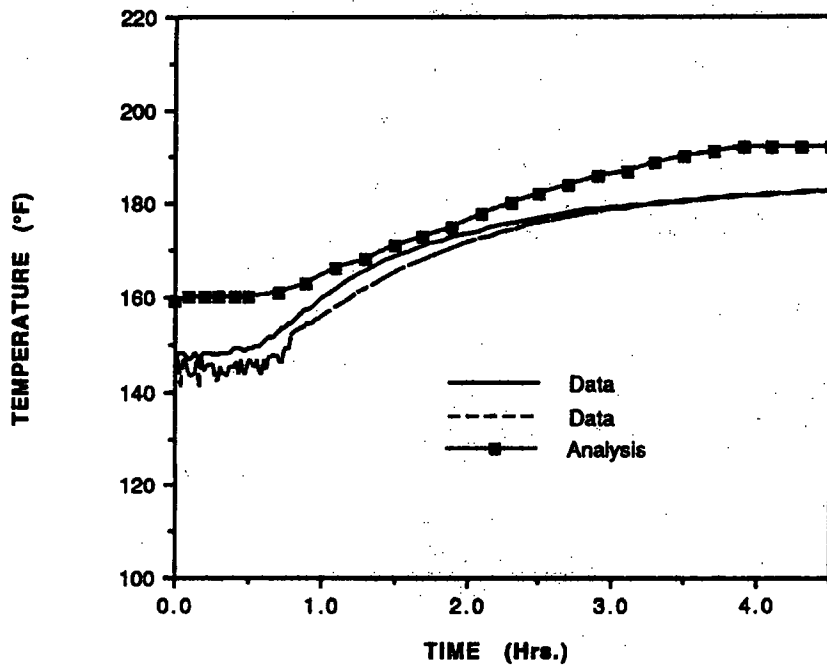


Figure 9

9975 SCV SIDE TEMPERATURE

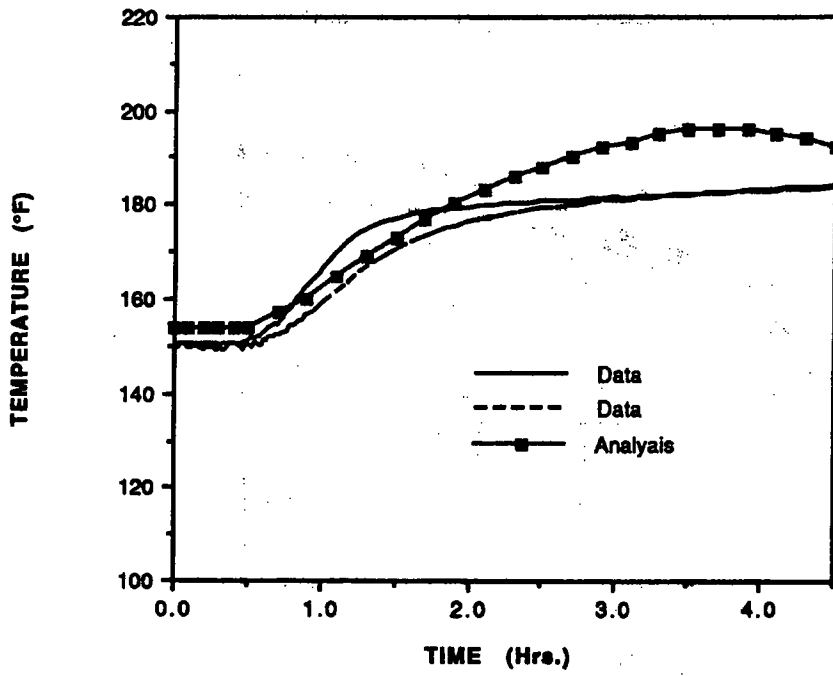


Figure 10

9975 PCV LID TEMPERATURE

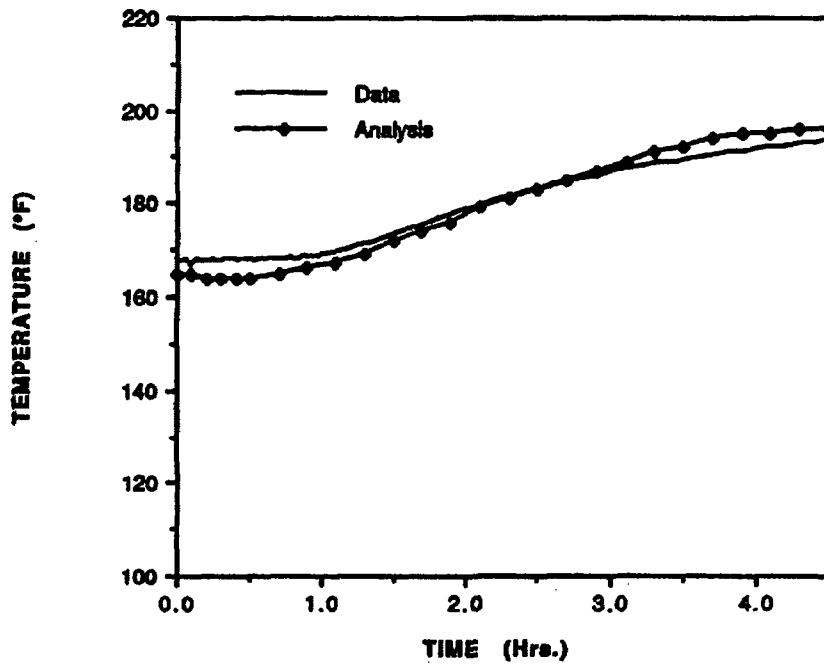


Figure 11

This Page Intentionally Left Blank

APPENDIX 3.3
THERMAL ANALYSIS OF THE 9975 PACKAGE
FOR
NORMAL CONDITIONS OF TRANSPORT
AND
HYPOTHETICAL ACCIDENT CONDITIONS

This Page Intentionally Left Blank

OSR 45-24# (Rev 5-19-2003)

ENGINEERING DOC. CONTROL - SRS



Calculation Cover Sheet

Project 9975 Packaging Certification		Calculation No. M-CLC-F-00590, Rev. 8		Project No. N/A	
Title Thermal Analysis of the 9975 Package for Normal Conditions of Transport and Accident Conditions		Functional Classification SC		Sheet 1 of <u>42</u>	
		Discipline Mechanical			
Calc Level <input checked="" type="checkbox"/> Type 1 <input type="checkbox"/> Type 2		Type 1 Calc Status <input type="checkbox"/> Preliminary <input checked="" type="checkbox"/> Confirmed			
Computer Program No. MSC/THERMAL <input type="checkbox"/> N/A		Version/Release No. 8.5			
Purpose and Objective This revision incorporates the thermal response of the LLNL Hex-Can configuration to support the configurations documented in the 9975 SARP. The revision also includes some additional observations in the results section from the existing and new analyses. Some missing emissivity values for the lead shield liner, PCV and SCV are included in Table 3. The calculation format is revised for consistency by putting all the tables and figures after the text .					
Summary of Conclusion The thermal response of the LLNL Hex-Can is bounded by the existing analyses in the 9975 SARP. The component temperatures for the Hex-Can configuration are below their limiting values. The average gas temperature (298°F) inside the PCV is less than 313°F used in the assessment of the structural integrity of the PCV in the 9975 SARP. There is no impact of the editorial and calculation format changes on the existing 9975 design.					
Revisions					
Rev No.	Revision Description				
0-7	See Revision sheet				
8	This revision includes analysis of the Hex-Can configuration and some editorial changes. See revision sheet.				
Sign Off					
Rev No.	Originator (Print) Sign/Date	Verification/ Checking Method	Verifier/Checker (Print) Sign/Date	Manager (Print) Sign/Date	
8	<i>N. K. Gupta</i> 10/27/03 N. K. GUPTA	Document Review	<i>S. Y. Lee</i> 10/20/03 S. Y. Lee	<i>C. B. HOLDING-SMITH</i> C. B. HOLDING-SMITH 10/28/03	
Design Authority — (Print)		Signature		Date	
N/A					
Release to Outside Agency — (Print)		Signature		Date	
N/A					
Security Classification of the Calculation Unclassified					

Revisions

Revision	Description
0	Original Issue
1	This includes revisions to respond to questions 3.33, 3.34, and 3.35 in the Q7 Review Questions.
2	Typographical error was corrected in the equation for natural convection, pre-fire Celotex density in Table 4 was corrected, and Tables 5 and 6 were updated.
3	This revision contains some typographical corrections to Revision 2, the addition of a spacer to the Rocky Flats configuration, and analysis of LLNL configuration.
4	This revision includes an addition of a note to Table 1 to clarify the use of carbon dioxide between PCV and SCV.
5	This revision includes thermal analyses for the Hanford product can configuration.
6	A typographical error for the LLNL configuration was corrected in Table 5. The maximum temperature for the SCV bottom was corrected from 132°C to 128°C.
7	This revision includes a load case with ambient temperature of -20°F, no solar insolation, and 19 watts of PuO ₂ contents. Resulting average gas temperature inside PCV is calculated.
8	This revision incorporates the results for the LLNL Hex-Can configuration and some additional observations in the 'results' Section 4.0 from the existing analyses. Some missing emissivity values are added in Table 3. Figure 18 is added as a 'worst case' configuration. All the tables and figures were moved after the text for consistency. Table 1 is revised to show the correct gas composition.

Thermal Analysis of the 9975 Package for Normal Conditions of Transport and Accident Conditions

1.0 Conclusions

This revision (Revision 8) contains thermal analyses for the LLNL Hex-Can configuration. The Hex-Can is designed to carry special Pu oxide material. Bounding NCT solar analyses are performed to include low density oxide (2 g/cc) and high density oxide (11 g/cc) contents. The power content is 19 watts in both cases. The analyses show that the low density oxide configuration is the limiting configuration. All the components temperatures are below their limiting temperatures. The average gas temperature inside the PCV is 298°F which is less than the maximum average of 313°F calculated for the foodcan configuration.

This revision (Revision 7) includes a load case where the ambient temperature is -20°F, no solar insolation, and the package has 19 watts of PuO₂ contents in the PCV. The analysis was performed to determine the PCV seal temperature, and to ensure that the resulting gas pressure would not be higher than the MNOP (365.4 psig). The analysis was performed for the LLNL configuration. The analysis shows that the MNOP at NCT bounds the temperatures and pressure inside PCV when the ambient is at -20°F.

This revision (Revision 5) contains thermal analyses for the Hanford convenience can configuration. This can configuration is similar to BNFL and Rocky Flats 3013 product can configurations. Table 1 lists the contents of the packagings and the Table 2 gives the external dimensions of the containers. The analyses show that the temperatures for the Hanford product can configuration with 19 watts of PuO₂ contents are bounded by the existing BNFL and Rocky Flats product cans analyses.

This revision (Revision 4) incorporates a note in Table 1 to clarify the impact of the consideration of CO₂ in analyzing the various content configurations listed in Table 1. CO₂ is required for the Food Can configuration only. The inclusion of this note will not impact the results and conclusions in this calculation.

This revision (Revision 3) contains some typographical corrections to Revision 2, addition of a spacer in the Rocky Flats configuration, and analysis results for the LLNL content configuration. Specifically, LLNL content configuration was added in Table 1, LLNL convenience can dimensions were added in Table 2, typographical errors in the thermal conductivity values of air in Table 4 were corrected, and thermal properties of CO₂ were added in Table 4. Justification is provided for the addition of the spacer in the Rocky Flats configuration which will not impact the conclusions from the Revision 2 analyses. Results for the LLNL can configuration are presented.

This revision contains corrections to Revision 1 which respond to questions 3.33, 3.34 and 3.35 in the "Q7 Review Questions, 9975 Packaging, Docket No. 93-4-9975" for the 9975 shipping package SARP. Specifically, a typographical error was corrected in the

equation for natural convection for $1.0 \times 10^9 < Ra$, the pre-fire density for Celotex[®] (fiberboard) in Table 4 was corrected and figures showing isotherms in the Celotex[®] were added. In addition, Tables 5 and 6 were updated to include the peak temperatures in the Celotex[®] and lead shield.

The thermal analysis of the 9975 package performed in Reference 1 has been revised to incorporate minor design modifications, revised content configurations, a revised food can configuration and an accident fire analysis. Three content configurations utilizing the 3013 vessel (two Pu metal and one Pu oxide) and one Pu oxide configuration with food cans were analyzed. All 9975 content configurations were analyzed for Normal conditions of Transport (NCT) and the Hypothetical Accident Conditions (HAC) fire. In all analyses, a 19 watt total decay power was uniformly distributed over the volume of the Pu metal and/or oxide.

For both the NCT and HAC analyses the 9975 drum was upright. In the steady-state NCT analysis, the drum was exposed to insolation heat flux of 800 W/m^2 on the drum top and 400 W/m^2 on the drum side ($253.6 \text{ Btu/hr-ft}^2$ and $126.8 \text{ Btu/hr-ft}^2$). The drum bottom was adiabatic for the NCT analyses and the 9975 package exchanged heat through natural convection and radiation to an ambient temperature of 100°F .

During the HAC transient, the ambient temperature was 1475°F for the first 30 minutes and 100°F thereafter. The initial condition for the HAC transient was identical to the steady-state NCT, except insolation was excluded. In the 30 minute fire phase, all sides of the drum (including the bottom) were heated by forced convection and radiation. The cooldown phase occurred immediately after the 30 minute fire. During this phase the drum was exposed to a 100°F ambient temperature, and insolation on the drum top and side (as in NCT) was included. The bottom of the drum transferred heat to the ambient via radiation only during cooldown. The entire HAC transient consisted of the 30 minute fire and 3 hours of cooldown.

The containment vessels, seals, and Pu temperatures were found to be higher during NCT (with insolation) than at any time during the 3 hour HAC transient. This result is expected because of the high thermal resistance of the Celotex[®] overpack in the 9975 package. Therefore, NCT (with insolation) temperatures bound the thermal conditions for the 9975 components of interest (e.g. outer drum not of interest) when 19 watts of payload are considered.

The most significant NCT temperature results are summarized to provide insight into the performance of the 9975 package. The middle Pu metal temperature is 423°F for the Rocky 3013 configuration and 314°F for the SRS 3013 configuration. The containment vessels and seals are below 300°F in all configurations, and the maximum peak fiberboard temperature of approximately 257°F occurs for 3013 oxide and the Rocky Flats configurations. The average primary containment vessel (PCV) gas temperatures for the 3013 oxide and food can configurations are 308°F and 313°F , respectively.

2.0 Input

Several minor changes to the design of the 9975 package and the addition of 3013 packing configurations required NCT and HAC thermal analyses to be revisited. In addition to three 3013 container storage configurations (two for Pu metal and one for Pu oxide), a thermal analysis was performed for a food can configuration. All configurations were analyzed under the Normal Conditions of Transport (NCT) and the Hypothetical Accident Conditions (HAC) fire. In the NCT analysis, the drum was exposed to insolation heat flux. The bottom of the drum was adiabatic and the top and sides of the 9975 package exchanged heat through natural convection and radiation to an ambient temperature of 100°F. The HAC analysis initiated from a steady state which was identical to the NCT analysis except that insolation was absent. For the HAC analysis, the drum was upright and exposed to an ambient temperature was 1475°F for the first 30 minutes and 100°F thereafter. For all analyses, a 19 watt total decay power was uniformly distributed over the volume of the Pu metal and/or oxide as an internal heat source.

2.1 Thermal Models

2.1.1 Geometry and Contents

Table 1 identifies all of the 9975 content configurations currently considered. A schematic of the contents of the 9975 package with the 3013 container and the Food Can containers is shown in Figure 1. The BNFL, Hanford, LLNL, and Rocky Flats configurations consist of three nested containers/cans within the PCV of the 9975. The Food Can configuration consists of two stacked cans within the PCV. The SRS 3013 and the Food Can configurations are double nested. LLNL Hex-Can configuration has one Hex-Can, two aluminum spacers, and an aluminum sleeve similar to the Food Can configuration. Dimensions of the containers/cans are shown in Table 2.

Figure 1 does not show the ingot can spacer [9] for the Rocky Flats configuration. LLNL configuration consists of BNFL outer can, BNFL inner can, and the LLNL convenience cans (1 or 2). Hanford configuration consists of BNFL outer can, Hanford BTS inner can, and the Hanford convenience can.

2.1.2 Axisymmetric Thermal Models

Based on the 9975 package geometry, axisymmetric models were developed in PATRAN and run with MSC/Thermal. A color representation of the material composition of a 9975 package, which does not include the finite element mesh, is shown in Figure 2. Figure 3 shows a detailed schematic of the axisymmetric model of the 9975 packaging with the BNFL configuration for Pu oxide contents. The four axisymmetric 9975 models (three 3013 and one food can) contain roughly 7300 nodes each. An example of the type of mesh used is shown in Figure 4. An ingot can spacer was added to the Rocky Flats configuration after the Rev. 2 of this calculation. The spacer is not an axisymmetric component and is not modeled in the model. The RFET spacer is fabricated from two

M-CLC-F-00590, Rev. 8, Pg.6 of 42

stainless steel pieces of sheet metal. Each sheet is 1/16 thick and approximately 2 inches high by 4 inches wide. The weight of the spacer is 0.285 lb (130 g). The mass and size of the spacer are such that it is not expected to alter the conclusions of the calculations that were performed without a spacer (see Item 8 of Results).

LLNL Hex-Can is modeled as a cylinder having the same internal volume (0.75 Liter) and height (4.08 inches) as the original geometry. This simplification is reasonable to maintain the axisymmetric nature of the model. Metal volume of the Hex-Can walls is small and is conservatively neglected. The walls maintain their radiative characteristics for radiation heat transfer.

Heat is transferred within the 9975 package by conduction and radiation. In all models, thermal radiation heat transfer was applied across all gaps filled with gas while natural convection was neglected in the internal gas spaces. Further, all gasses were assumed non-absorbing for thermal radiation and, hence, were treated as non-participating media in the radiation calculations. For the SRS and Rocky Flats models, the Pu metal buttons were modeled as disks 0.75 in. thick with flat tops and 5.125 in. radius of curvature bottoms (curved side down) as shown in Figure 5 [2]. Contact between the metal button and the container is at a point. In the case of the BNFL and Food Can models, the Pu oxide was assumed to completely fill the innermost container.

2.2 Normal Conditions of Transport

In 10 CFR-71.71(c) (1) the NCT are defined as an ambient temperature of 100°F in still air with solar heating of 800 W / m² on the top of the drum and 400 W / m² on the side. The 9975 drum is assumed to be upright and to have an adiabatic bottom surface. Heat transfer from the side and top of the drum to the ambient occurs via natural convection and radiation.

The convection coefficients used are functions of the temperature difference between the drum surfaces and the ambient temperature. Heat transfer coefficients for natural convection were obtained from correlations in the MSC/Thermal code. Specifically, the natural convection correlations are for isothermal plates and have the form:

1. For a vertical isothermal plate with $Ra < 1.0 \times 10^9$,

$$h = \left(\frac{k}{L} \right) \left(0.68 + \frac{0.670 \times Ra^{0.25}}{\left[1.0 + \left(\frac{0.492}{Pr} \right)^{9/16} \right]^{4/9}} \right)$$

2. For a vertical isothermal plate with $1.0 \times 10^9 < Ra$,

$$h = \left(\frac{k}{L} \right) \left(0.825 + \frac{0.387 \times Ra^{1/6}}{\left[1.0 + \left(\frac{0.492}{Pr} \right)^{9/16} \right]^{8/27}} \right)^2$$

3. For a horizontal hot isothermal plate facing upward with $1.0 \times 10^7 < Ra < 3.0 \times 10^{10}$,

$$h = \left(\frac{k}{L} \right) 0.15 \times Ra^{1/3}.$$

Where¹: Ra = Rayleigh number based on plate height.
 h = Convection heat transfer coefficient.
 k = Thermal conductivity of gas (air).
 L = Characteristic length of plate.

The thermal conductivity of fiberboard is based on previous heater experiments with the 9975 which showed the in-plane conductivity to be roughly twice the through-plane value [3].

A summary of the boundary conditions for the analyses follows:

1. The drum is in an upright position.
2. The bottom surface is adiabatic.
3. There is radiative heat transfer from drum sides and top to the ambient.
4. There is natural convection heat transfer from the drum sides and top to the ambient.
5. The ambient temperature is 100°F.
6. Insolation: 800 W/m² on drum top and 400 W/m² on drum side (solar absorptivity of the drum assumed unity).
7. Undamaged fiberboard properties are applied to all the fiberboard in the drum.
8. 19 watts total decay power.

2.3 Hypothetical Accident Conditions

During the HAC transient, the ambient temperature was 1475°F for the first 30 minutes and 100°F thereafter. The initial condition for the HAC transient was identical to the steady-state NCT, except insolation was excluded. In the 30 minute fire phase, all sides of the drum (including the bottom) are heated by forced convection and radiation. The cooldown phase occurs immediately after the 30 minute fire. During this phase the drum is exposed to a 100°F ambient temperature and insolation on the drum top and side (as in

¹ Note that all properties in the correlations are based on the film temperature.

M-CLC-F-00590, Rev. 8, Pg.8 of 42

NCT) is included. During the cooldown phase, the bottom of the drum transfers heat to the ambient by radiation only. The top and sides of the drum transfer heat to the ambient via both radiation and natural convection. The entire HAC transient consists of the 30 minute fire plus 3 hours of cooldown. The conditions for the three phases of the HAC are given below.

For the initial phase of the HAC:

1. The drum is in an upright position.
2. The bottom surface is adiabatic.
3. There is radiation heat transfer from the sides and top of the drum to the ambient.
4. There is natural convection heat transfer from the drum sides and top to the ambient. Convection coefficients were obtained from correlations for natural convection in MSC/Thermal.
5. The ambient temperature is 100°F.
6. No insolation.
7. Undamaged fiberboard properties are applied to all the fiberboard in the drum.
8. 19 watts total decay power.

For the fire phase of the HAC:

1. The drum is in an upright position.
2. There is forced convection from all surfaces of the drum. The convection coefficients, based on a 20 m/s air velocity, are:
 - i. 5.9 Btu/hr-ft² °F for the top and bottom of the drum.
 - ii. 3.0 Btu/hr-ft² °F for the side of the drum.
3. There is thermal radiation heat transfer from all surfaces of the drum to the ambient.
4. The ambient temperature is 1475°F.
5. No insolation.
6. Fire phase fiberboard properties are applied to all the fiberboard in the drum².
7. 19 watts total decay power.

For the fire post-fire phase of the HAC:

1. The drum is in an upright position.
2. There is thermal radiation from the top, sides and bottom of the drum to the ambient.
3. There is natural convection from the top and sides of the drum to the ambient. Convection coefficients were obtained from correlations for natural convection in MSC/Thermal.
4. The ambient temperature is 100°F.
5. Insolation: 800 W/m² on drum top and 400 W/m² on drum side (solar absorptivity of the drum assumed unity).

² The fiberboard properties used during the fire analyses were developed from extensive testing [4].

6. "Char layer" properties are applied to the outer 1.4 inch layer of the top, bottom and sides of the fiberboard contained in the drum².
7. Fire phase properties are applied to the all fiberboard not in the 1.4 inch outer layer².
8. 19 watts total decay power.

2.4 Thermal Properties

Conduction heat transfer through helium, carbon dioxide and air were considered (as appropriate) within the package, as indicated in Table 1. As mentioned previously, all gasses were assumed to be non-absorbing. The temperature ranges of the gasses were considered when assigning the constitutive properties, however, the gas pressure was assumed to remain at 1 atm.

The thermal properties of the packaging components used in the analyses are shown in Tables 3 and 4.

3.0 Analytical Methods and Computations

The general purpose conduction-radiation computer code MSC/Thermal (also known as P/Thermal) was used to perform the computations [5]. This computer code meets site nuclear safety QA requirements [6]. Work was performed in accordance with the WSRC E-7 manual [7]. The thermal models of the storage configurations were created using the general purpose finite element pre and post processor PATRAN [8].

4.0 Results

Steady state temperatures predicted by the models for NCT and HAC are shown in Tables 5 – 8. HAC transient temperatures are shown in Tables 9 - 24 and Figures 6 - 13. Temperature profiles in the fiberboard for NCT are shown in Figures 14 – 17. In the tables, temperatures at key locations are shown for each configuration. A review of the results shows that all the configurations have similar temperature distribution with minor differences for the different components. The BNFL oxide can configuration appears to have the higher temperatures than others. Figure 18 shows the PCV and SCV temperature contours for the BNFL oxide configuration during NCT. The following results are noteworthy:

1. The maximum predicted fiberboard temperature is approximately 257°F (125°C) and occurs with the Pu oxide in the BNFL 3013 configuration.
2. During NCT, the maximum SCV temperature is 268°F (131°C) and the maximum PCV temperature is 285°F (140°C). The maximum temperature occurs on the bottom of the containment vessels with the 3013 Rocky configuration (Pu metal).

M-CLC-F-00590, Rev. 8, Pg.10 of 42

3. During NCT, the maximum PCV seal temperature is 264°F (129°C) and the maximum SCV seal temperature is 252°F (129°C).
4. During NCT, the middle Pu centerline temperatures are 525°F (274°C), 423°F (217°C), 314°F (157°C) and 401°F (205°C) for the 3013 BNFL (Pu oxide), 3013 Rocky (Pu metal), 3013 SRS (Pu metal), and food can (Pu oxide) configurations, respectively.
5. During NCT, the average PCV gas temperature for the BNFL 3013 configuration (Pu oxide) is 308°F (153°C) and for the Food Can configuration (Pu oxide) is 313°F (156°C). Average gas temperatures were calculated by volume averaging of nodal temperatures at select nodal locations in the cavities within the PCV. The nodal temperatures were selected along the cavity centerlines and on cavity surfaces.
6. Except near the outer region of the package, temperatures at the end of the 30 minute HAC fire are lower than during NCT (with insolation). The temperatures are about 90°F cooler inside the PCV at the end of the HAC fire compared with NCT (with insolation).
7. For the BNFL (Pu oxide) configuration during NCT, the lead temperature near the axial midplane is approximately 253°F. The maximum lead temperature of approximately 257°F occurs at the bottom of the lead shield near the support for the SCV.
8. The Rocky Flats configuration will use a spacer [9] to raise Pu metal buttons in their convenience cans. This will raise the center of the buttons 2" from the analyzed condition. This shift in the location of the heat source will shift the higher PCV temperatures from the bottom of the vessel to the side of the vessel (see Tables 5, 11, and 12). However this shift still places the location of the maximum temperature well below the PCV O-rings and will not adversely impact the integrity of the O-rings.
9. The LLNL and BNFL Oxide configurations have similar packaging temperatures for the pre-fire and solar conditions. These are shown in Tables 5 and 7. Based on the closeness of these temperatures, it is concluded that the temperatures during the fire and post-fire transients will also be similar and were therefore not recalculated.
10. The Hanford Pu oxide can configuration has similar or lower temperatures than the LLNL and BNFL configurations for the pre-fire and solar conditions. These are shown in Tables 5 and 7. Based on the closeness of these temperatures, it is concluded that the temperatures during the fire and post-fire transients will also be similar and were therefore not recalculated. In general, the maximum temperatures with Pu metal contents are lower than with Pu oxide contents and, therefore, this configuration is also not reanalyzed.

11. The PCV seal temperature is 56°F and the average gas temperature inside the PCV is 68°F when the ambient temperature is -20°F with no insolation and the package has 19 watts of PuO₂ contents. The average gas temperature was calculated by volume averaging of nodal temperatures at select nodal locations in the cavities within the PCV. This gas temperature is less than the 313°F value for the NCT reported in Item #5 above. Since the average gas temperature is well below the gas temperature during NCT, the resulting gas pressure is bounded by the MNOP (365.4 psig).
12. The component temperatures for the LLNL Hex-Can configuration are below their limiting temperatures. The average gas temperature inside the PCV is 298°F, which is less than the maximum gas temperature of 313°F calculated for the SRS foodcan configuration. This configuration with the low density oxide as the contents and 19 watts power has the maximum content temperature of 641°F. This temperature is local and does not impact the integrity of the package. Since the component temperatures during NCT solar conditions are similar to the temperatures found in other configurations, it is expected that the thermal response during HAC will also be similar to other configurations. Therefore, no fire or post-fire analyses have been performed.
13. The temperature gradient through the PCV/SCV walls is less than 2°F.

The Rocky and SRS configurations have similar packaging temperatures, however the plutonium metal temperatures are lower for the SRS design. Heat generation by the plutonium contents affects the packaging and can temperatures. Further, the composition of the plutonium, as an oxide or metal, significantly affects its temperature within the package. Oxide yields significantly greater centerline Pu temperatures. In general, the packaging temperatures are quite consistent for all configurations during NCT. The design changes have a very small effect on the packaging temperatures (several degrees Fahrenheit).

Table 1: Content Configurations

Name	Outer Container	Inner Container	Convenience Container	Fill Gasses	Contents
BNFL	Yes BNFL 3013	Yes BNFL	Yes BNFL	O ₂ ≤ 5% and Helium in 3013, 75% CO ₂ between PCV& 3013, all other is air	Low density Pu Oxide (19 W total)
Rocky Flats (Rocky)	Yes BNFL 3013	Yes BNFL	Yes Rocky Flats	O ₂ ≤ 5% and Helium in 3013, 75% CO ₂ between PCV& 3013, all other is air	2 Pu metal buttons stacked directly on top of each other (19 W total)
SRS	Yes BNFL 3013	Yes SRS cans stacked two high	No	O ₂ ≤ 5% and Helium in 3013, 75% CO ₂ between PCV& 3013, all other is air	2 Pu metal buttons one in each of 2 containers (19 W total)
LLNL Can	Yes BNFL 3013	Yes BNFL 3013	Yes LLNL	O ₂ ≤ 5% and Helium in 3013, 75% CO ₂ between PCV& 3013, all other is air	2 Pu metal buttons like Rocky Flats. Low density Pu Oxide in each of two cans stacked directly on top of each other (19 W total)
LLNL Hex_Can	No	No	Yes Hex_Can	O ₂ ≤ 5% and 75% CO ₂ in PCV, all other is air	Pu Oxide (19 W total)
Food Can	Yes Food Can	Yes Food Can	No	O ₂ ≤ 5% and 75% CO ₂ in PCV, all other is air	Low density Pu Oxide in each of two cans stacked directly on top of each other (19 W total)
Hanford Can	Yes BNFL 3013	Yes Hanford BTS 3013	Yes Hanford	O ₂ ≤ 5% and Helium in 3013, 75% CO ₂ between PCV& 3013, all other is air	2 Pu metal buttons like Rocky Flats. Low density Pu Oxide in one convenience can. (19 W total)

Note for Table 1

A brief investigation was conducted on the sensitivity of package temperatures to the type of fill gasses used. It was found that the maximum temperature variation was less than 2°F when air was replaced by CO₂. This variation is small and it will not impact the structural integrity of the PCV or the SCV.

Table 2: External Dimensions of Containers

Container	Diameter X Height (in.) Used in Model	Diameter X Height (in.) From Drawing	Corresponding Drawing Number
BNFL Outer 3013	4.92 X 10.0	Max. 4.924 X 10.023 Min. 4.918 X 9.670	BNFL Drawing M-PV-F-0017, Rev 0
BNFL Inner Container	4.61 X 9.095 (top of lip) 4.61 X 8.80 (top of plug)	Max. to lip edge 4.625 X 9.094 Max. to plug 4.625 X 8.740 Max. to lip edge 4.580 X 9.094 Min. to plug 4.580 X 8.740	BNFL Drawing M-PV-F-0016, Rev 0
BNFL Convenience Can	4.29 X 8.435	Max. 4.420 X 8.396 Min. 4.398 X 8.333	BNFL Drawing M-PV-F-0015, Rev 0
Rocky Flats Convenience Can	4.11 X 5.46		Dynamic Machine Works, 1509-02
SRS Inner Container	4.6 X 4.625		WSRC Drawing R-R1-F-0039 Rev. 2
LLNL Convenience Cans	One 4.139 X 8.0 or Two 4.139 X 4.0		N/A
LLNL Hex-Can	One 3.724 X 4.08**	One (4.231/3.737) X 4.2	AAA00-104994 AAA00-107506
Food Can	4.25 X 7 Outer Can 4.0625 X 6.25 Inner Can		N/A
Hanford Convenience Can	One 4.27 X 8.093		Dynamic Machine Works, P/N 1900,1911- 1, and 1911-2
BTS Inner Can	4.6 X 9.0 Inner Can		EES-22726-R1-004

Table 3: Emissivity of Package Components

Component	Emissivity
Aluminum plates, honeycomb	0.20
Fiberboard	0.50
Lead	0.28
Lead/ Lead shield stainless steel liner	0.28
Drum Inner Surface	0.30
Drum Outer Surface (Initial HAC and NCT)	0.21
Drum Outer Surface (fire phase HAC)	0.90
Drum Outer Surface (post-fire phase HAC)	0.80
3013 Container	0.30
BNFL Middle Can	0.30
BNFL Convenience Can	0.20
Pu Oxide	0.90
Pu Metal	0.90
Rocky Convenience Can	0.20
SRS Convenience Can	0.20
PVC/SCV	0.30

Table 4: Constitutive Properties of Packaging Materials

Material	Density (lbm/ft ³) @ T(°F)	Conductivity (Btu/hr.-ft.- °F) @ T(°F)	Heat Capacity (Btu/lbm °F) @ T(°F)
Helium	0.010497	0.0910 @ 120 0.0985 @ 212 0.1226 @ 392	1.24
Air	0.080532	0.01396 @ 32 0.01839 @ 212 0.02238 @ 392 0.02593 @ 572	0.237 @ 212
Carbon Dioxide (CO ₂)	0.1122	0.00958 @ 80.0 0.01183 @ 170.0 0.01422 @ 260.0 0.01674 @ 350.0	2.0823E-01 @ 80.0 2.1517E-01 @ 170.0 2.2521E-01 @ 260.0 2.3429E-01 @ 350.0
Honeycomb energy absorber (radial)	16.2	3.82	0.22
Honeycomb energy absorber (axial)	16.2	7.62	0.22
Pre-fire fiberboard (radial)	16.86 @ 77 17.36 @ 187 17.86 @ 295	0.0723	0.306 @ 77 0.360 @ 187 0.417 @ 295
Pre-fire fiberboard (axial)	16.86 @ 77 17.36 @ 187 17.86 @ 295	0.031 @ 77 0.034 @ 187 0.029 @ 533	0.306 @ 77 0.360 @ 187 0.417 @ 295
During fire fiberboard (Fire Phase)	15.40 @ 80 15.40 @ 475 8.5 @ 810 3.5 @ 1500	0.035 @ 80 0.450 @ 170 0.550 @ 200 0.090 @ 210 0.070 @ 500	0.25 @ 80 0.50 @ 475 0.50 @ 810 0.50 @ 1500
Post-fire fiberboard (Char Layer)	8.1	0.07 @ 100 0.07 @ 140 1.0 @ 200 0.3 @ 300 0.07 @ 500	0.25
Aluminum	169.3	126.0	0.216
Stainless steel (304)	494.4	7.74 @ 32 9.43 @ 212 12.58 @ 932	0.12 @ 32 0.135 @ 752
Stainless steel (316)	514.3	8.79 @ 261 10.58 @ 621	0.12 @ 261 0.13 @ 621
Lead	708.5	19.6 @ 209 18.3 @ 400	0.0305 @ 32 0.0315 @ 212 0.0338 @ 621.5
Pu oxide	124.8	0.0460	0.022
Pu metal	1198.6	7.26 @ 207 7.74 @ 243 9.19 @ 266 18.39 @ 1112	0.032 @ 32 0.0328 @ 212 0.174 @ 257 0.0294 @ 347 0.0399 @ 842

Table 5: Solar Case Steady State Temperatures (°F/°C) with the 3013 Configuration

Location	19 Watt BNFL (Oxide) Configuration	19 Watt Rocky Flats Configuration	19 Watt SRS Configuration	19 Watt Hanford (Oxide) Configuration
Drum Top	254°F / 124°C	254°F / 124°C	254°F / 124°C	254°F / 124°C
Drum Bottom	235°F / 113°C	235°F / 113°C	234°F / 112°C	218°F / 103°C
Drum Side	206°F / 97°C	206°F / 97°C	206°F / 97°C	178°F / 81°C
Mid-Height Fiberboard	250°F / 121°C	247°F / 119°C	246°F / 119°C	231°F / 111°C
SCV O-ring	252°F / 122°C	249°F / 121°C	249°F / 121°C	237°F / 114°C
PCV O-ring	261°F / 127°C	256°F / 124°C	257°F / 125°C	249°F / 121°C
SCV Side	264°F / 129°C	250°F / 121°C	258°F / 126°C	246°F / 119°C
SCV Bottom	267°F / 130°C	268°F / 131°C	265°F / 129°C	247°F / 119°C
PCV Side	283°F / 139°C	272°F / 133°C	273°F / 134°C	263°F / 128°C
PCV Bottom	279°F / 137°C	285°F / 140°C	280°F / 138°C	261°F / 127°C
3013 Top	284°F / 140°C	272°F / 133°C	276°F / 136°C	260°F / 127°C
3013 Bottom	280°F / 138°C	287°F / 141°C	282°F / 139°C	261°F / 127°C
3013 Side	293°F / 145°C	276°F / 136°C	288°F / 142°C	273°F / 134°C
Pu-Can Interface	-----	398°F / 203°C	309°F / 154°C Top Button 291°F / 144°C Bottom Button	-----
Centerline Mid Height Pu	525°F / 274°C	423°F / 217°C Top Button 414°F / 212°C Bottom Button	314°F / 157°C Top Button 299°F / 148°C Bottom Button	485°F / 252°C
Maximum Fiberboard Temperature	257°F / 125°C	257°F / 125°C	254°F / 123°C	241°F / 116°C
Maximum Lead Temperature	257°F / 125°C	257°F / 125°C	255°F / 124°C	238°F / 114°C

Table 5 (Con'd): Solar Case Steady State Temperatures (°F/°C)
For LLNL Hex-Can and 3013 Configuration

Location	19 Watts Oxide LLNL Hex-Can Configuration	19 Watt Oxide LLNL 3013 Can Configuration
Drum Top	255°F / 124°C	253°F / 123°C
Drum Bottom	234°F / 112°C	234°F / 112°C
Drum Side	220°F / 104°C	206°F / 97°C
Mid-Height Fiberboard	250°F / 121°C	235°F / 113°C
SCV O-ring	254°F / 124°C	252°F / 122°C
PCV O-ring	265°F / 129°C	261°F / 127°C
SCV Side	260°F / 127°C	264°F / 129°C
SCV Bottom	264°F / 129°C	263°F / 128°C
PCV Side	272°F / 133°C	283°F / 139°C
PCV Bottom	275°F / 135°C	274°F / 134°C
3013 Top	N/A	288°F / 142°C
3013 Bottom	N/A	275°F / 135°C
3013 Side	N/A	294°F / 146°C
Centerline Mid Height Pu	641°F / 338°C	509°F / 265°C
Maximum Fiberboard Temperature	254°F / 124°C	256°F / 124°C
Maximum Lead Temperature	255°F / 124°C	251°F / 122°C

Table 6: Solar Case Steady State Temperatures (°F/°C) with the Food Can Configuration

Location	19 Watt Oxide Food Can Configuration
Drum Top	254°F / 124°C
Drum Bottom	231°F / 111°C
Side	206°F / 97°C
Mid-Height Fiberboard	244°F / 118°C
SCV O-ring	250°F / 121°C
PCV O-ring	264°F / 129°C
SCV Side	255°F / 124°C
SCV Bottom	258°F / 126°C
PCV Side	270°F / 132°C
PCV Bottom	268°F / 131°C
Top of Upper Pu Can	297°F / 147°C
Bottom of Lower Pu Can	269°F / 131°C
Side of PCV Sleeve (mid height of contents)	272°F / 133°C
Centerline Mid Height Pu (top can)	401°F / 205°C
Centerline Mid Height Pu (bottom can)	398°F / 203°C
Maximum Fiberboard Temperature	250°F / 121°C
Maximum Lead Temperature	250°F / 121°C

Table 7: Initial Pre-Fire Case Steady State Temperatures (°F/°C) with the 3013 Configuration

Location	19 Watt BNFL (Oxide) Configuration	19 Watt Rocky Flats Configuration	19 Watt SRS Configuration	19 Watt Oxide LLNL Can Configuration
Drum Top	103°F / 39°C	103°F / 39°C	103°F / 39°C	103°F / 39°C
Bottom	137°F / 58°C	137°F / 59°C	137°F / 58°C	135°F / 57°C
Side	109°F / 43°C	108°F / 42°C	108°F / 42°C	108°F / 42°C
Mid-Height Fiberboard	153°F / 67°C	149°F / 65°C	149°F / 65°C	149°F / 65°C
SCV O-ring	156°F / 69°C	153°F / 67°C	154°F / 68°C	153°F / 67°C
PCV O-ring	167°F / 75°C	161°F / 72°C	164°F / 73°C	162°F / 72°C
SCV Side	168°F / 76°C	153°F / 67°C	164°F / 73°C	166°F / 74°C
SCV Bottom	171°F / 77°C	174°F / 79°C	171°F / 77°C	166°F / 74°C
PCV Side	190°F / 88°C	179°F / 81°C	181°F / 83°C	190°F / 88°C
PCV Bottom	186°F / 86°C	192°F / 89°C	188°F / 87°C	180°F / 82°C
3013 Top	193°F / 90°C	179°F / 82°C	186°F / 86°C	197°F / 92°C
3013 Bottom	187°F / 86°C	195°F / 90°C	190°F / 88°C	181°F / 83°C
3013 Side	202°F / 94°C	183°F / 84°C	198°F / 92°C	202°F / 94°C
Pu-Can Interface	-----	324°F / 162°C	222°F / 106°C Top Button 200°F / 93°C Bottom Button	424°F / 218°C
Centerline Mid Height Pu	437°F / 225°C	355°F / 179°C Top Button 342°F / 172°C Bottom Button	228°F / 109°C Top Button 210°F / 99°C Bottom Button	424°F / 218°C

Table 7 (Cont'd): Initial Pre-Fire Case Steady State Temperatures (°F/°C) with the 3013 Configuration

Location	19 Watt Hanford (Oxide) Configuration
Drum Top	103°F /39°C
Bottom	133°F /56°C
Side	108°F /42°C
Mid-Height Fiberboard	146°F /63°C
SCV O-ring	152°F /67°C
PCV O-ring	167°F /75°C
SCV Side	163°F /73°C
SCV Bottom	164°F /73°C
PCV Side	182°F /83°C
PCV Bottom	179°F /82°C
3013 Top	180°F /82°C
3013 Bottom	180°F /82°C
3013 Side	193°F / 89°C
Pu-Can Interface	-----
Centerline Mid Height Pu	408°F /209°C

Table 8: Initial Pre-Fire Case Steady State Temperatures (°F/°C) with the Food Can Configuration

Location	19 Watt Oxide Food Can Configuration
Drum Top	103°F / 40°C
Drum Bottom	138°F / 59°C
Side	109°F / 43°C
Mid-Height Fiberboard	154°F / 68°C
SCV O-ring	162°F / 72°C
PCV O-ring	181°F / 83°C
SCV Side	169°F / 76°C
SCV Bottom	173°F / 78°C
PCV Side	188°F / 87°C
PCV Bottom	185°F / 85°C
Top of Upper Pu Can	224°F / 106°C
Bottom of Lower Pu Can	186°F / 85°C
Side of PCV Sleeve (mid height of contents)	190°F / 88°C
Centerline Mid Height Pu (top can)	324°F / 162°C
Centerline Mid Height Pu (bottom can)	319°F / 160°C

Table 9: Temperatures (°F) During the Fire Transient with the BNFL (Oxide) 3013 Configuration

Time (min)	Drum Top	Bottom	Side	Mid-Height Fiberboard	SCV O-ring	PCV O-ring	SCV Side	SCV Bottom	PCV Side	PCV Bottom	3013 Top	3013 Bottom	3013 Side	Mid Pu
0	103°F	137°F	109°F	153°F	156°F	167°F	168°F	171°F	190°F	186°F	193°F	187°F	202°F	437°F
5	1442°F	1188°F	1348°F	147°F	156°F	167°F	168°F	171°F	190°F	186°F	193°F	187°F	202°F	437°F
10	1444°F	1267°F	1384°F	148°F	155°F	167°F	168°F	171°F	190°F	186°F	193°F	187°F	202°F	437°F
15	1446°F	1303°F	1401°F	154°F	155°F	167°F	168°F	171°F	190°F	186°F	193°F	187°F	202°F	437°F
20	1447°F	1326°F	1412°F	161°F	155°F	167°F	168°F	171°F	190°F	186°F	193°F	187°F	202°F	437°F
25	1448°F	1341°F	1419°F	168°F	155°F	167°F	168°F	173°F	190°F	186°F	193°F	187°F	202°F	437°F
30	1449°F	1353°F	1424°F	174°F	156°F	167°F	169°F	175°F	190°F	187°F	193°F	187°F	202°F	437°F

Table 10: Temperature (°C) During the Fire Transient with the BNFL (Oxide) 3013 Configuration

Time (Min)	Drum Top	Bottom	Side	Mid-Height Fiberboard	SCV O-ring	PCV O-ring	SCV Side	SCV Bottom	PCV Side	PCV Bottom	3013 Top	3013 Bottom	3013 Side	Mid Pu
0	39°C	58°C	43°C	67°C	69°C	75°C	76°C	77°C	88°C	86°C	90°C	86°C	94°C	225°C
5	783°C	642°C	731°C	64°C	69°C	75°C	76°C	77°C	88°C	86°C	90°C	86°C	94°C	225°C
10	784°C	686°C	751°C	64°C	69°C	75°C	76°C	77°C	88°C	86°C	90°C	86°C	94°C	225°C
15	785°C	706°C	761°C	68°C	69°C	75°C	76°C	77°C	88°C	85°C	90°C	86°C	94°C	225°C
20	786°C	719°C	766°C	72°C	69°C	75°C	76°C	77°C	88°C	85°C	90°C	86°C	94°C	225°C
25	786°C	727°C	771°C	75°C	69°C	75°C	76°C	78°C	88°C	86°C	90°C	86°C	94°C	225°C
30	787°C	734°C	774°C	79°C	69°C	75°C	76°C	79°C	88°C	86°C	90°C	86°C	94°C	225°C

Table 11: Temperatures (°F) During the Fire Transient with the Rocky Flats 3013 Configuration

Time (min)	Drum Top	Bottom	Side	Mid-Height Fiberboard	SCV O-ring	PCV O-ring	SCV Side	SCV Bottom	PCV Side	PCV Bottom	3013 Top	3013 Bottom	3013 Side	Pu-Can Interface	Mid Pu (Top)	Mid Pu (Bottom)
0	103°F	137°F	108°F	149°F	153°F	161°F	153°F	174°F	179°F	192°F	179°F	195°F	183°F	324°F	355°F	342°F
5	1442°F	1187°F	1347°F	144°F	153°F	161°F	151°F	173°F	179°F	192°F	179°F	195°F	183°F	324°F	355°F	342°F
10	1444°F	1266°F	1384°F	145°F	153°F	161°F	150°F	173°F	179°F	192°F	179°F	194°F	183°F	324°F	355°F	342°F
15	1446°F	1303°F	1401°F	151°F	152°F	161°F	151°F	173°F	179°F	192°F	179°F	194°F	183°F	324°F	355°F	342°F
20	1447°F	1326°F	1411°F	158°F	152°F	161°F	153°F	174°F	179°F	192°F	179°F	194°F	183°F	324°F	355°F	342°F
25	1448°F	1341°F	1419°F	165°F	153°F	161°F	157°F	175°F	179°F	192°F	179°F	195°F	183°F	324°F	355°F	342°F
30	1448°F	1353°F	1424°F	171°F	153°F	161°F	162°F	177°F	179°F	193°F	179°F	195°F	183°F	324°F	355°F	342°F

Table 12: Temperatures (°C)) During the Fire Transient with the Rocky Flats 3013 Configuration

Time (min)	Drum Top	Bottom	Side	Mid-Height Fiberboard	SCV O-ring	PCV O-ring	SCV Side	SCV Bottom	PCV Side	PCV Bottom	3013 Top	3013 Bottom	3013 Side	Pu-Can Interface	Mid Pu (Top)	Mid Pu (Bottom)
0	39°C	59°C	42°C	65°C	67°C	72°C	67°C	79°C	81°C	89°C	82°C	90°C	84°C	162°C	179°C	172°C
5	783°C	642°C	731°C	62°C	67°C	72°C	66°C	79°C	81°C	89°C	82°C	90°C	84°C	162°C	179°C	172°C
10	784°C	686°C	751°C	63°C	67°C	72°C	66°C	78°C	81°C	89°C	82°C	90°C	84°C	162°C	179°C	172°C
15	785°C	706°C	761°C	66°C	67°C	72°C	66°C	78°C	81°C	89°C	82°C	90°C	84°C	162°C	179°C	172°C
20	786°C	719°C	766°C	70°C	67°C	72°C	67°C	79°C	81°C	89°C	82°C	90°C	84°C	162°C	179°C	172°C
25	786°C	727°C	770°C	74°C	67°C	72°C	70°C	79°C	81°C	89°C	82°C	90°C	84°C	162°C	179°C	172°C
30	787°C	734°C	773°C	77°C	67°C	72°C	72°C	80°C	81°C	89°C	82°C	91°C	84°C	162°C	179°C	172°C

Table 13: Temperatures (°F) During the Fire Transient with the SRS 3013 Configuration

Time (min)	Drum Top	Bottom	Side	Mid-Height Fiberboard	SCV O-ring	PCV O-ring	SCV Side	SCV Bottom	PCV Side	PCV Bottom	3013 Top	3013 Bottom	3013 Side (mid height of contents)	Pu Can Interface (top)	Pu Can Interface (bottom)	Mid Pu (top)	Mid Pu (bottom)
0	103°F	137°F	108°F	149°F	154°F	164°F	164°F	171°F	181°F	188°F	186°F	190°F	198°F	222°F	200°F	228°F	210°F
5	1442°F	1188°F	1347°F	145°F	154°F	164°F	164°F	171°F	181°F	188°F	186°F	190°F	198°F	222°F	200°F	228°F	210°F
10	1444°F	1267°F	1384°F	145°F	154°F	164°F	164°F	171°F	181°F	188°F	186°F	190°F	198°F	222°F	200°F	228°F	210°F
15	1446°F	1303°F	1401°F	151°F	153°F	164°F	164°F	170°F	181°F	188°F	186°F	190°F	198°F	222°F	200°F	228°F	210°F
20	1447°F	1326°F	1412°F	158°F	153°F	164°F	164°F	171°F	181°F	188°F	186°F	190°F	198°F	222°F	200°F	228°F	210°F
25	1448°F	1341°F	1419°F	165°F	153°F	164°F	164°F	173°F	181°F	188°F	186°F	190°F	198°F	222°F	200°F	228°F	210°F
30	1449°F	1353°F	1424°F	171°F	154°F	164°F	164°F	174°F	181°F	189°F	186°F	191°F	198°F	222°F	200°F	228°F	210°F

Table 14: Temperatures (°C) During the Fire Transient with the SRS 3013 Configuration

Time (min)	Drum Top	Bottom	Side	Mid-Height Fiberboard	SCV O-ring	PCV O-ring	SCV Side	SCV Bottom	PCV Side	PCV Bottom	3013 Top	3013 Bottom	3013 Side (mid height of contents)	Pu Can Interface (top)	Pu Can Interface (bottom)	Mid Pu (top)	Mid Pu (bottom)
0	39°C	58°C	42°C	65°C	68°C	73°C	73°C	77°C	83°C	87°C	86°C	88°C	92°C	106°C	93°C	109°C	99°C
5	783°C	642°C	731°C	63°C	68°C	73°C	73°C	77°C	83°C	87°C	86°C	88°C	92°C	106°C	93°C	109°C	99°C
10	784°C	686°C	751°C	63°C	68°C	73°C	73°C	77°C	83°C	87°C	86°C	88°C	92°C	106°C	93°C	109°C	99°C
15	785°C	706°C	761°C	66°C	67°C	73°C	73°C	77°C	83°C	87°C	86°C	88°C	92°C	106°C	93°C	109°C	99°C
20	786°C	719°C	766°C	70°C	67°C	73°C	73°C	77°C	83°C	87°C	86°C	88°C	92°C	106°C	93°C	109°C	99°C
25	786°C	727°C	770°C	74°C	67°C	73°C	73°C	78°C	83°C	87°C	86°C	88°C	92°C	106°C	93°C	109°C	99°C
30	787°C	734°C	774°C	77°C	68°C	73°C	73°C	79°C	83°C	87°C	86°C	88°C	92°C	106°C	94°C	109°C	99°C

Table 15: Temperatures (°F) During the Fire Transient with the Food Can Configuration

Time (min)	Drum Top	Bottom	Side	Mid-Height Fiberboard	SCV O-ring	PCV O-ring	SCV Side	SCV Bottom	PCV Side	PCV Bottom	Top of Upper Pu Can	Bottom of Lower Pu Can	Side of PCV Sleeve (mid height of contents)	Mid Pu (top can)	Mid Pu (bottom can)
0	103°F	138°F	109°F	154°F	162°F	181°F	169°F	173°F	188°F	185°F	224°F	186°F	190°F	324°F	319°F
5	1442°F	1188°F	1347°F	148°F	162°F	181°F	169°F	173°F	188°F	185°F	224°F	186°F	190°F	324°F	319°F
10	1444°F	1267°F	1384°F	149°F	162°F	181°F	169°F	172°F	188°F	185°F	224°F	185°F	190°F	324°F	319°F
15	1446°F	1303°F	1401°F	155°F	162°F	181°F	169°F	172°F	188°F	185°F	223°F	185°F	190°F	324°F	319°F
20	1447°F	1326°F	1412°F	162°F	162°F	181°F	169°F	173°F	188°F	185°F	223°F	185°F	190°F	324°F	319°F
25	1448°F	1341°F	1419°F	168°F	162°F	181°F	169°F	174°F	188°F	185°F	223°F	185°F	190°F	324°F	319°F
30	1449°F	1353°F	1424°F	174°F	162°F	181°F	169°F	176°F	188°F	185°F	223°F	186°F	190°F	324°F	319°F

Table 16: Temperatures (°C) During the Fire Transient with the Food Can Configuration

Time (min)	Drum Top	Bottom	Side	Mid-Height Fiberboard	SCV O-ring	PCV O-ring	SCV Side	SCV Bottom	PCV Side	PCV Bottom	Top of Upper Pu Can	Bottom of Lower Pu Can	Side of PCV Sleeve (mid height of contents)	Mid Pu (top can)	Mid Pu (bottom can)
0	40°C	59°C	43°C	68°C	72°C	83°C	76°C	78°C	87°C	85°C	106°C	85°C	88°C	162°C	160°C
5	783°C	642°C	731°C	65°C	72°C	83°C	76°C	78°C	87°C	85°C	106°C	85°C	88°C	162°C	160°C
10	784°C	686°C	751°C	65°C	72°C	83°C	76°C	78°C	87°C	85°C	106°C	85°C	88°C	162°C	160°C
15	785°C	706°C	761°C	68°C	72°C	83°C	76°C	78°C	86°C	85°C	106°C	85°C	88°C	162°C	160°C
20	786°C	719°C	766°C	72°C	72°C	83°C	76°C	78°C	86°C	85°C	106°C	85°C	88°C	162°C	160°C
25	786°C	727°C	771°C	76°C	72°C	83°C	76°C	79°C	86°C	85°C	106°C	85°C	88°C	162°C	160°C
30	787°C	734°C	774°C	79°C	72°C	83°C	76°C	80°C	86°C	85°C	106°C	86°C	88°C	162°C	160°C

Table 17: Temperatures (°F) During the Post-Fire Transient with the BNFL 3013 Configuration

Time (hr)	Drum Top	Bottom	Side	Mid-Height Fiberboard	SCV O-ring	PCV O-ring	SCV Side	SCV Bottom	PCV Side	PCV Bottom	3013 Top	3013 Bottom	3013 Side	Mid Pu
0.0	1449°F	1353°F	1424°F	174°F	156°F	167°F	169°F	175°F	190°F	187°F	193°F	187°F	202°F	437°F
0.5	249°F	346°F	217°F	191°F	160°F	167°F	176°F	187°F	192°F	192°F	194°F	193°F	203°F	438°F
1.0	249°F	265°F	202°F	196°F	167°F	169°F	184°F	195°F	196°F	199°F	195°F	200°F	207°F	440°F
1.5	249°F	221°F	202°F	198°F	173°F	172°F	191°F	199°F	201°F	205°F	197°F	206°F	211°F	443°F
2.0	249°F	203°F	202°F	198°F	178°F	176°F	195°F	202°F	206°F	209°F	201°F	210°F	216°F	447°F
2.5	249°F	201°F	202°F	199°F	182°F	180°F	198°F	204°F	209°F	212°F	204°F	213°F	219°F	451°F
3.0	249°F	201°F	202°F	199°F	185°F	183°F	201°F	206°F	213°F	214°F	208°F	215°F	223°F	454°F

Table 18: Temperatures (°C) During the Post-Fire Transient with the BNFL 3013 Configuration

Time (hr)	Drum Top	Bottom	Side	Mid-Height Fiberboard	SCV O-ring	PCV O-ring	SCV Side	SCV Bottom	PCV Side	PCV Bottom	3013 Top	3013 Bottom	3013 Side	Mid Pu
0.0	787°C	734°C	774°C	79°C	69°C	75°C	76°C	79°C	88°C	86°C	90°C	86°C	94°C	225°C
0.5	121°C	174°C	103°C	88°C	71°C	75°C	80°C	86°C	89°C	89°C	90°C	89°C	95°C	225°C
1.0	121°C	130°C	95°C	91°C	75°C	76°C	85°C	90°C	91°C	93°C	90°C	93°C	97°C	226°C
1.5	121°C	105°C	95°C	92°C	78°C	78°C	88°C	93°C	94°C	96°C	92°C	96°C	100°C	228°C
2.0	121°C	95°C	95°C	92°C	81°C	80°C	91°C	95°C	97°C	98°C	94°C	99°C	102°C	230°C
2.5	121°C	94°C	95°C	93°C	83°C	82°C	92°C	96°C	99°C	100°C	96°C	100°C	104°C	233°C
3.0	121°C	94°C	95°C	93°C	85°C	84°C	94°C	96°C	100°C	101°C	98°C	102°C	106°C	235°C

Table 19: Temperatures (°F) During the Post-Fire Transient with the Rocky Flats 3013 Configuration

Time (hr)	Drum Top	Bottom	Side	Mid-Height Fiberboard	SCV O-ring	PCV O-ring	SCV Side	SCV Bottom	PCV Side	PCV Bottom	3013 Top	3013 Bottom	3013 Side	Pu-Can Interface	Mid Pu (Top)	Mid Pu (Bottom)
0.0	1448°F	1353°F	1424°F	171°F	153°F	161°F	162°F	177°F	179°F	193°F	179°F	195°F	183°F	324°F	355°F	342°F
0.5	249°F	346°F	214°F	189°F	157°F	162°F	183°F	189°F	180°F	199°F	179°F	201°F	184°F	326°F	355°F	343°F
1.0	249°F	265°F	202°F	194°F	164°F	164°F	191°F	197°F	183°F	205°F	180°F	207°F	186°F	329°F	358°F	346°F
1.5	249°F	221°F	202°F	196°F	170°F	167°F	194°F	201°F	187°F	211°F	183°F	213°F	190°F	333°F	361°F	350°F
2.0	249°F	203°F	202°F	197°F	175°F	171°F	196°F	204°F	191°F	215°F	187°F	217°F	194°F	336°F	364°F	353°F
2.5	249°F	201°F	202°F	198°F	180°F	175°F	197°F	206°F	195°F	218°F	191°F	220°F	198°F	339°F	367°F	356°F
3.0	249°F	201°F	202°F	198°F	183°F	179°F	198°F	207°F	199°F	220°F	195°F	222°F	202°F	341°F	369°F	358°F

Table 20: Temperature (°C) During the Post-Fire Transient with the Rocky Flats 3013 Configuration

Time (hr)	Drum Top	Bottom	Side	Mid-Height Fiberboard	SCV O-ring	PCV O-ring	SCV Side	SCV Bottom	PCV Side	PCV Bottom	3013 Top	3013 Bottom	3013 Side	Pu-Can Interface	Mid Pu (Top)	Mid Pu (Bottom)
0.0	787°C	734°C	773°C	77°C	67°C	72°C	72°C	80°C	81°C	89°C	82°C	91°C	84°C	162°C	179°C	172°C
0.5	121°C	174°C	101°C	87°C	70°C	72°C	84°C	87°C	82°C	93°C	82°C	94°C	84°C	163°C	180°C	173°C
1.0	121°C	130°C	95°C	90°C	73°C	73°C	88°C	91°C	84°C	96°C	82°C	97°C	86°C	165°C	181°C	175°C
1.5	121°C	105°C	95°C	91°C	77°C	75°C	90°C	94°C	86°C	99°C	84°C	100°C	88°C	167°C	183°C	177°C
2.0	121°C	95°C	95°C	92°C	80°C	77°C	91°C	96°C	88°C	101°C	86°C	103°C	90°C	169°C	184°C	178°C
2.5	121°C	94°C	94°C	92°C	82°C	79°C	92°C	97°C	91°C	103°C	88°C	104°C	92°C	170°C	186°C	180°C
3.0	121°C	94°C	94°C	92°C	84°C	81°C	92°C	97°C	93°C	104°C	91°C	106°C	94°C	172°C	187°C	181°C

Table 21: Temperatures (°F) During the Post-Fire Transient with the SRS 3013 Configuration During Transport

Time (hr)	Drum Top	Bottom	Side	Mid-Height Fiberboard	SCV O-ring	PCV O-ring	SCV Side	SCV Bottom	PCV Side	PCV Bottom	3013 Top	3013 Bottom	3013 Side (mid height of contents)	Pu Can Interface (top)	Pu Can Interface (bottom)	Mid Pu (top)	Mid Pu (bottom)
0.0	1449°F	1353°F	1424°F	171°F	154°F	164°F	164°F	174°F	181°F	189°F	186°F	191°F	198°F	222°F	200°F	228°F	210°F
0.5	249°F	345°F	215°F	189°F	158°F	164°F	170°F	186°F	182°F	194°F	186°F	196°F	199°F	222°F	205°F	228°F	214°F
1.0	249°F	265°F	202°F	195°F	165°F	166°F	178°F	195°F	185°F	201°F	187°F	202°F	202°F	224°F	211°F	230°F	220°F
1.5	249°F	220°F	202°F	197°F	171°F	170°F	184°F	199°F	189°F	206°F	190°F	208°F	206°F	227°F	216°F	232°F	224°F
2.0	249°F	203°F	202°F	197°F	176°F	173°F	189°F	202°F	193°F	210°F	193°F	212°F	210°F	230°F	220°F	236°F	228°F
2.5	249°F	201°F	202°F	198°F	181°F	177°F	192°F	204°F	196°F	213°F	197°F	215°F	213°F	234°F	223°F	239°F	232°F
3.0	249°F	201°F	202°F	198°F	184°F	181°F	195°F	205°F	200°F	215°F	201°F	217°F	216°F	237°F	226°F	242°F	234°F

Table 22: Temperatures (°C) During the Post-Fire Transient with the SRS 3013 Configuration During Transport

Time (hr)	Drum Top	Bottom	Side	Mid-Height Fiberboard	SCV O-ring	PCV O-ring	SCV Side	SCV Bottom	PCV Side	PCV Bottom	3013 Top	3013 Bottom	3013 Side (mid height of contents)	Pu Can Interface (top)	Pu Can Interface (bottom)	Mid Pu (top)	Mid Pu (bottom)
0.0	787°C	734°C	774°C	77°C	68°C	73°C	73°C	79°C	83°C	87°C	86°C	88°C	92°C	106°C	94°C	109°C	99°C
0.5	121°C	174°C	102°C	87°C	70°C	74°C	77°C	86°C	84°C	90°C	86°C	91°C	93°C	106°C	96°C	109°C	101°C
1.0	121°C	129°C	95°C	90°C	74°C	75°C	81°C	90°C	85°C	94°C	86°C	95°C	94°C	107°C	99°C	110°C	104°C
1.5	121°C	105°C	95°C	91°C	77°C	76°C	84°C	93°C	87°C	97°C	88°C	98°C	96°C	108°C	102°C	111°C	107°C
2.0	121°C	95°C	95°C	92°C	80°C	78°C	87°C	94°C	89°C	99°C	90°C	100°C	99°C	110°C	104°C	113°C	109°C
2.5	121°C	94°C	95°C	92°C	83°C	81°C	89°C	95°C	91°C	100°C	92°C	101°C	101°C	112°C	106°C	115°C	111°C
3.0	121°C	94°C	94°C	92°C	84°C	83°C	90°C	96°C	93°C	102°C	94°C	103°C	102°C	114°C	108°C	117°C	112°C

Table 23: Temperatures (°F) During the Post-Fire Transient with the Food Can Configuration

Time (hr)	Drum Top	Bottom	Side	Mid-Height Fiberboard	SCV O-ring	PCV O-ring	SCV Side	SCV Bottom	PCV Side	PCV Bottom	Top of Upper Pu Can	Bottom of Lower Pu Can	Side of PCV Sleeve (mid height of contents)	Mid Pu (top can)	Mid Pu (bottom can)
0.0	1449°F	1353°F	1424°F	174°F	162°F	181°F	169°F	176°F	188°F	185°F	223°F	186°F	190°F	324°F	319°F
0.5	249°F	348°F	216°F	190°F	166°F	181°F	175°F	187°F	189°F	190°F	224°F	191°F	191°F	324°F	320°F
1.0	249°F	267°F	202°F	195°F	172°F	183°F	182°F	194°F	192°F	195°F	226°F	196°F	195°F	325°F	322°F
1.5	249°F	222°F	202°F	197°F	178°F	187°F	188°F	197°F	196°F	200°F	229°F	200°F	199°F	328°F	326°F
2.0	249°F	203°F	202°F	198°F	183°F	190°F	192°F	200°F	200°F	203°F	232°F	203°F	203°F	332°F	329°F
2.5	249°F	201°F	202°F	198°F	187°F	194°F	195°F	202°F	204°F	206°F	235°F	206°F	206°F	335°F	333°F
3.0	249°F	201°F	202°F	199°F	190°F	198°F	198°F	203°F	207°F	209°F	239°F	209°F	209°F	338°F	336°F

Table 24: Temperatures (°C) During the Post-Fire Transient with the Food Can Configuration

Time (hr)	Drum Top	Bottom	Side	Mid-Height Fiberboard	SCV O-ring	PCV O-ring	SCV Side	SCV Bottom	PCV Side	PCV Bottom	Top of Upper Pu Can	Bottom of Lower Pu Can	Side of PCV Sleeve (mid height of contents)	Mid Pu (top can)	Mid Pu (bottom can)
0.0	787°C	734°C	774°C	79°C	72°C	83°C	76°C	80°C	86°C	85°C	106°C	86°C	88°C	162°C	160°C
0.5	121°C	175°C	102°C	88°C	75°C	83°C	79°C	86°C	87°C	88°C	107°C	88°C	88°C	162°C	160°C
1.0	121°C	130°C	95°C	91°C	78°C	84°C	83°C	90°C	89°C	91°C	108°C	91°C	90°C	163°C	161°C
1.5	121°C	105°C	95°C	92°C	81°C	86°C	87°C	92°C	91°C	93°C	109°C	93°C	93°C	164°C	163°C
2.0	121°C	95°C	95°C	92°C	84°C	88°C	89°C	93°C	94°C	95°C	111°C	95°C	95°C	166°C	165°C
2.5	121°C	94°C	95°C	92°C	86°C	90°C	91°C	94°C	96°C	97°C	113°C	97°C	97°C	168°C	167°C
3.0	121°C	94°C	94°C	93°C	88°C	92°C	92°C	95°C	97°C	98°C	115°C	98°C	99°C	170°C	169°C

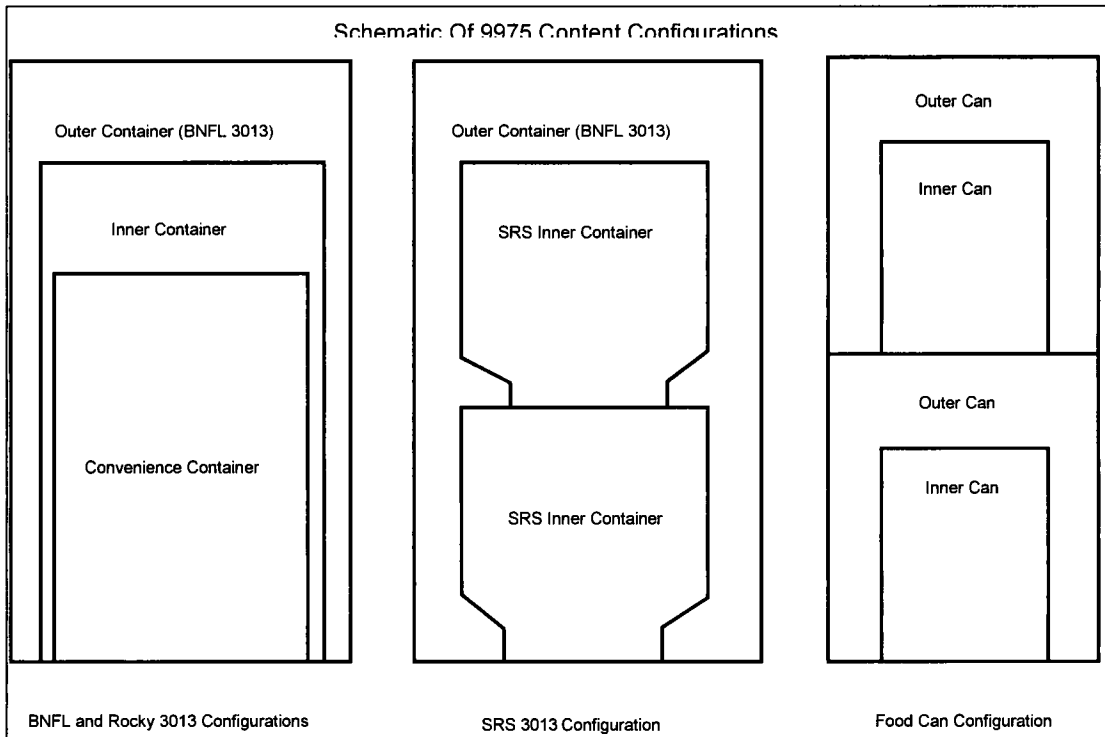


Figure 1. Schematic of 3013 and Food Can Configurations.

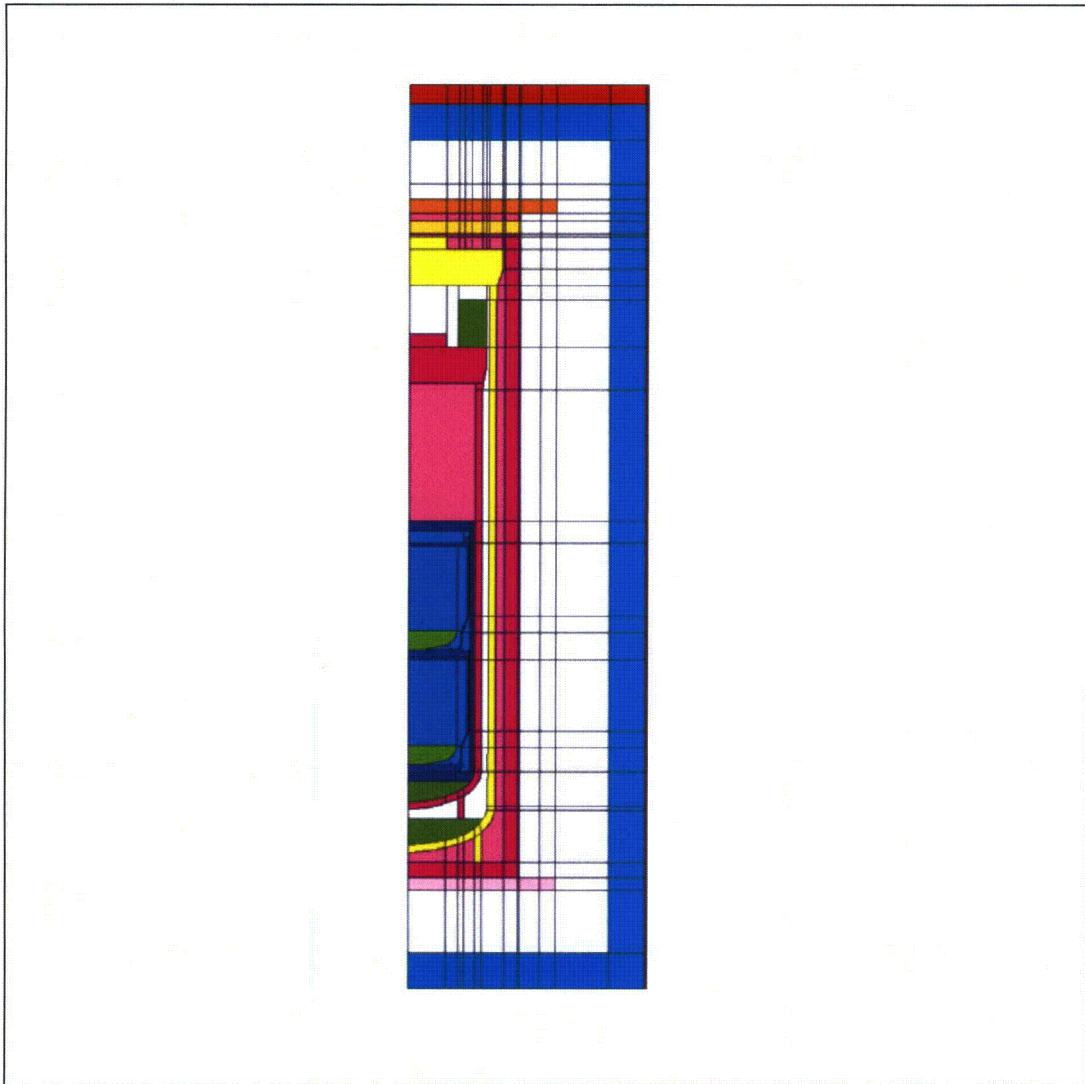


Figure 2. Color Representation of Material Location in SRS 3013 Configuration. (The mesh is not included).

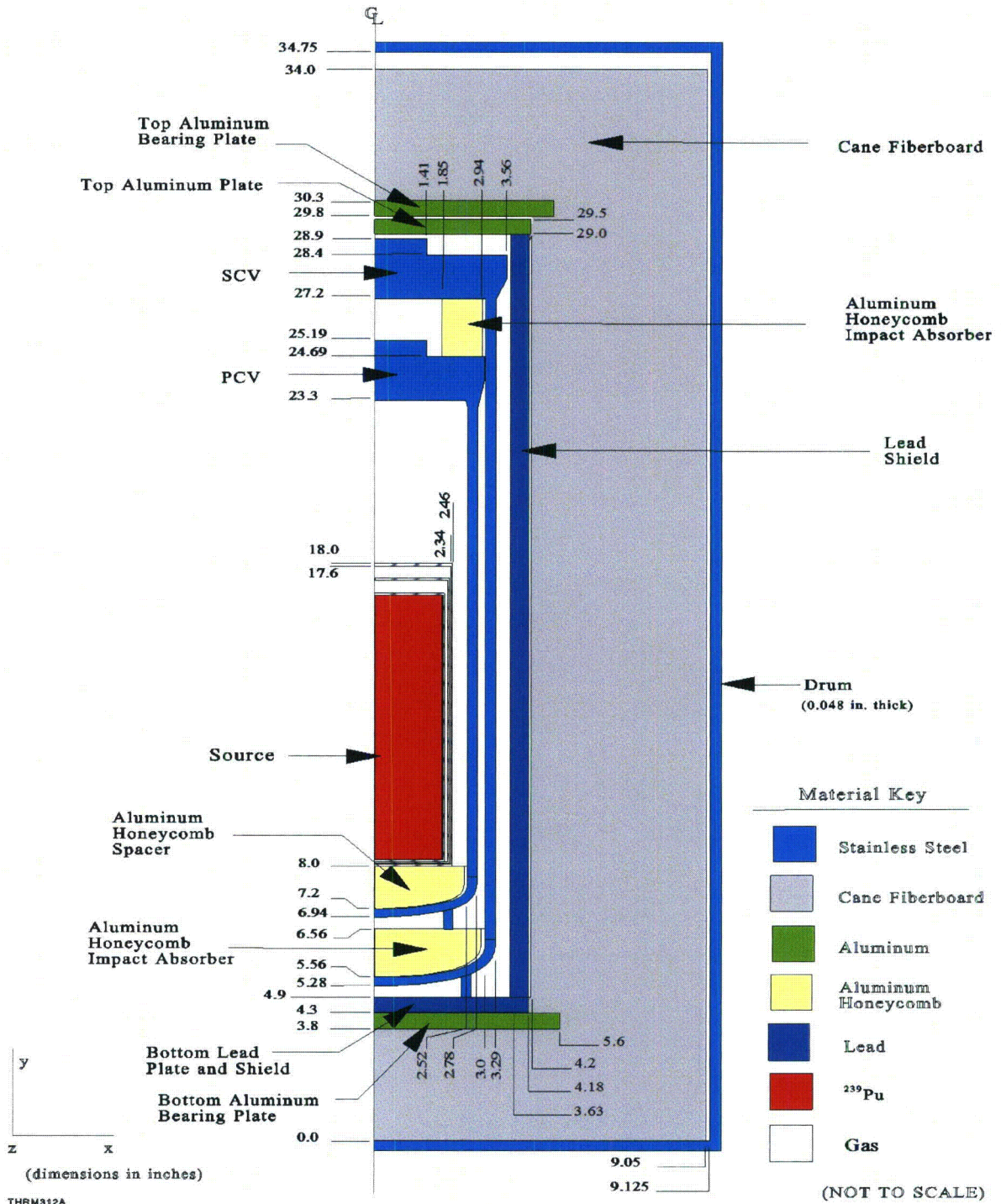


Figure 3. Schematic of 9975 package and contents for the BNFL 3013 Pu oxide configuration

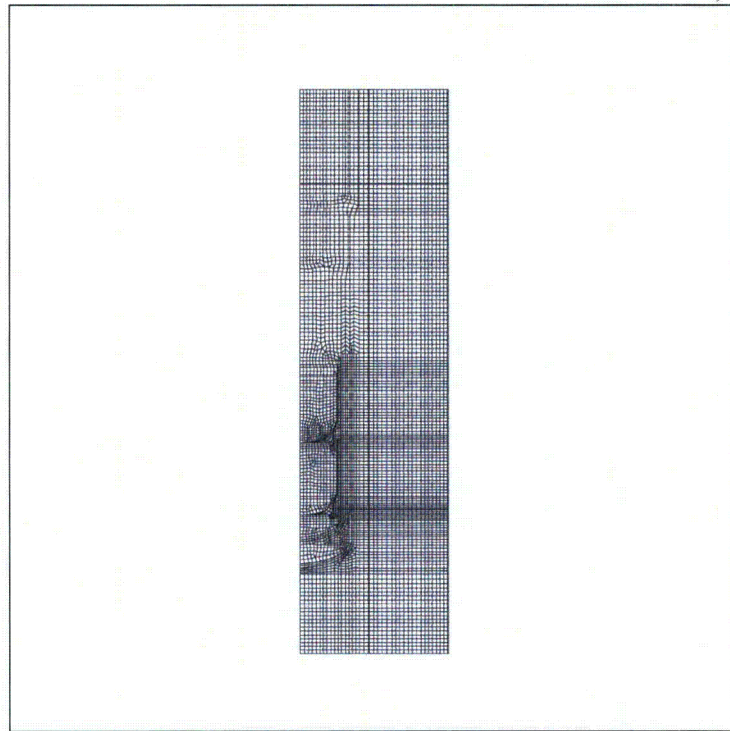


Figure 4. Typical mesh used in MSC/Thermal model.

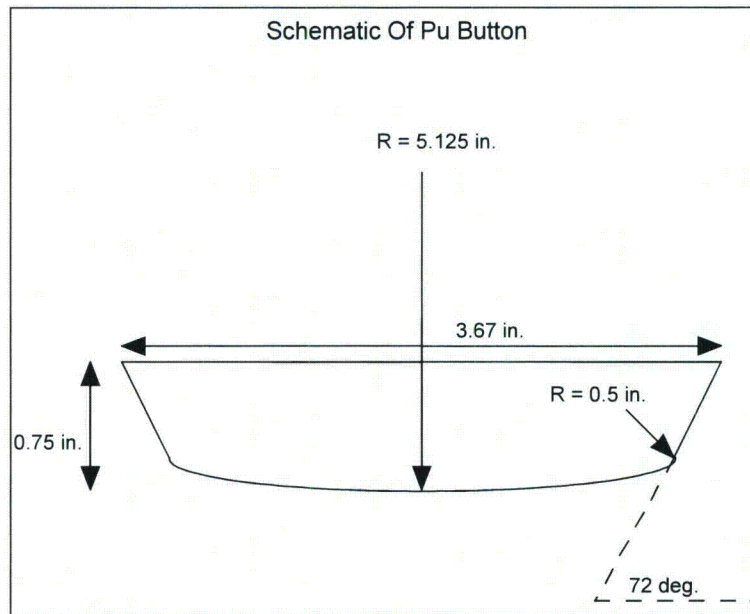


Figure 5. Schematic of Pu metal button.

Oxide Fire Transient

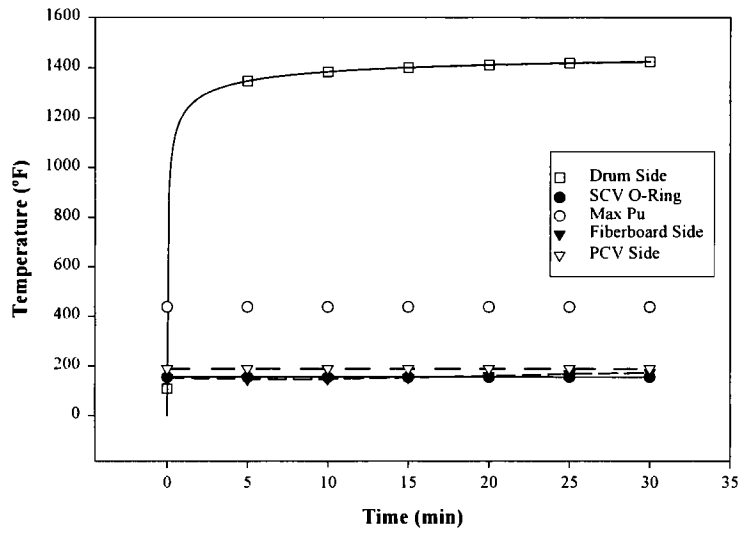


Figure 6. Temperature profile for the BNFL (Oxide) 3013 configuration fire transient.

Oxide Post-Fire Transient

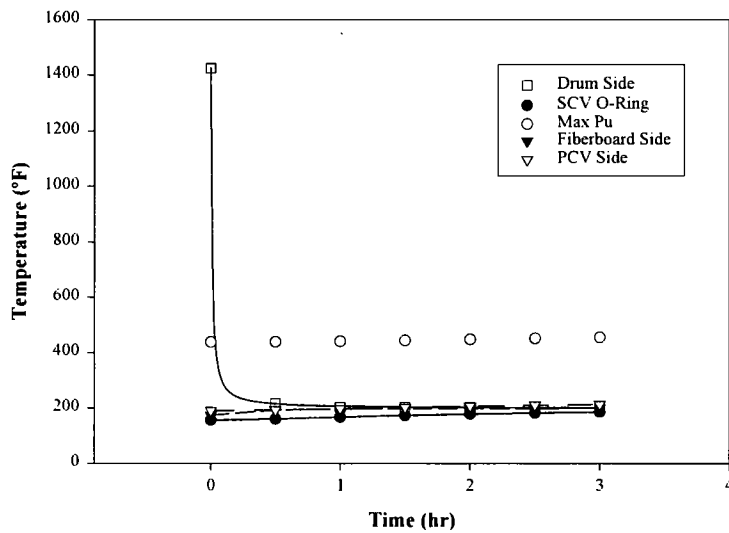


Figure 7. Temperature profile for the BNFL (Oxide) 3013 configuration post-fire transient.

Rocky Flats Fire Transient

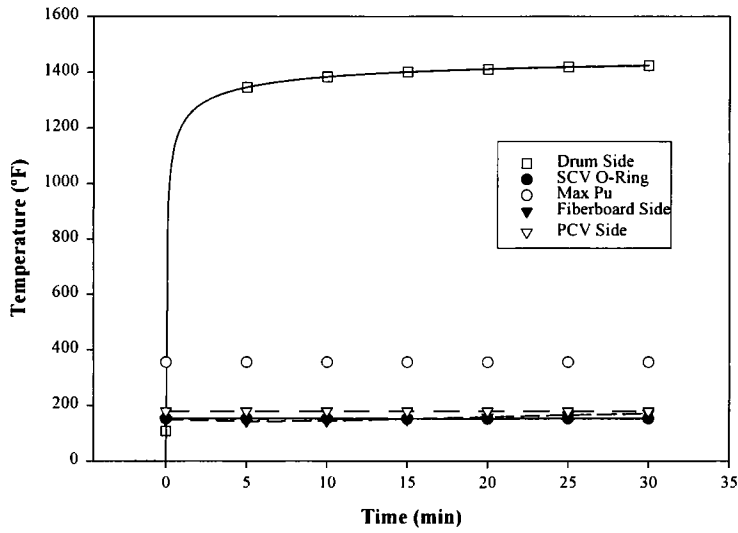


Figure 8. Temperature profile for the Rocky Flats 3013 configuration fire transient.

Rocky Flats Post-Fire Transient

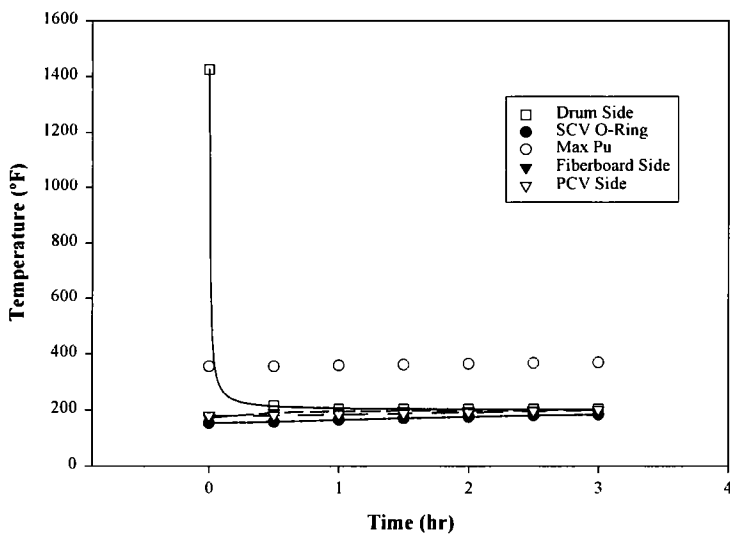


Figure 9. Temperature profile for the Rocky Flats 3013 configuration post-fire transient.

SRS (Bagless Transfer) Fire Transient

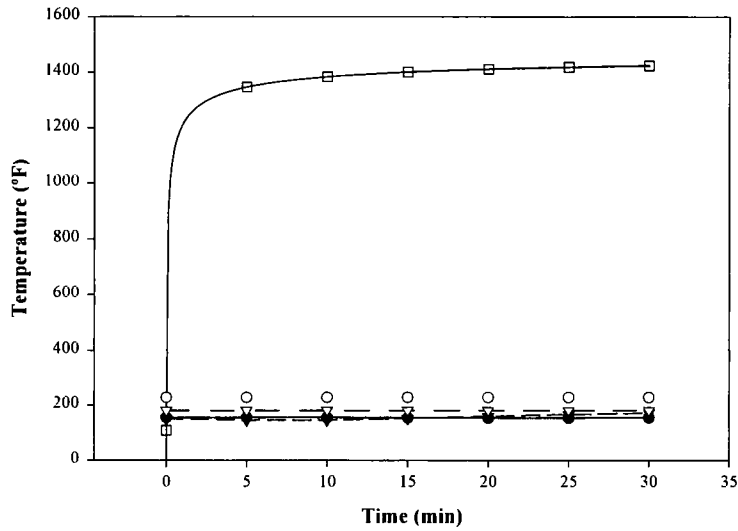


Figure 10. Temperature profile for the SRS 3013 configuration fire transient.
(For legends see Figure 9)

SRS (Bagless Transfer) Post-Fire Transient

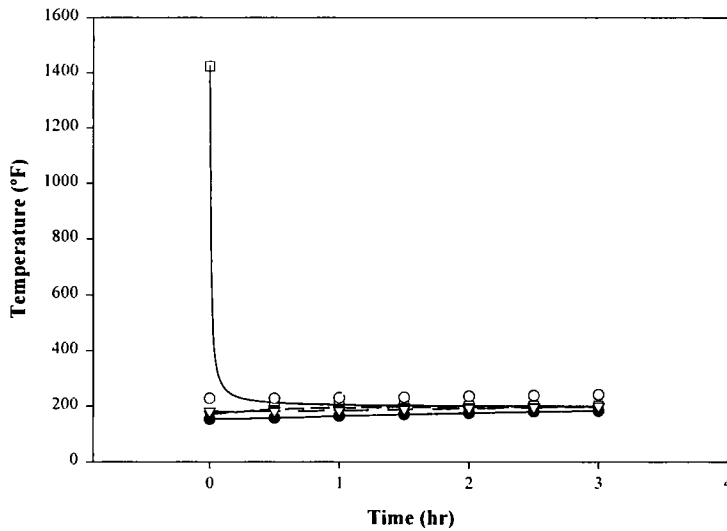


Figure 11. Temperature profile for the SRS 3013 configuration post-fire transient.
(For legends see Figure 9)

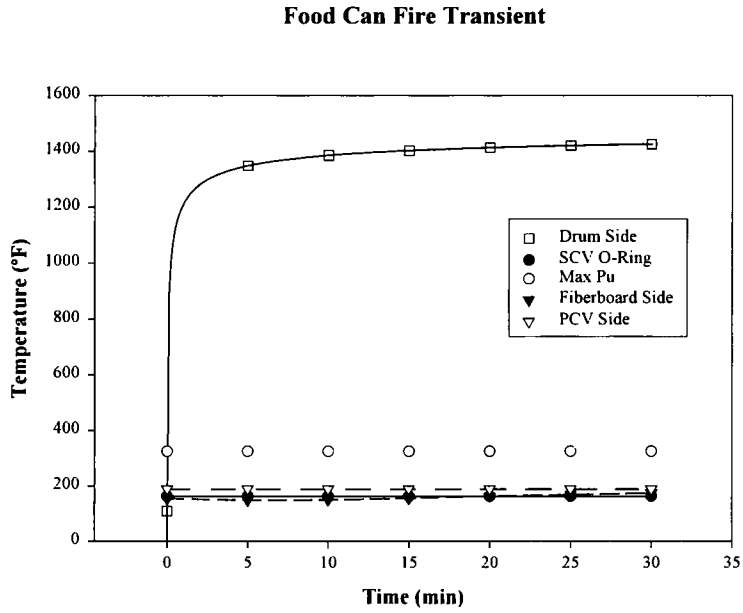


Figure 12. Temperature profile for the Food Can configuration fire transient.

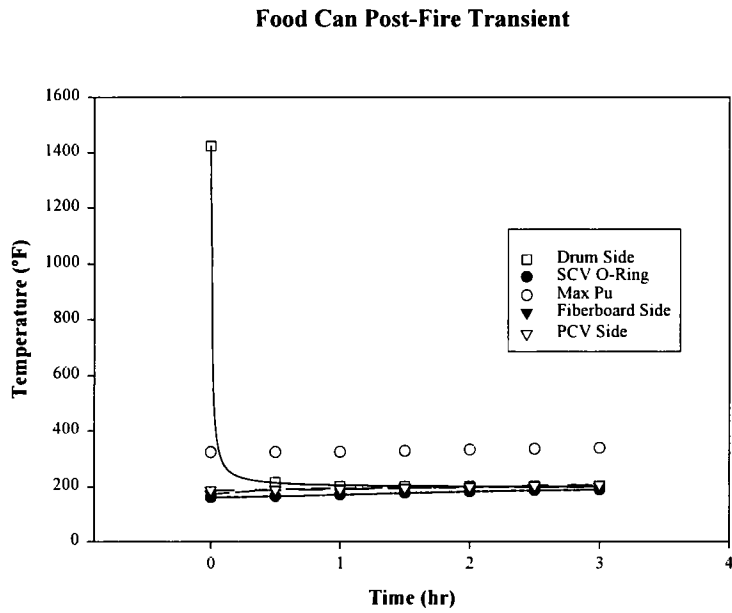


Figure 13. Temperature profile for the Food Can configuration post-fire transient.

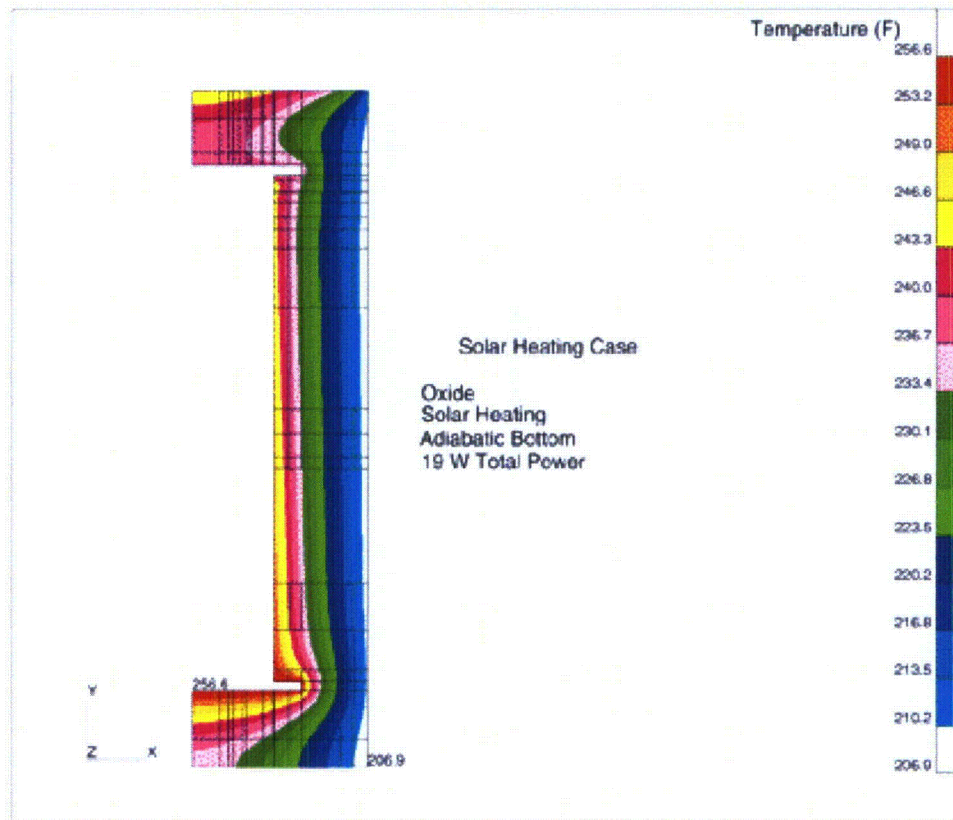


Figure 14. Fiberboard temperature profile for the BNFL (Oxide) configuration NCT. The locations of the maximum and minimum temperature are shown on the plot.

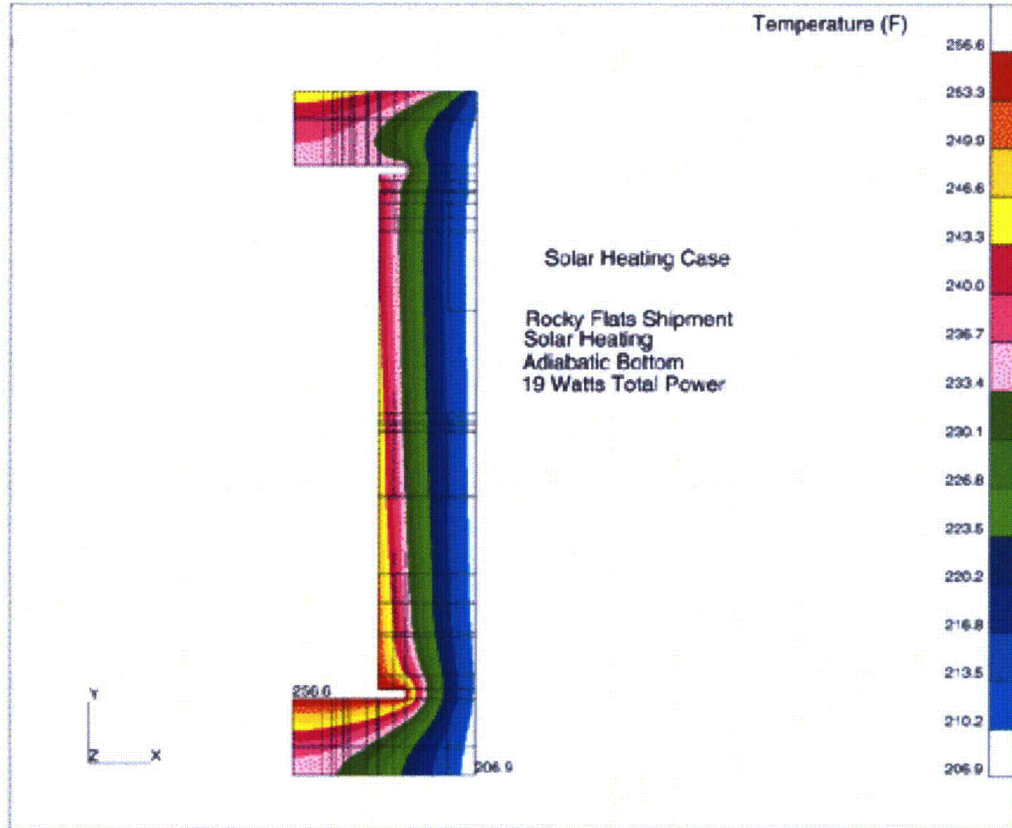


Figure 15. Fiberboard temperature profile for the Rocky Flats configuration NCT. The locations of the maximum and minimum temperature are shown on the plot.

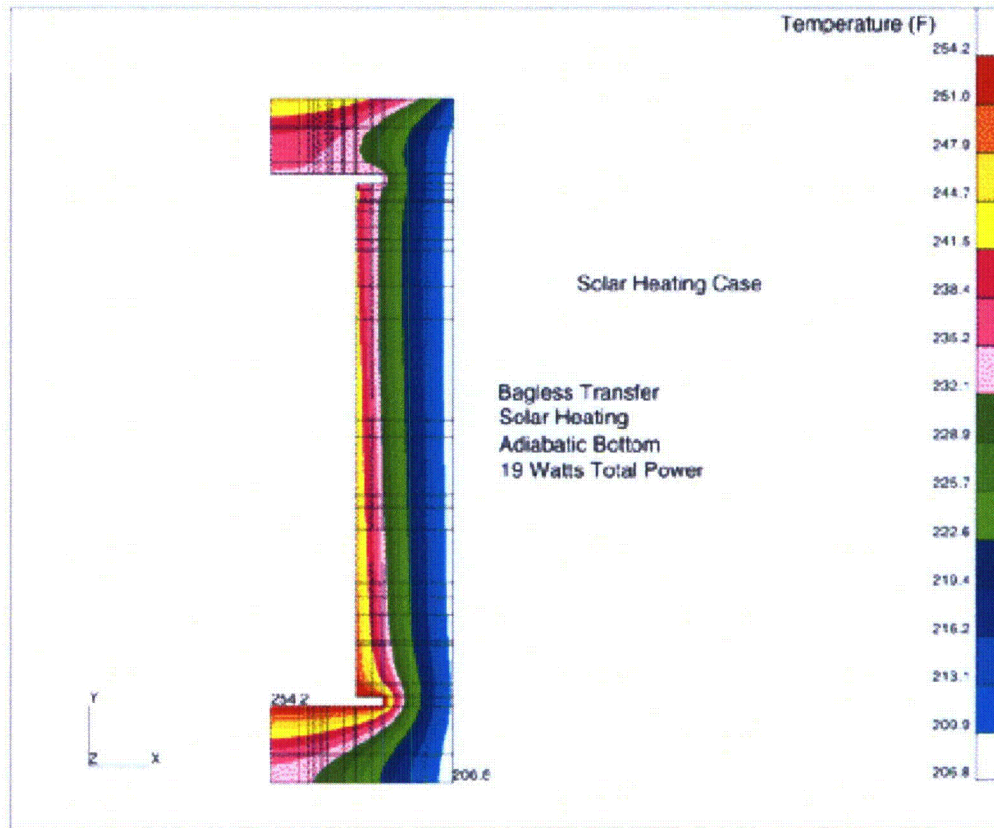


Figure 16. Fiberboard temperature profile for the SRS (Bagless Transfer) configuration NCT. The locations of the maximum and minimum temperature are shown on the plot.

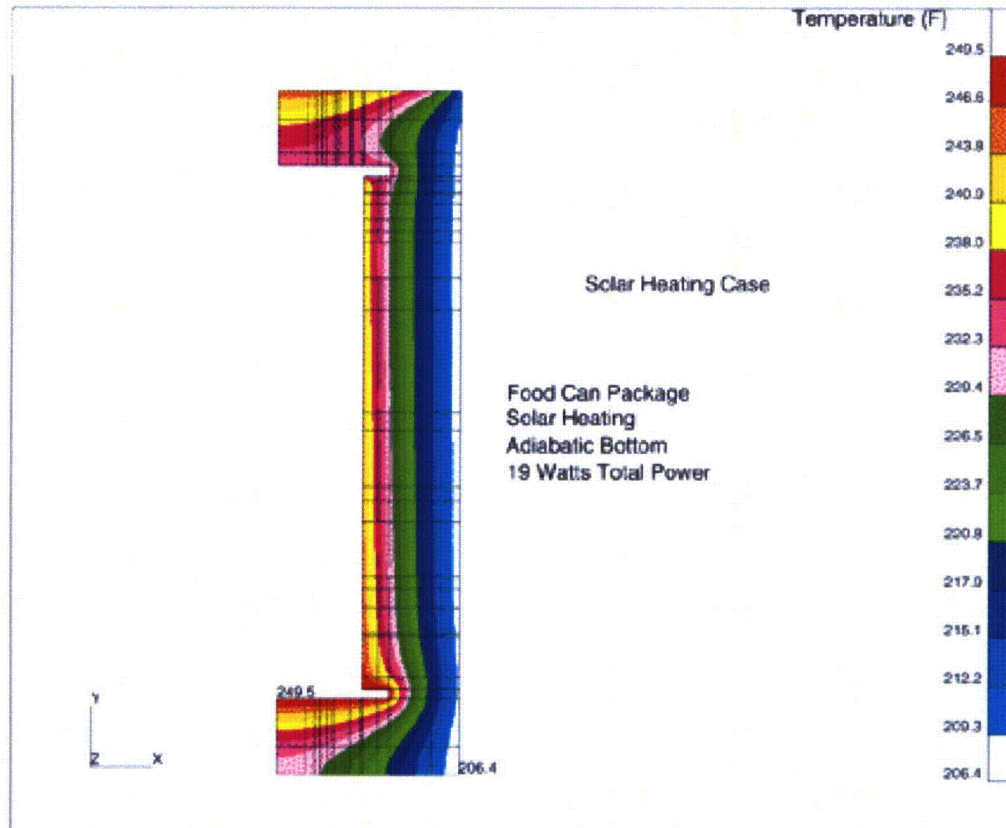


Figure 17. Fiberboard temperature profile for the Food Can configuration NCT. The locations of the maximum and minimum temperature are shown on the plot.

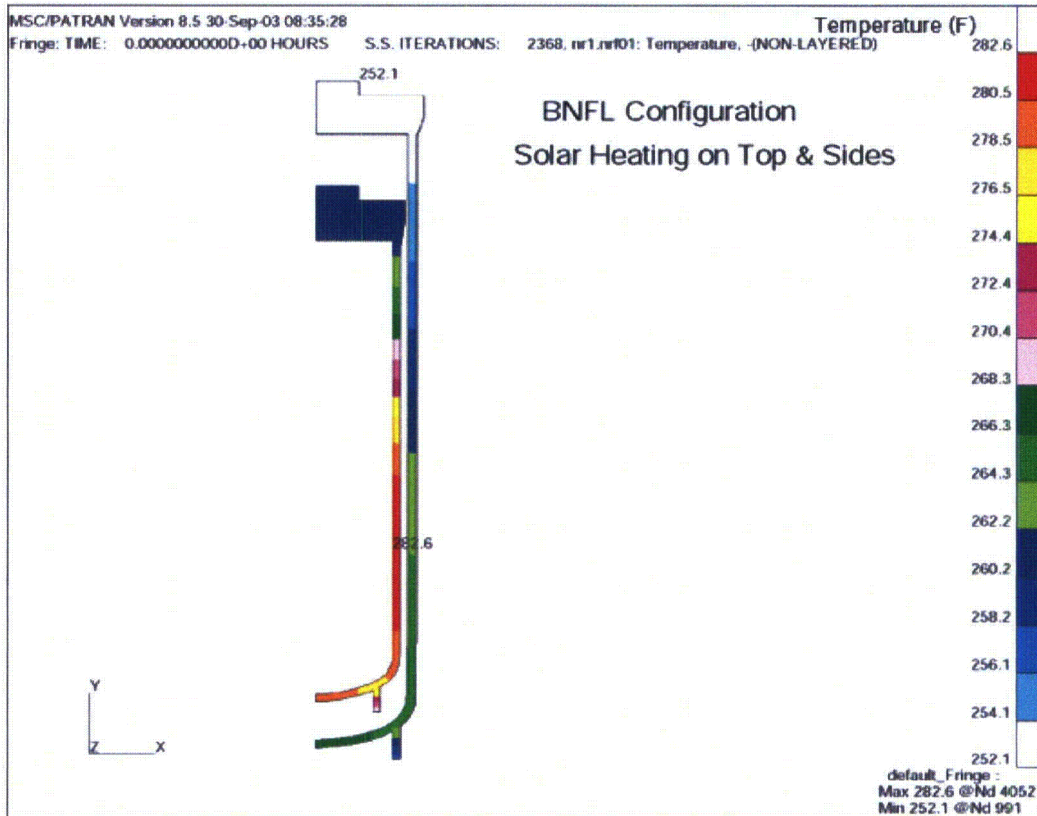


Figure 18. PCV/SCV Temperature Contours for the BNFL Configuration

5.0 References

1. Hensel, S. J., "Thermal Analyses Of The 9975 Package With the 3013 Configuration During Normal Conditions of Transport", WSRC-TR-98-00420.
2. Gray, L. W., "Kinetics Of The Ambient Temperature Dissolution Of Plutonium Metal In Sulfuric Acid", March 1978.
3. Jerrell, J. W., Van Alstine, M. N., and Gromada, R. J., Normal Conditions of Transport Thermal Analysis and Testing of a Type B Drum Package, PVP-Vol. 307, pp. 111-117.
4. Hensel, S. J., Van Alstine, M. N. and Gromada, R. J., "Hypothetical Accident Condition Thermal Analysis and Testing of a Type B Drum Package", ASME PVP Conference, PVP-Vol. 30, pp. 119-126, 1995.
5. MSC/Thermal, MacNeal-Schwendler Corporation, Los Angeles, CA 90041.
6. Gupta, N. K., "Validation of MSC/THERMAL Finite Element Software for Thermal Analysis at the Savannah River Site", G-VVR-G-00011, Rev. 0, 2001.
7. Westinghouse Savannah River Co., Conduct Of Engineering Manual, E-7, 1998.
8. Patran 8.5, MacNeal-Schwendler Corporation, Los Angeles, CA 90041.
9. Ingot Can Spacer Details and assembly, Rocky Flats Drawing No. 51651-9065 Rev. 0.


APPENDIX 3.4

**THE EFFECT OF A CELOTEX® GAP ON 9975 PACKAGE TEMPERATURES
DURING THE HAC-FIRE AND COOL-DOWN TRANSIENTS**

This Page Intentionally Left Blank

OSR 45-2# (Rev 10-28-93)

Calculation Cover Sheet

Project 9975 Packaging Certification		Calculation Number M-CLC-F-00667, Rev. 0	Project Number N/A 9975 ^{KC} 91100	
Title The Effect of a Celotex® Gap on the 9975 Package Temperatures During the Fire and Cooldown Transients (4)		Functional Classification SC	Sheet 1 of 15	
Discipline Mechanical				
<input type="checkbox"/> Preliminary <input type="checkbox"/> Committed <input checked="" type="checkbox"/> Confirmed				
Computer Program No. MSC/Thermal <input type="checkbox"/> N/A		Version/Release No. Version 8.5		
Purpose and Objective Calculate effect of gap in Celotex® on HAC fire transient temperatures.				
Summary of Conclusion The 9975 model with 1.38 inch Celotex® gap was run for the HAC fire transient including 4 hours of post fire cooling (with insulation). Even under the extremely conservative assumptions of the model, at no time did any components of the package closely approach their 9975 SARP (Rev. 10) temperature limits.				
Revisions				
Rev No.	Revision Description			
0	Original issue			
Sign Off				
Rev No.	Originator (Print) Sign/Date	Verification/ Checking Method	Verifier/Checker (Print) Sign/Date	Manager (Print) Sign/Date
	Bruce Hardy Pete Hardy 8/24/00		Steve Hensel Steve Hensel 8/24/00	C.B. HOLDING-SMITH C.B. Holding-Smith 8/24/00
Classification unclassified				
UNCLASSIFIED DOES NOT CONTAIN UNCLASSIFIED CONTROLLED TECHNICAL INFORMATION Bruce J. Hardy (Bruce J. Hardy) Fellow Engineer 8/24/00				
ENGINEERING DOC. CONTROL - SRS  00476620				

THE EFFECT OF A CELOTEX[®] GAP ON THE 9975 PACKAGE TEMPERATURES DURING THE FIRE AND COOL DOWN TRANSIENTS

1.0 Summary And Conclusions

As part of the Hypothetical Accident Conditions (HAC), 10 CFR 71.73 requires sequential tests in which a package is subjected to a fire with a flame temperature of 1475°C for 30 minutes. Following a drop test^[1] at Westinghouse Savannah River Company (WSRC), radiographs of a 9975 drum package showed that radial separations had formed in the Celotex[®]^[2]. The maximum radial gap observed in the radiographs was less than 1/8 inch thick. Because the Celotex[®] acts as a thermal insulator, concerns arose as to the effect gaps in the overpack would have on the packaging components during and after the fire transient. The importance of Celotex[®] gaps was investigated through the use of a thermal model and a transient fire thermal analysis.

The highest 9975 temperatures occur for Normal Conditions of Transport (NCT) for the Pu Oxide SRS food can configuration^[3]. For this reason, the 9975 package model with the SRS food can configuration was used as the basis for the calculations that address the thermal impact of gaps in the Celotex[®]. The components having the most significant affect on heat transfer during the fire and post-fire phases are the Celotex[®], the lead shield and the secondary containment vessel (SCV).

Celotex[®] sheets are oriented in layers normal to the axis of the drum. Hence, gaps produced from the drop test tend to be at small angle from the radial direction. From available radiographs, the gaps appear to subtend azimuthal angles much less than 360°. It has been estimated that the sum of all gap thicknesses will be less than 1 inch. This fact is important because attenuation of thermal radiation increases as the gap thickness decreases and as the angle of the gap to the radial direction increases. Due to uncertainties in the geometry of the gaps, an extremely conservative representation was used to bound the thermal model. The model assumed a gap that was 1.38 inch thick, extending over a 360° azimuthal angle (full circumference) and parallel to the radial direction.

The 9975 model with 1.38 inch Celotex[®] gap was run for the HAC fire transient including 4 hours of post fire cooling (with insolation). Even under the extremely conservative assumptions of the model, at no time did any components of the package closely approach their 9975 SARP (Rev. 10) temperature limits. The maximum package temperatures with their limits are listed in the following table.

Package Feature	Maximum Computed Temperature	SARP Thermal Limit
Lead	428°F	625°F
PCV	215°F	300°F
SCV	218°F	300°F
PCV air	244°F	313°F
SCV air	209°F	313°F

The thermal analysis supported the expectation that small separations in the fiberboard insulation will not degrade the thermal performance of the 9975 package in an HAC fire.

2.0 Model Description

2.1 Geometry, Mesh and Material Properties

The model was developed with the MSC/THERMAL[®] heat transfer software with the MSC/PATRAN[®] pre and post-processor^[4]. The package was modeled in 2-dimensions, radial and axial, as a body of rotation. The model had 7153 nodes and 7247 elements. The material location is shown in Figure 1.

The constitutive properties of the materials and the component dimensions, other than the gap, are given in Reference 3. The material configuration of the model is shown in Figure 1.

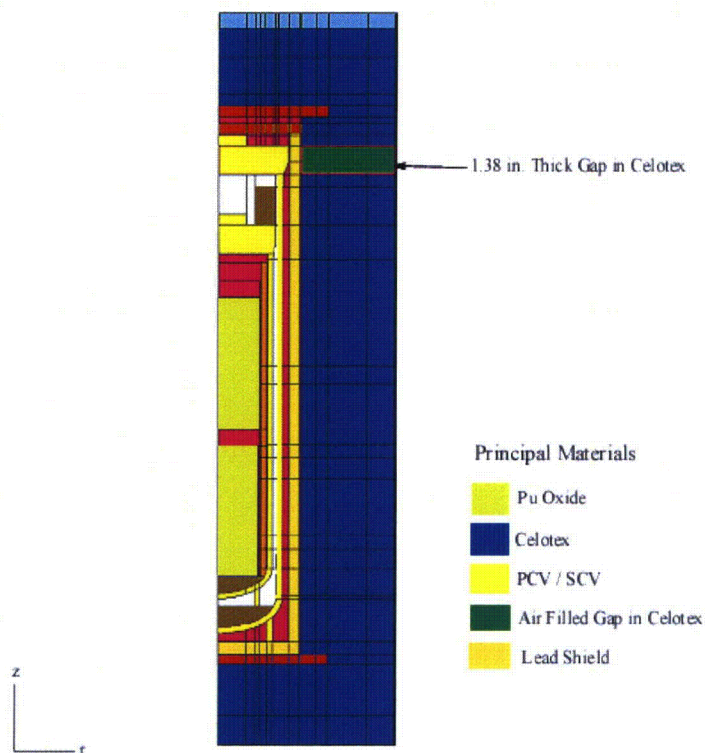


Figure 1. Material configuration for 2D (r-z) model.

The thermal model for the gap was a modification of the model used for the SRS Food can package configuration, see Reference 3. The gap was represented by replacing a 1.38 in. thick section of Celotex[®], as shown in Figure 1, with air. Thermal radiation and conduction were modeled within the gap, which extended from the inner surface of the drum to the lead radiation shield. As in Reference 3, convection within the cavities of the package was neglected.

2.2 Thermal Calculations

As the Celotex[®] is heated, it will release gasses and volatile species that may cause the gas space in the gap to have a much lower transmissivity than air. If the transmissivity of the gas is reduced during the transient, it will attenuate the radiation falling on the lead shield. Therefore, as a conservatism, the transmissivity of the gas in the gap is set to 1.

The accumulation of compounds released from the Celotex[®] during heating, as well as surface oxidation, will increase the emissivity of the inner surface of the drum. This will result in increased thermal radiation emitted from the inner surface of the drum to the lead surface across the gap. Hence, as a conservative measure, the emissivity of the drum surface facing the gap was increased from 0.3 to 0.9 during the fire transient.

Conversely, a lower emissivity on the inner surface of the drum adjacent to the gap will reduce the rate at which the lead cools. Therefore, the emissivity of the inner surface of

the drum, across from the gap, was reduced from 0.9 to 0.3 for the cool down phase of the post-fire transient.

Lead emissivity varies from 0.28 for a gray, oxidized surface to 0.63 for an oxidized surface at 300°F. To be conservative, for the lead surface facing the gap an emissivity of 0.7 was used during the fire transient and an emissivity of 0.28 was used for the post-fire cool down.

Thermal calculations were performed for the HAC fire transient discussed in Reference 3. The HAC fire transient consists of three phases, the initial phase, the fire phase and the post-fire phase. The conditions for the three phases are given below.

For the initial phase of the HAC:

1. The drum is in an upright position.
2. The bottom surface is adiabatic.
3. There is radiation heat transfer from the sides and top of the drum to the ambient.
4. There is natural convection heat transfer from the drum sides and top to the ambient. Convection coefficients were obtained from correlations for natural convection in MSC/THERMAL[®].
5. The ambient temperature is 100°F.
6. No insolation.
7. Undamaged Celotex[®] properties are applied to all the Celotex[®] in the drum.
8. 19 watts total decay power.
9. Emissivity of drum facing the gap is 0.3.
10. Emissivity of the lead facing the gap is 0.28.

For the fire phase of the HAC (duration 0.5 hour):

1. Restart from temperature profile in initial phase.
2. The drum is in an upright position.
3. There is forced convection from all surfaces of the drum. The convection coefficients, based on a 20 m/s air velocity, are:
 - i. 5.9 Btu/hr-ft² °F for the top and bottom of the drum.
 - ii. 3.0 Btu/hr-ft² °F for the side of the drum.
4. There is thermal radiation heat transfer from all surfaces of the drum to the ambient.
5. The ambient temperature is 1475°F.
6. No insolation.
7. Fire phase Celotex[®] properties are applied to all the Celotex[®] in the drum^[3].
8. 19 watts total decay power.
9. External drum surface emissivity of 0.9.
10. Emissivity of drum facing the gap is 0.9.
11. Emissivity of the lead facing the gap is 0.7.

For the fire post-fire phase of the HAC (duration 4 hours):

1. Restart from temperature profile at end of fire phase.
2. The drum is in an upright position.
3. There is thermal radiation from the top, sides and bottom of the drum to the ambient.
4. There is natural convection from the top and sides of the drum to the ambient. Convection coefficients were obtained from correlations for natural convection in MSC/Thermal.
5. The ambient temperature is 100°F.
6. Insolation: 800 W/m² on drum top and 400 W/m² on drum side (solar absorptivity of the drum assumed unity).
7. "Char layer" properties are applied to the outer 1.4 inch layer of the top, bottom and sides of the Celotex[®] contained in the drum^[3].
8. Fire phase properties are applied to the all Celotex[®] not in the 1.4 inch outer layer^[3].
9. 19 watts total decay power.
10. Emissivity of drum facing the gap is 0.3.
11. Emissivity of the lead facing the gap is 0.28.

3.0 RESULTS

The temperature profile prior to the start of the fire phase is shown in Figure 2. The temperature profile at the end of the fire phase (0.5 hours of a 1475°F fire) for the package is shown in Figure 3. Figure 4 shows the temperature profile in the lead and SCV at this time. The temperature profile in the package after 30 minutes of post fire cooling is shown in Figure 5, the profile in the lead and SCV at this time is shown in Figure 6.

Transient temperatures for the 30 minute fire phase, along with the limiting temperatures for each component are given in Table 1. The limiting temperatures listed in Tables 1 and 2 were given by the Radioactive Materials Packaging and Technology Group. The post-fire temperature in Table 1 are plotted in Figures 7 and 8.

Transient temperatures for 4 hours after the end of the fire phase, along with the limiting temperatures for each component are given in Table 2. The post-fire temperature in Table 2 are plotted in Figures 9 and 10.

The model for the gap was run for the HAC fire transient of Reference 3. Even under the extremely conservative assumptions of the model, at no time did any components of the package closely approach their temperature limits.

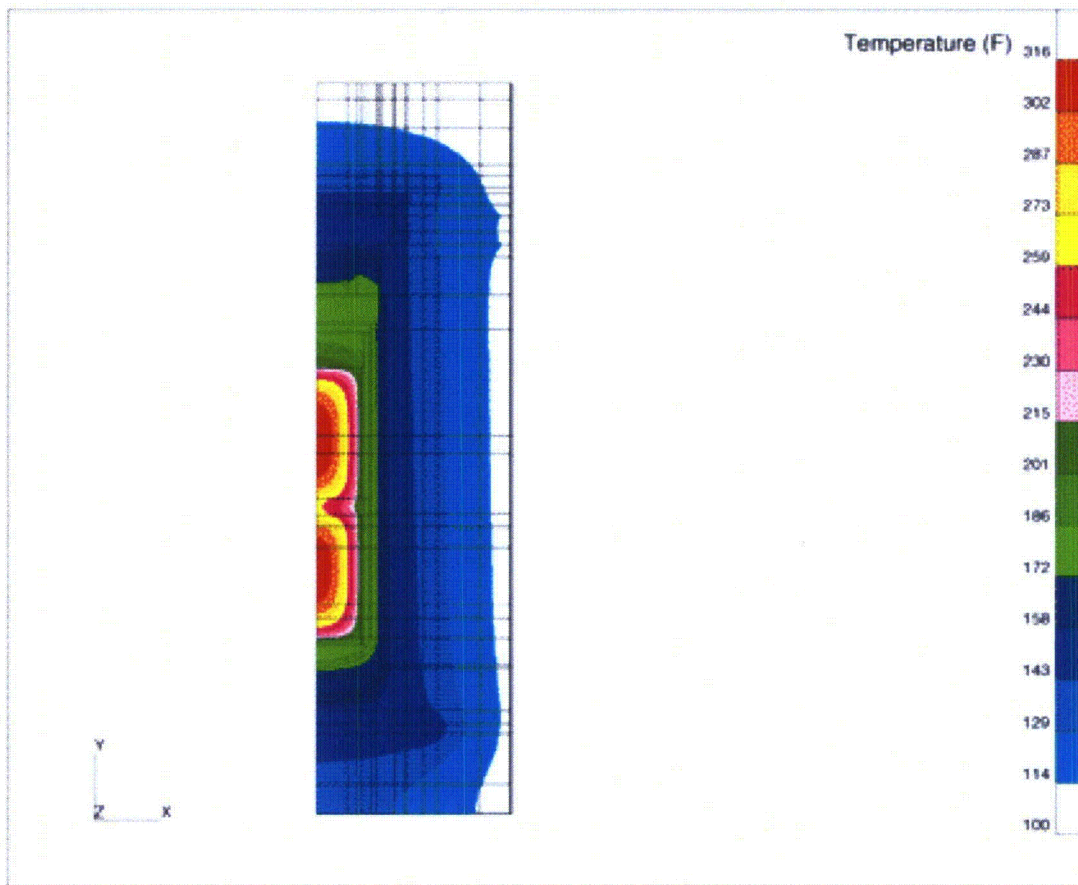


Figure 2. Temperature profile for the package prior to the fire phase.

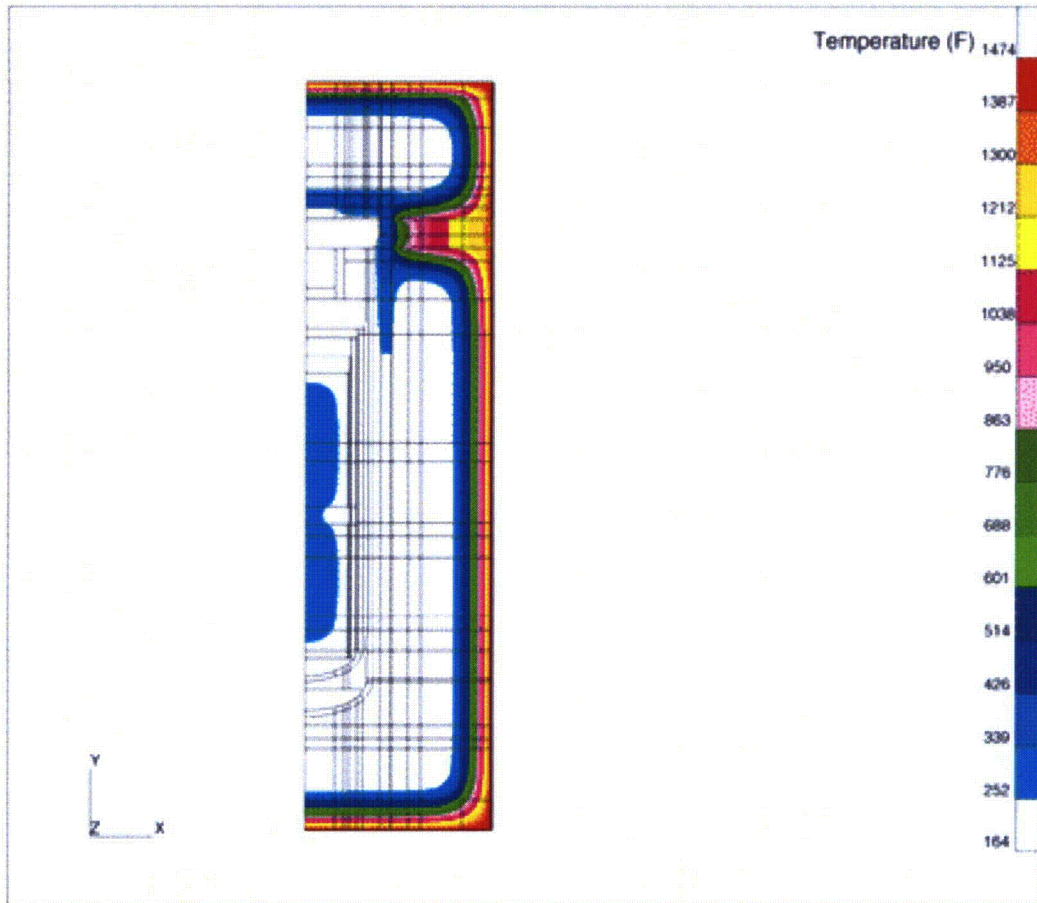


Figure 3. Temperature profile for the package after exposure to the 0.5 hr fire.

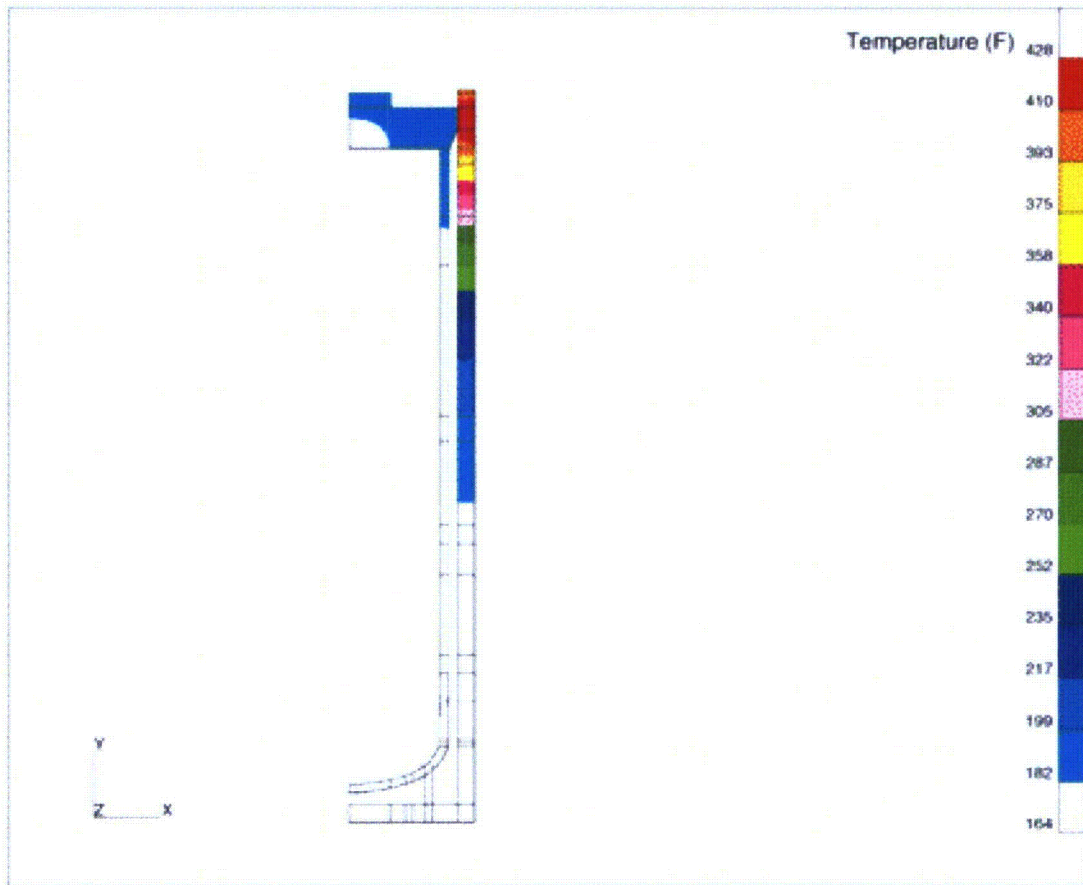


Figure 4. Temperature profile for lead shield and Secondary Containment Vessel (SCV) after exposure to the 0.5 hr fire.

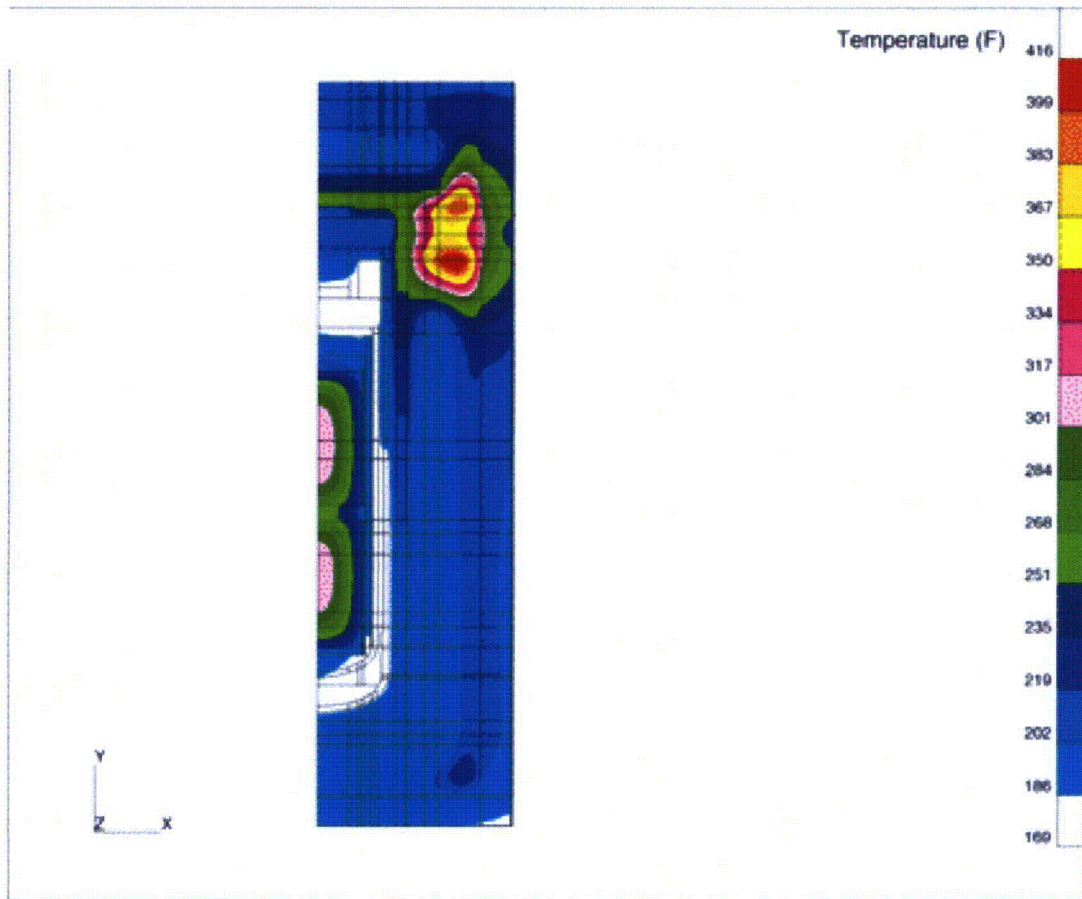


Figure 5. Temperature profile for the package 30 min. into the post-fire transient.

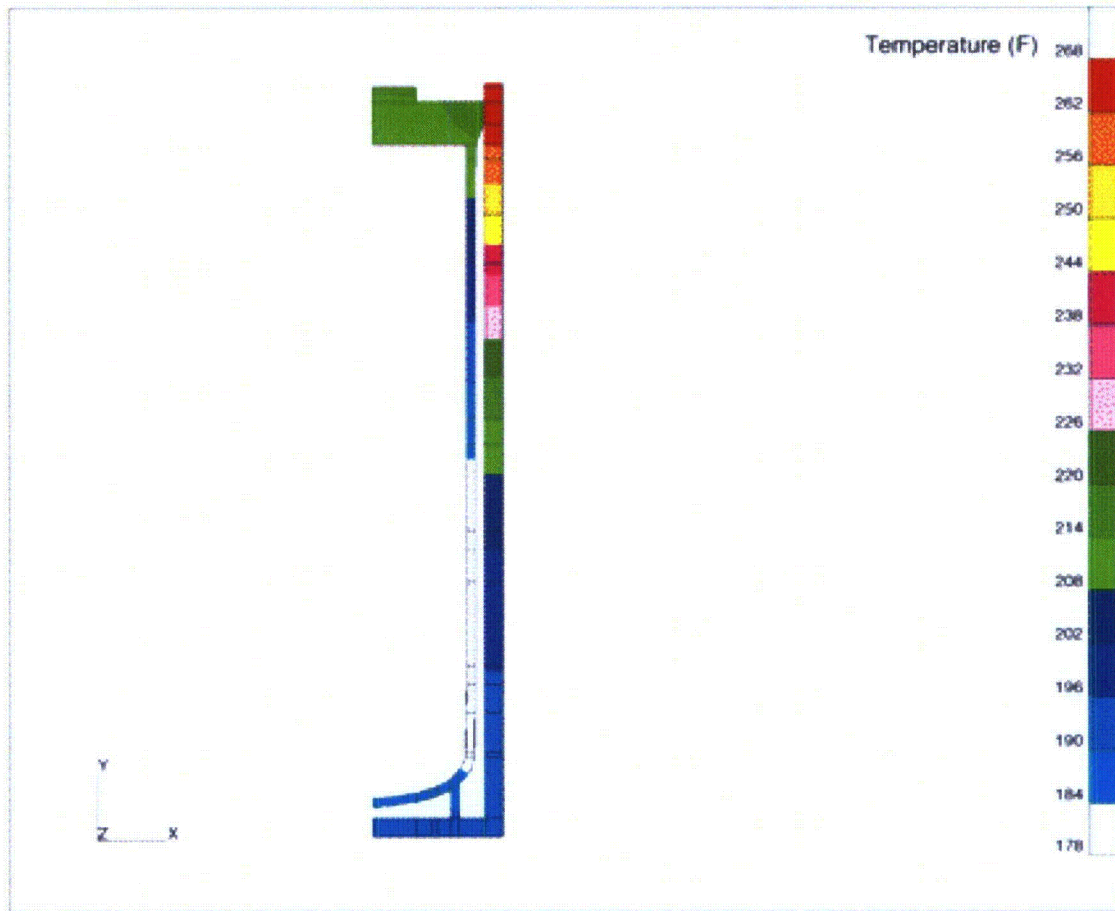


Figure 6. Temperature profile for lead shield and Secondary Containment Vessel (SCV) 30 min. into the post-fire transient.

Table 1
Temperatures for fire transient.

	Limit	Initial State	5 min	10 min	15 min	20 min	25 min	30 min
SCV O-Ring (Node 1255)	400 °F	155 °F	156 °F	159 °F	164 °F	171 °F	179 °F	190 °F
PCV O-Ring (Node 1890)	400 °F	173 °F	173 °F	173 °F	174 °F	174 °F	175 °F	175 °F
Max SCV	300 °F	165 °F	165 °F	165 °F	168 °F	176 °F	185 °F	197 °F
Max PCV	300 °F	180 °F	180 °F	180 °F	180 °F	180 °F	180 °F	181 °F
Max Lead	620 °F	146 °F	202 °F	251 °F	301 °F	349 °F	391 °F	428 °F
Max SCV Air	313 °F	172 °F	172 °F	172 °F	172 °F	173 °F	175 °F	176 °F
Max PCV Air	313 °F	212 °F	212 °F	212 °F	212 °F	212 °F	212 °F	212 °F
Max Component & Location	-	317 °F Pu Oxide	317 °F Pu Oxide	317 °F Pu Oxide	317 °F Pu Oxide	349 °F Lead Shield	391 °F Lead Shield	428 °F Lead Shield

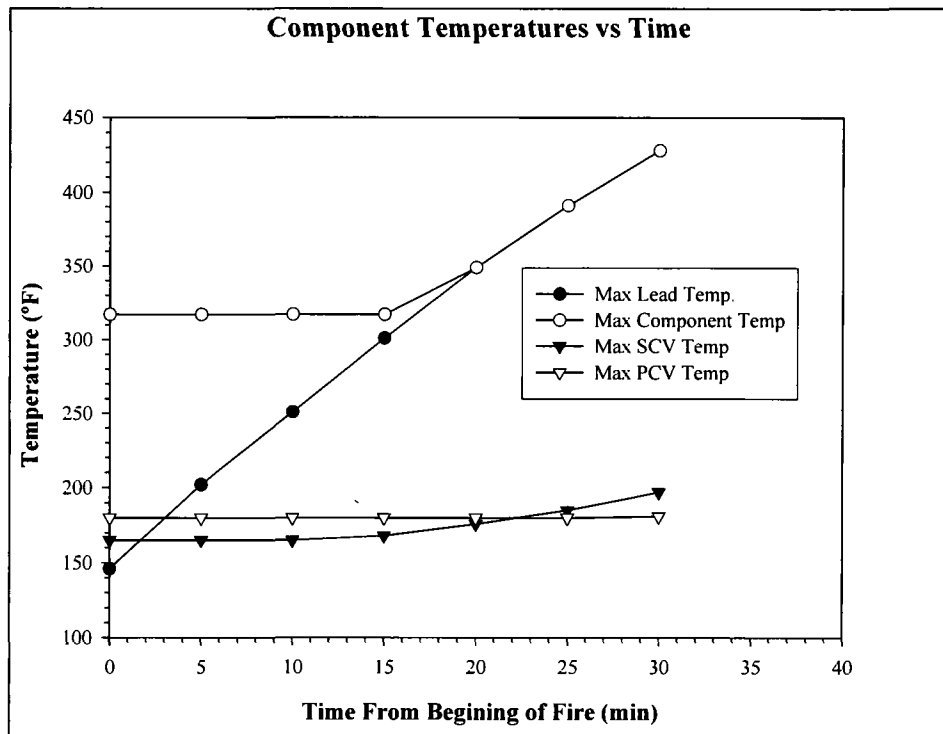


Figure 7. Maximum component temperatures for the 30 minute fire transient.

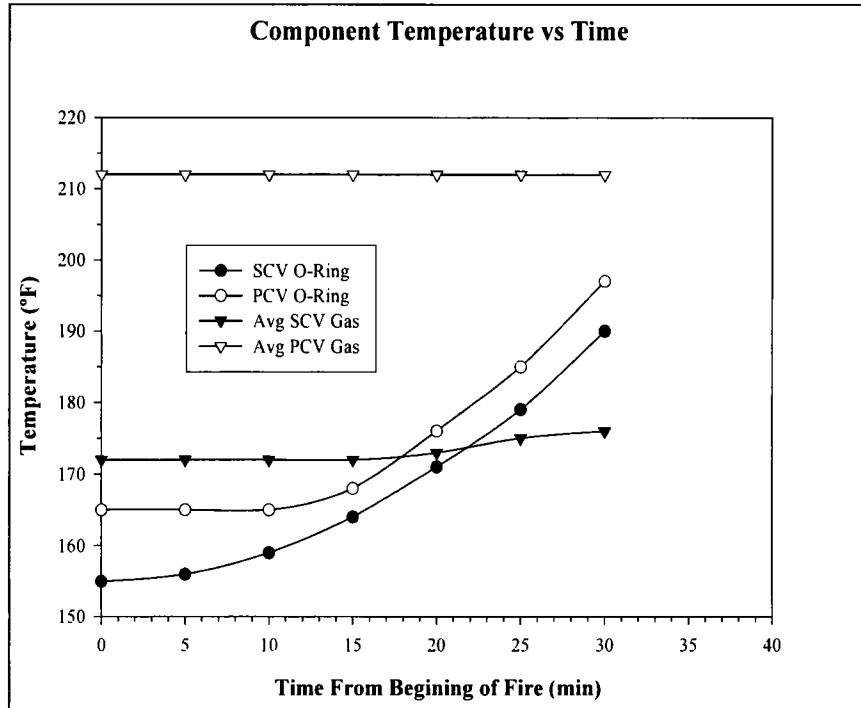


Figure 8. Component temperatures for the 30 minute fire transient.

Table 2
Temperatures for post-fire transient.

	Limit	End of Fire	10 min	20 min	30 min	40 min	50 min	1 hr	2 hr	3 hr	4 hr
SCV O-Ring (Node 1255)	400 °F	190 °F	203 °F	211 °F	215 °F	216 °F	217 °F	217 °F	213 °F	208 °F	206 °F
PCV O-Ring (Node 1890)	400 °F	175 °F	178 °F	180 °F	183 °F	186 °F	188 °F	191 °F	202 °F	208 °F	212 °F
Max SCV	300 °F	197 °F	207 °F	213 °F	216 °F	218 °F	218 °F	218 °F	214 °F	209 °F	206 °F
Max PCV	300 °F	181 °F	182 °F	184 °F	186 °F	189 °F	192 °F	194 °F	206 °F	212 °F	215 °F
Max Lead	620 °F	428 °F	336 °F	293 °F	268 °F	252 °F	242 °F	234 °F	213 °F	204 °F	202 °F
Max SCV Air	313 °F	176 °F	180 °F	184 °F	187 °F	190 °F	193 °F	195 °F	204 °F	206 °F	209 °F
Max PCV Air	313 °F	212 °F	213 °F	214 °F	216 °F	218 °F	220 °F	223 °F	234 °F	241 °F	244 °F
Max Component & Location	-	428 °F Lead Shield	317 °F Pu Oxide	317 °F Pu Oxide	318 °F Pu Oxide	318 °F Pu Oxide	320 °F Pu Oxide	321 °F Pu Oxide	334 °F Pu Oxide	343 °F Pu Oxide	348 °F Pu Oxide

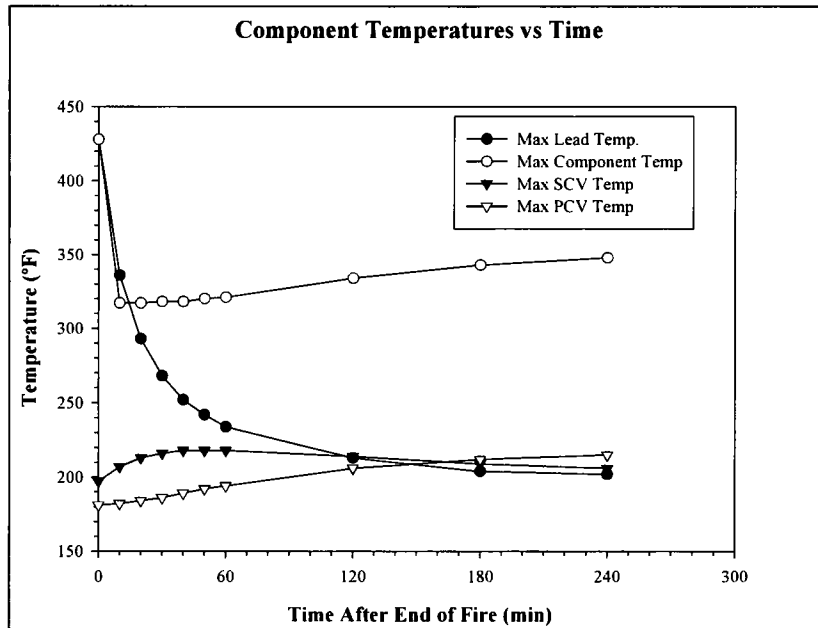


Figure 9. Maximum component temperatures for the 4 hours following the fire.

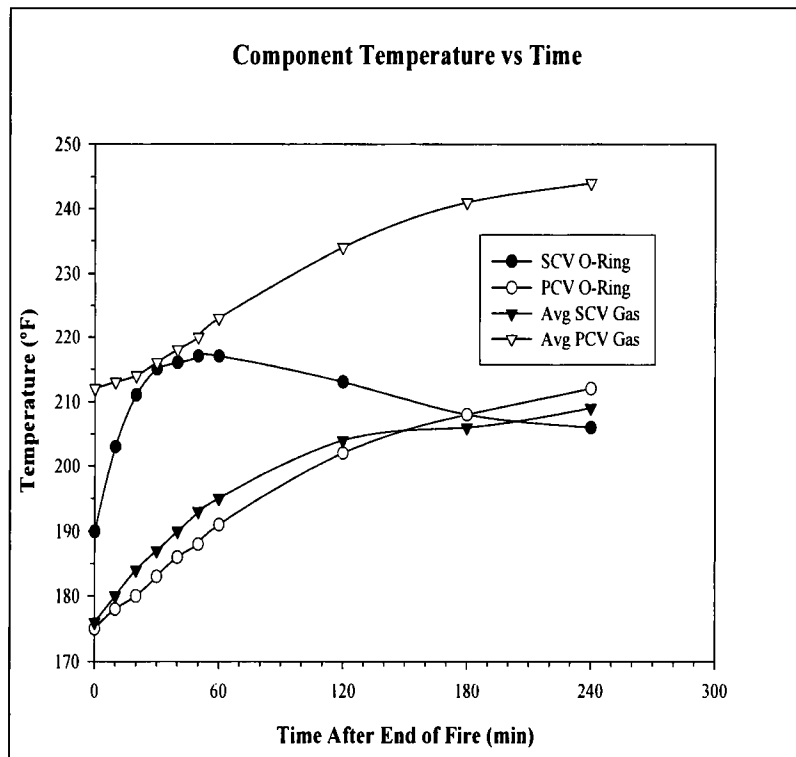


Figure 10. Component temperatures for the 4 hours following the fire.

5.0 REFERENCES

1. A.C. Smith. *Drop Tests of the Closure Ring for the 9975 Package*. Westinghouse Savannah River Company document, WSRC-TR-2000-00140 (2000).
2. B. Howard and D. Immel. *Radiography of a 9975 Shipping Container; Drop Test #4*. Westinghouse Savannah River Company document, SRT-IES-2000-034 (2000).
3. B. J. Hardy, S. J. Hensel. *Thermal Analysis of the 9975 Package for Normal Conditions of Transport and Accident Conditions*. Westinghouse Savannah River Company document, M-CLC-F-00590, Rev. 2 (1999).
4. MSC/PATRAN[®] and MSC/THERMAL[®] are licensed software from the MacNeal Schwendler Corporation.

This Page Intentionally Left Blank

APPENDIX 3.5
9973 AND 9975 PACKAGING HAC THERMAL TEST REPORT

This Page Intentionally Left Blank

**WESTINGHOUSE SAVANNAH RIVER COMPANY
INTER-OFFICE MEMORANDUM**SRT-PTG-94-0058
Page 1 of 58

July 25, 1994

TO: 730-A FILE ROOM
PROJECT FOLDER 22381 (QA/RIDS 4814))FROM: *MNA*
MARK N. VAN ALSTINE, 773-53AREVIEWED: *GC*
G. CADELLI, 773-53A**9973 AND 9975 PACKAGING THERMAL TEST REPORT (U)****INTRODUCTION**

Savannah River Site tested the 9973 and 9975 design variations of the 9972-series packagings. Testing of the 9973 was part of the regulatory hypothetical accident sequence defined in 10 CFR 71.73¹. Testing of the 9975 was primarily to provide benchmark data for analytical models. Summarized in this test report are test descriptions and results. Other supporting records are on file².

The selection of the 9973 and 9975 packagings as representative of the series is documented elsewhere³.

PACKAGING DESCRIPTION

The 9973 and 9975 test units are representative of the final packaging designs. Figures 1 and 2 show key packaging features. Significant thermal features are the thin walled drum and fiberboard insulation. A step at the fiberboard junction eliminates radial gaps through the fiberboard which otherwise may allow radiation heating of the containment vessel from the drum. The metal shield on the upper fiberboard eliminates air ingress into the fiberboard from the vent holes and lid during the thermal accident and subsequent cooling.

Packaging thermal acceptance criteria are listed below.

- containment vessel O-ring seals $\leq 400^{\circ}\text{F}$ rating
- lead $\leq 620^{\circ}\text{F}$ melting point (applicable to the 9975)
- fiberboard not burnt (burning is evidenced by loss of form and ash residue; charring is evidenced by retained form but carbonized structure, and is expected)
- containment vessels remain leak tight per ANSI N14.5-87⁴ ($\leq 1.96 \times 10^{-7}$ std cm³ He/sec at 14.7 psi differential)

730-A FILE ROOM, PROJECT FOLDER 22381
SRT-PTG-94-0058
Page 2 of 58
July 25, 1994

A thin ceramic blanket is used as required to fill between the lid and metal shield. The 9973 test unit had this blanket while the 9975 did not. The blanket has approximately the same thermal conductivity as fiberboard but has a much higher temperature rating.

During the thermal accident, the thin wall drum temperature will quickly rise, after which the fiberboard will slowly char inward. Significant internal temperature increases are expected only in the charred region. Fusible vent plugs will relieve drum pressurization. Eliminating air ingress, particularly in side orientations prone to chimney effects, prohibits fiberboard burning and smoldering. Both the vent plugs and lid gasket are assumed to be destroyed early in the accident.

PACKAGING PREPARATION

Instrumented assembly of the packagings is described in Appendix 1. Figures 3 and 4 show locations of the packaging thermocouples. All leads were routed from the packagings in flexible metal conduits.

The 9973 packaging included pressurized, leak tested containment vessels and content mass. Following assembly, it was subjected to the regulatory free drop and puncture tests, both impacting on the drum lid. Details of these impact tests are reported elsewhere. Expected damage was to minimize the fiberboard thickness and integrity in the upper packaging adjacent to the containment vessel seals. Internal damage was not assessed prior to the thermal test.

The 9975 packaging included content mass and an electric heater simulating a 21W content load. Both containment vessel walls were breached for instrumentation leads and the seals were not leak tested. Thermal testing was not preceded by any other hypothetical accident conditions.

PACKAGING TESTING

Thermal testing was performed at the Sandia National Laboratory in Albuquerque, New Mexico. Test requirements are documented in Appendix 2. Sandia's radiant heat facility was chosen for its test control capabilities. Heating was obtained by external quartz-electric heat lamps heating an upright cylindrical metal shroud which in turn radiated heat to the enclosed packaging. Coating on the shroud approximated a black-body source. Reradiant heating from insulation-backed thin metal plates provided top and bottom heating. Heat lamp power was controlled based on shroud temperatures.

Temperatures of the shroud and its upper and lower air plenums were recorded to demonstrate that the cool down environment was acceptable. An annular gap at the shroud bottom and a top baffle allowed for air flow around the packaging after the heat exposure. Conduit thermal protection was provided by insulation wrap and nitrogen purging.

A Sandia test report⁵ fully describes the facility and demonstrates that the required hypothetical accident environment was obtained.

730-A FILE ROOM, PROJECT FOLDER 22381
 SRT-PTG-94-0058
 Page 3 of 58
 July 25, 1994

The 9975 was tested upright in order to obtain uniform benchmark data. Prior to thermal accident testing, the 9975 internal heater was energized for 5 days, which raised packaging temperatures to realistic operating conditions. The heater remained energized during the accident heating and subsequent cool down. Manual heat lamp power control resulted in some early temperature fluctuations during the 9975 thermal accident test.

The 9973 was tested on its side to demonstrate that fiberboard burning would not occur due to air ingress. This orientation also maximized heating of the drop-damaged lid region. Heat lamp power was automatically controlled during the 9973 test. Heat lamp failures early in the 9973 test caused temperature fluctuations, but overall shroud temperatures were successfully compensated by remaining lamps.

TEST RESULTS

Following the tests, both packagings were disassembled at SRS. Appendix 3 provides disassembly observations. Table 1 summarizes fiberboard char depths.

Table 1. Fiberboard Char Summary

Packaging	Location	Char Depth*	Remaining Fiberboard
9973	Top center with drop damage	2.0 in.	1.1 in.
	Top without drop damage	2.0 in.	1.8 in.
	Side at cavity top	1.9—2.1 in.	3.2—3.4 in.
	Side at junction, top section	2.0 in.	3.3
	Side at junction, bottom section	2.1—2.3 in.	3.3—3.5 in.
	Side along main cavity	1.8 in.	3.8 in.
	Bottom	1.8 in.	1.7 in.
9975	Top center	1.4 in.	2.3 in.
	Side at cavity top	1.9 in.	2.6 in.
	Side at junction, top section	2.1 in.	2.4 in.
	Side at junction, bottom section	2.3 in.	2.5 in.
	Side along main cavity	1.8—2.3 in.†	2.5—3.0 in.
	Bottom	2.0 in.‡	2.0 in.

*Depth to stable board as indicated by rubbing the surface with a blunt probe.

†Greatest charring at unbonded glue joints.

‡Away from instrumentation conduit.

Test data for the 9973, 9975 preheat, and 9975 test are plotted on the ensuing pages. Table 2 defines data channel, thermocouple, and location correspondences. Plots show response over the entire test time and, where significant, magnification of the accident heat period.

730-A FILE ROOM, PROJECT FOLDER 22381
SRT-PTG-94-0058
Page 4 of 58
July 25, 1994

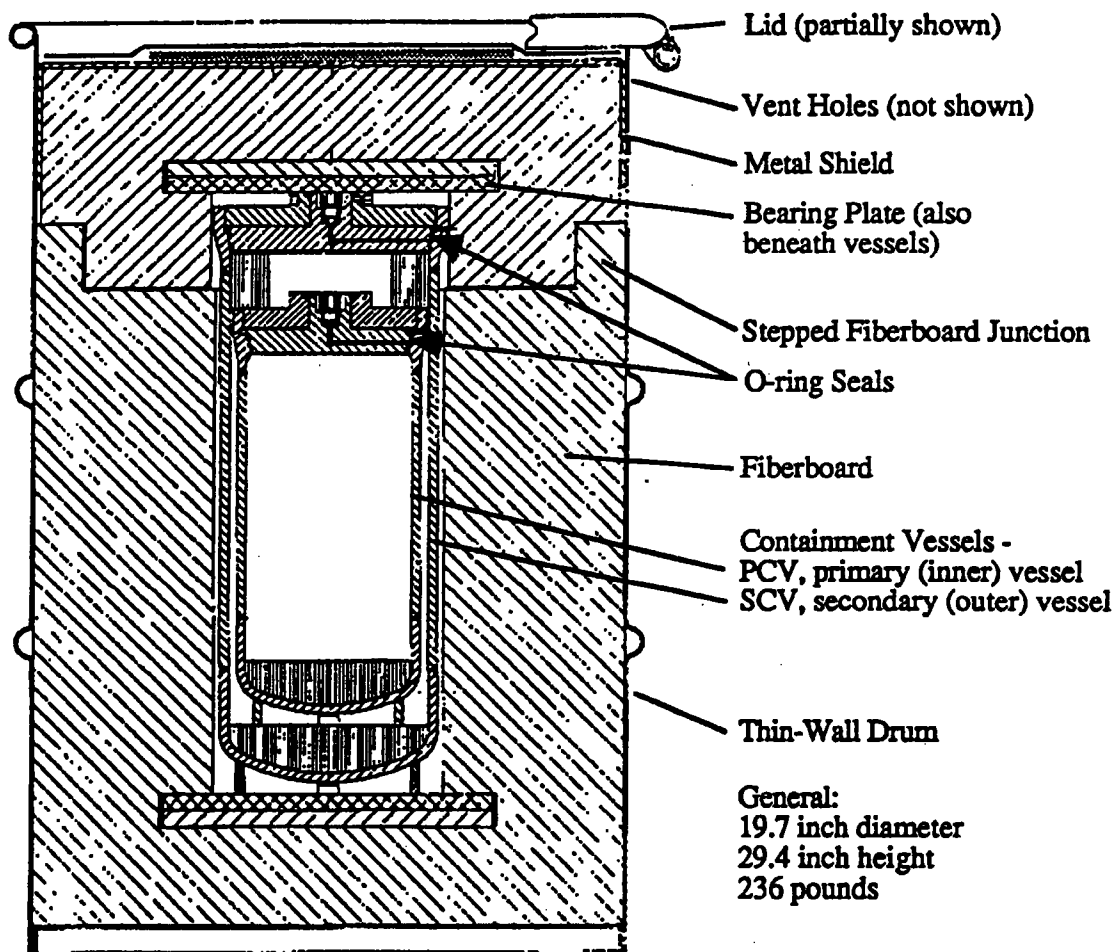


Figure 1. 9973 Packaging

730-A FILE ROOM, PROJECT FOLDER 22381
SRT-PTG-94-0058
Page 5 of 58
July 25, 1994

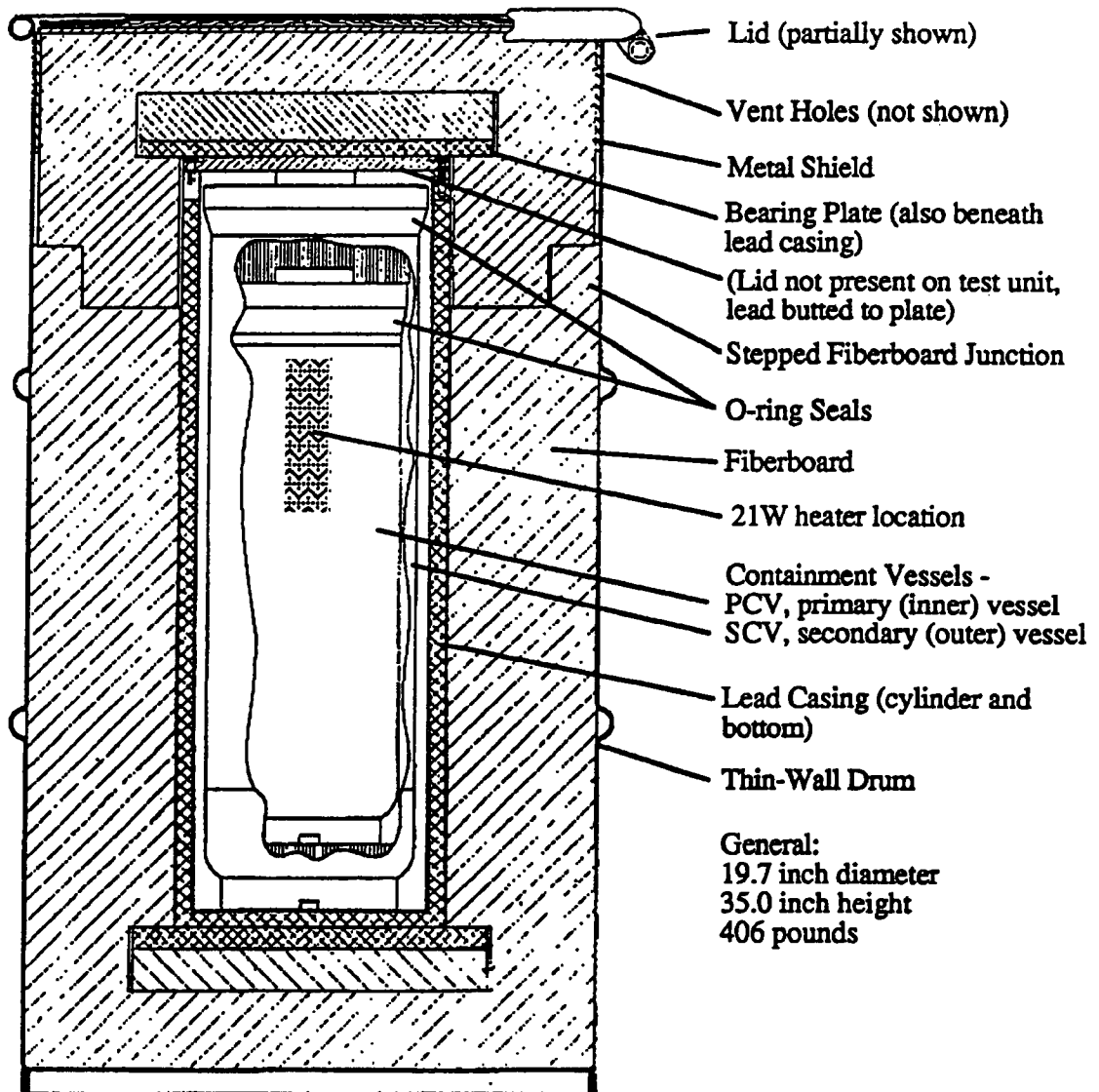


Figure 2. 9975 Packaging

730-A FILE ROOM, PROJECT FOLDER 22381
 SRT-PTG-94-0058
 Page 6 of 58
 July 25, 1994

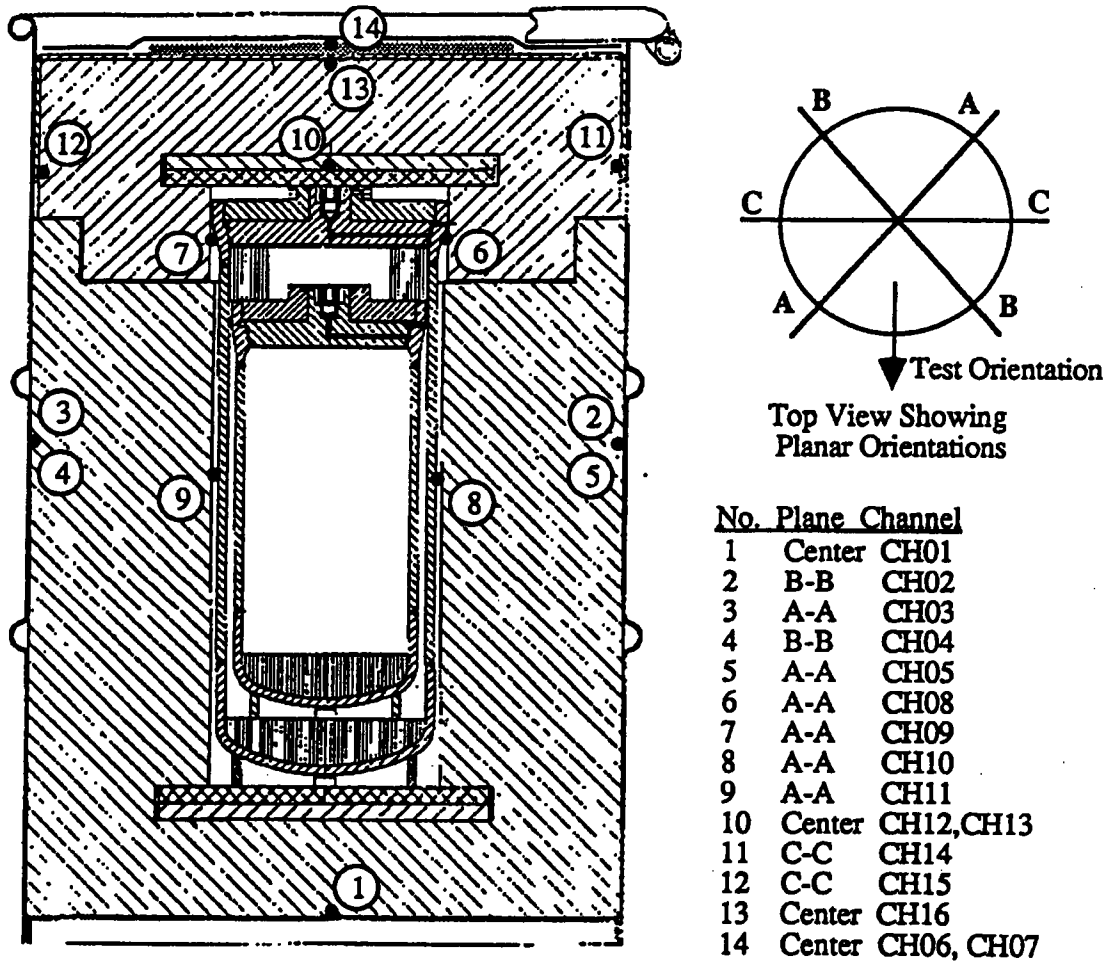


Figure 3. 9973 Packaging Thermocouple Locations

730-A FILE ROOM, PROJECT FOLDER 22381
 SRT-PTG-94-0058
 Page 7 of 58
 July 25, 1994

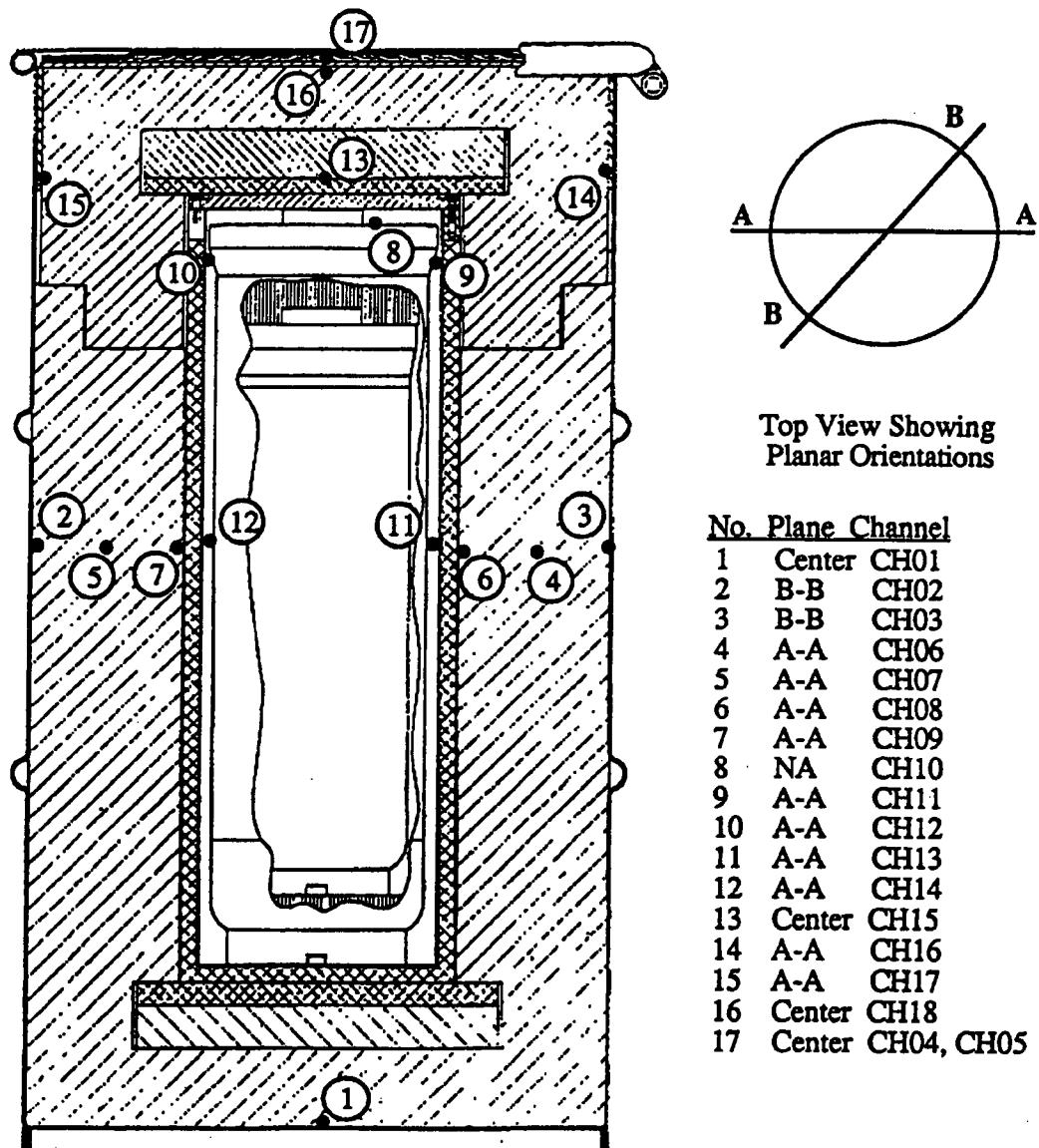


Figure 4. 9975 Packaging Thermocouple Locations

730-A FILE ROOM, PROJECT FOLDER 22381
 SRT-PTG-94-0058
 Page 8 of 58
 July 25, 1994

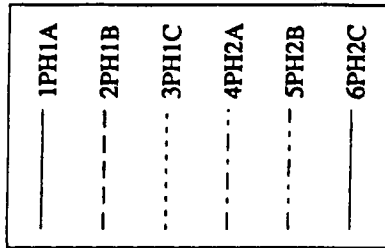
Table 2. Thermocouple Correspondences

Channel*	9973		9975	
	TC No.†	Location	TC No.†	Location
1PH1A	NR	Shroud front facing drum lid	NR	Shroud front
2PH1B	NR	Shroud, 60° right	NR	Shroud, 60° right
3PH1C	NR	Shroud, 120° right	NR	Shroud, 120° right
4PH2A	NR	Shroud, 180° right, facing drum bottom	NR	Shroud, 180° right
5PH2B	NR	Shroud, 240° right	NR	Shroud, 240° right
6PH2C	NR	Shroud, 300° right	NR	Shroud, 300° right
LPLENM	NR	Lower air plenum	NR	Lower air plenum
UPLENM	NR	Upper air plenum	NR	Upper air plenum
CH01	TR-3236	Drum bottom center	TR-3241	Drum bottom center
CH02	TR-3237	Drum side, down, 45° off vertical	TR-3242	Drum side
CH03	TR-3238	Drum side, down, 45° off vertical	TR-3243	Drum side, 180° apart
CH04	TR-3239	Drum side, up, 45° off vertical	TR-3246	Drum lid
CH05	TR-3240	Drum side, up, 45° off vertical	TR-3247	Drum lid, redundant
CH06	TR-3244	Drum lid	TR-3252	Fiberboard mid-wall
CH07	TR-3245	Drum lid, redundant	TR-3253	Fiberboard mid-wall, 180° apart
CH08	TR-3257	SCV seal	TR-3254	Lead side
CH09	TR-3258	SCV seal, 180° apart	TR-3255	Lead side, 180° apart
CH10	TR-3259	SCV side	TR-3256	PCV lid
CH11	TR-3260	SCV side, 180° apart	TR-3261	SCV seal
CH12	TR-3265	Upper bearing plate	TR-3262	SCV seal, 180° apart
CH13	TR-3266	Upper bearing plate, redundant	TR-3263	SCV side
CH14	TR-3268	Shield side	TR-3264	SCV side, 180° apart
CH15	TR-3269	Shield side, 180° apart	TR-3267	Upper bearing plate
CH16	TR-3270	Shield top	TR-3271	Shield side
CH17	NA	NA	TR-3272	Shield side, 180° apart
CH18	NA	NA	TR-3273	Shield top
CH19	NA	NA	NR	Preheat ambient
AMPS	NA	NA	NA	Heater amperage
VOLTS	NA	NA	NA	Heater voltage
PRESSR	NA	Drum pressure	NA	Drum Pressure

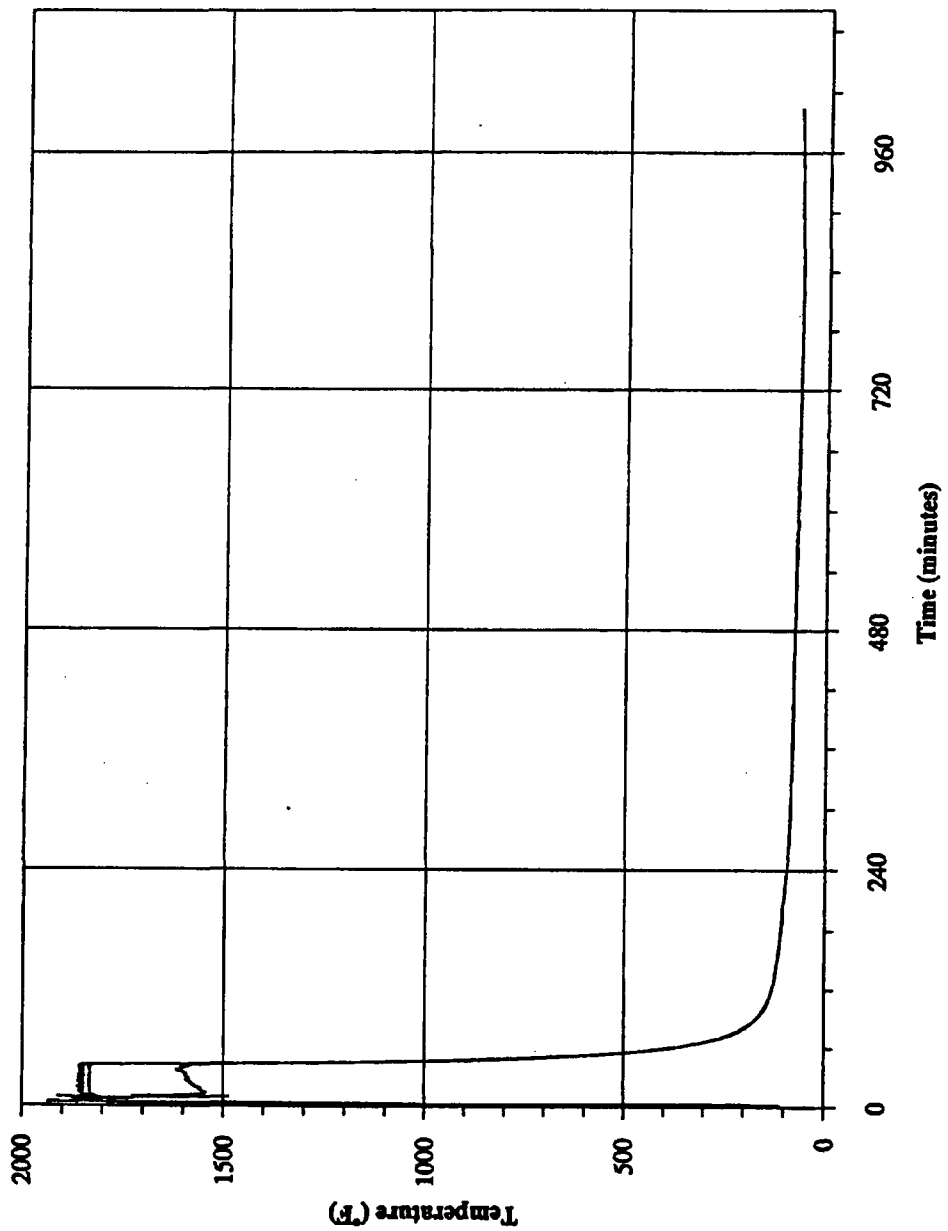
*Sandia data acquisition channel label.

†NR - not recorded, NA - not applicable.

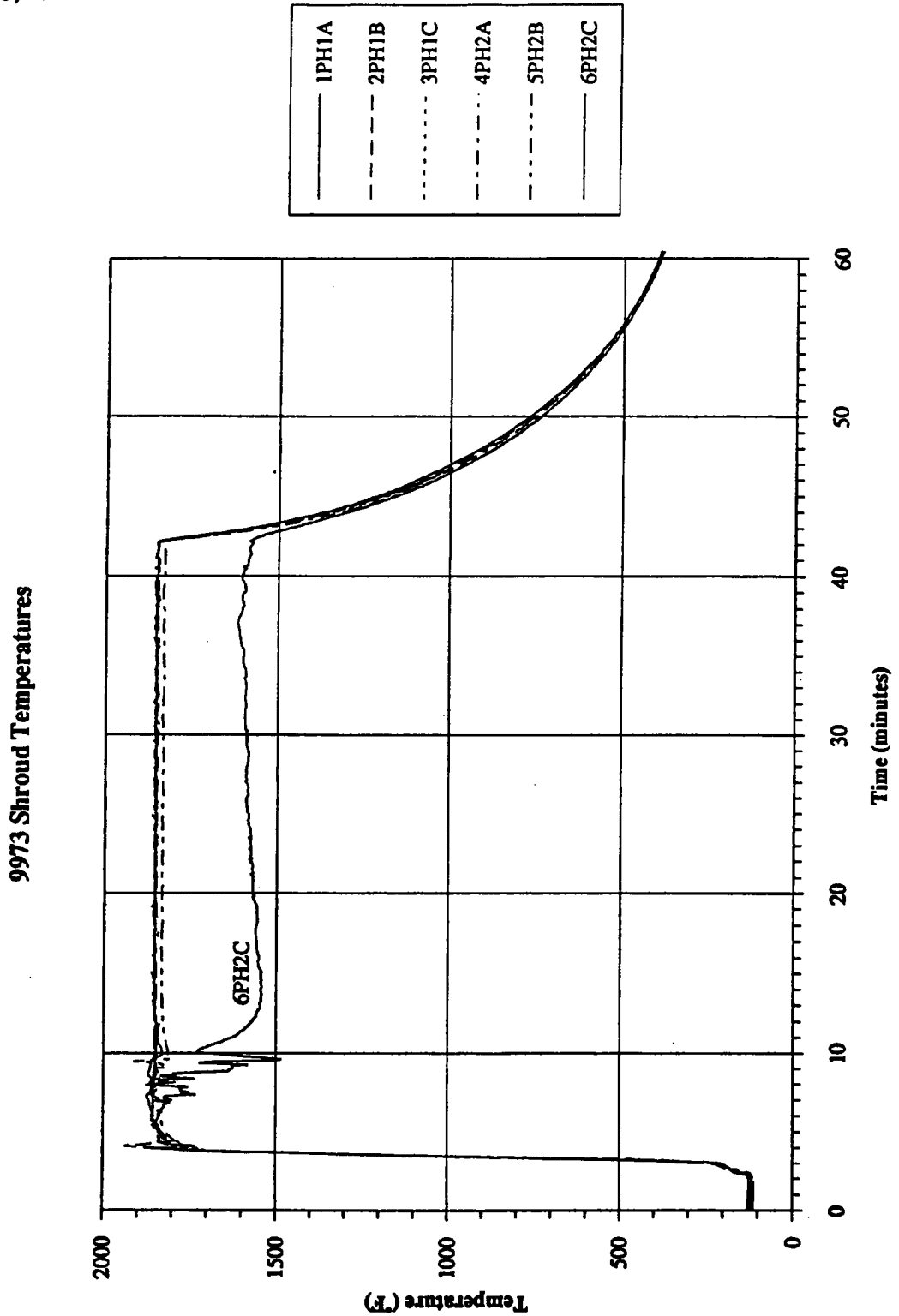
730-A FILE ROOM, PROJECT FOLDER 22381
SRT-PTG-94-0058
Page 9 of 58
July 25, 1994



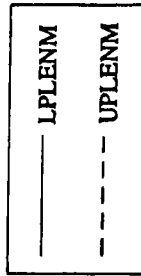
9973 Shroud Temperatures



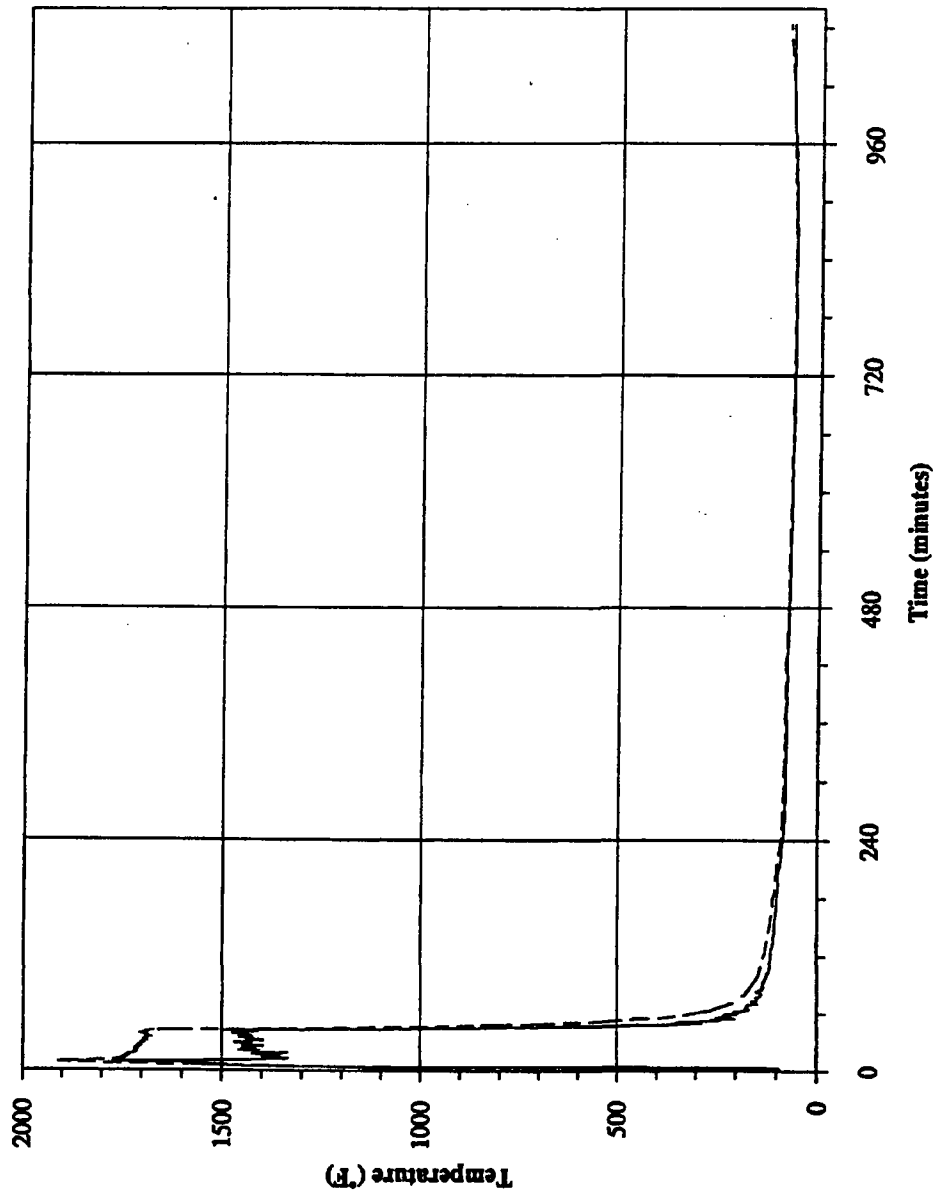
730-A FILE ROOM, PROJECT FOLDER 22381
SRT-PTG-94-0058
Page 10 of 58
July 25, 1994



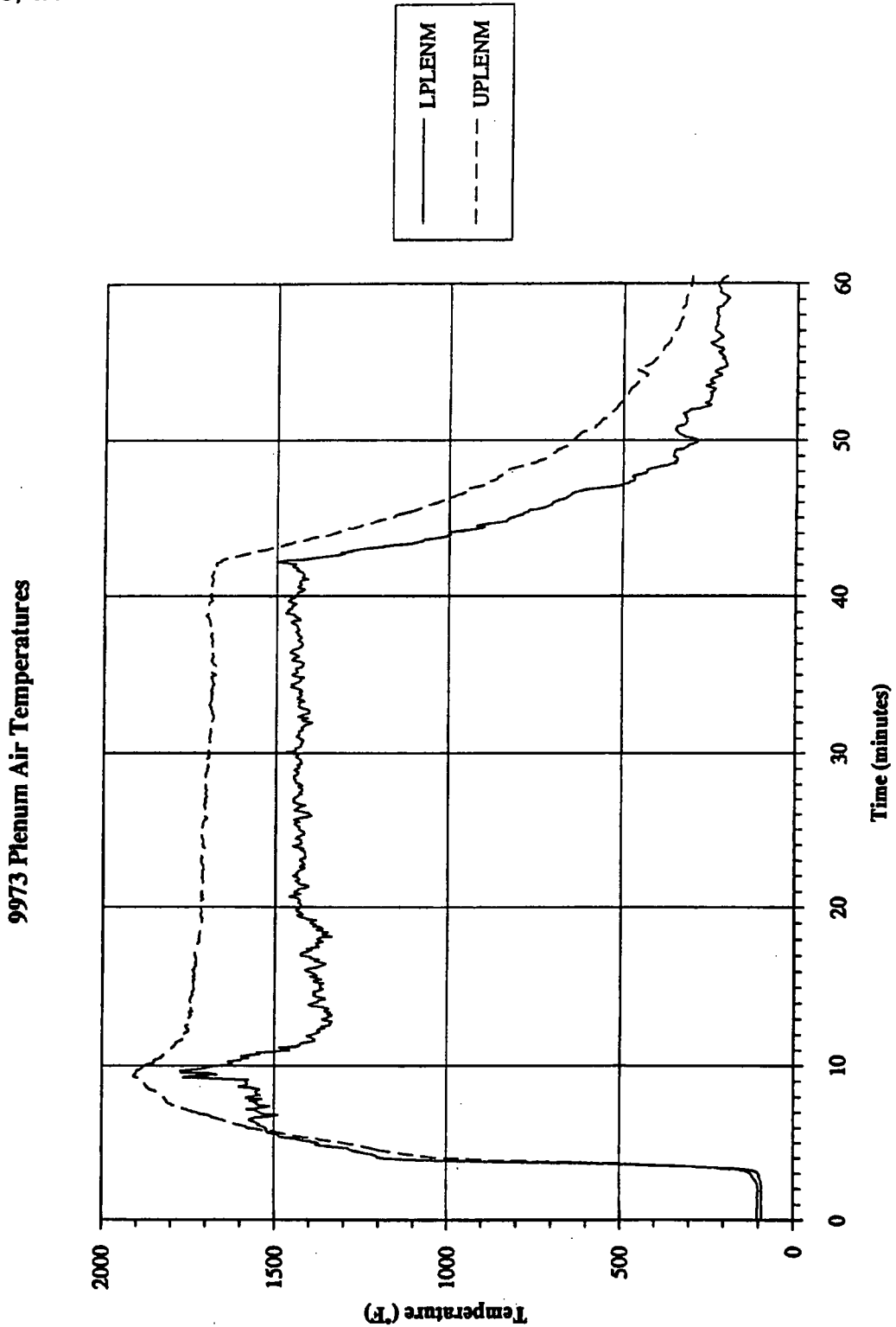
730-A FILE ROOM, PROJECT FOLDER 22381
SRT-PTG-94-0058
Page 11 of 58
July 25, 1994



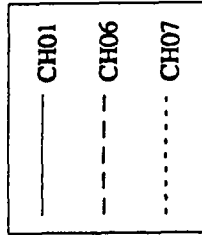
9973 Plenum Air Temperatures



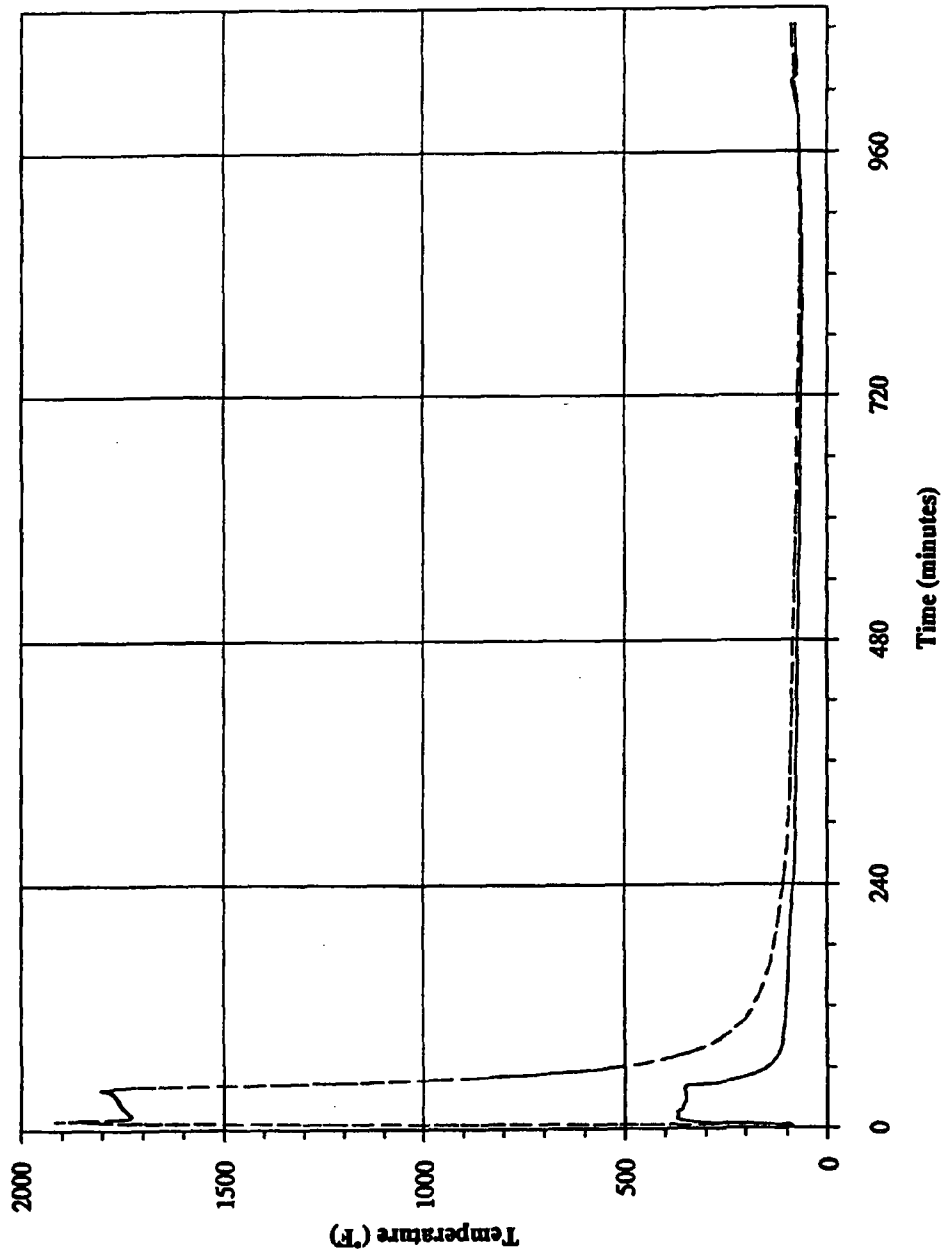
730-A FILE ROOM, PROJECT FOLDER 22381
SRT-PTG-94-0058
Page 12 of 58
July 25, 1994



730-A FILE ROOM, PROJECT FOLDER 22381
SRT-PTG-94-0058
Page 13 of 58
July 25, 1994

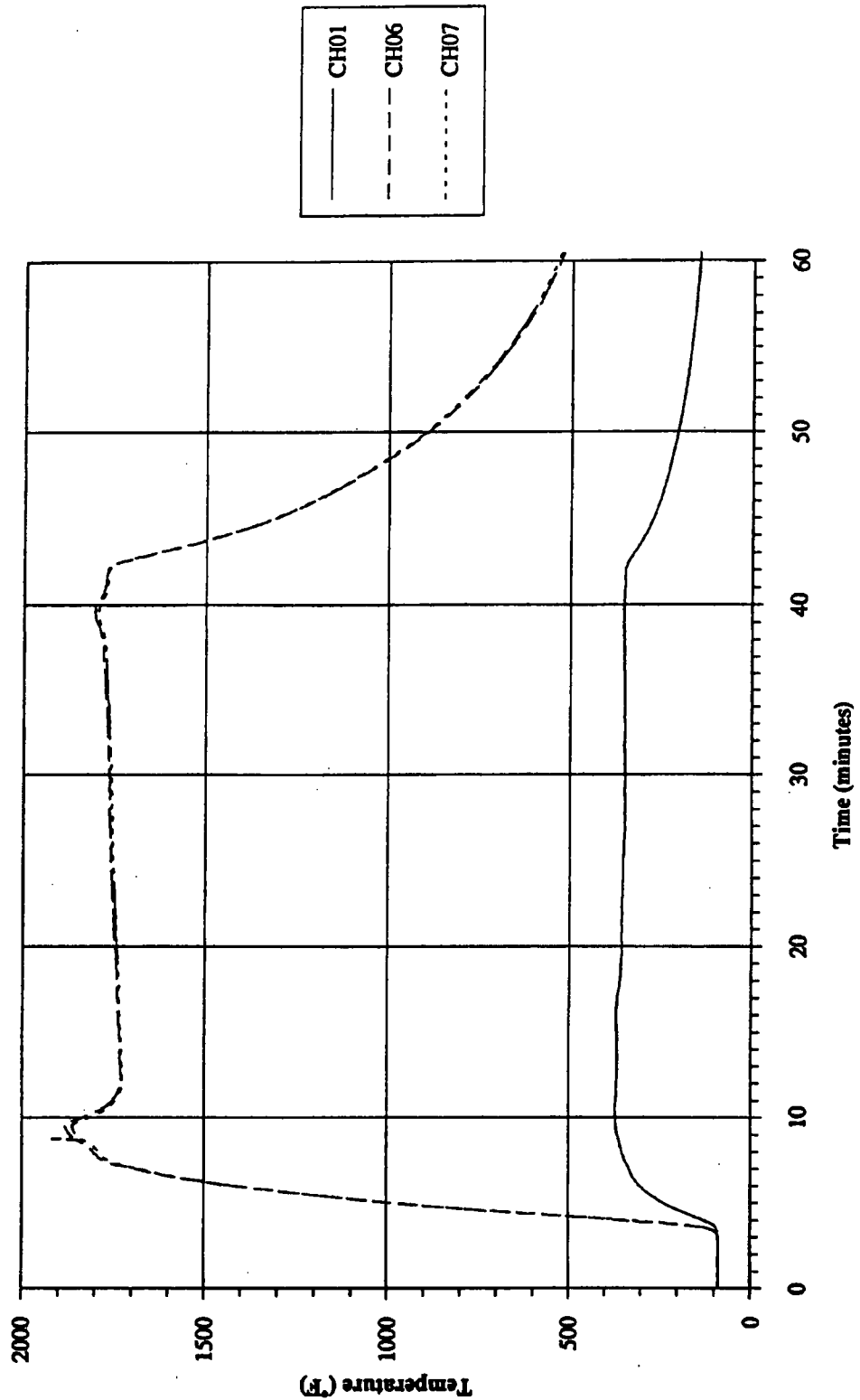


9973 Drum Lid and Bottom Temperatures

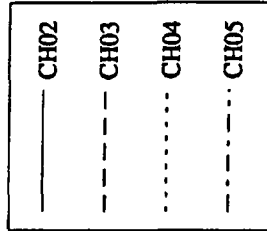


730-A FILE ROOM, PROJECT FOLDER 22381
SRT-PTG-94-0058
Page 14 of 58
July 25, 1994

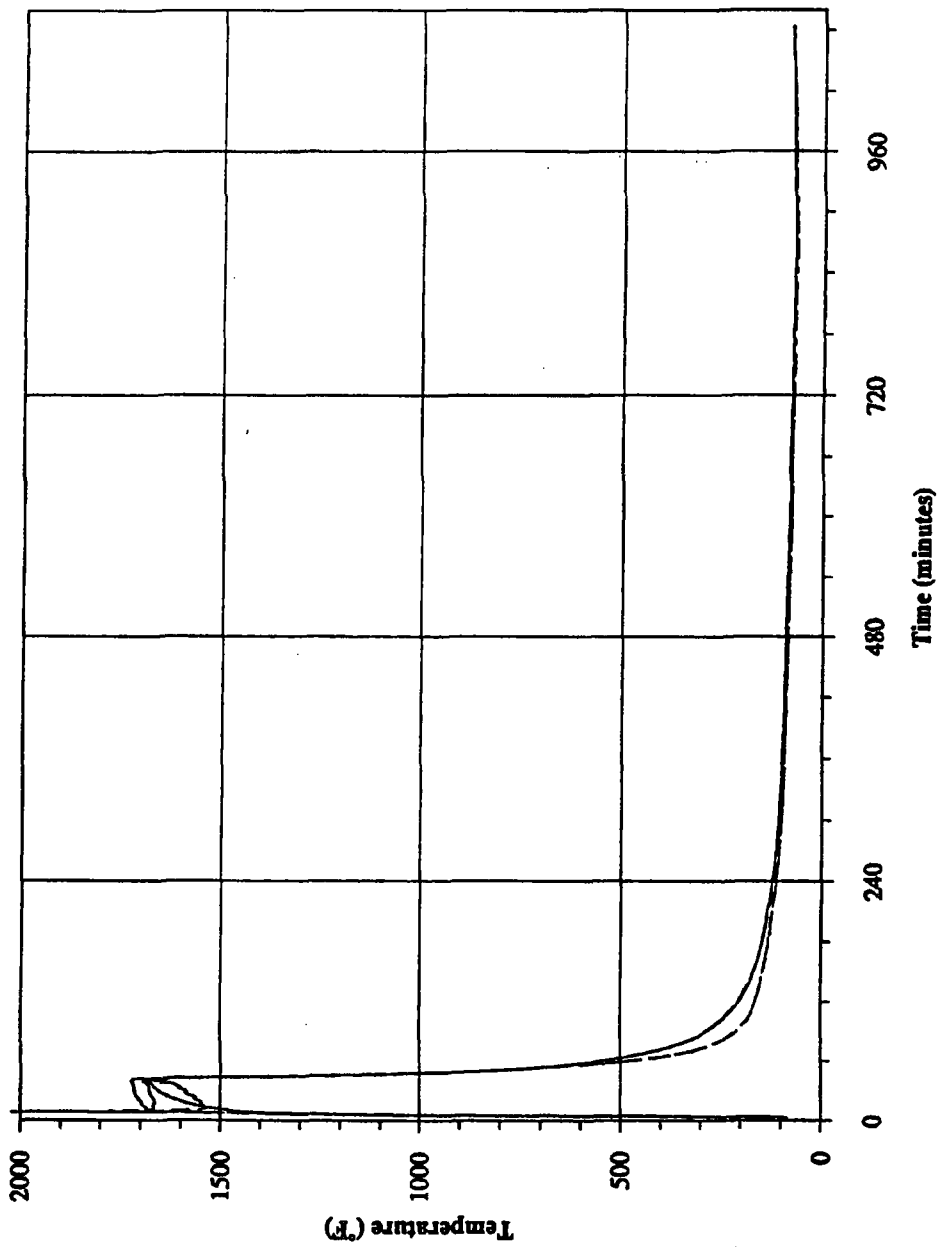
9973 Drum Lid and Bottom Temperatures



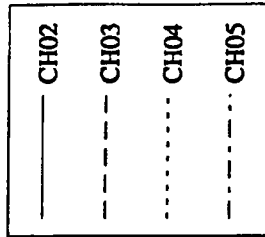
730-A FILE ROOM, PROJECT FOLDER 22381
SRT-PTG-94-0058
Page 15 of 58
July 25, 1994



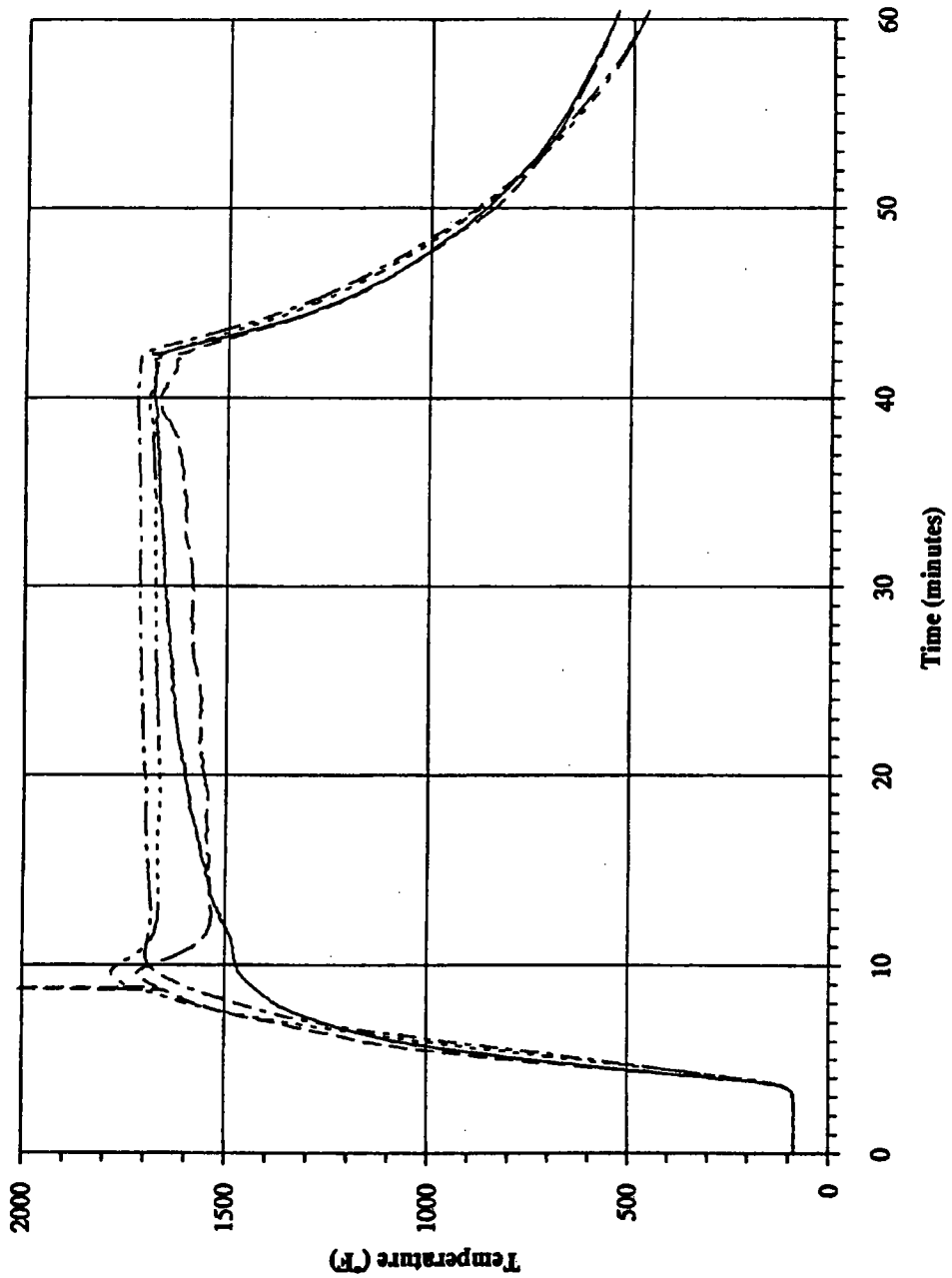
9973 Drum Side Temperatures



730-A FILE ROOM, PROJECT FOLDER 22381
SRT-PTG-94-0058
Page 16 of 58
July 25, 1994

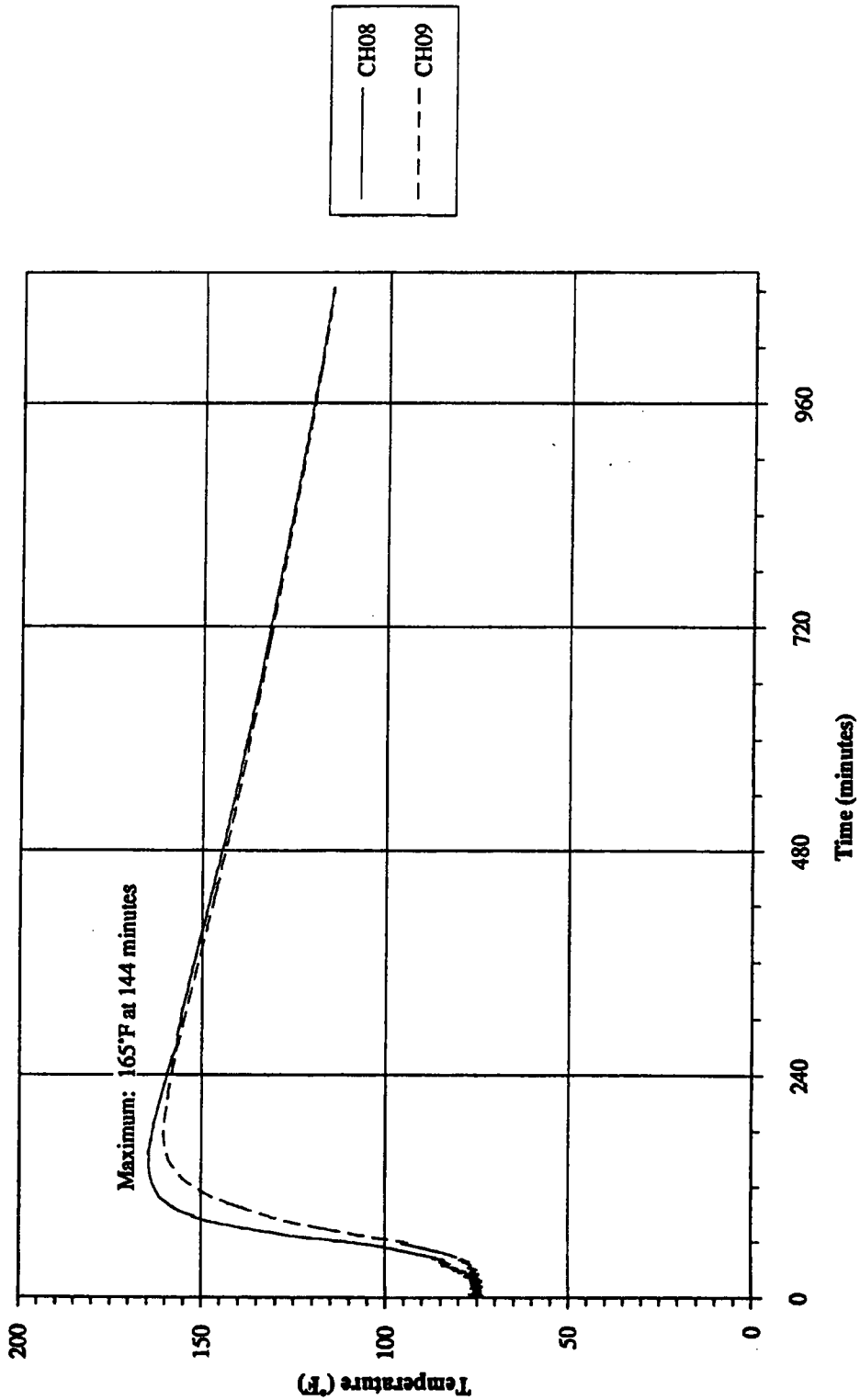


9973 Drum Side Temperatures



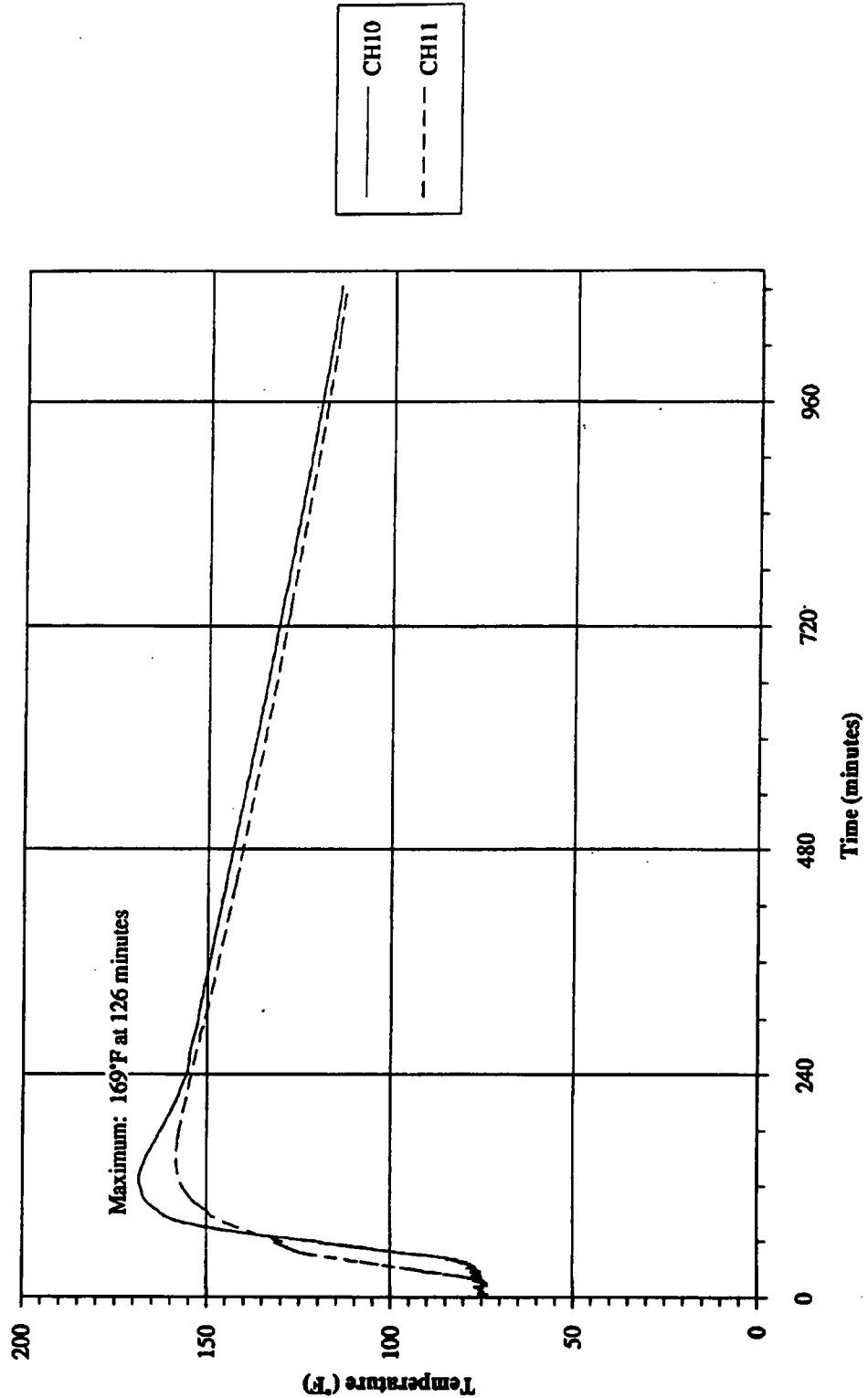
730-A FILE ROOM, PROJECT FOLDER 22381
SRT-PTG-94-0058
Page 17 of 58
July 25, 1994

9973 Secondary Containment Vessel Seal Temperatures



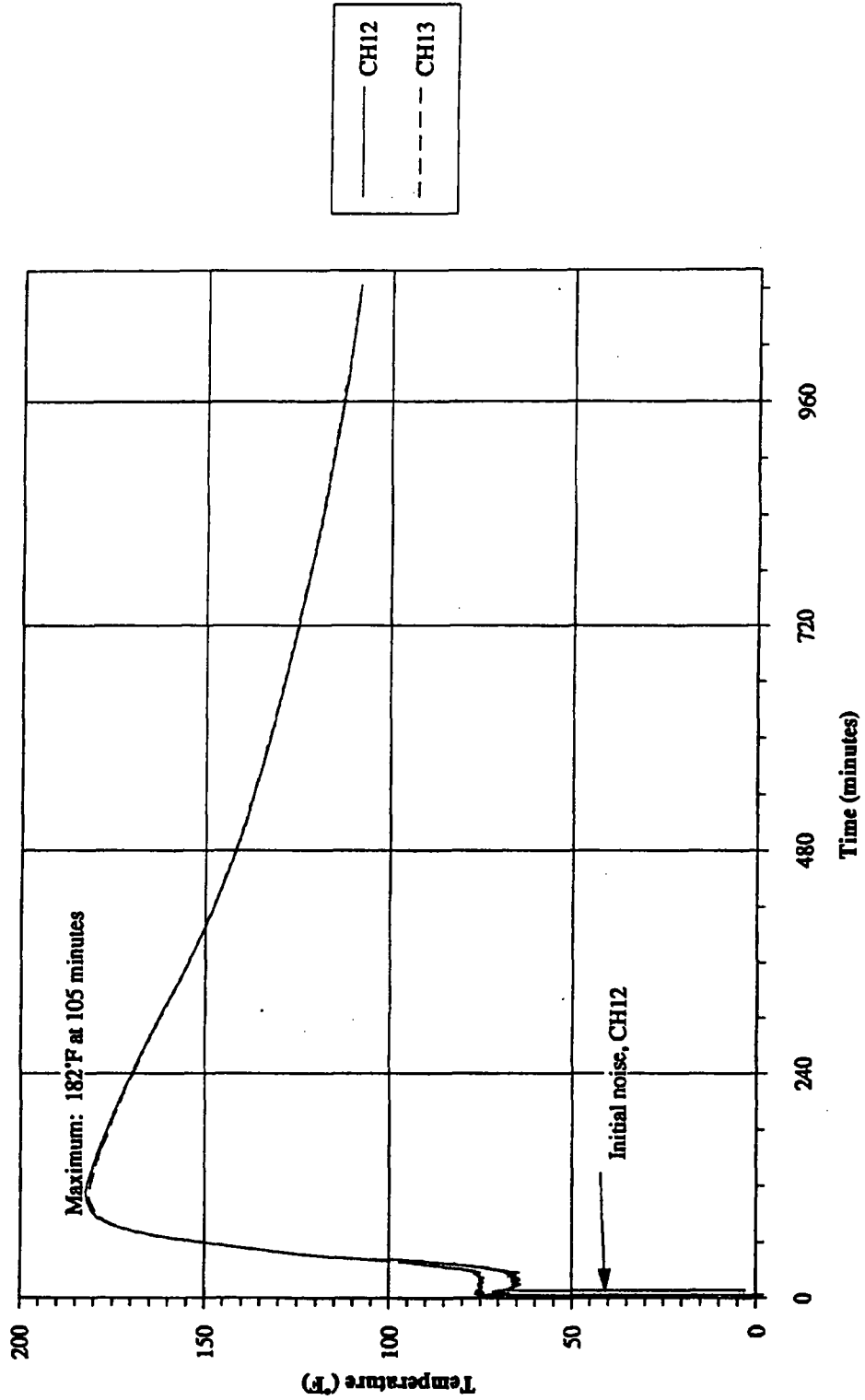
730-A FILE ROOM, PROJECT FOLDER 22381
SRT-PTG-94-0058
Page 18 of 58
July 25, 1994

9973 Secondary Containment Vessel Wall Temperatures

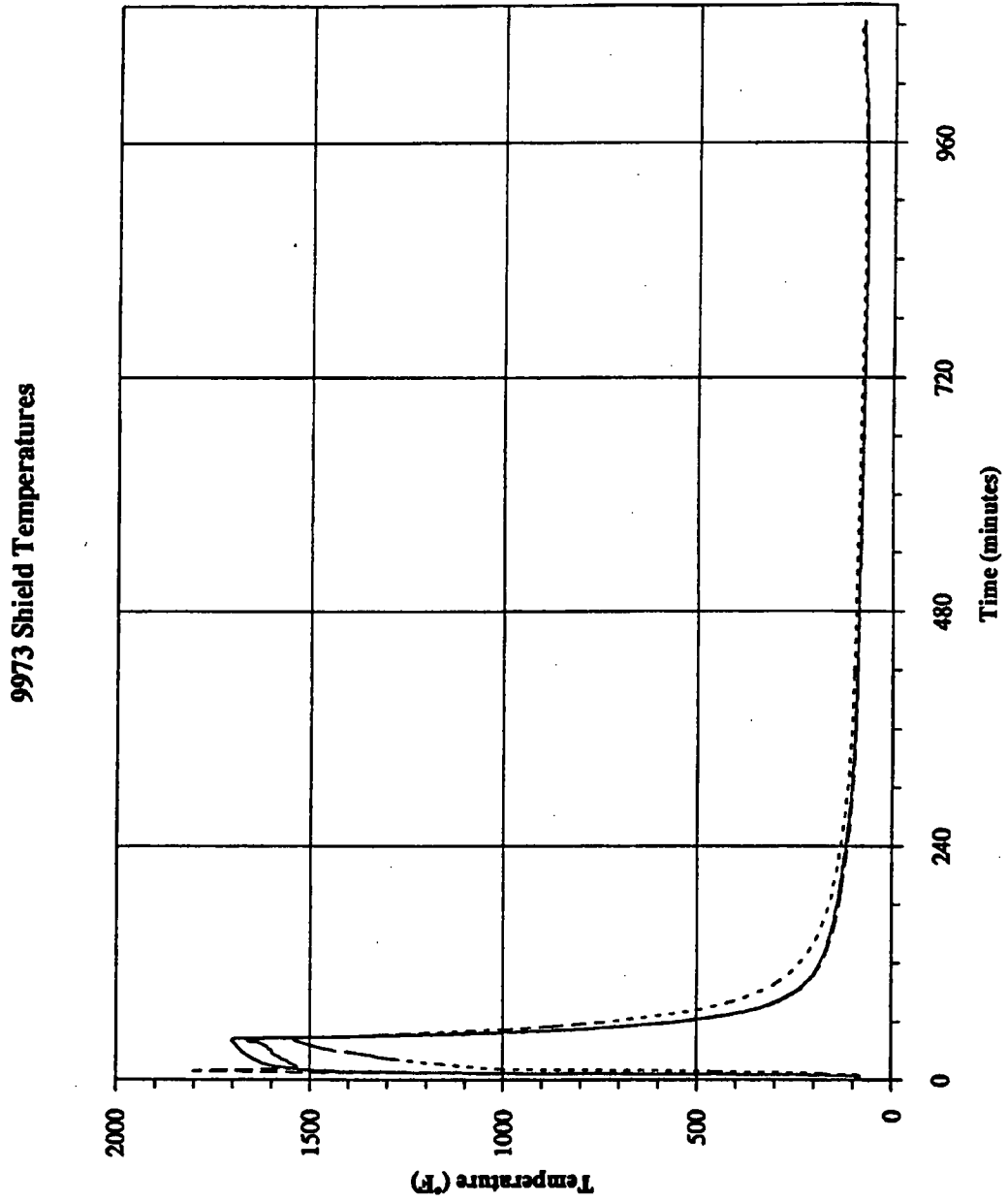
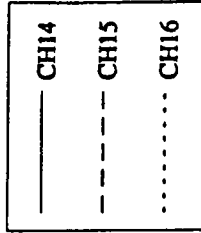


730-A FILE ROOM, PROJECT FOLDER 22381
SRT-PTG-94-0058
Page 19 of 58
July 25, 1994

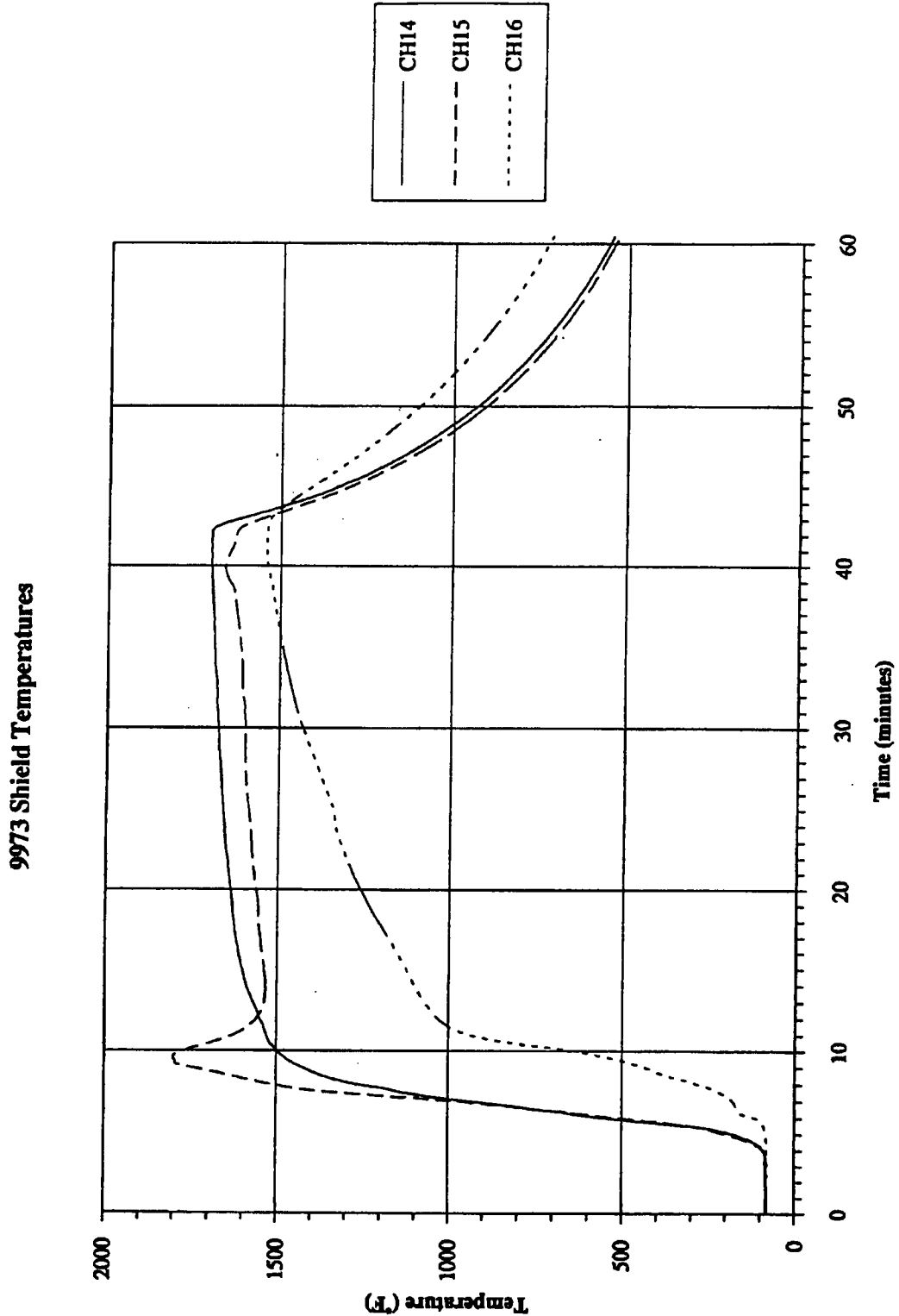
9973 Upper Bearing Plate Temperatures



730-A FILE ROOM, PROJECT FOLDER 22381
SRT-PTG-94-0058
Page 20 of 58
July 25, 1994

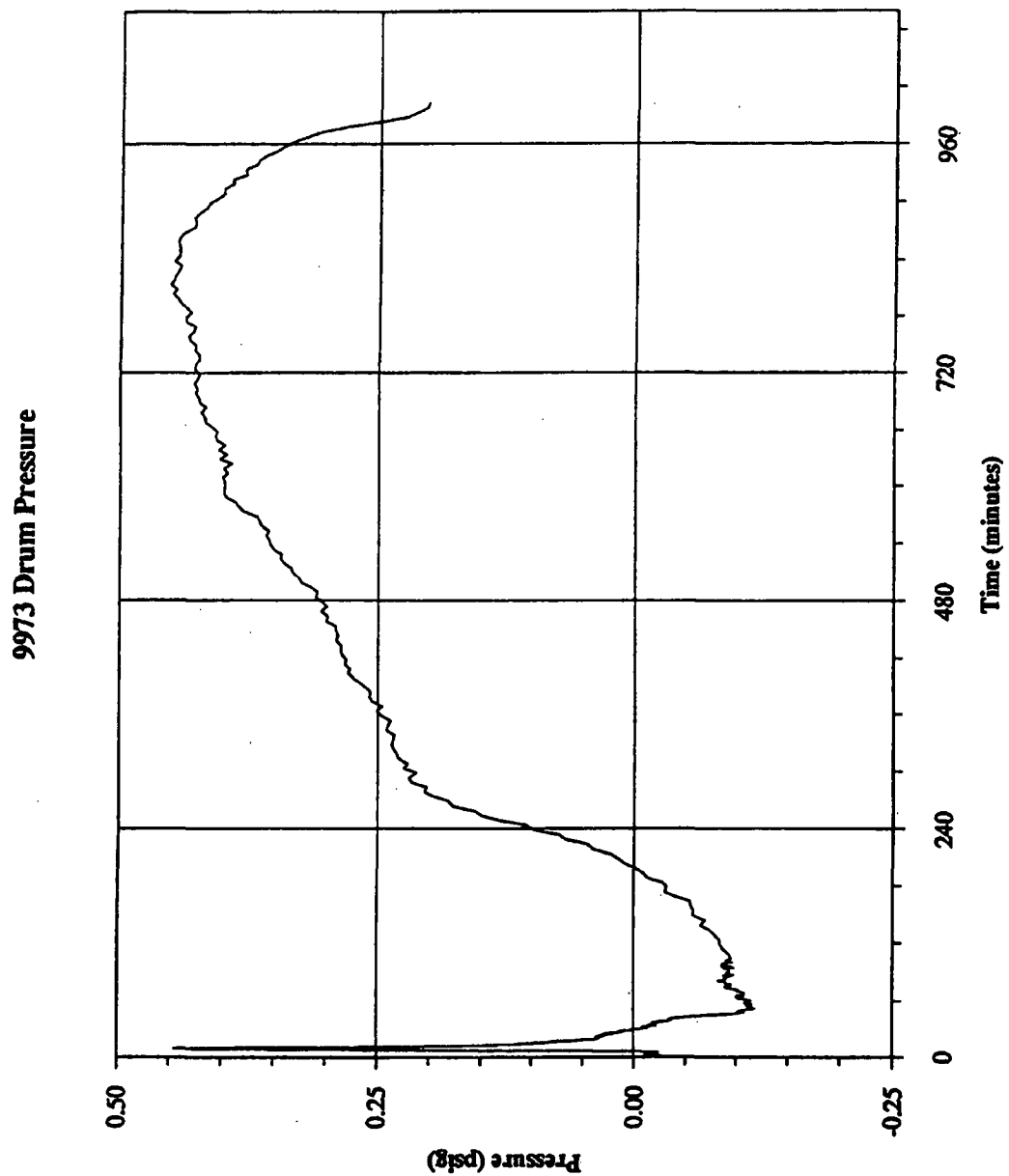


730-A FILE ROOM, PROJECT FOLDER 22381
SRT-PTG-94-0058
Page 21 of 58
July 25, 1994



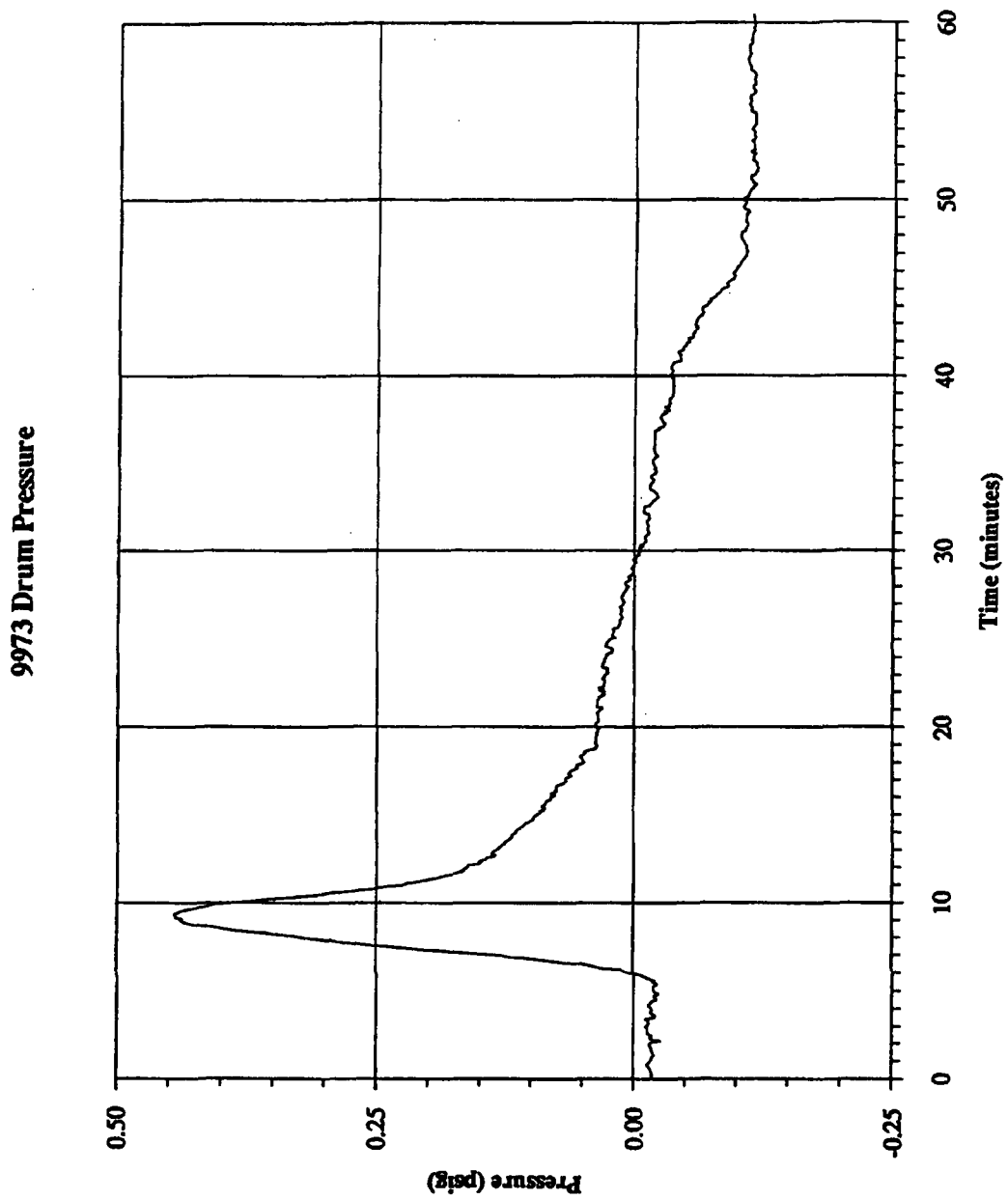
730-A FILE ROOM, PROJECT FOLDER 22381
SRT-PTG-94-0058
Page 22 of 58
July 25, 1994

— PRESSR

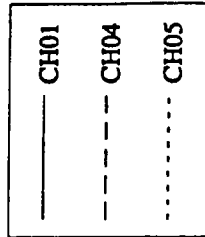


730-A FILE ROOM, PROJECT FOLDER 22381
SRT-PTG-94-0058
Page 23 of 58
July 25, 1994

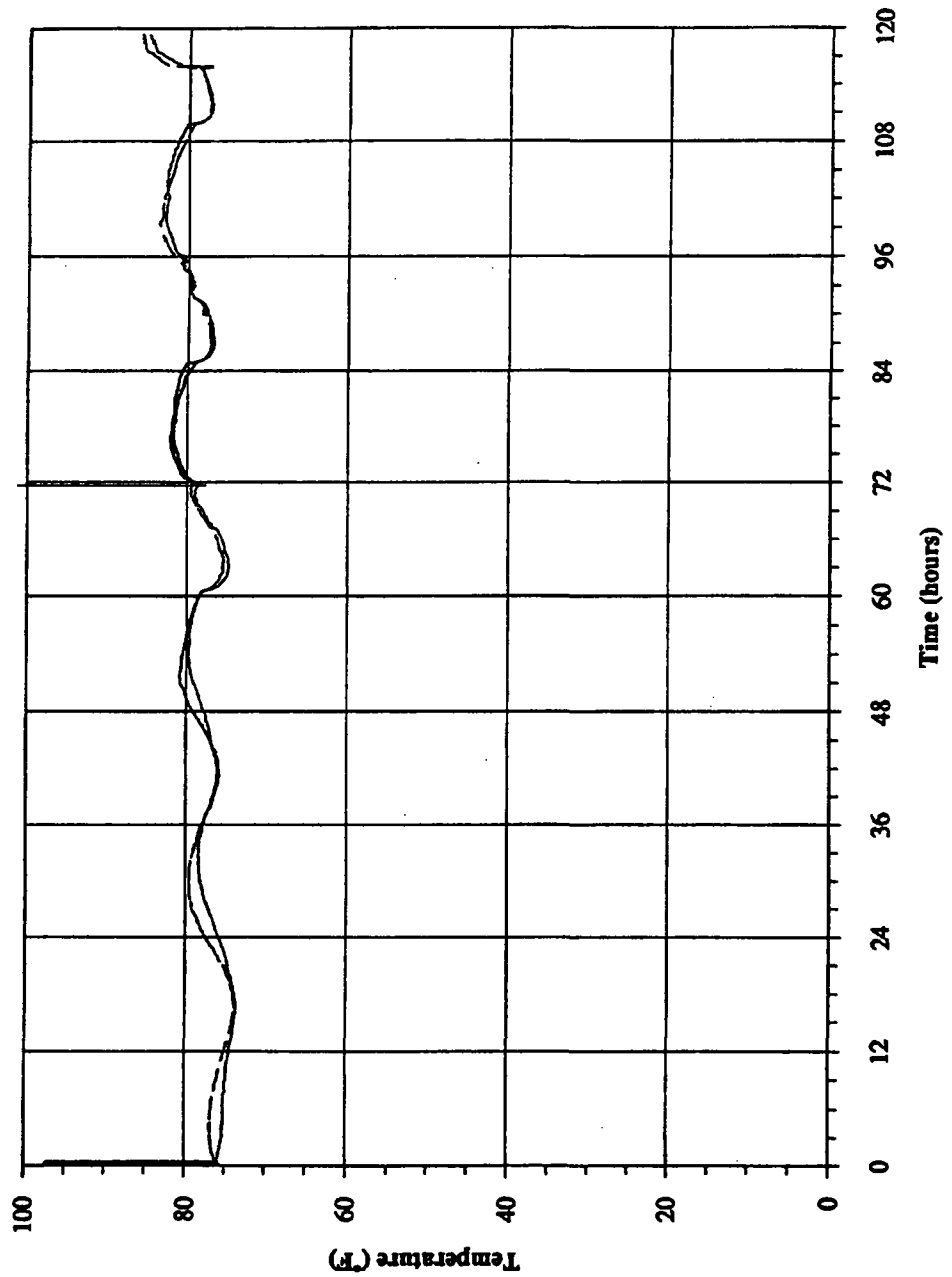
— PRESSR



730-A FILE ROOM, PROJECT FOLDER 22381
SRT-PTG-94-0058
Page 24 of 58
July 25, 1994

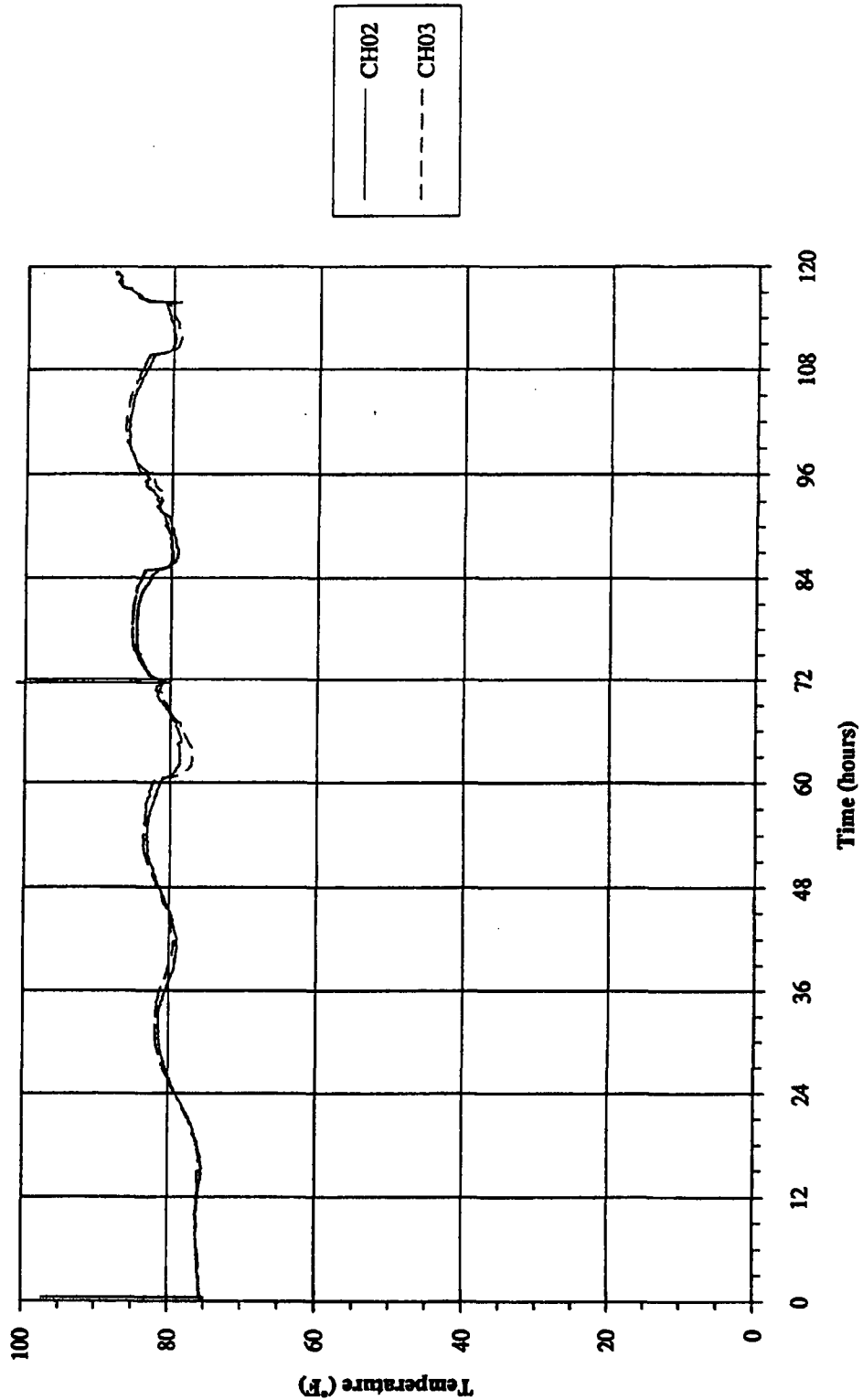


9975 Drum Lid and Bottom Preheat Temperatures



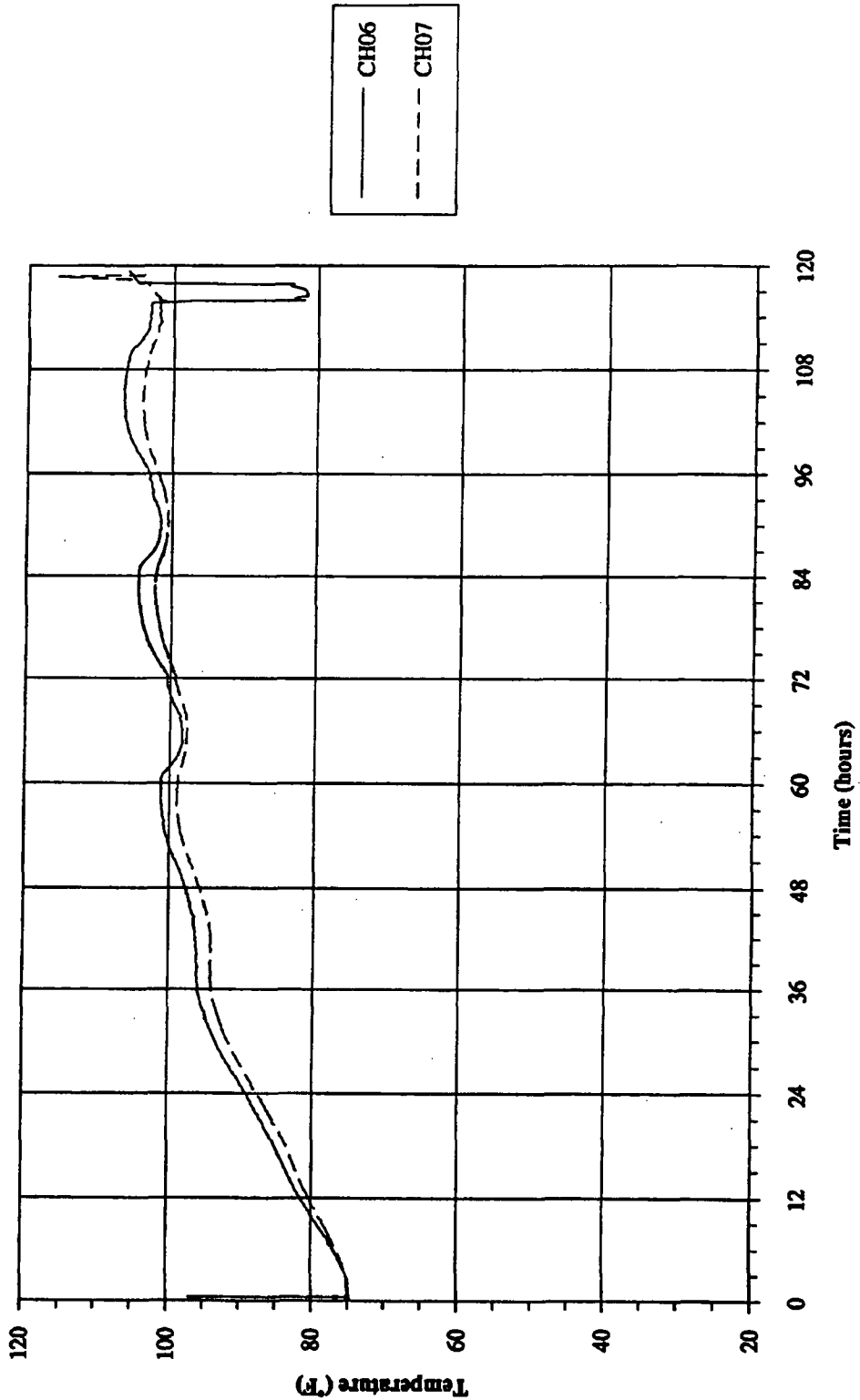
730-A FILE ROOM, PROJECT FOLDER 22381
SRT-PTG-94-0058
Page 25 of 58
July 25, 1994

9975 Drum Side Preheat Temperatures

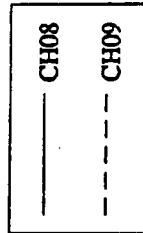


730-A FILE ROOM, PROJECT FOLDER 22381
SRT-PTG-94-0058
Page 26 of 58
July 25, 1994

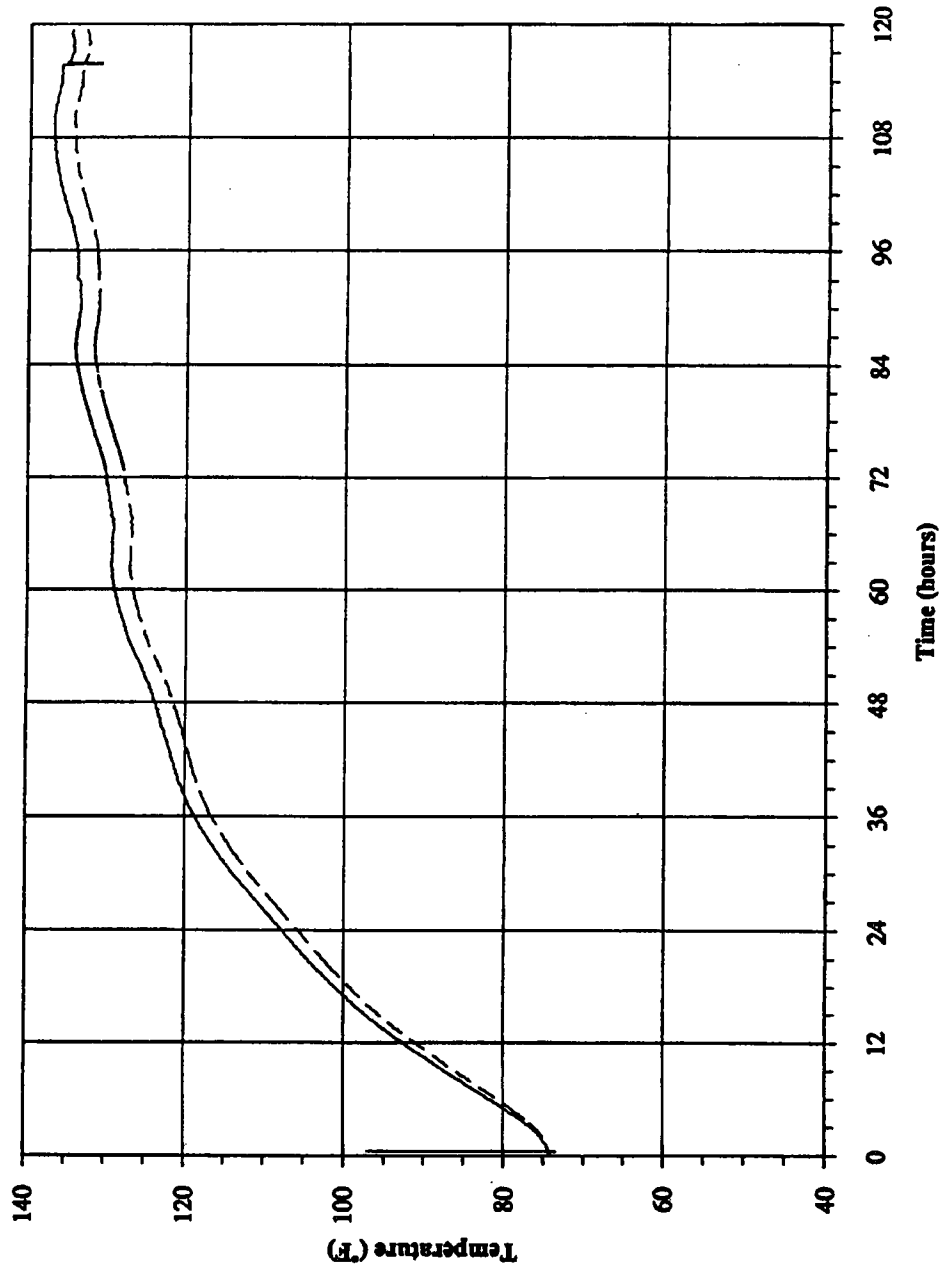
9975 Mid-wall Fiberboard Preheat Temperatures



730-A FILE ROOM, PROJECT FOLDER 22381
SRT-PTG-94-0058
Page 27 of 58
July 25, 1994



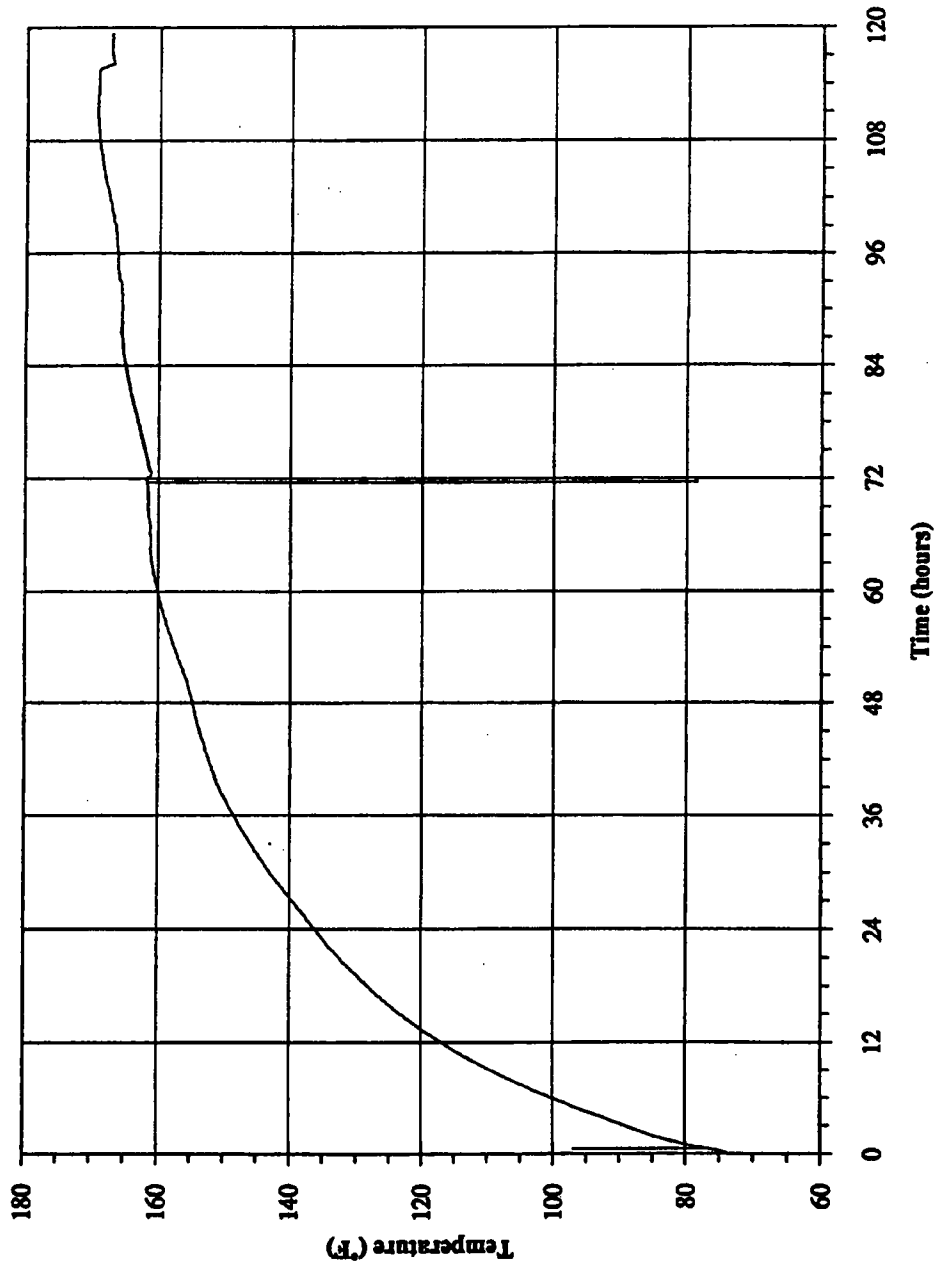
9975 Lead Preheat Temperatures



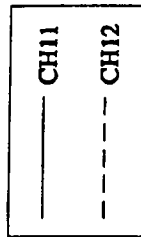
730-A FILE ROOM, PROJECT FOLDER 22381
SRT-PTG-94-0058
Page 28 of 58
July 25, 1994

CH10

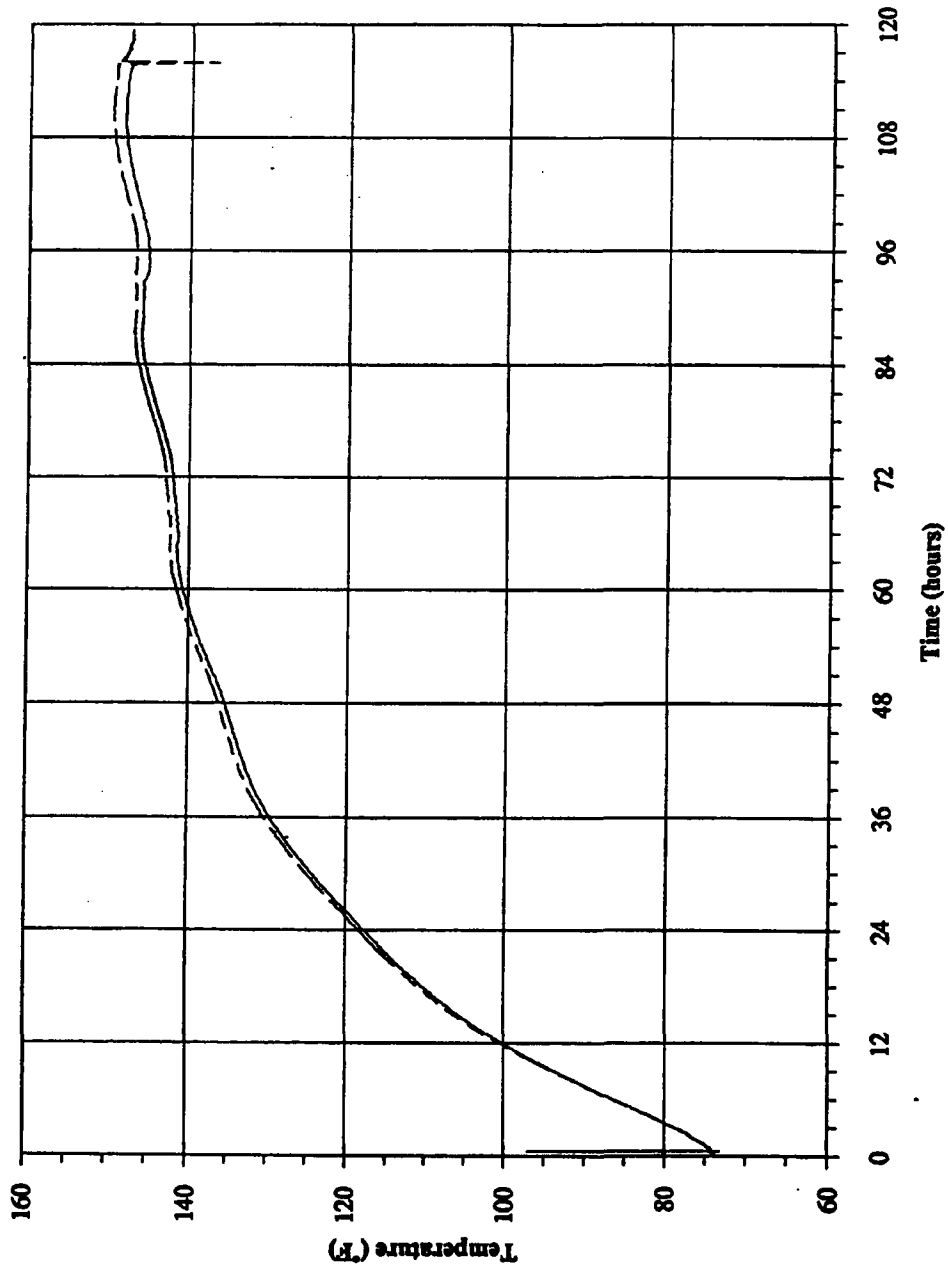
9975 Primary Containment Vessel Lid Preheat Temperatures



730-A FILE ROOM, PROJECT FOLDER 22381
SRT-PTG-94-0058
Page 29 of 58
July 25, 1994

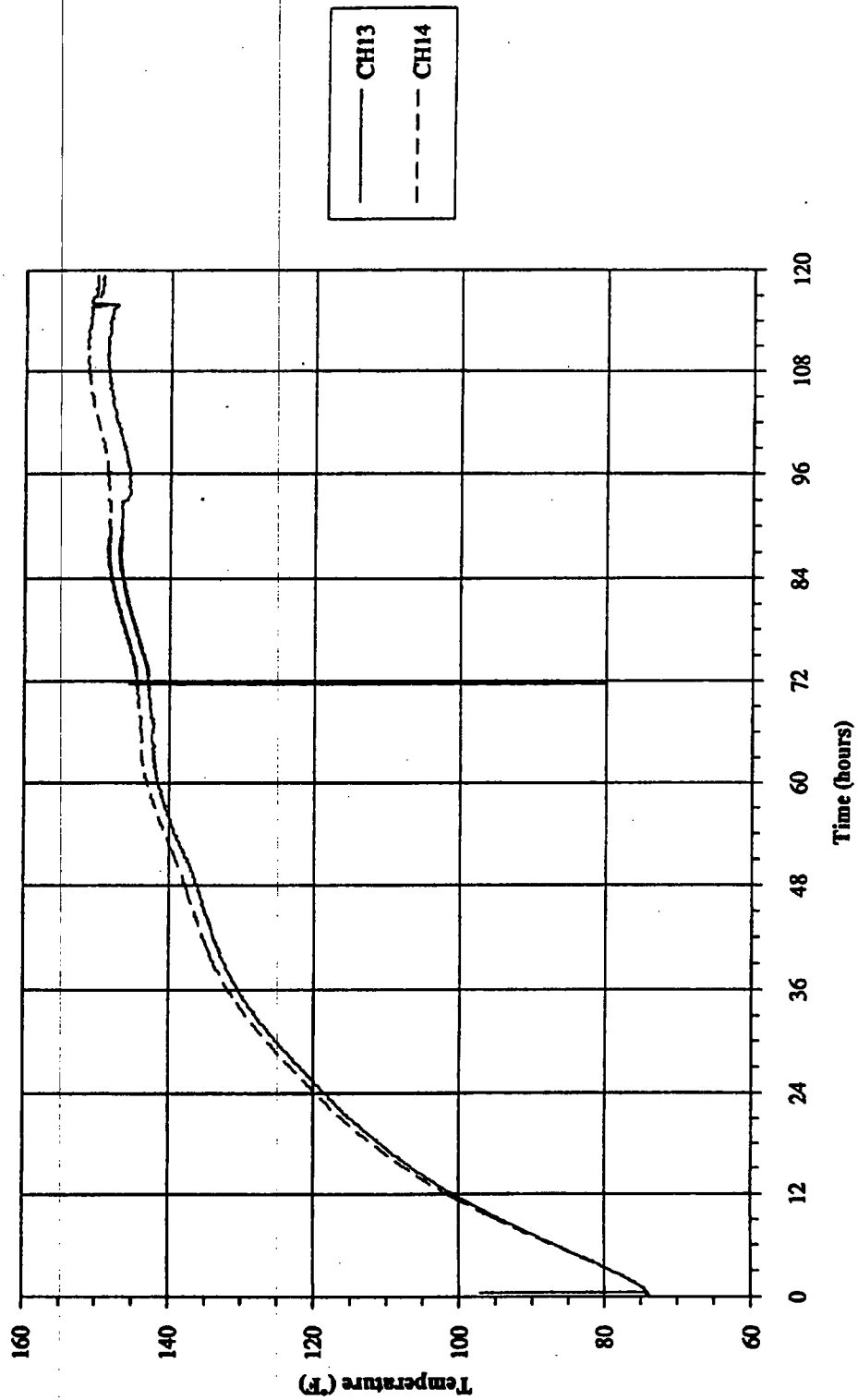


9975 Secondary Containment Vessel Seal Preheat Temperatures



730-A FILE ROOM, PROJECT FOLDER 22381
SRT-PTG-94-0058
Page 30 of 58
July 25, 1994

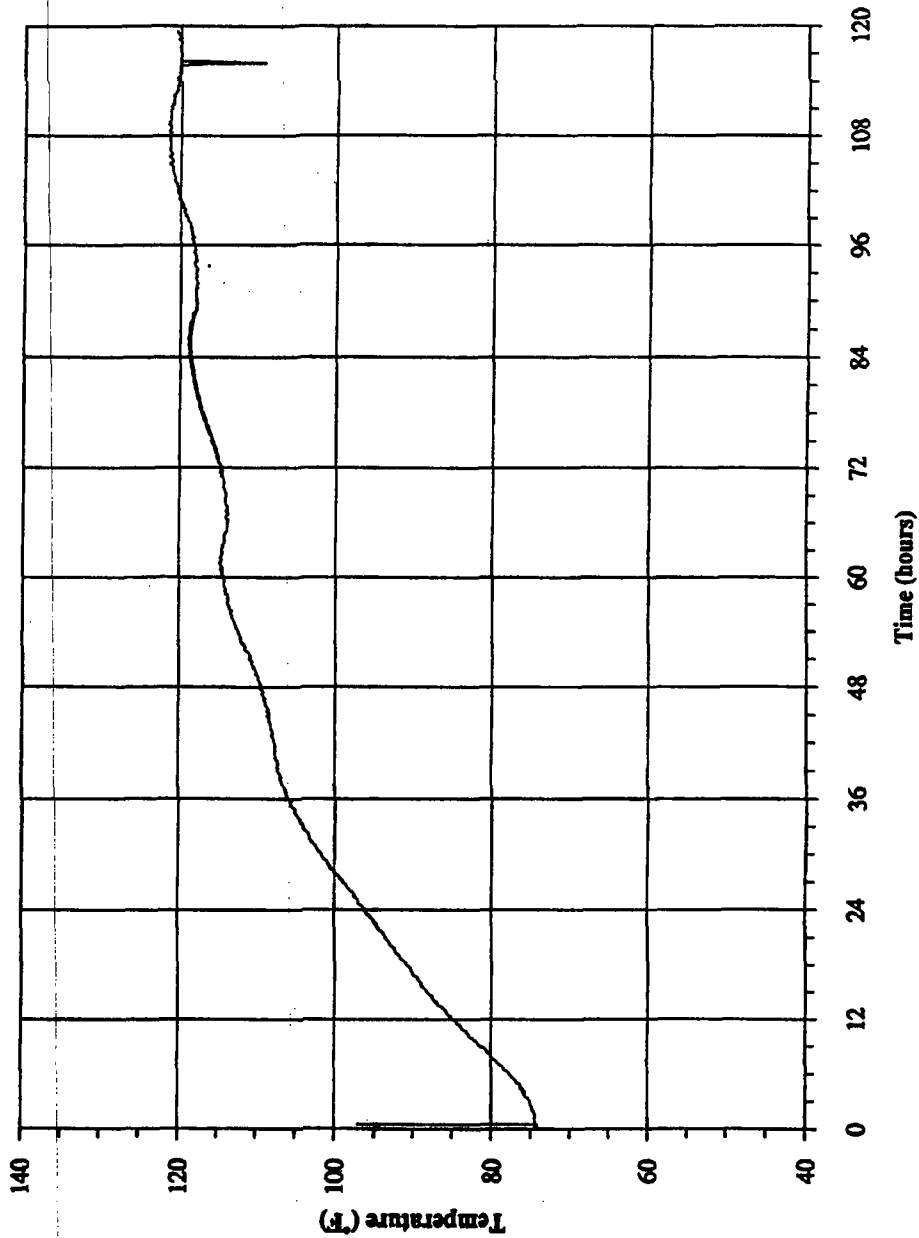
9975 Secondary Containment Vessel Wall Preheat Temperatures



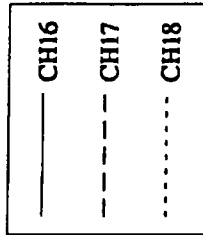
730-A FILE ROOM, PROJECT FOLDER 22381
SRT-PTG-94-0058
Page 31 of 58
July 25, 1994

CH15

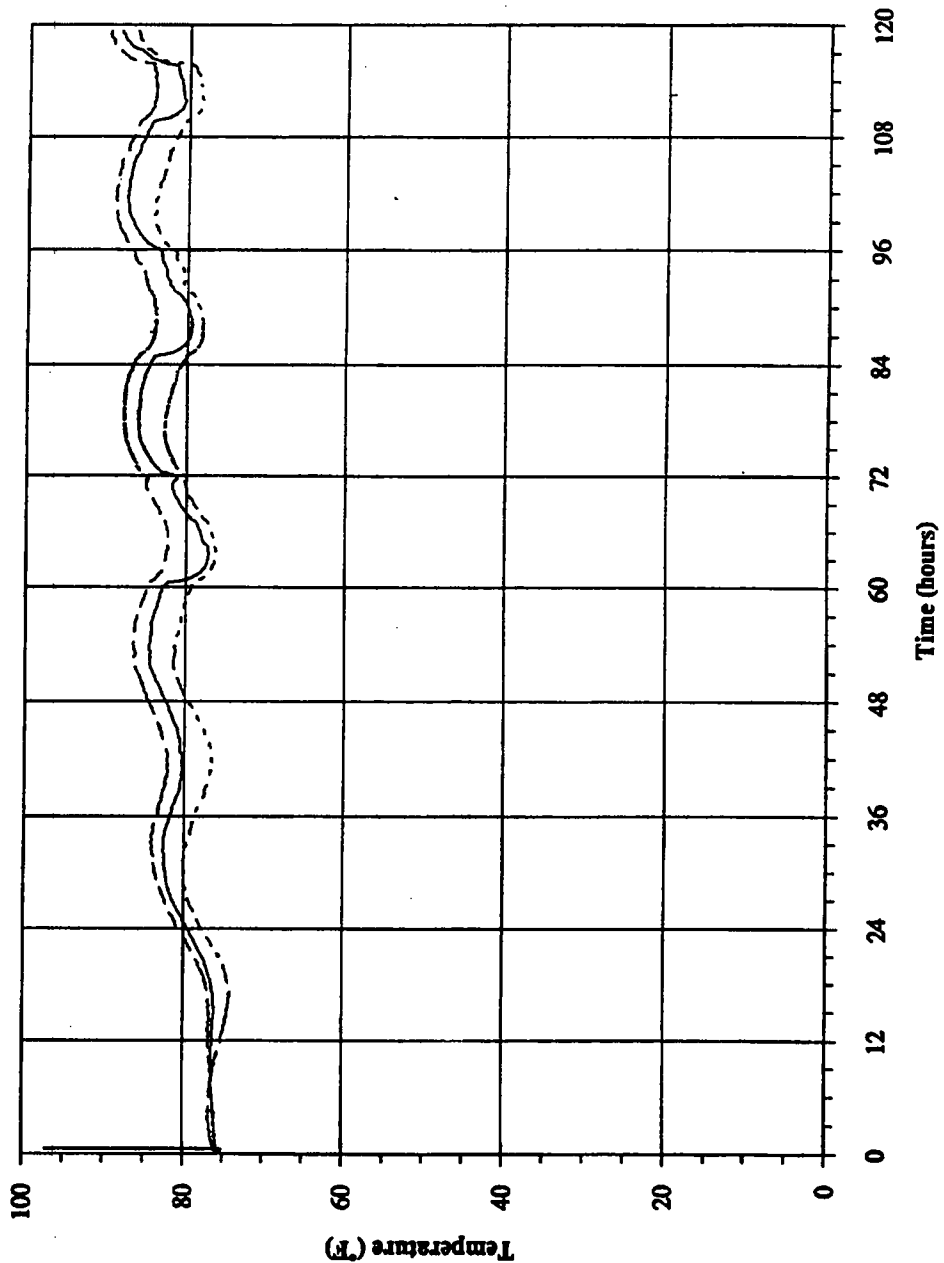
9975 Upper Bearing Plate Preheat Temperature



730-A FILE ROOM, PROJECT FOLDER 22381
SRT-PTG-94-0058
Page 32 of 58
July 25, 1994



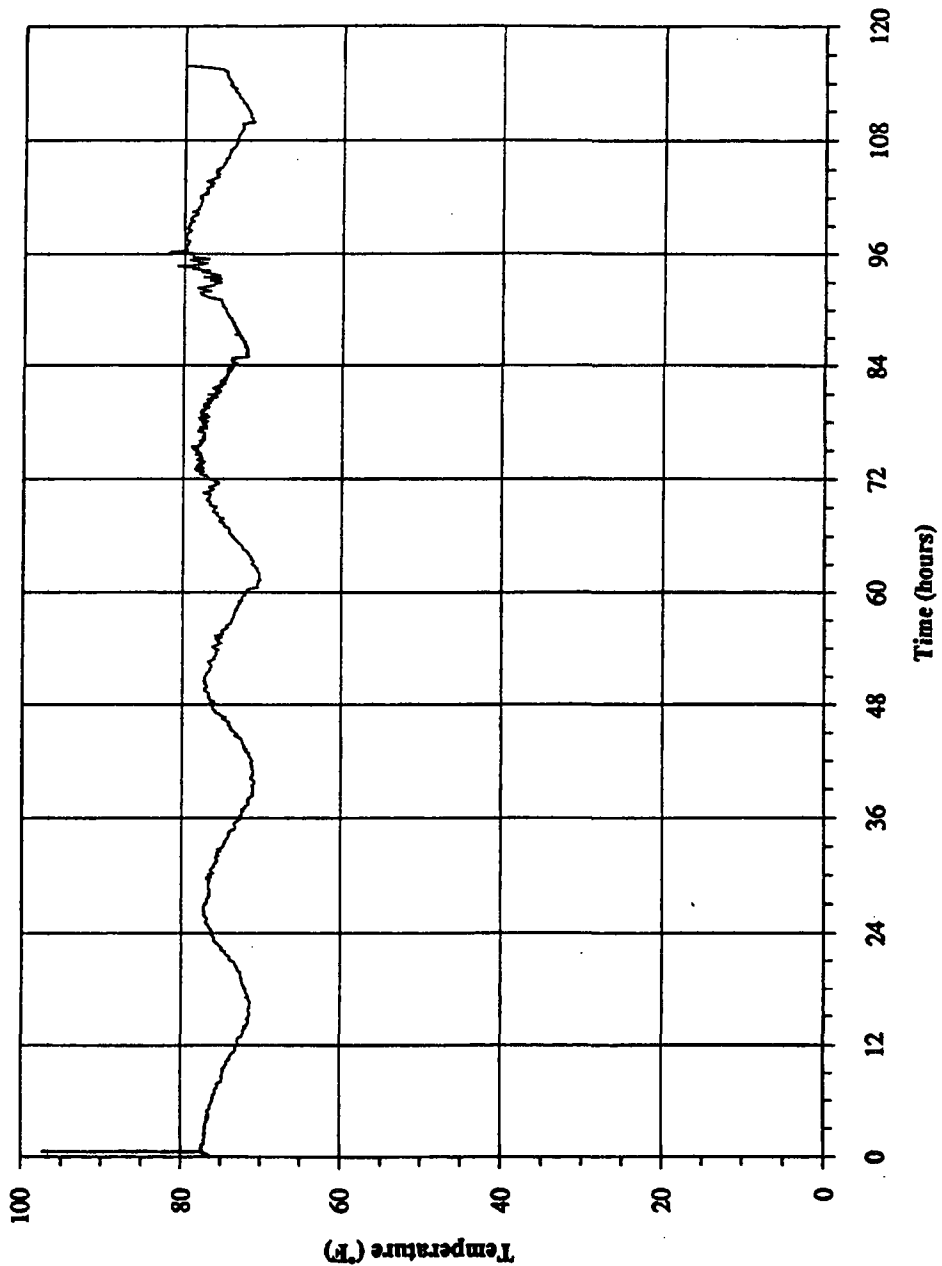
9975 Shield Preheat Temperatures



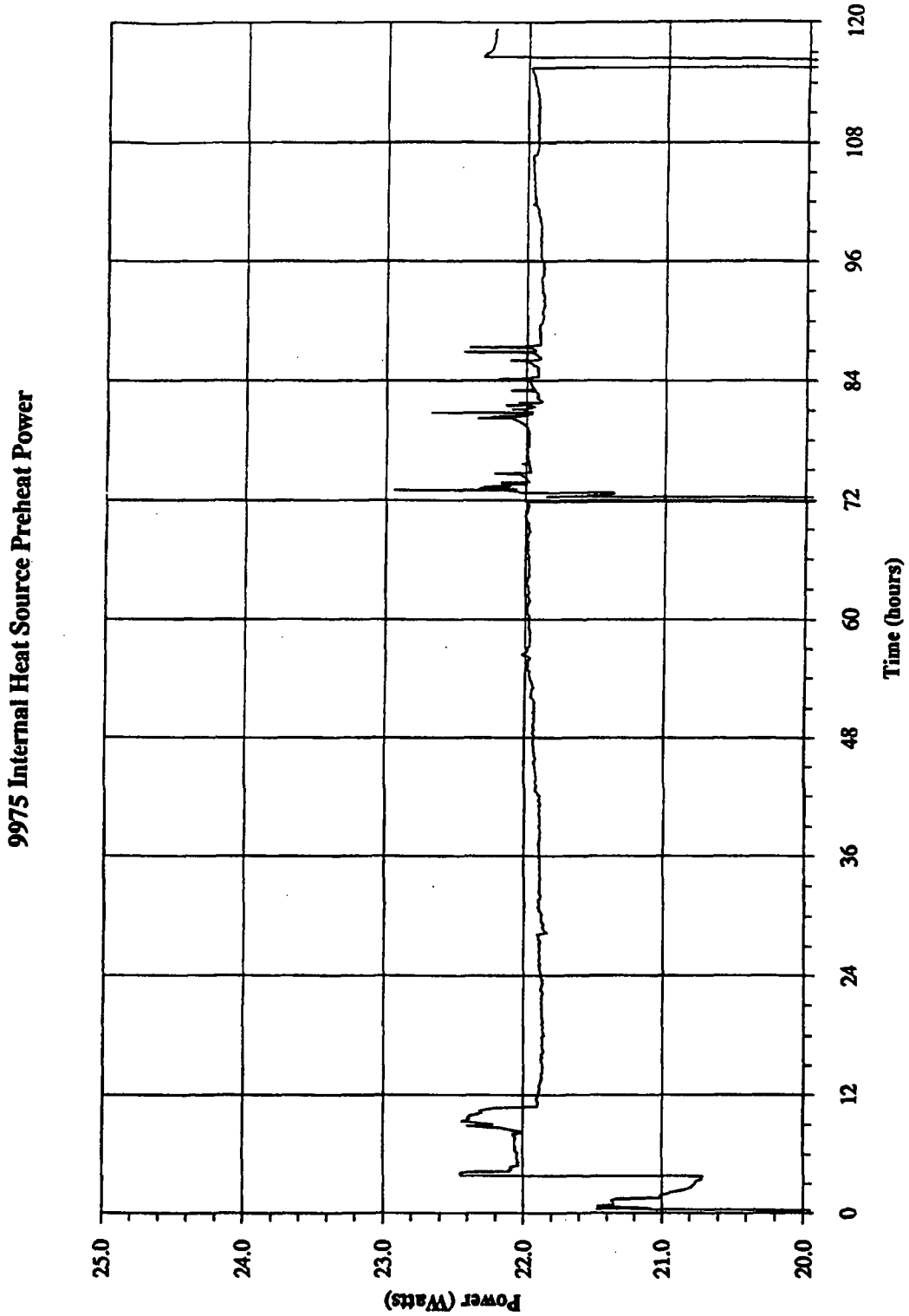
730-A FILE ROOM, PROJECT FOLDER 22381
SRT-PTG-94-0058
Page 33 of 58
July 25, 1994

CH19

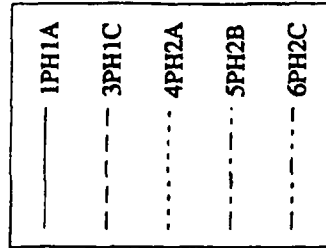
9975 Ambient Preheat Temperature



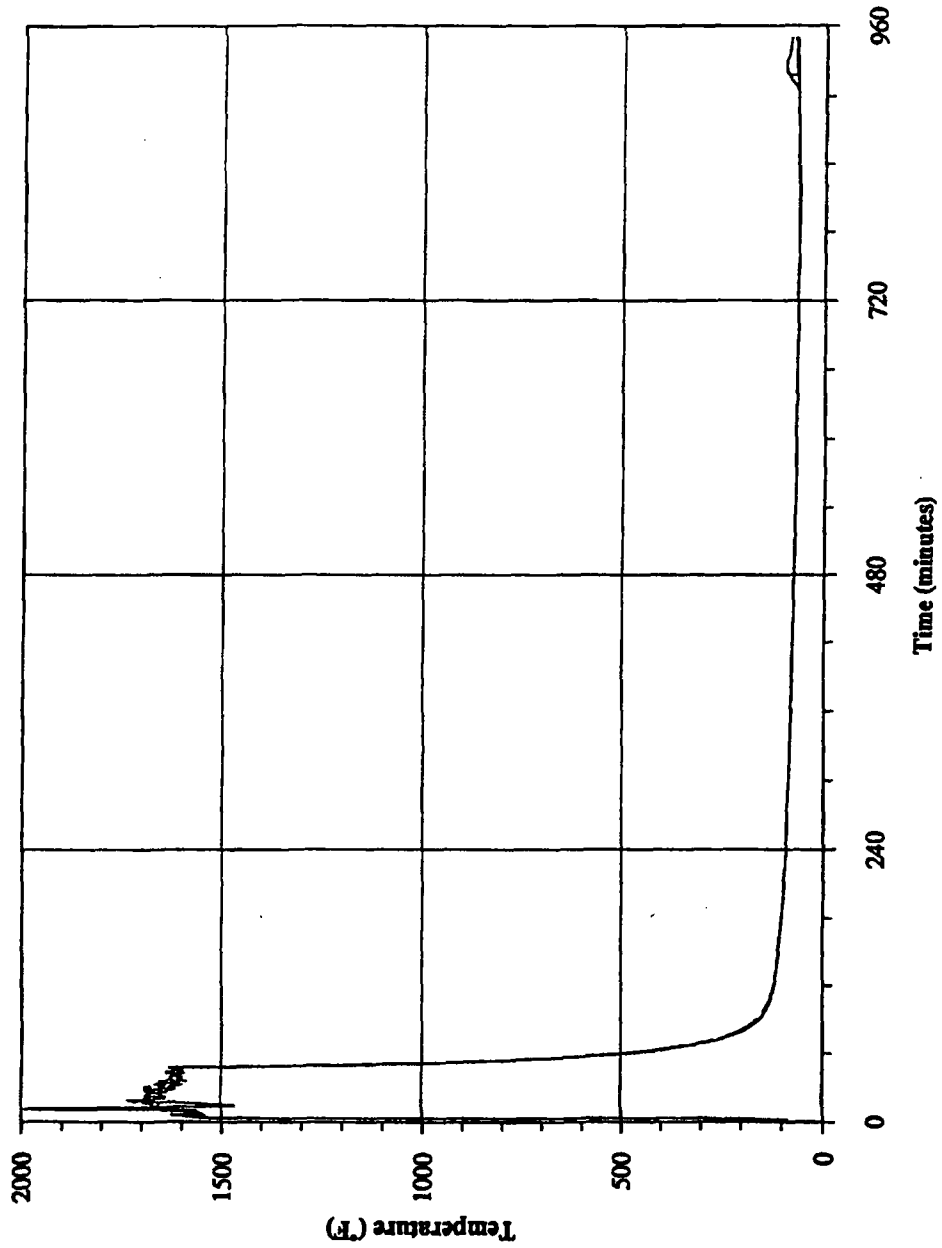
730-A FILE ROOM, PROJECT FOLDER 22381
SRT-PTG-94-0058
Page 34 of 58
July 25, 1994



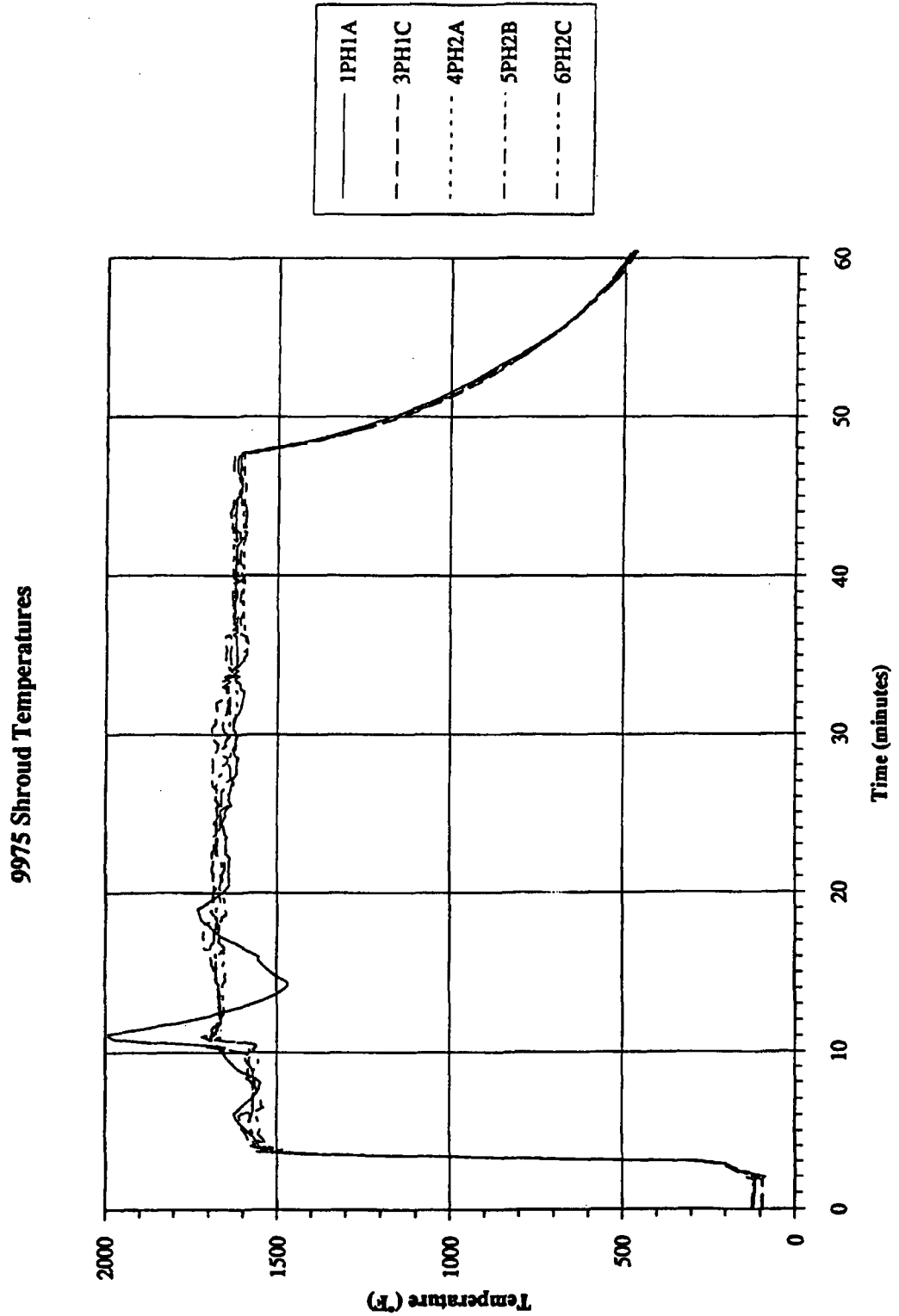
730-A FILE ROOM, PROJECT FOLDER 22381
SRT-PTG-94-0058
Page 35 of 58
July 25, 1994



9975 Shroud Temperatures

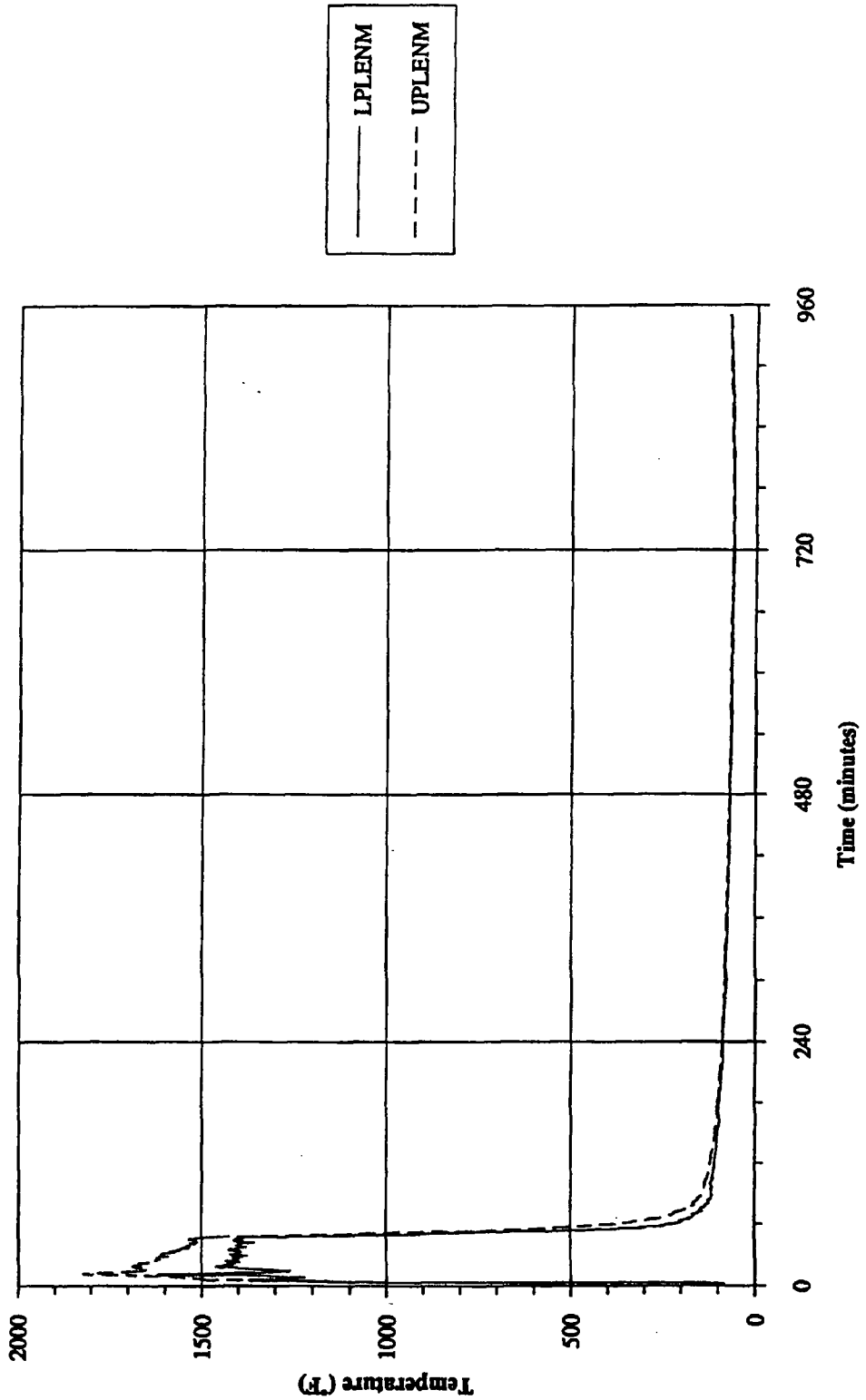


730-A FILE ROOM, PROJECT FOLDER 22381
SRT-PTG-94-0058
Page 36 of 58
July 25, 1994

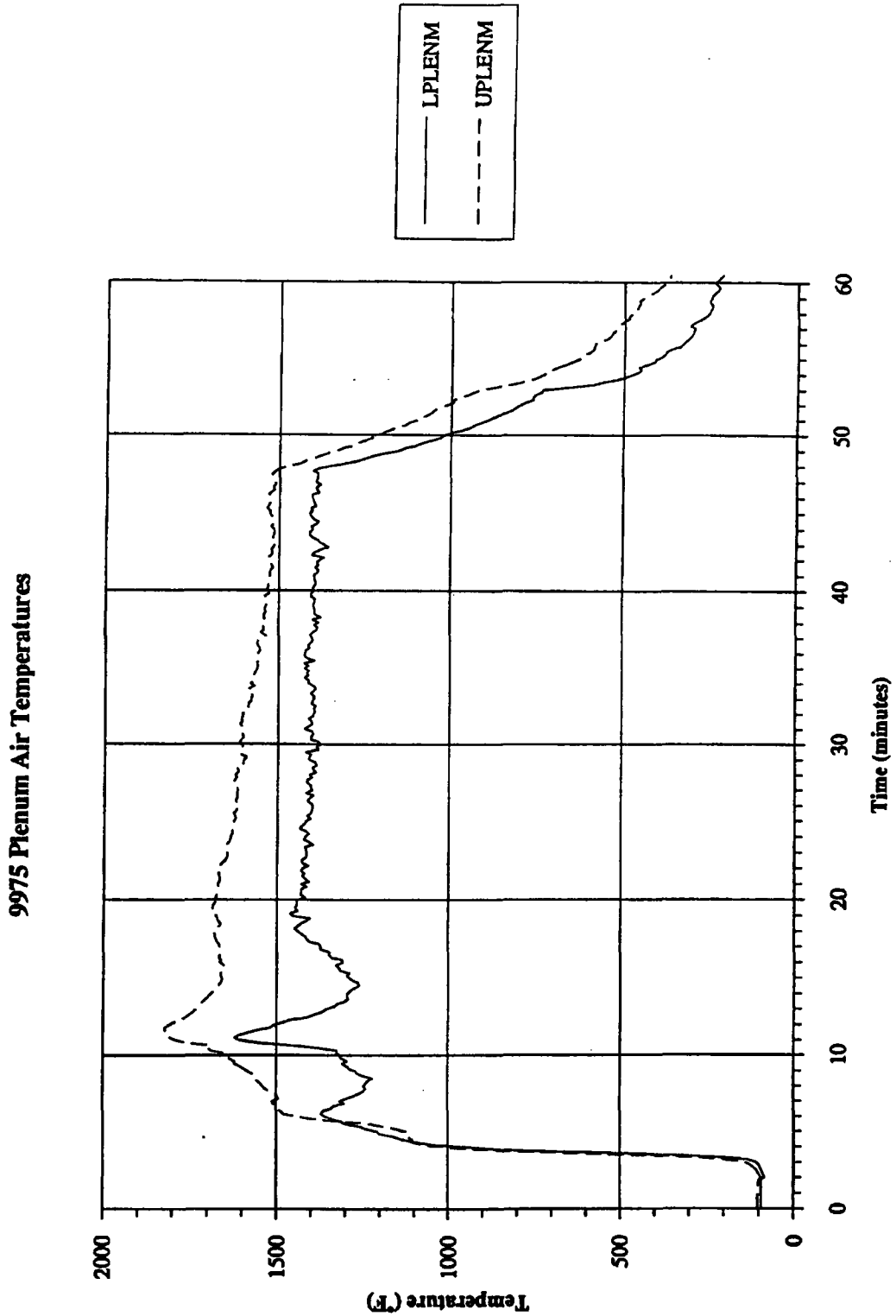


730-A FILE ROOM, PROJECT FOLDER 22381
SRT-PTG-94-0058
Page 37 of 58
July 25, 1994

9975 Plenum Air Temperatures

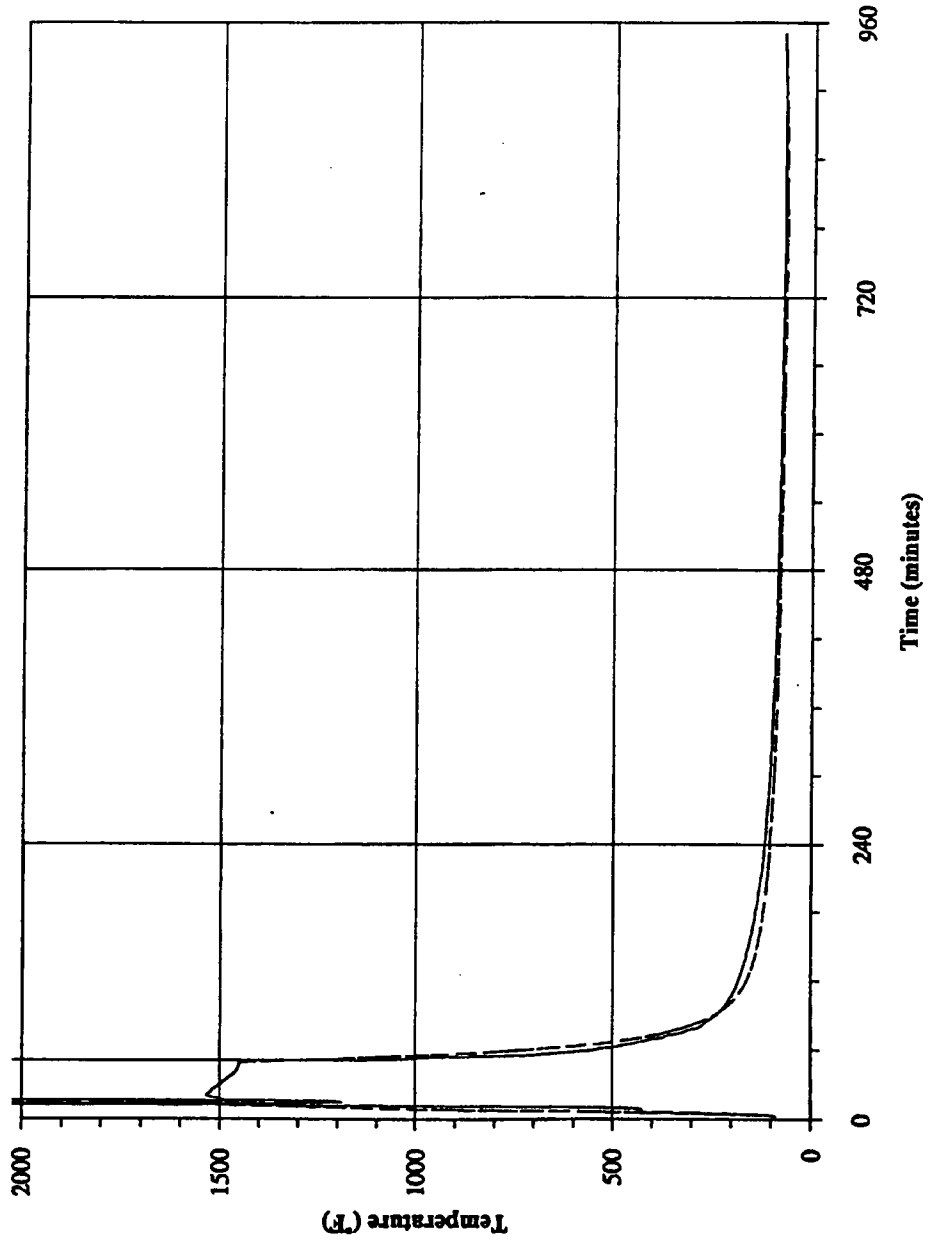


730-A FILE ROOM, PROJECT FOLDER 22381
SRT-PTG-94-0058
Page 38 of 58
July 25, 1994



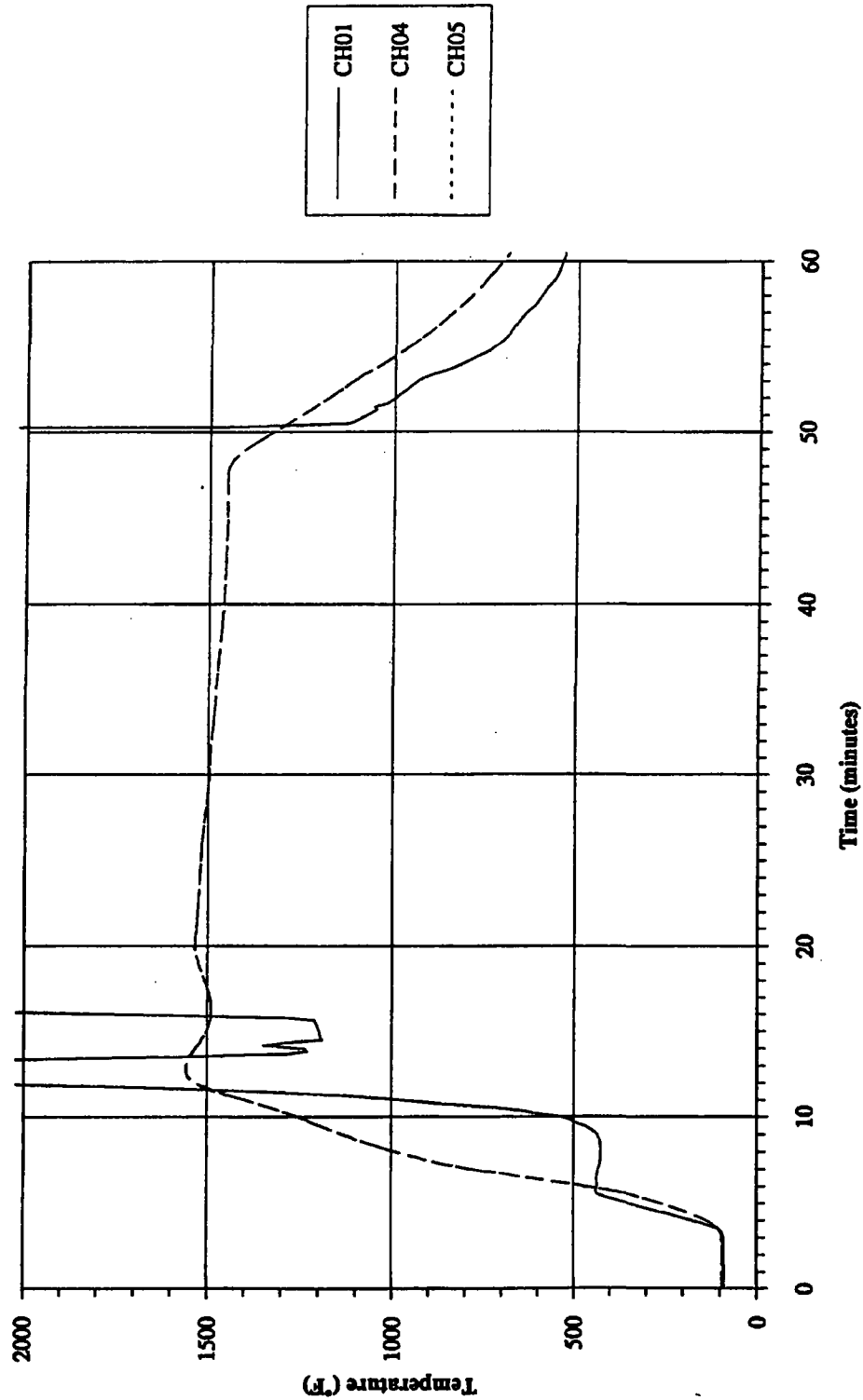
730-A FILE ROOM, PROJECT FOLDER 22381
SRT-PTG-94-0058
Page 39 of 58
July 25, 1994

9975 Drum Lid and Bottom Temperatures

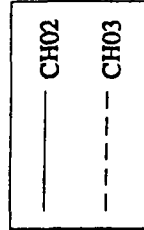


730-A FILE ROOM, PROJECT FOLDER 22381
SRT-PTG-94-0058
Page 40 of 58
July 25, 1994

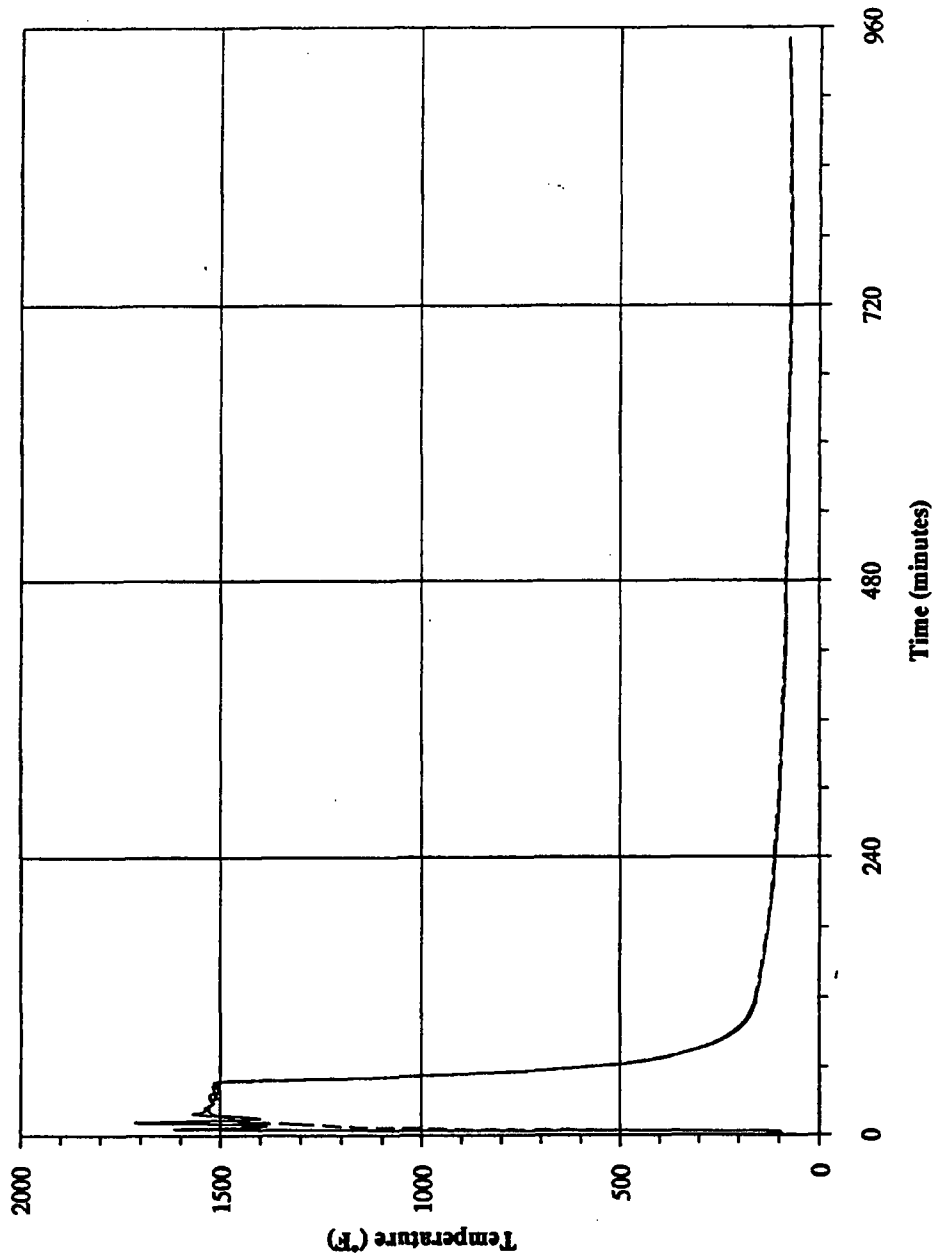
9975 Drum Lid and Bottom Temperatures



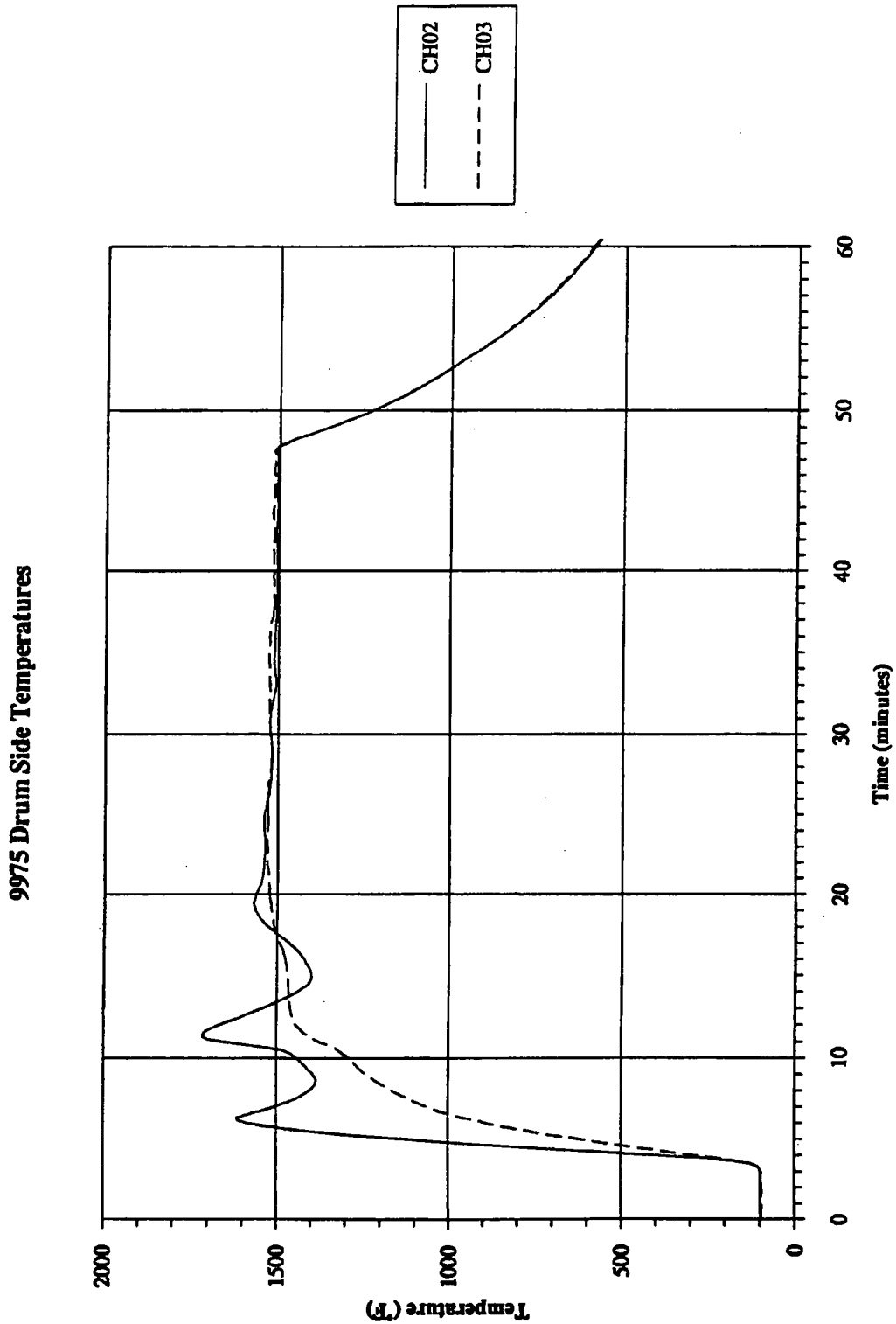
730-A FILE ROOM, PROJECT FOLDER 22381
SRT-PTG-94-0058
Page 41 of 58
July 25, 1994



9975 Drum Side Temperatures

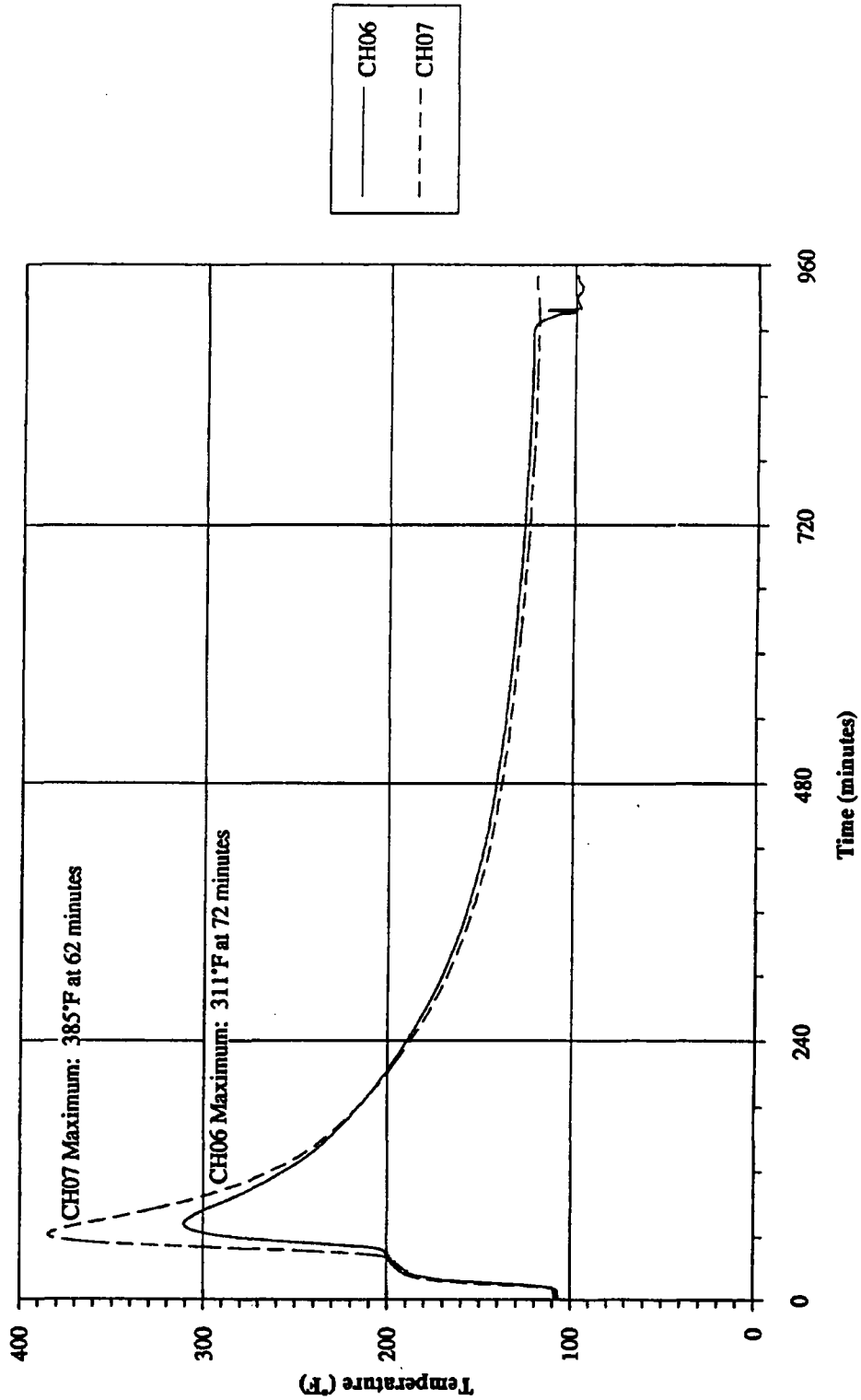


730-A FILE ROOM, PROJECT FOLDER 22381
SRT-PTG-94-0058
Page 42 of 58
July 25, 1994



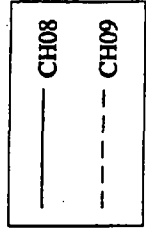
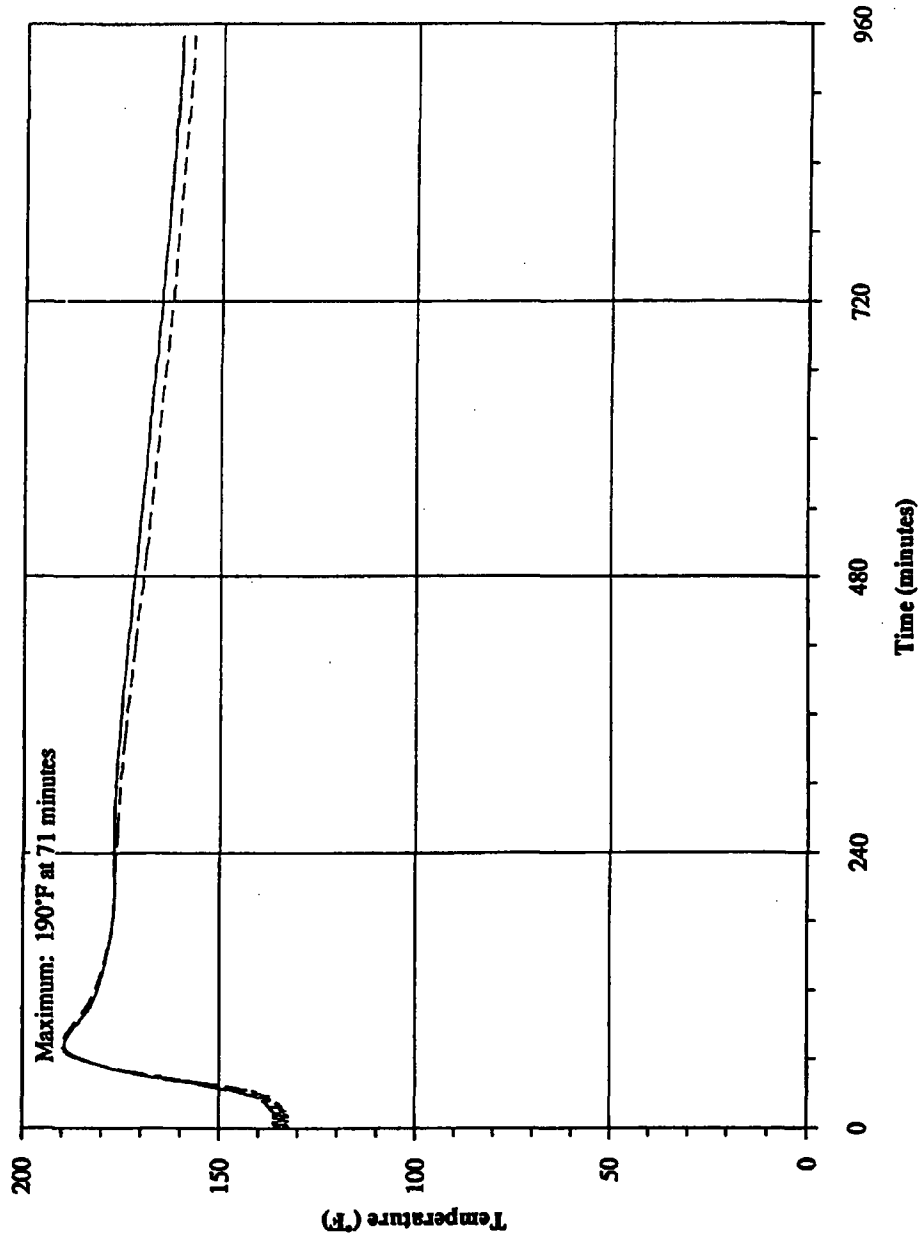
730-A FILE ROOM, PROJECT FOLDER 22381
SRT-PTG-94-0058
Page 43 of 58
July 25, 1994

9975 Mid-wall Fiberboard Temperatures



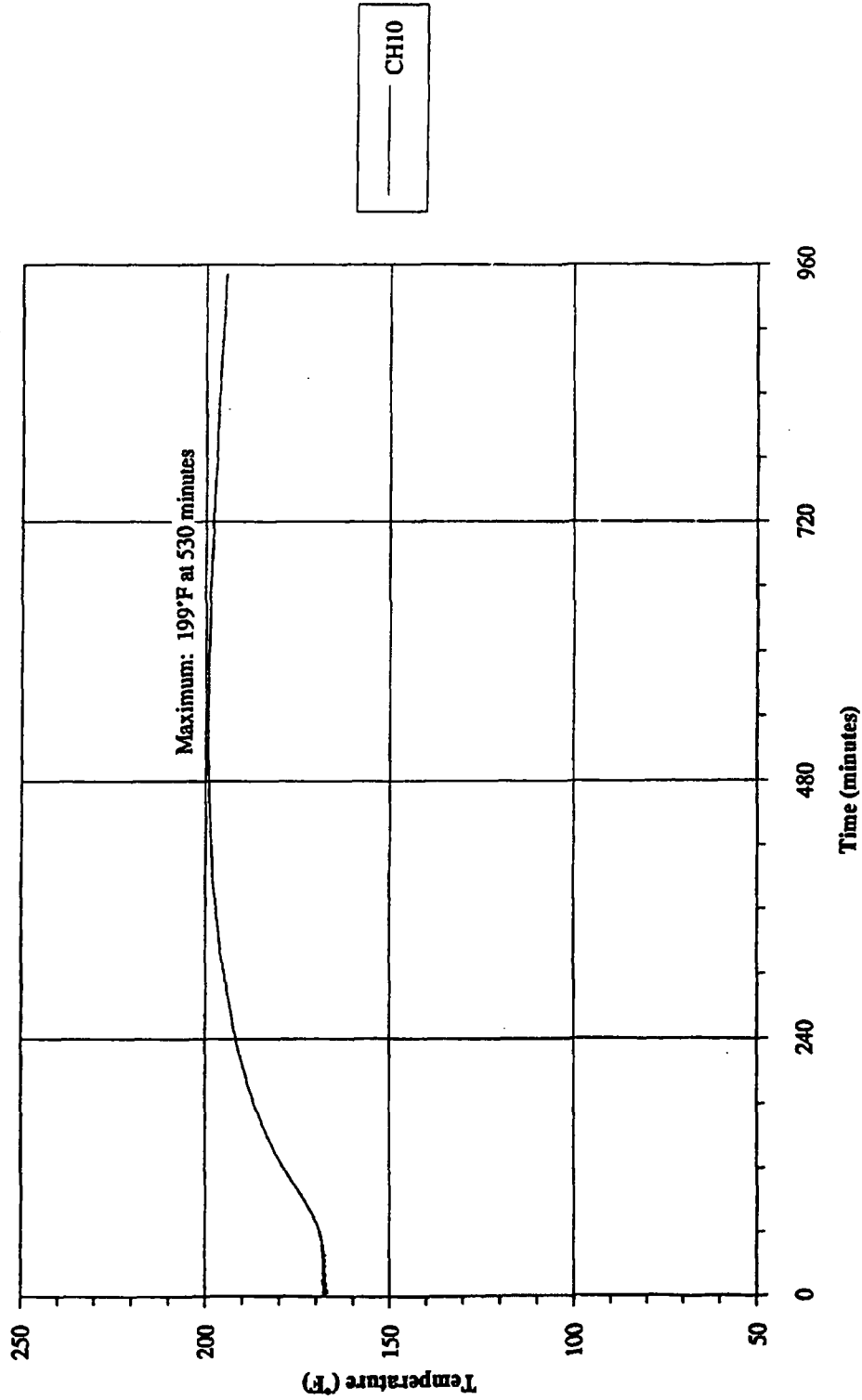
730-A FILE ROOM, PROJECT FOLDER 22381
SRT-PTG-94-0058
Page 44 of 58
July 25, 1994

9975 Lead Temperatures



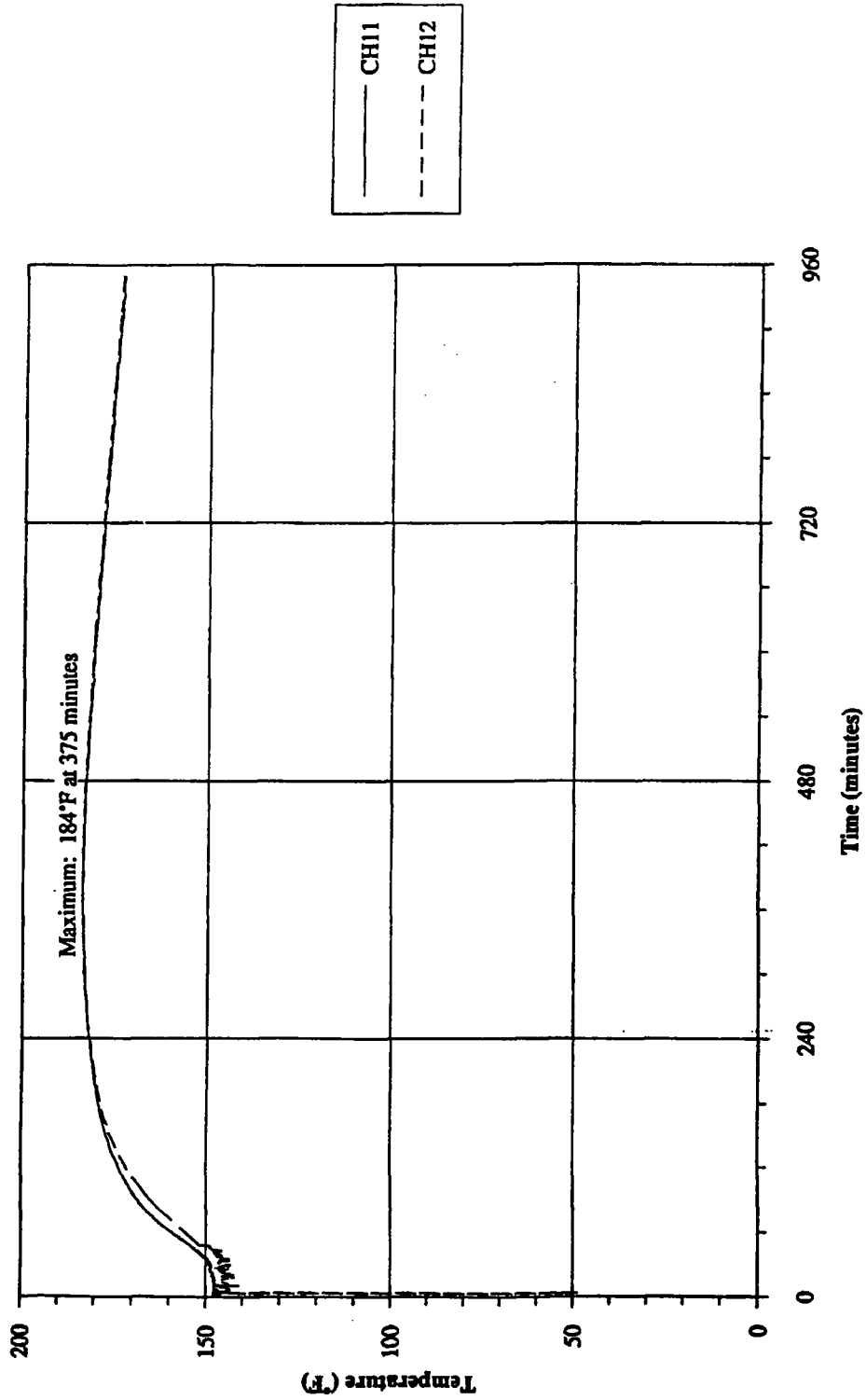
730-A FILE ROOM, PROJECT FOLDER 22381
SRT-PTG-94-0058
Page 45 of 58
July 25, 1994

9975 Primary Containment Vessel Lid Temperature

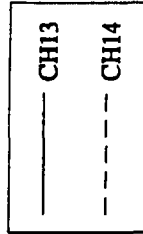


730-A FILE ROOM, PROJECT FOLDER 22381
SRT-PTG-94-0058
Page 46 of 58
July 25, 1994

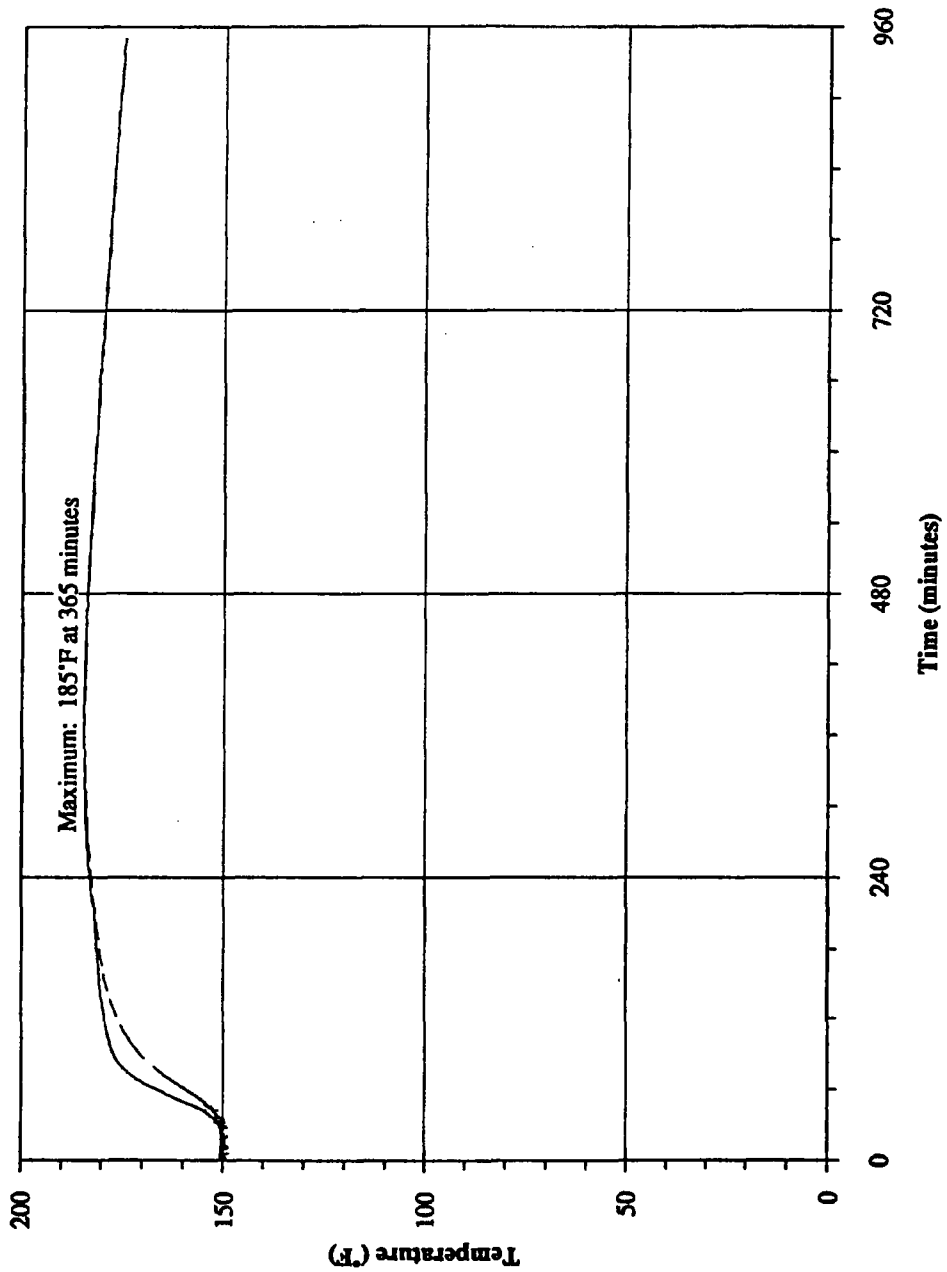
9975 Secondary Containment Vessel Seal Temperatures



730-A FILE ROOM, PROJECT FOLDER 22381
SRT-PTG-94-0058
Page 47 of 58
July 25, 1994



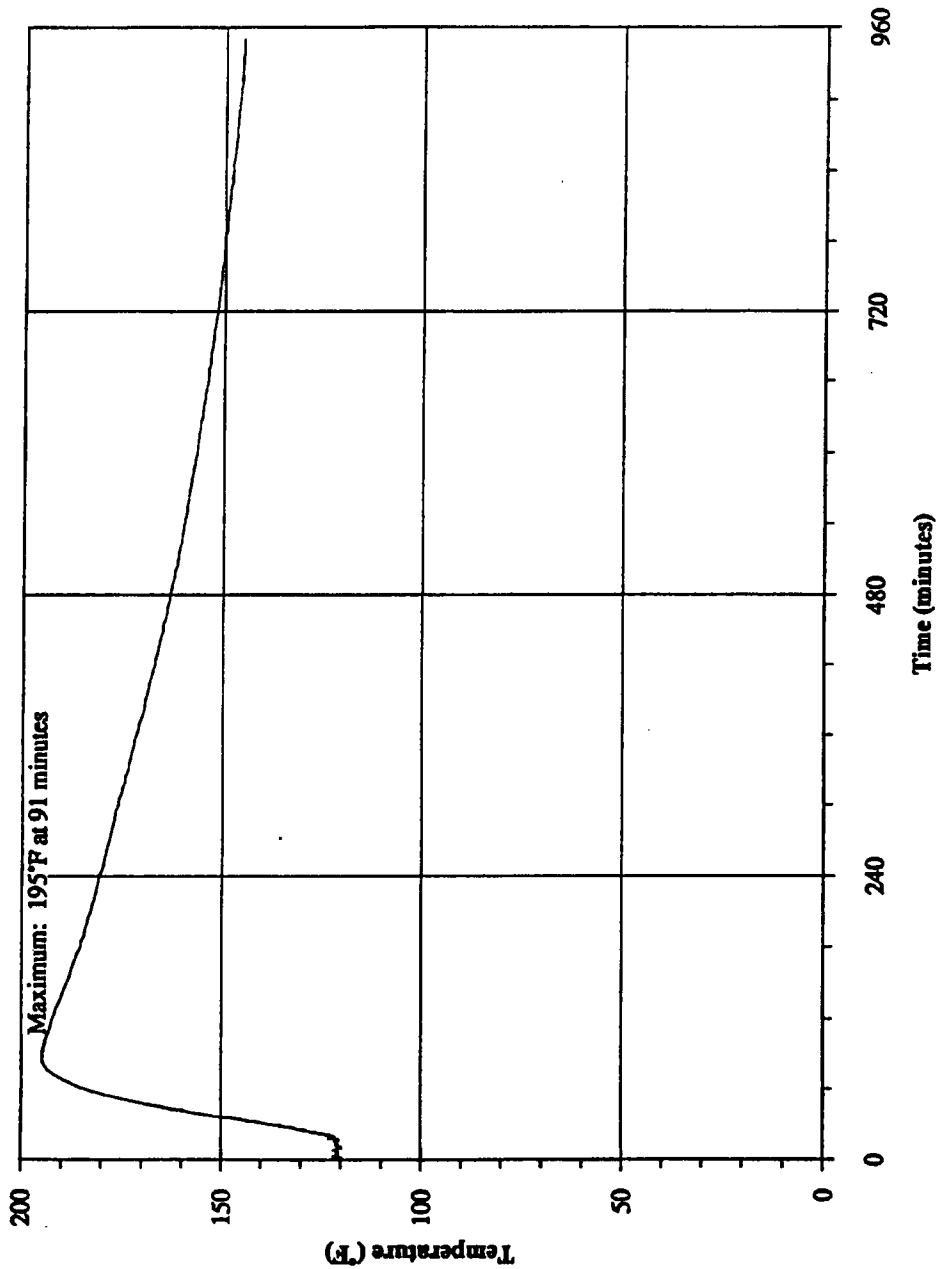
9975 Secondary Containment Vessel Wall Temperatures



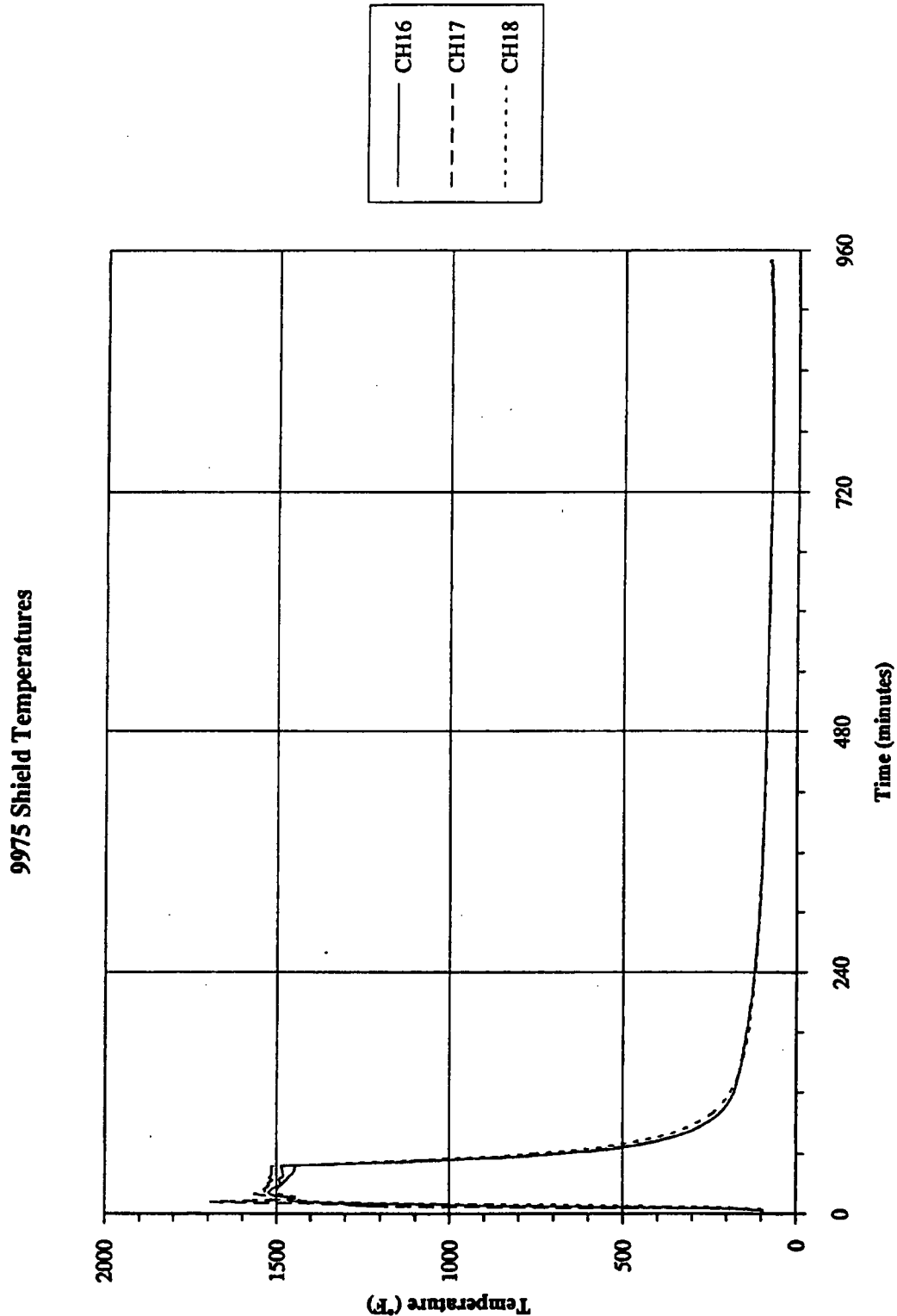
730-A FILE ROOM, PROJECT FOLDER 22381
SRT-PTG-94-0058
Page 48 of 58
July 25, 1994

CH15

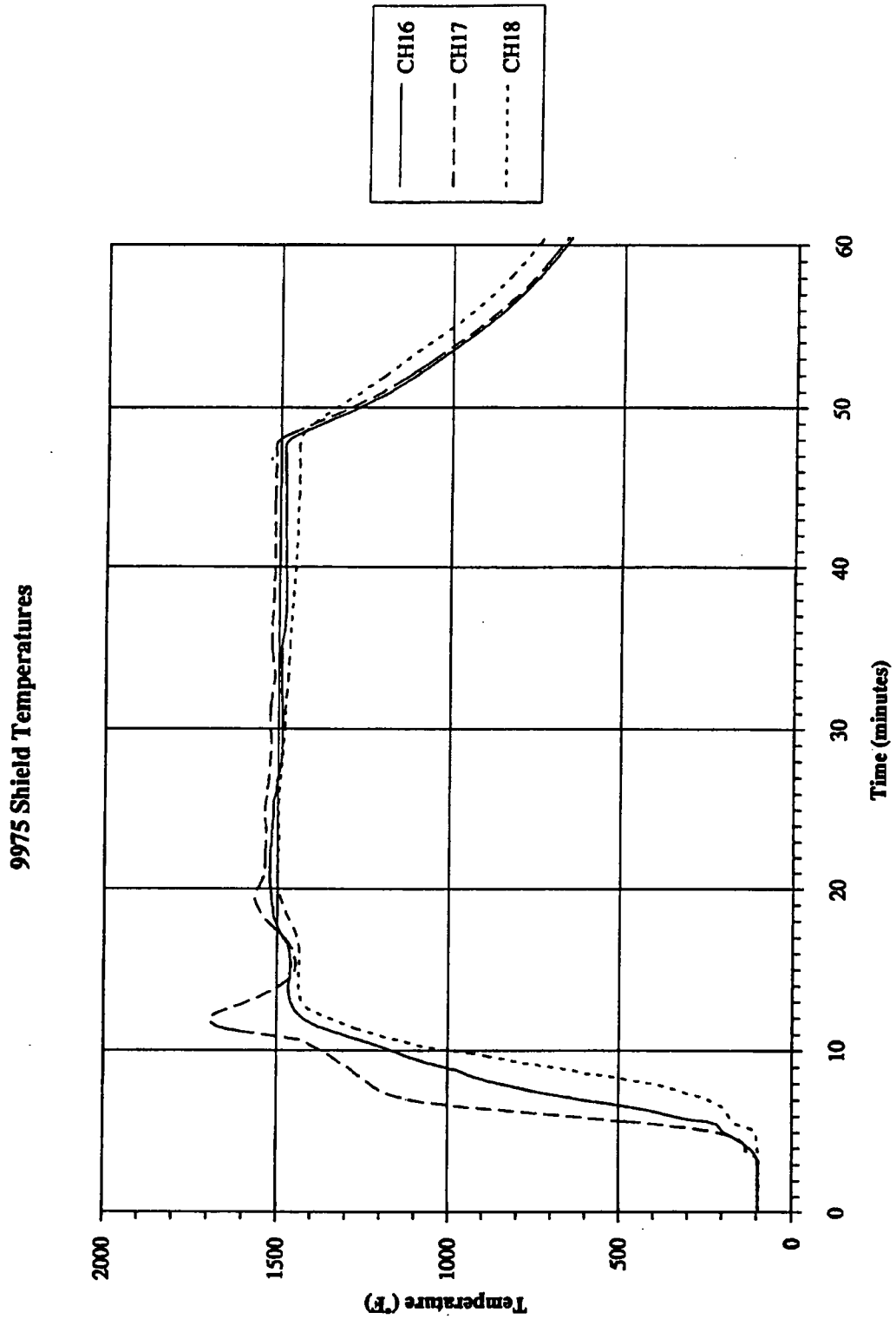
9975 Upper Bearing Plate Temperature



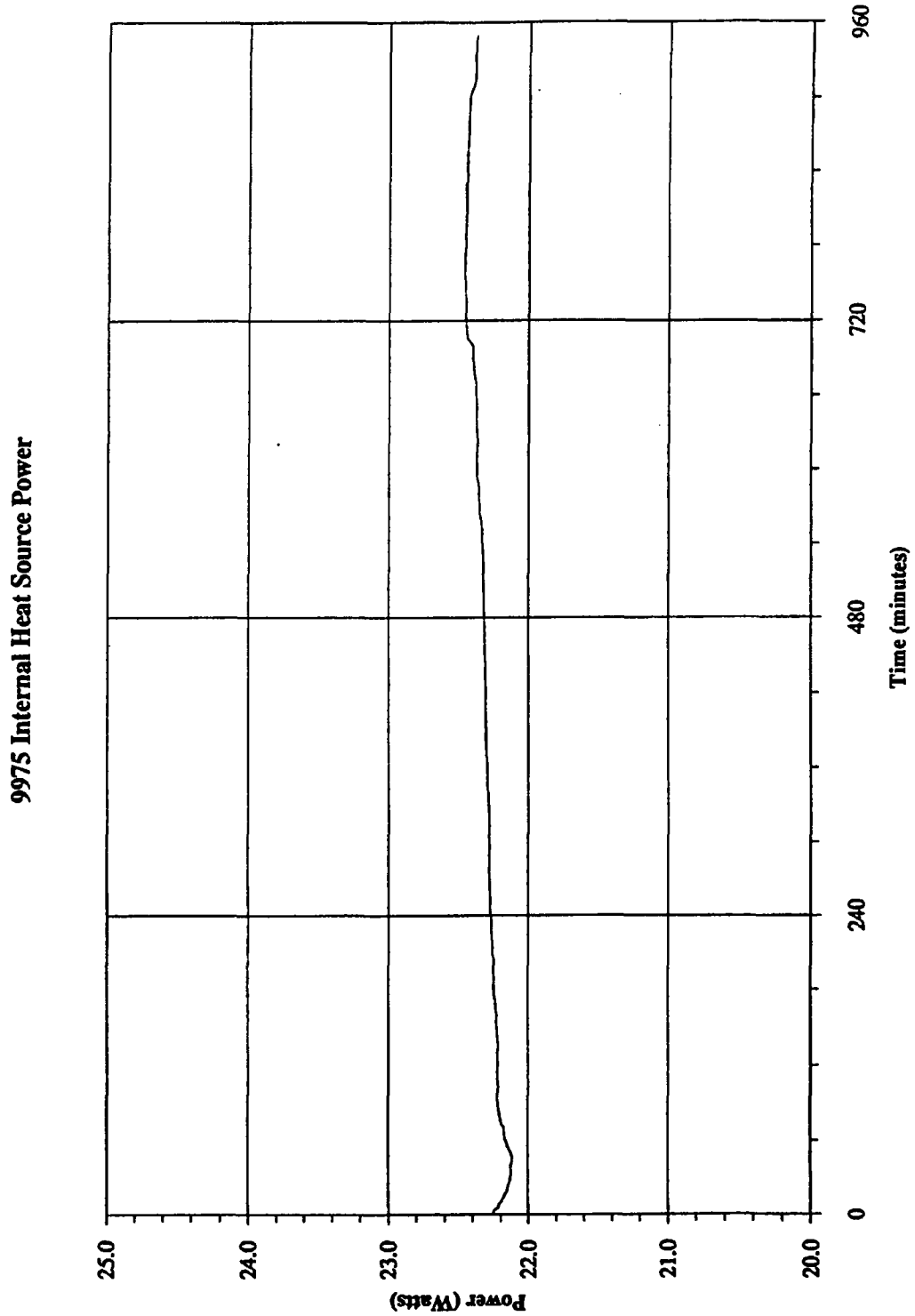
730-A FILE ROOM, PROJECT FOLDER 22381
SRT-PTG-94-0058
Page 49 of 58
July 25, 1994



730-A FILE ROOM, PROJECT FOLDER 22381
SRT-PTG-94-0058
Page 50 of 58
July 25, 1994

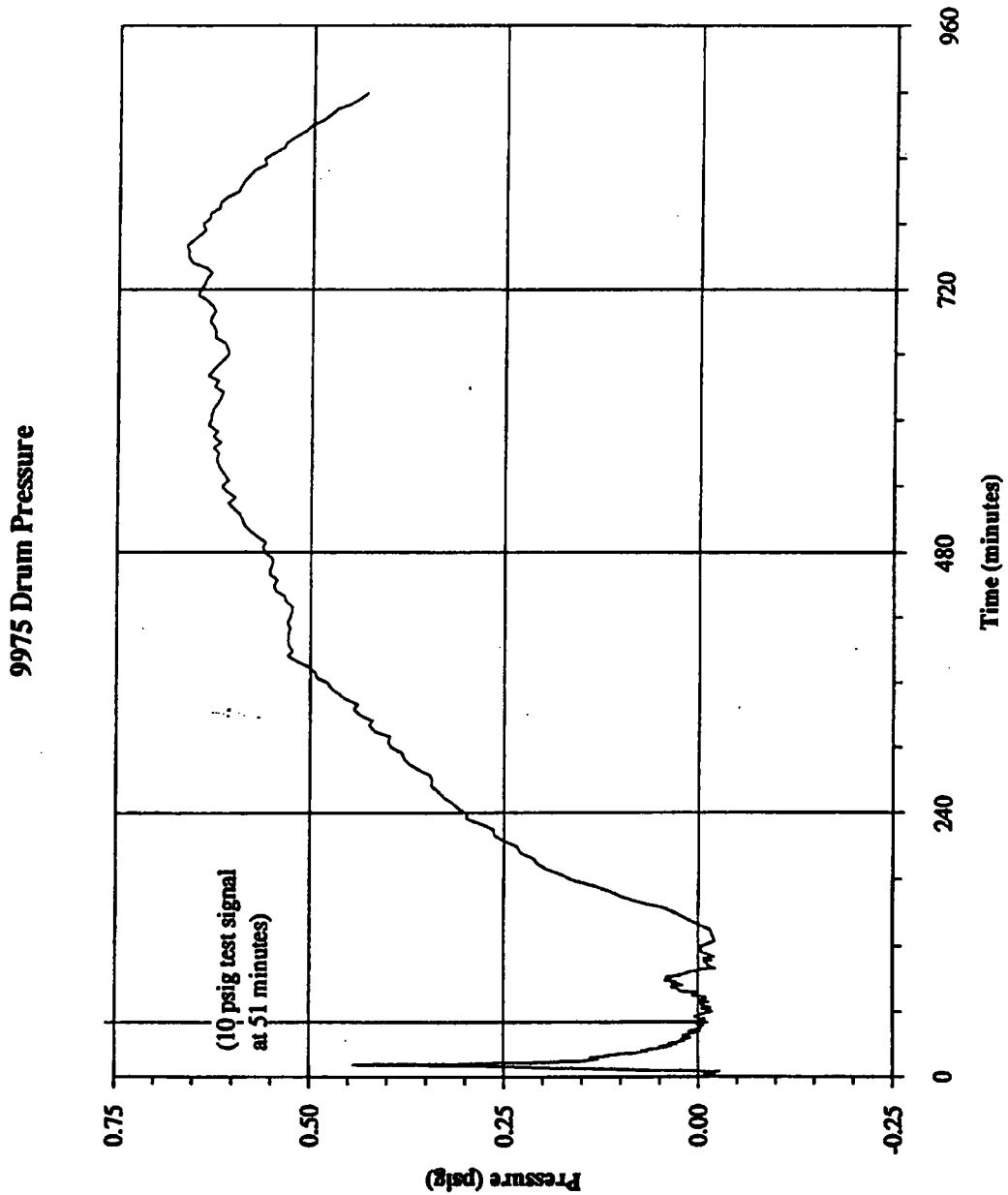


730-A FILE ROOM, PROJECT FOLDER 22381
SRT-PTG-94-0058
Page 51 of 58
July 25, 1994

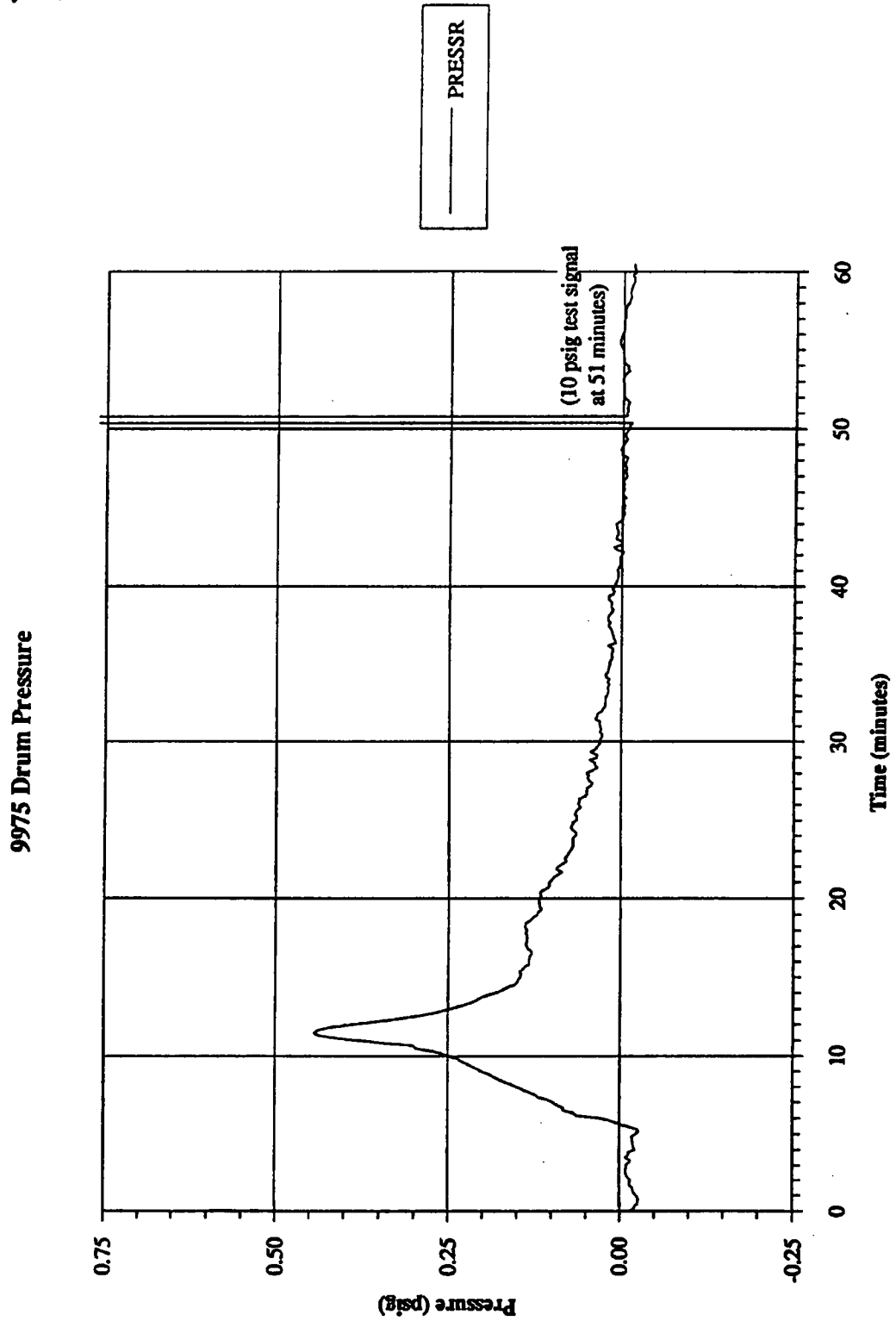


730-A FILE ROOM, PROJECT FOLDER 22381
SRT-PTG-94-0058
Page 52 of 58
July 25, 1994

— PRESSR



730-A FILE ROOM, PROJECT FOLDER 22381
SRT-PTG-94-0058
Page 53 of 58
July 25, 1994



730-A FILE ROOM, PROJECT FOLDER 22381
SRT-PTG-94-0058
Page 54 of 58
July 25, 1994

DISCUSSION

9973 Accident Test

This test was to fully comply with the regulatory test requirements. Consequently, acceptance was that during heating, the minimum drum temperature be at least 1500°F or greater for 30 minutes. Given the thin drum wall, this would ensure satisfying regulatory temperature and heat flux requirements. Following heating, the packaging was allowed to cool 17 hours while remaining in the test facility.

Shroud temperatures and plenum air temperatures indicate the thermal environment during heating and cooling. Heating began at 2 minutes and ended at 42 minutes. All shroud channels initially rose to approximately 1850°F; however, heat lamp failures at 7 minutes caused fluctuations and a decrease in channel 6PH2C to approximately 1575°F. Power compensations to the remaining heat lamps caused a localized melt-through of the shroud wall. Temperature spikes on some drum channels at 8 minutes are attributed to this power compensation. Again, the upper plenum was hotter than the lower plenum and rapid cooling of the facility environment indicated that the 9973 cooled as if in natural surroundings.

Drum bottom temperatures were again lost due to an apparent failure in channel CH01. Due to the horizontal packaging orientation, actual drum bottom temperatures are assumed to be the same as the drum top (CH06, CH07). Disassembly revealed essentially the same top and bottom test effects, further indicating that the temperatures were the same. Drum top temperatures remained above 1500°F for 38 minutes and above 1725°F during the 30 minute regulatory test period.

Lower drum side temperatures (CH02, CH03) were cooler than the upper drum side temperatures (CH04, CH05). CH02 controlled the test initiation. It reaching 1500°F at 12 minutes and gradually increased to 1684°F. Heat lamp failures caused CH03 to drop to 1534°F, which remained acceptable. Shield side temperatures (CH14, CH15) closely followed the drum side temperatures. However, the shield top temperature (CH16) heated much slower and peaked lower than did the drum lid. This is assumed to be caused by the thermal blanket between the lid and shield top.

Table 3 summarizes internal temperature peaks. Appendix 3 includes hardware evaluations.

Drum pressure was much less than expected. It reached a sharp peak of 0.45 psig at 9 minutes during heating, followed by a drop to -.012 psig at 51 minutes. Pressure then steadily increased, peaking at 0.45 psig at 859 minutes. It is not obvious whether the gradual increase was due to packaging behavior or facility conditions. The drum pressure tap fitting was observed to be loose following the test and was assumed to have loosened during the heating and subsequent cooling. No jetting marks were observed on the shroud, although the packaging orientation would have precluded direct impingement on the shroud.

Both the SCV and PCV were leak tight following the test and disassembly, as reported in Appendix 3.

730-A FILE ROOM, PROJECT FOLDER 22381
 SRT-PTG-94-0058
 Page 55 of 58
 July 25, 1994

Table 3. 9973 Peak Test Temperatures

Channel	Location	Peak and Time
CH08	SCV seal	165°F, 144 min.
CH09	SCV seal, 180° apart	160°F, 181 min.
CH10	SCV side	169°F, 126 min.
CH11	SCV side, 180° apart	158°F, 149 min.
CH12	Upper bearing plate	182°F, 105 min.
CH13	Upper bearing plate, redundant	181°F, 109 min.

9975 Preheat

The preheat, or 5 day period during which the internal heater brought the 9975 to normal operating temperatures, occurred in an air-conditioned building. Heater power was maintained at approximately 22W, slightly in excess of the design 21W. All 9975 preheat temperature plots show a calibration spike early in the first hour. Discontinuities at 72 hours were due to signal tests. Discontinuities after 114 hours were due to system changeover when the packaging was relocated to the test facility. Preheat was terminated when temperatures had reached nearly steady state as based on observation and preliminary analytical estimates.

Ambient temperatures (CH19) show the air temperature fluctuations starting at approximately 3:00 p.m., June 4, 1994. Daily peaks remained about 77°F until the last 2 days, which peaked at about 80°F. The drum skin temperatures (CH01 through CH05) were strongly influenced by the ambient. Heating caused skin temperatures to increase approximately 10°F in 5 days. Internal temperatures reflected ambient cycling, but to a gradually lesser extent further toward the packaging center. Temperature increases were greater closer to the packaging center (and heat source). Temperatures are summarized in Table 4.

9975 Accident Test

Immediately following the preheat, the 9975 was moved into the radiant heat facility and exposed to the thermal accident conditions. Acceptance was that the drum side temperatures be at 1500°F or greater for 30 minutes. Following the exposure, the packaging was allowed to cool 15 hours while remaining in the test facility.

Heater power remained approximately 22W the entire time. As with the 9973, shroud temperatures and plenum air temperatures indicate the thermal environment during heating and cooling. Heating began at 3 minutes and ended at 48 minutes. Shroud channel 1PH1A briefly rose to 2000°F at 11 minutes while heater power was being leveled. Shroud channel 2PH1B failed and was not reported. As expected, the upper plenum was hotter than the lower plenum. Rapid cooling of the facility environment indicated that the packaging was allowed to cool as if in natural surroundings. Shroud temperature increases at 900 minutes were due to solar heating during facility disassembly.

Drum bottom temperatures during heating were lost due to channel CH01 failing. When CH01 apparently recovered at 51 minutes, the drum bottom (CH01) was 1124°F while the drum top

730-A FILE ROOM, PROJECT FOLDER 22381
 SRT-PTG-94-0058
 Page 56 of 58
 July 25, 1994

(CH04 and CH05) was 1291°F. Bottom temperatures most likely remained 90.5% of the top temperature during the heating period, indicating that the drum bottom was then approximately 1350°F. The top varied from 1530°F to 1450°F during heating. Drum side temperatures (CH02 and CH03), which controlled the test, reached 1500°F at 18 minutes. Shield temperatures (CH16, CH17, CH18) were essentially the same as those of the drum.

Fiberboard temperature channel CH07 peaked 74°F higher than channel CH06. Upon disassembly, CH07 was found to be nearly at the char boundary, while CH06 was not. Appendix 3 includes pertinent measurements. Discontinuity in fiberboard channel CH06 after 900 minutes was due to disturbances during facility disassembly.

Table 5 summarizes internal temperature peaks. Appendix 3 includes hardware evaluations.

Table 4. 9975 Preheat Temperatures

Channel	Location	Initial (1 hr)	Peak and Time
CH01	Drum bottom center	76°F	83°F, 104 hr
CH02	Drum side	76°F	86°F, 101 hr
CH03	Drum side, 180° apart	75°F	87°F, 101 hr
CH04	Drum lid	76°F	84°F, 99 hr
CH05	Drum lid, redundant	76°F	84°F, 99 hr
CH06	Fiberboard mid-wall	75°F	107°F, 104 hr
CH07	Fiberboard mid-wall, 180° apart	75°F	104°F, 104 hr
CH08	Lead side	74°F	137°F, 110 hr
CH09	Lead side, 180° apart	74°F	134°F, 110 hr
CH10	PCV lid	76°F	169°F, 112 hr
CH11	SCV seal	74°F	148°F, 110 hr
CH12	SCV seal, 180° apart	74°F	150°F, 111 hr
CH13	SCV side	74°F	149°F, 110 hr
CH14	SCV side, 180° apart	74°F	152°F, 111 hr
CH15	Upper bearing plate	74°F	122°F, 109 hr
CH16	Shield side	76°F	88°F, 102 hr
CH17	Shield side, 180° apart	76°F	89°F, 101 hr
CH18	Shield top	76°F	84°F, 99 hr
CH19	Preheat ambient	77°F	80°F, 98 hr

Drum pressure was similar to that of the 9973. During heating, it peaked at 0.44 psig at 11 minutes, after which it returned to the initial value. However, it did not experience the negative pressure dip observed for the 9973. It again briefly increased and peaked at 0.04 psig at 60 minutes. Following a return to the initial value, the pressure gradually increased and peaked at 0.66 psig at 745 minutes. Again, it is not obvious whether the gradual increase was due to packaging behavior or facility conditions. While no vigorous gas emission was observed, markings on the shroud indicated some jetting occurred.

730-A FILE ROOM, PROJECT FOLDER 22381
 SRT-PTG-94-0058
 Page 57 of 58
 July 25, 1994

Disassembly revealed charring had penetrated greater at poorly adhered glue joints that at well adhered joints.

Table 5. 9975 Peak Test Temperatures

Channel	Location	Peak and Time
CH06	Fiberboard mid-wall	331°F, 72 min.
CH07	Fiberboard mid-wall, 180° apart	385°F, 62 min.
CH08	Lead side	189°F, 73 min.
CH09	Lead side, 180° apart	190°F, 71 min.
CH10	PCV lid	199°F, 530 min.
CH11	SCV seal	184°F, 380 min.
CH12	SCV seal, 180° apart	184°F, 375 min.
CH13	SCV side	185°F, 365 min.
CH14	SCV side, 180° apart	185°F, 375 min.
CH15	Upper bearing plate	195°F, 91 min.

CONCLUSION

Both the 9973 and 9975 packagings performed as intended and both tests were successfully accomplished. Test conditions were kept within acceptable limits. That the 9973 test environment satisfied regulatory requirements is documented in the Sandia test report⁵. Packaging acceptance criteria were satisfied, as summarized in Table 6.

Table 6. Acceptance Criteria Summary

Criteria	9973 Results	9975 Results
Containment vessel seals ≤ 400°F	PCV: NR SCV: 165°F†	PCV: 199°F† SCV: 184°F†
Lead ≤ 620°F melting point	Not applicable	190°F*
Fiberboard not burnt	No evidence of burning	No evidence of burning
Containment vessel leak ≤ 1.96 × 10 ⁻⁷ std cm ³ He/sec at 14.7 psid	PCV: 2.5 × 10 ⁻⁸ std cm ³ He/sec SCV: < 2.8 × 10 ⁻⁹ std cm ³ He/sec (both at 150 psid)	Not measured

† Actually vessel temperatures adjacent to seals.

* Outside wall at mid-height.

Having the thermal blanket present did significantly retard and limit the shield top temperature rise during accident heating. No fiberboard burning occurred, indicating that no air reached the

730-A FILE ROOM, PROJECT FOLDER 22381
SRT-PTG-94-0058
Page 58 of 58
July 25, 1994

heated fiberboard and further indicating that the shield functioned as intended. The vent plugs were completely consumed while the drum lid gasket, although fully charred, remained intact.

The fiberboard junction step, although fully charred, remained intact. There were no indications of radiant heating from the drum wall to the 9975 lead cylinder or 9973 SCV. Therefore, any gapping that may have occurred, particularly in the 9973 as a result of drop damages, was successfully overcome by the step. Poorly adhered glue joints allow greater char penetration than do well adhered joints.

As expected, the drum temperatures responded quickly to the heating and cooling environments, while large internal temperature increases occurred only in charred regions.

REFERENCES

1. *Packaging and Transportation of Radioactive Material*, Code of Federal Regulations, Title 10, Part 71, Washington, DC (January 1, 1991).
2. *9973 and 9975 Packagings Thermal Testing (U)*, WSRC Equipment and Materials Technology Department, Job Number 22381, (1994).
3. *Package Test Selection Justification (U)*, WSRC Memorandum SRT-ATS-940047, S. J. Hensel (July, 1994).
4. *American National Standard for Radioactive Leakage Tests on Packages for Shipment*. ANSI N14.5-87, American National Standards Institute, Inc., New York, NY (1987).
5. D. H. Schulze, R. Moreno, W. Gill, *Test Report, Simulated Fire Tests of the 9973 and 9975 Packagings*, 6324AK2801, Sandia National Laboratory, Albuquerque, NM (June 1994).

730-A FILE ROOM, PROJECT FOLDER 22381
SRT-PTG-94-0058
APPENDIX 1
July 25, 1994

APPENDIX 1

INSTRUMENTED ASSEMBLY OF THE 9973 AND 9975 SHIPPING PACKAGINGS (U),
WSRC SRTC E&MT Procedure FP 558, Rev. 0 (Performed May and June, 1994)

Savannah River Technology Center
E&MT Field Procedure

Procedure: FP 558, Rev 0
E&MT Job Folder: 22306
PTG Project File: PTG-PF-001
Category: 1
Effective: 5/17/94
Page: 1 of 22 23

Instrumented Assembly of the 9973 and 9975 Shipping Packagings

Instrumented Assembly of the 9973 and 9975 Shipping Packagings (U)

WORKING COPY
COPIED BY (S)
COPY DATE 5-17-94
EXP. DATE 6-17-94

Approvals

P&T Engineer M. N. Van... Date: 5/13/94
FT&OS Engineer E. R. Leader Date 5/13/94
P&T Task Leader R. J. ... Date 5/14/94
SRTC CQF J. Pardo Date 5/17/94
E&MT Manager [Signature] Date 5/17/94

Purpose

This procedure ensures proper, documented assembly of the 9973 and 9975 shipping packagings that will be subsequently thermally tested.

Scope

This procedure pertains to the task work supporting certification of the 9972-series packaging. This procedure applies to preparation of the 9973 shipping package that will be used for the certification drop, puncture, and thermal test, and applies to the 9975 shipping packaging that will be used for the benchmark thermal test. Prerequisite to this procedure are provision of the standard packaging hardware and, for the 9973, the containment vessel assembly. This procedure directs modification of the standard hardware for thermal test purposes.

Procedure performance assumes close cooperation of the test engineer and the fabrication shop. The test engineer will direct the work and be allowed substantial leeway during assembly. This is appropriate since this work is custom in nature.

Savannah River Technology Center
E&MT Field Procedure

Procedure: FP 558, Rev 0
E&MT Job Folder: 22306
Category: 1
Page: 2 of 23

Instrumented Assembly of the 9973 and 9975 Shipping Packagings

Terms and Definitions

9973 packaging - Drum-type radioactive materials packaging design defined in attachment 1, 3, and drawing S5-2-11039.

9975 packaging - Drum-type radioactive materials packaging design defined in attachment 2, 3, and drawing S5-2-13100.

Standard packaging hardware - Those items excluding radioactive materials necessary to assemble the packaging, including for the 9973 in this case an assembled, pressurized and leak tested containment system.

Responsibilities

FT&OS Engineer

The Equipment and Materials Technology (E&MT) Fabrication Technology and Operations Support (FT&OS) engineer is responsible for

- ensuring standard packaging hardware is available
- facilitating fabrication support, including shop access and manpower

P&T Task Leader

The E&MT Packaging and Transportation task leader is responsible for

- overall task coordination, including the work covered in this procedure

P&T Engineer

The E&MT Packaging and Transportation engineer is responsible for

- the test engineer role, including preparing this procedure
- initialing and dating each step upon satisfactory completion
- approving and noting within the procedure all deviations to this procedure

Shop Foreman

The Shop Foreman is responsible for

- providing qualified personnel to assist in executing this procedure
- providing a safe shop environment for doing this work

Safety

Shop personnel are to know and follow shop safety practices. E&MT personnel are responsible for heeding shop safety rules.

The 9975 sleeve may require special controls due to its being lead. Cadmium plating may be present when welding conduit fittings.

Savannah River Technology Center
E&MT Field Procedure

Procedure: FP 558, Rev 0
E&MT Job Folder: 22306
Category: 1
Page: 3 of 23

Instrumented Assembly of the 9973 and 9975 Shipping Packagings

Acceptance Criteria

The acceptance criteria is that the P&T engineer has initialed and dated each procedure step and any associated deviations.

Required Instrumentation and Equipment

The following equipment is necessary to perform this procedure:

- typical shop mechanical and fabrication tools (e.g., wrenches, drills, etc.)
- standard 9973 and 9975 packaging hardware with a 9973 containment vessel assembled per E&MT FP 516 and FP 519 and an unassembled 9975 containment vessel (supplied by the FT&OS engineer)
- mineral-insulated type K thermocouples, .63 in. dia. x 180 in., Gordon ABE000Q990UK30X, M&TE #TR-3236—TR-3251 calibrated to 1000°C and TR-3252—TR-3275 calibrated to 600°C (supplied by P&T Engineer)
- 3/4 in. flexible all-metal conduit, panel fittings, and end terminations (2 ea.)
- 4.7 min. dia. x 8.4 in. min. length bar (carbon or stainless steel)
- loose high temperature fiberglass insulation as required to fill small holes
- small nylon or similar wire ties
- 1/4 in. dia. thin wall copper tubing, approx. 22 feet
- .002-.003 in. stainless steel sheet sufficient for retaining thermocouples
- tack welding capability (likely via E&MT Equipment Engineering)
- electric heater element, Master Appliances HAS-041K or similar, and lead wires (supplied by P&T Engineer)
- ohmmeter with sensitivity to $1 \mu\Omega$ *not required - org. resistance ~ 66 Ω , Fluke model 25 multimeter acceptable, SN 44 30012*
- M&TE calibration no./exp. date: *N/A* *mm 5/19/94* *(From 786-A)*
- pressure tap fittings (supplied by P&T Engineer)
(Smegalok 1/4" 316ss union with one side removed mm 5/19/94)

*AWM 3069
20 RWG
5/19/94
150°C 600V
(mm 5/29)*

Procedure

1. General Instructions

1. DO NOT bend thermocouples smaller than a 3/16 in. inner bend radius.
2. Ensure each thermocouple M&TE number remains attached to the lead end.
3. DO NOT allow exposed thermocouple wires on lead ends to be broken. When routing thermocouples, a closed piece of tubing may be used as a protective casing.
4. Verify thermocouple calibrations and, per ASTM E-1350, measure the thermoelement loop resistance of each thermocouple prior to installation. Record the results in Table 1.

loop resistance measured by Don S. Hoang

Initials *mm* Date *5/19/94*

(P&T Tool Engineer - Mark M. Van Alstine)

Savannah River Technology Center
E&MT Field Procedure

Procedure: FP 558, Rev 0
E&MT Job Folder: 22306
Category: 1
Page: 4 of 23

Instrumented Assembly of the 9973 and 9975 Shipping Packagings

5. When cited, measure the post-installation thermoelement loop resistance per ASTM E-1350. If damage is indicated (measured before and after installation resistance difference is >5%), repeat the procedure steps necessary to replace the damaged thermocouple(s). Explain, reinitial, and redate repeated steps.
6. Minor notching of the fiberboard (width less than 1/4 in.) is allowed as necessary for routing leads.
7. Thermocouples should be attached such that at least 1.5 in. from the junction ends are in expected isotherms.
8. Attach thermocouples to steel surfaces by forming a small sheet metal retention strap over thermocouple and then tack welding the strap to the surface. See attachment 4 for example.

Attach thermocouples to lead and aluminum surfaces by grooving the surface 1 thermocouple dia. wide by 1.5 dia. deep and approximately 1.5 in. long or longer if necessary for retention, inserting the thermocouple, then peening the groove edges to retain the thermocouple.

WARNING - do not burn through the thermocouple sheath when welding or crush the sheath when peening!

2. Drum and Lower Fiberboard Preparation and Instrumentation

1. Drill a hole in the side of the 9973 drum for attachment of the 3/4 in. conduit bulk head fitting. The hole is to be such that its center will be at the elevation of the inner fiberboard step and is to be central in the quadrant of 2 adjacent vent holes.

Initials mmA Date 5/19/94

2. Drill a hole in the bottom of the 9975 drum for attachment of the 3/4 in. conduit bulk head fitting. The hole is to be eccentric from the axis 3.6 in. and is to be central in the quadrant of 2 adjacent vent holes.

Initials mmA Date 5/19/94

3. Attach the 9975 conduit fitting and seal weld it at the drum exterior.

Initials mmA Date 5/19/94

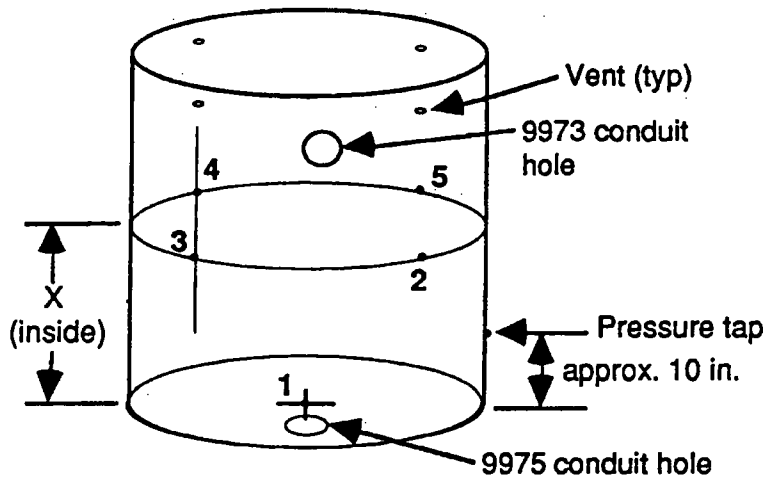
Savannah River Technology Center
E&MT Field Procedure

Procedure: FP 558, Rev 0
E&MT Job Folder: 22306
Category: 1
Page: 5 of 23

Instrumented Assembly of the 9973 and 9975 Shipping Packagings

- Using 1000°C calibrated thermocouples, attach the 9973 and 9975 drum interior thermocouples at the bottom center and mid-height per the sketch and complete the below table. Carefully route the leads out of the conduit hole.

NOTE - Bottom thermocouples may be omitted for later attachment at SNLA.



TC Location	9973		9975	
	M&TE No.	X (in.)	M&TE No.	X (in.)
1	TR-3236	—	TR-3241	—
2	TR-3237	13.5 (approx.)	(N/A)	(N/A)
3	TR-3238		TR-3242	17 in.
4	TR-3239		(N/A)	(N/A)
5	TR-3240		TR-3243	17 in.

Initials MMA Date 5/20/94

- Drill a hole for, and seal weld the pressure tap fitting to, each drum exterior at the location shown.

*8 1/2 in. up on 9973 to avoid drum rolling hoop.
mm 5/19/94*

Initials MMA Date 5/19/94

- Assemble the 9973 lower fiberboard in the drum using the assembly method defined by the FT&OS engineer. Cut a channel radially inward in the fiberboard 1.8 in. wide and .8 in. below the conduit hole center.

*(cut out smaller since conduit fitting flash inside
mm 5/24/94)*

WARNING - do not deform or dislocate the drum thermocouples!

Initials MMA Date 5/23/94

Savannah River Technology Center
E&MT Field Procedure

Procedure: FP 558, Rev 0
E&MT Job Folder: 22306
Category: 1
Page: 6 of 23

Instrumented Assembly of the 9973 and 9975 Shipping Packagings

- Attach the 9973 conduit fitting with existing leads passed through. Seal weld it at the drum exterior.

WARNING - do not ignite the fiberboard or excessively heat the leads.

Initials mt Date 5/19/94 (performed with step 2.1 since conduit fitting cut to be smooth with the drum interior surface - mt 5/19/94)

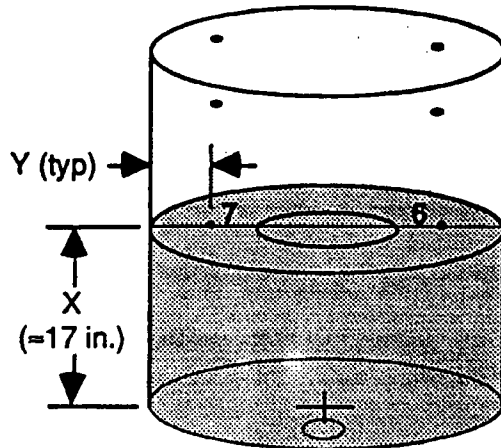
- Assemble the 9975 lower fiberboard in the drum to the layer nearest a 17 in. elevation. At the conduit fitting, counter bore the fiberboard 2 in. dia. by 1 in. depth. Drill a 3/4 in. hole up from the conduit hole through the bottom solid layers and lead bearing plate. Extend the cut to the top layer of fiberboard as a channel for instrumentation leads.
(no counterbore but 1" hole mt 5/24/94)

WARNING - do not deform or dislocate the drum thermocouples!

Initials mt Date 5/24/94

- Using 600°C calibrated thermocouples, attach the 9975 fiberboard thermocouples in the middle of the fiberboard as shown in the sketch below and complete the table. Carefully route the leads out of the conduit hole.

WARNING - ensure leads will not be crushed by the containment vessel.



TC Location	9975		
	M&TE No.	X (in.)	Y (in.)
6	TR- 3252	16.25	2.5
7	TR- 3253	16.25	2.5

Initials mt Date 5/24/94

Savannah River Technology Center
E&MT Field Procedure

Procedure: FP 558, Rev 0
E&MT Job Folder: 22306
Category: 1
Page: 7 of 23

Instrumented Assembly of the 9973 and 9975 Shipping Packagings

- Complete assembly of the 9975 lower fiberboard. Cut the channel through the added fiberboard layers.

Initials mut Date 5/26/94

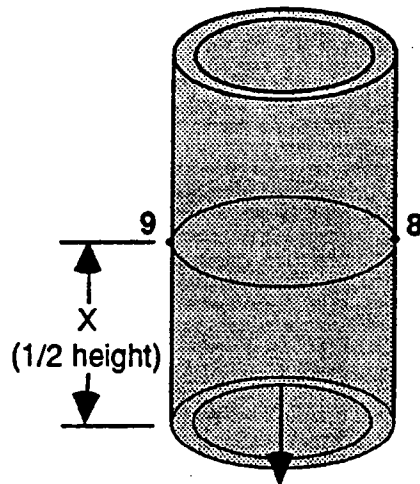
- Verify thermocouple operation per 1.5.

Initials _____ Date _____

*omitted - more likely to
damage thermocouples than
benefits gained. -mut
5/25/94*

3. Lead Sleeve Preparation and Instrumentation

- Using 600°C calibrated thermocouples, install the lead sleeve thermocouples as shown and complete the table.



TC Location	9975	
	M&TE No.	X (in.)
8	TR-3254	12.0
9	TR-3255	12.0

Initials mut Date 5/25/94

Savannah River Technology Center
E&MT Field Procedure

Procedure: FP 558, Rev 0
E&MT Job Folder: 22306
Category: 1
Page: 8 of 23

Instrumented Assembly of the 9973 and 9975 Shipping Packagings

2. Insert the lead sleeve into the 9975 packaging fiberboard. Align as shown in the preceding sketch. The hole in the lead bearing plate may require shaping to ensure passage of the leads and subsequent leads. Carefully route the leads out of the conduit hole.

WARNING - do not deform or dislocate the fiberboard thermocouples!

Initials MA Date 5/26/94

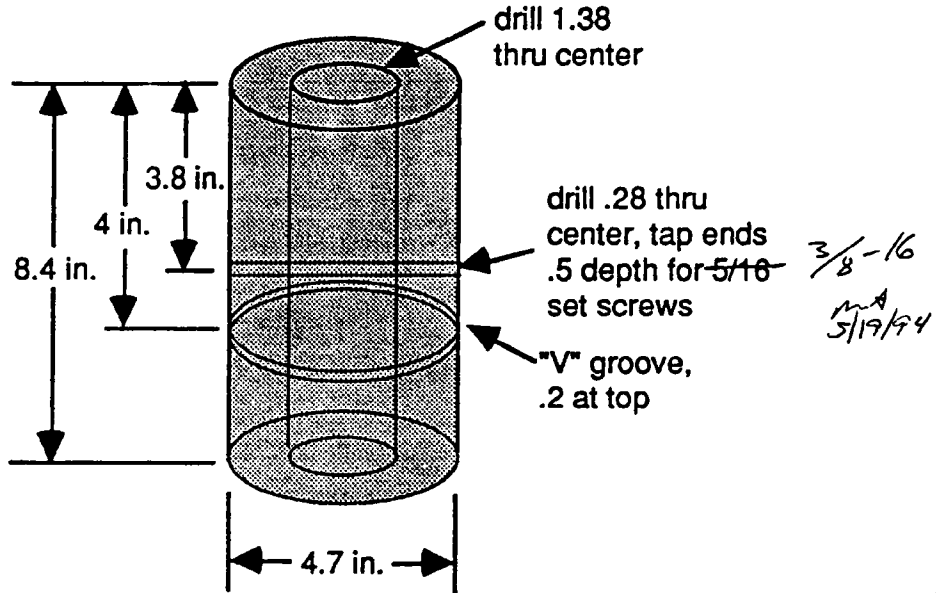
3. Verify thermocouple operation per 1.5.

*omitted - see step 2.11
MA 5/25/94*

Initials _____ Date _____

4. Containment Vessel Preparation and Instrumentation

1. Fabricate mock content mass of carbon or stainless steel as shown in the below sketch.
(used carbon tool steel bar stock - MA 5/19/94)



Initials MA Date 5/19/94

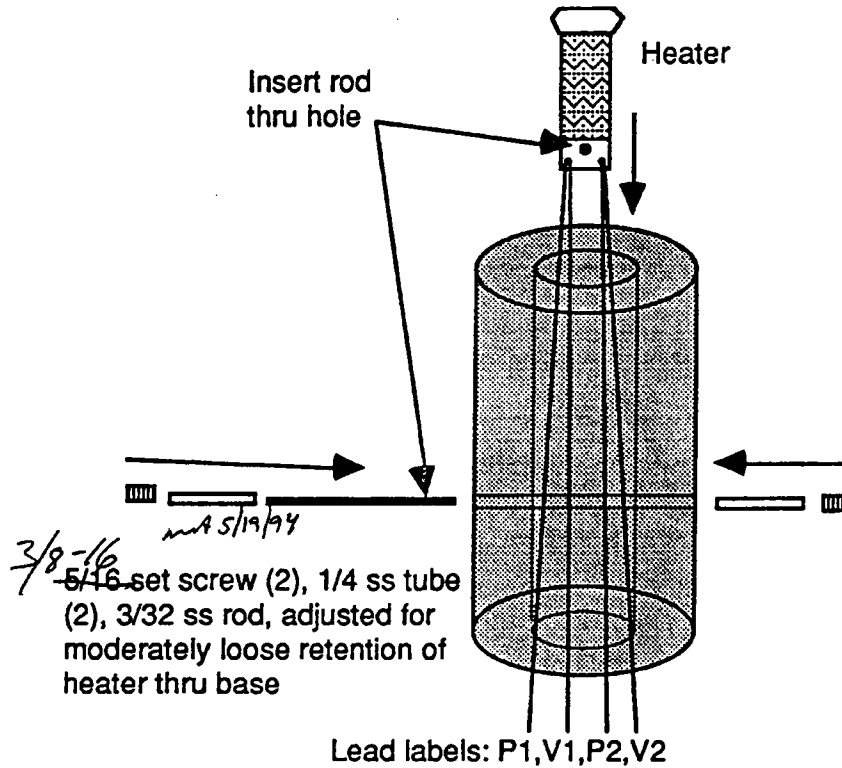
mechanist: WPA 5-19-94

Savannah River Technology Center
E&MT Field Procedure

Procedure: FP 558, Rev 0
E&MT Job Folder: 22306
Category: 1
Page: 9 of 23

Instrumented Assembly of the 9973 and 9975 Shipping Packagings

2. Install and label the electric heater leads and install the heater into the mock content mass as shown in the below sketch. Leads are to be 15 ft.



WARNING - ensure bare electrical leads are, and will remain, isolated!

Initials mm Date 5/24/94

3. Weigh the mock content assembly and record below.

Weight 17.262 (kg)

Initials mm Date 5/24/94

4. Drill a .5 in. hole in the 9975 inner containment vessel bottom center and smooth edges. Drill and tap two groups of 3 equally spaced set screw holes, one set at 5.8 in. from the vessel top rim and the other at 9.5 in. from the vessel top rim.

Initials mm Date 5/23/94

Savannah River Technology Center
E&MT Field Procedure

Procedure: FP 558, Rev 0
E&MT Job Folder: 22306
Category: 1
Page: 10 of 23

Instrumented Assembly of the 9973 and 9975 Shipping Packagings

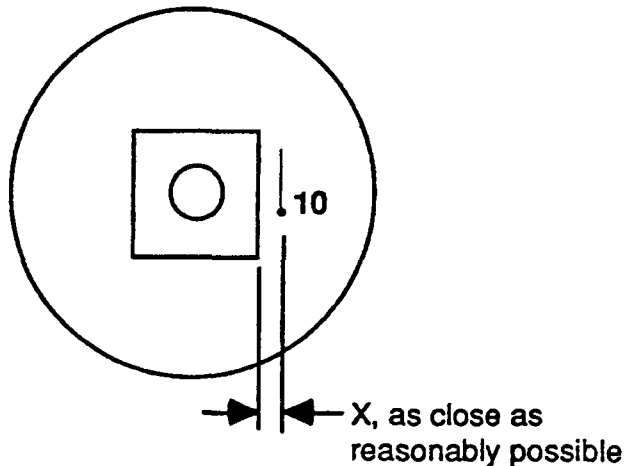
5. Install the mock content in the inner containment vessel. Axially align and retain it with the two groups of 3 set screws. The upper group is to set into the "V" groove in the mock content. Carefully route leads out the vessel bottom.

Initials MA Date 5/24/94

6. Complete assembly of the 9975 inner containment vessel using existing seals.

Initials MA Date 5/24/94 (only 1 O-ring provided and used)
nd 5/24/94

7. Using a 600°C calibrated thermocouple, attach a thermocouple to the 9975 inner containment vessel lid per the sketch and complete the below table.



Top View

TC	9975	
Location	M&TE No.	X (in.)
10	TR-3256	.38

Initials MA Date 5/24/94

8. Drill a 1/2 in. hole in the bottom center of the 9975 secondary containment vessel and the associated honeycomb. Round all hole edges.

Initials MA Date 5/23/94

Savannah River Technology Center
E&MT Field Procedure

Procedure: FP 558, Rev 0
E&MT Job Folder: 22306
Category: 1
Page: 11 of 23

Instrumented Assembly of the 9973 and 9975 Shipping Packagings

- 9. Insert the 9975 inner containment vessel into the outer containment vessel. Complete the 9975 secondary containment vessel assembly using existing seals and upper honeycomb. Carefully route leads out the vessel bottom.

(only upper O-ring provided and used mt 5/24/94) *(also used lower honeycomb mt 5/24/94)*
WARNING - do not deform or dislocate the inner vessel leads!

Initials mt Date 5/24/94

- 10. Retain the leads coming from within the 9975 vessel into one of the skirt notches by tack welding a stainless steel rod across the notch outside surface.

WARNING - do not excessively bend or heat the leads!

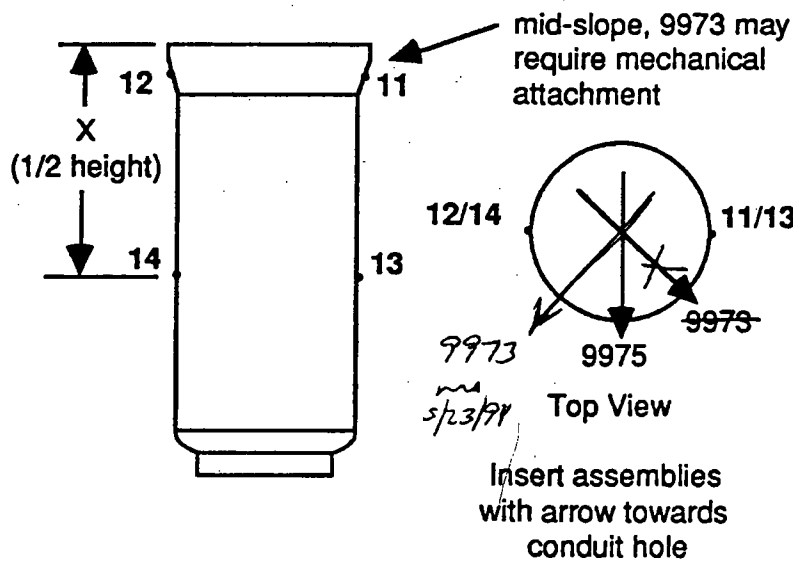
Initials mt Date 5/24/94

See page 16 mt 6/3/94

- 11. Verify heater lead continuities and no shorting to the vessel assembly.

Initials mt Date 5/24/94

- 12. Using 600°C calibrated thermocouples, install the 9973 and 9975 secondary vessel exterior thermocouples per the sketch and complete the below table. Install for routing of 9973 leads upward and 9975 leads downward in the indicated direction.



Savannah River Technology Center
E&MT Field Procedure

Procedure: FP 558, Rev 0
E&MT Job Folder: 22306
Category: 1
Page: 12 of 23

Instrumented Assembly of the 9973 and 9975 Shipping Packagings

TC Location	9973		9975	
	M&TE No.	X (in.)	M&TE No.	X (in.)
11	TR-3257	(N/A)	TR-3261	(N/A)
12	TR-3258	(N/A)	TR-3262	(N/A)
13	TR-3259	8.5	TR-3263	11.0
14	TR-3260	8.5	TR-3264	11.0

9973: *mt* 5/23/94
Initials *mt* Date 5/25/94

TR-3258 destroyed during conduit assembly (lead shield) - *mt* 5/21/94

13. Insert the 9973 and 9975 containment vessel assemblies into the respective lower drum assembly oriented per the preceding sketch. Carefully route the leads out of the conduit hole. For the 9973, ensure clearance between the vessel, existing thermocouples, and fiberboard is adequate for expected drop test movements. *see pg. 1*

WARNING - do not deform or dislocate any of the thermocouples!

9973: *mt* 5/23/94
Initials *mt* Date 5/26/94

14. Verify thermocouple operation per 1.5.

*omitted - see step 2-11
mt 5/25/94*

Initials _____ Date _____

5. Upper Insulation Preparation and Instrumentation

1. Using 600°C calibrated thermocouples, install 2 thermocouples on the upper center of the 9973 bearing plate (designated TC location 15 & 16) and 1 thermocouple on the upper center of the 9975 bearing plate. Complete the below table.

TC Location	9973	9975
	M&TE No.	M&TE No.
15	TR-3265	TR-3267
16	TR-3266	(N/A)

Initials *mt* Date 5/23/94

2. Assemble the 9973 and 9975 upper fiberboard, including the bearing plates. Route the 9973 leads radially outward through the fiberboard. Notch the 9975 inner cavity wall for the thermocouple leads and carefully route the 9975 leads around the plate edge and down the notch in the cavity wall.

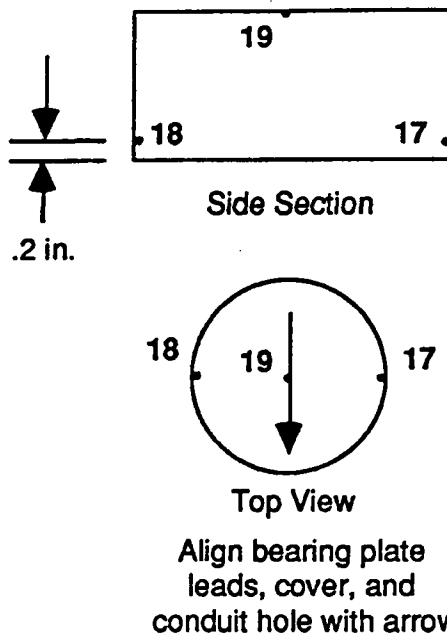
9973: *mt* 5/24/94
Initials *mt* Date 5/25/94

Savannah River Technology Center
E&MT Field Procedure

Procedure: FP 558, Rev 0
E&MT Job Folder: 22306
Category: 1
Page: 13 of 23

Instrumented Assembly of the 9973 and 9975 Shipping Packagings

3. Using 600°C calibrated thermocouples, install thermocouples on the inner surfaces of the insulation cover for the 9973 and 9975 packagings per the sketch. Complete the table.



TC	9973	9975
Location	M&TE No.	M&TE No.
17	TR-3268	TR-3271
18	TR-3269	TR-3272
19	TR-3270	TR-3273

Initials msd Date 5/20/94

4. Attach the insulation cover to the upper fiberboard oriented per the preceding sketch. Route leads to join with the existing bearing plate leads.

WARNING - do not dislocate the bearing plate or cover thermocouple leads!

Initials msd Date 5/25/94

Savannah River Technology Center
E&MT Field Procedure

Procedure: FP 558, Rev 0
E&MT Job Folder: 22306
Category: 1
Page: 14 of 23

Instrumented Assembly of the 9973 and 9975 Shipping Packagings

- 5. Using 1000°C calibrated thermocouples, route 2 thermocouples up from the conduit hole of each packaging. These will be later attached to drum lid.

9973: mt 5/25/94

Initials mt Date 5/26/94

- 6. Pack fiberglass insulation around the leads in the cut out region at the 9973 conduit hole and in the cut channel in the 9975.

9973: mt 5/28/94

Initials mt Date 5/27/94

For 9975, used refractory ceramic insulation. mt 5/27/94

- 7. Install the upper insulation assemblies in the orientation noted in the preceding sketch. Notch the insulation cover as necessary for the lid thermocouples. Notch the 9973 as necessary to ensure adequate room for thermocouple movement during the drop test. Carefully route leads through the conduit hole. Leave the lid thermocouples extending approximately 1 ft. from the upper surface.

WARNING - do not deform or dislocate existing thermocouple leads!

9973: mt 5/25/94

Initials mt Date 5/31/94

[9975: top reopened and closed at SNLA - mt 6/3/94]

9975: aluminum lid was not installed on top of lead sleeve mt 5/31/94

- 8. Verify thermocouple operation per 1.5.

Initials _____ Date _____

omitted, see step 2.11 mt 5/25/94

not required - mt 6/3/94

6. Drum Lid Preparation and Instrumentation

- 1. Centrally attach the 1000°C calibrated thermocouples to the inside of the drum lids (designated TC location 20 & 21). Complete the table.

TC Location	9973 M&TE No.	9975 M&TE No.
20	TR-3244	TR-3246
21	TR-3245	TR-3247

9973: mt 5/25/94

Initials mt Date 5/26/94

- 2. Install the 9973 drum lid such that the thermocouple leads have sufficient leeway for deforming during the drop test. Install both drum lids such that the thermocouple leads are not overlapping or severely bent. Tighten the drum closure ring as directed by the FT&OS engineer and note the method below.

WARNING - do not severely bend or dislocate the thermocouple leads!

Savannah River Technology Center
E&MT Field Procedure

Procedure: FP 558, Rev 0
E&MT Job Folder: 22306
Category: 1
Page: 15 of 23

Instrumented Assembly of the 9973 and 9975 Shipping Packagings

Ring tightening method: - done on 723-A prior to drop for 9973 - mt 5/25/94

9973: mt 5/25/94 9975: taken care of by Bob Maurer. mt 5/27/94

Initials mt Date 5/27/94 9975: redone at SNLA to 55 ft-lb using
calibrated torque wrench (SNLA-991, 03 2761-G,
exp. 4/24/95) - mt 6/17/94

3. Verify thermocouple operation per 1.5.

9973: mt 5/25/94 - #7R-3258 destroyed during conduit assembly -
see 7.6 - mt 5/25/94 mt 5/25/94

Initials mt Date 5/25/94
omitted - see 2.11 - mt 5/25/94

7. Protective Conduit Assembly

1. Ensure that each lead is tagged near the end so as to be identifiable after installing the protective conduit.

9973: mt 5/25/94

Initials mt Date 5/27/94

2. For each packaging, carefully align the leads so they are parallel. Add an approximately 11 ft. length of deburred copper tubing to each packaging lead grouping, terminating 2 in. from the conduit fitting. Tightly bundle each lead and tube grouping at the tube end near the drum and at 1 ft. intervals thereafter.

9973: mt 5/25/94 w/ 7 1/2' copper tube, 7' conduit

Initials mt Date 5/27/94 same length for 9975 or for 9973 - mt 5/27/94

3. For each packaging, tightly pack loose fiberglass insulation into the conduit lead hole.

WARNING - failure to tightly pack the hole could cause air ingress into the packaging during the test and subsequent test failure!

9973: mt 5/25/94

Initials mt Date 5/27/94

used refractory ceramic for

9975 - mt 5/27/94

also know as
F.11 - mt 6/3/94

4. Attach and tack weld a 4 ft. length of all-metal conduit to each packaging, carefully sliding the conduit over the bundled leads.

9973: mt 5/25/94 - used 7' for both 9973 and 9975.

Initials mt Date 5/27/94

9975 - redone at SNLA, not tack welded - mt 6/3/94

5. Attach the end termination fitting on the free conduit end. Do not tack weld this fitting to the conduit.

9973: mt 5/25/94

Initials mt Date 5/27/94

Savannah River Technology Center
E&MT Field Procedure

Procedure: FP 558, Rev 0
E&MT Job Folder: 22306
Category: 1
Page: 16 of 23

Instrumented Assembly of the 9973 and 9975 Shipping Packagings

*perform
step 6 at
SNLA after
attaching
plugs.
mt 5/27/94*

6. Perform a final thermocouple verification check per 1.5 and record the results in Table 1. For uninstalled thermocouples, merely note "NA".

*9973: mt 5/25/94 (TR-3258 destroyed at step 7.7 - Under steam)
Initials mt Date 6/3/94 mt 5/25/94 - see bottom of page.*

7. Carefully slip a length of heavy wall plastic or similar tube over the remaining exposed leads and join to the conduit with a union fitting or another suitable means. Fix this protective conduit assembly to the packaging sufficient for drop testing (9973) and shipment to Albuquerque. This may require fixing to the drums by tack welded wires and, for the 9973, making and tack welding a protective roll bar on the drum side at the conduit connection.

Initials mt Date 5/31/94

Records

The following documents shall be retained as records in accordance with SRTC L1 procedure 8.17:

1. This approved procedure (prior to use), per the E&MT procedure control system
2. This procedure once completed.

References

1. E&MT Procedure No. FP 516, Rev. 0, "Load Procedure for the Primary Containment Vessel of the 9973 & 9974 Shipping Containers."
2. E&MT Procedure No. FP 519, Rev. 0, "Load & Leak Test Procedure for Secondary Containment Vessel of the 9972 Family of Shipping Containers."
3. ASTM Standard E-1350-91, "Standard Test Methods for Testing Sheathed Thermocouples Prior to, During, and After Installation."

ref: steps 4.12, 7.6,

Thermocouple repair: TR-3236/37/58 all successfully repaired at SNLA and tested acceptably. - mt 6/3/94

step 4.11 - lead P1 not working at SNLA, removed to conduit, use V1 as power and voltage for terminal side 1. mt 6/3/94

Savannah River Technology Center
E&MT Field Procedure

Procedure: FP 558, Rev 0
E&MT Job Folder: 22306
Category: 1
Page: 17 of 23

Instrumented Assembly of the 9973 and 9975 Shipping Packagings

Table 1. Thermocouple Installation Verification Resistances

M&TE No. (786-A log)	Cal. Range (0°C to...)	Pre-Installation Resistance ($\mu\Omega$)	Post-Installation Resistance ($\mu\Omega$)
TR-3236	991°C	67.5	67.1 66.2
TR-3237		68.3	68.3 67.2
TR-3238		68.2	67.9 67.3
TR-3239		66.9	66.5 66.8
TR-3240		68.7	68.3 67.8
TR-3241		67.7	22.1 66.0
TR-3242		67.2	66.4
TR-3243		66.6	65.9
TR-3244		68.6	68.5 67.7
TR-3245		66.1	65.8 65.2
TR-3246		71.6	70.8
TR-3247		66.5	65.8
TR-3248		66.0	NA
TR-3249		67.3	NA
TR-3250		71.5	NA
TR-3251	991°C	68.7	NA
TR-3252	584°C	68.0	67.0
TR-3253	584	67.1	66.1
TR-3254	585	66.2	65.3
TR-3255	584	68.5	67.6
TR-3256	583	68.0	67.0
TR-3257	583	66.5	66.2 65.5
TR-3258	583	67.0	66.6 65.0
TR-3259	584	67.0	66.8 66.0
TR-3260	587	68.4	68.2 67.3
TR-3261	586	67.2	66.2
TR-3262	586	65.3	64.4
TR-3263	586	67.2	66.2
TR-3264	586	67.0	66.1
TR-3265	586	68.0	67.9 67.1
TR-3266	583	70.3	70.1 69.1
TR-3267	583	66.1	65.2
TR-3268	576	69.5	69.3 68.5
TR-3269	577	64.9	64.6 63.9
TR-3270	582	67.3	66.9 66.2
TR-3271	582	67.1	66.2
TR-3272	586	65.7	64.6
TR-3273	586	65.5	64.6
TR-3274	583	67.7	NA
TR-3275	575°C	65.6	NA

after installing plug
9973 and 9975
after repair at SNLCA and 6/13/94

* 32.1 was multimeter error
mt 6/3/94

All installed TC's within 5% of initial R_e after final assembly, therefore no internal damage suspected.
mt 6/6/94

* after repaired at SNLCA
mt 6/3/94

All installed TC's checked on TC reader and shown to be correctly junctioned (+/-) and reading ambient correctly - all ~ 78°F (reversed -/+ would cause all ~ 35°F)

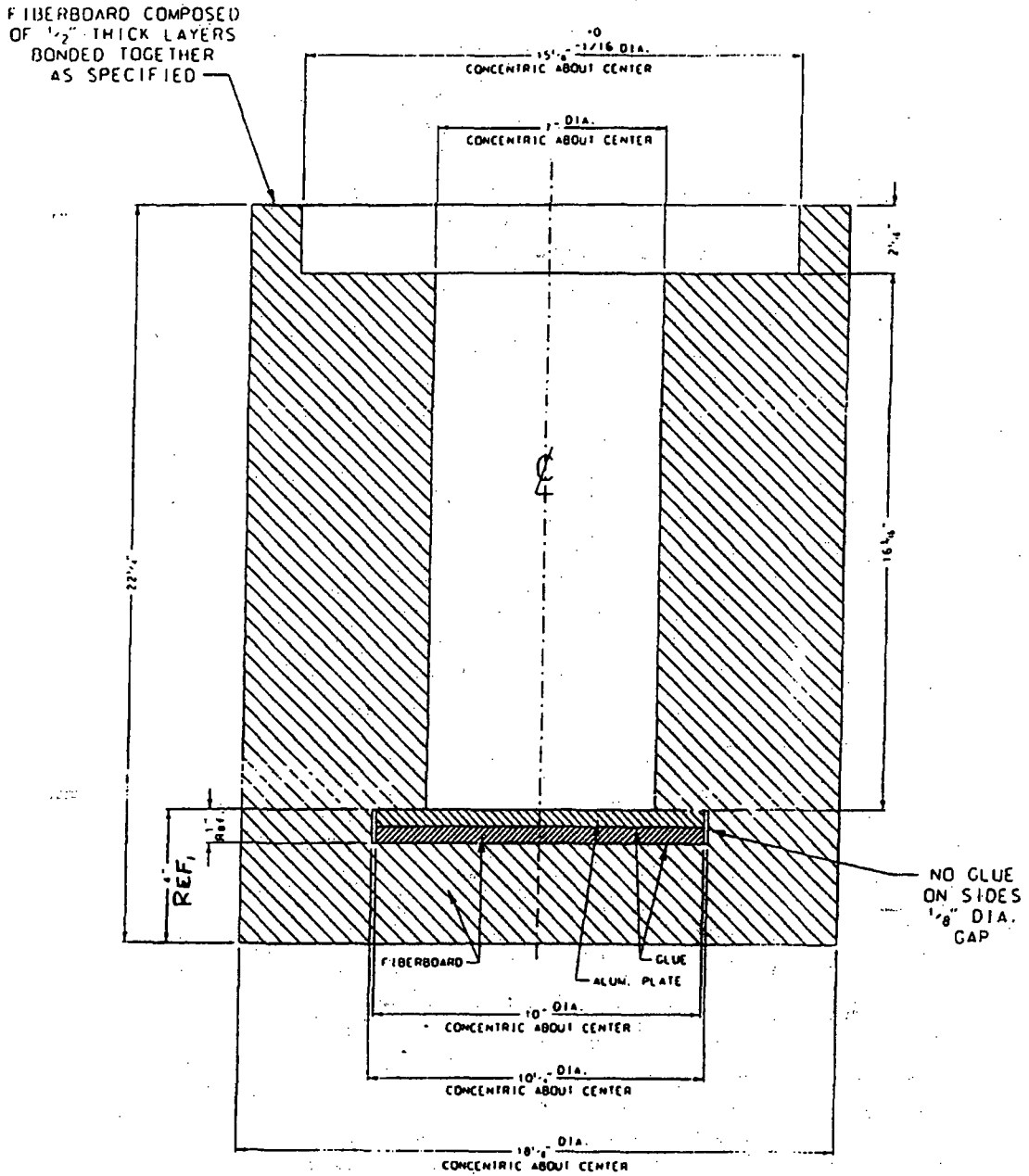
- mt
6/6/94

Savannah River Technology Center
E&MT Field Procedure

Procedure: FP 558, Rev 0
E&MT Job Folder: 22306
Category: 1
Page: 18 of 23

Instrumented Assembly of the 9973 and 9975 Shipping Packagings

Attachment 1



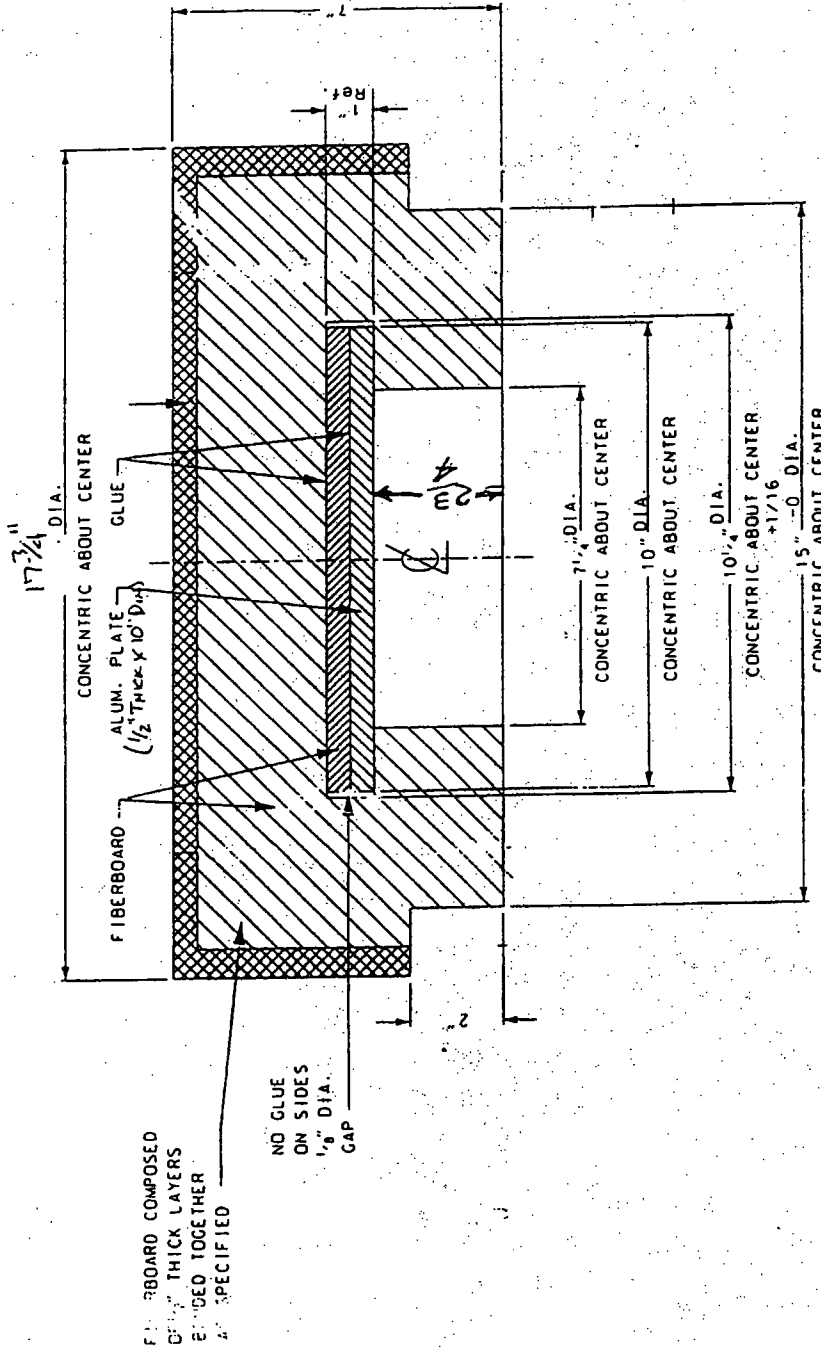
9973

Savannah River Technology Center
E&MT Field Procedure

Procedure: FP 558, Rev 0
E&MT Job Folder: 22306
Category: 1
Page: 19 of 23

Instrumented Assembly of the 9973 and 9975 Shipping Packagings

Attachment 1 (cont.)



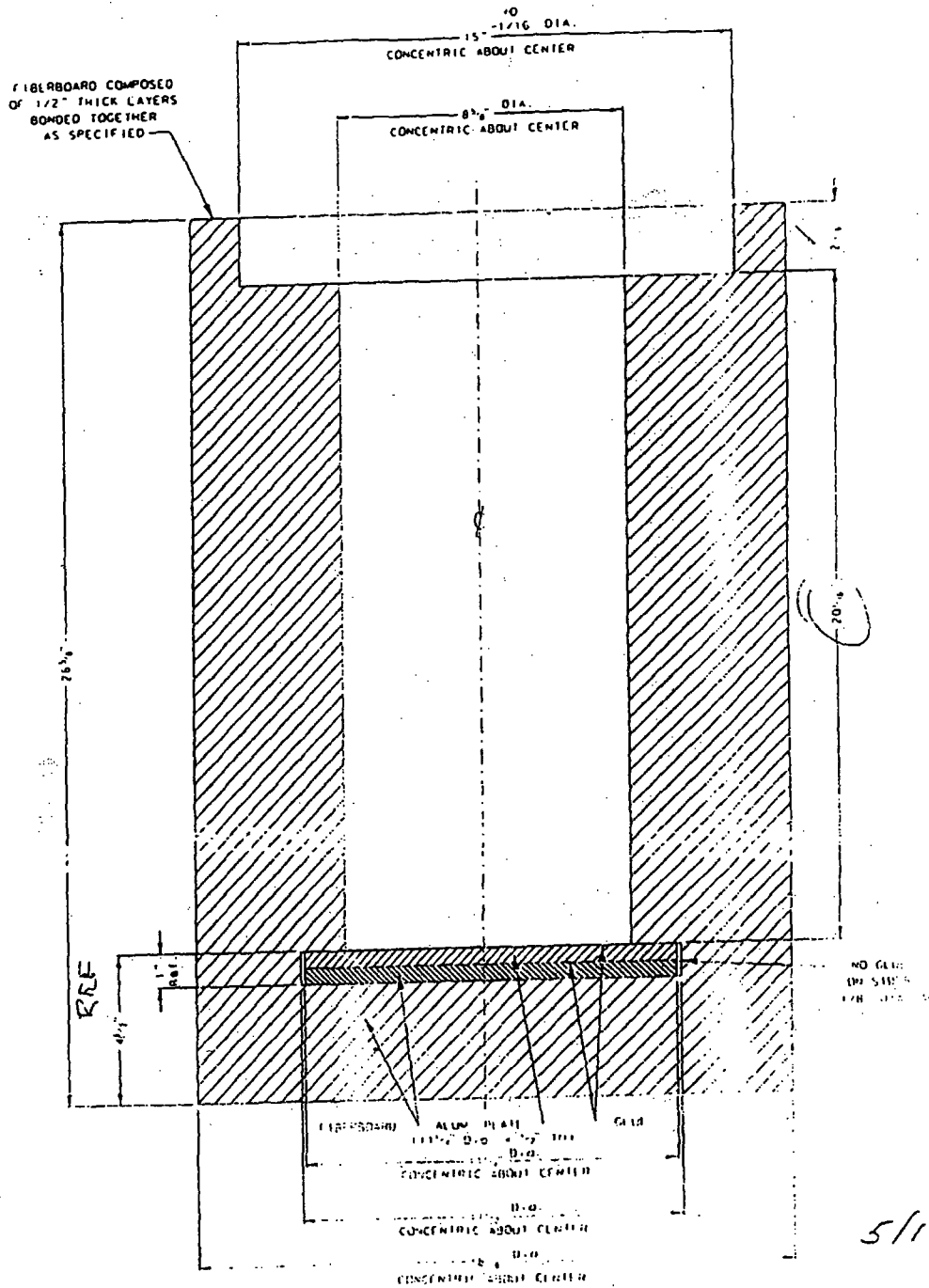
9973

Savannah River Technology Center
E&MT Field Procedure

Procedure: FP 558, Rev 0
E&MT Job Folder: 22306
Category: 1
Page: 20 of 23

Instrumented Assembly of the 9973 and 9975 Shipping Packagings

Attachment 2



5/14/94

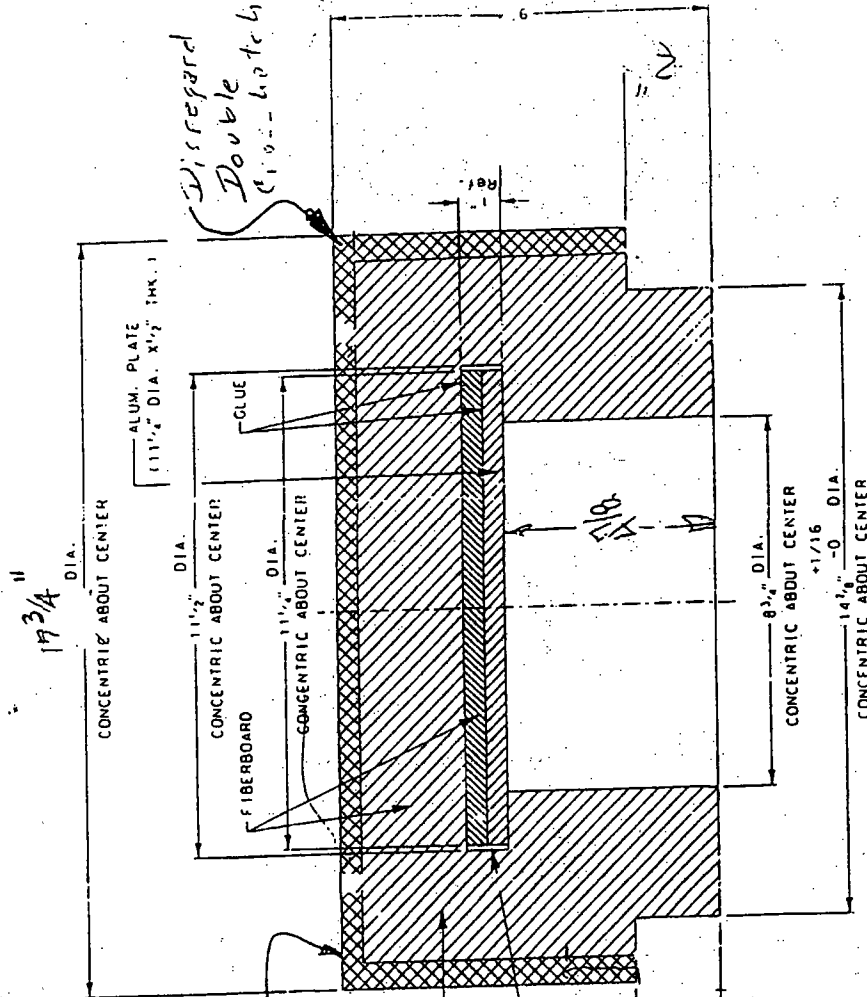
9975

Savannah River Technology Center
E&MT Field Procedure

Procedure: FP 558, Rev 0
E&MT Job Folder: 22306
Category: 1
Page: 21 of 23

Instrumented Assembly of the 9973 and 9975 Shipping Packagings

Attachment 2 (cont.)



Disregard
Double
Circle - hatched

BO. TO THIS SURFACE
ONLY TO INSIDE OF HEAT
SHIELD WITH "RTV"

FIBERBOARD COMPOSED
OF 1/2" THICK LAYERS
BOND TOGETHER
AS SPECIFIED

5/42/94

9975

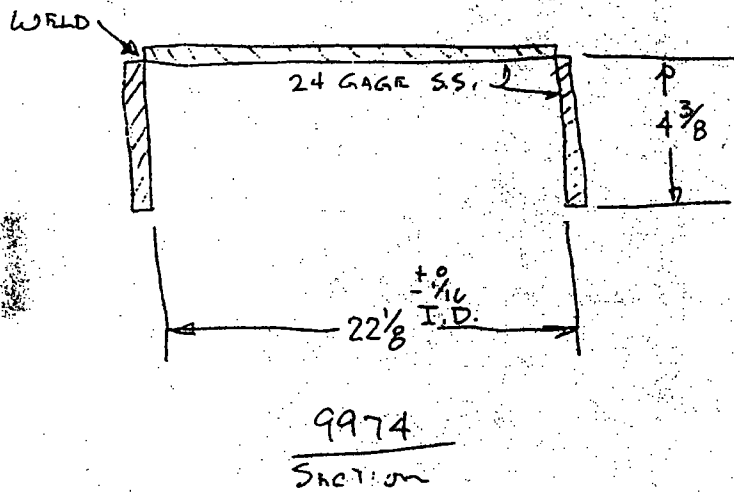
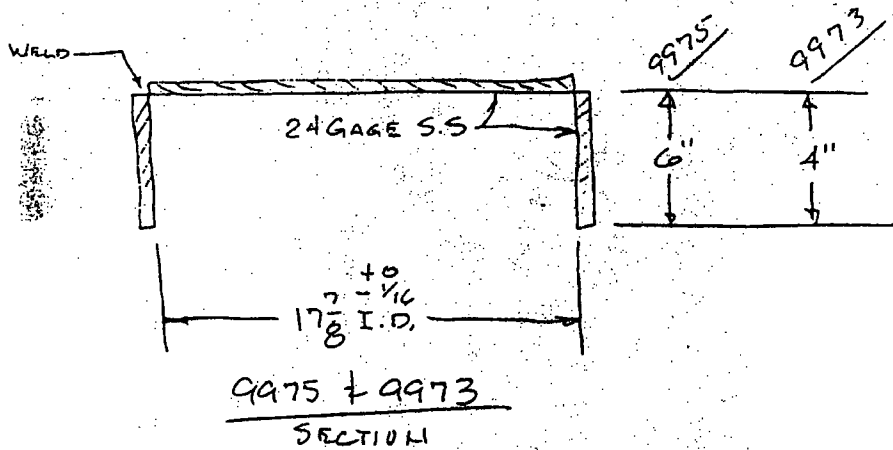
Savannah River Technology Center
E&MT Field Procedure

Procedure: FP 558, Rev 0
E&MT Job Folder: 22306
Category: 1
Page: 22 of 23

Instrumented Assembly of the 9973 and 9975 Shipping Packagings

Attachment 3

NOTE: FOR LIFTING, USE 8" OF SASH CHAIN
BOLTED TO HEAT SHIELD WITH TWO 10-32 BOLTS
6" APART.



MAKE ONE EACH.

HEAT SHIELD

DANNY PRIPPS
5-2832

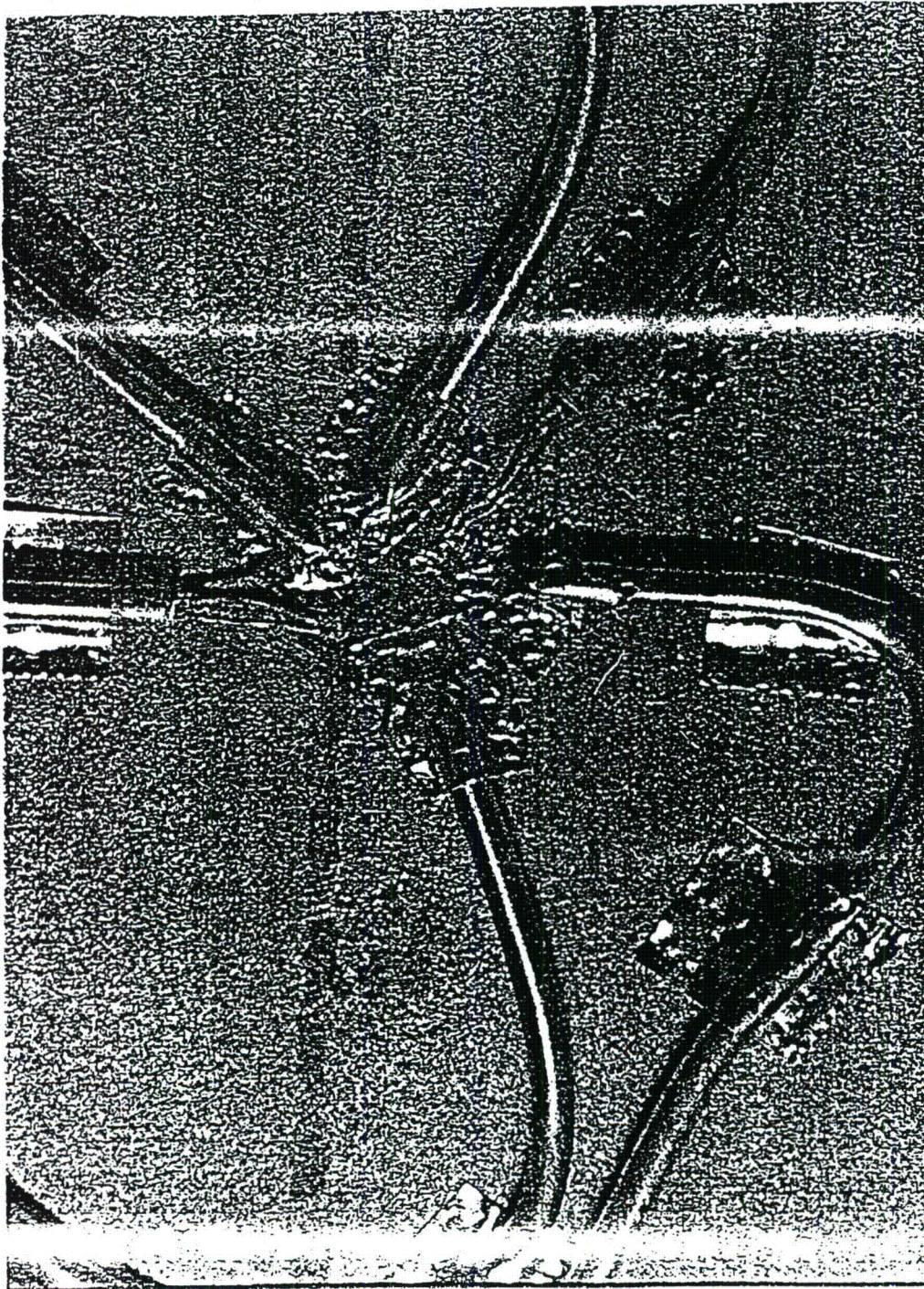
Savannah River Technology Center
E&MT Field Procedure

Procedure: FP 558, Rev 0
E&MT Job Folder: 22306
Category: 1
Page: 23 of 23

Instrumented Assembly of the 9973 and 9975 Shipping Packagings

Attachment 4

Example Thermocouple Attachments



730-A FILE ROOM, PROJECT FOLDER 22381
SRT-PTG-94-0058
APPENDIX 2
July 25, 1994

APPENDIX 2

**WSRC TEST REQUIREMENTS FOR 9973 AND 9975 PACKAGING TESTING (U),
WSRC Memorandum SRT-PTG-94-0033, M. N. Van Alstine to W. Gill, May 23, 1994.**



Westinghouse
Savannah River Company

P O Box 616
Aiken, SC 29802

SRT-PTG-94-0033

May 23, 1994

Mr. Walter Gill
Sandia National Laboratories
P. O. Box 5800
Mail Stop 1135
Albuquerque, NM 87185-1135

Attention: Mr. Walter Gill

Dear Walt:

WSRC TEST REQUIREMENTS FOR 9973 AND 9975 PACKAGING TESTING (U)

This memorandum identifies WSRC's test requirements for SNLA's thermal testing of the 9973 and 9975 packagings. In general, SNLA test work shall be planned, coordinated, controlled, and performed in accordance with approved written procedures or equivalent test planning documents developed and approved per SNLA work control implementing procedures. SNLA shall address the included WSRC test requirements.

WSRC will provide assembled and internally instruments packagings and additional thermocouples. WSRC is responsible for post-test disassembly and evaluation of the packaging hardware.

Test Planning

- SNLA shall prepare a test procedure or equivalent test planning documentation addressing the information identified in the attachment.
- The SNLA test procedure shall be uniquely identifiable, legible, and retrievable.
- SNLA shall document review of the test procedure for technical and administrative details prior to approval. SNLA should provide WSRC a draft by May 27, 1994.
- SNLA shall include myself or my designee and the WSRC Quality liaison, whom I will identify, on the test procedure approval.
- SNLA shall ensure that personnel performing test activities are trained and qualified.

Test Performance

- SNLA shall perform the test following the documents prepared during test planning.

Mr. Walter Gill
SRT-PTG-94-0033
Page 2 of 4

Evaluation of Test Results and Data

- SNLA shall evaluate and in the test report document the comparison of the results obtained to the acceptance criteria in the attachment. The test report is to also describe the test requirements, facilities, procedures, and test execution.
- The SNLA test report author shall sign and date the test report draft and forward it to myself or my designee. WSRC shall accept or reject the test report based on the evaluation adequacy. If WSRC rejects the test report, SNLA and WSRC shall work to resolve the deficiencies.
- Upon written WSRC acceptance of the test report, SNLA shall distribute the final report, including 10 copies to myself or my designee.

Post Test Hardware Disposition

- SNLA shall offer to WSRC custody of all test materials provided by WSRC, and shall assist WSRC in return transportation of materials.
- WSRC shall assume responsible for final disposition of all WSRC test materials.

Records

SNLA shall provide myself or my designee with the following records:

- Approved test procedure in prior to use condition
- Completed test procedure, including data records (3.5 in. diskettes)
- Test report as noted previously
- Any associated nonconformance documents indicating resolution of nonconforming conditions
- Any additional supporting documentation or documents deemed as records as prescribed within the SNLA test procedure

We tentatively are scheduled for performing these tests the week of June 5, 1994. Please schedule the SNLA test planning accordingly.

Sincerely,



Mark N. Van Alstine, Senior Engineer
Savannah River Technology Center

CC: R. J. Gromada, WSRC, 773-53A
E. K. Opperman, WSRC, 773-54A
J. Pardo, WSRC, 992-1W
S. J. Hensel, 773-42A
J. W. Jerrell, 773-42A

Mr. Walter Gill
SRT-PTG-94-0033
Page 3 of 4

ATTACHMENT

Objective

WSRC requires that 2 tests be performed. An undamaged 9975 packaging will be tested to provide bench marking support for WSRC analytical models. A damaged 9973 packaging will be tested as part of the 10 CFR 71.73 hypothetical accident condition (HAC) sequence.

SNLA is to provide this testing per the acceptance criteria and requirements below and is to document the degree that the acceptance criteria have been satisfied.

Acceptance Criteria

- For the 9973 HAC test, SNLA shall provide sufficient evidence that the heating environment satisfied 10 CFR 71.73 (c)(3) and that the minimum drum temperature was maintained at $\geq 815^{\circ}\text{C}$ for the regulatory time. The maximum drum temperature should not exceed 1040°C .
- For the 9975 preheat, SNLA shall report packaging and ambient temperatures and note ambient conditions relative to the shade and still air requirement.
- For the 9975 benchmark, SNLA shall provide sufficient evidence that the heating environment satisfied 10 CFR 71.73 (c)(3) but with the drum temperature sides maintained at $815 \pm 10^{\circ}\text{C}$ for the regulatory time. (The minimum drum temperature will likely be less than 800°C .)
- For the 9975, SNLA shall provide evidence that the heater power level remained $21 \pm 2.1 / - 0$ W except during brief periods (less than 1 hr) for packaging movement, during which power may be suspended.
- SNLA shall provide sufficient evidence that the remaining requirements of 10 CFR 71.73 (b) and (c)(3) have been satisfied.
- SNLA shall provide a conclusive assessment of the functionality of all thermocouples during the tests.

Hold Points

SNLA shall have approval of the WSRC test engineer

- prior to installing insulation on the instrumentation leads (WSRC shall verify that the nitrogen purge and instrumentation leads are connected).
- prior to initiating the thermal test (WSRC shall verify that the orientation is correct, the instrumentation leads are protected, the data acquisition system is ready with correct channel to thermocouple correspondence, and the packaging is at steady state).
- prior to test termination (WSRC shall verify that the packaging is at steady state).

Deviations

- SNLA shall obtain approval of the WSRC test engineer and quality assurance liaison prior to an otherwise not permitted deviation from the approved test procedure.

Test Requirements

- SNLA shall provide the packaging fixturing.
- SNLA shall provide a nitrogen purge with attachment for the 1/4 in. packaging tube.
- SNLA shall provide sufficient insulation to protect instrumentation leads.
- SNLA measuring and test equipment calibrations shall be current and traceable to NIST.
- SNLA shall allow test access to cleared WSRC personnel.

Mr. Walter Gill
SRT-PTG-94-0033
Page 4 of 4

- SNLA shall be amenable to installing external thermocouples as provided by WSRC.
- SNLA shall assess proper function of facility and packaging thermocouples prior to and following the tests.
- SNLA shall provide attachment of a pressure tap line (.25 in. dia. stainless steel tubing) to a tap in each packaging.
- SNLA shall provide and operate instrumentation and data acquisition with capabilities for
 - 22 channels of type K thermocouple couple input from each packaging
 - a controlled power supply for the 21W heater .
 - a 1 kPa pressure transducer for dead head pressure reading from a tap line (NIST traceability optional)
 - data acquisition with storage to DOS-formatted 3.5 in. diskettes.
- SNLA shall measure pre and post test drum diameters at consistent central locations.
- For the 9973, SNLA shall acquire ambient and packaging temperatures and pressure throughout the test duration at an interval of 10 seconds.
- For the 9975, SNLA shall acquire ambient and packaging temperatures at an interval of 10 minutes during the preheat and shall acquire ambient and packaging temperatures and pressure throughout the test duration at an interval of 10 seconds.
- SNLA shall preheat the 9975 by energizing the internal heater to the prescribed power and perform the preheat in a shaded, still air environment.
- SNLA shall test the 9973 packaging on its side with the instrumentation conduit down.
- SNLA shall test the 9975 packaging upright with maximum thermal symmetry.
- SNLA shall initiate each test when the packaging temperatures reach steady state in a normal (approx. 25°C) ambient. This may take up to 5 days for the 9975 preheat.
- SNLA shall terminate each test when post-heat temperatures cool to steady state.

730-A FILE ROOM, PROJECT FOLDER 22381
SRT-PTG-94-0058
APPENDIX 3
July 25, 1994

APPENDIX 3

DISASSEMBLING THE 9973 AND 9975 THERMAL TEST PACKAGINGS (U), WSRC
SRTC E&MT Procedure FP 570, Rev. 0 (Performed June and July, 1994)

Savannah River Technology Center
E&MT Field Procedure

Procedure: FP 570, Rev 0
E&MT Job Folder: 22306
PTG Project File: PTG-PF-001
Category: 1
Effective: 6/16/94
Page: 1 of 12

Disassembling the 9973 and 9975 Thermal Test Packagings

Disassembling the 9973 and 9975 Thermal Test Packagings (U)

Approvals

P&T Engineer Wade N. Vata Date: 6/16/94

P&T Task Leader P.J. Branda Date 6/16/94

SRTC CQF J. Pardo Date 6/16/94

E&MT Manager Eric O. [Signature] Date 6/16/94

Purpose

This procedure ensures that test data is recovered during disassembly of the 9973 and 9975 shipping packagings that have been thermally tested.

Scope

This procedure specifically applies to the 9973 and 9975 packagings that have been assembled per procedure FP 558, rev. 0, and have been tested at Sandia National Laboratory the week of June 5, 1994.

Procedure performance assumes close cooperation of the test engineer and shop personnel. The test engineer will direct the work and be allowed substantial leeway during disassembly. This is appropriate since this work is custom in nature.

Terms and Definitions

9973 and 9975 packagings - Prototype drum-type radioactive materials packagings produced by execution of procedure FP 558, rev. 0.

WORKING COPY
COPIED BY Tom Woodson
COPY DATE 6-16-94
EXP. DATE 7-16-94

Savannah River Technology Center
E&MT Field Procedure

Procedure: FP 570, Rev 0
E&MT Job Folder: 22306
Category: 1
Page: 2 of 12

Disassembling the 9973 and 9975 Thermal Test Packagings

Responsibilities

P&T Task Leader

- The E&MT Packaging and Transportation task leader is responsible for
- overall task coordination, including the work covered in this procedure
 - allowing work past engineering witness points (if this waives other witnesses, he shall note this in the procedure next to their names).

P&T Engineer

- The E&MT Packaging and Transportation engineer is responsible for
- the test engineer role, including preparing this procedure
 - initialing and dating each step upon satisfactory completion
 - obtaining task leader approval before passing engineering witness points
 - approving and noting within the procedure all deviations to this procedure other than engineering witness point waivers

Shop Foreman

- The Shop Foreman is responsible for
- providing qualified personnel to assist in executing this procedure
 - providing a safe shop environment for doing this work

Safety

Shop personnel are to know and follow shop safety practices. E&MT personnel are responsible for heeding shop safety rules.

The 9975 sleeve may require special controls due to its being lead.

Acceptance Criteria

The acceptance criteria is that the P&T engineer has initialed and dated each procedure step and any associated deviations.

Required Instrumentation and Equipment

The following equipment is necessary to perform this procedure:

- typical shop mechanical and fabrication tools (e.g., wrenches, drills, etc.)
- 9973 and 9975 packagings
- VHS video camera and 35mm still camera

Savannah River Technology Center
E&MT Field Procedure

Procedure: FP 570, Rev 0
E&MT Job Folder: 22306
Category: 1
Page: 3 of 12

Disassembling the 9973 and 9975 Thermal Test Packagings

Procedure

1. General

1. During disassembly, mark the relative locations of all parts using a highly visible, durable marker. Someone should be able to reassemble the parts based on the markings.
2. All parts are to be retained and stored inside as directed by the P&T engineer.
3. Observations must include the following as applicable:
 - when relative to a thermocouple (TC) location, the TC M&TE number
 - TC attachment condition
 - note char depths relative to inner undamaged surface
 - traces of water condensation
 - effects of conduit penetration
 - drop damage effects to 9973
 - movement (collapse, etc.) of parts
 - heat marks and exhaust patterns
 - evidence of burning
 - effects of adjacent features.
4. Cut TC and wire leads as necessary for disassembly.
5. Take enough video and still pictures throughout for complete reference.

2. 9973 Disassembly

1. Remove the conduit cover up to the drum fitting. Record observations below.

Strong residue smell initially at conduit end, then along conduit-covered section of lead bundle. All discolored brown/black at conduit fitting, insulation plug intact but permeated with stain, sealed in place. Taped wire ties missing until ~1 1/2 ft. from open conduit end. Purge line not plugged. Tar/soot deposits on leads progressively heavier out up to fitting end.

Initials *ima* Date *6/17/94*

2. Remove the drum lid using the closure bolt and ring. Record observations below.

Light gray dust (decomposed gasket) fell out during removal. Bolt was quite loose. TCs held as new. Dap damage evident - lid chain marks on shield (unired TCs - not crushed). Top liner very brittle, broke when dropped. Aluminum coating on liner seemed to have vaporized & redeposited on

Savannah River Technology Center
E&MT Field Procedure

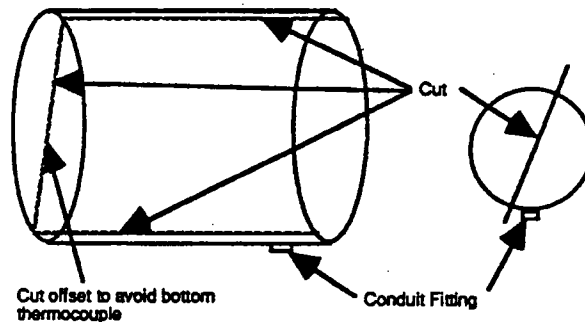
Procedure: FP 570, Rev 0
E&MT Job Folder: 22306
Category: 1
Page: 4 of 12

Disassembling the 9973 and 9975 Thermal Test Packagings

on drum lid and shield, was likely some of what was observed at the vent holes. White caked material at closure bolt was likely decomposed gasket material. Rust-colored run marked marks evident on the lid in the downward direction.

Initials mt Date 6/17/94

3. Cut the drum laterally and across the bottom as shown below and remove the upper half. Records observations below.



Cut side near fitting and bottom with jig saw, cut both sides adjacent to shield and side opposite fitting with grinder (less vibration and penetration than saw). Shiny coating on inside top of drum (w.r.t. burn orientation) - assumed due to aluminum on liner. Fiberboard uniformly shrunk, left gap at shield (~1 1/2 in. less ϕ than shield). Consistently, every other glue joint opened in char region, were our joints - mfg. joints held well. Char cracked like wood does, but no wide cracked areas. Opened glue joints typically 1/4 in. deep, but ranged from 1 in. to 1 3/4 in. Was no evidence of burning anywhere on fiberboard. Drum side TCs held well. Bottom TC loose, but was hit by saw blade (not cut or punctured) - may have been loose in test.

Initials mt Date 6/17/94

Savannah River Technology Center
E&MT Field Procedure

Procedure: FP 570, Rev 0
E&MT Job Folder: 22306
Category: 1
Page: 5 of 12

Disassembling the 9973 and 9975 Thermal Test Packagings

ENGINEERING WITNESS POINT

Request the following to witness, initial, and date:

S. J. Hensel Initials SH Date 6-17-94

E. M. Majzlik Initials R.S.M Date 6-17-94 For E. M. Majzlik

R. J. Gromada Initials RJ Date 6-17-94
(approval to proceed)

P&T Engineer Initials mt Date 6/17/94

4. Remove the upper fiberboard assembly. Remove the shield if it is loose of the fiberboard. Record observations below, particularly noting charring at insulation interface, shield effects, impact damages, and conduit effects.

Char by conduit broken up during disassembly, but no burning or significant char variation at lead entrance from conduit. Fiberboard browned slightly along lead path between upper and lower fiberboard assemblies. Outer fiberboard step fully charred and was broken up, but char depth in general penetrated little more than ring thickness. Shield not attached. Top fiberboard layer intact but fragile. RTV marks evident. All shield TCS well-attached.

Impact marked significant on bearing plate. No brownning on exposed SF part, but some on part in lower fiberboard. Charred parts

Initials mt Date 6/17/94 Breaking off, losing original condition in charred regions.

5. Quarter the upper fiberboard assembly, including the bearing plate and, if attached, the shield. Record observations below, particularly noting char depths, shield effects, and impact damages.

Only halved assembly, then quartered one half. Char at junction with lower assembly: discoloration $2\frac{3}{4}$ in. from ID, blackening $3\frac{1}{4}$ in. from ID. Charring rounded at top corner with approx. $1\frac{1}{2}$ in. radius. Drop damage very evident - top aluminum plate deformed with square of vessel top imprinted. Plate/board original height from base: $2\frac{3}{4}$ in., at deformed center: $3\frac{7}{16}$ in., visible compression of board. Measuring from base to top on relatively undeformed side (see drawing) have $4\frac{3}{4}$ in. to brownning, 5 in. to blackened char, radially have $3\frac{3}{16}$ in. - $3\frac{3}{8}$ in. of sound (but discolored at outer bound) board. No significant

Initials mt Date 6/20/94 radial char difference in shield to unshielded areas.

Savannah River Technology Center
E&MT Field Procedure

Procedure: FP 570, Rev 0
E&MT Job Folder: 22306
Category: 1
Page: 6 of 12

Disassembling the 9973 and 9975 Thermal Test Packagings

6. Remove the containment vessel assembly and provide to P&T person(s) responsible for leak testing per FP 531. Record observations below.

Is rust colored coating on vessel below insulation assembly junction, heaviest on side including thermocouple TR-3259. Fiberboard cavity had some rust colored coating as well. All thermocouples as-new. Heaviest discoloration on vessel was ~~at~~ where fiberboard was nearest.

Initials nmA Date 6/17/94

7. Obtain the primary and secondary containment vessel seal leak test data sheets from the responsible P&T engineer. Record the results below for each and note the responsible engineer. Attach the data sheets to this procedure.

*Secondary: SRT-SPS-94014F54, Record 238, 6/25/94,
responsible engr: R S Maurer.*

result: $< 2.8 \times 10^{-9}$ std cc He/sec, 150 psid

Primary: SRT-SPS-940154, Record 285, 7/2/94.

responsible engr: R S Maurer

result: 2.5×10^{-8} std cc He/sec, 150 psid

Initials nmA Date 7/13/94

Both satisfy stated acceptance of $\leq 2.0 \times 10^{-7}$ std cc He/sec.

8. Quarter the lower fiberboard assembly including the bearing plate. Record observations below, particularly noting char depths, conduit effects, and impact damages.

Cut edge cylinder part in half, then halved bottom layers (after cutting from cylinder parts) and quartered one bottom piece. Bottom 2 layers destroyed due to fragile nature, top insulation strip originally intact but totally lost due to fragile nature of char. Negligible conduit effects - browsing where leads crossed insulation junction, no difference in charring. No impact effects. On cylinder: 4 in to full char, 3 3/4 in to stable board (from ID). At top, char was deeper: 3 1/4 in. to 3 1/2 in. stable, 3 1/2 in. + fully charred (from ID). With respect to horizontal burn, bottom corner radius of char is approx 1 in. on bottom, 2 in. on top. Base charred evenly to approx. 1 1/16 in. Stable board

Savannah River Technology Center
E&MT Field Procedure

Procedure: FP 570, Rev 0
E&MT Job Folder: 22306
Category: 1
Page: 7 of 12

Disassembling the 9973 and 9975 Thermal Test Packagings

plus 1/2 in. aluminum plate. Side cylinder char uniform along length between base on top junction. Bottom TC apparently was intact during test as indicated by rust-colored deposits at attachment.

Initials nut Date 6/20/94

9. Record observations of the lower drum half with the conduit fitting.

All thermocouples remained well-attached. Drum essentially the same as the other half. No noticeable marks at conduit opening.

Initials nut Date 6/20/94

10. Gather the 9973 parts for later storage.

Initials nut Date 6/30/94

3. 9975 Disassembly

1. Remove the conduit cover up to the drum fitting. Record observations below.

Lots of powdered black material in conduit and in purge line at drum end - likely vibrated down in shipment. No tar at drum end, some with odor, far from drum. Only 1st wire tie lost. Drum hole appears to be still plugged, although fully blackened. Much different condition than 9973.

Initials nut Date 6/22/94

2. Remove the drum lid using the closure bolt and ring. Record observations below.

Contents settled in shipment approx. 3/4 in. gauged from vent-hole observations at SNL. Total settling from original height approx. 2 3/16 in - 2 1/2 in. Carbon layer on all surfaces, not shiny like 9973 (had no aluminum blanket). Ring bolt loose, but not as

Savannah River Technology Center
E&MT Field Procedure

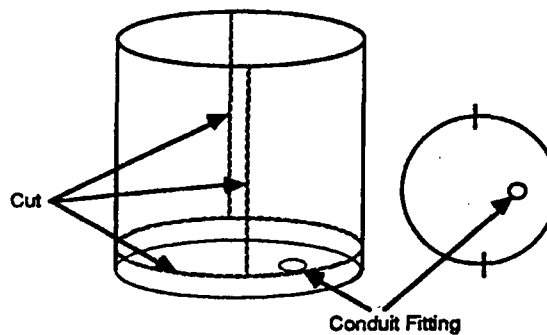
Procedure: FP 570, Rev 0
E&MT Job Folder: 22306
Category: 1
Page: 8 of 12

Disassembling the 9973 and 9975 Thermal Test Packagings

loose as 9973. Much of the lid gasket structure was intact but carbonized. Thermocouples attached as-new.

Initials MMW Date 6/22/94

3. Cut the drum laterally and around the bottom as shown below. Remove the upper pieces. Record observations below.



Saber-sawed all but adjacent to shield, ground this. Very uniform charring. Outer insulation step fully charred approx. 18 in. at thermocouple pass-through broken off during disassembly (pieces either settled down to drum bottom or were removed and placed aside). Glue pattern char-cracking as with 9973, but now every 2 in. (cylinder was re-used). Gap between upper assembly and outer ring axially 1/4 in. (possibly due in part to shrinkage of fully charred ring). Approx. 1/2 in. radial shrinkage at shield, 3/8 in. to 1/2 in. radial shrinkage at drum wall (measured at bottom). Drum walls coated on lower 2/3 with rust-colored deposits, drain marks evident from location of shield base downward. All TC attachments good. Shield obviously loose from fiberglass. No effect at pressure

Initials MMW Date 6/22/94 port. No burning, although one region approx. opposite conduit side and 2/3 up wall was grey high lighted, possibly due to carbon being flattened at disassembly. Outer step ring height measured - $1\frac{3}{16}$ in.

Savannah River Technology Center
E&MT Field Procedure

Procedure: FP 570, Rev 0
E&MT Job Folder: 22306
Category: 1
Page: 9 of 12

Disassembling the 9973 and 9975 Thermal Test Packagings

ENGINEERING WITNESS POINT

Request the following to witness, initial, and date:

S. J. Hensel Initials SH Date 6-22-94

R. J. Gromada Initials RJG Date 6-23-94
(approval to proceed)

P&T Engineer Initials mm Date 6/23/94

- 4. Remove the upper fiberboard assembly. Remove the shield if it is loose of the fiberboard. Record observations below, particularly noting charring at insulation interface, shield effects, and signs of lead melting. Also, observe any reasons why the 1/2 in. thick aluminum lid did not fit above the lead sleeve at assembly.

Shield cleanly lifted off - black caked material on top of fiberboard, likely RTV char. Top 2 board layers intact but loose, fell off when lifted. Outside height of max. OD section: 6 3/8 - 6 5/8 in. Top board contours matched warped shield. Lower board surface black, as-supplied by Celotex. Lead and lid cavity discolored black at TC hole/channel. Lead discolored light tan on much of its exposed surface. Lead elevation from boards 4 7/8 in., cavity in lid: 4 15/16 in., or 1/16 in. gap. About 1/16 in. gap in lead top elevation to SEV top.

Initials mm Date 6/24/94

- 5. Quarter the upper fiberboard assembly, including the bearing plate and, if attached, the shield. Record observations below, particularly noting char depths and shield effects.

Unstable fiberboard: easily crumbles away, including all black char and much of the darker brown partial char.

Halved top at TC path plane, then quartered one half. At bottom, char depth slightly deeper than top near aluminum plate. At bottom: 2 3/8 in. From ID to stable board, 2 5/8 in. At cavity top radial near plate. At top: 2 3/4 in. From bottom of plate (1/2 in. AL) to top of stable board. All 4 TC's on shield attached as-new. Char radius at corner approx. 1 in.

Initials mm Date 6/24/94

Savannah River Technology Center
E&MT Field Procedure

Procedure: FP 570, Rev 0
E&MT Job Folder: 22306
Category: 1
Page: 10 of 12

Disassembling the 9973 and 9975 Thermal Test Packagings

6. Remove the containment vessel assembly with heater leads intact. Record observations below.

Top leads - too tight at bottom of lead to allow pull-through. PCV TC fractured at exit from SCV, apparently stress concentration related. Some tar deposited on SCV at TC channel, otherwise SCV appears as-new, TC's attached as-new. Lead is fully seated at the bottom. Retention bar holding internal leads into bottom SCV slot lost during disassembly.

Initials WRS Date 6/24/94

7. Remove the primary containment vessel with heater leads intact. Record observations below.

SCV seal ring still moist, no test effects visible. Top honeycomb as-new. Bottom honeycomb stuck in SCV. TC on PCV attached as-new. No rattling in PCV, no discoloring anywhere on PCV. Heater leads not fully intact, sheared 2 and severely damaged 11/12 in prior step.

Initials MVA Date 6/24/94

8. Remove the heater assembly and determine what went wrong with the bad lead. Also, check the heater resistance. Record observations below, particularly noting the above items.

Could not determine lead fault due to disassembly damage. Resistance measured at 10.3Ω using Fluke model 77 Form 786-A. Lead insulation yellowed, heaviest at heater connections, fading to white base color at approx. 10 in. from heater. No evidence of any arcing, shorts, or other failures. No heater discoloration (some rust-colored specs in upper insulation may have been when new). No discoloration of the carbon steel dummy canker mass inside or outside. All fracturing as-installed, no abnormalities.

Initials MVA Date 6/29/94

Savannah River Technology Center
E&MT Field Procedure

Procedure: FP 570, Rev 0
E&MT Job Folder: 22306
Category: 1
Page: 11 of 12

Disassembling the 9973 and 9975 Thermal Test Packagings

- 9. Remove the lead sleeve. This may be done during quartering of the lower fiberboard assembly. Record observations below, particularly noting evidence of lead melting. Also, observe any reasons why the 1/2 in. thick aluminum lid did not fit above the lead sleeve at assembly.

Pulled lead out with 4 people using cross-bars to hold bottom board down. Heavy white coat on lead, apparently mastic from the board (only on lead adjacent to mastic). Stripes on lead at 2 in. intervals matching layers of board that cracked in char. Some blacken regions on side, not clear if from char vibrating into joint or from TC channel (or otherwise). No distinct trace up TC channel region. Lead sleeve length: 24 in.

Initials *MS* Date *6/24/94*

- 10. Quarter the lower fiberboard assembly including the bearing plate and cut at the plane of the included TCs. Record observations below, particularly noting char depths, conduit effects, and the state of the region near each fiberboard TC. Also, observe any reasons why the 1/2 in. thick aluminum lid did not fit above the lead sleeve at assembly.

cut same as 9973, then further sectioned to location TC planes.



Cavity depth: 19 13/16 in., to be 20 1/16 in., undersize 1/4 in. Pulled lead plate first - slight discoloration at TC groove, discolored ring on top between sleeve I.D. and SCV O.D. Plate thickness at edge: 3/16 in. - 1/16 in., to be 1/2 in. Thickness increased during assembly due to hammering down AD. Therefore, aluminum 1/2 in. plate did not fit due to 3/16 in. cavity + lead dimensional error.

Char on board board wall not uniform due to poor joints at 2 in. layers, some layers not adhered in areas across entire radius. From ID to unstable board: 2 1/2 in. at top, 2 5/8 in. at 3 1/2 in. down, 2 7/8 in. at 7 1/4 in. down, 2 1/2 in. at bad glue joint 10 in. down, 3 in. at 17 in. down; at another quadrant: varied from 2 1/2 in. at glue joints (12) to 2 3/4 in. top. ~ 2 1/16 in. Striping on lead apparently due to gas passing through poor joints. TR-3252: 2 3/8 in. to char junction, 3 in. to char, heavy glue line; TR-3253: 2 3/8 in. to junction, 2 3/4 in. to char. Char

penetration uniform at both TCs. Bottom less charred at conduit, likely due to insulation. Balance of bottom 2 1/2 in. with aluminum 1/2 in. plate;

- 11. Record observations of the bottom drum part with the conduit fitting.

TC intact as new. Originally flat bottom warped at conduit, some likely due to welding. Originally 3/4 in. from bottom lip to flat bottom.

sharp (< 1/2 in.) corner char, but 3 in. at conduit and 1 in. corner char - radius. Ceramic/fiber plug intact, no charring in TC hole, little discoloration in hole or channel. OD at aluminum plate: 14 5/8 in. stable, no discoloration on surface.

Savannah River Technology Center
E&MT Field Procedure

Procedure: FP 570, Rev 0
E&MT Job Folder: 22306
Category: 1
Page: 12 of 12

Disassembling the 9973 and 9975 Thermal Test Packagings

*reduced to 1/2 in. at conduit. 4-point test stand apparently
keep bottom from bowing out further. Rust-colored in inside
corner perimeter and on areas of the wall. Signs of char sticking
to bottom surface.*

Initials WA Date 6/29/94

12. Gather the 9975 parts for later storage.

Initials WA Date 6/30/94

Records

The following documents shall be retained as QA records:

1. This approved procedure in the E&MT procedure control system
2. This procedure once completed, including leak test data sheets.

References

1. E&MT Procedure No. FP 558, Rev. 0, "Instrumented Assembly of the 9973 and 9975 Shipping Packagings", (as performed 5/94 through 6/94).
2. E&MT Procedure No. FP 531, current Rev., "Unloading, Inspecting, & Leak Testing the 9972 Family of Shipping Packages."

** ACCEPTABLE **

06/25/94
PAGE 1 OF 2
Record No.: 238

Basis No.: SRT-SPS-940154
RETENTION: LIFE

CC: BOB MAURER
Laboratory Copy
File Room, 730-A
SRL Records, 773-A

773-54

EES PROOF/LEAK TEST DATA SHEET (U)

Test Item: 9973B SECONDARY SHIPPING CONTAINER
Test Item Serial Number: 203
Test Date: 06/28/94
Body: Leakage Rate, std cc He/sec: < 2.8 x 10⁻⁹

Leak Test Pressure (psig): 150

Acceptable Maxium Leak Rates, std cc He/sec:
Body: 2.0 X 10⁻⁷

EES Test Engineer: D. J. TRAPP Phone: 725-7284

Results verified by: Dale C. Alexander

Certified L.T. L.J. Sperry II Date: 6-28-94
Signature/Level

COMMENTS

ACTUAL LEAK TEST PRESSURE - 155 PSIG.

PAGE 2 OF 2
Record No.: 238

TEST DESCRIPTION

Technician: DALE C. ALEXANDER
Procedure No.: FP-516
Revision No.: 0
Proof Test Time (min):
Proof Test Fluid:
Leak Test Method: BELL JAR
Leak Test Time (min): 3
Leak Test Fluid: HE
% Concentration: 100

TEST EQUIPMENT

<u>M&TE Description</u>	<u>No.</u>	<u>Cat.</u>	<u>Expires</u>
Leak Detector	3-1221	1	B/A
Strip Chart Recorder	L41005		
Pressure Gauge/Transducer	3-1101	1	1-1-95
Thermometer	EA-974	1	12-14-94

PRELIMINARY CALIBRATION

Preliminary Standard Leak Rate, std cc He/sec: 2.93×10^{-8}
Standard Leak M&TE Cat 1 #: 3-1078 Expires: 01/01/95
Preliminary Standard Leak Cal. Temp, oC: 26.7
Room Temperature, oC: 24.4
Preliminary Temp Corrected Standard Leak Rate, std cc He/sec:
 2.7×10^{-8}
Preliminary Cal Background, Divisions: 0.1
Preliminary Cal Meter Reading, Divisions: 10.0
Preliminary Sensitivity (std cc He/sec/Division): 2.8×10^{-9}

FINAL CALIBRATION

Final Standard Leak Rate, std cc He/sec: 2.9×10^{-8}
Standard Leak M&TE Cat 1 #: 3-1078 Expires: 01/01/95
Final Standard Leak Cal Temp, oC: 26.7
Final Temp Corrected Standard Leak Rate, std cc He/sec: 2.7×10^{-8}
Final Cal Background, Divisions: 0.1
Final Cal Meter Reading, Divisions: 10.0
Final Sensitivity (std cc He/sec/Division): 2.8×10^{-9}

LEAK MEASUREMENTS

Body Sample Background, Divisions: 0.1
Sample Meter Reading, Divisions: 0.1

** ACCEPTABLE **

07/02/94
PAGE 1 OF 2
Record No.: 285

Basis No.: SRT-SPS-940154
RETENTION: LIFE

CC: BOB MAURER 773-54
Laboratory Copy
File Room, 730-A
SRL Records, 773-A

EES PROOF/LEAK TEST DATA SHEET (U)

Test Item: 9973-B PRIMARY SHIPPING CONTAINER
Test Item Serial Number: 203
Test Date: 07/08/94
Body: Leakage Rate, std cc He/sec: 2.5 x 10⁻⁸

Leak Test Pressure (psig): 150

Acceptable Maxium Leak Rates, std cc He/sec:
Body: 2.0 X 10⁻⁷

EES Test Engineer: D. J. TRAPP Phone: 725-7284

Results verified by: *L. J. Spivey*

Certified L.T. *T. Simpson II* Date: 7-8-94
Signature/Level

COMMENTS

ACTUAL LEAK TEST PRESSURE - 154 PSIG.

PAGE 2 OF 2
Record No.: 285

TEST DESCRIPTION

Technician: T.SNIPES
Procedure No.: FP-531
Revision No.: 0
Proof Test Time (min):
Proof Test Fluid:
Leak Test Method: BELL JAR
Leak Test Time (min): 3
Leak Test Fluid: HE
% Concentration: 100

TEST EQUIPMENT

<u>M&TE Description</u>	<u>No.</u>	<u>Cat.</u>	<u>Expires</u>
Leak Detector	8-1098	1	B/A
Strip Chart Recorder	L41004	0	N/A
Pressure Gauge/Transducer	3-1068	1	1-1-95
Thermometer	EA-974	1	12-14-94
		0	
		0	

PRELIMINARY CALIBRATION

Preliminary Standard Leak Rate, std cc He/sec: 2.93×10^{-8}
Standard Leak M&TE Cat 1 #: 3-1078 Expires: 01/01/95
Preliminary Standard Leak Cal. Temp, oC: 26.7
Room Temperature, oC: 25.4
Preliminary Temp Corrected Standard Leak Rate, std cc He/sec:
 2.8×10^{-8}
Preliminary Cal Background, Divisions: 5.4
Preliminary Cal Meter Reading, Divisions: 33.0
Preliminary Sensitivity (std cc He/sec/Division): 1.0×10^{-9}

FINAL CALIBRATION

Final Standard Leak Rate, std cc He/sec: 2.9×10^{-8}
Standard Leak M&TE Cat 1 #: 3-1078 Expires: 01/01/95
Final Standard Leak Cal Temp, oC: 26.7
Final Temp Corrected Standard Leak Rate, std cc He/sec: 2.8×10^{-8}
Final Cal Background, Divisions: 5.4
Final Cal Meter Reading, Divisions: 33.0
Final Sensitivity (std cc He/sec/Division): 1.0×10^{-9}

LEAK MEASUREMENTS

Body Sample Background, Divisions: 5.4
Sample Meter Reading, Divisions: 30.0

APPENDIX 3.6
DETERMINATION OF PRESSURES IN THE 9975 PACKAGE
FOR IMPURE PU OXIDE CONTENTS

This Page Intentionally Left Blank

Calculation Cover Sheet

Project 9975 Package Certification		Calculation Number M-CLC-F-00630	Project Number	
Title Determination Of Pressures In The 9975 Package For Impure Pu Oxide Contents		Functional Classification SC	Sheet 1 of 11	
		Discipline Mechanical		
<input type="checkbox"/> Preliminary <input type="checkbox"/> Committed <input checked="" type="checkbox"/> Confirmed				
Computer Program No. <input checked="" type="checkbox"/> N/A		Version/Release No.		
Purpose and Objective To evaluate the 3013 vessel and 9975 shipping package containment vessel maximum normal operating pressures (MNOP) during Normal Conditions of Transport (NCT). Impure Pu oxide packed in both food cans and 3013 configurations are considered.				
Summary of Conclusion The 3013, PCV, and SCV allowable pressures are 699, 900, and 800 psig, respectively, regardless of content configuration. During Normal Conditions of Transport (NCT) the pressures in the 9975 containment vessels for impure Pu oxide packed in either food cans or the 3013 vessel result in pressures below the allowables. The pressures for impure Pu oxide are bounding relative to pure Pu oxide due to free volume differences. The BNFL 3013 configuration results in the greatest pressures of the three (BNFL, LLNL, and LANL) 3013 configurations. The maximum calculated pressures in the 3013, PCV, and SCV are 646.4, 365.4, and 165.8 psig, respectively.				
Revisions				
Rev No.	Revision Description			
0	Original issue			
Sign Off				
Rev No.	Originator (Print) Sign/Date	Verification/ Checking Method	Verifier/Checker (Print) Sign/Date	Manager (Print) Sign/Date
0	Steve Hensey Alan Hensey 2/12/00	Individual	PRAN K. PAUL Prank Paul 1/12/00	S.P. HOLDING-SMITH S.P. Holding-Smith 1/7/00
Classification Unclassified				

Determination of Pressures in the 9975 Package for Impure Pu Oxide Contents

1.0 Conclusions

The maximum normal operating pressure (MNOP) in the 9975 package during Normal Conditions of Transport (NCT) was computed for the primary containment vessel (PCV) and the secondary containment vessel (SCV) for impure Pu oxide contents packed in food cans. For Pu oxide packed in the 3013 vessel, the MNOP was computed for the 3013 and PCV. Two layers of pressure containment are evaluated for both configurations. The results are summarized in Table 1. The pressures for Pu oxide contents which satisfy the material requirements in DOE-STD-3013-99 (packed in food cans or in the 3013 container within the 9975 PCV) were computed by applying the storage standard for gas generation via radiolysis of the adsorbed moisture [1]. The maximum amount of hydrogen generated is based on a 0.5% (25 g) total absorbed moisture limit on the contents (5.0 kg maximum Pu oxide) [1]. The 3013, PCV, and SCV allowable pressures are 699 [1, p. 7], 900 [2, p. 1-30], and 800 [2, p. 1-31] psig, respectively. The pressures in the 9975 containment vessels for impure Pu oxide packed in either food cans or the 3013 vessel result in pressures below the allowable. The pressures for impure Pu oxide are bounding relative to pure Pu oxide due to free volume differences. The BNFL 3013 configuration results in the greatest pressures of the three (BNFL, LLNL, and LANL) 3013 configurations.

Table 1: Pressures And Allowables In The 9975 With Impure Pu Oxide Contents

Vessel	Configuration	MNOP (psig)	Allowable (psig)
PCV	food cans	365.4	900
SCV*	food cans	165.8	800
3013	3013 vessel	646.4	699
PCV*	3013 vessel	258.2	900

* pressure assumes inner vessel leaks

2.0 Input

2.1 Free Volumes

The free volume available in the PCV can be computed based on the volume of the impure Pu oxide, cans, bags (if applicable), honeycomb, and PCV cylindrical sleeve or spacer. The content volume excludes the free volume available due to the porosity of the materials, because that space is available for gas to occupy. The volume occupied by the impure oxide is presented in Table 2. Three 3013 configurations are considered (BNFL [1], LANL [3], and LLNL [4]). The volume occupied by the impure Pu oxide is determined using the statistical density method in DOE-STD-3013-99 [1] where the ratio of bulk to particle density is given by:

$$F_p = 0.3928 + 0.05673\rho_{\text{bulk}} \text{ (DOE-STD-3013-99, p. 59)}$$

where ρ_{bulk} is given in g/cc (assume 5.0 kg contents within convenience can) and the volume occupied by the contents in cc is $(M/\rho_{\text{bulk}})*F_p$, with M as content mass in grams.

Table 2: Determination Of Volume Occupied By Pu Oxide Contents

Quantity	Food Cans*	BNFL 3013**	LANL 3013***	LLNL 3013****
convenience can volume (cc)	2987 (from can size)	1839 [1]	1801 (from can size)	1543 (from can size)
oxide mass (g)	5000	5000	5000	5000
ρ_{bulk} (g/cc)	1.67	2.72	2.78	3.24
F_p (g/cc)	0.4875	0.5471	0.5505	0.5766
volume (cc)	1460	1006	1001	890
volume (ft. ³)	0.0516	0.0355	0.0353	0.0314

* bounding configuration is with three 4 1/16 in. X 4 11/16 in. (DIA X height) inner cans

** Volume of convenience can found in DOE-STD-3013-99, p. 55

*** Convenience can is 4.00 in. X 8.76 in. (DIA X Height) [3]

**** Convenience can is 4.139 in. X 7.0 in. (DIA X Height) [4]

The free volumes in the 3013, PCV, and SCV are derived in Table 3.

Table 3: Volumes of Components and Net Free Volume In 3013, PCV, & SCV (ft.³)

Components (#)	Food Cans	BNFL 3013	LANL 3013	LLNL 3013
Gross 3013 (1)	-----	0.0919 [1, p. 55]	0.0919 [1, p. 55]	0.0919 [1, p. 55]
Contents (2)	0.0516	0.0355	0.0353	0.0314
Cans/bags/foil (3)	0.0106 (see note)	0.0141 (see note)	0.0089 (see note)	0.0089 (see note)
Net 3013 (1-2-3)	-----	0.0423	0.0477	0.0516
3013 vessel (4)	-----	0.0178 [1, p. 55]	0.0178 [1, p.55]	0.0178 [1, p. 55]
PCV sleeve or spacer (5)	0.039 [5, see calculation below]	0.0116 [5, see calculation below]	0.0116 [5, see calculation below]	0.0116 [5, see calculation below]
PCV honeycomb (6)	0.0016 [2, p. 3-53]	0.0016 [2, p. 3-53]	0.0016 [2, p. 3-53]	0.0016 [2, p. 3-53]
Gross PCV (7)	0.1811 [2, p. 3-53]	0.1811 [2, p. 3-53]	0.1811 [2, p. 3-53]	0.1811 [2, p. 3-53]
Net PCV (7-6-5-4-3-2)	0.0783	0.1005	0.1059	0.1098
Between PCV & SCV (8)	0.1020 [2, p. 3-53]	0.1020 [2, p. 3-53]	0.1020 [2, p. 3-53]	0.1020 [2, p. 3-53]
SCV honeycomb (9)	0.0039 [2, p. 3-53]	0.0039 [2, p. 3-53]	0.0039 [2, p. 3-53]	0.0039 [2, p. 3-53]
Net SCV (8+7-9-6-5-4-3-2)	0.1764	0.1986	0.2040	0.2079

Note: the Pu oxide in food can configuration allows up to 900 grams of steel cans (7.83 g/cc), 100 grams of low density polyethylene (0.92 g/cc) or nylon bagging (1.14 g/cc), and 200 grams of aluminum foil (2.7 g/cc); volumes occupied by inner containers for 3013 configurations are based on data in DOE-STD-3013-99, the ARIES inner can (1600 gram mass assumed, same as BNFL inner 3013 container), and a convenience can mass of 400 grams for both LLNL and LANL configurations was assumed (all 3013 configurations are free of polyethylene or nylon bagging, and crushed aluminum foil).

M-CLC-F-00630, Rev. 0
p. 5 of 11

A cylindrical sleeve is required for food can shipments and a cylindrical spacer is required for shipments utilizing the 3013 vessel [5].

Cylinder sleeve used in PCV with food can shipments:

Cylinder design: 4.385 in. ID and 5.0 in. OD

Volume of cylinder (14.9 in. tall): $3.14159(2.5*2.5 - 2.1925*2.1925)*14.9 = 67.5 \text{ in.}^3$
(0.0390 ft.³)

Cylinder spacer used in PCV with 3013 vessel shipments:

Cylinder design: 4.38 in. ID and 4.92 in. OD [5]

Volume of cylinder (5.06 in. tall): $3.14159(2.46*2.46 - 2.19*2.19)*5.06 = 20.0 \text{ in.}^3$
(0.0116 ft.³)

2.2 Gas mixtures and temperatures

2.2.1 Pu oxide in food cans

Plutonium oxide contents with a decay power of 19 W are considered.

Conditions in the Primary Containment Vessel (PCV) during NCT with solar:

Temperature 313°F (772.6 R) [6, p. 2]

Free volume within PCV is 0.0783 ft.³

Content has up to 0.5 % wt. moisture (25 grams moisture)

M-CLC-F-00630, Rev. 0
p. 6 of 11

Hydrogen gas generation from radiolysis of the moisture is conservatively determined by applying the 50 year storage standard for plutonium oxides [1]. This results in 1.389 gram-moles of hydrogen gas (complete radiolysis of the moisture). The radiolysis is assumed to occur instantaneously once the PCV is closed. In addition, gas (in the form of water vapor) can be generated by the thermal breakdown of nylon bagging. An additional 32.1 psia was measured from FB-Line nylon bagging when a sample was heated to 350°F (sample size to test container volume was 793 g/ft.³) [7]. Using a PCV temperature of 313°F and a bag mass to free volume ratio of 100 g to 0.1145 ft.³ free volume (873 g/ft.³) results in an equivalent 33.7 psia increase in pressure due to gas generation. FB-Line nylon bagging was found to out gas more than RFETS nylon or low density polyethylene [8,9].

Conditions in Secondary Containment Vessel (SCV) during NCT with solar:

Temperature 313°F (772.6 R) [6, p. 2]

Free volume within the combined PCV and SCV is 0.1764 ft.³

2.2.3 Pu oxide in 3013 container

Plutonium oxide contents with a decay power of 19 W are considered. The BNFL configuration results in the least free volume inside the 3013 vessel and therefore pressures in the BNFL 3013 configuration bound those in the LLNL and LANL configurations.

Conditions in the 3013 vessel during NCT with solar:

Temperature 360°F (819.6 R) (estimate of volume average of temperatures reported in [6])

Free volume within PCV is 0.0423 ft.³

Content has up to 0.5 % wt. moisture (25 grams moisture)

M-CLC-F-00630, Rev. 0
p. 7 of 11

Hydrogen gas generation from radiolysis of the moisture is determined by conservatively applying the 50 year storage standard for plutonium oxides [1]. This results in 1.389 gram-moles of hydrogen gas (complete radiolysis of the moisture). The radiolysis is assumed to occur instantaneously once the PCV is closed.

Conditions in Primary Containment Vessel (PCV) during NCT with solar:

Temperature 308°F (767.6 R) [6, p. 2]

Free volume within the combined 3013 and PCV is 0.1005 ft.³

3.0 Analytical Methods and Computations

3.1 Pu oxide in food cans

The total composition of gas in the PCV consists of:

Fill gas initially in the free space within the PCV (including food cans)-

$$M_{\text{gas}} = (14.7 \text{ psia})(0.0783 \text{ ft.}^3)/[(10.73 \text{ psi-ft.}^3/\text{lb-moles-R})(529.6 \text{ R})]$$

$$M_{\text{gas}} = 2.025\text{E-}04 \text{ lb-moles}$$

Helium generated via radioactive decay- consider 19 W of Pu-239 decaying for 2 years (see [1], eq. 23) (R=547 psi-liters/lb-moles-K)

$$7.517\text{E-}05 * 19 * 2 / 547 = 5.22\text{E-}06 \text{ lb-moles}$$

$$M_{\text{helium}} = 5.22\text{E-}06 \text{ lb-moles}$$

Hydrogen generated via radiolysis of 25 g moisture (1.389 gram-moles)-

$$M_{\text{hydrogen}} = 3.062\text{E-}03 \text{ lb-moles}$$

The partial pressure from thermal decomposition of low density polyethylene, nylon bagging used at Rocky Flats, and nylon bagging used at FB-Line Savannah River Site

M-CLC-F-00630, Rev. 0
p. 8 of 11

results in an additional pressure due to thermal decomposition. The greatest contribution is from the FB-Line Nylon bagging material (33.7 psia).

$$M_{\text{bag}} = (33.7 \text{ psi})(0.0783 \text{ ft.}^3)/[(10.73 \text{ psi-ft.}^3/\text{lb-moles-R})(772.6 \text{ R})]$$

$$M_{\text{bag}} = 3.18\text{E-}04 \text{ lb-moles}$$

Total gas in the PCV is:

$$M_{\text{total PCV}} = M_{\text{gas}} + M_{\text{helium}} + M_{\text{hydrogen}} + M_{\text{bag}}$$

$$M_{\text{total PCV}} = 2.03\text{E-}04 + 5.22\text{E-}06 + 3.062\text{E-}03 + 3.18\text{E-}04 \text{ lb-moles}$$

$$M_{\text{total PCV}} = 3.59\text{E-}03 \text{ lb-moles (85\% of gas is hydrogen)}$$

During NCT the resulting pressure is:

$$P_{\text{PCV}} = (3.59\text{E-}03 \text{ lb-moles})(10.73 \text{ psi-ft.}^3/\text{lb-moles-R})(772.6 \text{ R})/(0.0783 \text{ ft.}^3)$$

$$P_{\text{PCV}} = 380.1 \text{ psia}$$

$$P_{\text{PCV}} = 365.4 \text{ psig}$$

Assuming the PCV leaks as a requirement for double containment, the total gas in the PCV & SCV is that in the PCV plus the original fill gas solely in the SCV:

$$M_{\text{SCVgas}} = (14.7 \text{ psia})(0.1764 - 0.0783 \text{ ft.}^3)/[(10.73 \text{ psi-ft.}^3/\text{lb-moles-R})(529.6 \text{ R})]$$

$$M_{\text{SCVgas}} = 2.54\text{E-}04 \text{ lb-moles}$$

$$M_{\text{total SCV}} = 3.59\text{E-}03 + 2.54\text{E-}04 \text{ lb-moles}$$

$$M_{\text{total SCV}} = 3.84\text{E-}03 \text{ lb-moles (80\% of gas is hydrogen)}$$

During NCT the resulting pressure is:

$$P_{\text{SCV}} = (3.84\text{E-}03 \text{ lb-moles})(10.73 \text{ psi-ft.}^3/\text{lb-moles-R})(772.6 \text{ R})/(0.1764 \text{ ft.}^3)$$

$$P_{\text{SCV}} = 180.5 \text{ psia}$$

M-CLC-F-00630, Rev. 0
p. 9 of 11

$$\underline{P_{SCV} = 165.8 \text{ psig}}$$

3.2 Pu oxide in 3013

The total composition of gas in the 3013 consists of:

Gas initially in the free space within the 3013 (including 3013 and interior vessels)-

$$M_{\text{gas}} = (14.7 \text{ psia})(0.0423 \text{ ft.}^3)/[(10.73 \text{ psi-ft.}^3/\text{lb-moles-R})(529.6 \text{ R})]$$

$$M_{\text{gas}} = 1.09\text{E-}04 \text{ lb-moles}$$

Helium generated via radioactive decay- consider 19 W of Pu-239 decaying for 2 years:

5.22E-06 lb-moles of helium

$$M_{\text{helium}} = 5.22\text{E-}06 \text{ lb-moles}$$

Hydrogen generated via radiolysis of 25 g moisture (1.389 gram-moles)-

$$M_{\text{hydrogen}} = 3.062\text{E-}03 \text{ lb-moles}$$

Total gas in the 3013 is:

$$M_{\text{total 3013}} = M_{\text{gas}} + M_{\text{helium}} + M_{\text{hydrogen}}$$

$$M_{\text{total 3013}} = 1.09\text{E-}04 + 5.22\text{E-}06 + 3.062\text{E-}03 \text{ lb-moles}$$

$$M_{\text{total 3013}} = 3.18\text{E-}03 \text{ lb-moles (96\% of gas is hydrogen)}$$

During NCT the resulting pressure is:

$$P_{3013} = (3.18\text{E-}03 \text{ lb-moles})(10.73 \text{ psi-ft.}^3/\text{lb-moles-R})(819.6 \text{ R})/(0.0423 \text{ ft.}^3)$$

$$P_{3013} = 661.1 \text{ psia}$$

$$\underline{P_{3013} = 646.4 \text{ psig}}$$

M-CLC-F-00630, Rev. 0

p. 10 of 11

Assuming the 3013 leaks (although this is incredible as both the inner and 3013 vessel are leak tested after welded closure) the total gas in the PCV is that in the 3013 plus the original fill gas solely in the PCV:

$$M_{PCV_{gas}} = (14.7 \text{ psia})(0.1005 - 0.0423 \text{ ft.}^3) / [(10.73 \text{ psi-ft.}^3/\text{lb-moles-R})(529.6 \text{ R})]$$

$$M_{PCV_{gas}} = 1.51\text{E-}04 \text{ lb-moles}$$

$$M_{\text{total PCV}} = M_{\text{total 3013}} + M_{PCV_{gas}}$$

$$M_{\text{total PCV}} = 3.18\text{E-}03 + 1.51\text{E-}04 \text{ lb-moles}$$

$$M_{\text{total PCV}} = 3.33\text{E-}03 \text{ lb-moles (92\% of gas is hydrogen)}$$

During NCT the resulting pressure in the PCV is:

$$P_{PCV} = (3.33\text{E-}03 \text{ lb-moles})(10.73 \text{ psi-ft.}^3/\text{lb-moles-R})(767.6 \text{ R}) / (0.1005 \text{ ft.}^3)$$

$$P_{PCV} = 272.9 \text{ psia}$$

$$P_{PCV} = 258.2 \text{ psig}$$

4.0 Results

The results are summarized in Table 4.

Table 4: Pressures And Allowables In The 9975 Containment Vessels

Vessel	Configuration	MNOP (psig)	Allowable (psig)
PCV	food cans	365.4	900
SCV*	food cans	165.8	800
3013	3013 vessel	646.4	699
PCV*	3013 vessel	258.2	900

* pressure assumes inner vessel leaks

5.0 References

1. DOE Standard, "Stabilization, Packaging, and Storage of Plutonium-Bearing Materials", DOE-STD-3013-99, November 1999.
2. WSRC-SA-7, Safety Analysis Report Packages 9965, 9968, 9972-75, Rev. 8, 1999.
3. Los Alamos drawing 90Y-219959.
4. Sketch of 94-1 LLNL Canning System, convenience can is 404X700 Can Manufacturers Institute (CMI) three piece sanitary can.
5. Westinghouse Savannah River Company drawing R-R4-F-0055 Rev. 2.
6. Hardy, B. J., "Thermal Analysis of the 9975 Package for Normal Conditions of Transport and Accident Conditions", M-CLC-F-00590, Rev. 0.
7. Skidmore, T. E., and Vormelker, P. R., "Off-Gas Pressure Evaluation of FB-Line Nylon Bagging Material", SRT-MTS-99-4031, April, 1999.
8. Skidmore, T. E., "Off-Gas Pressure Evaluation of RFETS Nylon Bagging Material", SRT-MTS-98-4112, Rev. 2.
9. Vormelker, P. R., "Polymer Film Out gassing Tests for Shipping Containers", SRT-MTS-94-5190, February, 1995.

This Page Intentionally Left Blank.

APPENDIX 3.7

**PRESSURE IN THE 9975 PACKAGE
WITH THE 3013 CONTAINER, PCV, AND SCV GAS SPACES IN COMMUNICATION**

This Page Intentionally Left Blank.

OSR 45-24# (Rev 1-10-2000)

Calculation Cover Sheet

Project 9975 Package Certification		Calculation Number M-CLC-A-00176	Project Number N/A	
Title Pressure in the 9975 Package with the 3013 Container, PCV, and SCV Gas Spaces in Communication (47)		Functional Classification SC	Sheet 1 of 4	
		Discipline Mechanical		
<input type="checkbox"/> Preliminary <input checked="" type="checkbox"/> Confirmed				
Computer Program No.		<input checked="" type="checkbox"/> N/A		
Version/Release No.				
Purpose and Objective To evaluate the 9975 shipping package containment vessel maximum normal operating pressure (MNOP) during Normal Conditions of Transport (NCT). The 3013 configuration, with the case where both the 3013 container and PCV leak, is considered. This calculation extends the analysis in calculation note M-CLC-F-00630.				
Summary of Conclusion The allowable pressure in the SCV is 800 psig, regardless of content configuration. During NCT the pressure in the 9975 SCV for impure Pu oxide packed in the 3013 container results in a pressure below the allowable. The calculated pressure in the SCV is 132.6 psig. In calculation note M-CLC-F-00630 NCT pressures were calculated for the cases in which the 3013 container either leaked or did not leak. The case where the PCV leaked as well as the 3013 container was not addressed. This calculation is documented herein.				
Revisions				
Rev No.	Revision Description			
0	Original Issue			
Sign Off				
Rev No.	Originator (Print) Sign/Date	Verification/ Checking Method	Verifier/Checker (Print) Sign/Date	Manager (Print) Sign/Date
0	Martin A. Shaddy Jr. <i>[Signature]</i> 6/20/01	DOCUMENT REVIEW	N. K. GUPTA <i>[Signature]</i> 6/20/01	C. B. HOLDING SMITH <i>[Signature]</i> 6/20/01
Release to Outside Agency – Design Authority (Print)		Signature		Date
NA				
Security Classification of the Calculation				
Unclassified				

ENGINEERING DOC. CONTROL - SRS



00640032

Pressure in the 9975 Package with the 3013 Container, PCV, and SCV Gas Spaces in Communication

Introduction and Summary

In reference [1] the results of maximum normal operating pressures (MNOP) during Normal Conditions of Transport (NCT) calculations are presented. Pressures were determined for two scenarios of the 3013 configuration of the 9975 package, cases where the 3013 container does and does not leak. The case where both the 3013 container and the PCV leak, and the contents of the gas spaces of the two containers mix with the contents of the gas space of the SCV, is not addressed in reference [1]. This scenario is addressed herein.

Plutonium oxide in a 9975 shipping package can generate hydrogen by radiolysis of absorbed water vapor, and alpha decay can generate helium. These gasses as well as heating of the gas by plutonium decay will pressurize the gas spaces inside of the SCV. If the 3013 container and the PCV leak, the internal gas space pressures will equilibrate. The calculated steady state pressure, consistent with the assumptions in reference [1] is 132.6 psig.

Input

The 3013 configuration of the 9975 shipping package contains three nested containers. From the inside going out, the nested containers are: the 3013 container, the primary containment vessel (PCV), and the secondary containment vessel (SCV). The volumes of the gas spaces in the three containers are [1]:

$$\begin{aligned}V_{3013} &= 1.1978 \times 10^{-3} \text{ m}^3 \\V_{\text{PCV}} &= 1.6480 \times 10^{-3} \text{ m}^3 \\V_{\text{SCV}} &= 2.7779 \times 10^{-3} \text{ m}^3\end{aligned}$$

The PCV volume is the volume of gas space inside of the PCV and outside of the 3013 container. The SCV volume is the volume of gas space inside of the SCV and outside of the PCV.

The 9975 shipping package is packed by loading the plutonium oxide in the 3013 container and then sequentially loading the nested containers, each in the next larger container, until the package is assembled. The initial temperature and pressure of the container gas spaces are assumed to be 70°F and 14.7 psia. The initial composition of the fill gas is immaterial with respect to the final pressure.

The 9975 package internals will heat-up during shipping and storage due to radioactive decay of the contents. The final temperatures of the gas spaces were determined with

steady-state heat transfer modelling of the 9975 package during NCT with insolation [2]. The 3013 container gas space temperature is an estimate of the volume average gas space temperature [1,2]. The PCV and SCV gas space temperatures are conservatively assumed to be equal to the peak surface temperatures of the gas space boundaries [2]. The assumed temperatures are:

$$T_{3013} = 360^{\circ}\text{F} = 455.2 \text{ K}$$

$$T_{\text{PCV}} = 293^{\circ}\text{F} = 418.2 \text{ K}$$

$$T_{\text{SCV}} = 283^{\circ}\text{F} = 412.6 \text{ K}$$

The internal gas space pressures will rise due to gas production as well as the radioactive heating. Hydrogen is produced by radiolysis of absorbed water vapor in the plutonium oxide. Alpha decay of the plutonium also produces helium. The hydrogen and helium source terms [1] are:

$$N_{\text{H}_2} = 1.389 \text{ mols H}_2$$

$$N_{\text{He}} = 2.3679 \times 10^{-3} \text{ mols He}$$

All of the hydrogen and helium is produced within the 3013 container. Gas space pressures for the two scenarios where the 3013 container does and does not leak are presented in reference [1]. For the scenario in which the 3013 container leaks, the contents of the 3013 container and the PCV gas spaces are assumed to mix freely and the two gas space pressures equilibrate. The scenario in which the PCV also leaks was not addressed, and this is the objective of this document. The contents of all three gas spaces are assumed to be well mixed after the initial loading and the 3013 hydrogen and helium is produced. The steady-state temperature distribution in the 9975 package is assumed to be independent of the gas mixing. This is reasonable and the only assumption that can be made with the available information [2].

Analytical Methods and Computations

The number of moles in the three gas spaces initially at 70°F and atmospheric pressure, is determined with the ideal gas relation. The total gas space volume of the three vessels is used. Note that this quantity is independent of the gas composition.

$$n = \frac{PV}{RT} \quad (1)$$

$$n_{\text{initial}} = \frac{(101300)(5.6237 \times 10^{-3})}{(8.314)(294.3)} = 0.23283 \text{ mols}$$

The final value for the number of moles of gas in the three gas spaces is the sum of the initial gas loading and the hydrogen and helium produced in the 3013 container:

$$n_{final} = .23283 + 1.389 + 2.3679 \times 10^{-3} = 1.6242 \text{ mols}$$

The pressures in the three gas spaces will be equal after mixing, but the temperatures will differ. To determine the pressure, solve the continuity equation and the ideal gas relation for each of the gas spaces simultaneously.

$$PV_{3013} = n_{3013} \bar{R} T_{3013} \quad (2)$$

$$PV_{PCV} = n_{PCV} \bar{R} T_{PCV} \quad (3)$$

$$PV_{SCV} = n_{SCV} \bar{R} T_{SCV} \quad (4)$$

$$n_{3013} + n_{PCV} + n_{SCV} = n \quad (5)$$

By judicious substitution these simultaneous equations can be reduced to a single equation for the pressure:

$$P = \frac{n \bar{R} T_{3013}}{V_{3013} + V_{PCV} \frac{T_{3013}}{T_{PCV}} + V_{SCV} \frac{T_{3013}}{T_{SCV}}} \quad (6)$$

Results

The steady state pressure inside of the 3013 container, the PCV, and the SCV with the gas spaces communicating through leaks in the 3013 container and the PCV is calculated with equation (6).

$$P = \frac{(1.6242)(8.314)(455.2)}{1.1978 \times 10^{-3} + 1.648 \times 10^{-3} \frac{455.2}{418.2} + 2.7779 \times 10^{-3} \frac{455.2}{412.6}} = 1014946.5 \text{ Pa}$$

$$P = 147.3 \text{ psia (132.6 psig)}$$

References

1. Hensel, S. J., "Determination of Pressures in the 9975 Package for Impure Pu Oxide Contents", M-CLC-F-00630, January 2000.
2. Gupta, N. K., "Thermal Analysis of the 9975 Package for Normal Conditions of Transport and Accident Conditions", M-CLC-00590, Rev. 3, January 2000.

APPENDIX 3.8

DEFLAGRATION CALCULATIONS FOR THE 9975 PACKAGE WITH INERTING

This Page is Intentionally Blank.

OSR 45-24# (Rev 1-10-2000)

Calculation Cover Sheet

10/21/03

Project 9975 Package Certification		Calculation Number M-CLC-A-00201	Project Number <i>MRS</i>
Title Deflagration Calculations for the 9975 Package with Inerting		Functional Classification SC	Sheet 1 of 45 <i>47</i>
Discipline Mechanical			
<input type="checkbox"/> Preliminary <input checked="" type="checkbox"/> Confirmed			
Computer Program No.		<input checked="" type="checkbox"/> N/A	Version/Release No.
Purpose and Objective Determine the deflagration pressures inside of the 9975 package containment vessels, with helium diluting of the 3013 container and the food pack cans and CO ₂ diluting of the PCV.			
Summary of Conclusion Deflagration pressures in the 9975 package have been determined when the gas spaces of the food pack cans or 3013 container are diluted to 5% oxygen with helium, and when the PCV gas space is diluted with 75% CO ₂ . Scenarios involving the 3013 container, food pack cans, and the PCV that either leak or are intact have been considered. The scenarios that involve just the gas spaces of the two inner containers, which are inerted, result in bounding pressures less than 100.0 psia. The two scenarios in which the PCV gas space mixes with that of the SCV, which is not inerted, result in bounding pressures of 165.6 and 207.1 psia for the 3013 and food pack can configurations respectively. In addition to the deflagration pressures, the internal energies of combustion have been calculated.			
Revisions			
Rev No.	Revision Description		
0	Original Issue		
Sign Off			
Rev No.	Originator (Print) Sign/Date	Verification/ Checking Method	Verfier/Checker (Print) Sign/Date
0	<i>M.A. Shadday 10/20/03</i> <i>MRS</i>	Document Review	<i>Bruce J. Harkins, 10/20/03</i> <i>Tom J. [unclear]</i>
			<i>C.P. HOLDING SMITH</i> <i>[Signature]</i>
Release to Outside Agency -- Design Authority (Print)		Signature	Date
Security Classification of the Calculation			

Deflagration Calculations for the 9975 Package with Inerting

Table of Contents

Introduction and Summary	3
Input	3
Analytical Methods and Computations	4
Results and Discussion	6
Conclusion	7
References	8
Nomenclature	8
Appendix	9

Introduction and Summary

Plutonium oxide in a 9975 shipping package can generate hydrogen by radiolysis of adsorbed water vapor. The gas spaces of the inner container, either a 3013 container or food pack cans, and the primary containment vessel (PCV) are inerted with helium and CO₂ respectively to preclude the possibility of detonable hydrogen/air mixtures, [1]. The criteria used to preclude detonations are based on detonation cell widths, and do not necessarily preclude flammable mixtures. The pressures that would be generated by deflagrations in the various gas spaces, for the several possible scenarios involving container integrity, have been calculated. The scenarios that involve just the two inner containers result in bounding pressures less than 100.0 psia because, due to inerting, there is very little available oxygen. The two scenarios in which the PCV leaks into the secondary containment vessel (SCV) result in bounding pressures of 165.6 psia for the 3013 configuration and 207.1 psia for the food can configuration, because the SCV is not inerted. In all cases the calculations were carried out at the upper flammability limit (UFL), which is bounding. In addition to the pressure, the available energies for heating container vessels and components are also calculated.

Input

The 9975 shipping package consists of nested containers. In the 3013 configuration, the containers from the inside out are: the 3013 container, the PCV, and the SCV. The food pack can configuration consists of two stacked cans, one on top of the other, inside of the PCV, which is inside of the SCV. The gas spaces of the 3013 container and the food pack cans are filled with sufficient helium to reduce the volume fraction of oxygen to 5%. The gas space of the PCV is filled with air mixed with 75% CO₂ by volume, and the gas space of the SCV is filled with air. These containers are assumed to have been sealed at atmospheric pressure and 70°F. “α” radiation can produce a further 2.3815×10^{-3} mols of helium, [2]. The plutonium oxide can have up to 25 g of adsorbed water vapor available for the production of hydrogen by radiolysis, [3]. The oxygen is assumed to not

be released as a gas. Complete dissociation of the water vapor will produce 1.3877 mols of H₂, more than enough to produce flammable mixtures in all three of the nested gas spaces.

Three scenarios with the 3013 configuration are considered, and two with the food pack can configuration. The first 3013 scenario is the integrity of the 3013 container is assumed to be intact and the hydrogen-air-helium mixture in the gas space burns. In the second scenario, the 3013 container leaks and the gas spaces of the 3013 and the PCV are considered as a single control volume with a hydrogen-air-helium-carbon dioxide mixture that burns. The third scenario has the PCV also leaking, so all three gas spaces are treated as a single control volume. The initial temperature of the gas spaces in the three 3013 scenarios is 308° F, [4]. The volumes of the three gas spaces are, [5]:

$$\begin{aligned}V_{3013} &= 0.0516 \text{ ft}^3 \\V_{PCV} &= 0.0582 \text{ ft}^3 \\V_{SCV} &= 0.0981 \text{ ft}^3\end{aligned}$$

No credit is taken for the integrity of the food cans, so the gas mixtures in the cans and the PCV mix freely. The second food pack can scenario has the PCV leaking and hydrogen mixture in the PCV mixing with the air in the SCV. The initial temperature in of the gas spaces in the food pack can scenarios is 313° F, [4]. The three gas space volumes are, [5]:

$$\begin{aligned}V_{fp\ cans} &= 0.05535 \text{ ft}^3 \\V_{PCV} &= 0.02295 \text{ ft}^3 \\V_{SCV} &= 0.0981 \text{ ft}^3\end{aligned}$$

The two stacked outer food pack cans are assumed to be cylinders, each with an outside diameter of 4.25 in. and a height of 7.0 in. Plastic bags enclose the plutonium oxide inside the food pack cans, and the cans are wrapped in aluminum foil. These facts are required to calculate the food can and PVC volumes. These calculations are included in the hand written notes that constitute the appendix.

Analytical Methods and Computations

The pressure resulting from a deflagration of a gaseous mixture in a closed vessel can be calculated with the ideal gas relation:

$$PV = n\bar{R}T \quad (1)$$

The temperature of the products of combustion is determined from the first law of thermodynamics. The combustion process is rapid and therefore reasonably approximated as adiabatic. For this case, the first law states that the internal energy of the products of combustion equals that of the reactants:

$$\sum_r n_i (\bar{h}_f^0 + \Delta\bar{h} - \bar{R}T)_i = \sum_p n_e (\bar{h}_f^0 + \Delta\bar{h} - \bar{R}T)_e \quad (2)$$

Equation (2) is expressed in terms of enthalpy because tabulated values of the ideal gas enthalpies for various gases [6], as functions of temperature, are more readily available than tables for internal energy. The enthalpies all have a common basis temperature of 25° C, at which the enthalpies of all elements are assumed to be zero. Since the enthalpies are functions of temperature, the solution of equation (2) is necessarily iterative. Subtracting the product of the universal gas constant and the temperature from the enthalpy converts the property to internal energy.

The gaseous mixtures in the five scenarios are well mixed. The composition of the reactants in each container gas space, minus hydrogen and helium due to “α” decay, is specified at the time of packing. The container gas spaces are then mixed in accordance with the scenario under consideration, and sufficient hydrogen is added to put the gaseous mixture at the upper flammability limit (UFL). While the highest combustion products temperature occurs with stoichiometric hydrogen, the added moles of hydrogen at the UFL more than compensate for the lower combustion temperature and result in a higher pressure. Complete combustion is assumed in all calculations. This assumption is conservative in that it results in the highest combustion products temperature, and is quite reasonable for the low flame temperatures of these inerted gaseous mixtures. Below 2000 K, dissociation of the products of combustion is negligible.

In addition to the temperature and pressure of the products of combustion, the internal energy of combustion is also calculated for each deflagration scenario. The internal energy of combustion is the difference in internal energies of the products of combustion at the completion of the reaction and the products cooled to the initial temperature of the reactants prior to the deflagration. This is the available energy for heating surrounding surfaces and internals within the vessel.

The H₂ volume fraction at UFL varies with both type and volume fraction of inert gas. The adiabatic flame temperature at UFL is 1200 K, [7], and this characteristic is used to determine the required H₂ for a specified air plus inert gasses mixture. The adiabatic flame temperature is defined for a steady-flow process, and the appropriate form of the first law is:

$$\sum_r n_i (\bar{h}_f^0 + \Delta\bar{h})_i = \sum_p n_e (\bar{h}_f^0 + \Delta\bar{h})_e \quad (3)$$

Figure 1 shows the UFL for hydrogen-air plus inert gas as a function of added volume fractions of N₂ or CO₂. CO₂ is a more effective inerting gas than N₂ because of its higher molecular weight. The O₂ volume fraction controls the reaction at the UFL. Figure 2 shows the O₂ volume fractions for the same hydrogen-air-inert gas mixtures as shown in Figure 1. For the N₂ cases the percent oxygen is constant at 5.5%, and with CO₂ the

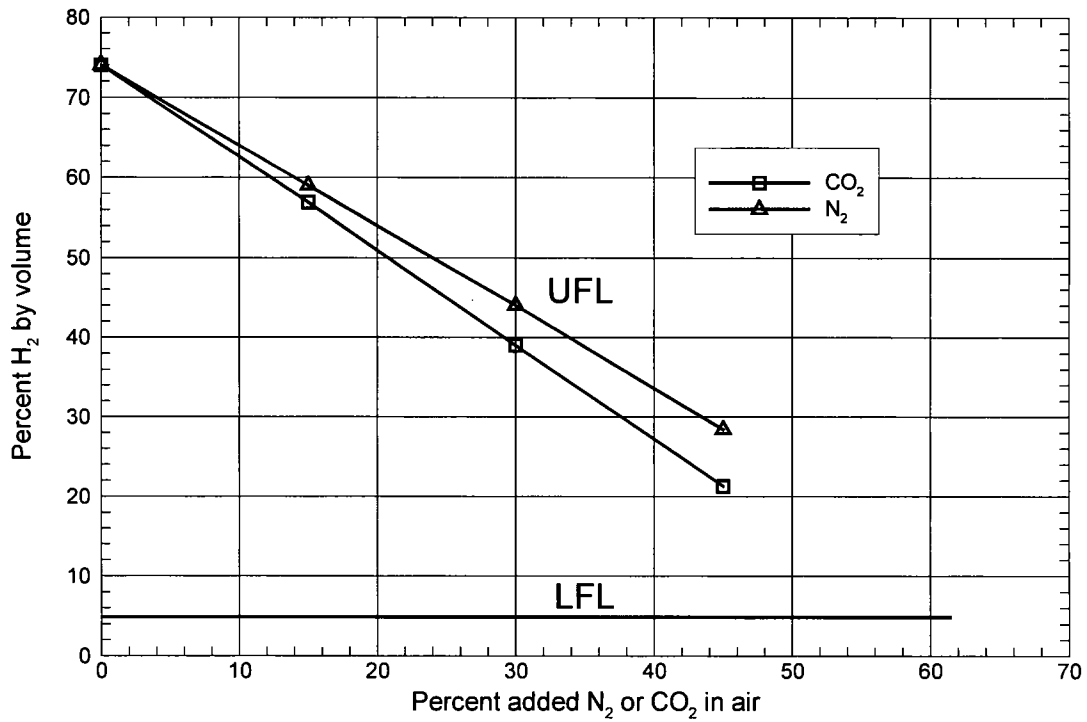


Fig. 1: Flammability limits of hydrogen in air diluted with nitrogen or carbon dioxide.

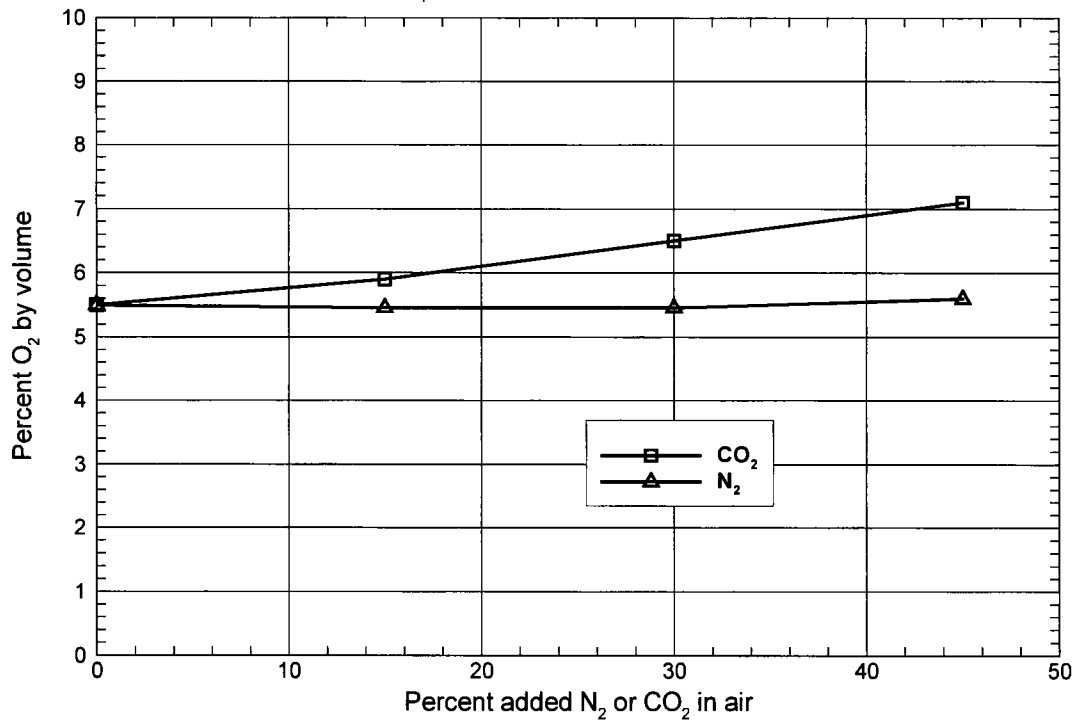
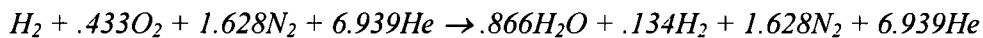


Fig. 2: Percent oxygen at UFL of hydrogen in air diluted with nitrogen or carbon dioxide.

percent oxygen increases with increasing percent CO₂. These results are consistent with the discussion in reference [7].

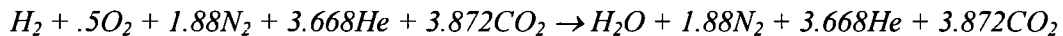
Results and Discussion

Hand written notes, showing all of the calculations that were done, are in the appendix. For scenario #1 of the 3013 configuration, the 3013 container only, the reaction for complete combustion at the UFL, per mole of H₂, is:



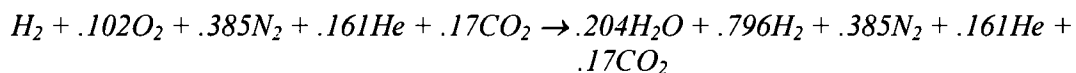
The mole fractions of the reactants are respectively: 10% H₂, 4.3% O₂, 16.3% N₂, and 69.4% He. The temperature and pressure of the products of combustion, and the internal energy of combustion are: 1743 K, 96.2 psia, and 1459.7 J.

For scenario #2 of the 3013 configuration, the 3013 container and the PCV combined, the reaction for complete combustion of stoichiometric H₂, is:



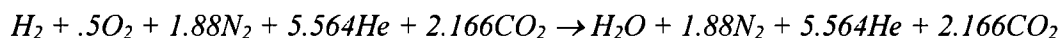
The mole fractions of the reactants are respectively: 9.2% H₂, 4.6% O₂, 17.2% N₂, 33.6% He, and 35.5% CO₂. This mixture has an adiabatic flame temperature of 981 K, and therefore is not flammable. There is, of course, some uncertainty in the flammability limits, and therefore combustion calculations were carried out. The temperature and pressure of the products of combustion, and the internal energy of combustion are: 1267 K, 67.7 psia, and 3190.9 J.

For scenario #3 of the 3013 configuration, the 3013 container the PCV and the SCV combined, the reaction for complete combustion at the UFL, per mole of H₂, is:



The mole fractions of the reactants are respectively: 55% H₂, 5.6% O₂, 21.2% N₂, 8.8% He, and 9.4% CO₂. The temperature and pressure of the products of combustion, and the internal energy of combustion are: 1566 K, 165.6 psia, and 14804 J.

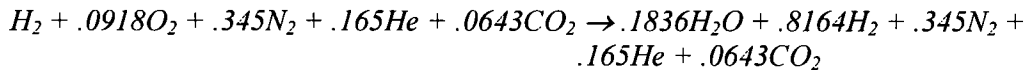
For scenario #1 of the food pack can configuration, the food pack cans and the PCV combined, the reaction for complete combustion of stoichiometric H₂, is:



The mole fractions of the reactants are respectively: 9% H₂, 4.5% O₂, 16.9% N₂, 50.1% He, and 19.5% CO₂. This mixture has an adiabatic flame temperature of 1065 K, and therefore is probably not flammable, but combustion calculations were carried out

anyway. The temperature and pressure of the products of combustion, and the internal energy of combustion are: 1428 K, 76.8 psia, and 2247 J.

For scenario #2 of the food pack can configuration, the food pack cans and the PCV and the SCV combined, the reaction for complete combustion at the UFL, per mole of H₂, is:



The mole fractions of the reactants are respectively: 60% H₂, 5.5% O₂, 20.7% N₂, 9.9% He, and 3.9% CO₂. The temperature and pressure of the products of combustion, and the internal energy of combustion are: 1640 K, 207.1 psia, and 14276.7 J.

Conclusions

As long as the gas tight integrity of the PCV is maintained, hydrogen generated by radiolysis of adsorbed water vapor in the plutonium oxide can result in gaseous mixtures that are at best only marginally flammable. Wall effects, which retard the propagation of a flame front, are completely ignored in this analysis. With narrow passages inside of the nested containers and the consequent large surface areas, it is unlikely that a deflagration could occur with a mixture that is within the flammability limits, such as scenario #1 with the 3013 configuration. Treating the gas spaces of nested containers that leak as a single volume is also conservative. Constrictions in passages tend to quench flame fronts, so a deflagration in the 3013 container would not necessarily propagate into the PCV.

The SCV gas space is not inerted, and this is the source of a considerable amount of oxygen when the inner containers leak. The two deflagration scenarios involving the SCV are considerably more energetic than the scenarios that take place within the PCV.

Higher molecular weight gasses are more effective inerting agents. The oxygen volume fraction at UFL for hydrogen-air with added nitrogen is approximately 5.5%. With carbon dioxide added to hydrogen-air, the oxygen volume fraction at UFL increases above 5.5% with increasing amounts of CO₂. The hydrogen-air-helium mixture in the 3013 container has 10% H₂ and 4.3% O₂ at UFL.

References

1. Shadday, M. A., "Detonation Cell Widths in the 9975 Package with CO₂ Diluting of the PCV Gas Space", M-CLC-A-00175, Rev. 1
2. Hensel, S. J., "Determination of Pressures in the 9975 Package", M-CLC-F-00491, Rev. 1.
3. DOE Standard, "Criteria for Preparing and Packaging Plutonium Metal and

Oxides for Long Term Storage”, DOE-STD-3013-2000.

4. Hardy, B. J., “Thermal Analysis of the 9975 Package for Normal Conditions of Transport and Accident Conditions”, M-CLC-F-00590, Rev. 0.
5. M-CLC-F-00630, Rev. 0.
6. Van Wylen, G. J., & Sonntag, R. E., “Fundamentals of Classical Thermodynamics”, 2nd Edition, John Wiley & Sons, New York, 1978.
7. Drell, I. L., & Belles, F. E., Survey of Hydrogen Combustion Properties”, NACA Report 1383.

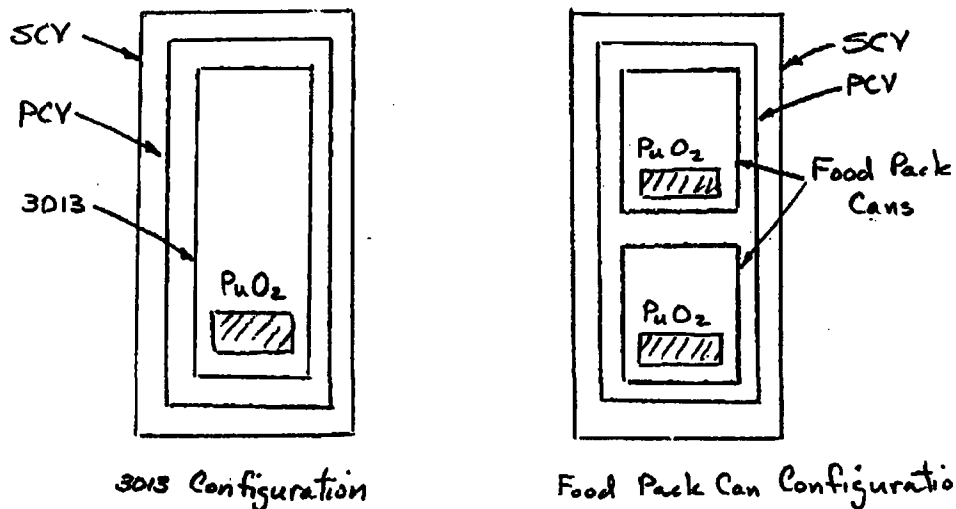
Nomenclature

\bar{h}_f^0	Enthalpy of formation, (J/mol)
$\Delta\bar{h}$	Ideal gas enthalpy difference (T-298 K), (J/mol)
n_i	Number of moles of the i th constituent
P	Pressure
\bar{R}	Universal gas constant
T	Temperature
V	Volume

Appendix: Calculation Notes

Flammability of 9975 Shipping Package Gas Spaces Inerted with Helium and Carbon Dioxide

Consider two configurations:



The 3013 container and the Food Pack cans are inerted to 5% O_2 with He.

The air in the PCY is mixed with 75% CO_2

The SCY initially contains air

The initial conditions are atmospheric pressure at 70°F.

The PuO_2 contains up to 25g of H_2O that can produce H_2 by radiolysis. The O_2 is not released as a gas. This H_2 is generated in the 3013 container or the Food Pack Cans.



$$M_{\text{H}_2\text{O}} = 18.015 \frac{\text{g}}{\text{mol}}$$

$$M_{\text{H}_2} = 2.016 \frac{\text{g}}{\text{mol}}$$

Each mole of H_2O radiolyzed releases one mole of H_2 :

$$\eta_{\text{H}_2\text{O}} = \frac{m}{M} = \frac{25\text{g}}{18.015 \frac{\text{g}}{\text{mol}}} = 1.388 \text{ mols of } \text{H}_2\text{O} = 1.388 \text{ mols } \text{H}_2$$

up to 1.388 mols of H_2 can be released.

Gas Space Volumes : (see the enclosed e-mail from Kurt Houghtaling)

$$V_{3013} = .0516 \text{ ft}^3 \quad .001461149 \text{ m}^3$$

$$V_{\text{PCV}} = .1098 \text{ ft}^3 - .0516 \text{ ft}^3 = .0582 \text{ ft}^3 \quad (.001648041 \text{ m}^3)$$

$$V_{\text{scv}} = .2079 \text{ ft}^3 - .0582 \text{ ft}^3 - .0516 \text{ ft}^3 = .0981 \text{ ft}^3 \quad (.002777883 \text{ m}^3)$$

These three gas space volumes are for the LLNL 3013 configuration which has the largest volumes and therefore can burn the most hydrogen.

Food Pack Can Configuration :

Each Food Pack Can has an outside diameter of 4.25" and a height of 7".

$$\text{Inner Volume PCV} = .1811 \text{ ft}^3 \quad V_{\text{gas space}} = .0783 \text{ ft}^3$$

$$V_{\text{steel in cans}} = \frac{900\text{g}}{7.83 \frac{\text{g}}{\text{cc}}} = 114.94 \text{ cm}^3 \times 3.5315 \times 10^{-5} \frac{\text{ft}^3}{\text{cc}} = .004059 \text{ ft}^3$$

$$V_{\text{foil}} = \frac{200\text{g}}{2.7 \frac{\text{g}}{\text{cc}}} \times 3.5315 \times 10^{-5} \frac{\text{ft}^3}{\text{cc}} = .0026159 \text{ ft}^3$$

Kurt Houghtaling

To: Martin Shadday/WSRC/Srs@Srs

cc: Nick Gupta/WSRC/Srs@Srs, Cynthia Holding-Smith/WSRC/Srs@Srs,
Paul Blanton/WSRC/Srs@Srs, Glenn Abramczyk/WSRC/Srs@Srs,
Steve Hense/WSRC/Srs@Srs

09/29/03 11:26 AM

Subject: Cleanup of Deflagration Calculations

Andy,

As promised, here are the input parameters for your revision (or new issue) of the Calc-Note supporting deflagration/detonation in the 9975 package.

Given in Blue typeface are free volumes and tablenotes copied from M-CLC-F-00630, Rev. 0 (9975 SARP Appendix 3.6).

Table 3: Volumes of Components and Net Free Volume In 3013, PCV, & SCV (ft.3)

Components (#)	Food Cans	BNFL 3013	LANL 3013	LLNL 3013
Gross 3013 (1)	-----	0.0919 [1, p. 55]	0.0919 [1, p. 55]	0.0919 [1, p. 55]
Contents (2)	0.0516	0.0355	0.0353	0.0314
Cans/bags/foil (3)	0.0106 (see note)	0.0141 (see note)	0.0089 (see note)	0.0089 (see note)
Net 3013 (1-2-3)	-----	0.0423	0.0477	0.0516
3013 vessel (4)	-----	0.0178 [1, p. 55]	0.0178 [1, p. 55]	0.0178 [1, p. 55]
PCV sleeve or spacer (5)	0.039 [5, see calculation below]	0.0116 [5, see calculation below]	0.0116 [5, see calculation below]	0.0116 [5, see calculation below]
PCV honeycomb (6)	0.0016 [2, p. 3-53]	0.0016 [2, p. 3-53]	0.0016 [2, p. 3-53]	0.0016 [2, p. 3-53]
Gross PCV (7)	0.1811 [2, p. 3-53]	0.1811 [2, p. 3-53]	0.1811 [2, p. 3-53]	0.1811 [2, p. 3-53]
Net PCV (7-6-5-4-3-2)	0.0783	0.1005	0.1059	0.1098
Between PCV & SCV (8)	0.1020 [2, p. 3-53]	0.1020 [2, p. 3-53]	0.1020 [2, p. 3-53]	0.1020 [2, p. 3-53]
SCV honeycomb (9)	0.0039 [2, p. 3-53]	0.0039 [2, p. 3-53]	0.0039 [2, p. 3-53]	0.0039 [2, p. 3-53]
Net SCV (8+7-9-6-5-4-3-2)	0.1764	0.1986	0.2040	0.2079

Note: the Pu oxide in food can configuration allows up to 900 grams of steel cans (7.83 g/cc), 100 grams of low density polyethylene (0.92 g/cc) or nylon bagging (1.14 g/cc), and 200 grams of aluminum foil (2.7 g/cc); volumes occupied by inner containers for 3013 configurations are based on data in DOE-STD-3013-99, the ARIES inner can (1600 gram mass assumed, same as BNFL inner 3013 container), and a convenience can mass of 400

grams for both LLNL and LANL configurations was assumed (all 3013 configurations are free of polyethylene or nylon bagging, and crushed aluminum foil).

Notice that the table above provides three set of 3013-related volumes. Which 3013 free volume is the worst case must be determined by you before running the series of six analysis cases given below. Is it the smallest volume to receive deflagration pressure or largest volume to maximize deflagration fuel?

Gas temperature used in your old Calc-Note revision M-CLC-F-00499, Rev. 3 (SARP Appendix 3.8) is unchanged. However the gas compositions have. Gas mixtures to be evaluated are the following.

SCV = Normal air

PCV = Normal air diluted by 75% CO₂

Can = Normal air diluted to 5% O₂ by helium (Can is either a 3013 can or a Food-pack can)

Hydrogen presence is limited by full dissociation of the 25g of water present inside the Can (be it 3013 or FPC).

Cases to be analyzed are the following.

- 1 Burn inside 3013
- 2 3013 leaks freely into PCV and gas mixture burns.
- 3 3013 and PCV leak freely into SCV and gas mixture burns.

- 4 Burn inside Food-pack can (FPC)
- 5 FPC leaks freely into PCV and gas mixture burns.
- 6 FPC and PCV leak freely into SCV and gas mixture burns.

Please charge Activity Code LSLDHBLNP

Thank you for your service.

-

Kurt Houghtaling 803/725-3360

kurt.houghtaling@srs.gov

$$V_{\text{bags}} = .0106 - .0026159 - .004059 = .0039251 \text{ ft}^3$$

$$V_{\text{contents}} = .0516 \text{ ft}^3$$

$$V_{\text{can}} = \frac{\pi D^2}{4} H = .057967 \text{ ft}^3 \quad 2(V_{\text{can}}) = .114934 \text{ ft}^3$$

V_{inner} - gas space volume inside of cans

V_{outer} - gas space volume outside cans and inside PCV

note: the plastic bags are inside of the cans and the foil is outside of the cans

$$V_{\text{outer}} = .1811 - .0016 - .039 - .0026159 - .114934 = .0229501 \text{ ft}^3$$

$$V_{\text{inner}} = .114934 - .0516 - .0039251 - .004059 = .0553499 \text{ ft}^3$$

$$V_{\text{outer}} + V_{\text{inner}} = .0783 \text{ ft}^3 \quad (.002217201 \text{ m}^3)$$

$$V_{\text{scv}} = .0981 \text{ ft}^3 \quad (\text{same as 2013 configuration})$$

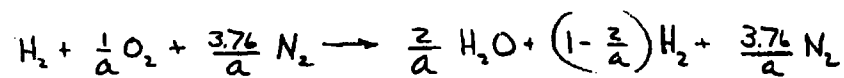
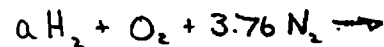
Upper Flammability Limit

Deflagration calculations will be made at the upper flammability limit for gaseous mixtures with multiple inert gasses.

Drell & Belles Report 1383 shows a plot of the flammability limits hydrogen-air with added N_2 or CO_2 . The plot cannot be used quantitatively, the plots for UFL are inconsistent with the associated text description. UFL occurs with an adiabatic flame temperature of 1200k

and this observation will be used as the defining characteristic in calculating UFL.

Determine the volume percent H_2 for air such that $T_p = 1200 \text{ K}$:



note The adiabatic flame temperature is defined for a steady-flow process.

$$H_R = H_P$$

$$\sum_R \gamma_i (\bar{h}_f^0 + \Delta \bar{h})_i = \sum_P \gamma_e (\bar{h}_f^0 + \Delta \bar{h})_e$$

Assume an initial temperature of 25°C $\therefore H_R = 0$

$$\frac{2}{a} (\bar{h}_f^0 + \Delta \bar{h})_{H_2O} + \frac{a-2}{a} \Delta \bar{h}_{H_2} + \frac{3.76}{a} \Delta \bar{h}_{N_2} = 0$$

$$a \Delta \bar{h}_{H_2} = 2 (\Delta \bar{h}_{H_2} - \Delta \bar{h}_{H_2O} - \bar{h}_f^0_{H_2O}) - 3.76 \Delta \bar{h}_{N_2}$$

$$a = \frac{2 (\Delta \bar{h}_{H_2} - \Delta \bar{h}_{H_2O} - \bar{h}_f^0_{H_2O}) - 3.76 \Delta \bar{h}_{N_2}}{\Delta \bar{h}_{H_2}}$$

$$\text{@ } 1200 \text{ K} \quad \bar{h}_f^0(H_2O) = -241827 \text{ J/mol}$$

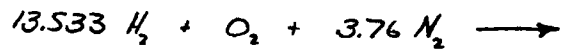
$$\Delta \bar{h}_{N_2} = 28108$$

$$\Delta \bar{h}_{H_2O} = 34476$$

$$\Delta \bar{h}_{H_2} = 26794$$

} J/mol

$$a = \frac{2(26794 + 241827 - 34476) - 3.76(28108)}{26794} = 13.533 \frac{\text{mols } H_2}{\text{mol } O_2}$$



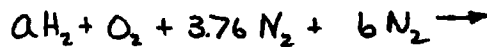
$$\eta_{\text{total}} = 13.533 + 4.76 = 18.293 \frac{\text{mols}}{\text{mol } O_2}$$

$$\frac{\eta_{H_2}}{\eta} = \frac{13.533}{18.293} = .73979 \quad (74\% H_2 \text{ by volume})$$

$$\frac{\eta_{O_2}}{\eta} = \frac{1}{18.293} = .05467 \quad (5.5\% O_2 \text{ by volume})$$

(These results agree with Report 1383)

Look at 15% excess N_2 : (What is $\frac{\eta_{H_2}}{\eta}$ such that $T_p = 1200k$?)



$$x = \frac{\eta_{H_2}}{\eta} = \frac{a}{4.76 + a + b} \quad y = \frac{\eta_{N_2 \text{ excess}}}{\eta} = \frac{b}{4.76 + a + b}$$

$$a = (4.76 + a + b)x \quad b = (4.76 + a + b)y$$

$$a(1-x) = (4.76 + b)x \quad ay = b - 4.76y - by$$

$$a = \frac{x}{1-x} (4.76 + b) \quad a = \frac{b(1-y) - 4.76y}{y}$$

$$\frac{x}{1-x} (4.76 + b) = \frac{b(1-y) - 4.76y}{y}$$

$$\frac{xy(4.76+b)}{y(1-x)} = \frac{[b(1-y) - 4.76y](1-x)}{y(1-x)}$$

equate numerators

$$xy(4.76+b) = [b(1-y) - 4.76y](1-x)$$

$$xyb - (1-x)(1-y)b = -4.76y(1-x) - 4.76xy$$

$$xyb - (1-x-y+xy)b = -4.76y + 4.76xy - 4.76xy$$

$$(x+y-1)b = -4.76y$$

$$b = \frac{4.76y}{1-x-y} \quad a = \frac{x}{1-x}(4.76+b)$$

given "y" and with an assumed value of "x" the coefficients of H_2 and excess N_2 in the reactants can be calculated

$$y = .15 \quad \text{guess } x = .65$$

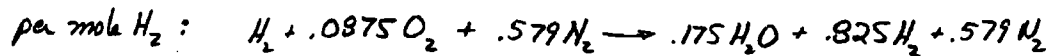
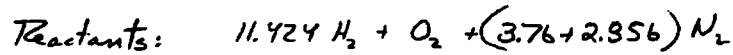
$$b = \frac{4.76(.15)}{1-.15-.65} = 3.57 \quad a = \frac{.65}{1-.65}(4.76+3.57) = 15.47$$

$$\frac{\%_{O_2}}{\%} = \frac{1}{3.57+15.57+4.76} = .042 \quad (\text{too low should be } \sim 5.5\%)$$

$$\text{guess } x = .6$$

$$b = \frac{4.76(.15)}{1-.15-.6} = 2.856 \quad a = \frac{.6}{1-.6}(4.76+2.856) = 11.424$$

$$\frac{n_{H_2}}{n} = \frac{1}{2.856 + 11.424 + 4.76} = .053 \quad \text{close}$$



$$\text{Try } T_p = 1200 \text{ K:}$$

$$.175(34476) + .825(26794) + .579(28108) - .175(241827) = 2093.2$$

$$\text{Try } T_p = 1100 \text{ K:}$$

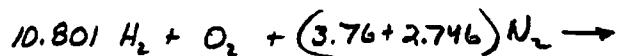
$$.175(30167) + .825(23723) + .579(24757) - 42319.7 = -3134.7$$

$$100 \left[\begin{array}{cc|c} 1100 & -3134.7 & 3134.7 \\ T_p & 0 & \\ \hline 1200 & 2093.2 & \end{array} \right] 5227.9 \quad \begin{array}{l} \alpha = 59.96 \\ T_p = 1160 \text{ K} \end{array}$$

$$\text{guess } \chi = .59$$

$$b = \frac{4.76(.15)}{1 - .15 - .59} = 2.746 \quad a = \frac{.59}{1 - .59} (4.76 + 2.746) = 10.801$$

$$\frac{n_{O_2}}{n} = \frac{1}{4.76 + 2.746 + 10.801} = .0546$$



$$\text{Try } T_p = 1200 \text{ K:}$$

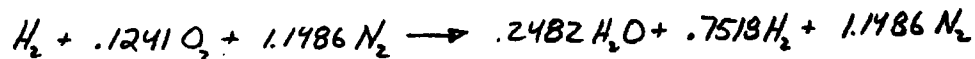
$$.1852(34476) + .8148(26794) + .6024(28108) - .1852(241827) = 362.6$$

(this is pretty close)

$$30\% \text{ excess } N_2: \quad y = .3 \text{ guess } x = .44$$

$$b = \frac{4.76(.3)}{1 - .3 - .44} = 5.492 \quad a = \frac{.44}{1 - .44} (4.76 + 5.492) = 8.055$$

$$\frac{n_{O_2}}{n} = \frac{1}{4.76 + 5.492 + 8.055} = .0546$$



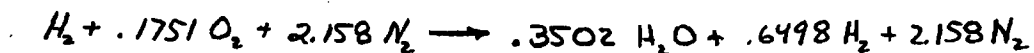
$$.2482(34476) + .7518(26794) + 1.1486(28108) - .2482(241827) = 964$$

$$T_p \sim 1175 \text{ K (close enough)}$$

$$45\% \text{ excess } N_2: \quad y = .45 \text{ guess } x = .3$$

$$b = \frac{4.76(.45)}{1 - .45 - .3} = 8.568 \quad a = \frac{.3}{1 - .3} (4.76 + 8.568) = 5.712$$

$$\frac{n_{O_2}}{n} = \frac{1}{4.76 + 8.568 + 5.712} = .053$$



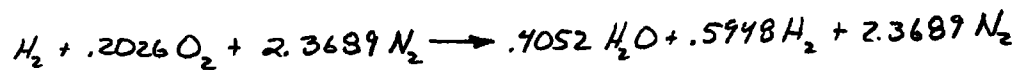
@ $T_p = 1200\text{K}$:

$$.3502(34476) + .6498(26794) + 2.158(28108) - .3502(241827) = 5453$$

guess $x = .28$

$$b = \frac{4.76(.45)}{1-.45-.28} = 7.933 \quad a = \frac{.28(4.76 + 7.933)}{1-.28} = 4.936$$

$$\frac{\eta_{O_2}}{\eta} = \frac{1}{4.76 + 7.933 + 4.936} = .057$$



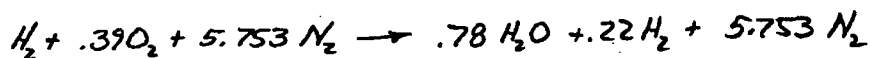
$$.4052(34476) + .5948(26794) + 2.3689(28108) - .4052(241827) = -1497$$

$$.02 \begin{bmatrix} x & \begin{bmatrix} .28 & -1497 \\ & 0 \end{bmatrix} & 1497 \\ & .30 & 5453 \end{bmatrix} \begin{matrix} 6950 \\ \\ \end{matrix} \quad \begin{matrix} x = .0043 \\ x = .284 \end{matrix} \quad \frac{\eta_{O_2}}{\eta} = 5.59\%$$

60% excess N_2 : $y = .6$ guess $x = .14$

$$b = \frac{4.76(.6)}{1-.6-.14} = 10.985 \quad a = \frac{.14(4.76 + 10.985)}{1-.14} = 2.563$$

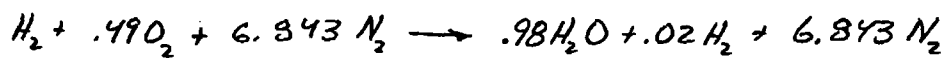
$$\frac{\eta_{O_2}}{\eta} = \frac{1}{4.76 + 10.985 + 2.563} = .0546$$



$$.78(34476) + .22(26794) + 5.753(28108) - .78(241827) = 5866.2$$

(too much excess H_2)

$$\left. \begin{array}{l} y = .6 \\ x = .12 \end{array} \right\} \quad a = 2.04 \quad b = 10.2 \quad \frac{\eta_{O_2}}{\eta} = \frac{1}{4.76 + 10.2 + 2.04} = .059$$



$$.98(34476) + .02(26794) + 6.843(28108) - .98(241827) = -10325$$

$$.02 \begin{bmatrix} .12 & -10325 \\ .14 & 5866.2 \end{bmatrix} \begin{bmatrix} 10325 \\ 1491.2 \end{bmatrix} \quad x = .133$$

$$b = 10.697 \quad a = 2.371$$

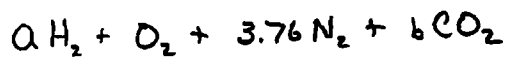


$$.844(34476) + .156(26794) + 6.097(28108) - .844(241827) = 550$$

(close)

$$\frac{\eta_{O_2}}{\eta} = .056$$

look at CO_2 as the inerting gas



$$x = \frac{a}{a+b+4.76} \quad y = \frac{b}{a+b+4.76}$$

a & b are defined in exactly the same fashion

$$y = .15 \quad \text{guess} \quad x = .62$$

$$b = 3.104 \quad \frac{\eta_{O_2}}{\eta} = \frac{1}{4.76 + 12.831 + 3.104} = 4.93 \quad (\text{too low})$$

$$a = 12.831$$

$$y = .15 \quad \text{guess} \quad x = .55$$

$$b = 2.39 \quad \frac{\eta_{O_2}}{\eta} = \frac{1}{4.76 + 8.727 + 2.39} = .063$$

$$a = 8.727$$



$$\bar{h}_f^\circ(CO_2) = -393522 \text{ J/mol} \quad (\text{heat of formation } CO_2 \text{ cancels})$$

$$@1200K \quad \bar{\Delta}h_{CO_2} = 44484 \text{ J/mol}$$

$$.23 \bar{\Delta}h_{H_2O} + .77 \bar{\Delta}h_{H_2} + .431 \bar{\Delta}h_{N_2} + .273 \bar{\Delta}h_{CO_2} + .23 \bar{h}_f^\circ_{H_2O} = 0$$

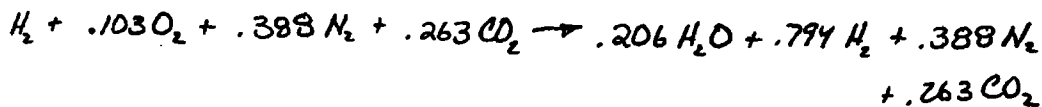
$$.23(34476) + .77(26794) + .431(28108) + .273(44484) - .23(241827) = -14915$$

($T_p > 1200K$ need more H_2)

$$y = .15 \quad \text{guess} \quad x = .57$$

$$b = 2.55 \quad \frac{\eta_{O_2}}{\eta} = .059$$

$$a = 9.69$$



$$.206(34476) + .794(26794) + .388(28108) + .263(44484) - .206(241827) = 1165$$

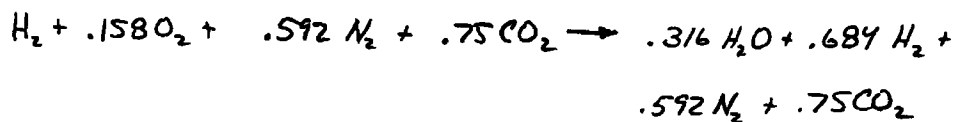
$$.02 \begin{bmatrix} \kappa \begin{bmatrix} .55 & -14915 \\ 0 & 14915 \end{bmatrix} \\ .57 & 1165 \end{bmatrix} 16080 \quad \kappa = .0186$$

$$\chi = .569 \sim .57$$

$$y = .3 \quad \text{guess } \chi = .4$$

$$b = 4.76 \quad \frac{\eta_{O_2}}{\eta} = .063$$

$$a = 6.347$$



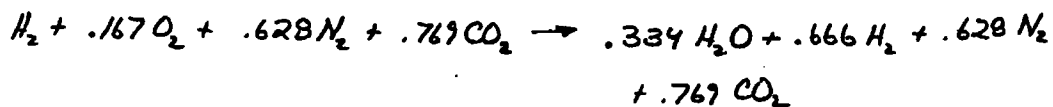
$$-207351$$

$$.316 (34476 - 241827) + .684 (26794) + .592 (28108) + .75 (44484) = 2807$$

$$\text{guess } \chi = .39$$

$$b = 4.606 \quad \frac{\eta_{O_2}}{\eta} = .065$$

$$a = 5.988$$



$$-.334 (207351) + .666 (26794) + .628 (28108) + .769 (44484) = 449.6$$

(close enough)

$$y = .45 \quad \text{guess } \chi = .22$$

$$b = 6.12 \quad \frac{\eta_{O_2}}{\eta} = .074$$

$$a = 2.72$$

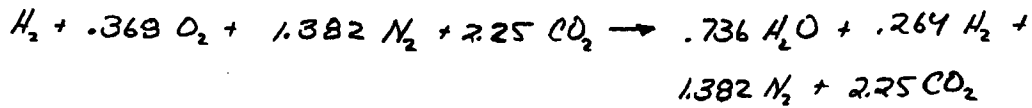


$$-.63(207351) + .37(26794) + 1.185(28108) + 2.046(44484) = 3605$$

$$y = .45 \quad \text{guess } x = .2$$

$$b = 6.12 \quad \frac{\% O_2}{\eta} = .074$$

$$a = 2.72$$



$$-.736(207351) + .264(26794) + 1.382(28108) + 2.25(44484) = -6602$$

$$.02 \begin{bmatrix} x & \begin{bmatrix} .2 & -6602 \\ 0 & 6602 \end{bmatrix} \\ .22 & 3605 \end{bmatrix} \begin{matrix} 10207 \\ 10207 \end{matrix} \quad \begin{matrix} K = .013 \\ x = .213 \sim .21 \end{matrix}$$

$$y = .45 \quad x = .21$$

$$b = 6.3 \quad \frac{\% O_2}{\eta} = .071$$

$$a = 2.94$$

% Excess Inert gas	% H ₂ (N ₂ Case)	% O ₂ (N ₂ Case)	% H ₂ (CO ₂ Case)	% O ₂ (CO ₂ Case)
0	74	5.5	74	5.5
15	59	5.46	57	5.9
30	44	5.46	39	6.3
45	28.4	5.59	21	7.1
60	13.3	5.6	—	—

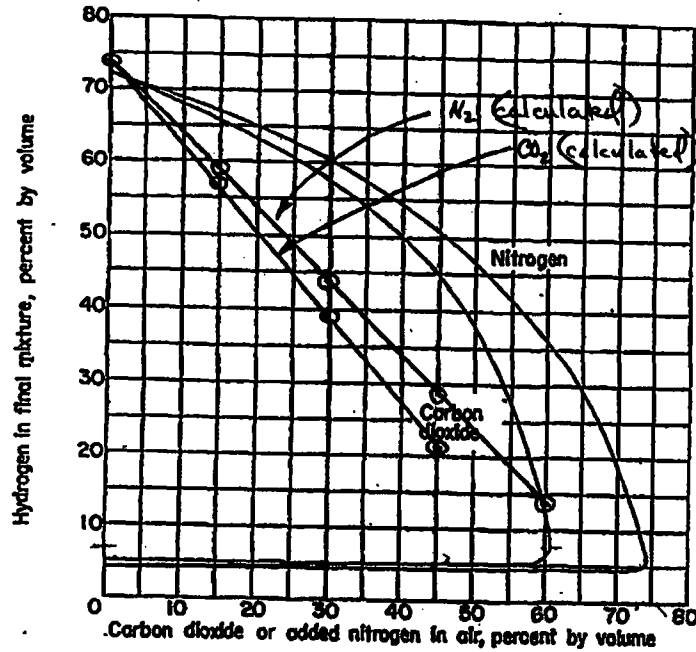


FIGURE 15.—Flammability limits of hydrogen in air diluted with nitrogen or carbon dioxide (ref. 48).

This is the figure in Drull & Belles Report 1383 of the H_2 -air-inertgas flammability limits. Also shown are the upper flammability limits calculated from an adiabatic flame temperature of 1200K. The calculated limits are not in agreement with the plot. The calculated % O_2 values (5.5% for N_2 & 5.5 to 7.1% for CO_2) agree with the writeup in the report and are inconsistent with figure 15 in the report. An adiabatic flame temperature of 1200K defining UFL is valid.

Deflagrations in a 9975 package (3013 configuration):

$$V_{3013} = .0516 \text{ ft}^3 (.001461149 \text{ m}^3)$$

$$n = \frac{PV}{RT}$$

$$P = 101300 \text{ Pa}$$

$$T = 294.3 \text{ K (70°F)}$$

$$\bar{R} = 8.314 \frac{\text{J}}{\text{mol K}}$$

$$n = \frac{101300 (.001461149)}{8.314 (294.3)} = .0604928 \text{ mols}$$

This mixture is 5% O_2 (air inerted with He)

$$O_2 + 3.76 N_2 + x He \quad \frac{1}{4.76 + x} = .05$$

$$x = \frac{1 - .05(4.76)}{.05} = 15.24$$

$$\frac{n_{O_2}}{n} = .05 \quad \therefore n_{O_2} = .05 (.0604928) = .00302464 \text{ mols } O_2$$

$$n_{N_2} = 3.76 (.00302464) = .011372646 \text{ mols } N_2$$

$$n_{He} = 15.24 (.00302464) = .0460955 \text{ mols He}$$

" α " radiation can produce 5.25×10^{-6} lb-mols He

$$5.25 \times 10^{-6} \text{ lb-mols} \left(\frac{4.003 \text{ lb}_3}{\text{lb-mol}} \right) = 2.1016 \times 10^{-5} \text{ lb}_3 = 9.533 \times 10^{-6} \text{ kg}$$

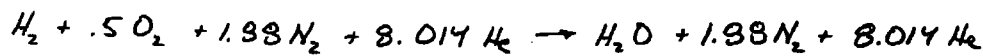
$$= 9.533 \times 10^{-3} \text{ g}$$

$$n_{He} = \frac{9.533 \times 10^{-3} \text{ g He}}{4.003 \text{ g/mol}} = 2.38146 \times 10^{-3} \text{ mols} \quad \left(\text{This is additional Helium} \right)$$

$$\therefore \left. \begin{array}{l} n_{O_2} = .00302464 \text{ mols} \\ n_{N_2} = .011372646 \text{ mols} \\ n_{He} = .04847696 \text{ mols} \end{array} \right\} \left(\begin{array}{l} \text{gas in 3013} \\ \text{minus } H_2 \end{array} \right)$$

Determine the adiabatic flame temperature for stoichiometric H_2 :

$$n_{H_2} = 2(.00302464) = .00604928 \text{ mols}$$



$$\left(\bar{h}_f^\circ + \Delta \bar{h} \right)_{H_2O} + 1.88 \bar{\Delta h}_{N_2} + 8.014 \bar{\Delta h}_{He} = 0$$

$\bar{\Delta h}_{He}$ is not tabulated but monoatomic hydrogen should be very close see fig. B5 of the "KABOOM" document (WSRC-TR-2000-00492)

Assume $T_p = 1200 \text{ K}$:

$$(34476 - 241827) + 1.88(28109) + 8.014(18749) = -4253$$

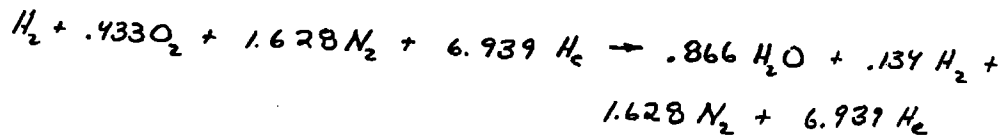
$T_p > 1200 \text{ K} \therefore$ the mixture is deflagrable

$$\begin{aligned} n_{total} &= n_{H_2} + .00302464 + .011372646 + .04847696 \\ &= n_{H_2} + .062874 \end{aligned}$$

$$\frac{n_{H_2}}{n_T} = \frac{.00604928}{.00604928 + .062874} = .088$$

Determine UFL: guess $\frac{n_{H_2}}{n_T} = .1 = \frac{n_{H_2}}{n_{H_2} + .062874}$

$$.9 n_{H_2} = .0062874 \quad n_{H_2} = .006986$$

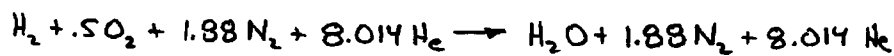


$$-.866(207351) + .134(26794) + 1.628(28103) + 6.939(18799) = -116.4 \quad (\text{close})$$

calculate the deflagration pressure for stoichiometric H_2 and at UFL :

$$T_{\text{initial}} = 308^\circ\text{F} = 153.3^\circ\text{C} = 426.48\text{K}$$

Stoichiometric H_2 :



$$\sum_R \eta_i (\bar{h}_f^\circ + \Delta\bar{h} - \bar{R}T_R)_i = \sum_P \eta_e (\bar{h}_f^\circ + \Delta\bar{h} - \bar{R}T_P)$$

$$T_R = 426.5\text{K} : \quad \Delta\bar{h}_{\text{N}_2} = 3750 \text{ J/mol} \quad \Delta\bar{h}_{\text{O}_2} = 3840 \text{ J/mol}$$

$$\Delta\bar{h}_{\text{H}_2} = 3733 \text{ J/mol} \quad \Delta\bar{h}_{\text{H}_2\text{O}} = 2668 \text{ J/mol}$$

$$\eta_R = 1.5 + 1.88 + 8.014 = 11.394 \text{ mols/mol H}_2$$

$$\eta_P = 2.98 + 8.014 = 10.994 \text{ mols/mol H}_2$$

$$U_R = 3733 + .5(3840) + 1.88(3750) + 8.014(2668) - 11.394(8.314)426.5 = -6317.9 \text{ J/mol H}_2$$

$$\begin{aligned} \text{Assume } T_p = 1800 \text{ K :} \quad \Delta \bar{h}_{\text{H}_2\text{O}} &= 62609 \text{ J/mol} \\ \Delta \bar{h}_{\text{N}_2} &= 48982 \text{ J/mol} \\ \Delta \bar{h}_{\text{He}} &= 31217 \text{ J/mol} \end{aligned}$$

$$\begin{aligned} (62609 - 241827) + 1.88(48982) + 8.014(31217) - 10.894(8.314)/1800 \\ + 6317.9 = 6328 \\ \text{(too hot)} \end{aligned}$$

$$\begin{aligned} \text{Assume } T_p = 1700 \text{ K :} \quad \left. \begin{aligned} \Delta \bar{h}_{\text{H}_2\text{O}} &= 57685 \\ \Delta \bar{h}_{\text{N}_2} &= 45430 \\ \Delta \bar{h}_{\text{He}} &= 29142 \end{aligned} \right\} \text{ J/mol} \end{aligned}$$

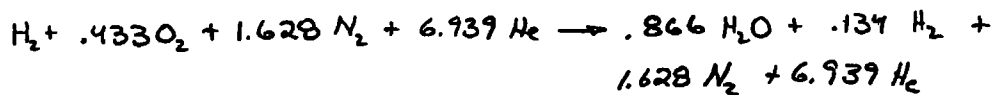
$$57685 - 241827 + 6317.9 + 1.88(45430) + 8.014(29142) - 90.5727(1700) = -12845$$

$$100 \left[\begin{array}{cc|c} 1700 & -12845 & 12845 \\ \hline 2 & 0 & 19173 \\ 1800 & 6328 & \end{array} \right] \quad \begin{aligned} \alpha &= 67 \\ T_p &= 1767 \text{ K} \end{aligned}$$

$$P = \frac{n \bar{R} T}{V} \quad \gamma_p = 10.894 \frac{\text{mols}}{\text{mol H}_2} (.00604928) = .065900856 \text{ mols}$$

$$P = \frac{.065900856 (8.314) 1767}{.001461149} = 662587 \text{ Pa} \\ \text{(96.2 psia)}$$

H₂ @ UFL :



$$\eta_R = 1 + .433 + 1.628 + 6.939 = 10 \frac{\text{mols}}{\text{mol H}_2}$$

$$\eta_p = .866 + .134 + 1.628 + 6.939 = 9.567 \frac{\text{mols}}{\text{mols H}_2}$$

$$U_R = 3733 + .433(3840) + 1.628(3750) + 6.939(2668) \\ - 10(8.314)(426.5) = -5445 \frac{\text{J}}{\text{mol H}_2}$$

Assume $T_p = 1700\text{K}$:

$$.866(57685 - 241827) + .134(42815) + 1.628(45430) + 6.939(29142) \\ - 9.567(8.314)(1700) + 5445 = -7326$$

Assume $T_p = 1800\text{K}$:

$$.866(62609 - 241827) + .134(46150) + 1.628(48982) + 6.939(31217) \\ - 9.567(8.314)(1800) + 5445 = 9612$$

$$100 \left[\begin{array}{cc|c} 1700 & -7326 & 7326 \\ \hline 1800 & 9612 & \end{array} \right] 16938 \quad \begin{array}{l} \alpha = 43.25 \\ \underline{T_p = 1743\text{K}} \end{array}$$

$$\eta_p = 9.567 \frac{\text{mols}}{\text{mols H}_2} (.006986) = .066835 \text{ mols}$$

$$P = \frac{.066835(8.314)1743}{.001461149} = 662852 \text{ Pa} \\ (96.2 \text{ psia}) \\ \text{essentially the same} \\ (\text{slightly higher})$$

The internal energy of combustion is the difference in internal energies for the products at the combustion temperature and the initial temperature &

Products: $.866 \text{ H}_2\text{O} + .134 \text{ H}_2 + 1.628 \text{ N}_2 + 6.939 \text{ He}$

$$\Delta U = U_{1743\text{K}} - U_{426.5\text{K}}$$

$$\text{@ } 426.5\text{K} \quad \Delta \bar{h}_{\text{H}_2\text{O}} = 4371 \quad \text{@ } 1743\text{K} \quad \Delta \bar{h}_{\text{H}_2\text{O}} = 59802$$

$$\Delta \bar{h}_{\text{H}_2} = 3733 \quad \Delta \bar{h}_{\text{H}_2} = 44249$$

$$\Delta \bar{h}_{\text{N}_2} = 3750 \quad \Delta \bar{h}_{\text{N}_2} = 46957$$

$$\Delta \bar{h}_{\text{He}} = 2668 \quad \Delta \bar{h}_{\text{He}} = 30034$$

$$\begin{aligned} \Delta U = & .866(59802 - 4371) + .134(44249 - 3733) + 1.628(46957 - 3750) \\ & + 6.939(30034 - 2668) - 9.567(8.314)(1743 - 426.5) = \\ & 208951.6 \frac{\text{J}}{\text{mole H}_2} \end{aligned}$$

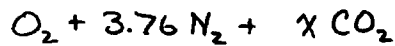
$$\Delta U_{\text{total}} = 208951.6 (.006986) = 1459.7 \text{ J}$$

Scenario #2 Allow the 3013 gas to mix freely with the PVC gas

$$V_{\text{PVC}} = .001648041 \text{ m}^3$$

$$n_{\text{PVC}} = \frac{101300 (.001648041)}{8.314 (294.3)} = .06823027 \text{ mols}$$

This gas mixture consists of 75% CO_2 and air:



$$\frac{x}{4.76 + x} = .75 \quad x = \frac{.75(4.76)}{.25} = 14.28 \frac{\text{mols CO}_2}{\text{mol O}_2}$$

$$n_{\text{CO}_2} = .75(.06823027) = .051172703 \text{ mols CO}_2$$

$$n_{\text{O}_2} = \frac{.051172703 \text{ mols CO}_2}{14.28 \frac{\text{mols CO}_2}{\text{mol O}_2}} = .003583523 \text{ mols O}_2$$

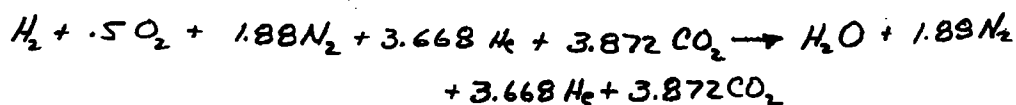
$$n_{\text{N}_2} = 3.76(.003583523) = .013474045 \text{ mols N}_2$$

Combine the 3013 ft³ PVC gas spaces: ($V = .00310919 \text{ m}^3$)

$$\left\{ \begin{array}{l} n_{\text{O}_2} = .00302464 + .003583523 = .006608163 \text{ mols} \\ n_{\text{N}_2} = .00372646 + .013474045 = .024846691 \text{ mols} \\ n_{\text{He}} = .04847696 \text{ mols} \\ n_{\text{CO}_2} = .051172703 \text{ mols} \end{array} \right.$$

Determine the adiabatic flame temperature for stoichiometric hydrogen:

$$n_{\text{H}_2} = 2(.006608163) = .013216326 \text{ mols}$$



Assume $T_p = 1200\text{ K}$:

$$(34476 - 241827) + 1.88(28108) + 3.668(18749) + 3.872(44484) \\ = 86505.4$$

$T_p < 1200\text{ K}$ { this should not be a
flammable mixture

Assume $T_p = 1000\text{ K}$:

$$(25978 - 241827) + 1.88(21460) + 3.668(14590) + 3.872(33405) \\ = 7356$$

Assume $T_p = 900\text{ K}$:

$$(21924 - 241827) + 1.88(18221) + 3.668(12510) + 3.872(28041) \\ = -31186$$

$$100 \left[\begin{array}{cc} 900 & -31186 \\ 1000 & 7356 \end{array} \right] \begin{array}{l} 31186 \\ 38572 \end{array} \quad \begin{array}{l} \alpha = 80.9 \\ T_p = 981\text{ K} \end{array} \left\{ \begin{array}{l} \text{adiabatic} \\ \text{flame temperature} \end{array} \right.$$

Assume a deflagration occurs :

$$T_R = 426.5 : \quad \bar{h}_{\text{CO}_2} = 5149 \text{ J/mol}$$

$$U_R = 3733 + .5(3840) + 1.88(3750) + 3.668(2668) + 3.872(5149) \\ - 10.92(8.314)(426.5) = 3705$$

Assume $T_p = 1200\text{ K}$:

$$(34476 - 241827) + 1.88(28108) + 3.668(18749) + 3.872(44484) - 3705 - 10.42(8.314)(1200) = -21158$$

Assume $T_p = 1300\text{ K}$:

$$(38903 - 241827) + 1.88(31501) + 3.668(20824) + 3.872(50158) - 3705 - 10.42(8.314)(1300) = 10566$$

$$100 \left[\alpha \begin{bmatrix} 1200 & -21158 \\ 1300 & 10566 \end{bmatrix} \begin{matrix} 21158 \\ 31724 \end{matrix} \right] \alpha = 66.69 \\ T_p = 1267\text{ K}$$

$$\eta_p = 10.42 \frac{\text{mols}}{\text{mol H}_2} (0.013216326 \text{ mols H}_2) = .137714 \text{ mols}$$

$$P = \frac{.137714(8.314)(1267)}{.00310919} = 466570.7 \text{ Pa} \quad (67.7 \text{ psia})$$

Calculate internal energy of combustion

Products: $\text{H}_2\text{O} + 1.88\text{N}_2 + 3.668\text{He} + 3.872\text{CO}_2$

$$\left. \begin{array}{l} T = 426.5 \\ \Delta \bar{h}_{\text{CO}_2} = 5149 \text{ J/mol} \end{array} \right\} T = 1267\text{ K} : \left. \begin{array}{l} \Delta \bar{h}_{\text{H}_2\text{O}} = 37442 \\ \Delta \bar{h}_{\text{N}_2} = 30381 \\ \Delta \bar{h}_{\text{He}} = 20139 \\ \Delta \bar{h}_{\text{CO}_2} = 48286 \end{array} \right\} \text{ J/mol}$$

$$\Delta U = (37472 - 4371) + 1.88(30381 - 3750) + 3.668(20139 - 2668) \\ + 3.872(48286 - 5149) - 10.42(8.314)(1267 - 426.5) = \\ 241433 \frac{\text{J}}{\text{mol H}_2}$$

$$\Delta U = 241433 (.013216326 \text{ mols H}_2) = \underline{3190.9 \text{ J}}$$

Scenario #3: Allow the 3013, PVC, & SCY gas spaces to mix freely

$$V_{\text{scv}} = .002777883 \text{ m}^3$$

$$n_{\text{scv}} = \frac{101300 (.002777883)}{8.314(294.3)} = .11500669 \text{ mols}$$

The SCY gas space is filled with air:

$$\text{O}_2 + 3.76 \text{ N}_2 \quad \frac{n_{\text{O}_2}}{n} = \frac{1}{4.76} = .21008$$

$$n_{\text{O}_2} = .21008 (.1150069) = .024161 \text{ mols}$$

$$n_{\text{N}_2} = n - n_{\text{O}_2} = .1150069 - .024161 = .0908456 \text{ mols}$$

Combine the three gas spaces:

$$n_{\text{O}_2} = .006608163 + .024161 = .030769 \text{ mols}$$

$$n_{\text{N}_2} = .024846691 + .0908456 = .1156923 \text{ mols}$$

$$n_{\text{H}_2} = .04847696 \text{ mols}$$

$$n_{\text{CO}_2} = .051172703 \text{ mols}$$

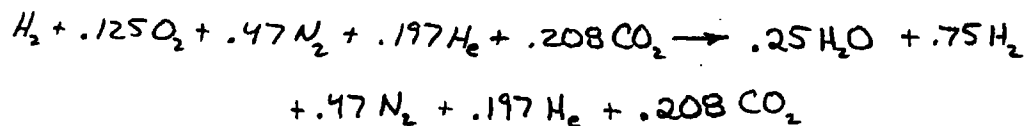
$$\eta = .030769 + .1156923 + .04847696 + .051172703$$

$$\eta = .246110963 \text{ mols}$$

Determine the H_2 required to bring the mixture to UFL:

$$\frac{\eta_{H_2}}{\eta} = x = \frac{\eta_{H_2}}{\eta_{H_2} + .246110963} \quad \eta_{H_2} = \frac{x(.246110963)}{1-x}$$

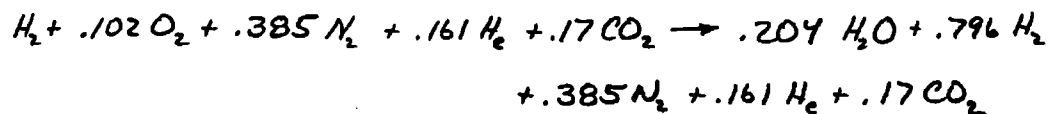
Assume $\frac{\eta_{H_2}}{\eta} = .5$ $\eta_{H_2} = \frac{.5(.246110963)}{1-.5} = .246049 \text{ mols}$



$$T_p = 1200 \text{ K:}$$

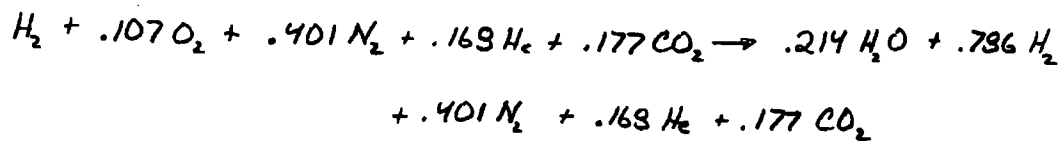
$$-.25(207351) + .75(26794) + .47(28108) + .197(18749) \\ + .208(44484) = -5585$$

Assume $\frac{\eta_{H_2}}{\eta} = .55$ $\eta_{H_2} = \frac{.55(.246110963)}{1-.55} = .300726 \text{ mols}$



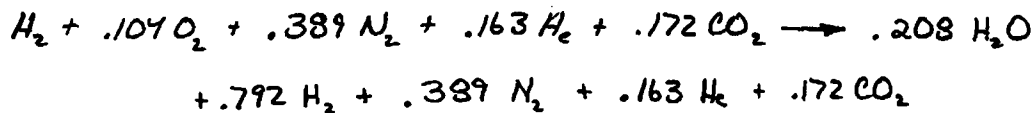
$$-.204(207351) + .796(26794) + .385(28108) + .161(18749) \\ + .17(44484) = 431 \text{ (close)}$$

Assume $\frac{\eta_{H_2}}{\eta} = .54$ $\eta_{H_2} = .28884 \text{ mols}$



$$-.214(207351) + .796(26794) + .401(28108) + .168(18749) \\ + .177(44484) = -1018$$

$$.02 \left[\begin{array}{cc|c} .54 & -1018 & 1013 \\ & 0 & \\ \hline .55 & 431 & \end{array} \right] 1449 \quad \frac{\eta_{H_2}}{\eta} = .547 \\ \eta_{H_2} = .297105 \text{ mols}$$



$$-.208(207351) + .792(26794) + .389(28108) + .163(18749) \\ + .172(44484) = -267$$

$\frac{\eta_{H_2}}{\eta} \sim .548$ I will use .55

UFL 8 $\frac{\eta_{H_2}}{\eta} = .55$ $\eta_{H_2} = .300726 \text{ mols}$

$$\eta_R = 1 + .102 + .385 + .161 + .17 = 1.818 \text{ mols/mol H}_2$$

$$\eta_P = .204 + .796 + .385 + .161 + .17 = 1.716 \text{ mols/mol H}_2$$

$$U_R = 3733 + .102(3840) + .385(3750) + .161(2668) \\ + .17(5149) - 1.818(8.314)426.5 = 427$$

Assume $T_p = 1600 \text{ K}$:

$$.204(52844 - 241827) + .796(39522) + .385(41903) + .161(27062) \\ + .17(67580) - 1.716(8.314)(1600) - 427 = 1631$$

Assume $T_p = 1500 \text{ K}$:

$$.204(48095 - 241827) + .796(36267) + .385(38405) + .161(24983) \\ + .17(61714) - 1.716(8.314)(1500) - 427 = -3180$$

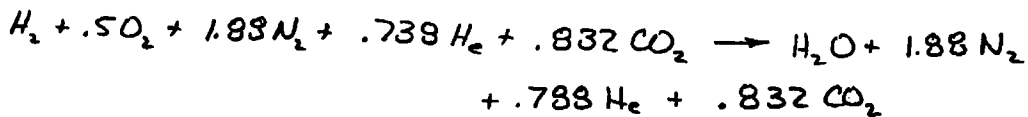
$$100 \left[\alpha \begin{bmatrix} 1500 & -3180 \\ & 0 \end{bmatrix} \begin{bmatrix} 3180 \\ 1631 \end{bmatrix} \right]_{4211} \quad \alpha = 66.1 \\ T_p = 1566 \text{ K}$$

$$\eta_P = 1.716 \frac{\text{mols}}{\text{mol H}_2} (.300726 \text{ mols H}_2) = .51605 \text{ mols}$$

$$P = \frac{.51605(8.314)1566}{.00588707} = 1141286 \text{ Pa} \\ (165.6 \text{ psia})$$

Look at stoichiometric H_2 to demonstrate that UFL is limiting

$$n_{H_2} = 2n_{O_2} = 2(0.030769) = 0.061538 \text{ mols } H_2$$



$$n_p = 1 + 1.88 + .738 + .832 = 4.5 \frac{\text{mols}}{\text{mol } H_2}$$

$$n_p = 4.5(0.061538) = 0.276921 \text{ mols}$$

$$T_p = \frac{p\psi}{n_p R} = \frac{1141286(0.00588707)}{0.276921(8.314)} = 2918 \text{ K}$$

This is the combustion temperature for stoichiometric H_2 such that the pressure is the same as that for UFL. This temperature is too high so the stoichiometric pressure will be lower. Stoichiometric H_2 -air with an initial temperature of 298K has a combustion temperature of 2772 K. If 128 K is added to this temperature to compensate for an initial temperature of 426K vs 298K, the combustion temperature is 2900 K. The gas mixture in the SCV is significantly inerted with He & CO_2 and this will substantially lower the combustion temperature

Calculate the internally energy of combustion:

Products: $.204 \text{ H}_2\text{O} + .796 \text{ H}_2 + .385 \text{ N}_2 + .161 \text{ H}_2 + .17 \text{ CO}_2$

$$T_p = 1566: \left. \begin{array}{l} \Delta \bar{h}_{\text{H}_2\text{O}} = 51229 \\ \Delta \bar{h}_{\text{H}_2} = 38415 \\ \Delta \bar{h}_{\text{N}_2} = 40714 \\ \Delta \bar{h}_{\text{H}_2} = 26355 \\ \Delta \bar{h}_{\text{CO}_2} = 65586 \end{array} \right\} \text{ J/mol}$$

$$\begin{aligned} \Delta U = & .204 (51229 - 4371) + .796 (38415 - 3733) \\ & + .385 (40714 - 3750) + .161 (26355 - 2668) \\ & + .17 (65586 - 5149) - 1.716 (8.314) (1566 - 426.5) = \\ & 49228 \frac{\text{J}}{\text{mol H}_2} \end{aligned}$$

$$\Delta U = 49228 (.300726) = 14804 \text{ J}$$

Deflagrations in a 9975 package (Food Pack Can configuration)

$$V_{\text{cans}} = .001567335 \text{ m}^3$$

$$P = 101300 \text{ Pa}$$

$$T = 294.3 \text{ K (70}^\circ\text{F)}$$

$$n = \frac{PV}{RT} = \frac{101300 (.001567335)}{8.314 (294.3)} = .06488979 \text{ mols}$$

The gas spaces inside of the cans are inerted to 5% O_2

with He: $\text{O}_2 + 3.76 \text{N}_2 + x \text{He} \left\{ \begin{array}{l} \frac{1}{4.76+x} = .05 \\ x = 15.24 \frac{\text{mols He}}{\text{mols O}_2} \end{array} \right.$

$$n_{\text{O}_2} = .05 (.06488979) = .003244449 \text{ mols}$$

$$n_{\text{N}_2} = 3.76 (.003244449) = .012199128 \text{ mols}$$

$$n_{\text{He}} = 15.24 (.003244449) = .049445402 \text{ mols}$$

The PCY gas space outside the cans is inerted with 75% CO_2 by volume

$$\text{O}_2 + 3.76 \text{N}_2 + x \text{CO}_2 \quad \frac{x}{4.76+x} = .75$$

$$x = 14.28 \frac{\text{mols CO}_2}{\text{mol O}_2}$$

$$V = .000649875 \text{ m}^3$$

$$n = \frac{101300 (.000649875)}{8.314 (294.3)} = .026905352 \text{ mols}$$

$$n_{\text{CO}_2} = .75 (.026905352) = .020179014 \text{ mols}$$

$$n_{\text{O}_2} = \frac{.020179014 \text{ mols CO}_2}{14.28 \frac{\text{mols CO}_2}{\text{mol O}_2}} = .001413096 \text{ mols}$$

$$n_{\text{H}_2} = 3.76 (.001413096) = .005313242 \text{ mols}$$

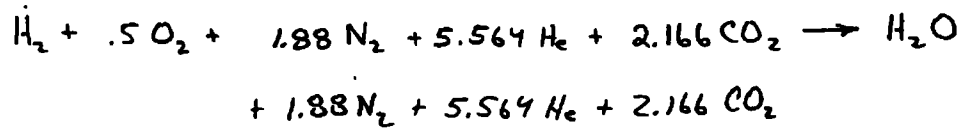
The gas in the food pack cans and the PCV gas spaces mix freely and the helium due to " α " decay is added:

$$\left\{ \begin{array}{l} n_{\text{O}_2} = .00324449 + .001413096 = .004657545 \text{ mols} \\ n_{\text{N}_2} = .012199128 + .005313242 = .01751237 \text{ mols} \\ n_{\text{He}} = .049445402 + .00238146 = .051826862 \text{ mols} \\ n_{\text{CO}_2} = .020179014 \text{ mols} \end{array} \right.$$

$$n_{\text{total}} = .094175791 \text{ mols}$$

Look at stoichiometric H_2 :

$$n_{\text{H}_2} = 2 (.004657545) = .00931509 \text{ mols}$$



Calculate the adiabatic flame temperature:

assume $T_p = 1200 \text{ k}$:

$$34476 - 241827 + 1.88(28108) + 5.564(18749) + 2.166(44484) \\ = 46164 \\ T_p < 1200 \text{ k}$$

assume $T_p = 1000 \text{ k}$:

$$25978 - 241827 + 1.88(21460) + 5.564(14590) + 2.166(33405) \\ = -21970$$

$$200 \left[\begin{array}{cc|c} 1000 & -21970 & 21970 \\ \hline & 0 & \\ 1200 & 46164 & \end{array} \right] 68134 \quad \alpha = 64.5 \\ \underline{\underline{T_p = 1064.5 \text{ k}}}$$

This mixture is probably not flammable but a deflagration analysis will be done anyway:

$$T_{\text{initial}} = 313^\circ \text{F} (429.3 \text{ K})$$

$$\begin{aligned}
 T_R = 429.3 \text{ K} : \quad \Delta \bar{h}_{\text{H}_2} &= 3815 \text{ J/mol} & \Delta \bar{h}_{\text{He}} &= 2726 \text{ J/mol} \\
 \Delta \bar{h}_{\text{O}_2} &= 3925 \text{ J/mol} & \Delta \bar{h}_{\text{CO}_2} &= 5270 \text{ J/mol} \\
 \Delta \bar{h}_{\text{N}_2} &= 3833 \text{ J/mol} & \Delta \bar{h}_{\text{H}_2\text{O}} &= 4468 \text{ J/mol}
 \end{aligned}$$

$$\begin{aligned}
 U_R &= 3815 + .5(3925) + 1.88(3833) + 5.564(2726) \\
 &\quad + 2.166(5270) - 11.11(8.314)(429.3) = -88
 \end{aligned}$$

Assume $T_p = 1400$:

$$\begin{aligned}
 43447 - 241827 + 1.88(34936) + 5.564(22903) + 2.166(55907) \\
 - 10.61(8.314)(1400) + 88 = -7582
 \end{aligned}$$

Assume $T_p = 1500$:

$$\begin{aligned}
 48095 - 241827 + 1.88(38405) + 5.564(24983) + 2.166(61714) \\
 - 10.61(8.314)(1500) + 88 = 17728
 \end{aligned}$$

$$100 \left[\begin{array}{cc} 1400 & -7582 \\ & 0 \end{array} \right] \begin{array}{c} 7582 \\ 27310 \end{array} \quad \alpha = 27.8$$

$$\underline{T_p = 1428 \text{ K}}$$

$$\gamma_p = 10.61 \frac{\text{mols}}{\text{mol H}_2} (.00931509) = .098833 \text{ mols}$$

Combine the three gas spaces:

$$n_{O_2} = .004657545 + .024161 = .028818545 \text{ mols}$$

$$n_{N_2} = .01751237 + .0908456 = .10835797 \text{ mols}$$

$$n_{H_2} = .051826862 \text{ mols}$$

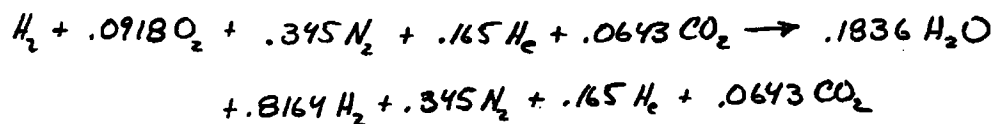
$$n_{CO_2} = .020179014 \text{ mols}$$

$$n_T = .209182391 \text{ mols}$$

Determine the required amount of H_2 for the UFL:

$$\text{Assume } \frac{n_{H_2}}{n} = .6 = \frac{n_{H_2}}{n_{H_2} + .209182391}$$

$$n_{H_2} = \frac{.6 (.209182391)}{1-.6} = .313773587 \text{ mols}$$



$$-.1836(207351) + .8164(26794) + .345(28108) + .165(18749)$$

$$+ .0643(44484) = -544$$

$T_p > 1200K$ need more H_2 (close)

$$P = \frac{.098833 (8.314)(1428)}{.002217209} = 529216.7 \text{ Pa} \\ (76.8 \text{ psia})$$

Determine the internal energy of combustion:

$$\begin{array}{l} @ T_p = 1428 \text{ K} \\ \left. \begin{array}{l} \Delta \bar{h}_{\text{H}_2\text{O}} = 44748 \\ \Delta \bar{h}_{\text{N}_2} = 35907 \\ \Delta \bar{h}_{\text{H}_2} = 23485 \\ \Delta \bar{h}_{\text{CO}_2} = 57533 \end{array} \right\} \text{ J/mol} \end{array}$$

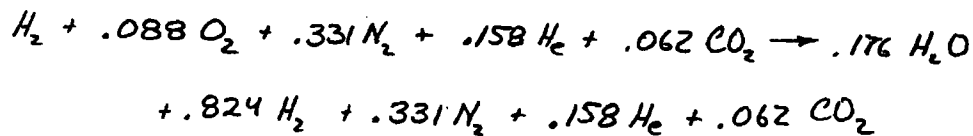
$$\begin{aligned} & (44748 - 4468) + 1.88 (35907 - 3833) + 5.564 (23485 - 2726) \\ & + 2.166 (57533 - 5270) - 10.61 (8.314) (1428 - 429.3) = \\ & \qquad \qquad \qquad 241187 \frac{\text{J}}{\text{mol H}_2} \end{aligned}$$

$$\Delta U = 241187 (.00931509) = \underline{\underline{2247 \text{ J}}}$$

Scenario #2: combine the FP can/PCV with the SCV

$$\left. \begin{array}{l} V_{\text{SCV}} = .002777883 \text{ m}^3 \\ n_{\text{O}_2} = .024161 \text{ mols} \\ n_{\text{H}_2} = .0908456 \text{ mols} \end{array} \right\} \text{ same as for the 3013 configuration}$$

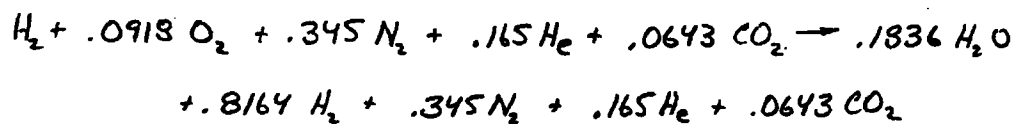
$$\text{Assume } \frac{\eta_{H_2}}{\eta} = .61 \quad \eta_{H_2} = \frac{.61(.209182391)}{1-.61} = .327182714 \text{ mols}$$



$$-.176(207351) + .824(26794) + .331(28108) + .158(18749)$$

$$+ .062(44484) = 609$$

$$\therefore \text{UFL } \frac{\eta_{H_2}}{\eta} = .6 \quad \eta_{H_2} = .313773587 \text{ mols}$$



$$\eta_R = 1 + .0918 + .345 + .165 + .0643 = 1.6661 \frac{\text{mols}}{\text{mol } H_2}$$

$$U_R = 3815 + .0918(3125) + .345(3833) + .165(2726)$$

$$+ .0643(5270) - 1.6661(8.314)(421.3) = 340$$

$$\text{Assume } T_p = 1600K :$$

$$.1836(52844 - 241827) + .8164(39522) + .345(41903) + .165(27062)$$

$$+ .0643(67580) - 1.6661(8.314)(1600) - 340 = -1667$$

Assume $T_p = 1700\text{K}$:

$$\begin{aligned} &.1836 (57685 - 241827) + .8164 (42815) + .345 (45430) \\ &+ .165 (29142) + .0643 (73492) - 1.6661 (8.314) (1700) - 340 = \\ &2465 \end{aligned}$$

$$100 \begin{bmatrix} \alpha \begin{bmatrix} 1600 & -1667 \\ & 0 \end{bmatrix} 1667 \\ 1700 & 2465 \end{bmatrix} 4132 \quad \alpha = 40.3$$

$$\underline{\underline{T_p = 1640\text{K}}}$$

$$\mathcal{V}_p = 1.6661 \frac{\text{mols}}{\text{mol H}_2} (.313773587) = .522778 \text{ mols}$$

$$v = .004995092 \text{ m}^3$$

$$P = \frac{.522778 (8.314) (1640)}{.004995092} = 1427012 \text{ Pa} \quad (207.1 \text{ psia})$$

$$T_p = 1640\text{K} : \left. \begin{array}{l} \Delta \bar{h}_{\text{H}_2\text{O}} = 54780 \\ \Delta \bar{h}_{\text{H}_2} = 40839 \\ \Delta \bar{h}_{\text{N}_2} = 45755 \end{array} \right\} \text{J/mol} \quad \left. \begin{array}{l} \Delta \bar{h}_{\text{H}_2} = 27894 \\ \Delta \bar{h}_{\text{CO}_2} = 69945 \end{array} \right\} \text{J/mol}$$

$$\begin{aligned} \Delta U &= .1836 (54780 - 4468) + .8164 (40839 - 3815) + .345 (45755 - 3833) \\ &+ .165 (27894 - 2726) + .0648 (69945 - 5270) \\ &- 1.6661 (8.314) (1640 - 429.3) = 45499.86 \frac{\text{J}}{\text{mol H}_2} \end{aligned}$$

$$\Delta U = 45499.86 (.313773587) = \underline{\underline{14276.7 \text{ J}}}$$

This Page is Intentionally Blank

APPENDIX 3.9
DETONATION CELL WIDTHS IN THE 9975 PACKAGE
WITH CO₂ DILUTING OF THE PCV GAS SPACE

This Page Intentionally Left Blank

CSR 43-24# (Rev. 1-10-2000)

Calculation Cover Sheet

Project 9975 Package Certification		Calculation Number M-CLC-A-00175	Project Number N/A	
Title Detonation Cell Widths in the 9975 Package with CO ₂ Diluting of the PCV Gas Space <i>u</i>		Functional Classification SC	Sheet 1 of 13	
		Discipline Mechanical		
<input type="checkbox"/> Preliminary <input checked="" type="checkbox"/> Confirmed				
Computer Program No. detcs.1 (a code developed by the author) <input type="checkbox"/> N/A		Version/Release No. (Reference: WSRC-TR-2001-00265)		
Purpose and Objective To determine the detonation cell widths in the 9975 package containment vessels with CO ₂ diluting of the PCV. The impact of a 75% diluting of the 3013 container with either helium, argon, or additional nitrogen on the cell width is also assessed.				
Summary of Conclusion Detonation cell widths in the 3013 container, the PCV, and the SCV of the 9975 package have been determined for four diluting scenarios of the 3013 container and the PCV. Scenarios in which the PCV is diluted with 50% and 75% CO ₂ by volume are considered, with and without a 75% diluting of the 3013 container. Both the 3013 container and the PCV are assumed to leak, so the gas mixtures within all three containment vessels mix freely. Sufficient hydrogen is assumed to be generated after the 9975 package is sealed to form a stoichiometric hydrogen-air-diluent mixture. With 50% CO ₂ initially in the PCV, the cell widths are approximately 18 mm and 28 mm respectively without and with helium diluting of the 3013 container. With 75% CO ₂ initially in the PCV, the cell widths are approximately 61 mm and 98 mm respectively without and with helium diluting of the 3013 container. Since the bounding radial gap is 20.3 mm, 75% CO ₂ diluting of the PCV effectively precludes a detonation in the 9975 package. Cell width considerations also preclude a detonation in the head spaces.				
Revisions				
Rev No.	Revision Description			
0	Original Issue			
1	The lower threshold percent CO ₂ diluting of the PCV is calculated for a bounding gap of 20.3 mm instead of 18.6 mm.			
Sign Off				
Rev No.	Originator (Print) Sign/Date	Verification/ Checking Method	Verifier/Checker (Print) Sign/Date	Manager (Print) Sign/Date
0				
1	<i>M.A. Shadday</i> <i>M.A. Shadday</i> 6/21/01	Document Review	<i>N.K. Gupta</i> <i>N.K. Gupta</i> 6/21/01 <i>Steve Hensley</i> <i>John Hermal</i> 6/21/01	<i>C.P. HOLDING SMITH</i> <i>C.P. HOLDING SMITH</i> 6/21/01
		Customer review		
Release to Outside Agency -- Design Authority (Print)		Signature		Date
Security Classification of the Calculation Unclassified				

DETONATION CELL WIDTHS IN THE 9975 PACKAGE WITH CO₂ DILUTING OF THE PCV GAS SPACE

Introduction and Summary

Plutonium oxide in a 9975 shipping package can generate hydrogen by radiolysis of absorbed water vapor. If the hydrogen is released into the gas space it can form a combustible and potentially detonable mixture with the oxygen in the air. The detonation cell width is a measure of the sensitivity of a particular flammable mixture to the onset and propagation of a detonation wave. A large cell width, depending on the characteristic channel dimension, can preclude the propagation of a detonation down a channel. As long as the detonation cell width is greater than the gap width, a detonation cannot propagate down a channel. Detonation cell widths have been determined for the nested containers in the 9975 package under several scenarios in which the air is diluted with the inert gases helium, or argon, or excess nitrogen, and/or carbon dioxide. Carbon dioxide is an especially effective diluent with respect to increasing the gaseous mixture cell width. Filling the PCV gas space with 51.8% CO₂ by volume will result in a gaseous mixture with 11.2% CO₂ when the gas spaces of the 3013 container, the PCV, and the SCV are connected by leaks and sufficient hydrogen is generated to render the hydrogen and oxygen stoichiometric. The cell width for this mixture is approximately 20.3 mm and the worst case radial gap, following a deforming impact, has a width of 20.3 mm. As long as the PCV is diluted with more than 51.8% CO₂, a detonation is precluded in the radial gaps. Filling the PCV with 75% CO₂ results in a gaseous mixture with 16.6% CO₂, when the contents of the three gas spaces mix, and the resultant cell width is approximately 61.0 mm. There is sufficient margin between the detonation cell width and the bounding gap width to conclude that a detonation is not possible in 3013 configuration of the 9975 shipping package if the PCV gas space is filled with 75% CO₂. Cell width considerations also preclude a detonation in the axial head spaces between the nested vessels.

Input

The 3013 configuration of the 9975 shipping package contains three nested containers. From the inside going out, the nested containers are: the 3013 container, the primary containment vessel (PCV), and the secondary containment vessel (SCV). The volumes of the gas spaces in the three containers are [1]:

$$\begin{aligned}V_{3013} &= 1.1978 \times 10^{-3} \text{ m}^3 \\V_{\text{PCV}} &= 1.6480 \times 10^{-3} \text{ m}^3 \\V_{\text{SCV}} &= 2.7779 \times 10^{-3} \text{ m}^3\end{aligned}$$

The PCV volume is the volume of gas space inside of the PCV and outside of the 3013 container. The SCV volume is the volume of gas space inside of the SCV and outside of the PCV.

The 9975 shipping package is packed by loading the plutonium oxide in the 3013 container and then sequentially loading the nested containers, each in the next larger container, until the package is assembled. The gas spaces of the containers are assumed to be filled with air at 70°F and 14.7 psia, unless filled with an inert gas. A proposal to fill the PCV gas space with CO₂, to prevent the possibility of a detonation, is under consideration. Since the fraction of PCV gas space that can be filled with CO₂ during the 9975 packing phase is unknown, two scenarios are considered, 50% and 75% by volume of the PCV gas space initially filled with CO₂. The balance of the PCV gas space will be filled with air, and again the initial temperature and pressure are assumed to be 70°F and 14.7 psia. There are also plans to fill the 3013 container with an inert gas (most likely helium but possibly argon or nitrogen), so the two PCV fill scenarios are considered, each with and without a 75% diluent fill of the 3013 container. The plutonium oxide is stored inside of the 3013 container, and all of the hydrogen is generated within this container. As long as the gas tight integrity of the 3013 container is maintained, only the inside of the 3013 container need be considered for a possible detonation. There will be no fuel in the gas spaces of the outer containers. Since the integrities of the 3013 container and the PCV cannot be guaranteed, it is conservatively assumed that they leak and that the contents of the gas spaces of the three nested containers mix. Mixing is not assumed to dilute the hydrogen fuel. There is sufficient absorbed water vapor in the plutonium oxide to generate enough hydrogen to result in stoichiometric hydrogen-oxygen-inert gas mixtures in all three gas spaces. The oxygen generated by dissociation of water is assumed to remain absorbed in the plutonium oxide, and it is therefore not released to the gas space. The hydrogen will be generated after the 9975 package is sealed, so it will increase the pressure in the gas spaces. Mixing will dilute the 3013 container diluent and the PCV CO₂.

Once the 9975 package is sealed the contents will be heated by plutonium decay. The steady-state temperature distribution in a 9975 package has been calculated numerically [2]. The gas space temperatures are conservatively assumed to be the peak surface temperature for each gas space. The assumed gas space temperatures are:

$$T_{3013} = 324^{\circ}\text{F} = 435.4 \text{ K}$$

$$T_{\text{PCV}} = 293^{\circ}\text{F} = 418.2 \text{ K}$$

$$T_{\text{SCV}} = 282^{\circ}\text{F} = 412.0 \text{ K}$$

Only stoichiometric hydrogen-oxygen gaseous mixtures are considered. This is a bounding approach from the detonation cell width viewpoint. The cell width is very sensitive to the fuel-oxygen ratio, with a sharp minimum for stoichiometric mixtures. The cell width is a much weaker inverse function of pressure. If more hydrogen than that required by a stoichiometric mixture is generated, the pressure will be greater than that for a stoichiometric mixture, but the fuel rich mixture will have a larger cell width because of the non-optimum hydrogen-oxygen composition. To get to a fuel rich

composition, the mixture would necessarily pass through the bounding stoichiometric composition point. The minimum cell width for a stoichiometric mixture also bounds those of fuel lean mixtures, in which there is less hydrogen. The amount of absorbed water in the plutonium oxide is irrelevant with respect to this analysis, as long as there is sufficient water to generate the hydrogen to make the hydrogen-air mixture stoichiometric. This criterion is easily satisfied, and as mentioned above an analysis of a stoichiometric mixture bounds analysis of fuel lean mixtures.

Helium generation due to alpha decay is neglected in this analysis. This is a negligible contributor to the total number of moles of gas in the mixture, and helium is an inert diluent that increases detonation cell widths. Ignoring this source is conservative.

Analytical Methods and Computations

Given the pressure, temperature, and constituency of the gaseous mixture that results from the mixing of the contents of the three container gas spaces, the detonation cell width can be calculated with the semi-empirical model described in reference [3]. This model relates the Zeldovich, Doring, and Von Neumann (ZND) induction length [4] to the cell width. Detonation cell width data was used to determine the correlation factor "A" between the theoretical ZND induction length and the cell width "λ".

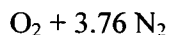
$$\lambda = AL_{ZND} \quad (1)$$

For all hydrogen-air mixtures with helium, argon, or excess nitrogen the value of the correlation factor is assumed to be 51.0. For mixtures with CO₂ the value of the correlation factor is a function of the percent CO₂ by volume in the mixture.

To determine the final state of the hydrogen-air-CO₂ mixture in the three connected gas spaces, the number of moles of each of the constituents in each of the gas spaces, initially at 70°F and atmospheric pressure, is determined. First the total number of moles in each of the gas spaces is determined with the ideal gas relation:

$$n = \frac{PV}{RT} \quad (2)$$

The number of moles of each constituent is the product of the constituent mole fraction and the total number of moles. For example, if the volume is filled with air



the number of moles of oxygen and nitrogen are respectively:

$$n_{\text{O}_2} = \frac{1}{4.76} n \quad \& \quad n_{\text{N}_2} = \frac{3.76}{4.76} n$$

To determine the constituency of the final mixture when the contents of the three gas spaces mix, the numbers of moles of each constituent in each gas space are summed and sufficient hydrogen is added to make the mixture stoichiometric. The pressures in the three gas spaces will be equal after mixing, but the temperatures will differ. To determine the pressure, solve the continuity equation and the ideal gas relation for each of the gas spaces simultaneously.

$$PV_{3013} = n_{3013} \bar{R} T_{3013} \quad (3)$$

$$PV_{PCV} = n_{PCV} \bar{R} T_{PCV} \quad (4)$$

$$PV_{SCV} = n_{SCV} \bar{R} T_{SCV} \quad (5)$$

$$n_{3013} + n_{PCV} + n_{SCV} = n \quad (6)$$

By judicious substitution these simultaneous equations can be reduced to a single equation for the pressure:

$$P = \frac{n \bar{R} T_{3013}}{V_{3013} + V_{PCV} \frac{T_{3013}}{T_{PCV}} + V_{SCV} \frac{T_{3013}}{T_{SCV}}} \quad (7)$$

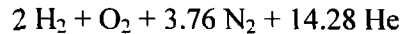
With the gas mixture constituency the pressure and the three gas space temperatures known, the gas space cell widths can be determined by the semi-empirical model [3]. As a result of the temperature differences, each gas space will have a different value for the cell width.

Results and Discussion

Four scenarios, in which the PCV is partially filled with CO₂ and the 3013 container is or is not partially filled with an inert diluent, are considered. The 3013 container and the PCV are assumed to leak, allowing the contained gas mixtures to mix with that in the SCV. From the detonation standpoint this is a conservative assumption, since the air initially in the SCV is not diluted with an inert gas and it supplies oxygen to the final mixture. Since it is assumed that there is sufficient hydrogen available to match any available oxygen, the more oxygen the more hydrogen and the volume percentage of inert diluents is reduced. Since all of the hydrogen is generated in the 3013 container, if this container does not leak it alone will contain a combustible gaseous mixture. Inerting the 3013 will preclude the possibility of a detonation in the container, as long as it does not leak. With 75% helium and 25% air initially in the container the initial gaseous mixture is:

$$\text{O}_2 + 3.76 \text{N}_2 + x \text{He} \quad \text{where} \quad \frac{x}{4.76 + x} = 0.75$$

The stoichiometric coefficient of helium is $x = 14.28$. Adding sufficient hydrogen to make a stoichiometric mixture results in the following mixture:



$$\% \text{H}_2 = (2/21.04) \times 100 = 9.5\%$$

This mixture is 9.5% hydrogen by volume. This is just above the lean flammable limit for hydrogen-air mixtures (9.0%, [5]). The lean hydrogen detonable limit will be greater than the flammable limit, so the conjecture that the hydrogen-air-helium mixture will not detonate is reasonable.

At 14.7 psia and 70°F, the initial helium mixture will have 0.04959 moles, equation (2). The number of moles of oxygen is 0.0026045. Twice this number of moles of hydrogen is added to make the hydrogen-air-helium mixture stoichiometric. The ideal gas relation is used to calculate the final pressure (24.03 psia). With a temperature of 324°F, the predicted detonation cell width [3] is 26.6 mm. This calculated cell width is independent of the flammability limit. The model will calculate a cell width, irrespective of whether the mixture is within the flammability limits. The cell width alone precludes a detonation since the cell width is greater than the bounding radial gap (6.5 mm inside of the 3013 container following an impact [6,8]).

$$n = \frac{PV}{RT} = \frac{101300(0.001197803)}{8.314(294.3)} = 0.04959 \text{ mols}$$

$$n_{\text{O}_2} = \frac{0.04959}{19.04} = 0.0026045 \text{ mols}$$

$$n_{\text{stoic}} = n + 2n_{\text{O}_2}$$

$$P = \frac{n_{\text{stoic}} \bar{R} T}{V} = \frac{0.054799(8.314)(435.4)}{0.0011978} = 165610.08 \text{ Pa} \quad (24.03 \text{ psia})$$

If only the 3013 container leaks, the helium-air in the 3013 container will mix with the CO₂-air mixture in the PCV. This mixture will not be detonable because CO₂ is a very effective diluent for raising the cell width. There is no diluent in the SCV, so mixing the SCV air with the contents of the other two containers is conservative. The additional oxygen in the SCV air allows more hydrogen in the final stoichiometric mixture.

Scenario #1: 50% CO₂ in the PCV and no Dilution of the 3013 Container

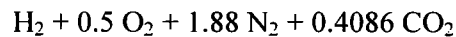
The first scenario considered is the one in which the PCV is initially filled with 50% CO₂ and the 3013 container is initially filled with air. The number of moles of oxygen, nitrogen, and CO₂ initially in each of the three containers are shown in Table 1 along

with the total for the combined mixture. The number of moles of hydrogen added to make the mixture stoichiometric is twice the total number of moles of oxygen.

Table 1: Number of moles of oxygen, nitrogen, and carbon dioxide initially in the 3013 container, the PCV, and the SCV at 70°F and 14.7 psia. The PCV is filled with 50% by volume CO₂.

Container	$n(\text{O}_2)$	$n(\text{N}_2)$	$n(\text{CO}_2)$
3013	0.010418	0.03917	-
PCV	0.007167	0.026948	0.034115
SCV	0.024161	0.090846	-
Combined	0.041746	0.156964	0.034115

The final constituency of the mixture, based on a mole of hydrogen, is:



This mixture is 10.8% CO₂ by volume. The pressure from equation (7) is 28.4 psia. The predicted cell widths are:

$$\begin{aligned}\lambda_{3013} &= 18.1 \text{ mm} \\ \lambda_{\text{PCV}} &= 18.5 \text{ mm} \\ \lambda_{\text{SCV}} &= 18.6 \text{ mm}\end{aligned}$$

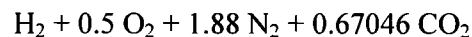
Scenario #2: 75% CO₂ in the PCV and no Dilution of the 3013 Container

The second scenario considered is the one in which the PCV is initially filled with 75% CO₂ and the 3013 container is initially filled with air. The number of moles of oxygen, nitrogen, and CO₂ initially in each of the three containers are shown in Table 2 along with the total for the combined mixture. The number of moles of hydrogen added to make the mixture stoichiometric is twice the total number of moles of oxygen.

Table 2: Number of moles of oxygen, nitrogen, and carbon dioxide initially in the 3013 container, the PCV, and the SCV at 70°F and 14.7 psia. The PCV is filled with 75% by volume CO₂.

Container	$n(\text{O}_2)$	$n(\text{N}_2)$	$n(\text{CO}_2)$
3013	0.010418	0.03917	-
PCV	0.003584	0.01347	0.051173
SCV	0.024161	0.090846	-
Combined	0.038163	0.14349	0.051173

The final constituency of the mixture, based on a mole of hydrogen, is:



This mixture is 16.6% CO₂ by volume. The pressure from equation (7) is 27.8 psia. The predicted cell widths are:

$$\lambda_{3013} = 59.5 \text{ mm}$$

$$\lambda_{PCV} = 61.6 \text{ mm}$$

$$\lambda_{SCV} = 62.3 \text{ mm}$$

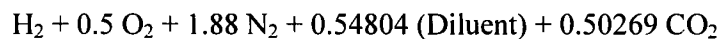
Scenario #3: 50% CO₂ in the PCV and 75% Diluent in the 3013 Container

The third scenario considered is the one in which the PCV is initially filled with 50% CO₂ and the 3013 container is initially filled with 75% diluent, either helium, argon or additional nitrogen. The numbers of moles of oxygen, nitrogen, diluent, and CO₂ initially in each of the three containers are shown in Table 3, along with the total for the combined mixture. The number of moles of hydrogen added to make the mixture stoichiometric is twice the total number of moles of oxygen.

Table 3: Number of moles of oxygen, nitrogen, helium, and carbon dioxide initially in the 3013 container, the PCV, and the SCV at 70°F and 14.7 psia. The 3013 container is filled with 75% by volume He and the PCV is filled with 50% by volume CO₂.

Container	<i>n</i> (O ₂)	<i>n</i> (N ₂)	<i>n</i> (Diluent)	<i>n</i> (CO ₂)
3013	0.0026045	0.00979298	0.0371925	-
PCV	0.007167	0.026948	-	0.034115
SCV	0.024161	0.090846	-	-
Combined	0.0339325	0.127587	0.0371925	0.034115

The final constituency of the mixture, based on a mole of hydrogen, is:



This mixture is 11.3% CO₂ by volume. The pressure from equation (7) is 27.0 psia. The predicted cell widths for the three different diluents are shown in Table (4).

Table 4: Cell widths in the 3013 container, the PCV, and the SCV with 75% diluting of the 3013 container with either helium, argon, or additional nitrogen and 50% diluting of the PCV with CO₂.

Container	Cell Width (He)	Cell Width (Ar)	Cell Width (N ₂)
3013	25.5 mm	23.4 mm	32.8 mm
PCV	26.1 mm	24.0 mm	33.9 mm
SCV	26.4 mm	24.2 mm	34.4 mm

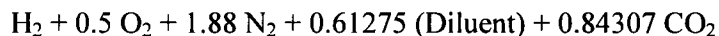
Scenario #4: 75% CO₂ in the PCV and 75% Dilution of the 3013 Container

The fourth scenario considered is the one in which the PCV is initially filled with 75% CO₂ and the 3013 container is initially filled with 75% diluent. The numbers of moles of oxygen, nitrogen, diluent, and CO₂ initially in each of the three containers are shown in Table 5, along with the total for the combined mixture. The number of moles of hydrogen added to make the mixture stoichiometric is twice the total number of moles of oxygen.

Table 5: Number of moles of oxygen, nitrogen, helium, and carbon dioxide initially in the 3013 container, the PCV, and the SCV at 70°F and 14.7 psia. The 3013 container is filled with 75% by volume He and the PCV is filled with 75% by volume CO₂.

Container	<i>n</i> (O ₂)	<i>n</i> (N ₂)	<i>n</i> (Diluent)	<i>n</i> (CO ₂)
3013	0.0026045	0.00979298	0.0371925	-
PCV	0.0035836	0.013474	-	0.05117
SCV	0.024161	0.090846	-	-
Combined	0.0303491	0.114113	0.0371925	0.05117

The final constituency of the mixture, based on a mole of hydrogen, is:



This mixture is 17.4% CO₂ by volume. The pressure from equation (7) is 26.4 psia. The predicted cell widths for the three different diluents are shown in Table (6).

Table 6: Cell widths in the 3013 container, the PCV, and the SCV with 75% diluting of the 3013 container with either helium, argon, or additional nitrogen and 75% diluting of the PCV with CO₂.

Container	Cell Width (He)	Cell Width (Ar)	Cell Width (N ₂)
3013	94.4 mm	86.9 mm	126.0 mm
PCV	98.2 mm	90.4 mm	132.4 mm
SCV	99.6 mm	91.7 mm	134.8 mm

Consideration of Axial Gaps

In addition to the radial gaps between nested containers that form long channels through which a detonation wave could travel, there are axial gaps between the containers. The largest open space occurs between the lid of the 3013 container and the inner surface of the PCV lid, and inside of the annular spacer that maintains this gap. The annular spacer has an inside diameter of 111.25 mm (4.38 in.) and a height of 128.52 mm (5.06 in.). The appropriate criterion for the onset of a detonation from a weak ignition source in an enclosure is; the enclosure characteristic length is greater than seven times the detonation cell width [7].

$$L > 7\lambda \quad (8)$$

The characteristic length for a room [7] is defined as the average of the width and height. For the cylindrical space inside of the 3013 top spacer, the characteristic length is the average of the diameter and axial length:

$$L = \frac{1}{2}(D + H) = 119.9 \text{ mm}$$

$$\lambda = \frac{119.9}{7} = 17.1 \text{ mm}$$

Therefore, the threshold cell width for a detonation is 17.1 mm. If the cell width is greater than this value, a detonation will not occur in the axial space above the 3013 container lid. In scenario #1 above with 50% diluting of the PCV with CO₂ and no diluting of the 3013 container, the PCV cell width is 18.5 mm. This is above the threshold, but by only a small margin. The more realistic case, scenario #4 above with 75% diluting of the PCV with CO₂ and 75% diluting of the 3013 container, has a PCV cell width of 90.4 mm with argon diluting of the 3013 container. A detonation is precluded with plenty of margin.

Lower Threshold Percent CO₂ Dilution of the PCV

The lower threshold allowable percent CO₂ dilution of the PCV is that which results in a detonation cell width of 20.3 mm [6,8], the bounding radial gap in the 9975 package. During normal conditions of transport (NCT) the largest radial gap (16.9 mm) occurs between the PCV and the SCV. This is a bounding NCT value for this gap. Following a drop, deformation of the vessels can increase the gaps, and a 16.9 mm gap could become 20.3 mm [6,8]. To preclude a detonation in this gap, the cell width must be greater than 20.3 mm, and this value will also preclude a detonation in the axial head space between the 3013 container and the PCV. The threshold cell width for this space is 17.1 mm.

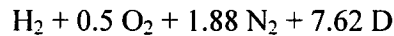
The percent diluting of the PCV with CO₂, and with no diluting of the 3013 container, that results in a SCV cell width of 20.3 mm was calculated iteratively. A value for percent CO₂ dilution of the PCV was assumed and the SCV cell width was calculated. This process was repeated until the calculated cell width converged with the desired cell width of 20.3 mm. This is the lower threshold value of CO₂ dilution of the PCV that precludes a detonation in the 9975 package if the 3013 container leaks. No credit was taken for inert gas dilution of the 3013 container, and if the 3013 container is diluted this threshold value will drop.

3013 Container Dilution Considerations, (no leak)

If the leak-tight integrity of the 3013 container is maintained, the CO₂ diluting of the PCV will not benefit the 3013 container, and the initial diluting of the 3013 container alone will impact the cell width. The 3013 container will be loaded and assembled in an atmosphere with less than 5.0% oxygen. Calculations of the cell widths for dilutions of the 3013 container that result in 5.0% by volume oxygen at loading follow. Dilutions with helium, argon, and hydrogen are considered. The initial oxygen mole ratio is 0.05:

$$\text{O}_2 + 3.76 \text{N}_2 + X_D \text{D} \Rightarrow \frac{n_{\text{O}_2}}{n} = \frac{1}{4.76 + X_D} = 0.05 \Rightarrow X_D = 15.24$$

With the addition of sufficient hydrogen to make the hydrogen-oxygen mixture stoichiometric, the composition of the mixture on the basis of a mole of hydrogen is:



The final pressure (P_f) is calculated with the ideal gas relation. The initial temperature is 294.3 K and the final temperature is 435.4 K.

$$P_f = P_i \frac{n_f}{n_i} \frac{T_f}{T_i} = 164854.3 \text{ Pa (23.92 psia)} \quad (9)$$

The detonation cell widths [3] for the three possible diluents are:

$$\begin{aligned} \lambda_{\text{argon}} &= 15.9 \text{ mm} \\ \lambda_{\text{helium}} &= 29.7 \text{ mm} \\ \lambda_{\text{nitrogen}} &= 195.2 \text{ mm} \end{aligned}$$

The initial percent volume of diluent in all three cases is 76.2%.

The bounding radial gap in the 3013 container following an impact that results in deformations of the nested vessels is 6.5 mm. Calculations of the percent diluents, and the associated percent oxygen, that result in cell widths of 6.5 mm follow. The procedure is necessarily iterative. The compositions of the gaseous mixtures at loading, and after closing and hydrogen generation are respectively:

Initial composition: $0.5 \text{O}_2 + 1.88 \text{N}_2 + X_D \text{D}$

Final composition: $\text{H}_2 + 0.5 \text{O}_2 + 1.88 \text{N}_2 + X_D \text{D}$

The final pressure is determined with the ideal gas relation, equation (9), where the final to initial mole ratio is:

$$\frac{n_f}{n_i} = \frac{3.38 + X_D}{2.38 + X_D} \quad (10)$$

The initial and final temperatures are again 294.3 K and 435.4 K respectively.

The iterative procedure is to first assume a value for the final pressure and then use the cell width model [3] to determine the diluent stoichiometric coefficient (X_D) that results in a cell width of 6.5 mm. The final pressure is checked and updated with equations (9 & 10), and the procedure is repeated until the final pressure converges. Results are presented in Table (7).

Table 7: Initial percent diluents and oxygen for diluting of the 3013 container such that the cell width is 6.5 mm.

Diluent	X_D	Pf (psia)	Initial % Diluent	Initial % Oxygen
helium	1.822	26.91	43.4	11.9
argon	3.23	25.63	57.6	8.9
nitrogen	0.753	28.69	84.0 (total)	16.0

Conclusions

Of the four PCV and 3013 container dilution scenarios considered in the previous section, the smallest cell size occurs with 50% CO₂ in the PCV and no diluent in the 3013 container. Going from 50% CO₂ to 75% CO₂ in the PCV dramatically increases the cell width. Adding 75% diluent to the 3013 container also increases the cell widths for both cases of 50% CO₂ and 75% CO₂ added to the PCV. These increases in cell width are due primarily to the serendipitous increases in percentage CO₂ in the final mixtures because the diluent displaces some of the oxygen in the 3013 container. With less total oxygen in the final mixture, there will be less hydrogen added to make the mixture stoichiometric. The number of moles of CO₂ is independent of the diluent added to the 3013 container, but the diluent reduces the total number of moles of gas in the final mixture. This increases the volume percent CO₂ in the final mixture, and the cell width is very sensitive to the percent CO₂ in the mixture. For increasing the detonation cell width, CO₂ is a much more effective inert diluent than the other three diluents considered. Additional nitrogen is a more effective diluent than either helium or argon.

References

1. "Safety Analysis Report – Packages 9972-9975 Packages", WSRC-SA-7, Rev. 11, p. 3.5-6, December 2000.
2. Gupta, N. K., "Air Temperatures in the 9975 Package", Interoffice Memorandum SRT-EMS-2001-00010, March 29, 2001.

3. Shadday, M. A., "A Semi-Empirical Model for Detonation Cell Widths", WSRC-TR-2001-00265, May 2001.
4. Kumar, R. K., "Detonation Cell Widths in Hydrogen-Oxygen-Diluent Mixtures", *Combustion and Flame*, 80(2): 157-169 (1990).
5. Drell, I. L., & Belles, F. E., "Survey of Hydrogen Combustion Properties", NACA Report 1383.
6. Wu, T. T., "Analysis of Gap Sizes between Components of 9975 Package subjected to 55-Foot Drop", M-CLC-00746, Rev. 0, June 2001.
7. Breitung, W., et. al., "Flame Acceleration and Deflagration to Detonation Transition in Nuclear Safety", NEA/CSNI/R(2000)7, August 2000, available at <http://www.galcit.caltech.edu/~jesup/SOAR/index.html>.
8. Abramczyk, G. A., "Stack-up Dimensions of the 9975 Packaging Components in Normal Conditions of Transport (NCT) and Hypothetical Accident Conditions (HAC)", M-CLC-00177, Rev. 0, June 2001.

This Page Intentionally Left Blank